

20  
NIDK - 00  
*Analysis*

# TELSTAR I

FACILITY FORM 602

N67 12301	N67 12320
(ACCESSION NUMBER)	(THRU)
448	1
(PAGES)	(CODE)
(NASA OR OTHER AGENCY USE ONLY)	07



NASA SP-32  
VOLUME 4  
DECEMBER 1965

OLD PRICE \$ \_\_\_\_\_

CURRENT PRICE(S) \$ \_\_\_\_\_

Quantity (MP) \$ 7.45

Quantity (MP) 2.00

WITH A  
SUPPLEMENT ON  
TELSTAR II

# 650 July 65

NATIONAL AERONAUTICS AND SPACE ADMINISTRATION  
GODDARD SPACE FLIGHT CENTER

## Preface

Volume IV of NASA Special Publication SP-32 was originally intended to contain only those papers published outside of the Bell System Technical Journal that were pertinent to the Telstar I project. However, since that time, the results of Telstar II have been reported to NASA by the Bell Telephone Laboratories. It was then decided that this report should also be included.

I would like to express my appreciation to Mr. E. F. O'Neill, the Bell Telephone Laboratories Telstar Project Manager, for the understanding and cooperation that he gave me during this project. As well, I would like to express my appreciation to the principal international participants: M. Rene Sueur of CNET, PTT, France; Mr. F. J. D. Taylor, Engineering Department, GPO, United Kingdom; and Dr. Piero Fanti, Telespazio, Italy, for making possible their nations' contributions to this report.

CHARLES P. SMITH, JR.  
*NASA Telstar Project Manager*

Contents, Part 4

TELSTAR I

FUCINO, ITALY

Project Telstar — Fucino Earth Station Operation Analysis 1941 ✓

PLEUMEUR-BODOU, FRANCE

Description of the Installations at the Pleumeur-Bodou Space  
Communications Station M. J. DAUTREY 1951 ✓

Results of Tests Performed with the Telstar I Satellite at the  
Pleumeur-Bodou Satellite Communication Station  
L. BOURGEAT, A. DYEVE AND J. P. HOUSSIN 1999 ✓

GOONHILLY DOWNS, ENGLAND

The Post Office Satellite Communication System Ground Station  
at Goonhilly, Cornwall W. J. BRAY AND F. J. D. TAYLOR 2059 ✓

The Goonhilly 85-ft Steerable Dish Aerial C. N. KINGTON 2077 ✓

Computing and Data Transmission for the Prediction Steering  
of the Goonhilly Satellite-Communication Aerial  
E. C. SEAMAN AND W. E. THOMPSON 2091 ✓

Digital Techniques Used in the Steering Apparatus of the GPO  
Steerable Aerial at Goonhilly Downs J. E. MARSHALL,  
R. J. COULTER AND J. K. BINKS 2101 ✓

Beam-Swinging Facilities for the Goonhilly Satellite-Communi-  
cation Aerial C. F. DAVIDSON AND W. A. RAWLINSON 2117 ✓

A 4/6 Gc/s Circularly-Polarized Diplexer for the Goonhilly  
Satellite-Communication Aerial  
D. CHAKRABORTY AND G. F. D. MILLWARD 2127 ✓

Primary Feeds for the Goonhilly Satellite-Communication Aerial  
I. A. RAVENSCROFT 2141 ✓

Waveguide Feeder System for the Goonhilly Satellite-Communi-  
cation Earth Station I. F. MACDIARMID AND S. C. GORDON 2157 ✓

The Travelling Wave Maser Amplifier in the Goonhilly Radio  
Station J. C. WALLING AND F. W. SMITH 2167 ✓

The Helium System of the Maser Installation at the Goonhilly Satellite-Communication Earth Station	H. N. DAGLISH AND M. R. CHILD	2183	✓
A Low-Temperature Thermal Noise Source for Use at the Goon- hilly Satellite-Communication Earth Station	H. N. DAGLISH	2195	✓
Demodulation Techniques for Use at Goonhilly Satellite-Com- munication Earth Station	R. N. WHITE AND R. J. WESTCOTT	2201	✓
A High Power Travelling Wave Tube for Satellite Communica- tions	M. O. BRYANT, A. THOMAS AND P. W. WELLS	2211	✓
The Output Stage for the Ground Transmitter at Goonhilly	A. R. PETHERHAM	2219	✓
Results of Tests at Goonhilly Using the Experimental Communi- cation Satellites Telstar I and Telstar II	W. J. BRAY, F. J. D. TAYLOR AND R. W. WHITE	2229	✓

### *TELSTAR II*

Communications and Radiation Experiments with Telstar II		2261	✓
--	--	------	---

**TELSTAR I**

**FUCINO, ITALY**

# Project Telstar

N67 12302

## Fucino Earth Station Operation Analysis

Telstar I was employed in communication experiments from the pass 1627, January 4th 1963 until February 16th, when the satellite ceased functioning for communication. During this period 23 experiments were performed, about half of which were of wideband type.

### THE FUCINO EARTH STATION

The Fucino Earth Station, owned by Telespazio, has been operational, during the period when communication experiments were conducted via Telstar I, only for the reception.

The Telespazio Station is located in the Fucino Valley, about 80 miles East of Rome. Geographical coordinates are as follows: Latitude,  $41^{\circ} 58' 40.55''$  North; Longitude,  $13^{\circ} 36' 04.21''$  East.

The Station is equipped with a 30 ft steerable dish, azimuth-elevation mount, equipped with a Cassegranian sub-reflector and with a primary feed assembly consisting of a four port horn for the 4 kMc band, used both for the monopulse beacon autotrack receiver and the communication receiver.

The communication receiver consists of a two stage parametric amplifier, the first stage being liquid nitrogen refrigerated. A conversion is made to a 70 Mc IF, the IF amplifier being followed by either of two frequency following demodulators, one for the wideband experiments and one for the narrow band experiments.

The Station is also equipped with video band equipment and instrumentation and test equipment. Fig. 1 shows a general view of the Station. Fig. 2 is a block diagram of the receiving system.

### EQUIPMENT PERFORMANCE

#### *Antenna*

Gain at 4170 Mc/s =  $48,7 \pm 0,5$  db



Fig. 1 — A general view of the Telespazio Station.

#### *Communication Receiver*

3 db Bandwidth	: 24 Mc/s
Noise Bandwidth	: 26 Mc/s
RF Gain	: 28 db

Reference noise temperature (dry atmosphere) : 220°K

#### *Wideband threshold*

The threshold occurs when the carrier to noise ratio equals 18 db in 1 Mc/s bandwidth. In these conditions the received power is about -97,5 dbm and the weighted video S/N is about 40 db;

#### *Narrowband threshold*

It occurs when the carrier to noise ratio equals 6,75 db for the group A (12—60 kc), 10 db for the group B (60—108 kc) in 1 Mc/s bandwidth.

In these conditions the received power is -108,5 dbm for the group A and the signal to noise ratio on the highest channel is about 35 db.

Using the CCIR emphasis and psophometrically weighting the noise, this ratio is about 41 db, to which corresponds a 80,000 pW noise in any channel. For group B the signal to noise ratio in the highest channel at the threshold is about 41,5 db; using the CCIR emphasis psophometrically weighting the noise, this ratio becomes 46 db and the relative noise 12,000 pW.

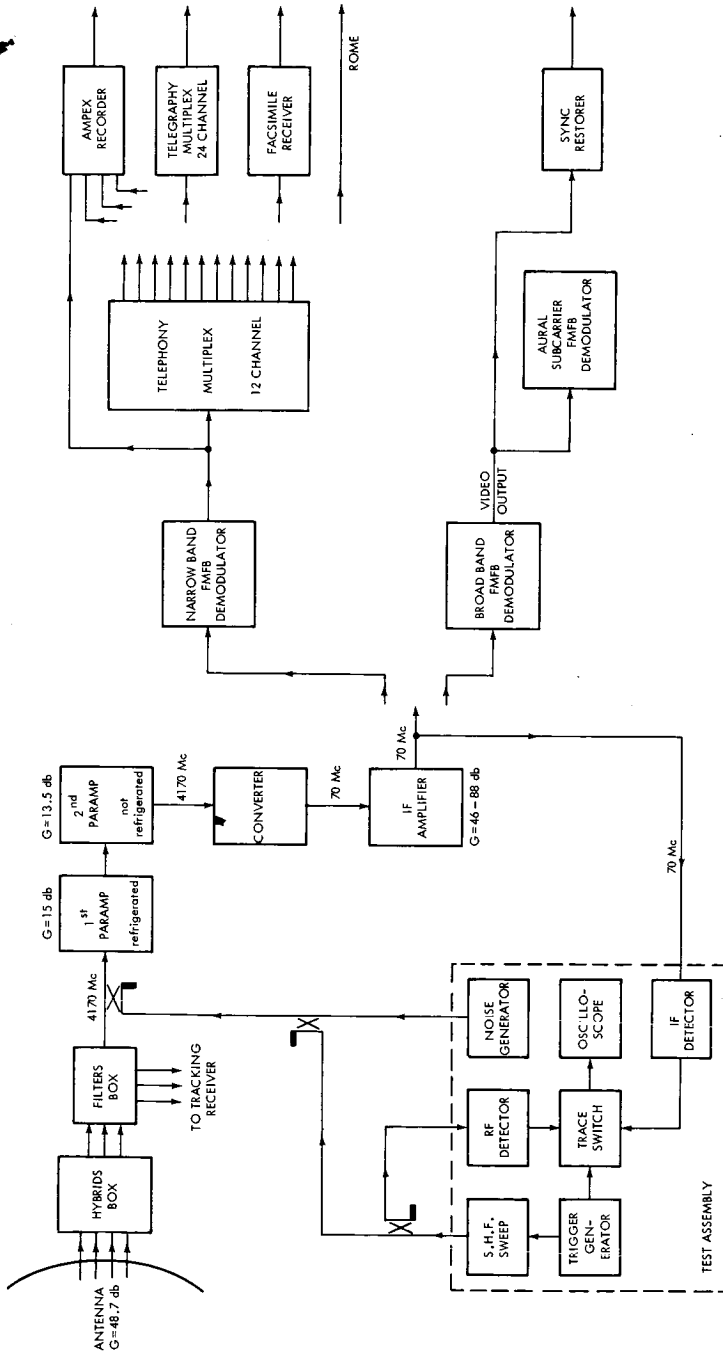


Fig. 2 — Communication receiver system.

## OPERATION ANALYSIS

*Noise Temperature*

The reference noise temperature, measured immediately before and after every pass, varied from 220 to 260°K, depending on weather conditions.

*Received Signal Strength*

In Fig. 3 are shown some values of the received power, referred to a 10,000 km range. It has been assumed, as a reference for this range, a  $-104.5$  dbm received power level, which corresponds to a satellite transmitting antenna gain of  $-1$  db.

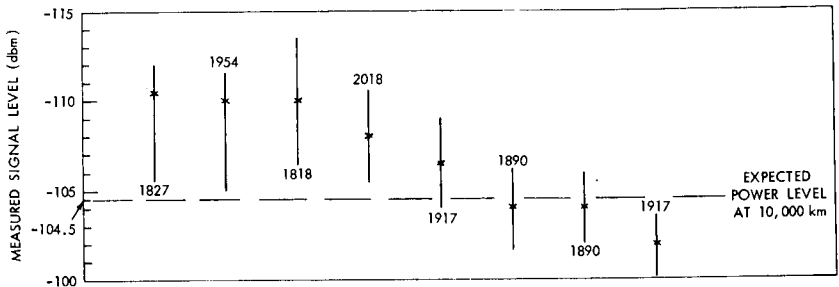


Fig. 3 — Power levels referred to the 10,000 km range.

In Figs. 4 and 5 the signal strengths received during two experiments are shown. It has been observed that the measured power differs, from the expected one, by as much as 6 db. The average is about 3 db below the expected value. These differences may be attributed to errors in the power test system, particularly for low signal levels, and also to the spacecraft look angle. The maximum measured power was  $-99$  dbm, the minimum  $-110$  dbm. The maximum observed spin modulation was about 2 db.

*Insertion Gain*

This test is typical of the loop configuration in which the Earth Station itself checks the transmitted and received signal levels.

Considering that Fucino Station is not yet equipped with the transmitter, this test is of little interest. Anyway, the results have been fairly good.

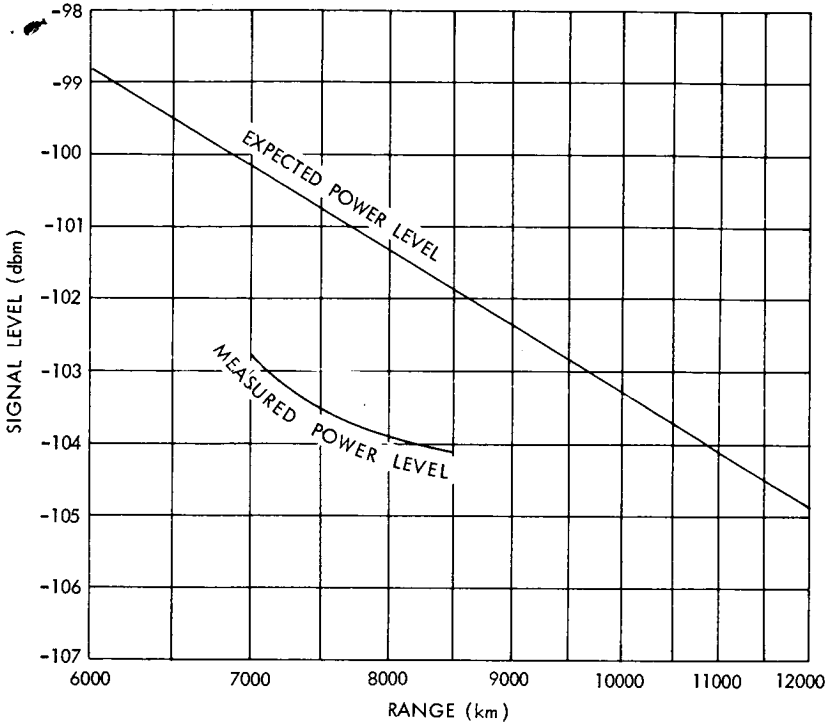


Fig. 4 — Telstar—Pass 1890: Received signal level versus range.

*Continuous Random Noise*

In Table I are shown some results of a typical noise test, on 12th channel, group A, performed during the Telstar I 1917 pass. This experiment has been conducted without preemphasis, and the noise has not been psophometrically weighted. The main part of the differences from expected values may be attributed to the imprecision in measurements, and also to the multiplex adjustment.

TABLE I

Measured signal strength (dbm)	Expected S/N (db)	Measured S/N (db)
- 104	39	37
- 101	42	38.5
- 99	44	39

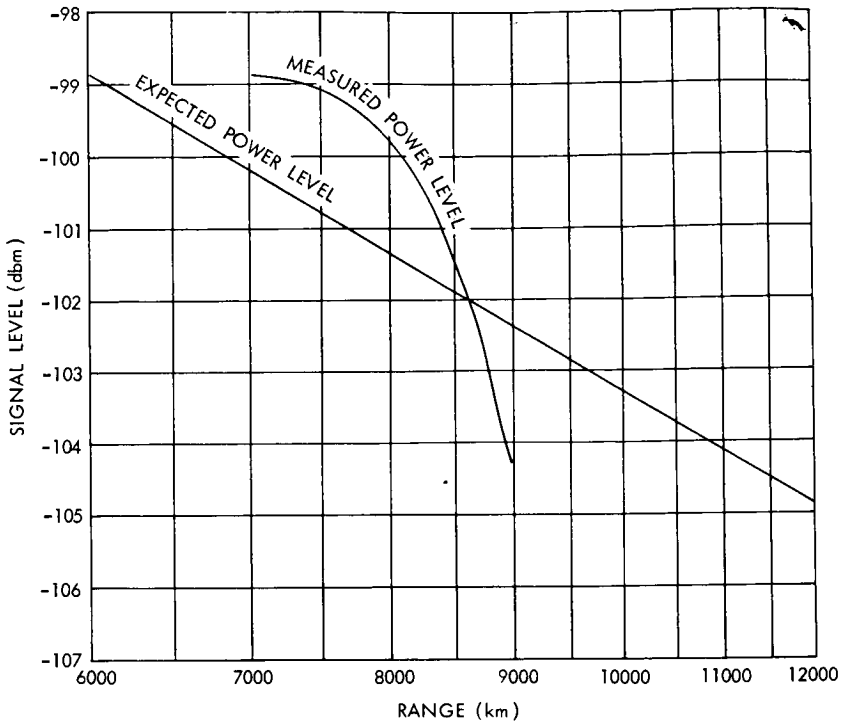


Fig. 5 — Telstar—Pass 1917: Received signal level versus range.

During these narrowband experiments voice narrations, telephone demonstrations, and teletype signals, have been received. The signal was quite always over the threshold.

#### *Wideband Experiments*

The absolutely first reception conducted by Fucino Earth Station was a TV test, the "window", transmitted from Andover, via Telstar, during the revolution 1627 of the January 4th 1963.

Several other wideband reception tests via Telstar have been successively conducted; owing to the small dimensions of our Station which had been basically dimensioned for 12 telephone channels, the signal level was always below the threshold. Nevertheless these experiments have been very useful.

## TRACKING PERFORMANCE

The employed tracking system, of monopulse type, yielded good results and confirmed that, owing to its simplicity and reliability, it is very suitable.

During the first days of the experiments some difficulties in acquisition and tracking were experienced. These troubles, due to damages in the tachymetric loop, were quickly removed and, since then, the system performance was excellent.

The minimum power level for the 4080 Mc beacon acquisition is -129 dbm.

**PLEUMEUR-BODOU, FRANCE**

# Description of the Installations at the Pleumeur-Bodou Space Communications Station

N67 12303

M. J. DAUTREY

CENTRE NATIONAL D'ETUDES DES TELECOMMUNICATIONS

*The Pleumeur-Bodou Ground Station, the research center of the National Center for Telecommunications Studies in the field of space telecommunications, is equipped to study all problems connected with active satellites: link performance, acquisition, tracking, telemetry, and command. This station is also intended for possible future commercial applications.*

A ground Station constitutes the basic facility for experimental studies of space communications systems. In the Pleumeur-Bodou ground station, CNET (National Center for Telecommunication Studies) has a group of installations which will permit the acquisition of extensive experience in the field of communication by active satellites.

However, these installations have not been designed solely for experimental purposes: the operational status of the station has been planned for. The station is able to accommodate the equipment required for practical application of a communications system by satellite.

The establishment of a ground station at Pleumeur-Bodou was decided upon within the framework of the American projects Relay and Telstar. In the spring of 1961, the French Government signed an agreement with NASA, to associate with project Relay by putting into service a station capable of providing communication links through the satellite.

In consideration of the very short notice allowed by the announcement of the planned satellite launch date, the Ministere des Postes et Telecommunications decided to ask for the cooperation of AT and T (American Telephone and Telegraph). This company had in fact undertaken to set up an original project for communications by active satellite, the Telstar project, which included construction of a ground

station which was the subject of special studies at Andover. In December 1961, AT and T signed a contract with the Administration des Postes et Telecommunications and undertook to furnish the essential elements for a station identical to the one at Andover, as well as technical assistance. CNET was to be responsible for the overall operation. The Compagnie Generale d'Electricite (CGE) participated in the capacity of industrial architects. After a period of preparation, the first construction work started in October 1961 on the selected site. On July 8, 1962, all the equipment was installed and on 9 July the system tests demonstrated that the station was operational.

The various characteristics of the ground station will be discussed: (1) The site; (2) Overall design; (3) Buildings and substructure; and (4) Operating equipment.

A more detailed description will follow of some of the equipment which is characteristic of the Pleumeur-Bodou station: (5) The command tracker; (6) Terminal equipment; (7) Simulator equipment of l'Île Losquet (boresite tower); and (8) Power supply equipment.

#### THE SITE

The search for a suitable site, begun in 1961, was confined to Brittany, which, being in the westernmost part of France, would give the longest periods of visibility from both sides of the Atlantic. Also, the temperate climate of this region was an attractive consideration.

Pleumeur-Bodou was finally chosen for the location of the site for the following reasons (Fig. 1 and 2):

1. The proximity of the CNET laboratories, situated near Lan-nion (Research Center—Flight Testing).
2. Within easy reach of the telephone and television networks.
3. Rapid acquisition, in a sparsely populated area, of a large area on a stable granite base, affording a potential for expansion.
4. Radio interference minimized (distance from r-f beams, airports, seaports, and sea lanes) and monitored by systematic control measures.
5. Overall topography in the shape of a basin, the edges of which act as a screen which increases protection against radio interference, but which is low enough (less than 5°) not to raise the horizon.
6. Proximity of a resort-type coastal zone which offers pleasant surroundings for employees.



Fig. 1—Location of the ground stations in Brittany and Cornwall.

The surface area of the site is 105 hectares. The geographical coordinates of the center of the antenna are:

Latitude  $48^{\circ} 47' 13''$  N

Longitude  $03^{\circ} 31' 20''$  W.

The average altitude is 40 meters. A general view of the station is shown in Fig. 3.

#### OVERALL DESIGN OF THE STATION

The performance characteristics of the station were determined by those of the Telstar satellite, and by the desired link.

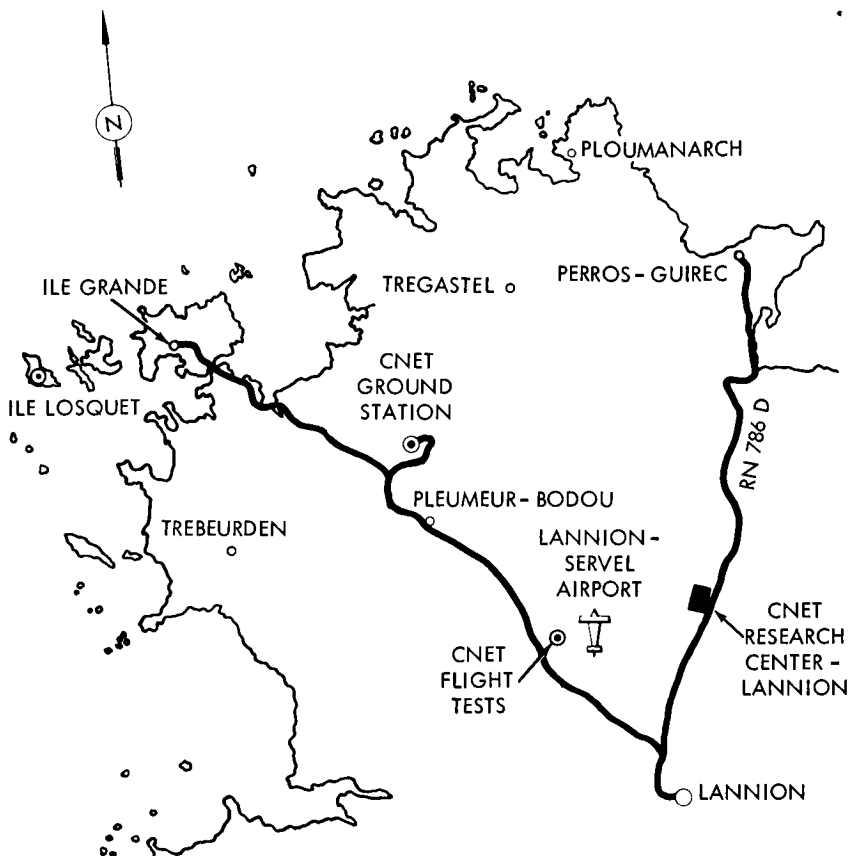


Fig. 2 — The Pleumeur-Bodou region.

The two basic characteristics of this type of link are the great distances which the signal must travel without amplification, and the fact that the transponder (i.e., the satellite) is in motion. Thus a very large and heavy antenna, which can be aimed with extreme precision, is needed.

In order for such a large facility to be commercially profitable, it must be ready to operate at all times. It must be sheltered from atmospheric conditions which might inhibit its action, the wind in particular. This is the function of the radome. Its capabilities for acquiring and tracking the satellite must be reliable; this is brought about by an acquisition and tracking system in which the antenna

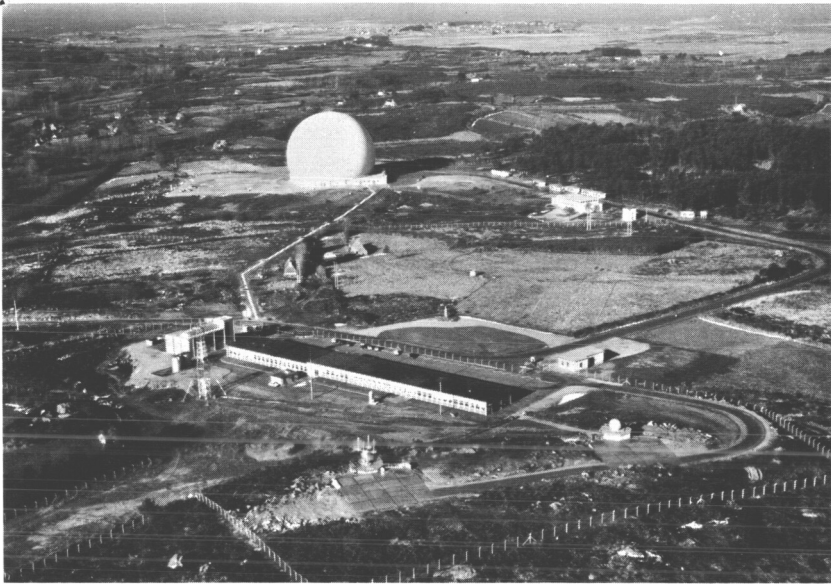


Fig. 3 — General view of the station.

equipment is complemented by coarse and fine trackers. Finally, basic equipment mentioned above must be supported by reliable auxiliary equipment.

To be able to take advantage of all the experimental possibilities of this system, the station must have facilities for receiving the satellite telemetry, and for command.

The Pleumeur-Bodou station has consequently been equipped with the following main installations:

1. Under the radome, a horn antenna with transmitter and receiver, the Vernier-Autotrack, the antenna control, and the servo amplifier for the steering motors.
2. An acquisition and command tracker, with its antenna
3. A precision tracker and its antenna
4. In the main building (centrally located):  
Antenna control systems  
Terminal equipment for connection to the telephone and television networks.
5. Facilities for testing the equipment:  
A test tower for tracking equipment.  
A satellite simulator tower for use with the horn antenna.

## 6. Auxiliary installations:

- Power supply
- Heating
- Air-conditioning
- Pressurization for the radome

The individual characteristics of the antenna and its steering gear will be discussed below.

### *The Horn Antenna*

Since the antenna requires a very high gain and a very low noise, the Bell Laboratories decided on a horn antenna with cylindrical reflector, with an opening about 20 meters in diameter.

The antenna characteristics are:

	<i>Gain</i>	<i>Beam Width</i>
Transmission 6000 Mc	60 db	0.12°
Reception 4000 Mc	57 db	0.23°

Thermal noise, including the radome, is 19°K.

The nominal level of the signal at the entry of the receiver is -94 dbm, the threshold being -104 dbm. The antenna has a very large bandwidth and can be used for frequencies up to 10,000 Mc.

### *The Receiver*

Nominal frequency: 4169.72 Mc.

To reduce the noise added by the receiving equipment to a minimum, the incoming signal is amplified by a maser, which operates in liquid helium and has a noise temperature of only 4°K.

The frequency excursion of the incoming signal being very large, the threshold of the receiver is reduced to its lowest value by frequency compression.

### *The Transmitter*

Nominal frequency: 6389.58 Mc.

The transmitter power can be adjusted in relation to the distance of the satellite, from 20 w to 2 kw.

### *Antenna Pointing*

The operation of tracking the satellite is made very critical by the great inertia of the antenna (weight: 340 tons) and by the small beam-width ( $\pm 0.12^\circ$ ). The antenna must be oriented both in azimuth and in elevation with an accuracy of a few hundredths of a degree.

Such precision can be obtained only with the help of digital computers. In normal operation, a data reduction center computes, from the orbital parameters, antenna pointing data at 4 second intervals. This data is recorded on magnetic tape.

At the desired time, given by the station clock, a block of data is transferred to the antenna control which stores it in a memory and interpolates at the rate of 128 points per second; the antenna control makes manual or automatic corrections to these points, and compares the result with the actual position of the antenna so as to determine the necessary corrections. These corrections, when translated into analog signals, will act as servo-mechanical commands.

The vernier autotrack (VAT) receives the 4079.73 Mc signals from the satellite beacon, evaluates the pointing deviations and adds a vernier pointing correction.

The necessary elements for establishing ephemerides are supplied from the Andover station or the NASA computing center. They can also be computed by the station computing center from data recorded during a pass.

This system of pointing, which is the operational mode when the satellite's orbit is known, is inadequate for experimentation.

Therefore, a precision tracker (PT) would be needed for use in case the magnetic tape fails. Its beam angle being  $2^\circ$  it can, with the aid of the coarse tracker (beam angle  $20^\circ$ ) if necessary, acquire the satellite 4079.73 Mc beacon and track it with an accuracy greater than 0.01 deg. A track encoder processes the pointing data, translates it into digital commands, and transmits it to the antenna drive which controls the orientation of the horn antenna. The horn antenna can then either lock onto the satellite by the vernier autotrack, or continue tracking from the data supplied by the precision tracker.

The pointing data is sent by the track encoder to the computation center, where it is recorded on tape from which the orbital parameters can be computed.

By means of the two independent pointing systems, a very high degree of steadiness in satellite tracking has been provided.

#### BUILDINGS—THE SUBSTRUCTURES

##### *Station Layout*

The arrangement of the existing installations within the site leaves a large open area for future expansion (Fig. 4).

The tracking antennas, the main building, and the heating plant are

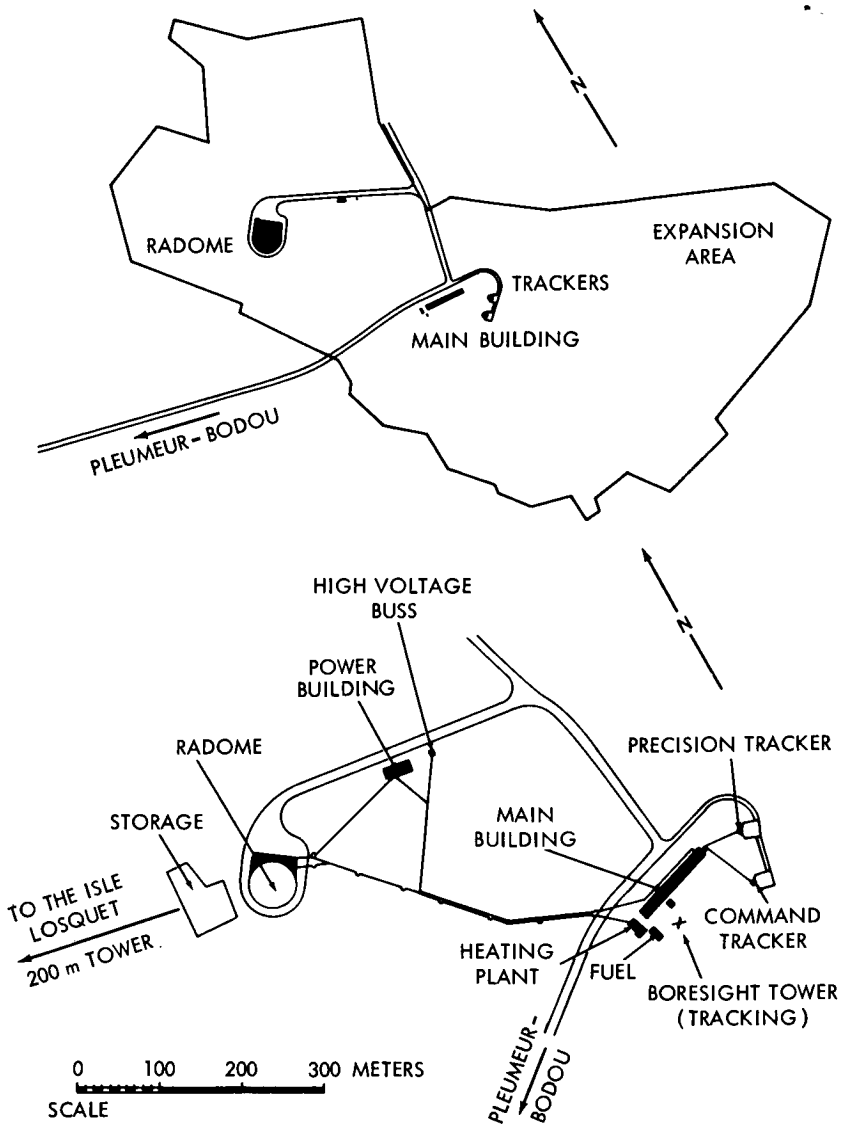


Fig. 4 — General plan of the station and location of the buildings.

centrally located with regard to the radome and the planned locations of future antennas.

To avoid air pollution from diesel exhaust affecting the radome

blowers, the power plant has been located at some distance from the radome.

*Radome*

The radome (Fig. 5) is built in an unobstructed location. It acts as a very stable base for the antenna (track diameters: 22 and 41 meters), and insures weather protection (spherical envelope with a diameter of 64 meters—supported by a surrounding wall of 58.50 meters).

Pivot, tracks and wall foundations have large anchor sole plates imbedded in 0.50 meter of solid granite.

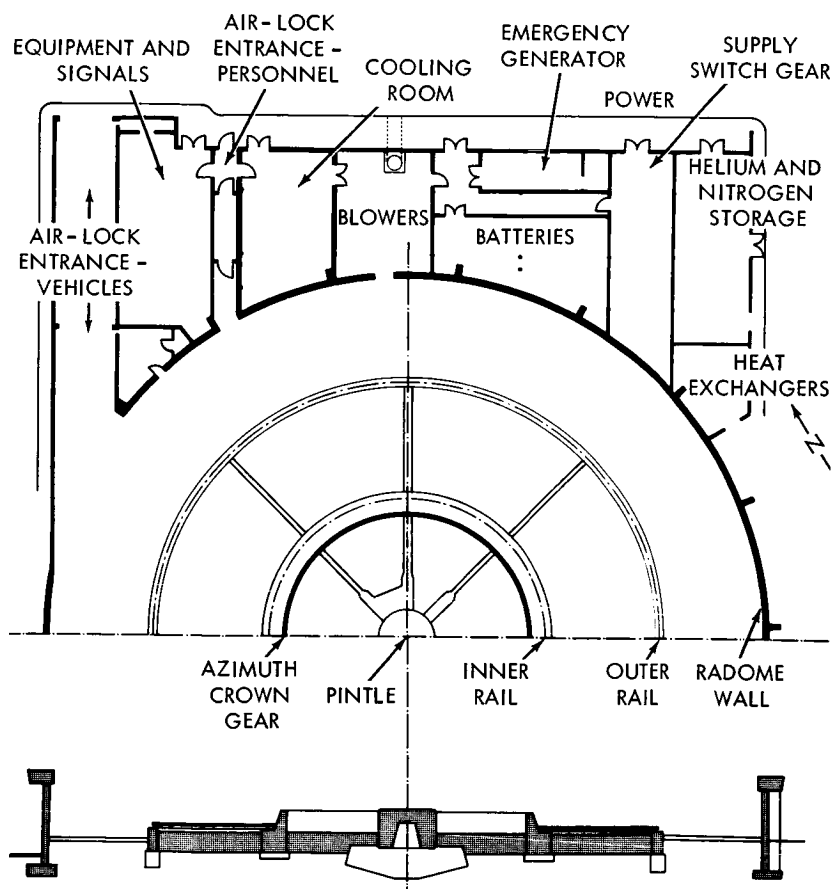


Fig. 5—The radome foundations (bottom) and floor plan of the radome and its auxiliary building.

Under normal conditions, the radome structure is supported by an air pressure of 3.8 cm of water; with the air pressure raised to 14.00 cm of water, it can resist winds of 160 km per hour.

### *Radome Auxiliary Building*

Entrance air-locks, one for personnel and one for motor vehicles, are located in an auxiliary building of 500 m<sup>2</sup> adjoining the radome. This building also shelters facilities for:

1. The five radome pressurizing blowers and their emergency power supply generator.
2. The switch gear for power supply.
3. Racks for connecting cables to the main building.
4. The refrigeration plant (water is at 4°C).
5. The heat-exchangers for the 8 radome heaters.
6. Storage facilities for liquid helium and nitrogen.

### *The Main Building*

The two tracking antennas, over their respective technical buildings, are supported by concrete piles located on a granite hill which is exceptionally unobstructed. The main building (Figs. 6, 7, and 8) is built at the foot of the antennas, level with the ground; its area is 1500 m<sup>2</sup> (dimensions: 111 × 14 meters).

The equipment room (340 m<sup>2</sup>), the computing center, the two principal facilities, have been specially constructed: a flooring of movable wooden sections with plastic covering is supported at 30 cm from the ground by a metal frame on adjustable screw supports.

The open space beneath the floor is utilized for cables and air-conditioning ducts. The windows do not open. An air conditioning plant, consisting of two refrigerating units of 110,000 calories per hour each, recycles the air in two supply and return systems. One system is for the computation center (16,200 kg/hr of air at 16°C, 62% humidity), the other for the equipment room (35,500 kg/hr of air at 16°C, 73% humidity). The desired environments are respectively: 22°C, 43% humidity and 24°C, 45% humidity.

The other facilities within the main power supply building are the 50 cycle station, the switchboard, the batteries, and the LGD (long distance lines) switchboard. There are also facilities for the telephone and teleprinters, a supply store, a conference room, and offices for engineers and administrative services.

Near the main building, a boresight tower 25 m high and especially rigid (motion at the top: less than ±1.5 mm with winds of 120 km/hr),



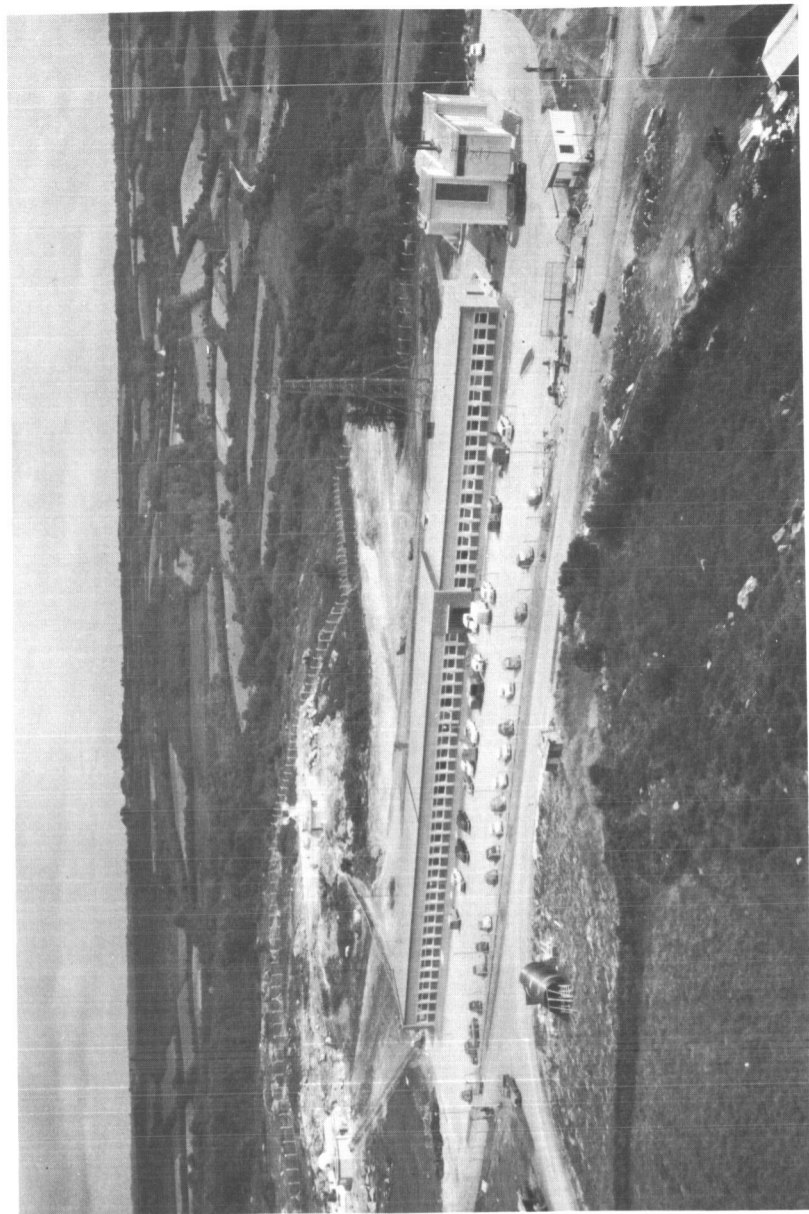


Fig. 7 — The main building area.



Fig. 8—View of the main building at night.

supports the antennas which broadcast the signals used for tracking tests, as well as the anemometer which controls the air pressure within the radome.

Three posts support the wire receiving antenna for 18 Mc signals.

#### *The Power Supply Building—The Generators*

The delivery station receives two power supply lines from the national network.

The dimensions of the power supply building (Figs. 9 and 10) are as follows: length, 35 m; width, 12 m; and height, 5 m. This building houses chiefly a 50-cycle station, 2 50/60-cycle converters, 4 60-cycle generators. For disassembling the motors, there is a 5-ton overhead crane.

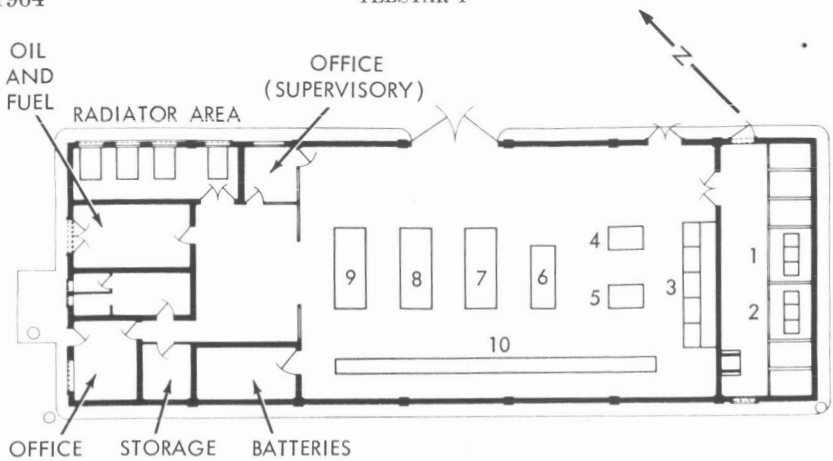
#### *Heating Plant*

The heating plant, 22 m long, 10 m wide and 6 m high, shelters 2 boilers which supply superheated water, ( $180^{\circ}$ —10 kg/cm<sup>2</sup>) which is pumped to the radome heat exchangers through pipes of 125 mm diameter.

The output of  $3 \times 10^6$  calories per hour is ample to insure proper heating of the radome in winter, and obviates the accumulation of snow or frost. This power may be tripled by the addition of a third boiler.

1964

TELSTAR I



- 1, 2 15,000/380 - 220 V - 630 KVA TRANSFORMERS
- 3 50 cps PANEL
- 4, 5 50/60 cps CONVERTERS
- 6 GE1 - 60 cps - 75 KVA - EMERGENCY GENERATOR
- 7, 8, 9 GE2 - GE3 - GE4 - 60 cps - 250 KVA GENERATORS
- 10 60 cps DISTRIBUTION PANEL

Fig. 9 — Floor plan of the power building.

### *External Conduits and Cable*

External conduits with special compartments connect the different buildings. They are used by medium power, low voltage electric cables;



Fig. 10 — Outside view of the power supply building.

command, communication, and telephone cables; and the water and heating ducts.

Overhead cables connect the tracking antennas to one another and to the main building; they also connect the main building to the test tower (Fig. 11).



Fig. 11 — Routing of the cables to the command tracker.

### *Ile Losquet*

The satellite simulator (beacon and transponder) is located on a tower 200 m high which is built on a small deserted island 6342 m from the center of the antenna. An elevation of  $1.4^\circ$  is obtained in this way for a beam going from the axis of the horn antenna to the simulator. The tower is very stable; with a wind of 120 km/hr, the motion at the top is less than 0.50 m.

The isolation of the island has necessitated the establishment of a separate power supply. The various equipment are commanded and monitored from the main building by radio.

### OPERATIONAL EQUIPMENT

The equipment responsible for the operation of the station will be described in their own location.



Fig. 12 — View of the Ile Losquet and the 200 m tower.

### *The Communications Antenna*

Located within the radome, the entire structure of the antenna rotates in azimuth on 2 concentric rails (Fig. 13).

#### The Horn Antenna

This antenna includes a horn-shaped reflector (Fig. 14) which consists of a conical HF horn about 36 m long, a parabolic reflector, the focal point of which coincides with the apex of the cone, and a cylindrical reflector with an opening area of 334 m<sup>2</sup>. The antenna is oriented in elevation by rotation about its horizontal axis. Positioning of the antenna is done by means of pinions engaging racks. Vickers hydraulic motors (2 in azimuth and 2 in elevation) drive the pinions.

#### The Upper Cabin

The antenna throat is enclosed in the upper cabin; a rotary joint insures the connection between the apex and the rest of the horn.

The upper cabin (Fig. 15) contains:

Near the top, the Vernier Auto Track (VAT), the mode coupler and the 4080 Mc receiver.

The communication receiver which changes the 4170 Mc wide-band signal into the baseband, the maser and its pump, the cooling

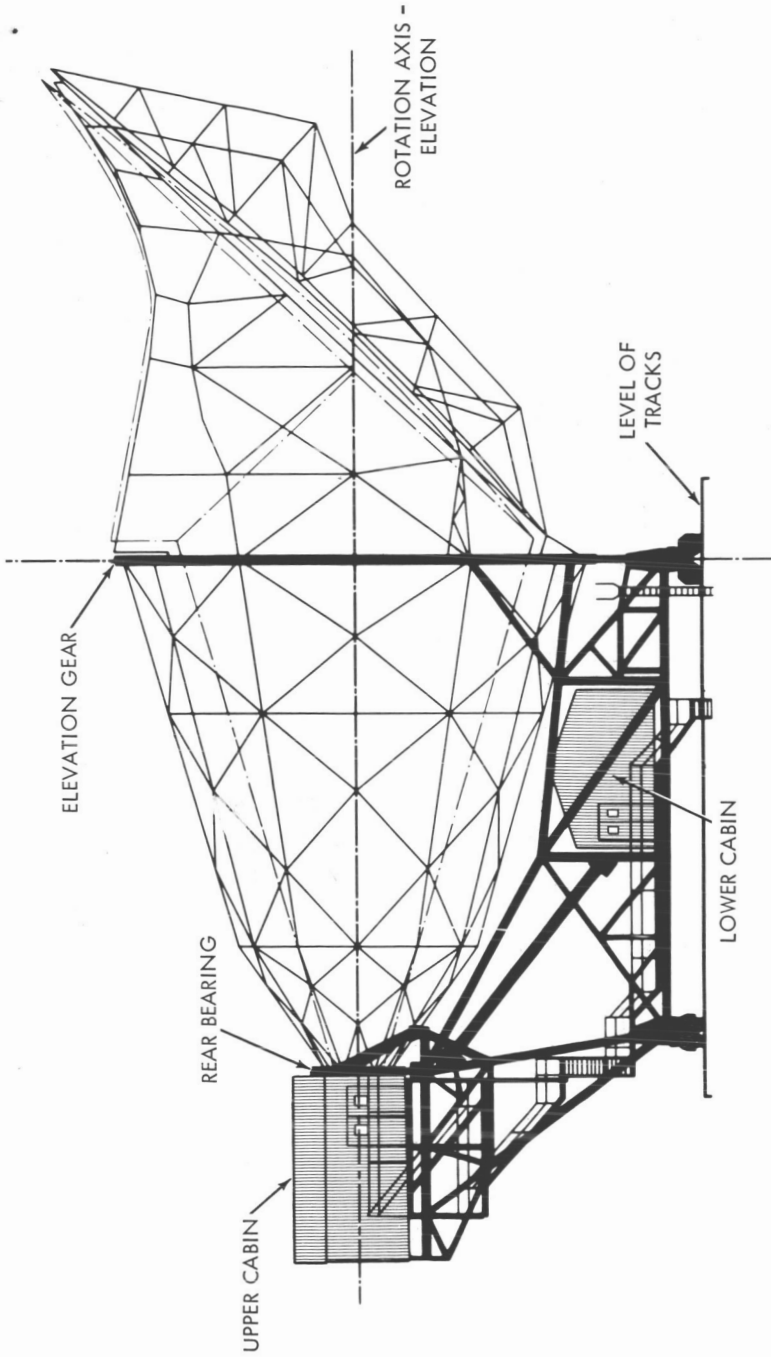


Fig. 13—Lateral view of the antenna.

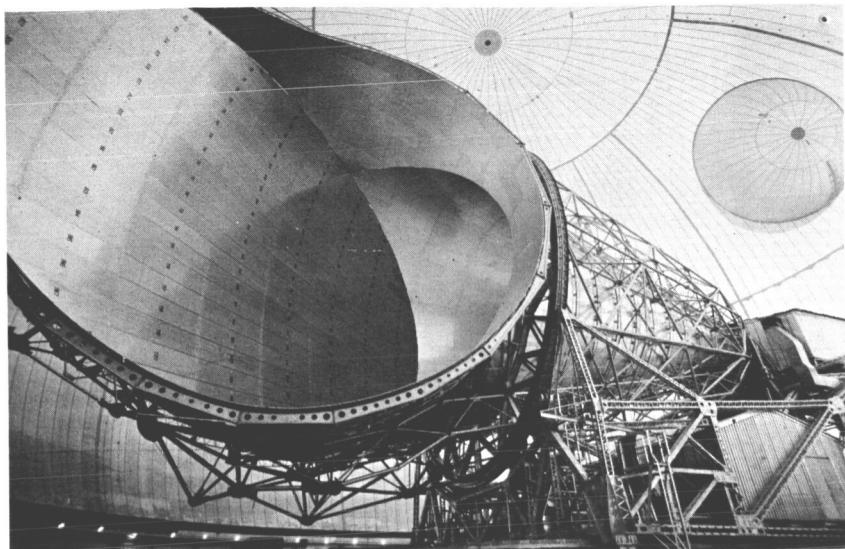


Fig. 14 — The horn reflector.

system using liquid helium and liquid nitrogen, the if amplifier, and the frequency compression loop.

The Telstar transmitter which changes the baseband signal into the 6390 Mc wideband signal, with the power amplifier which has a range of 20 w to 2 kw.

The measurement equipment, radiometric equipment, and antenna drive equipment (coder-resolver—VAT coordinate converter).

#### The Lower Cabin

The lower cabin contains the antenna steering equipment (Fig. 16):

The X and Y receivers of the Vernier Auto Track equipment.

The antenna control equipment which calculates the error signals.

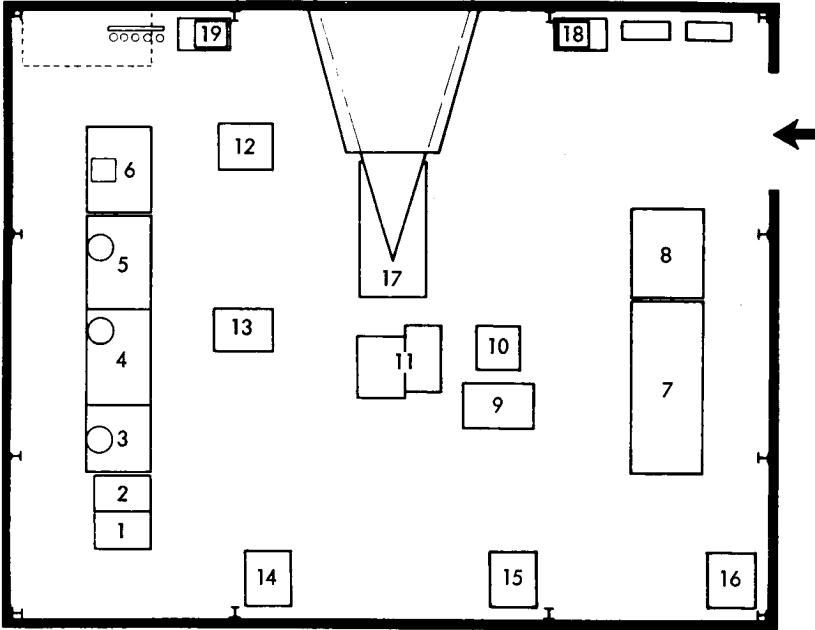
The servo amplifier which drives the hydraulic motors.

The recording and monitoring assemblies.

Also housed in this building: High voltage power for the power amplifier and its stabilizer, the bays for alarm, intercommunication, and multiplex equipment, and the installation for retrieving the helium gas after its evaporation in the maser (Fig. 17).

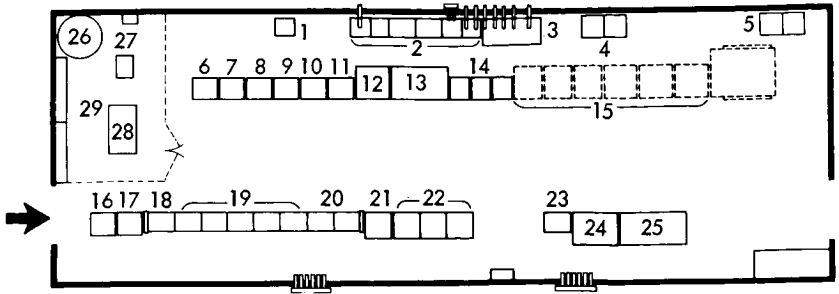
#### Cables

The radome and the main building are connected by the following cables: 1 cable of six coaxial pairs 1.2/4.4 and 69 sets of four 0.9 wires;



- 1 LOCAL OSCILLATOR
- 2 FM GENERATOR
- 3 HF BAY TRAVELING WAVE TUBE
- 4 CONTROL AND REGULATION
- 5 LOW VOLTAGE POWER SUPPLY
- 6 FM DEVIATOR
- 7 RECEIVER
- 8 MISCELLANEOUS EQUIPMENT (RADIOMETRY)
- 9 MASER HIGH FREQUENCY PUMP
- 10 MASER
- 11 LIQUID NITROGEN AND HELIUM STORAGE
- 12 TRANSMITTER-RECEIVER TESTS
- 13 FM TERMINAL SET
- 14 TV TRANSMISSION BAY
- 15 TV RECEIVER BAY
- 16 SPARE TRAVELING WAVE TUBE
- 17 VERNIER AUTOTRACK RF EQUIPMENT
- 18 RESOLVER ENCODER
- 19 VAT COORDINATE CONVERTER

Fig. 15 — Floor plan of the upper cabin.



- |        |   |
|--------|---|
| 1      | 420 cps POWER SOURCE                            |
| 2      | ANTENNA DRIVE CONTROL CENTER                    |
| 3      | POWER PANEL                                     |
| 4      | RECTIFIERS - 48 V                               |
| 5      | RECTIFIERS - 130 V                              |
| 6      | TEST SIGNAL                                     |
| 7      | VAT FREQUENCY                                   |
| 8      | VAT ERROR - X AXIS                              |
| 9      | VAT CONTROL                                     |
| 10     | VAT ERROR - Y AXIS                              |
| 11     | VAT POWER SUPPLY                                |
| 12, 13 | HIGH VOLTAGE POWER SUPPLY - TELSTAR TRANSMITTER |
| 14     | SIGNAL DISTRIBUTION PANEL                       |
| 15     | RELAY TRANSMITTER                               |
| 16     | ANTENNA CONTROL EQUIPMENT - 28 V POWER SUPPLY   |
| 17     | ANTENNA CONTROL EQUIPMENT - 12 V POWER SUPPLY   |
| 18     | ANTENNA CONTROL EQUIPMENT - MONITOR GROUP       |
| 19     | ANTENNA CONTROL GROUP                           |
| 20     | ANTENNA CONTROL TESTING                         |
| 21     | ANTENNA RECORDER GROUP                          |
| 22     | SERVO - MECHANISM - CONTROL                     |
| 23     | INTERCOMMUNICATION                              |
| 24     | CARRIER AND ALARM                               |
| 25     | CARRIER TELEGRAPH CONTROL                       |
| 26     | GAS TANK  |
| 27     | PURIFIER  |
| 28     | COMPRESSOR                                      |
| 29     | BOTTLES   |
- } HELIUM RETRIEVAL

Fig. 16 — Floor plan of the lower cabin.

1 cable of 100 pairs 0.9, shielded; and 74 coaxial cables RF 11 A/U. In the radome auxiliary building is a bay for an equalizer-amplifier assembly, and a switching system for television signals.



Fig. 17 — Installation for retrieving helium.

### *Main Building—Trackers*

All controls for the entire assembly are located in the main building as well as the connections with the national telephone and television networks.

#### Command and Tracking Room

The control console for the station is centered in this room (Fig. 18). All information from the various units converges here; the operations of acquisition and tracking are directed from this point. Three video receivers (2 transmission, 1 reception) are used for monitoring the TV transmission.

The precision tracker consists of:

The frequency acquisition receiver which receives the signals from the antenna.

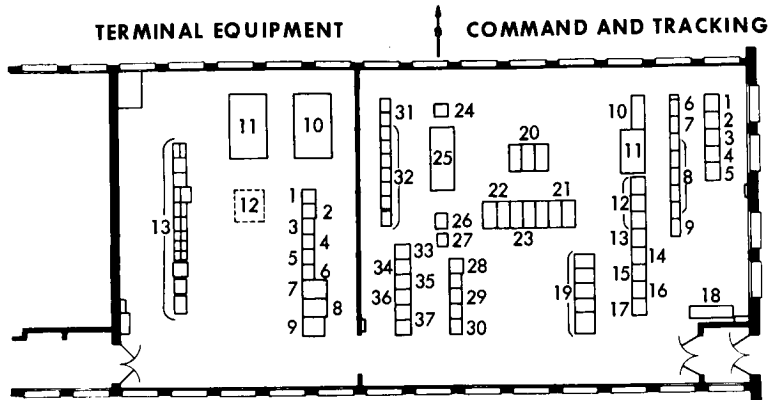
The tracking receiver.

The frequency standard and station clock are regulated by the 18 kc signals from NBA-Panama (crossing duration error 35 ms).

The test generator with 4080 Mc signals.

The track encoder which is also part of the direction system of the horn antenna.

The acquisition tracking equipment will be described in detail in a



### COMMAND AND TRACKING

- |    |  |        |   |
|----|--|--------|---|
| 1  | CLOCK OSCILLATOR                                       | 19     | POWER PANEL   |
| 2  | CLOCK POWER SUPPLY                                     | 20     | DIRECTOR CONSOLE                                      |
| 3  | TEG - POWER SUPPLY - 250 V                             | 21     | STATION CONTROL CONSOLE                               |
| 4  | TEG - POWER SUPPLY - 12 V                              | 22     | RECORDERS   |
| 5  | TEG - POWER SUPPLY - 28 V                              | 23     | TV RECEIVERS  |
| 6  | CLOCK GROUP  | 24     | INTERCOM  |
| 7  | TEG TEST GROUP   | 25, 26 | CABLE DISTRIBUTION FRAME                              |
| 8  | TRACK ENCODER GROUP (TEG)                              | 27     | ALARMS  |
| 9  | AUXILIARY STATION CONTROL<br>CONSOLE BAY               | 28     | TELEMETRY RECORDER                                    |
| 10 | POWER SUPPLY - PRECISION TRACKER                       | 29     | TELEMETRY   |
| 11 | PRECISION TRACKER CONSOLE                              | 30     | COMMAND   |
| 12 | COMBINED FILTERS                                       | 31     | N1 TERMINAL   |
| 13 | PRECISION TRACKER LOGIC                                | 32     | 43A CARRIER TELEGRAPH                                 |
| 14 | PRECISION TRACKER RECEIVER                             | 33     | COMMAND TRACKER                                       |
| 15 | PRECISION TRACKER FREQUENCY<br>RECEIVER                |        | POWER AMPLIFIERS - AZIMUTH<br>AND ELEVATION SERVOS    |
| 16 | PRECISION TRACKER FREQUENCY                            | 34     | COMPUTER AMPLIFIERS - AZIMUTH<br>AND ELEVATION SERVOS |
| 17 | PRECISION TRACKER TEST SIGNAL                          | 35     | ELECTRONIC AND MECHANICAL<br>REPEATERS                |
| 18 | LINK WITH THE BORESIGHT TOWER<br>(SATELLITE SIMULATOR) | 36     | PHASE-LOCK RECEIVER                                   |
|    |  | 37     | TEST EQUIPMENT  |

### TERMINAL EQUIPMENT

- |      |   |        |                                  |
|------|---|--------|----------------------------------|
| 1, 2 | STILL PICTURE ANALYZERS                   | 7, 8   | MEASURING EQUIPMENT              |
| 3    | 60 cps MODULE - SYNCHRO-<br>STABILIZATION | 9      | FRENCH TELEVISION NETWORK<br>BAY |
| 4    | VIDEO SWITCHING                           | 10, 11 | AMPEX VIDEO RECORDER             |
| 5    | TRANSMISSION MONITOR                      | 12     | AMPEX FR 100 RECORDER            |
| 6    | RECEIVING MONITOR                         | 13     | TELEPHONE RACK                   |

Fig. 18 — Command and tracking-terminal equipment rooms.

later section. It provides for telemetry reception and satellite command operations.

Communications with the antenna are handled by a 43 A1 telegraph, N carrier multiplex equipment, permitting a small number of circuits, and therefore, of commutator rings. The radio link to the Ile Losquet tower is handled by special equipment.

#### Terminal Equipment Room

The terminal equipment provides a link between the communication antenna, the main building and the networks (Fig. 18).

The television rack handles signal distribution and measuring operations (Figs. 19, 20, and 21). Two coaxial cables connect it with the Pleumeur-Bodou microwave link for picture transmission. The telephone lines carry the sound. Two Ampex Videotape magnetic recorders make it possible to record or retransmit the TV signals handled by the station.

The telephone rack will be described in detail in a later chapter. 2 coaxial cables connect it with the Pleumeur-Bodou microwave link.

The above mentioned telephone installation is completed by an Ampex FR 100 8-track recorder.

Fig. 22 shows how the national networks are used for both telephone and television.

#### Computation Center

The IBM 16 20 computer (see Fig. 23) with its special floating decimal point device, is equipped with a supplementary IBM 16 23 memory. The input and output of large quantities of information is effected by an IBM 16 22 reader card punch.

The computer can be connected to 6 model 729 II high speed tape drives. The use of the tapes is made very flexible by a switching system. Complementary equipment consists of Alphabetic Printing Multiperforator IBM 026, Tabulator IBM 407, and Tape Punch IBM 046.

#### Service Communications

Three semiduplex machines with tape punches provide for links with

- The NASA network, through London,
- BTL (Murray Hill), and
- The Telex network of France.

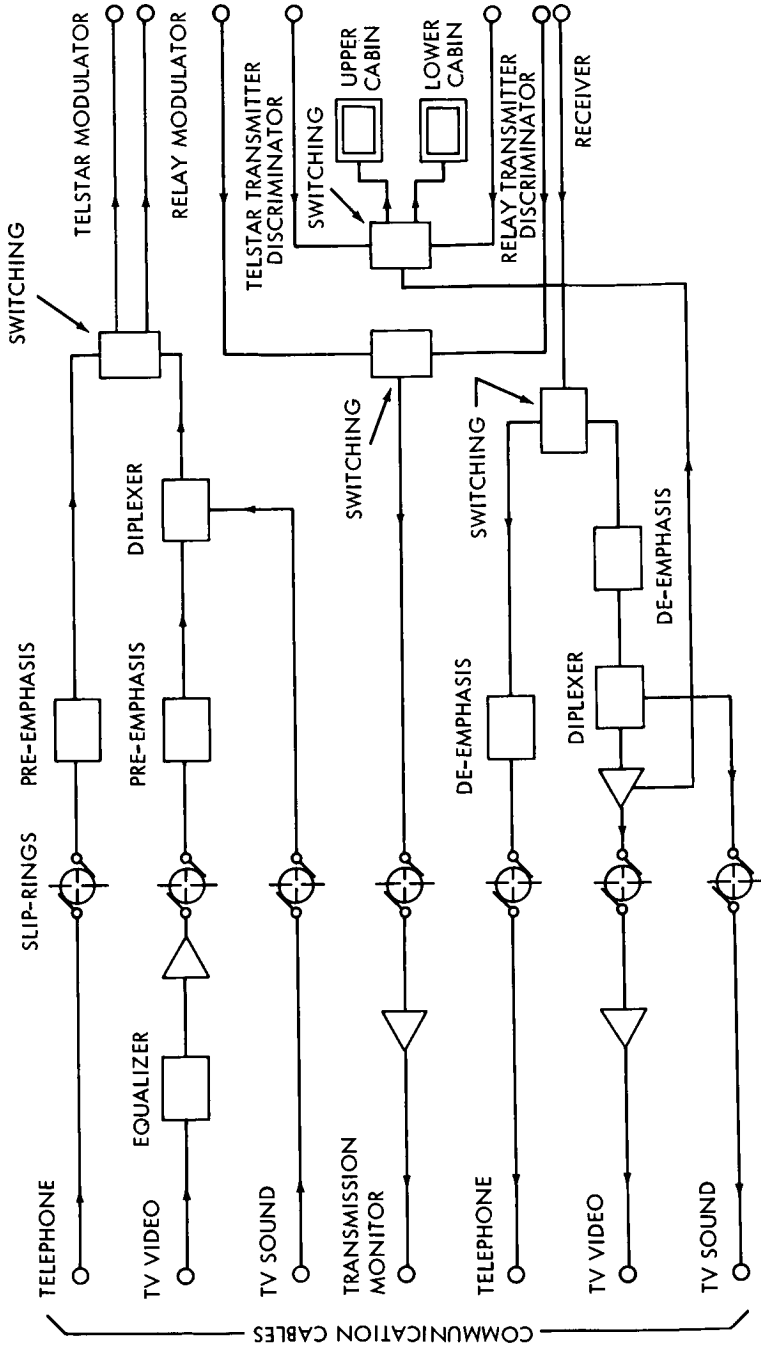


Fig. 19 — Communications between the station and the telephone and television networks.

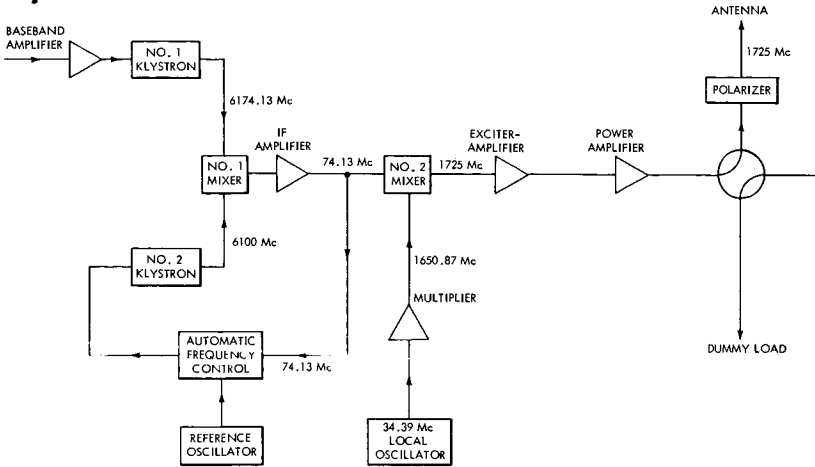


Fig. 20 — Transmission circuits—Functional block diagram.

The telephone switchboard is connected with the French network, and has direct lines to CNET in Paris, NASA at Goddard Space Flight Center, and Andover. An automatic internal system serves the entire station area.

THE COMMAND TRACKER

The command and telemetry assemblies developed by the CNET laboratories perform the following functions:

- Acquisition and tracking of the satellite Telstar, using the 136 beacon.

- Receiving telemetry data transmitted by the satellite.

- Sending of command signals from the station to the satellite.

The equipment chiefly responsible for the performance of these functions is located in or near the main building.

*The Antenna and HF Circuits*

The antenna (Fig. 24) consists of 4 helicoidal elements (7 coils of 0.50 m in diameter) located on the top side of a square 2.80 m on a side. One side of the square moves in a horizontal plane for the rotation in azimuth, and the other in a vertical plane for the rotation in elevation.

The 3-db beamwidth of the main radiating lobe is 18° at 136 Mc, 22.5° at 123 Mc (Fig. 25).

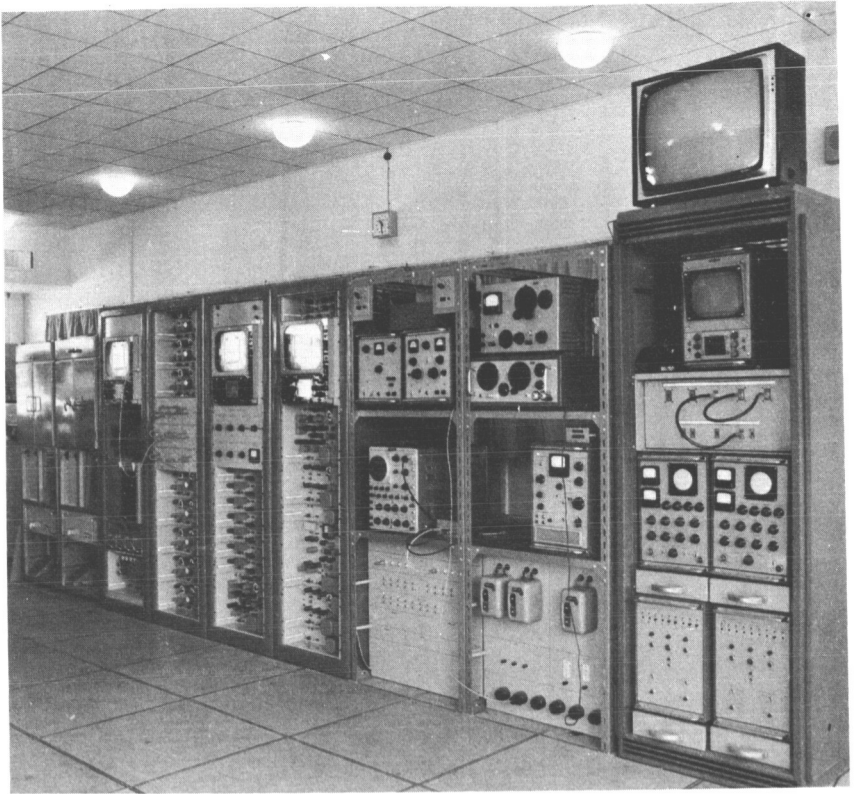


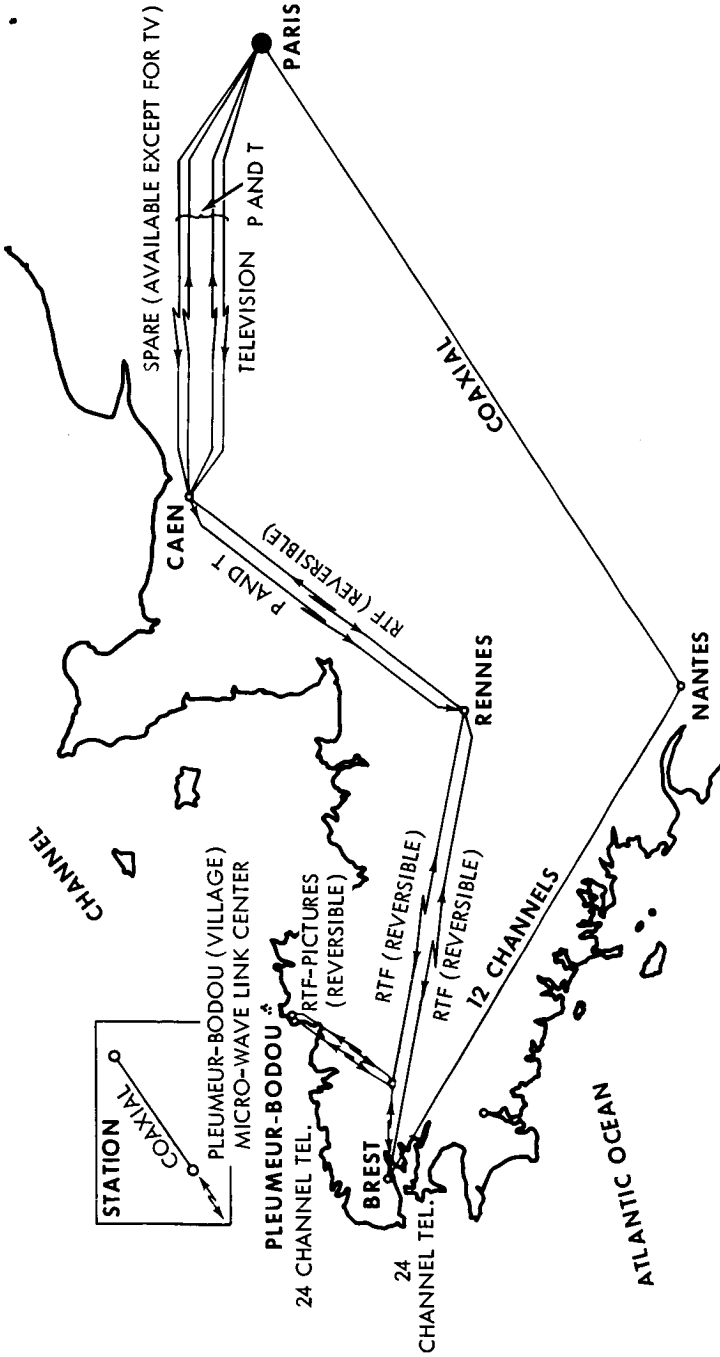
Fig. 21 — View of the television bay.

If the signals received by each helix are called A, B, C, D (Fig. 26), in a monopulse system of three  $6\lambda/4$  phase loops, the following signals are developed.

- A + B - (C + D) elevation error signal
- A + D - (B + C) azimuth error signal
- A + B + C + D reference sum signal

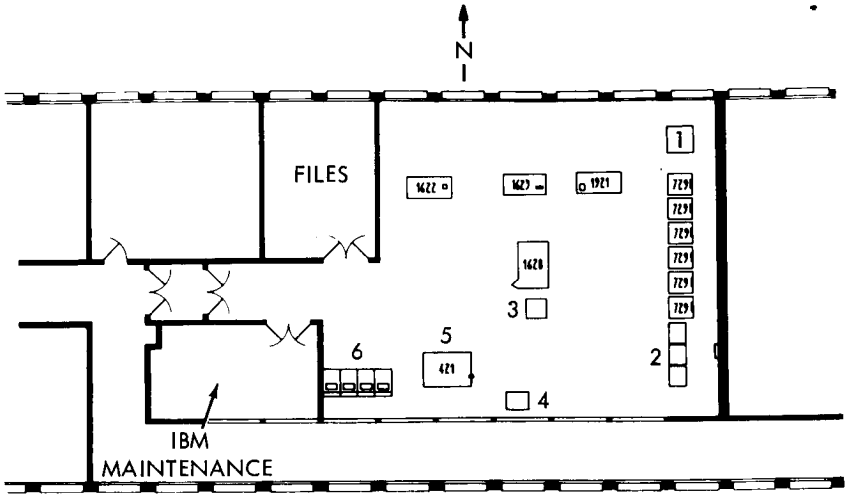
Each signal is directed toward the corresponding preamplifier, through a passband filter of 5 cavities, centered on 136.5 Mc, with a 3-db bandwidth of 2 Mc and attenuation of about 80 db at  $\pm 10$  Mc. The insertion loss is less than 3 db.

Upstream of this filter, in the path of the reference signal, a directional coupler is inserted which permits the injection of command transmission at 123 Mc. Thanks to the 130 Mc filters, the preamplifiers



RTF - RADIOTELEVISION FRANCAISE (NATIONAL TV NETWORK)  
P AND T - POSTS AND TELECOMMUNICATIONS (NATIONAL TELEPHONE NETWORK)

Fig. 22 — Television terminal equipment interconnections.



- 1 IBM 046 UNIT
- 2 TAPE SWITCHING UNIT
- 3 TAPE SWITCHING CONSOLE
- 4 IBM 026 UNIT
- 5 TABULATOR - IBM 421 OR 407
- 6 POWER DISTRIBUTION PANEL

Fig. 23 — Floor plan of the computation center.

present a very high impedance for the command signal which is radiated in its entirety by the 4 antennas in parallel.

The preamplifiers located at the base of the antenna, as near as possible to the monopulse system, are fed and controlled from the main building. The signal is amplified in one stage at 136 Mc, then converted to a first if of 20.25 Mc. The local oscillator is the same for the 3 preamps; it is situated in the main building. Its frequency is transmitted and multiplied inside the preamps. The overall noise factor is below 2 db.

#### *The Receiver*

The receiver (Fig. 27), situated in the main building, is composed of 3 chains which are quite distinct, but as similar as possible. The 20.25 Mc signals from the preamps are amplified, converted to 500 kc, amplified again and detected. The reference signal is used to drive a phase-coherent loop which determines the frequency of the local

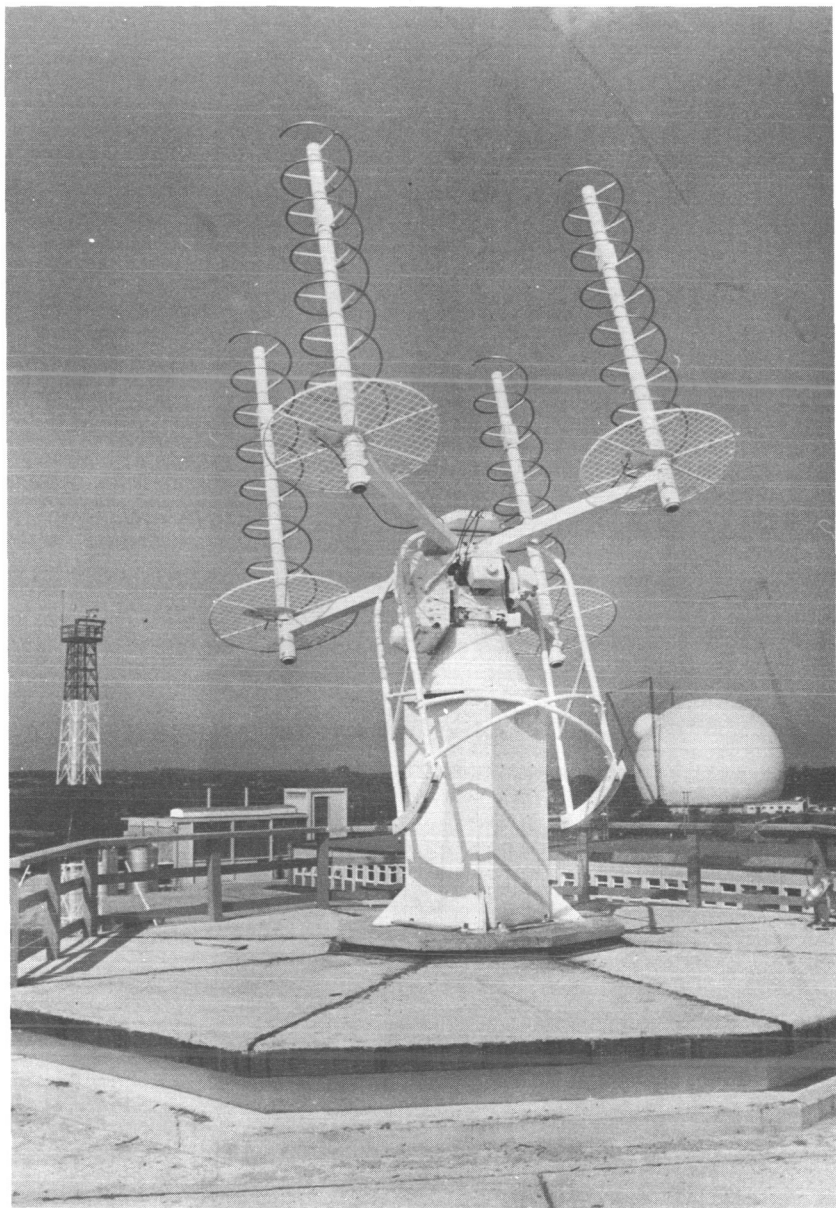


Fig. 24 — The command tracker antenna.

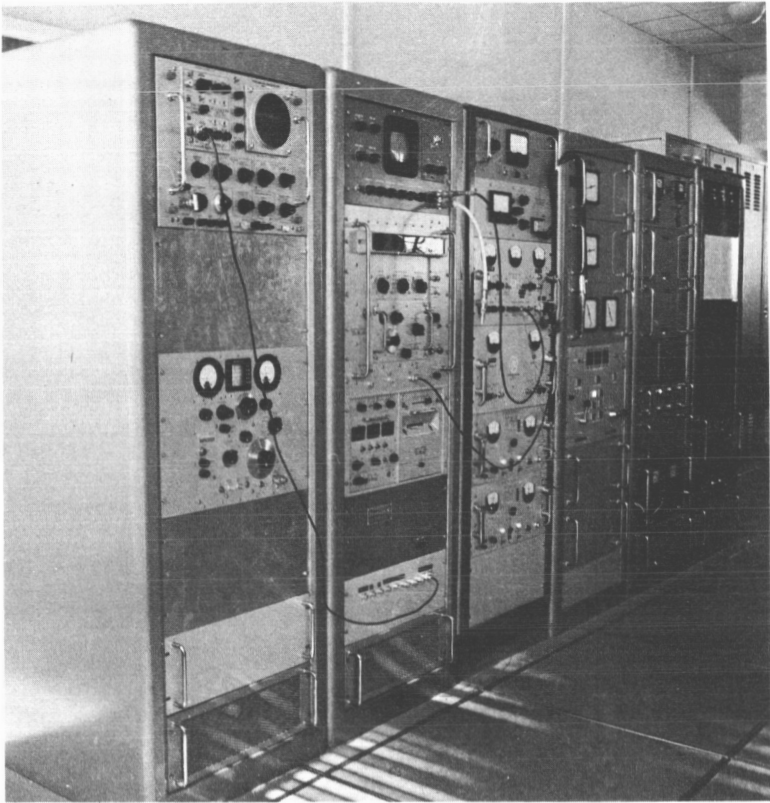


Fig. 25—View of the command tracker cabinets.

oscillator, which, after various multiplications, is used for all frequency changes. In 3 synchronous detectors fed by the local reference oscillator, a signal proportional to the level of the received signal is developed and sent to the automatic gain control circuits of the 3 channels, and two error signals, suitably filtered and amplified, are sent to the antenna servomechanism.

The receiver's principal characteristics are:

Variation of the output level as a function of the input level.

Efficiency of the AGC: 0 db from  $-130$  dbm to  $-80$  dbm

10 db from  $-150$  dbm to  $-125$  dbm

Difference in gain between the three amplification chains, less than 1 db.

Phase drive as a function of the input level in each chain.

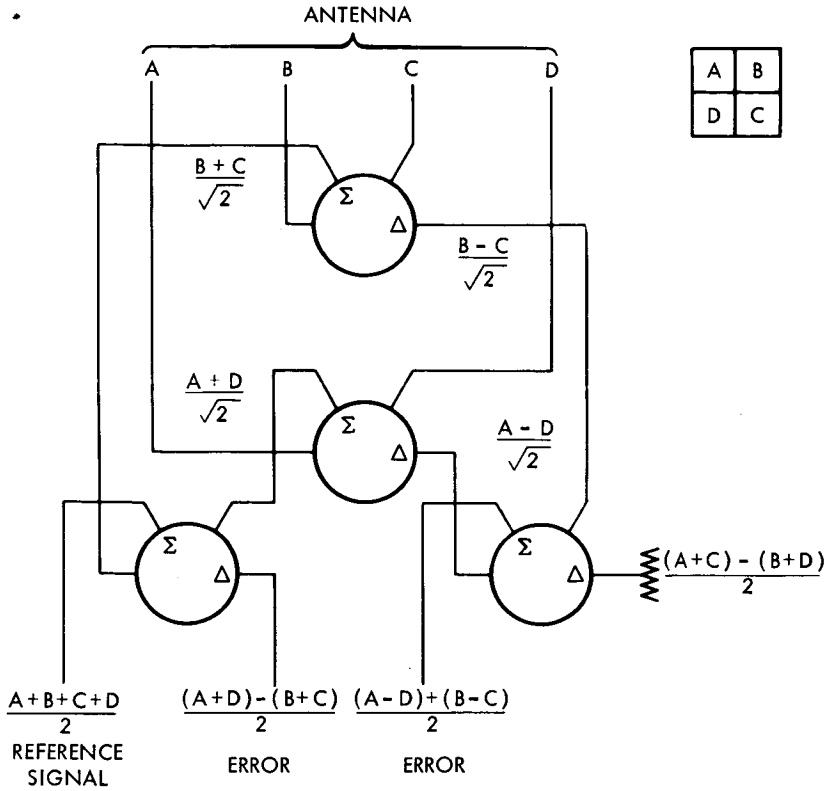


Fig. 26 — The command tracker monopulse system.

0° from -125 dbm to -80 dbm.

3° from -150 dbm to -125 dbm.

Differences between the phase errors introduced by the 3 chains: less than 4°.

Passband of the receiver: adjustable from 10 cycles to 1 Mc.

*Servomechanism*

The error voltages are led to the two servo drive chains in elevation and azimuth.

The modes of operation (Fig. 28) are as follows:

Waiting: voltage is applied to the drive, but the power amplifier is grounded and the antenna is free.

Manual: the antenna can be oriented in any direction by two manual controls.

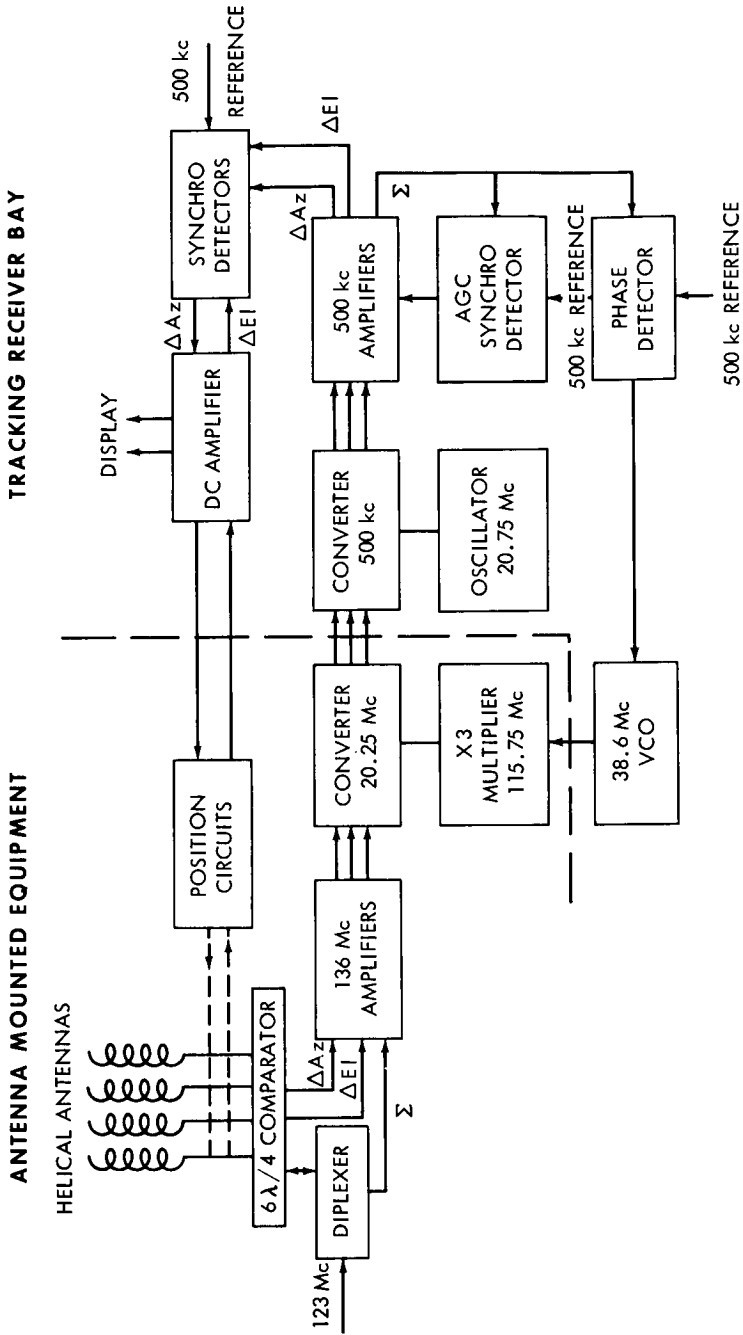


Fig. 27 — Schematic diagram of the command tracker.



When these controls are stopped, the antenna is commanded to hold its position by means of a repeating mechanism which can be locked in position; this is the position of waiting for the satellite.

Autotrack: the servo drive is connected to the tracking receiver which supplies it with the error voltages.

Slaved to the precision tracker antenna: In this mode in particular, the antenna can be driven by program through the precision tracker.

Conversely, in the acquisition phase, if no correct program is available, the precision tracker can be slaved and pointed toward the satellite by the command tracker.

Various synchro-transmitting and synchro-receiving devices give the antenna position and display elevation and azimuth angles with an accuracy of  $1/10^\circ$ .

### *Telemetry*

The telemetry data transmitted by the 136 Mc carrier of the satellite are received and recorded.

The binary groups frequency modulate a 3-kc subcarrier.

This subcarrier is extracted from the 136 Mc by a synchronous demodulator, after which it can be recorded directly on a FR 1100 tape recorder. It can also be processed by a phase-lock discriminator which extracts the telemetry pulses. After being reshaped, the pulses are transmitted by telephone circuit to the CNET laboratories in Paris, where they are reduced.

### *The Encoder and the Command Transmitter*

Commands to the satellite can be generated either by the encoder or by the station control console.

In the encoder circuitry, each command is transformed into a sequence consisting of a digital group repeated five times and followed by three "silent" groups. The entire sequence provides all-or-nothing modulation to the 5.45 kc subcarrier produced by a crystal oscillator. The oscillator frequency is also used as a reference for the generation of groups and of pulses modulated in duration. The subcarrier in turn modulates the 123-Mc transmitter.

## TELEPHONE TERMINAL EQUIPMENT

### *Communications*

The telephone terminals serve the following communication lines:

60 circuits between Pleumeur-Bodou and Andover via the Satellite.

12 circuits Pleumeur-Bodou—Brest.

12 circuits Pleumeur-Bodou—Paris via Brest.

These circuits use the Pleumeur-Bodou (village)—Brest microwave link.

Between the main building and the radome, the 60 Andover circuits utilize 2 of the coaxial pairs from the 6-pair cable; 3 other pairs are used for television picture transmission, the sound using one four wires set.

The connection to the microwave station of Pleumeur-Bodou by the two coaxial autocarrier cables, together with the microwave link, can support the operation of the 60 circuits.

#### *Instruments*

The telephone equipment consists of the items listed below and is mounted on racks assembled into a bay (Fig. 29).

The Pleumeur-Bodou—Andover Circuits are (Fig. 30):

5 systems of 12 channels forming 5 primary B groups (60-108 kc) connected to the distributor in primary groups.

5 primary group modulator-demodulators (GP 1, 2, 3, 4, 5) connected on the 60-108 kc side to the primary group distributor, and on the other side, after coupling, to the secondary group distributor, form in this way a basic secondary group (312-552 kc).

4 primary group modulator-demodulators (GP 2, 3, 4, 5) connected on the 60-108 kc side to the primary group distributor, and connected separately on the other side to the secondary group distributor.

5 secondary group modulator-demodulators (GS 2, 4, 6, 8, 11) which, connected on the 312-552 Mc side to the secondary groups repartitor, terminate after coupling at the transmitting and receiving amplifiers.

A transmitter amplifier and a receiver amplifier, each equipped with an equalizer and an artificial line, compensating the attenuation of the coaxial pairs in both directions, and at all frequencies in the band between 12 kc and 13 Mc. In the upper cabin the coaxial pairs are directly connected, one to the modulator (transmission) and the other to the demodulator (receiving).

A 120 kc primary group modulator-demodulator, a coupler and amplifiers make it possible to take this group from the distributor and to use it either in the 60-108 kc or the 12-60 kc positions.

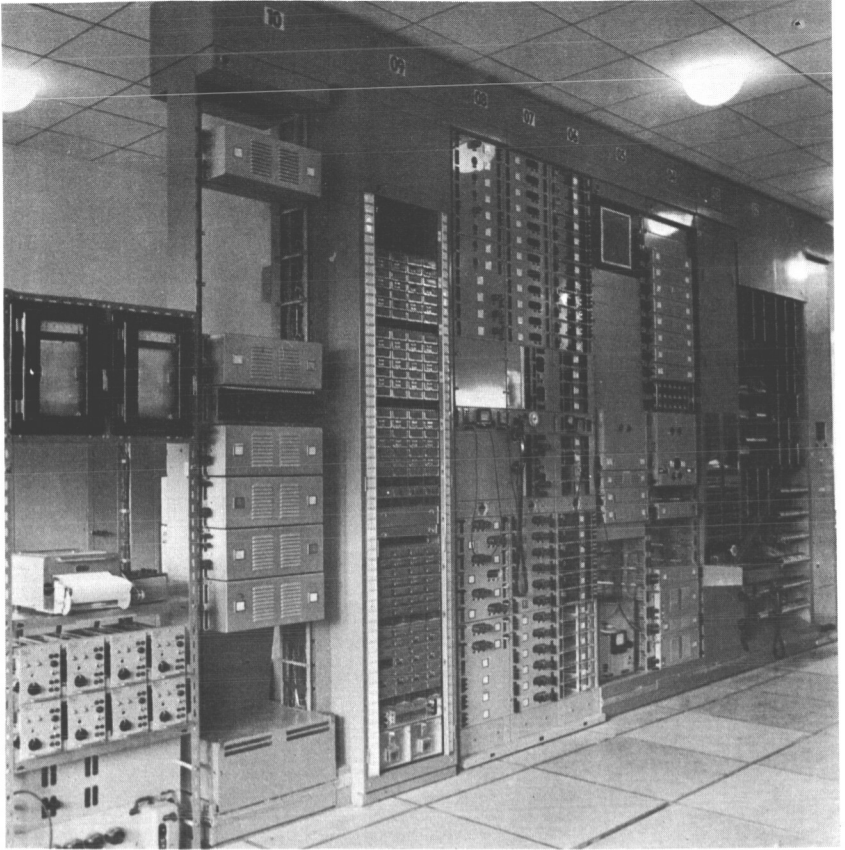


Fig. 29 — View of the telephone terminal equipment.

Both primary and secondary group distributors are equipped with jacks, so that with patch cords quick access is available to the following combinations:

60 circuits occupying one of the following frequency-bands:

312-552 kc	secondary group 2
812-1052 kc	secondary group 4
1308-1548 kc	secondary group 6
1804-2044 kc	secondary group 8
2548-2788 kc	secondary group 11

60 circuits divided into 5 groups of 12 (5 primary groups) each of these groups being situated in one of the above mentioned secondary groups.

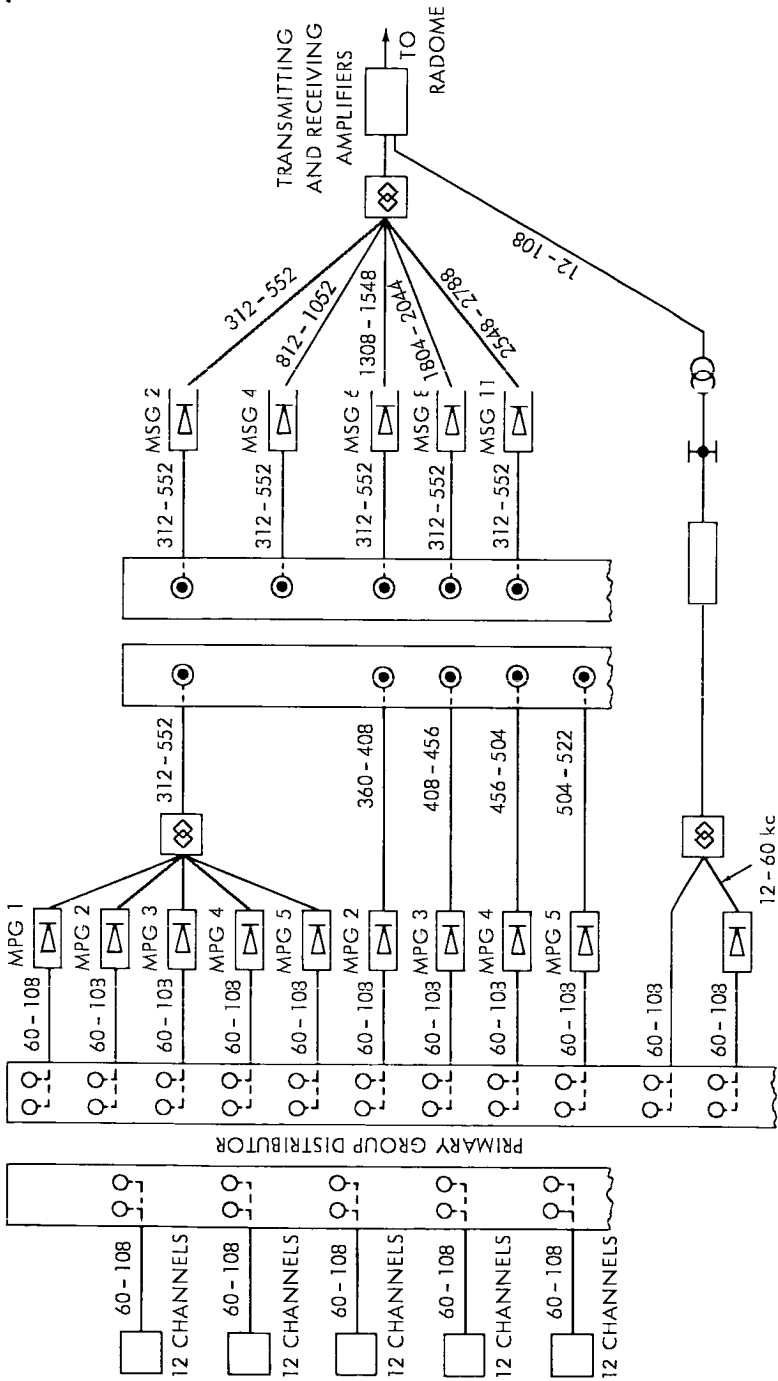


Fig. 30 Telephone equipment—Functional diagram.

or, 12 circuits occupying either the 12-60 kc band or the 60-108 kc band.

The Brest Pleumeur-Bodou Circuits (Fig. 30) are:

2 systems of 12 channels each, constituting 2 base B primary groups.

2 primary group modulator-demodulators (GP 4 and 5) which place these two groups of 12 channels in the 456-504 and 504-552 kc bands.

A transmission modulator and a receiver amplifier together with equalizers and artificial lines. This assembly compensates the attenuation of the overhead coaxial pairs in both directions, and at all frequencies between 60 and 300 kc.

Twelve of these 24 channels constitute the Pleumeur-Bodou-Brest circuits; the other 12 go on to Paris as a primary group. Channels 4, 5, and 6 of these last group can be used either separately as telephone lines or together as the "sound" circuit for TV. For this purpose, these three channels are switched in Paris and Pleumeur-Bodou to special equipment which provides a circuit with a pass band of 30 to 10,000 cps.

The components of the equipment for these 24 circuits are connected to the various distributors in normal fashion, with no provision for rapid changeovers. However, the 12 Paris channels as well as the satellite transmission channels go through a patchboard where they are hooked up in such a way as to be easily connected on 4 wires, thus making Paris-Andover circuits.

### *General Equipment*

There are: a central generator; generators for the primary group carriers; generators for the secondary group carriers; and generators and transmitters for the 60 and 30 kc pilot signals.

All the telephone equipment parts are standard, but their configuration has been planned in a special way to accommodate the necessary measurements and transmission tests (Fig. 30).

### BORESIGHT TOWER EQUIPMENT

Equipment which simulates all the essential functions of the satellite has been placed on top of the 200 m tower built on the Ile Losquet: a beacon with an unmodulated 4080 Mc signal and a transponder which receives the 6390 Mc signal of the horn antenna; the 6390 Mc signal is transmitted at 4170 Mc.

The problems presented to the CNET laboratories in the building

of this equipment were very different from those encountered by the developers of Telstar. There were no serious limitations as to weight, size, or power supply to be considered; the environment, however, called for protection against rain, dampness and salt air. This was achieved by cases of lightweight alloys, and rubber-sealed joints.

On the other hand, the equipment being approximately 1000 times closer to the antenna than the satellite, its signals had to be a million times weaker than those of the satellite; also, the signals received by the transponder are a million times stronger and it must transmit less power than it receives.

### *The Beacon*

The beacon (Figs. 31, 32, and 33) was designed entirely with semi-conductors, whence its highly dependable operation. A two-stage multiplier, the two stages of which are separated by amplifiers, is driven by a crystal oscillator with a resonance frequency of approximately 50 Mc. This assembly is located within a thermally insulated area for greater stability.

A solid-state generator of high harmonics produces the 4080 Mc signal. A parabolic antenna (Diam: 60 cm), fed at its focus by a small plane reflector, directs the 4080 Mc signal toward the radome. The circularly polarized signal is brought to this point by a circular waveguide filled with dielectric.

To simulate a Doppler effect ( $\pm 140$  kc in 10 minutes) the frequency of the oscillator can be varied continuously over a range of about  $\pm 2$  kc by means of a semiconductor diode with variable capacitance. The command voltage is obtained by a remotely controlled motor. A high frequency attenuator controls the beacon output level ( $-50$  dbm to  $-70$  dbm). The stability for 1 minute is better than  $10^{-7}$ .

### *Repeater*

It was possible to simplify the repeater very much because the signals going through it require no amplification. The frequency is simply changed by a semiconductor diode (Fig. 34). The transposition frequency of 2220 Mc is a harmonic amplified by electronic tubes of the same resonant frequency as a crystal oscillator. The passband is very wide,  $\pm 25$  Mc, and a wideband filter provides that only the 4170 Mc signal is sent to the antenna, which are helical (Fig. 35). The insertion gain between omnidirectional antennas is  $-11.6$  db, and can be adjusted by means of a variable attenuator.

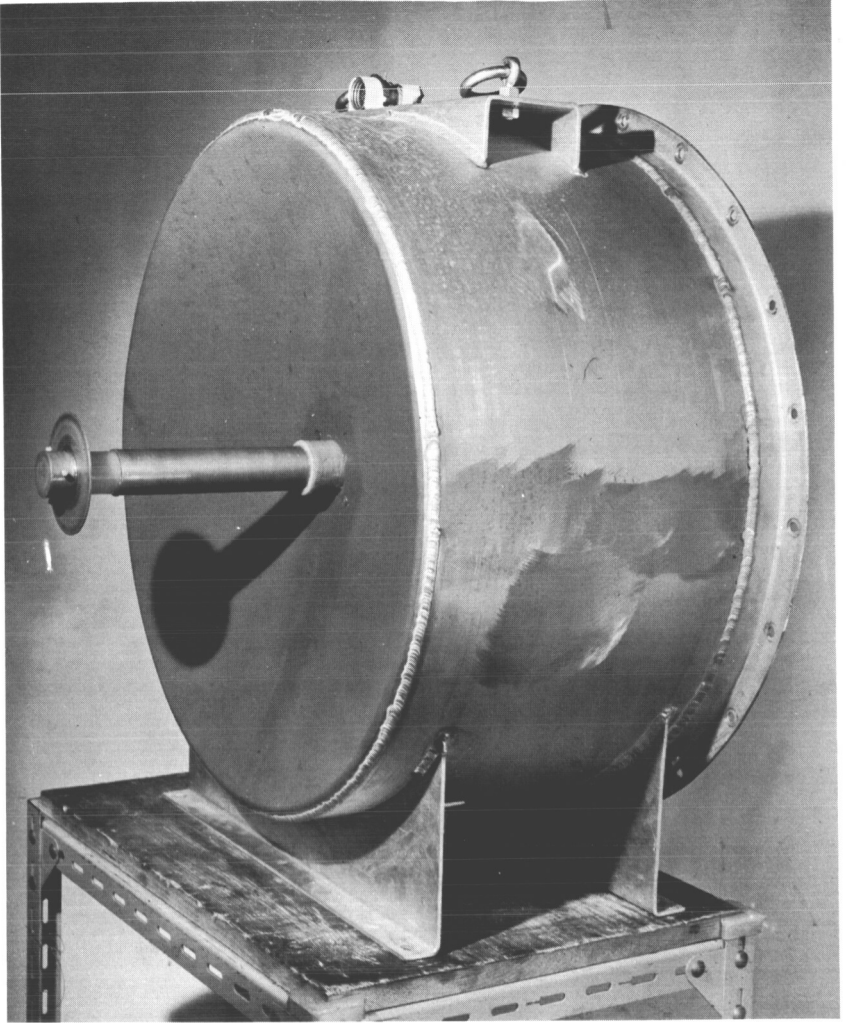


Fig. 31 — View of the Telstar Simulator 4080 Mc Beacon.

For a 2-kw transmitted power of the horn antenna the received signal level is  $-0.8$  dbm, and the transmitted power is  $-12.4$  dbm. The power level at the horn antenna input is  $-133.4$  dbm.

#### ELECTRICAL POWER

The electrical power equipment is distributed in the various areas and buildings already described (Fig. 36).



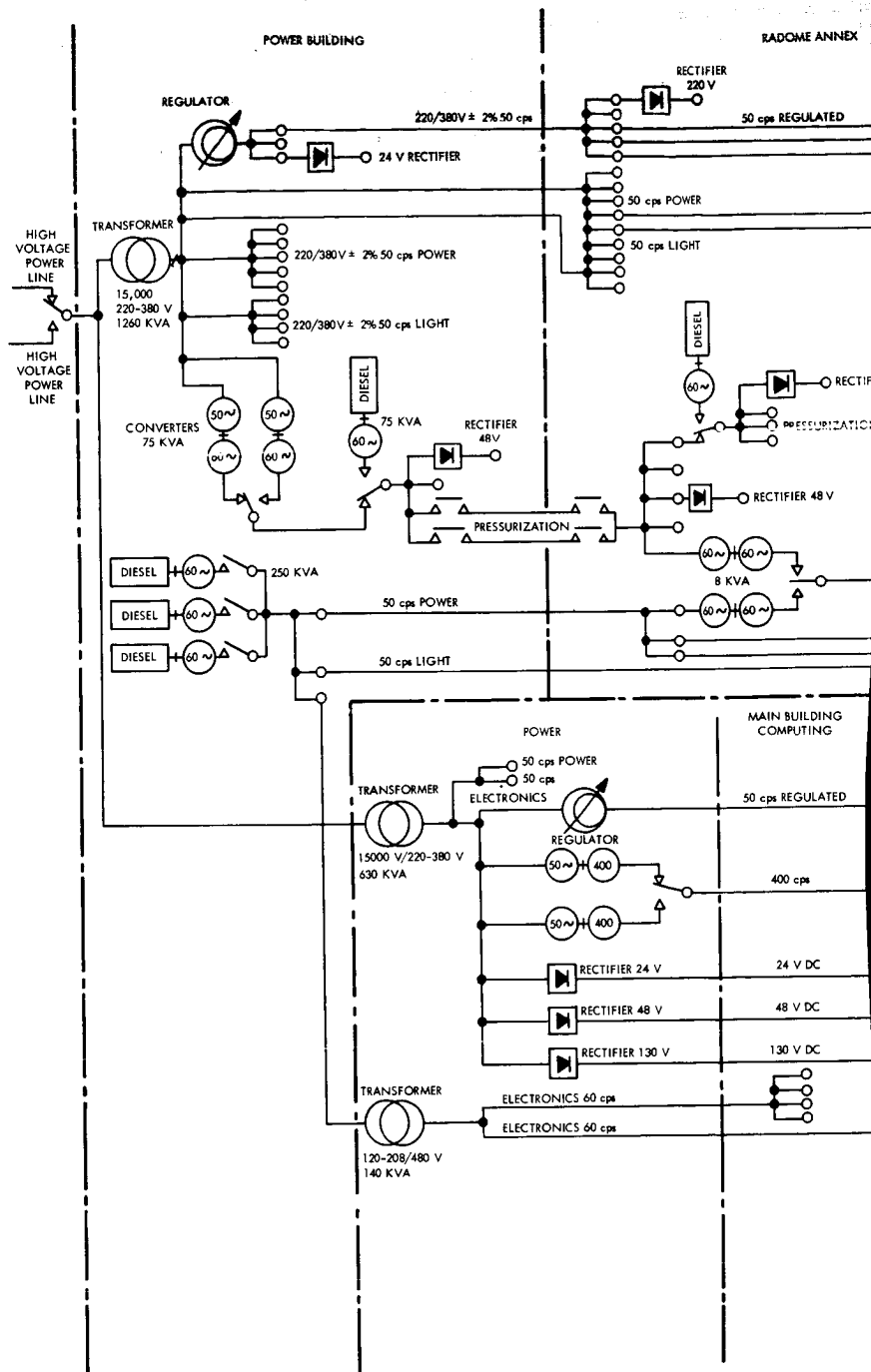
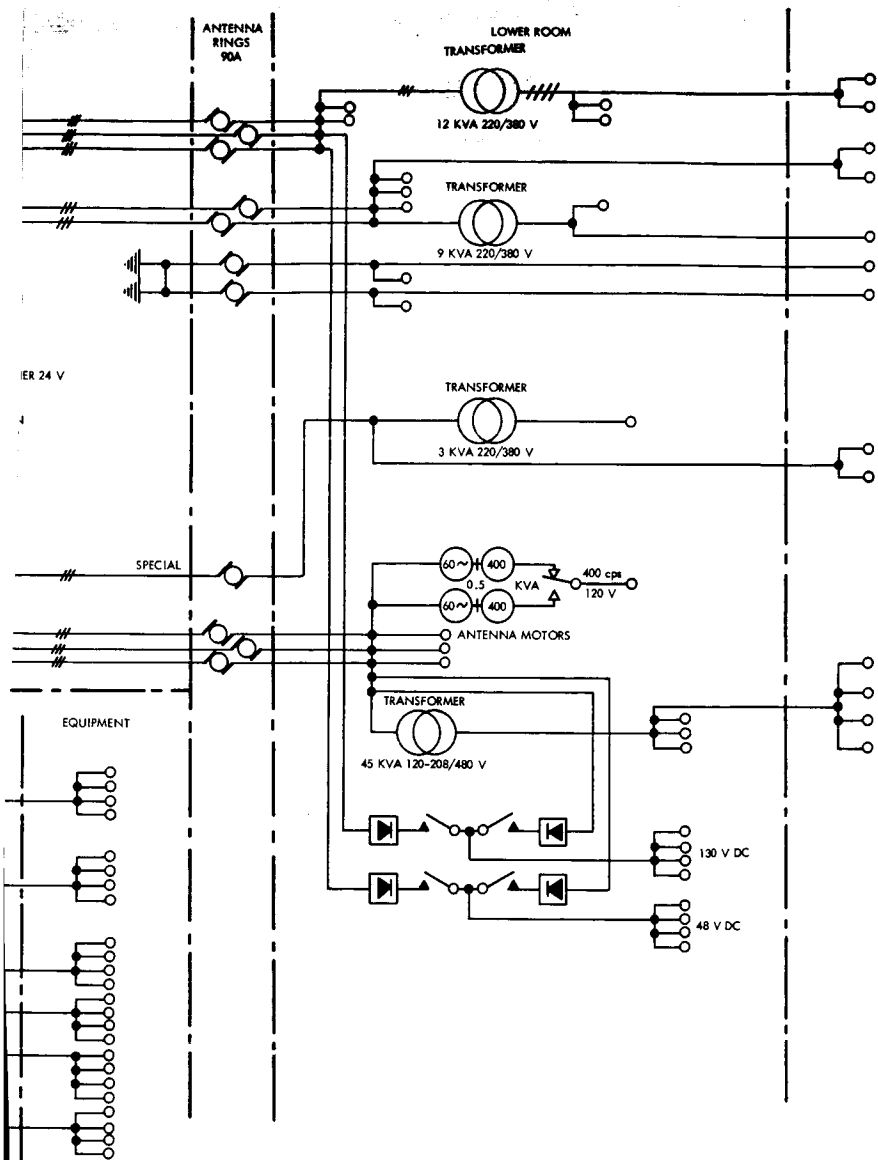


Fig. 36 — The electrical install

2



tion—General diagram.

3

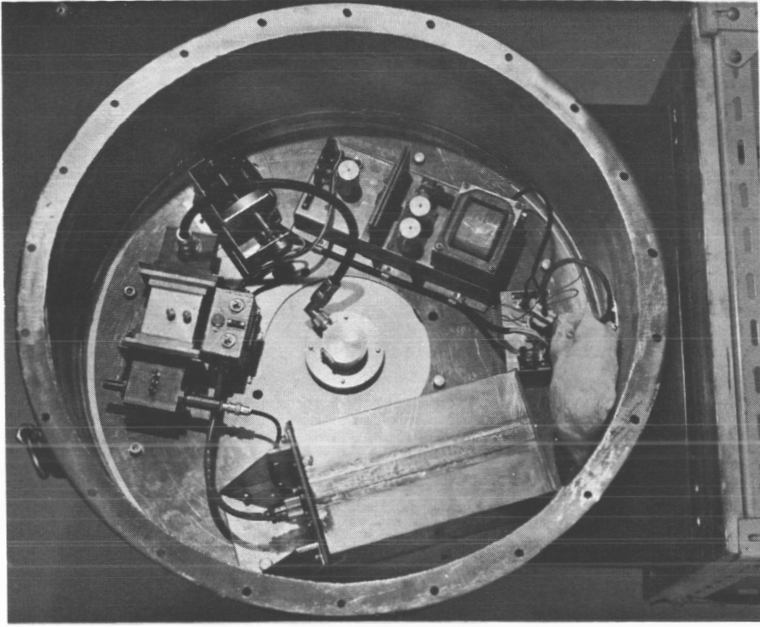


Fig. 33 — Interior view of the beacon.

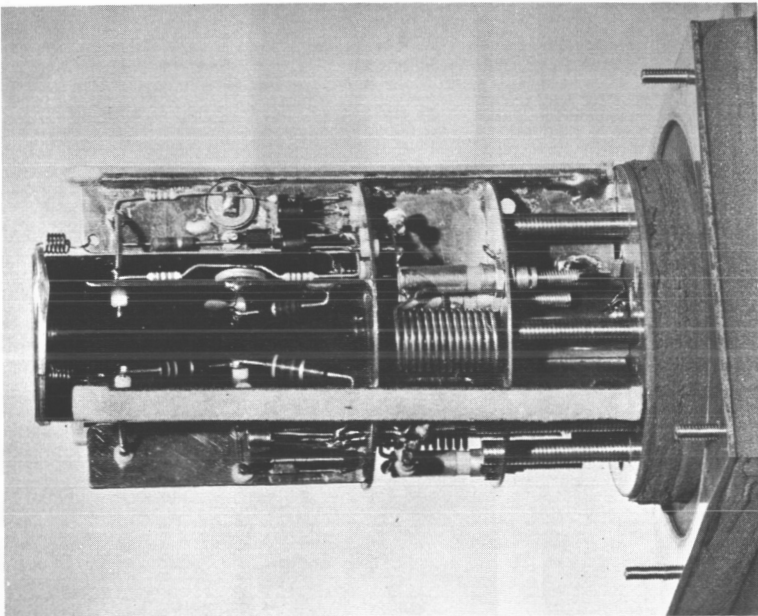


Fig. 32 — View of the thermostatic controlled oscillator providing 200 Mc to the simulator beacon.

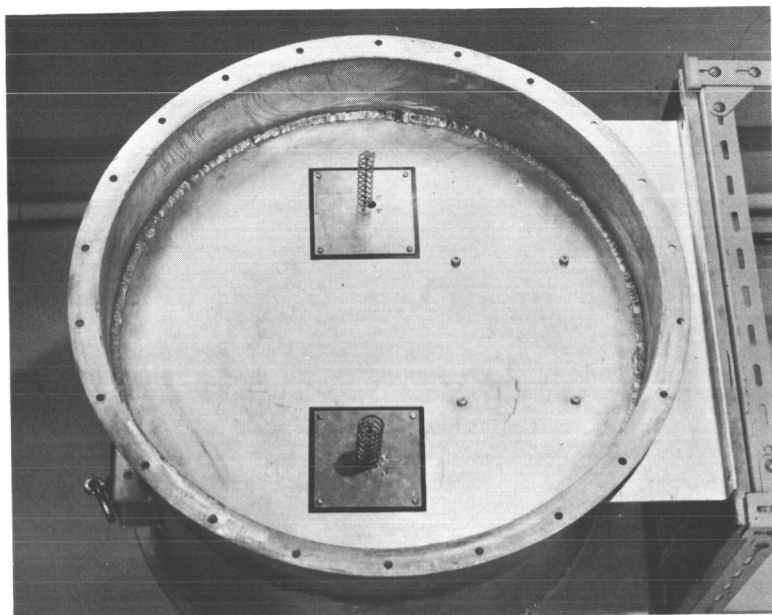


Fig. 35 — View of the Telstar simulator transponder antennas.

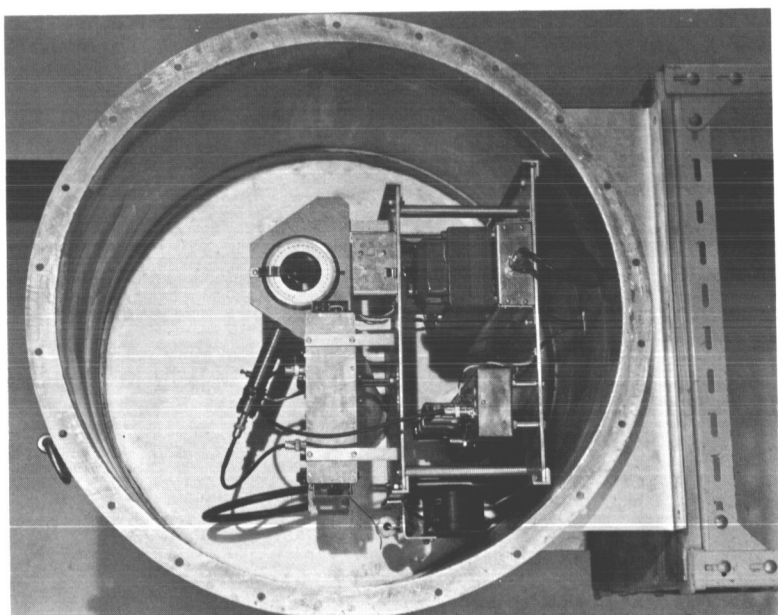


Fig. 34 — Interior view of the transponder.

### *The 50-Cycle Alternating Current: 220/380 volts*

The 50-cycle power from the national network of L'Electricite de France is carried by 2 medium voltage supply lines. One of these is for regular use and the other is on standby for emergency use; both are connected to the main power switchboard. Since a distance of more than 500 m separates the main building from the power supply building, it was necessary to install at these two points 2 transformers of 630 and 1260 KVA, both of which supply power at 220/380 v. They are complemented by 2 induction regulators which produce a regulated voltage at  $\pm 2\%$  for electronic equipment of French origin.

### *60-Cycle Alternating Current*

#### *60-Cycle Blowers, 272/470 volts*

The power for the pressurizing equipment of the radome, consisting of five 5 KVA blowers (Fig. 37), is provided by special circuits.

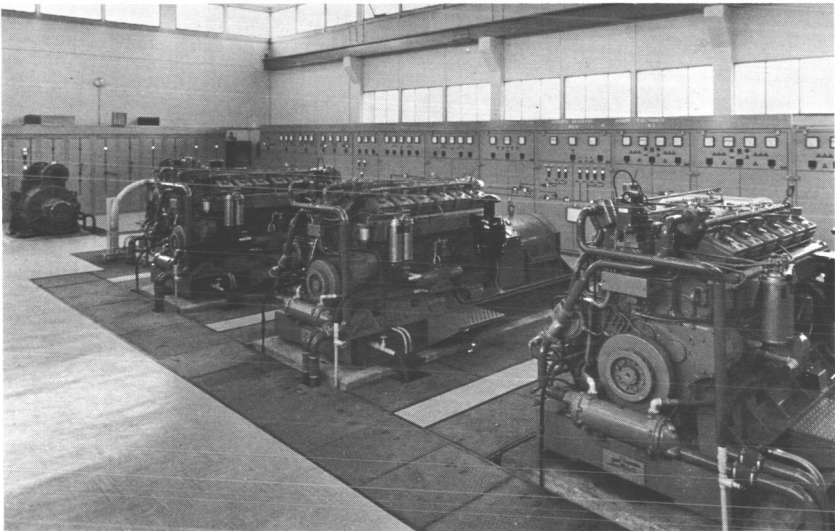


Fig. 37 — Interior view of the power supply building.

In the power supply building, 2 groups of 50/60 cycle converters ordinarily supply the necessary power through 2 lines, one of these being a standby.

In case of power failure from the network, one 75 KVA diesel generator (GE1), in reserve for emergencies, starts up automatically.

Finally a second emergency generator (GE5) of the same power, is held in emergency reserve in the radome auxiliary building. This second group is only capable of operating 4 of the blowers. This obviates the risk of total loss of pressure from a simple switching failure in the control cabinet of this group.

#### 60-Cycle General, 272/470 volts

In the power supply building, 3 250 KV diesel generators, GE2, GE3, and GE4 provide the regular supply.

Normally, the power is supplied by GE2 or GE3 which have manual starters, GE4 being an automatically started stand by.

At critical times, GE2 or GE3 is coupled in parallel with GE4.

The frequency tolerance of  $\pm 1\%$  is obtained by a speed regulator of the wattmeter type. The alternators have voltage regulators with an accuracy of  $\pm 1\%$ .

The power is sent to the radome via 2 separate circuits (for motors and electronic equipment respectively), and to the main building, where two transformers (one exclusively for the computing center) reduce the voltage to 120/208 volts.

#### 60-Cycle Special

Some components of the antenna require a regular power supply of 230 volts at 60 cycles, single phase, with subharmonics less than 0.5/1000.

2 converter groups of 60/60 cycles—8 KVA—1800 rpm with automatic starters, provide this power.

One of the groups is powered by the 60-cycles coming from the 50/60 conversion, the other by the 60-cycle general supply.

At critical times, the two groups are in operation, one carrying the load, the other unloaded on automatic standby; the load transfer can be effected within 0.25 seconds.

These groups fulfill exactly the necessary requirements: no harmonic is above 3%. No matter what the load (from 4/4 to zero) with a power factor varying from 1 to 0.7, the value of the subharmonics remains below 0.5/1000. With the same variations of load and power factor, the voltage is regulated at  $\pm 1\%$ .

#### *The Power Supply for the Antenna*

Power is supplied to the rotating structure through 28 commutator rings on the pivot.

• The neutral of the 3-phase a-c supply is omitted; this has no effect on the motors, but creates a need for transformers in the lower cabin for the single-phase circuits.

The commutator rings are protected at the radome annex switch-board by electronically triggered circuit-breakers (Nominal load 90 A) and by special fuses for short-circuits. At the antenna input, circuit-breakers with overload relays break the circuit when the load exceeds 100 A. These circuit-breakers release in case of general power failure, to avoid arcing when the power is re-established.

All the circuit-breakers have the usual thermal overload cutoff which is kept as an emergency provision.

#### *420-400 Cycle Power Supply*

In the antenna, two 0.3 KVA groups supply single-phase current at 120 v—420 cycles  $\pm 0.25\%$  to the antenna servo loops.

In a small building near the central building, 2 groups produce for the trackers 120/208 volt current at 400 cycles  $\pm 2\%$ .

#### *DC Sources*

The special sources are:

24 volt current  $\pm 5\%$ —filtering 1/1000.

2 batteries in the main building supply the station clock (80 amps) and the telephone switchboard (15 amps).

130 volt current  $\pm 4\%$ —filtering 1/1000.

For electronic equipment,

1 battery in the main building.

2 rectifier assemblies in the antenna lower cabin.

220 v—60 amps power for emergency lighting of the radome.

Various sources insure, at 24 volts, the starting of the motor-generators, and at 48 volts, the power for the distribution switchboards (switching and indicators).

#### *Power Supply for the Telephone Transmission Equipment*

The telephone terminal equipment of the main building is supplied by a special system (battery-emergency generator—switchboard) standardized for long distance lines (LGD).

#### *Ile Losquet*

An autonomous power supply station, composed of a permanent source of single-phase 220 v 50-cycle current from 3 motor-generators

which are rotated daily, is installed besides the 200 m tower. Batteries supply the remote monitoring equipment. These batteries can also act as a spare power supply to the beacon lights for the safety of aircraft.

#### *Distribution Switchboards*

These have been constructed in a unique design, being made of identical and matching modules, equipped with switches, and mounted on plug-in frames (Fig. 38).

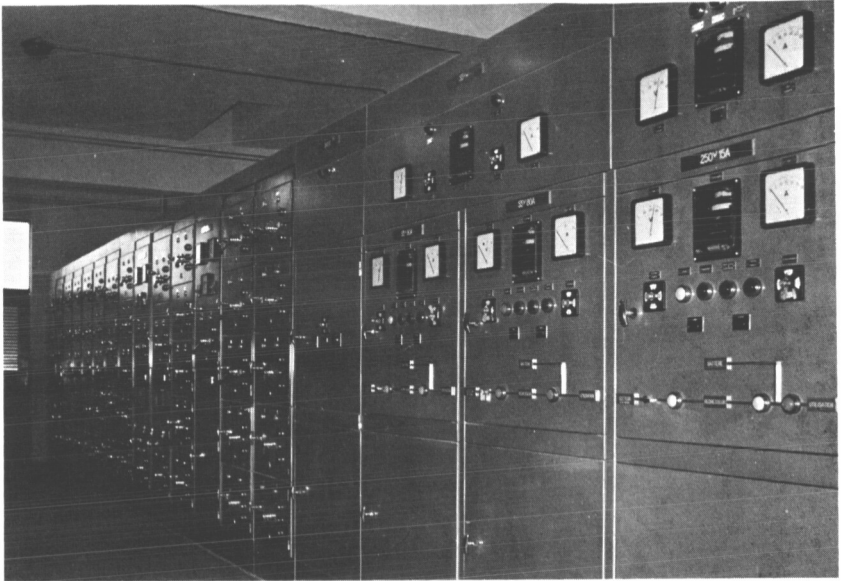


Fig. 38 — Radome auxiliary building—View of the power switch gear.

Beside the switch, each frame carries the usual safety devices: indicating fuses and thermal relays.

#### CONCLUSION

The Pleumeur-Bodou station has been in operation without failure for all the orbit revolutions which it supported.

Its use has contributed, as well as test data, invaluable experience concerning the functional characteristics of a system both novel and complex.

CNET thus have available sound information for the planning of an operational ground station.

N67 12304

# Results of Tests Performed with the Telstar I Satellite at the Pleumeur-Bodou Satellite Communication Station

L. BOURGEAT, A. DYEURE, and J. P. HOUSSIN

CENTRE NATIONAL D'ETUDES DES TELECOMMUNICATIONS

*Tests performed at the Pleumeur-Bodou satellite communications station with Telstar I are described.*

*These tests have made possible an analysis of the feasibility of acquisition and tracking of a satellite by an antenna of very narrow beamwidth and of the good and bad features of the transmission channel established in this manner. These tests were completely satisfactory and have enabled us to determine the methods which will be economically and technically valid for establishing a commercially practical system for satellite communications.*

Tests of communications through an active satellite began at the French station at Pleumeur-Bodou on the day the Telstar I satellite was launched—10 July 1962. They continued with this satellite until 21 February 1963, when the satellite transmissions were broken off.

These tests were performed during more than 110 revolutions and were intended to explore and analyze the feasibility of establishing and keeping in operation a communication link via satellite, in other words, the feasibility of acquiring and tracking a satellite and the good and bad features of the transmission channel established in this way.

From the first pass of the satellite, during its sixth orbit about the earth, the quality of the television pictures transmitted by the AT and T station at Andover and received at Pleumeur-Bodou showed that the entire station was operating perfectly well and the link was of very satisfactory quality. The tests described in the following pages were performed to enable us to determine the optimum characteristics and the limits of capability of each part of the equipment and to provide us with the experience which would be indispensable for future develop-

ments leading to the establishment and use of satellite communication links.

### ACQUISITION AND TRACKING TESTS

During the 115 passes of Telstar I utilized by the Pleumeur-Bodou station, corresponding to 40 hours of traffic across the Atlantic, the total time during which the link was interrupted or delayed by reason of a failure of the equipment or personnel of the antenna control amounts to 22 minutes, distributed over 5 passes. Three of these interruptions are related to operator error, one to misadjustment of a circuit before the pass, and one to a power failure. The percentage of time during which the tracking of the satellite was correct and permitted television and telephony demonstrations or technical tests amounts to over 99 percent. It should be noted that during these first hours of space communications, which must be considered from many points of view as part of an experimental period, there was no serious equipment failure.

Since the main purpose of the antenna drive is to assure correct pointing of the horn reflector antenna in the direction of the satellite to provide for transmission and reception of communications or any related tests, we made an effort during the various passes to determine the acquisition capability of the different kinds of tracking equipment and of their capability for maintaining contact with the satellite in the various modes of operation. In the light of the results of these observations, some modifications or additions were made to the equipment.

We call attention to the fact that, with one exception, the components which went into the command antenna were supplied by Bell Laboratories and are identical to those in operation at Andover. The exception is the 136 Mc command and telemetry equipment, referred to as the "command tracker", produced by CNET.

We shall analyze the various components successively. They are shown in block diagram form in Fig. 1.

#### COMMAND TRACKER TESTS

##### *Tracking Tests*

We recall that the tracking equipment receives the satellite beacon signal, which is transmitted at a frequency of about 136 Mc. In the case of Telstar I, the frequency is 136.05 Mc.

The many measurements which have been made have shown us that

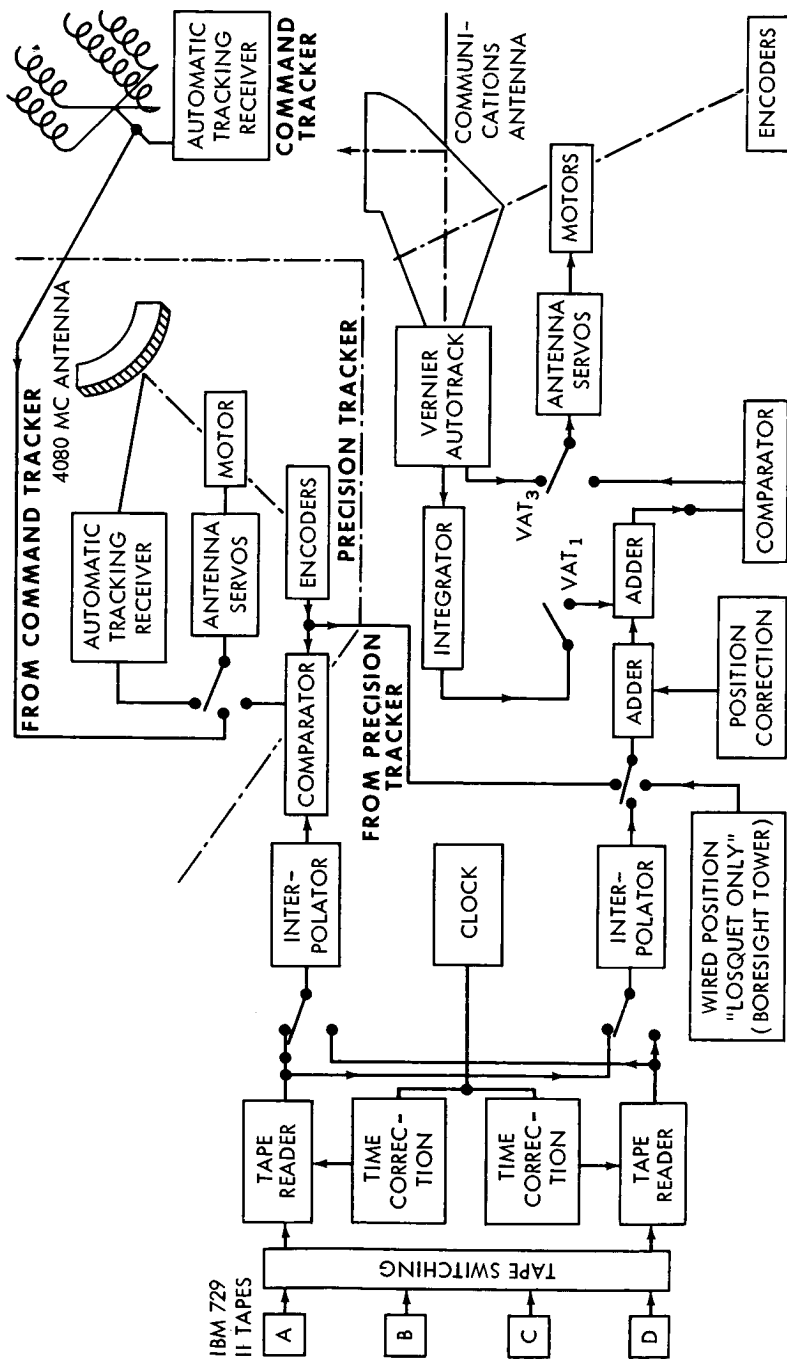


Fig. 1 — Functional block diagram of the antenna drive.

acquisition could be achieved at the time of the apparent rise of the satellite above the horizon. Taking into account the phenomena of refraction at elevations which permit reception of the first beacon signals at geometrical elevations of between  $-0.5$  and  $-1$  degree and of the time necessary for the receiver to achieve frequency lock, it is always possible to drive the antenna in the automatic tracking mode at elevations below  $2^\circ$ .

However, on account of ground reflections and the width of the antenna pattern ( $20^\circ$  at 3 db) some important errors appear between the real positions of the satellite and the information supplied by the encoders. These differences are more evident in elevation for angles of less than  $20^\circ$ : the rapid fluctuations of the antenna can attain  $\pm 5^\circ$  without causing the autotrack to lose lock. For higher elevations the pointing accuracy improves and attains  $\pm 1^\circ$  at  $40^\circ$ . The azimuth data is only very slightly affected by reflections, but due to the size of the antenna and its mechanical structure, errors of about  $2^\circ$  can appear under the buffeting of winds over 60 kilometers per hour. Due to the exposure of the antenna site, such wind velocities were experienced fairly frequently during the winter of 1962-1963.

In Fig. 2 we have reproduced the recording of a tracking operation. During this pass the signal/noise ratio was 25 db and the wind speed 50 Km/hr.

To make this chart, we used for measuring equipment some components of the tracking encoder in the precision tracker.

With the precision tracker slaved to the command tracker, the position information given by its encoders is compared at each instant with the precomputed tape corresponding to the pass. The validity of this tape is continuously checked against the data given by the horn reflector antenna tracking the 4080 Mc beacon.

Furthermore, for the 15, 20, and 30 degree positions, a control was provided by shifting the precision tracker to autotrack.

Following the conclusions indicated above, the use of the command tracker as a means of acquisition for the communications antenna is limited to confirming the presence of the satellite as well as the time when the satellite rises above the horizon. The positions indicated by the computed tapes are more accurate, as we shall see later on, than those given by the command tracker.

### *Telemetry*

The reception of Telstar I telemetry data is always accurate and all the recorded magnetic tapes have been easily decoded.

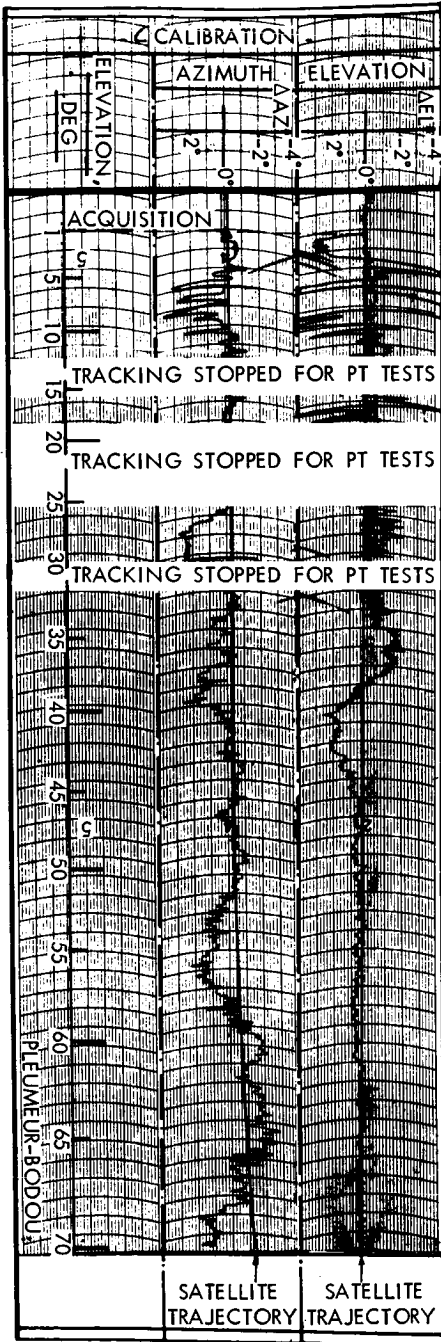


Fig. 2 — Plot from the 136 Mc tracker: S/N = +25db.

The quality of this data is such that it could have been used for monitoring the satellite during the various command operations.

After some difficulty with the reception of the Telstar II telemetry on 7 and 8 May 1963, an equipment modification (reducing the receiver bandwidth from 50 Kc to 8 Kc) allowed very satisfactory use of the data from this satellite, despite the low received level due to the range, often from 15,000 to 16,000 Km.

#### TESTS WITH THE 4080 MC PRECISION TRACKER

##### *Acquisition*

Acquisition by the precision tracker of the 4079.73 Mc satellite beacon takes place in two steps:

1. Acquisition in position.
2. Acquisition in frequency.

##### Acquisition in Position

Acquisition is considered achieved to the extent that the pointing of the antenna corresponds to the real position of the satellite within  $\frac{1}{2}$  degree. The 3-db beamwidth of the antenna being 2 degrees, a pointing error of 0.5 degree corresponds to an attenuation by 1 db.

Some series of tests were made with a view to adapting the method to any circumstances which might arise, and to the training of operators.

It became apparent that the problem is not the same in the case of the beacon being ON when the satellite rises above the horizon as it is for elevations other than zero.

1. In the case of the beacon being ON when the satellite comes up over the horizon, acquisition can be achieved by means of
  - a. Computed magnetic tapes which, acting through the tracking encoder, operate the azimuth and elevation equipment, to the extent that the available information furnished regarding time and position can be considered accurate.
  - b. Manual positioning in elevation at elevation zero, with the beacon moved slowly through a small sweep (approximately  $2^\circ$ ) in azimuth, around the calculated position. This method has the great advantage of practically eliminating the acquisition time parameter, an accurate trajectory with a slight shift in time still permitting the solution of the problem of acquisition.

- It is to be noted that acquisition by slaving to the command tracker was not used. In the event of the pointing information appearing doubtful, the presence of the satellite is confirmed by this equipment which provides sufficient indication to avoid gross errors.
- 2. If the beacon is not ON when the satellite rises above the horizon, acquisition is achieved by servo drive with precomputed magnetic tape, plus a search in azimuth and elevation about this position.

Series of tests were made with the antenna slaved to the command tracker. Due to the rapid variations of about  $\pm 5^\circ$  (see Paragraph I.1.1) it was not possible to obtain satisfactory results for elevations below  $20^\circ$ . On the other hand, for elevations above about  $30^\circ$ , a trained operator may effect acquisition by this mode of operation.

It should be noted that the 4080 Mc beacon is practically always ON for elevations below  $20^\circ$ .

### Frequency Acquisition

When acquisition has been effected, phase lock of the automatic frequency control oscillator\* must be achieved. Depending on the received signal level, this operation either is automatic and almost instantaneous, or calls for the intervention of the operator. Taking into consideration Doppler effect, thermal drift of the beacon, or any other disturbance within the satellite, the range of frequencies within which the frequency can be located is 150 Kc around the nominal value.

The automatic method, making use of the comb filter of 300 outputs, is usable for practical purposes for received powers of  $-139$  dbm at the level of the parametric amplifiers, corresponding to a signal/noise ratio of  $+2$  db in the receiving circuit used.

This operational mode of acquisition was always usable for Telstar I, for which acquisition ranges varied between 9000 and 4000 km, corresponding to received powers between  $-137$  dbm and  $-130$  dbm.

This no longer held true for Telstar II, for which the received power is often in the vicinity of  $-141$  dbm (range of 16.000 km). In this case we had to use manual acquisition routinely, consisting of prepositioning the 3-Kc bandwidth receiver channel on the frequency received by the equipment. Taking into account the Doppler frequency information supplied by the computing center, a small amplitude search around the predetermined frequency, together with an aural

\* In the tracking receiver.

analysis of the beat signal, makes it possible to obtain acquisition-for signal/noise ratios in the 3 Kc bandwidth as poor as  $-8$  db.

Actually, for Telstar II this acquisition was achieved most of the time at a signal/noise ratio of  $-5$  db.

As soon as acquisition has been achieved the oscillator phase-lock reduces the equivalent passband to 100 cps, which brings the noise level to  $-151$  dbm.

It should be noted that allowing for the refraction at 4080 Mc (a systematic study of which will be found in Paragraph I.3.3), the acquisition is completed and the precision tracker turned over to autotrack almost certainly at geometrical elevations below  $2^\circ$ , whatever the method used, whether automatic or manual, providing of course that the beacon is ON when the satellite comes up over the horizon.

### *Tracking*

When the satellite has been acquired, the accuracy with which it can be followed will depend upon random variations in tracking as well as on systematic errors due to mechanical imperfections of the system.

#### Random Errors

These errors depend both on the elevation above the horizon, and on the signal/noise ratio in the receiving channel after phase lock.

The direction of the received signal suffers far fewer disturbances than is the case with the command tracker.\* As a consequence of the width of the antenna lobe, the accuracy obtained is around  $0.2^\circ$  for elevations less than  $2^\circ$ . For higher elevations, this accuracy improves rapidly until at  $3^\circ$  it depends solely on the signal/noise ratio.

The fluctuations due to ground reflections have been noted by recording on magnetic tape the data from the position encoder outputs and comparing it to the theoretical trajectories.

To achieve measurements of tracking characteristics at elevations above  $3^\circ$ , we made use of the horn-reflector antenna with its vernier autotrack as a necessary instrument.

To perform these tests we took into consideration the fact that the precision of angular measurements by this equipment is markedly superior to those of the precision tracker. This results from the dimensions of the horn reflector antenna, and the fact that the signal/noise

---

\* In fact it is the reflections which activate the command tracker at low elevations because of the width of the antenna lobe.

ratio in the receiving channel of the vernier autotracker is always superior by 10 db to that of the precision tracker.

On the other hand, the overall response characteristics in position of the two systems are essentially comparable in the region utilized.

With the horn antenna slaved to the precision tracker antenna, via the encoders and the digital equipment, the angular deviation between the pointing of this antenna and the true position of the satellite is measured at each instant by the vernier autotracker circuits operating in open loop (Fig. 3).

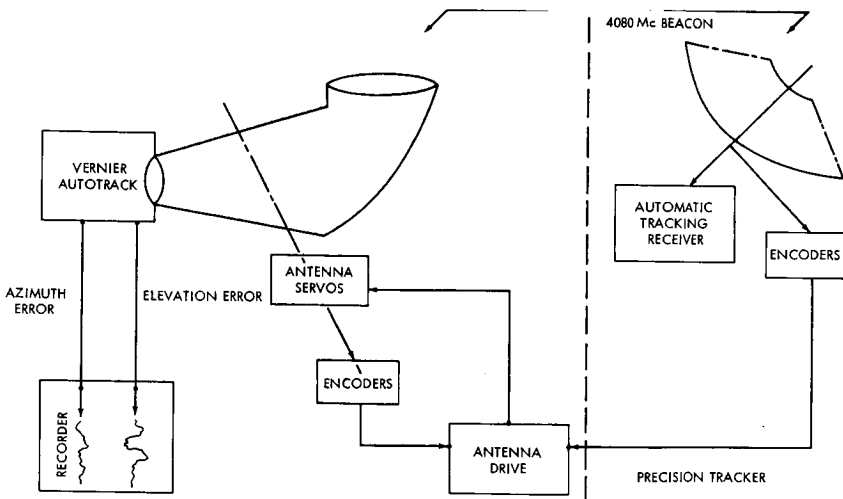


Fig. 3—The horn reflector antenna.

In Figure 4 are shown tracings of recordings corresponding to signal/noise ratios of 27 db and 12 db for a servo noise bandwidth of 0.2 cps.

An analysis of these results brings us to an RMS noise jitter of:

$$10^{-4} \text{ radians for } \frac{\text{signal}}{\text{noise}} = 27 \text{ db}$$

$$3 \times 10^{-4} \text{ radians for } \frac{\text{signal}}{\text{noise}} = 12 \text{ db}$$

It should be noted that these measurements take into account thermal noise, and also the potential digital error ( $0.5 \times 10^{-4}$  rad) of the encoders and the mechanical imperfections about the position used.\*

\* i.e., mechanical biases as a function of angular position.

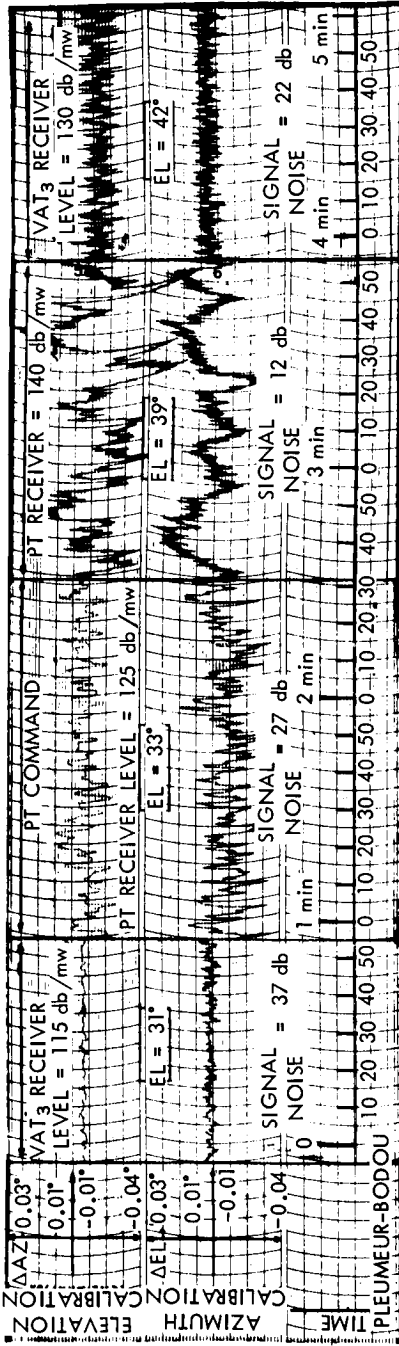


Fig. 4 — Plot from the 4080 Mc precision tracker.

We have shown in this figure the recordings, made during the same passes, of the output errors of the vernier autotrack operating in closed loop.

### Systematic Errors

These errors can be the result of imperfections in fabrication or wear of the elevation and azimuth drive mechanisms of the antenna and the associated encoders, or of shifts in the position of the antenna base.

The only systematic checks were to verify that the base was level; they revealed a settling of the foundations during the first three months, resulting in an angular variation of the reference plane of  $0.015^\circ$ . The monthly measurements now performed do not indicate the need for any adjustments.

In any case, no noteworthy mechanical error was detected with respect to variations in elevation or azimuth in the course of the passes which were studied.

### Operation

During all of the operational passes which were utilized, the precision tracker was operated. The reliability and accuracy of this equipment, together with its relatively wide practical acquisition angle (width of the antenna beam associated with the search about the computed position), led to its being considered, while not essential to the smooth running of the operations, an element of functional reliability.

The data received and recorded on magnetic tape during these passes was not utilized in any useful way for the determination of orbital parameters. It should be noted that the average duration of the passes which included the acquisition phase, is 20 minutes.

To facilitate the use of the equipment and to reduce the operating personnel of the station, the main controls of the tracking encoder were mounted on the precision tracker operator's console.

Information concerning the difference between the taped position and the antenna pointing is displayed at the central station console. This information, shown on a dial after conversion into analog form and amplification, informs the chief of operations of the difference to within  $0.01^\circ$ . A time correction adder identical to the one used in the antenna drive located in the lower cabin under the radome provides time corrections to the tape used for the tracking encoder. With the error indications supplied by the central console, this allows optimum

adjustment of the time and position information on the tape driving the horn antenna, and helps in the establishment of the link.\*

A computer unit which can be hooked up between the precision tracker and the antenna drive was designed and built so that when the horn antenna is directly slaved to the precision tracker (through the encoders) an accurate pointing of the radio beam carrying the communications information can be achieved despite deformations of the antenna.

We shall define the theory of this equipment in Paragraph 1.3.2.2.

#### TESTS WITH THE COMMUNICATIONS ANTENNA

The tests concerned the different possible modes of acquisition and tracking, requiring therefore the measurement of the intrinsic characteristics of the antenna in relation to the particular conditions which prevail at the time of the mission.†

For this reason we were led to an examination of the following parameters:

The radiation patterns of the horn reflector antenna in the communications receiving band, centered on the normal frequency of 4169.72 Mc, and at the vernier autotrack frequency of 4079.73 Mc.

The azimuth errors as a function of elevation.

Refraction at low elevations.

#### *Antenna Patterns*

These tests were performed with a view to learning the patterns of the secondary lobes near the antenna and verifying that when the antenna is in the vernier autotrack mode. The pointing corresponds to the maximum of the pattern for the communications receiving frequency.

These measurements were carried out by receiving the signal from the satellite for elevations included between 20° and 30°. It was not possible to take these readings using the simulator on the boresight tower because the ground effects are not negligible, the elevation at which the horn reflector antenna sees the simulator being 1.35°.

#### Method of Measurement

The satellite is illuminated by an auxiliary station transmitting a pure frequency. The signal is received at Pleumeur-Bodou by the com-

\* Manual offsets of time and position information can be inserted in order to eliminate systematic errors.

† The schematics of the digital drive circuits of the antenna drives of the precision tracker and the communications antenna are shown in Figures 10 and 11.

communications equipment at the frequency of 4170 Mc and the auto-track equipment at 4079.73 Mc.

The frequency band of the communications receiver used for the measurement is a compromise based on the stability of the transmitter, the receiver circuits, and the level at which the pattern must be traced.

Tracking of the satellite is performed by tape, the relative deviation between the position of the satellite and the direction of the antenna being obtained by the insertion of position corrections into the antenna drive chain. The tape chosen is checked in advance to make sure that it is satisfactory; if not, fixed position and time corrections are made to make the computed trajectory and the actual trajectory coincide.

This test is a dynamic one, with the receiver level to be measured recorded continuously and position corrections applied to the constant speed of 65.76 deg/min. The receiver levels in both the VAT channels and the communication channel are determined from the previously calibrated AGC level; the zero of the VAT error corresponding to the pointing direction in automatic tracking is obtained by recording "errors" in the azimuth and elevation channels.

Relative variations in range on the order of 1 percent per minute are disregarded during the test.

The transmitter power of the satellite is assumed constant over the duration of any pointing error.

After each pattern trace the zero level at the pattern maximum is taken again.

The accuracy of the measurement, dependent both on the calibration accuracy of the recording and on the accuracy of reading the recording, is on the order of  $\pm 0.25$  db.

### Results

Figures 5 and 6 are pattern traces obtained on the communication channel. Pointing errors from  $-10^\circ$  to  $+10^\circ$  were measured; only those angles for which the received level is detectable are plotted. Various series of tests resulted in half-power widths.

#### 1. Variable elevation minus zero azimuth error.

Allowing for the accuracy of  $\pm 0.25$  db, we obtain for 3 db beam-width for 3 different pointing errors:

$$0.208 < 3 \text{ db } W^\circ < 0.225$$

$$0.208 < 3 \text{ db } W^\circ < 0.23$$

$$0.205 < 3 \text{ db } W^\circ < 0.225$$

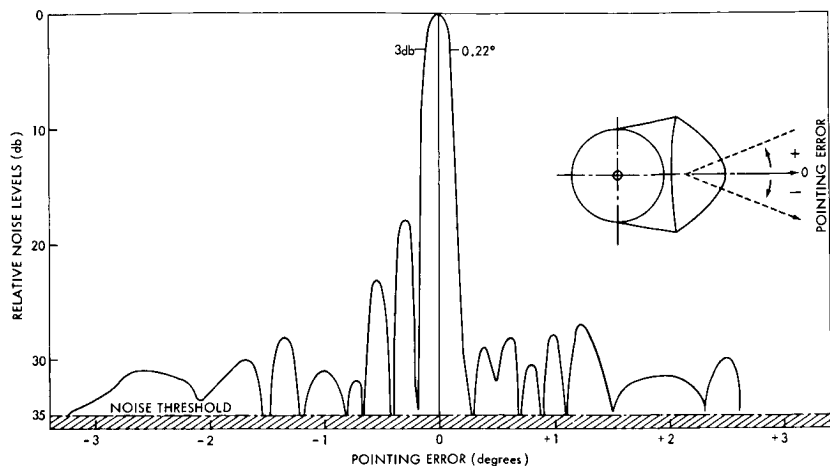


Fig. 5 — Communications antenna pattern, elevation plot.

Taking the mean value,

$$3 \text{ db beamwidth} = 0.215^\circ$$

2. Variable azimuth. Zero elevation error.

As above, for 3 different pointing errors we obtain:

$$0.235 < 3 \text{ db } W^\circ < 0.25$$

$$0.235 < 3 \text{ db } W^\circ < 0.25$$

$$0.241 < 3 \text{ db } W^\circ < 0.26$$

Hence the mean value

$$3 \text{ db beamwidth} = 0.245^\circ$$

Comparison of the null command of the VAT to the maximum radiation shows that within the accuracy of measurement these two points coincide.

In Fig. 7 are shown traces of the patterns seen by the X and Y channels of the VAT. Because of the sensitivity of the equipment, the measurement could only be made up to 15 db.

The patterns traced for the 4080 Mc frequency are perceptibly different from the patterns traced at 4170 Mc. This difference corresponds to a slight misadjustment of the hyperfrequency circuits resulting in insufficient decoupling of the TM 01 and TE 11 channels. The low

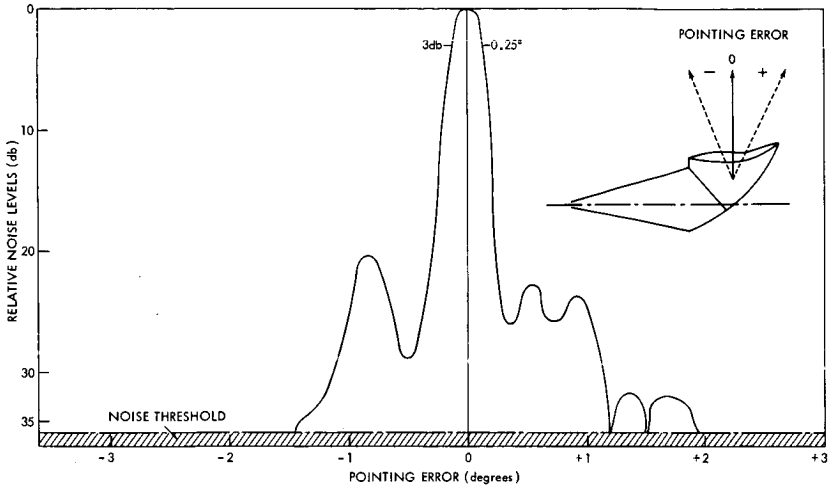


Fig. 6 — Communications antenna pattern, azimuth plot.

amplitude of this perturbation does not affect in any way the overall operation of the system.

#### *Study of Azimuth-Elevation Coupling*

After the first month of operation of the station with Telstar I, it became evident that there was a systematic error in azimuth whenever the elevation of the satellite was above the horizon. A control check performed by calibration on stars showed an error of about  $0.20^\circ$  for an elevation of  $62^\circ$ . A series of measurements was therefore undertaken to establish the curve of azimuth-elevation coupling, so that a distortion correction could be applied to the communications antenna drive tapes.

The method used consisted in tracking the satellite separately with the precision tracker and with the large antenna positioned by the vernier autotrack. The positions were recorded on magnetic tape during the entire pass and subsequently compared. The information obtained, together with the star calibration and the precomputed theoretical trajectories of the satellite, enabled us to establish a curve providing the azimuth errors as a function of elevation. The tests performed for different azimuths showed that this law of variation remains valid for any azimuth.

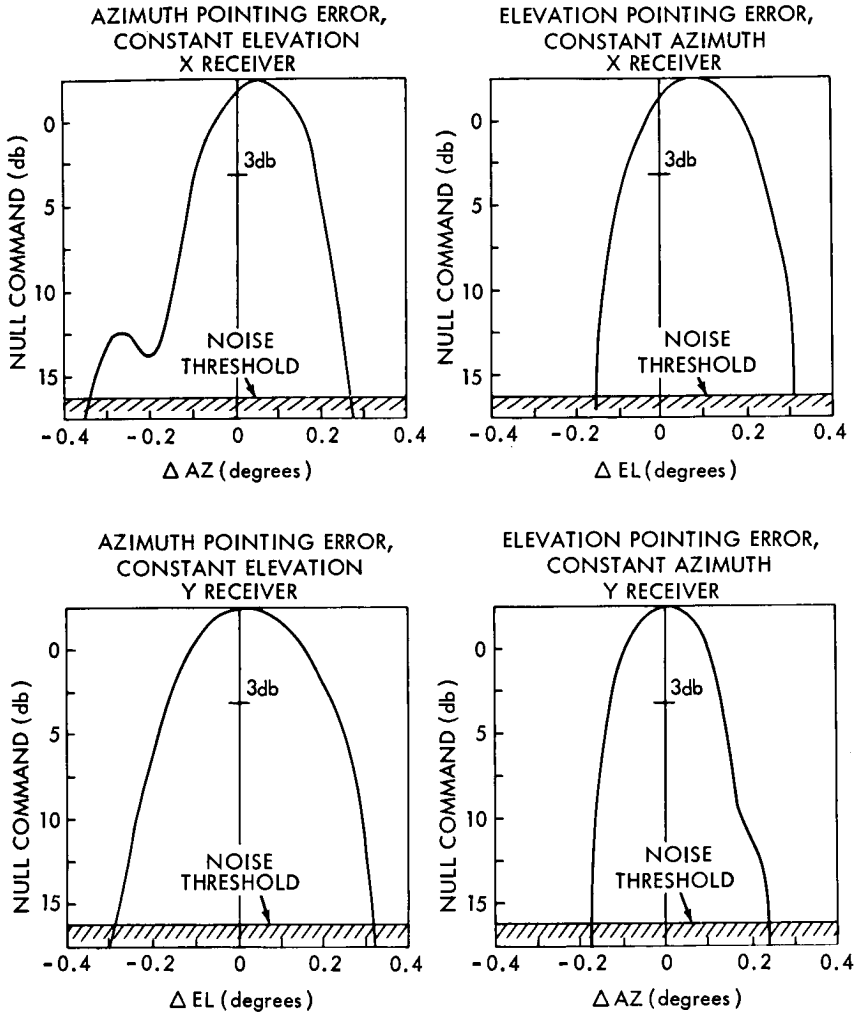


Fig. 7 — Vernier autotrack receiver levels.

### Results

A first series of tests performed up to 15 December 1962 enabled us to determine the relation (Fig. 8):

$$\tan Az = \frac{1}{570} \tan El$$

which is equivalent to the variation contributed by the antenna pat-

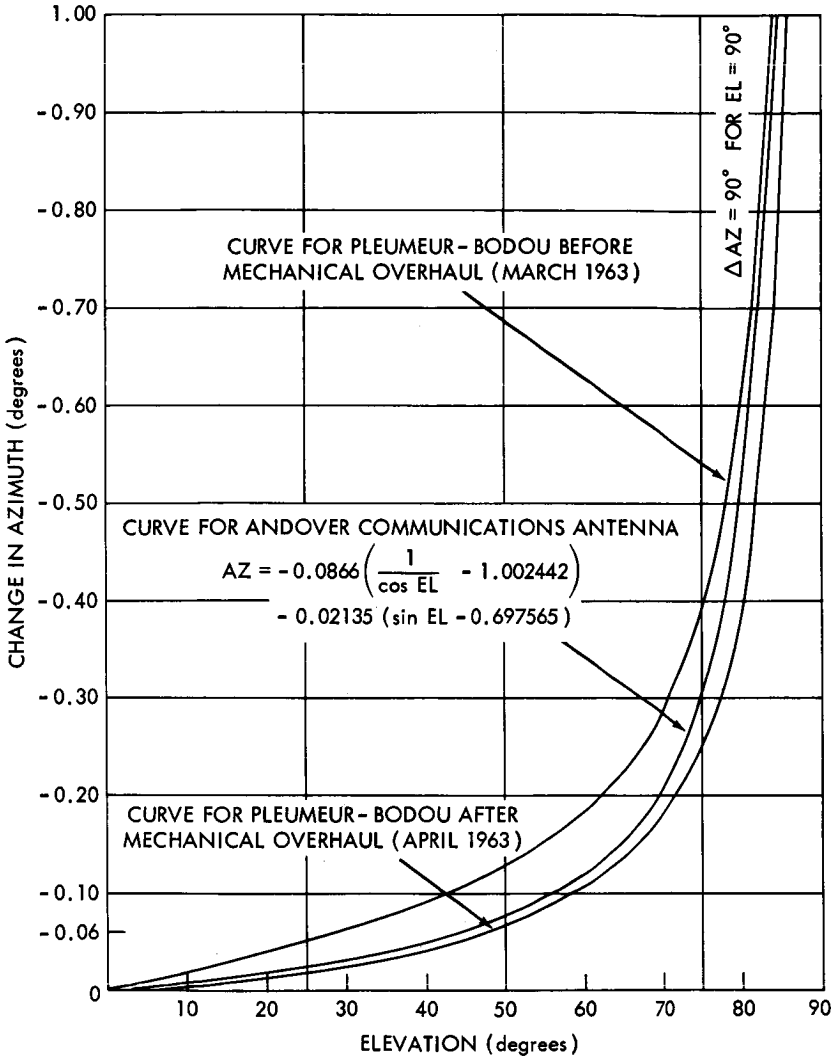


Fig. 8—Communications antenna, azimuth error versus elevation.

tern in a plane which is not perpendicular to the axis of rotation in elevation, but in a plane shifted from that plane by  $0.1^\circ$ . A check of the antenna structure failed to show any systematic error of that order of magnitude, but enabled us to see that a very large percentage of the structure bolts were loose, leading to an excessive deformation as a function of variations in elevation.

A general overhaul of the structure was carried out in April, 1963.

With Telstar II, a new series of tests was undertaken, resulting in a new law of variation. A mathematical analysis of this curve, made so that it could be applied to the antenna drive tapes, led to:

$$Az = -0.06 \left( \frac{1}{\cos El} - 1 \right) - 0.05 \sin El$$

This law is to be compared to that which was provided us by BTL and which was applied to the Andover antenna (Tracking Program Document, 15 October 1962: Program Description):

$$Az = 0.0866 \left( \frac{1}{\cos El} - 1.002442 \right) - 0.02135 (\sin El - 0.697565)$$

#### Direct Slaving to the Precision Tracker

It thus appeared that because of this coupling there would be some difficulty in slaving the communications antenna directly to the precision tracker. The positions displayed by the encoders of the two antennas did not have the same value during satellite tracking. A computer unit was therefore designed and built to permit application of this correction between the encoders of the precision tracker and the antenna drive. The purpose of the unit, which is mounted in available space in the tracking encoder unit, is to effect an automatic correction by means of a wired program which determines the value to be added to the azimuth information:

$$Az = -a \left( \frac{1}{\cos El} - 1 \right) - b \sin El$$

$$\text{with } a = 0.06 \text{ and } b = 0.05$$

which corresponds to the measurements made and holds for elevations up to  $85^\circ$ .

The computer, of the series type, computes the successive powers of the elevation expressed in radians to the seventh term, performs the modifications of these terms as a function of the coefficients  $a$  and  $b$ , and then adds the partial results, in such a way that a cycle of operation is completed in  $1/64$  second.

The polynomial retained is of the form

$$Az = \frac{5}{3} bx + \frac{b}{6} x^3 - \frac{b}{120} x^5 - \frac{45a}{720} x^6 + \frac{bx^7}{7040}$$

The deviations between this function and the theoretical function are always less than the noise in the data provided by the precision tracker.

### *Study of Refraction*

Since the satellite is commanded from the Andover station, the relative positions of the Pleumeur-Bodou and Andover stations result, for the trajectory of Telstar I, in the fact that the TWT of the satellite is very often in operation when the satellite rises above the theoretical horizon at Pleumeur-Bodou. The favored location of this station, for which the theoretical horizon is in many directions the same as the actual horizon because of the proximity of the sea, led to the performance of tests of the refraction of electromagnetic waves at low elevations. These measurements were made for frequencies in the vicinity of 4000 Mc.

Many passes were used for the performance of these tests. It should be noted that no appreciable variation in the results was noted as a function of the seasons: this stability must be considered as resulting from the proximity of the sea above which the satellite rises, and from the fairly constant climatic conditions of the region.

Two methods were used:

1. For elevations above  $1^\circ$ , we used magnetic recordings of the antenna position in automatic tracking of the satellite. This operation requires all the attention and the skill of the operators because of the fluctuations in received signal levels at elevations up to  $3^\circ$ . The data obtained, corresponding to apparent elevations, is later compared with the geometrical elevations of the theoretical trajectory, reconstructed from trajectory data taken during the entire pass.
2. For elevations below  $1^\circ$ , the antenna is prepositioned in elevation at the value chosen for performance of the measurement, the azimuth drive being made by tape. For this condition, the desired pass is one for which the azimuth varies only slightly with respect to time, in order to eliminate any time error in pointing. When the satellite rises, the time of passage through the antenna lobe permits determination of the geometric elevation corresponding to this apparent elevation.

The two methods enabled us to plot, point by point, the curve for refraction correction as a function of geometric elevation (Fig. 9).

This law of variation enabled us, after it was applied to the program for preparation of magnetic antenna drive tapes, to acquire the satellite at apparent elevations of  $0.2^\circ$ , corresponding to a geometric elevation of  $-0.6^\circ$ . We did not consider in this acquisition the quality of the communication link, which is subject to large fluctuations in level.

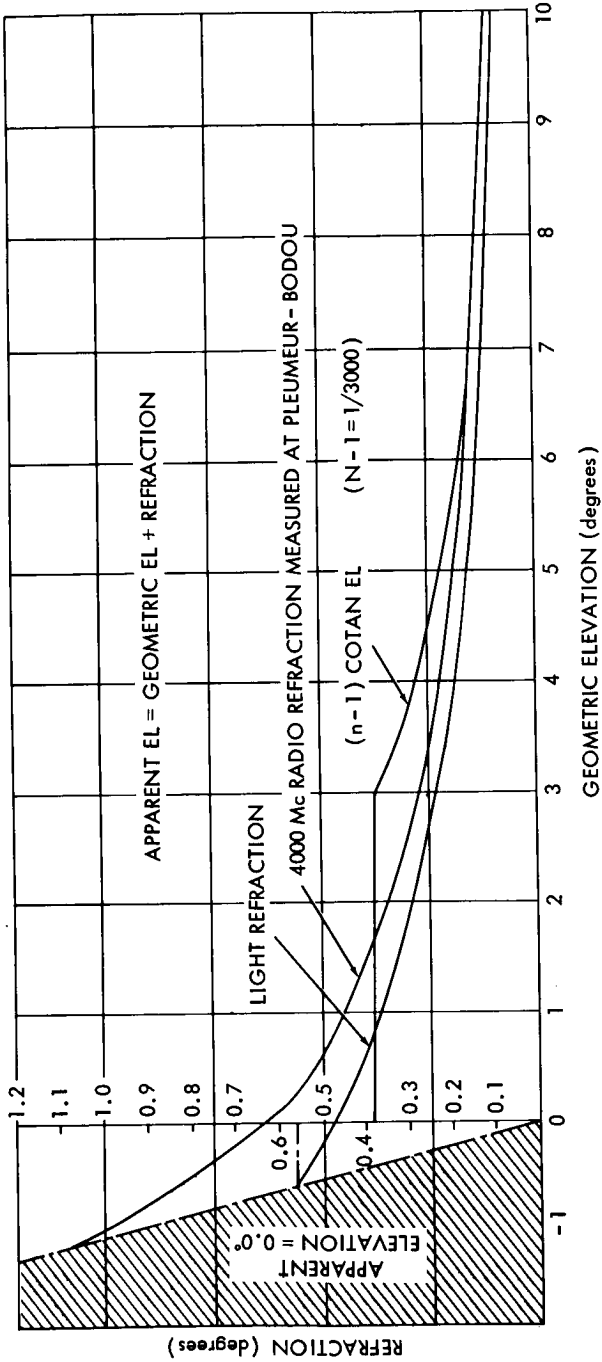


Fig. 9 — Tropospheric refraction.

We plotted on the same figure the following curves:

1. Light refraction law.
2. Law of  $(n-1) \cot E_l$ , with  $(n-1) = 3.3 \times 10^{-4}$ .
3. Law derived at Pleumeur-Bodou for 4000 Mc.

Analysis of the results shows the following:

1. The refraction measured at 4000 Mc, which is slightly greater than light refraction to  $3^\circ$ , is clearly greater for smaller angles, with a limiting value of  $1.05^\circ$  for  $0.55^\circ$ .
2. The measured refraction law coincides with the  $(n-1) \cot E_l$  law with  $(n-1) = \frac{1}{3000}$  for angles above  $7^\circ$ .
3. The use of the  $(n-1) \cot E_l$  law limited to the value of  $E_l = 3^\circ$  corresponds, for the rise of the satellite, to an error of  $0.6^\circ$  and delays acquisition with the tapes which have been computed with allowance for this information.

### *Acquisition and Tracking Modes*

We have summarized here the experience we acquired during 115 passes of Telstar. This experience has enabled us to define general line of operation with respect to the various circumstances which may arise.

#### Acquisition

During the period of waiting for the satellite to rise, or for turn-on of the beacon in the event it is not illuminated at the time the satellite appears, the antenna is nominally driven by the magnetic tape computed from the osculating orbital parameters furnished by BTL. During the 115 passes of Telstar I, the reduction of the output data from the precision tracker and from the communications antenna monitor led to a determination that there was a time error on the precomputed tapes of an average value of 5 sec, with the extreme not exceeding 12 sec. The position errors are negligible after application of the time corrections to the antenna drive chain (Figure 10).

It should be noted that the information provided for Telstar II led to errors which were appreciably greater in time and in position. The use of the uncorrected tape often corresponds to deviations greater than one degree.

The mean orbital parameters determined by NASA do not enable us, with the computer programs in our possession, to drive the antenna in a usable manner, since the results of the computations are too far

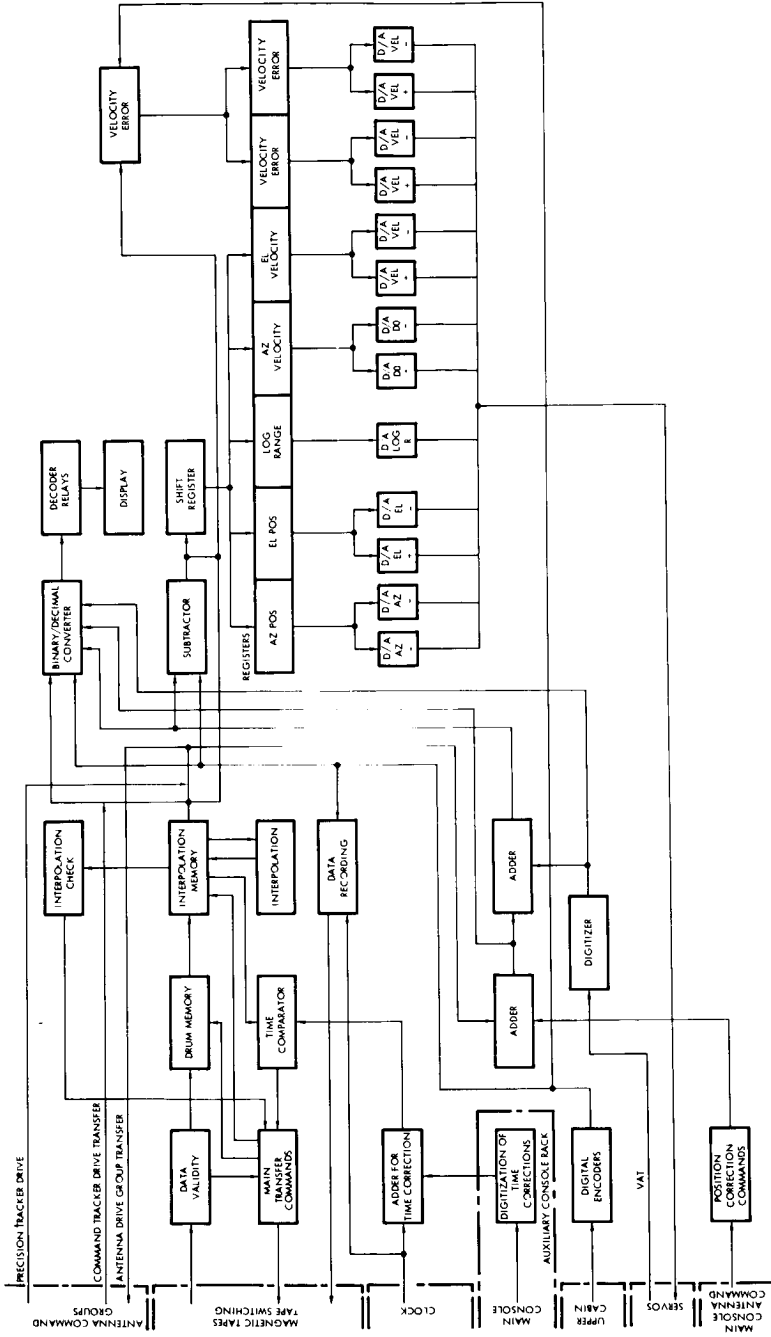


Fig. 10 — Block diagram of the antenna drive.

from the actual positions. On the other hand, the topocentric coordinates received from this agency are particularly satisfactory, giving a position error less than 0.05 during the entire pass.

The criterion of acquisition is the locking on in phase of the VCO of the VAT receiver, assuming of course satisfactory operation of all the equipment.

Two cases are possible for such acquisition:

1. The precision tracker acquires the satellite first, and goes over to automatic tracking. The acquisition delay for the horn antenna may arise either from the fact of a poor position of the frequency of the phase-lock oscillator of the VAT receiver or from the fact that the data tapes do not correspond to sufficiently accurate pointing of the antenna. In either case, phase lock of the oscillator is not achieved.

The chief of operations can, by checking the AGC level of the communications receiver displayed on the main console, determine which of these two errors is at fault.

As a result:

1. The VAT goes over to being slaved in frequency to the precision tracker.
2. The precision tracker/tape error displayed on the console is reduced to a minimum by insertion of time corrections.

If, after these two operations, the satellite has not been acquired, and if the elevation of the satellite is above  $2^\circ$ , the horn antenna is slaved to the precision tracker. The  $2^\circ$  limit results from the fact that below this value the oscillations of the precision tracker make it impossible to use it for very long to drive the horn reflector antenna.

Under these conditions, acquisition should be achieved very quickly:

1. Acquisition is effected by the VAT or at the same time as the precision tracker. In this case the tracking phase is started immediately.
2. It should be noted that acquisition by spiral scan about the position given by the magnetic tapes has never been utilized. The use of this mode of operation assumes that the precision tracker has not acquired, and requires a simultaneous search in frequency and in position. Considering the rates of the spiral scan and the range of frequencies to be covered, the problem cannot practically be solved.

### Tracking

As soon as the beacon has been acquired in frequency the method generally used is the tracking mode called VAT 3. In this mode of operation the antenna is directly slaved to the satellite without use of the tapes. It is thus possible to compare the pointing information given by the satellite to the information provided by the tapes and to apply time and position corrections to make the two identical. Once this is done, it is possible to maintain this tracking mode or to utilize the VAT 1 mode, which makes use of both the data tapes and the pointing errors furnished by the VAT. This mode has the advantage of greater reliability, since a break in the signal receiver by the VAT receiver does not interrupt tracking: the antenna continues to be driven by the updated tapes.

In practice, these two modes (VAT 1 and VAT 3) were used during the tests with Telstar I with no loss of the satellite directly attributable to either.

Tracking by direct slaving to the precision tracker was used for test purposes. This method gave very good results after installation of the computer for antenna distortion. The oscillations caused by the tracking noise of the precision tracker (see Fig. 4) do not lead to any fluctuation in the communications channels, since the angular deviations are comparable to the  $0.23^\circ$  width of the lobe at 3 db.

This tracking mode may be used if required in the event that the magnetic tapes have not been prepared and that acquisition has nonetheless been effected by the precision tracker. In order to facilitate these tests, the circuits of the antenna drive group (Fig. 10) were modified to permit insertion of position corrections between the precision tracker encoders (Fig. 11) and the horn antenna.

The tests taken as a whole prove that acquisition of the satellite is virtually certain and that subsequent tracking is accurate enough that communication links can be established and tests performed without any degradation due to pointing errors.

Trained operators who are thoroughly familiar with the equipment can, making use of various circuits for pointing the antenna in the direction of the satellite, handle any minor incidents which may occur during a pass without interrupting the link.

### TRANSMISSION TESTS

Transmission tests with the Telstar I satellite were performed at the Pleumeur-Bodou station during 113 passes with mutual visibility for Andover and Pleumeur-Bodou. These passes are spread over the

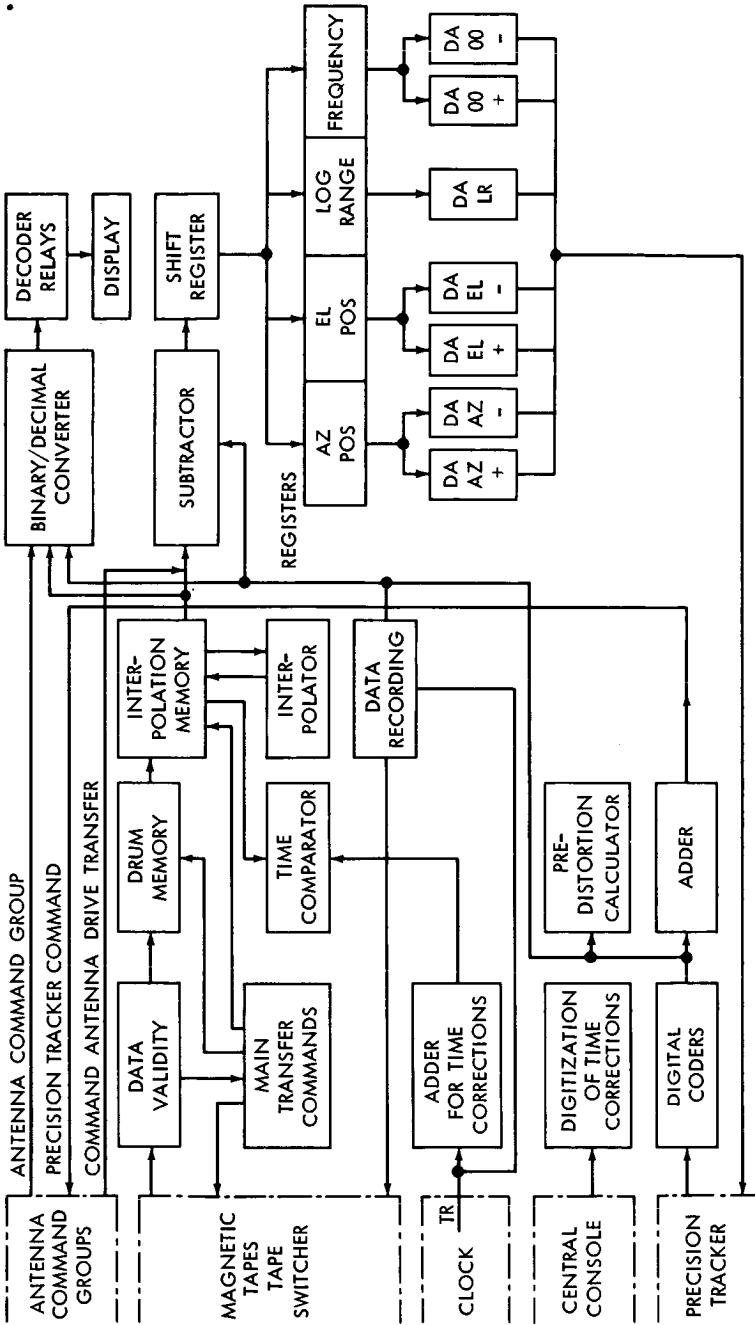


Fig. 11 — Block diagram of the tracking encoder.

periods 10 July to 2 November 1962 and 3 January to 21 February 1963. Technical tests were performed during 69 of these passes. For most of these tests the satellite was utilized in loop, with the station receiving back the signal it had transmitted. The conditions are in almost all the cases identical to those existing for a station-to-station link, and the tests are easier to perform. A few tests were, however, carried out in collaboration with the Andover station. System or demonstration tests were carried out in addition during 59 passes.\*

The technical tests were concerned with measurements of the received carrier power and of the receiving equipment; these parameters define the capability of the station for receiving the transmitted information. Our studies also dealt with the noise in the transmission channel and the distortions of the transmitted signal. Studies were made of some effects which are peculiar to satellite communications and do not exist in other modes of transmission presently in use. We also describe a few of the most interesting of the system tests.

#### RECEIVED CARRIER POWER

We measured the power of the received carrier during each of the passes utilized, recording the variations in the AGC current of the receiver. This current is calibrated before and after each pass by sending into the receiver input a signal of known power provided by a hyperfrequency generator. These measurements can be compared to the value calculated on the basis of the distance of the satellite from the station. For these calculations we used the following mean values:

Power level of the signal transmitted by the satellite:

33.5 dbm for a one-way link.

30.5 dbm for a two-way link, assuming that the two carriers radiated by the satellite are equal.

Satellite antenna gain: 0 db.

Station antenna gain at 4170 Mc: 58 db.

Receiving system losses: 0.4 db.

We examined the mean value and the fluctuations of the received carrier power.

#### *Mean Value of Received Carrier Power*

Figure 12 shows an example of the mean value of the received carrier power as a function of the range of the satellite for a one-way link

\* Some technical tests were performed at the same time as system or demonstration tests in the different telephone channels of the multiplex system.

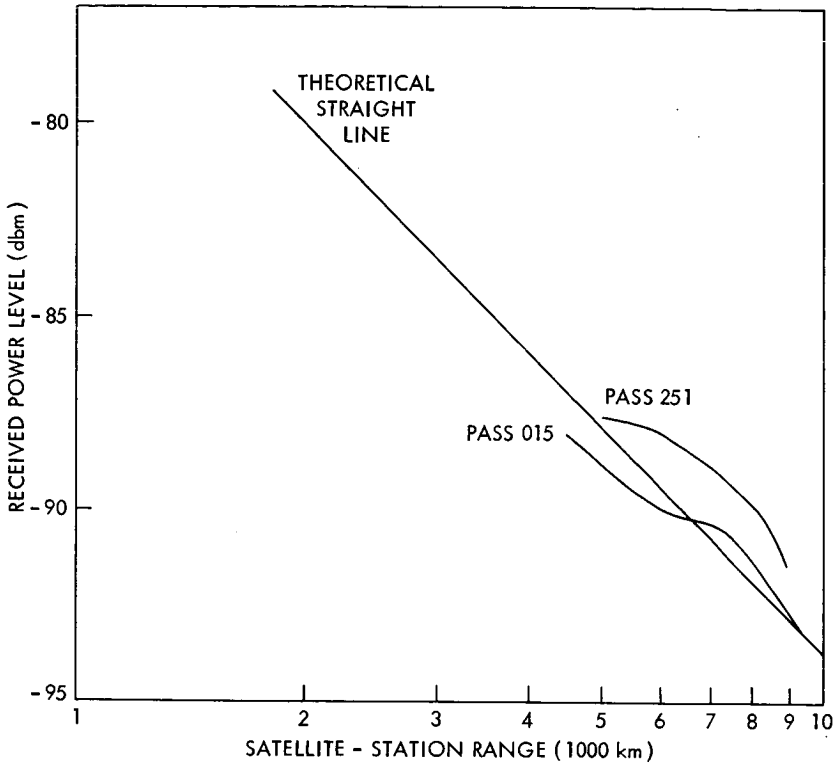


Fig. 12 — Received power at receiver input (1-way link).

for two different passes. Noting that the calculation does not take into account the satellite transmitting antenna gain, which varies with the look angle from the station, we see good agreement between the theoretical and experimental results. In Fig. 13, the same quantities are plotted for two two-way passes. For pass 1974, good agreement is seen between the theoretical and experimental values; on this pass special precautions were taken to see that the satellite received the same power from each station. On pass 33, on the other hand, where no such precautions were taken, a large difference can be seen. If the two carriers received by the satellite are at different levels, the two signals which it transmits are at different levels. This phenomenon was studied during tests performed in collaboration with the Andover station.

The radiated powers of the two stations were altered with programmed variations corresponding to the range of the satellite for each station. After it was determined that the powers of the two

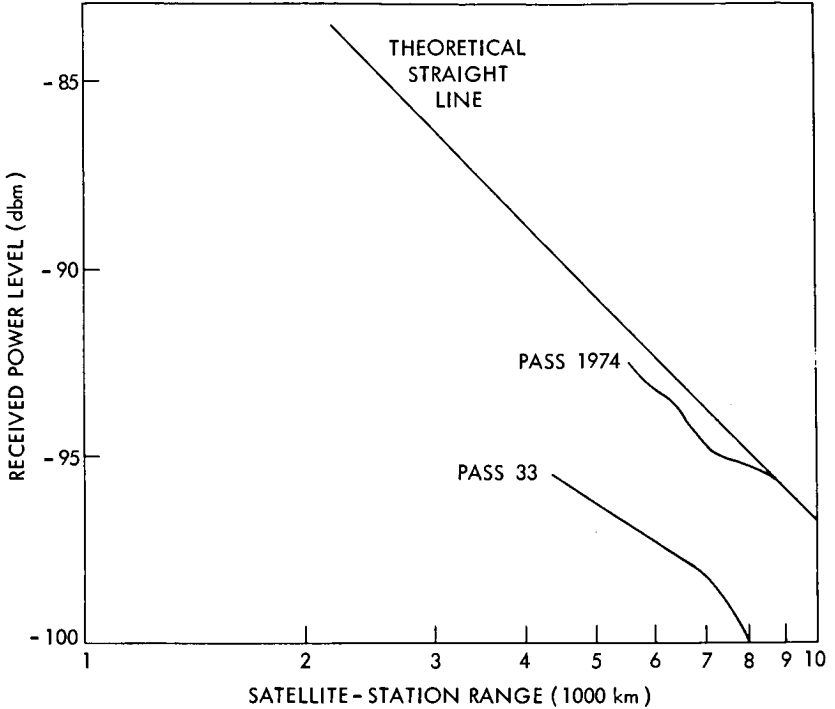


Fig. 13 — Received power at receiver input (2-way link).

carriers received by the satellite were equal, the Andover station made its radiated power vary by a known quantity from the programmed value. The variations in received power at Pleumeur-Bodou are given in Fig. 14. It can be seen that the power radiated by the satellite at the frequency of the carrier received at Pleumeur-Bodou is divided in the same ratio as the power of the corresponding carrier which it receives. The power radiated by the satellite on the other carrier, however, varies simultaneously in the inverse direction although the corresponding power it is receiving remains constant. Consequently, the ratio of radiated carrier powers at the satellite is greater than the ratio of the carrier powers it receives.

#### *Fluctuations of Received Carrier Power*

##### Fluctuations Due to the Receiving System

Figure 15 shows reproductions of received carrier power recordings made for a one-way link at low elevation angles, and Fig. 16, the same

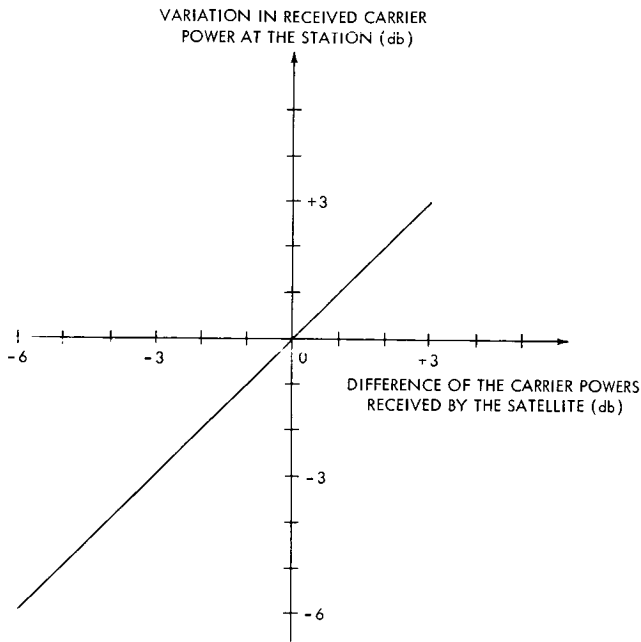


Fig. 14— Variations in the power of a carrier radiated by the satellite (2-way link).

data for high elevation angles. The value given for elevation is the geometrical elevation of the satellite. The value of received power based on satellite orbital data is shown in a dashed line. The tracking mode used was VAT 1, which makes use simultaneously of the calculated data and corrections furnished by the VAT. It can be seen that the fluctuations were of large amplitude for elevations below  $3^\circ$ , but that above this value they do not exceed  $\pm 2$  db and remain below 0.5 db above  $10^\circ$ . We saw in the first part that the pointing accuracy of the antenna is adequate even at low elevations (errors less than 2-3 tenths of a degree) to preclude a reduction in the received power. We feel that the fluctuations of received power at low elevations are due to multipath propagations and to reflection of the waves from the ground at points near the antenna where the pattern lobes are not yet closed. At elevations greater than a few degrees the only variations are those of the radiated power at the satellite, resulting from the irregularities in the satellite transmitting antenna pattern as it rotates on its axis. In any case, the tracking of the satellite, with regard to

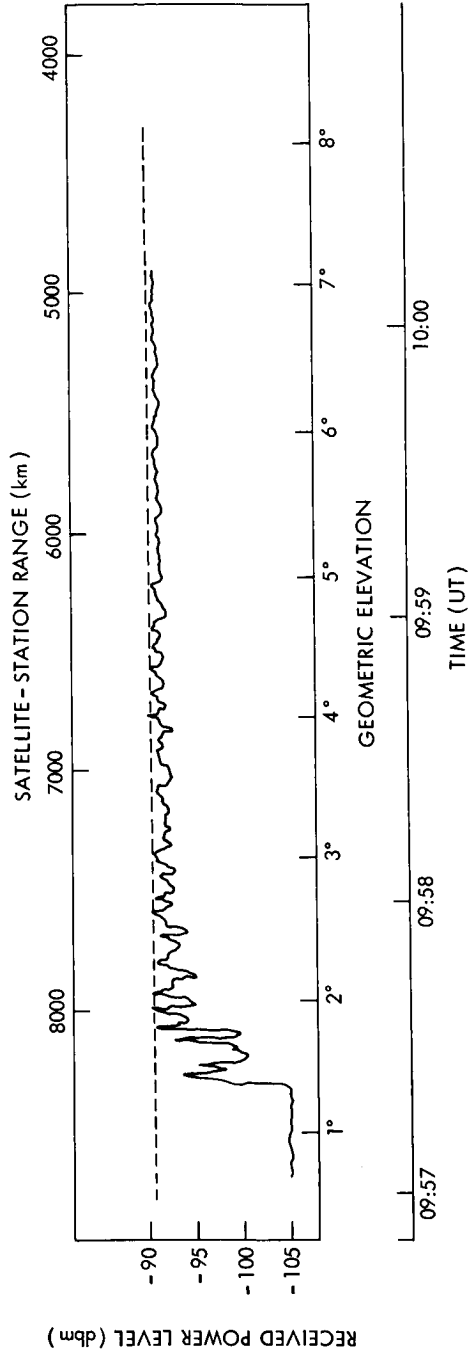


Fig. 15 — Received power at receiver input for low elevations (Pass 996).

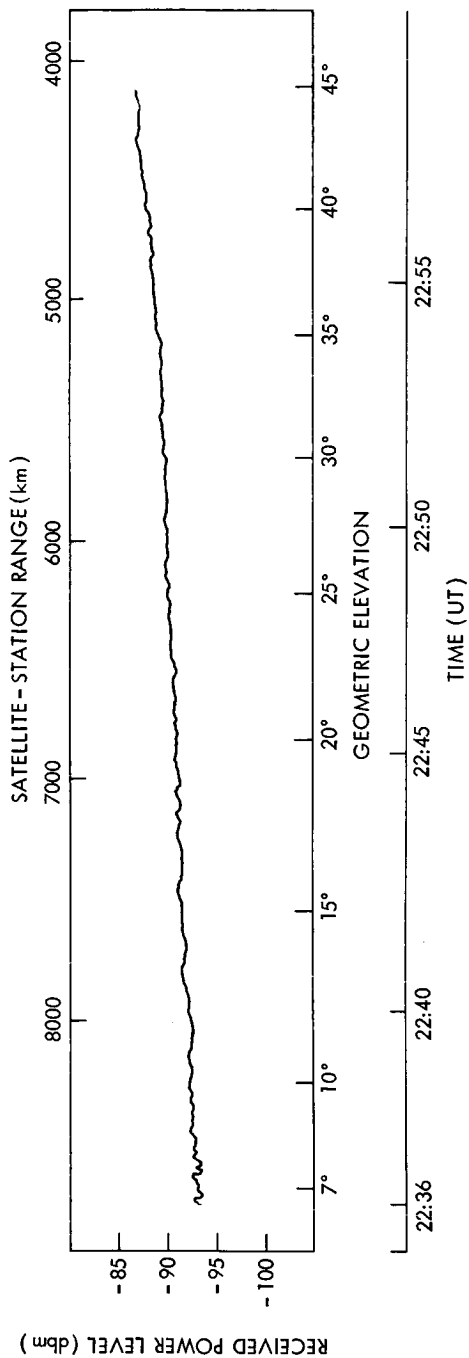


Fig. 16 — Received power at receiver input for high elevations (Pass 252).

the power of the received carrier and thus to the signal-to-noise ratio of the transmitted information, is quite satisfactory when the elevation of the satellite is above  $3^\circ$ .

#### *Fluctuations Due to the Rotation of the Satellite About Its Axis*

Since the radiation pattern of the transmitting antenna is not strictly constant as the satellite rotates on its axis, fluctuations of the received power are observed at the rotation rate of the satellite. For the one-way link the amplitude of the observed fluctuations is for most passes below  $\pm 0.5$  db. For the two-way link this amplitude increases with the difference of the power of the two carriers received by the satellite (Fig. 17).

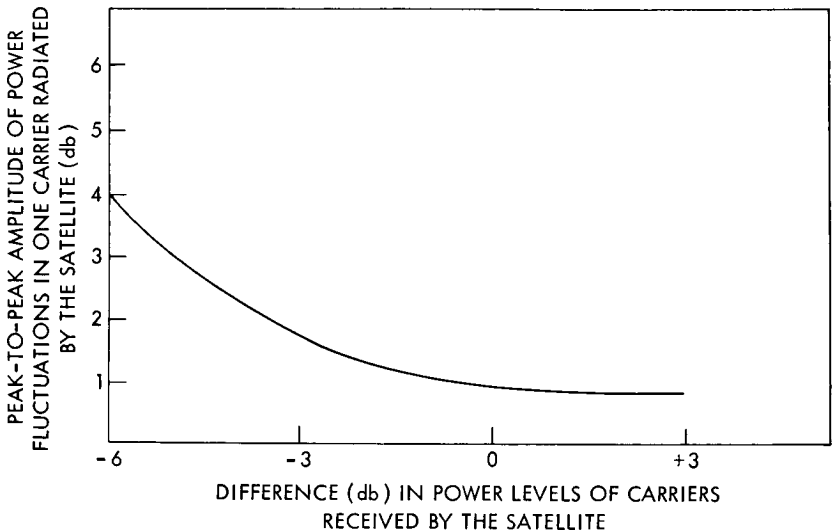


Fig. 17 — Fluctuations in received power due to illumination of the satellite (2-way link).

When the two carriers have quite different powers there are large fluctuations of the weaker carrier. It is noted that the amplitude of these fluctuations varies slightly from one pass to another because of the variation of the angle between the spin axis of the satellite and the satellite station line, with the consequent variation in the radiation from the satellite antenna. These fluctuations are probably due to irregularities in the spacecraft receiving antenna pattern as it rotates

about its axis, together with the tendency of the satellite TWT to provide relatively more power to the signal which has the greater input level.

NOISE TEMPERATURE OF THE RECEIVING SYSTEM

Measurement of the noise temperature of the receiving system is performed after the maser amplifier and the first IF stages, since the noise contributed by the following components can be considered negligible. For this purpose a measurement is made of the difference in noise power level of the receiving equipment alone and the receiving equipment with a known noise power added by coupling at the maser input. The known noise power is provided by a calibrated white noise generator.

*Measurement of Noise Temperature at the Zenith*

Systematic measurements were made of the noise temperature with the antenna pointed at the zenith. A curve (Fig. 18) was plotted of the distribution based on 331 measurements. It is seen that for 50

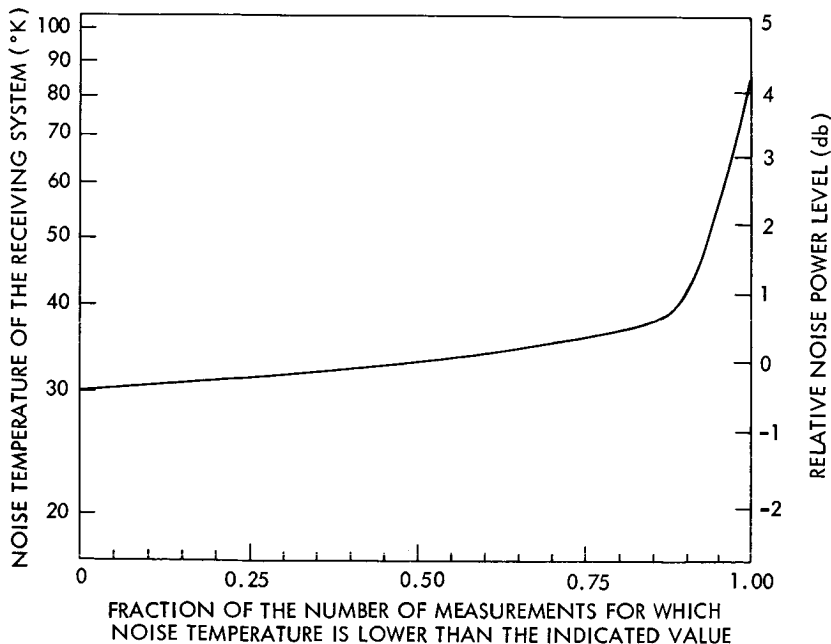


Fig. 18 — Distribution of noise temperature measured at the zenith.

percent of the measurements the noise temperature is equal to or less than  $33^{\circ}\text{K}$ . The lowest value measured was  $27^{\circ}\text{K}$  and the highest,  $92^{\circ}\text{K}$ . For 80 percent of the measurements the noise temperature was in the range of 27 to  $38^{\circ}\text{K}$ , with variation in noise power of the receiving system of less than 1 db. For 99 percent of the measurements the total variation of noise power does not exceed 4 db.

*Measurement of Noise Temperature as a Function of Antenna Elevation*

Figure 19 shows the variation of noise temperature as a function of elevation in dry weather. This curve is the average of a set of measurements for which the maximum deviations are less than  $0.5^{\circ}$ . Under these conditions the noise temperature at the zenith is  $30.5^{\circ}\text{K}$ , is only  $44^{\circ}\text{K}$  for an elevation of  $5^{\circ}$ , and reaches  $55^{\circ}\text{K}$  for an elevation of  $3^{\circ}$ , when the noise power is 2.5 db greater than the noise power at the zenith.

We have also shown on the same figure two examples of variations in noise temperature in the presence of perturbations. These two examples are characteristic of the two typical cases which were observed:

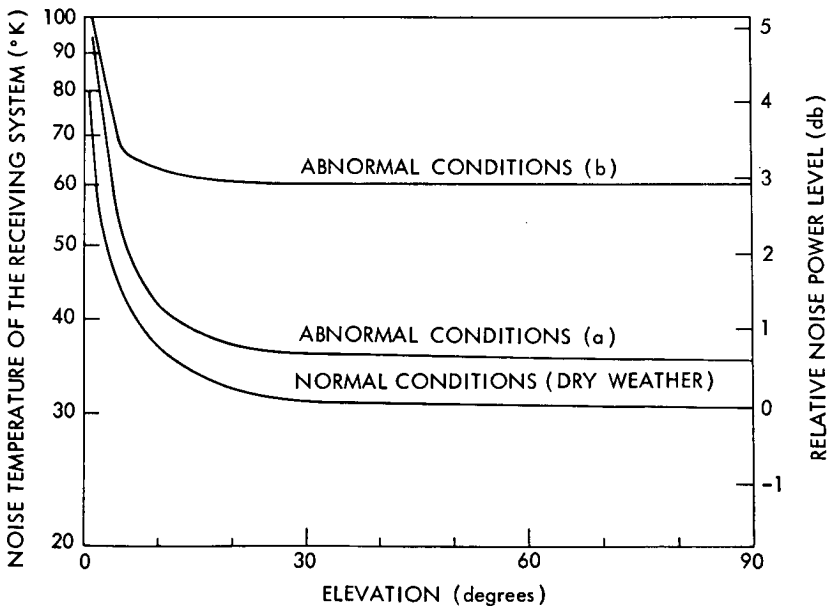


Fig. 19 — Noise temperature as a function of antenna elevation.

1. The increase in noise power level with respect to the dry-weather case is constant as a function of elevation, but small—about 0.5 db.
2. The increase in noise temperature is large, but variable with elevation. A decrease is even observed sometimes when the elevation decreases. For elevations of a few degrees, the increase in noise power level is relatively less than at the zenith (about 1 db).

#### NOISE IN THE TRANSMISSION CHANNEL

One measurement of the quality of the transmission channel is the amount of noise it contains. We measured this noise for each frequency and then studied its effect in the telephone channels and in the audio and video channels of the television signal.

##### *Analysis of Noise in the Transmission Channel*

The analysis of noise as a function of frequency in the transmission channel is performed with a selective analyzer having an equivalent pass band of 4 kc. We determined the curve obtained on the basis of measurements made on the wideband link (Fig. 20) and the curve for the narrowband link (Fig. 21). We plotted on these figures the signal power as a function of frequency, which enabled us to determine the pass band of the receiver. The dashed line is the curve calculated for noise power on the basis of the measured values of noise temperature and received power. The value of the measured noise power is in good agreement with the computed value for intermediate frequencies, but is higher for the lower frequencies because of the fact that the noise in the ground equipment becomes preponderant. It decreases rapidly at high frequencies because of the limiting of the RF band.

##### *Impulsive Noise in the Transmission Channel*

In order to determine the magnitude of impulsive noise which might appear in the link, we performed transmission tests with very short pulses at a rate of 875,000 bits per second, by direct modulation of the carrier. The transmission lasted for 20 minutes, which represents a billion transmitted bits. The quality of the transmission was exceptional, since only a single error was observed. It can therefore be concluded that no discernible impulsive noise appears in the link.

##### *Noise in the Telephone Channels*

###### Noise in the Telephone Channels on One-Way Links

When the link is one way, it is possible to equip some of the 600

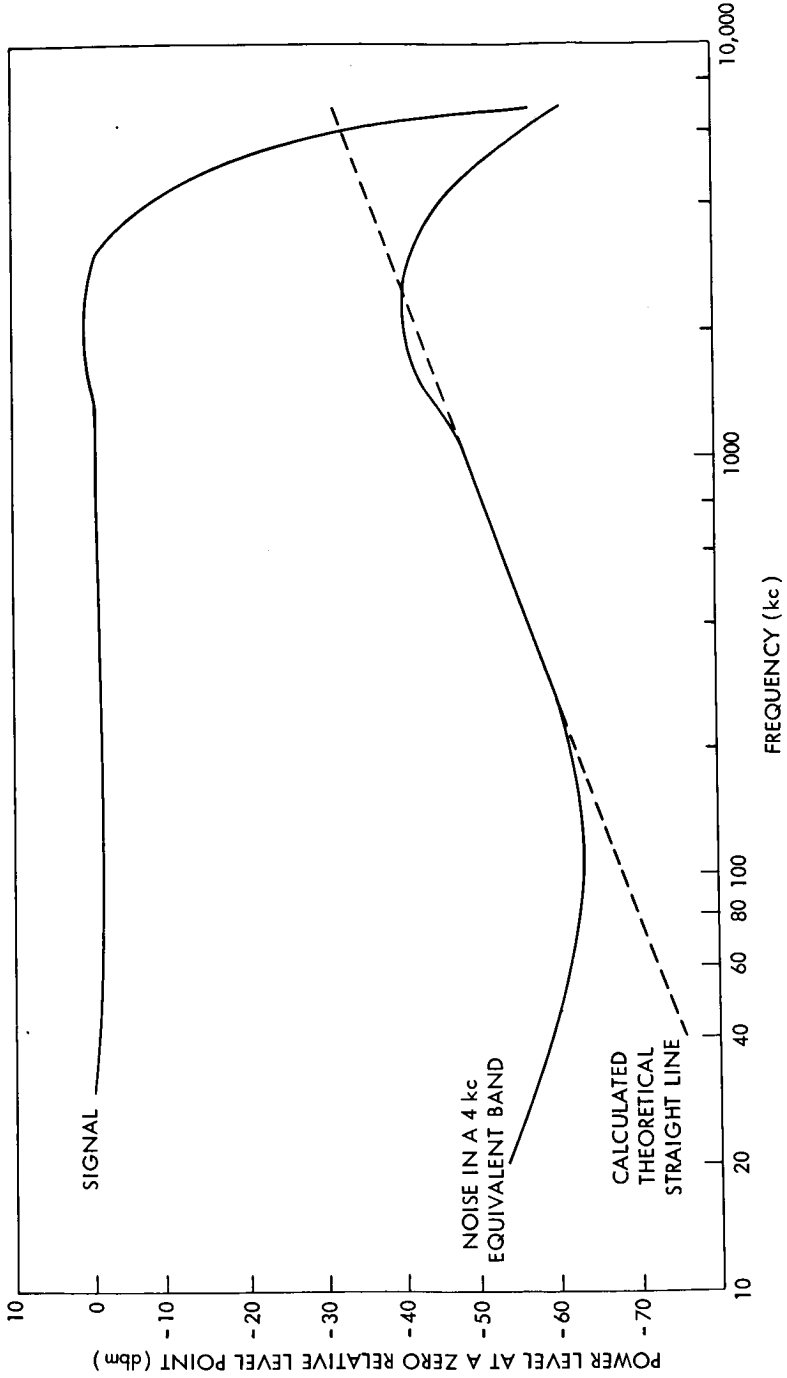


Fig. 20 — Noise analysis for the wideband link (Pass 705).

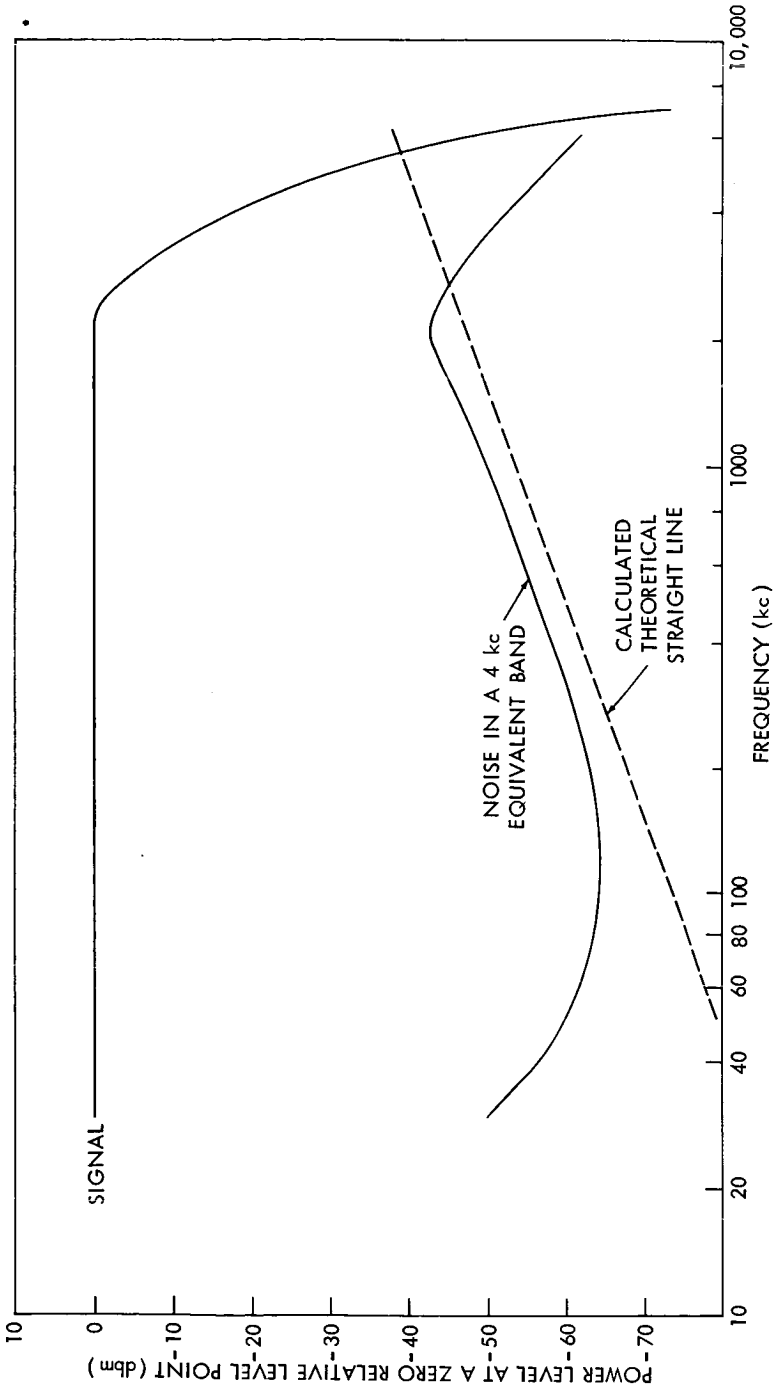


Fig. 21 — Noise analysis for the narrowband link (Pass 832).

telephone channels with a frequency-division multiplex system. After measurement of the equivalent channel a measurement is made of the psophometric noise. Figure 22 shows the results of measurements performed in loop on the satellite without pre-emphasis. The ratio of the signal to the psophometric noise, and the psophometric noise power, are plotted as functions of the frequency of the various channels measured. Corrections were made for the difference between the theoretical and measured equivalents of each channel. There is also shown the theoretical curve based on the received carrier power and the receiving system noise temperature. Very good agreement can be seen with the results of the measurements. For the pass shown here, the conditions were close to the most unfavorable conditions observed, and the noise power in the least favorable channel was on the order of 50,000 pw.

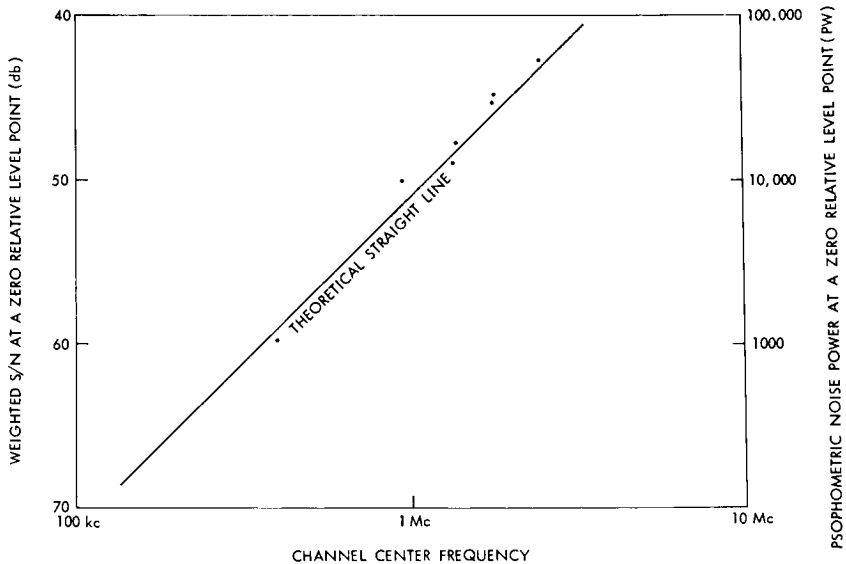


Fig. 22—Psophometric noise power in the telephone channel, one-way link without pre-emphasis.

The rapid variations of noise power in the telephone channels were also measured and recorded. Variations of less than  $\pm 0.25$  db were observed. These variations are essentially due to the rotation of the satellite about its axis and to the irregularities in the pattern of its transmitting antenna.

• Noise in the Telephone Channels on Two-Way Links

Psophometric thermal noise was measured for different carrier power levels received by the satellite on a 12-channel two-way link in the 60-108 kc band in collaboration with the Andover station.

Each station radiated a variable power which was adjusted automatically as a function of the satellite range, so that the satellite would receive the same power on each carrier. After checking the equality of these powers by telemetry, the Andover station varied its radiated power by a known quantity with respect to the programmed value. The Pleumeur-Bodou station continued to transmit in accordance with the planned program. For each value of the difference in received power at the satellite, a measurement was made of the psophometric noise power in channels 1 and 11 of the 12-channel multiplex telephony equipment. The nominal value for effective frequency deviation per channel (110 kc) had been used.

The results of this test are shown in Fig. 23 with respect to the received carrier power at Pleumeur-Bodou or, which amounts to the same thing, as we have already seen, with respect to the difference between the carriers received at the satellite.

It can be seen that the noise power in the telephone channels varies less rapidly than the received carrier power. This arises probably from

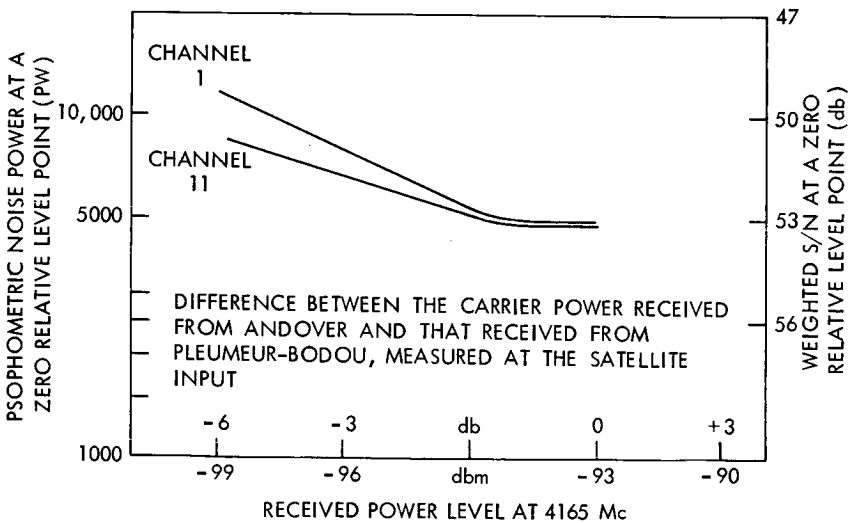


Fig. 23 — Weighted thermal noise for 12 two-way telephone channels (Pass 1014).

the noise generated in the equipment, since the measured noise power is very low. It will be noted that even for large differences of carrier powers received at the satellite, the weighted noise power is less than 10,000 pw.

### *Noise in the Television Channel*

#### Noise in the Video Channel

Measurements were made of the ratio of the peak-to-peak signal to effective noise in television for received carrier powers in the range of  $-85$  to  $-92$  dbm. Noise temperatures in the receiving system were measured over the range  $30^{\circ}\text{K}$  to  $70^{\circ}\text{K}$ . A weighting network conforming to the network recommended by the CCIR for the 405-line standard (maximum transmitted frequency, 3 Mc) was used for certain measurements. The noise is limited between 10 kc and 3 Mc. Under these conditions the ratio of peak-to-peak signal to effective weighted noise always remained within the range 51 to 55 db. Comparison of the measured results with the values calculated theoretically from received power and receiver noise temperature was satisfactory only for the lowest measured values, corresponding to a very low received power. We were able to determine that this is due to noise in the ground equipment, which becomes preponderant when the signal-to-noise ratio reaches 55 db. For the same reason, the improvement effected by the weighting network is only about 10 db rather than the theoretical value of 12.3 db, computed for triangular noise.

The same measurements were made in two-way television, with the received carrier power lower and the frequency deviation reduced by 12 db. The ratio of peak-to-peak signal to effective weighted noise was measured for average conditions at about 41 db. No pre-emphasis was used, and the measured value is in very good agreement with the calculated value. In this case the above-mentioned noise in the ground equipment becomes negligible with respect to the noise contributed by the rest of the link.

#### Noise in the Sound Channel

Measurements were made of the ratio of peak-to-peak signal to effective unweighted noise in the television sound channel on a one-way link. The received carrier power was in the range of  $-85$  to  $-93$  dbm and the noise temperature approximately  $35^{\circ}\text{K}$ . The peak frequency deviation produced by a 1000 cps signal on the sound sub-carrier at 4.5 Mc was 50 kc. A pre-emphasis network of the RC type, favoring the highs and with a time constant equal to  $75\ \mu\text{s}$  was used.

The peak frequency excursion produced by the subcarrier on the carrier was 1.4 Mc. The ratio of peak signal to effective unweighted noise remained in the range 50-56 db. Comparison with the calculated values indicates a slight deterioration of the signal-to-noise ratio, due probably to equipment noise. Nevertheless, the quality of the link is satisfactory.

In addition, no impulsive noise was observed.

The rapid variations of noise level are on the order of  $\pm 0.25$  db. They are due mainly to the rotation of the satellite on its axis and to the irregularities of the pattern of its transmitting antenna.

#### DISTORTION IN THE TRANSMISSION CHANNEL

It is important not to deform the signal in the course of transmission. The most important deformation arises from variations of group propagation time in the RF band by FM signal. In telephony this produces intermodulation between channels; we also studied the deformation of television test signals.

#### *Envelope Delay Distortion vs Intermediate Frequency*

Distortions in frequency modulation are caused in particular by variations in group propagation time in the RF link of the transmission channel. The variations are measured in the following manner: At the input of the modulator a 50 cps sinusoidal signal is applied, causing a frequency deviation of  $\pm 7$  Mc about the center frequency. On this signal is superimposed a 200 Kc sinusoidal wave which causes a low-amplitude (about 100 kc) frequency excursion. In the receiver the 50-cps signal is filtered out and the 200-kc signal is sent to a phase discriminator. This unit gives for each instant, and thus for a given value of the mean frequency, a voltage proportional to the deviation between its phase at that instant and the mean phase of the received signal. This error voltage is applied to the vertical deviation plates of an oscilloscope for which the horizontal sweep is synchronized to the 50-cps signal. The curve obtained on the screen thus represents the variation of group propagation time as a function of the intermediate frequency. Figure 24 reproduces the results obtained by loop tests with the satellite and the satellite simulator.

No appreciable difference can be observed between the results obtained with the simulator and with the satellite itself. The distortion is mostly parabolic. For a frequency deviation of  $\pm 7$  Mc the measured value is about 25 ns. No delay equalizer was inserted in this measurement.

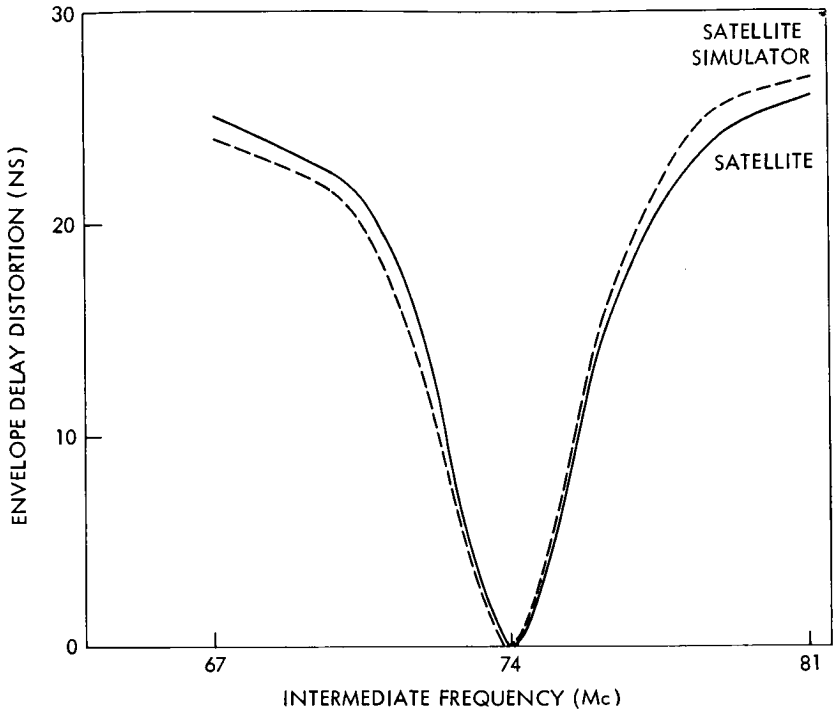


Fig. 24 — Envelope delay distortion as a function of intermediate frequency.

### *Intermodulation Noise in One-Way Telephony*

#### DISTORTION IN THE TRANSMISSION CHANNEL

Intermodulation noise in one-way telephony was measured in loop on the satellite for a system of 600 telephone channels. Measurements were made for different effective frequency deviation per channel with or without the pre-emphasis network defined by the CCIR in recommendation No. 275. On Fig. 25 are plotted the values taken by the signal-to-unweighted-noise ratio in the channels centered on 70, 1248, and 2438 kc as a function of the effective frequency deviations per channel. The link was loaded by the uniform spectrum signal defined by CCIR recommendation No. 275 for 600 channels. The curves in dotted lines represent the values taken by the signal-to-unweighted-noise ratio with no modulation (thermal noise only). The solid lines represent the values taken by the signal-to-unweighted-noise ratio with modulation (thermal noise plus intermodulation noise). It can be seen that the effect of pre-emphasis is quite satisfactory and that

it would be possible to increase by about 4 db the effective frequency excursion per channel, initially chosen at 512 kc, or to about 800 kc. The ratio of signal to unweighted noise would then be in all channels equal to or greater than 44 db for average conditions of received carrier power and noise temperature of the receiving system. This corresponds to a weighted noise power at a zero relative level point in the worst channel on the order of 15,000 pw.

*Intermodulation Noise in Two-Way Telephony*

Far-end and Near-end Crosstalk

In cooperation with the Andover station, measurements were made of far-end and near-end crosstalk for a multiplex system of 60 tele-

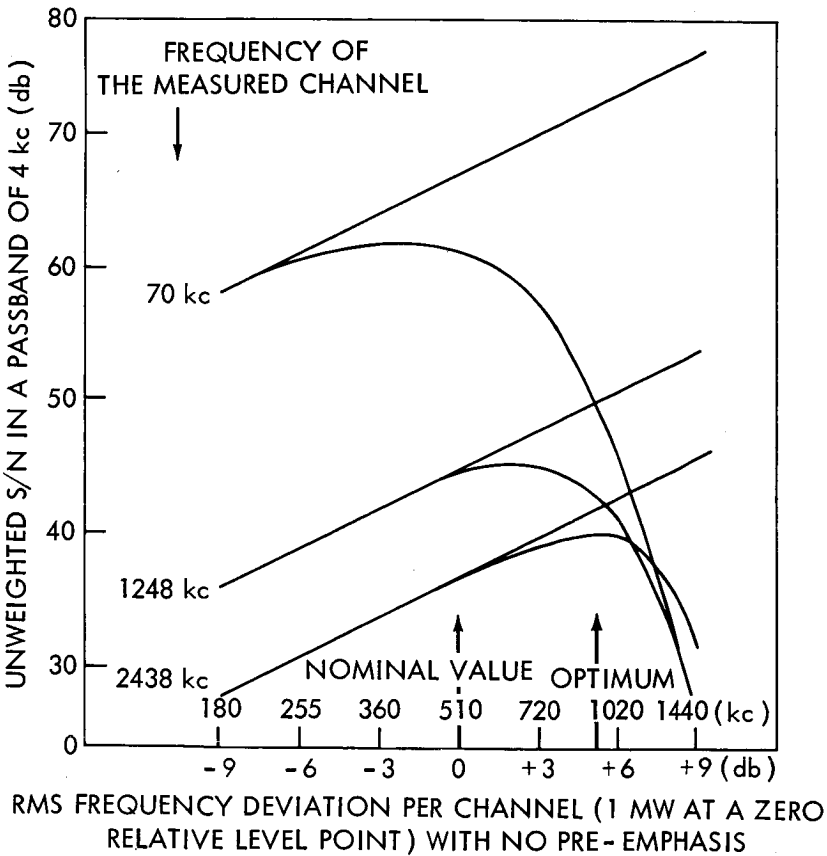


Fig. 25 — Intermodulation noise for 600 one-way channels.

phone channels in two-way link. The RF band was limited by a filter of 6 Mc bandwidth at mid power. No pre-emphasis was used.

For far-end crosstalk, the results are shown graphically as a function of effective frequency excursion per channel (Fig. 26). The curves in dotted lines represent the values taken by the signal-to-unweighted-noise ratio in the channels centered on 70 and 270 kc with no modulation (thermal noise only). The solid-line curves represent the values taken by the signal-to-unweighted-noise ratio when the link is loaded by the continuous uniform spectrum signal defined in CCIC recommendation No. 294 for 60 channels (thermal noise and intermodulation noise). It can be deduced from these measurements that the optimum effective frequency deviation per channel is 180 kc, slightly less than the 200 kc initially chosen, and that beyond this value the intermodu-

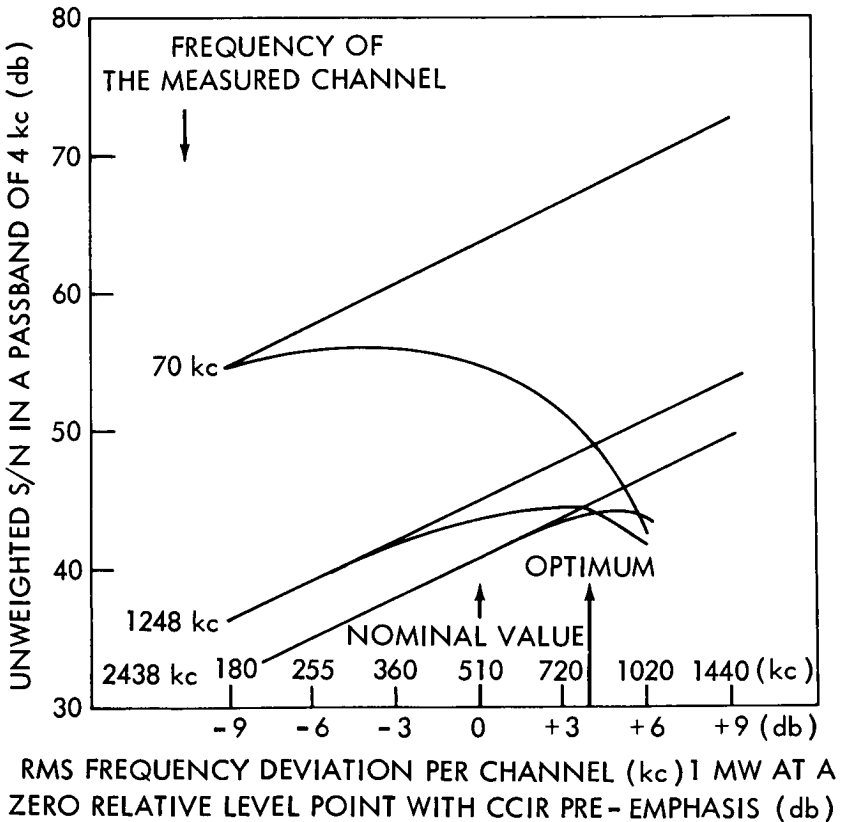


Fig. 25 (cont.) — Intermodulation noise for 600 one-way channels.

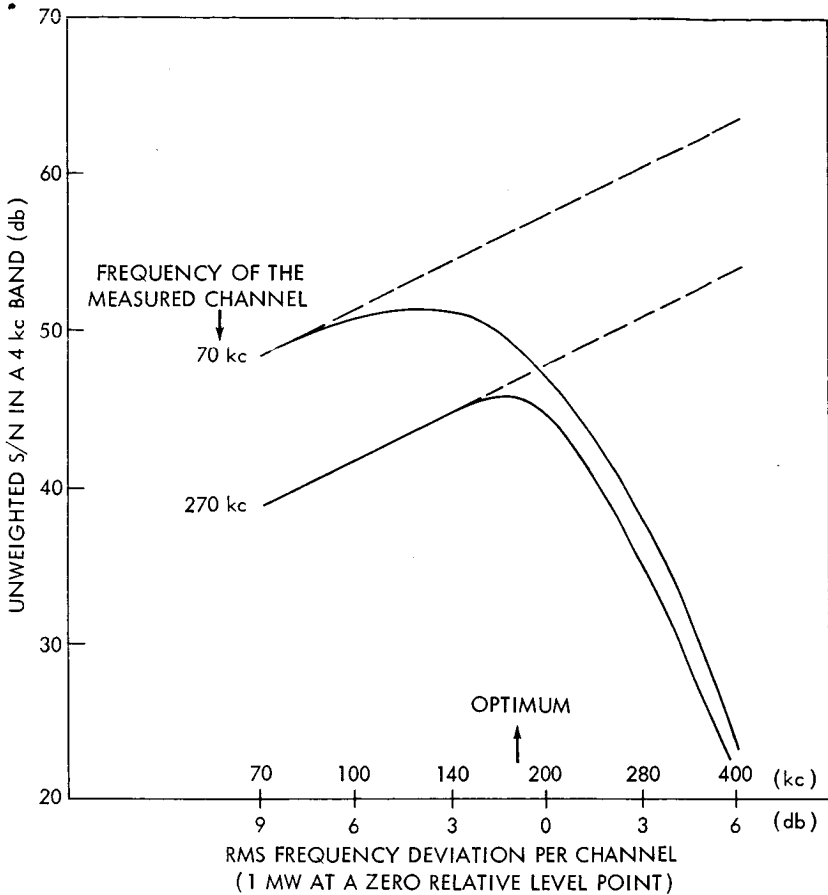


Fig. 26—Intermodulation noise for 60 two-way channels.

lation noise increases rapidly. The ratio of the signal to unweighted noise in the worst channel is under optimum conditions, 45 db, corresponding to a psophometric noise power at a zero relative level point for each channel of less than 15,000 pw.

The near-end study shows that the signal-to-unweighted-noise ratio experiences a constant deterioration of about 2 db when the effective frequency deviation per channel varies from 100 to 400 kc.

#### Intelligible Crosstalk

It is possible to measure intelligible intermodulation between the two directions of transmission in two-way telephony in this way. By

modulating one of the two carriers with a 100 kc sinusoidal signal, we studied the different frequency excursions produced by this signal, also with respect to the difference in power of the carriers at the satellite input.

The measurements listed in Table 1 were performed at Pleumeur-Bodou on a link with Andover.

The 100-kc signal was transmitted by the Andover station by modulation of the 6395 Mc carrier. After translation in the satellite the signal was retransmitted to the ground at 4175 Mc. The Pleumeur-Bodou station transmitted an unmodulated carrier at 6386 Mc, which was retransmitted by the satellite at 4165 Mc. The nominal values of the signal level received by selection of the 4174 Mc carrier at the measurement point for the deviations chosen (1 Mc peak-to-peak, 0.5 Mc peak-to-peak, and 0.25 Mc peak-to-peak) are shown on the first line of the table.

TABLE I — INTELLIGIBLE INTERMODULATION TWO-WAY TELEPHONY\*

CARRIER		$\Delta F = 1 \text{ Mc P-P}$	$\Delta F = 0.25 \text{ Mc P-P}$	$\Delta F = 0.5 \text{ Mc P-P}$
NOMINAL VALUE	CARRIER AT 4175 Mc	-2.20 N†	-2.90 N	-3.60 N
CARRIER POWER EQUAL AT SATELLITE INPUT	CARRIER AT 4175 Mc	-2.15 N	-2.80 N	-3.50 N
	CARRIER AT 4165 Mc	-8.60 N	-9.55 N	-9.50 N
POWER AT 6395 Mc (ANDOVER) 3 db LOWER THAN AT 6385 Mc AT SATELLITE INPUT	CARRIER AT 4175 Mc	-2.15 N		-3.55 N
	CARRIER AT 4165 Mc	-9.20 N		-9.65 N

\* Andover transmits at 6395 Mc a carrier modulated at 100 kc with a peak-to-peak frequency excursion  $\Delta F$ . Pleumeur-Bodou transmits at 6385 Mc an unmodulated carrier.

† N = Neper.

• The power transmitted by each station is automatically adjusted for the range of the satellite and the power received from each station is determined from the telemetry and adjusted before the actual tests.

We have shown, when the power of the carriers received by the satellite are equal, the signal level received for each carrier. For the two lowest frequency deviations the parasite signal is lost in the noise. The carrier power received was  $-93$  dbm for the two carriers and the noise temperature of the receiver was  $33^{\circ}\text{K}$ . For the greatest frequency excursion the presence of a parasite signal due to intermodulation can be observed; this increases the measured noise in a 300 cps band by about 0.9 neper.

When the power of the carrier with the signal, as measured at the satellite, is reduced by 3 db the power of the corresponding carrier received on the ground decreases by 3 db also ( $-96$  dbm at Pleumeur-Bodou); the power of the other carrier received on the ground increases by 1 to 2 db (about  $-91.5$  dbm at Pleumeur-Bodou). In fact, it can be seen that the 100-kc noise received after demodulation has decreased by about 0.15 N.\* The parasite signal obtained by intermodulation is still lost in the noise at the smallest frequency excursion. For the greatest frequency excursion, on the other hand, the parasite signal is still present but increases the noise by only about 0.4 N.

There is thus some intermodulation occurring in the amplification equipment common to the two carriers (satellite equipment, maser amplifiers and first IF stages of the station), and it appears above the noise for the large frequency excursions (above 0.5 Mc peak-to-peak).

#### *Distortion in the Television Channel*

The study of linear and nonlinear distortion in the video channel was carried out by using the test signals recommended by the CCIR. The reconstituted signals remain within the limits defined by the CCIR for each test signal. The same tests were performed in loop on the cable link between the measurement room of the main building and the radome, without using the modulation equipment. The results were practically the same as those obtained with the satellite. From the point of view of distortion in the video channel, then, the television link is of satisfactory quality.

The total distortion of a sinusoidal signal in the sound channel was measured as a function of frequency for a sinusoidal signal at 1000 cps which produced in the 4.5 Mc subcarrier at peak frequency excursion

---

\* Neper.

of 17.7 or 50 kc. In both cases the total distortion remained below 3 percent for all the frequencies of the useful band.

In order to examine the intermodulation of the video channel on the sound channel, the ratio of peak signal to effective noise in the sound channel was measured, with the video carrier unmodulated or modulated with the following test signals: CCIR test signals Nos. 1, 2, and 3 (Recommendation No. 267), high-frequency rectangular signal with 14 square pulses per line, test pattern, and a taped television program. It could be seen that when video and audio pre-emphasis networks are used the intermodulation can be considered negligible. Without pre-emphasis, however, the deterioration of the peak signal to effective noise ratio may reach 20 db. We feel that this deterioration comes from the ground equipment, since a similar result is observed when the transmitting equipment is looped to the receiving equipment at intermediate frequency.

#### SPECIAL EFFECTS ON THE LINK

Studies were made of two effects peculiar to satellite links; these do not appear in classical microwave links.

##### *Absolute Measure of Propagation Time*

The absolute measurement of propagation time is performed in loop on the satellite by measuring the interval of time which separates the leaving and the arrival of a square pulse after going through the satellite. A first series of measurements was made by transmitting the appropriate pulse in a telephone channel, the accuracy of the measurement in this case being  $\pm 0.2$  ms. A second series of measurements, made by sending pulses with steeper sides in the video frequency band, enabled us to achieve an accuracy of  $\pm 0.2$   $\mu$ s. A comparison of measured values with those obtained by calculation based on the range of the satellite as determined by orbital data and allowing for propagation time in the equipment shows a remarkable agreement.

##### *Influence of the Doppler Effect in Baseband*

The frequency shift produced by the variation of transmission time on the frequencies transmitted in baseband is measured in loop on the satellite.

Figure 27 shows a comparison of the values measured at different times for the deviation between the received and transmitted fre-

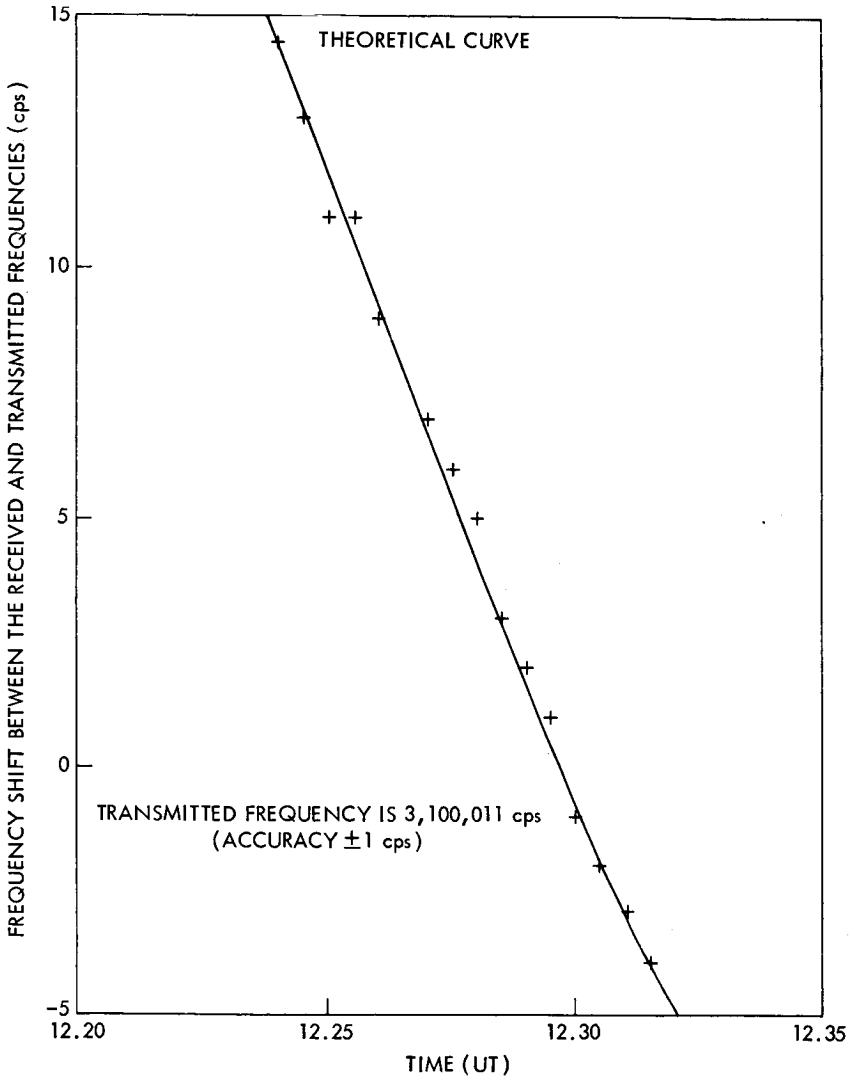


Fig. 27 — Doppler effect measurement (Pass 723).

quencies, with the transmitted frequency being 3,100,011 cps stable to 1 part in  $10^8$ , with the theoretical curve based on orbital data. The accuracy of the measurement, made with a frequency counter, was  $\pm 1$  cps.

## SYSTEM TESTS

System tests of the link are for the most part qualitative tests of the transmission of a certain number of different types of information.

*System Tests of the Telephone Channels*

In addition to qualitative tests of telephony between talkers, the telephone channels were used for the transmission of certain information.

## System Tests of Facsimile Transmission

When the satellite communication link was used for a system of multiplex telephone channels, some channels were used for the transmission of facsimile.

The first facsimile received from the United States at Pleumeur-Bodou on pass 97 was on a two-way link is reproduced in Fig. 28. A slight deformation of the corners can be observed due to the Doppler effect.

The link could also be one way. Under this condition, in loop on the satellite, we tested a system for Doppler effect correction, using a pure frequency linked with the rotational velocity of the transmitter drum and transmitted by frequency modulation of a subcarrier in the same telephone channel as the picture. Two photographs are reproduced (Figs. 29 and 30), one received with the use of the correction equipment designed for this purpose and the other received on an ordinary facsimile apparatus. The correction system, which requires very little change of normal equipment, corrects completely for the Doppler effect. The quality of the resulting photograph is excellent.

## System Tests of Data Transmission

It is possible to use the telephone channels of the telephone multiplex system of a two-way link for the transmission of data at medium speeds.

The first system test, which took place during pass 97, consisted in transmitting some text from Pleumeur-Bodou to Andover and then from Andover to Pleumeur-Bodou at the rate of 1200 bands. The error-correction system of the machines used for the test did not operate during this test and errors were noted.

A measurement was also made of the quality of transmission at 2400 bands in different channels of a 600-channel multiplex system used on a one-way link in loop on the satellite. In the first test a channel in the lower part of the frequency band was utilized. No error was observed to 2.5 million bits transmitted. During a second test, the channel which

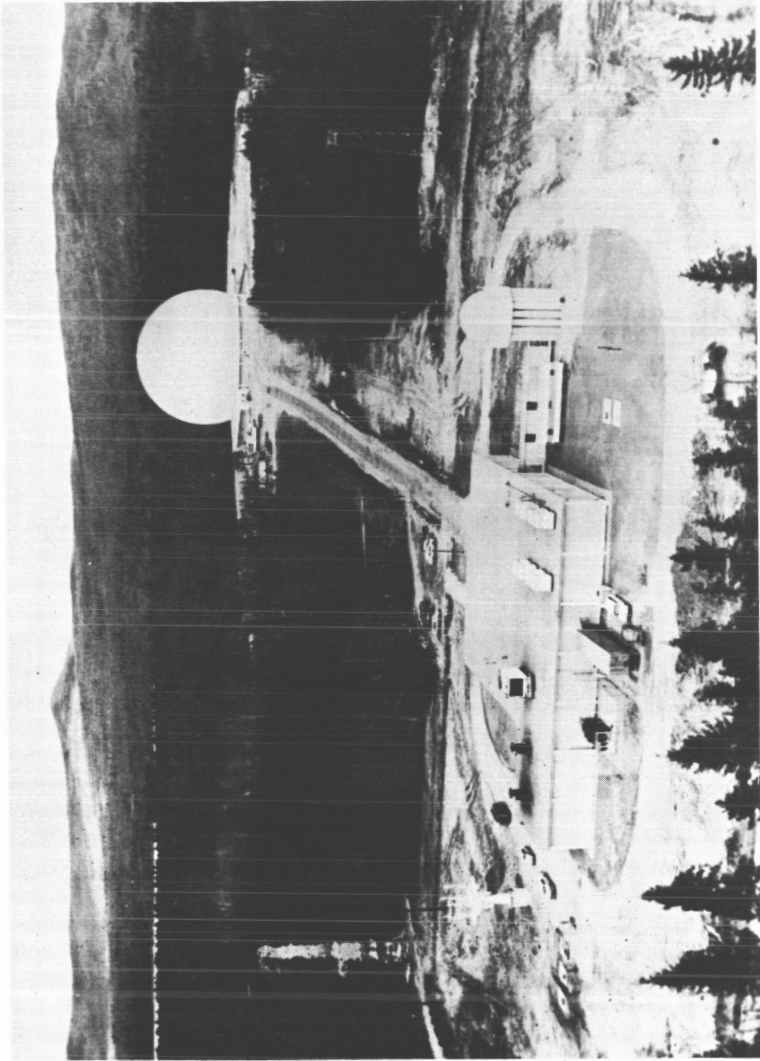


Fig. 28 — First facsimile photograph transmitted at New York and received at Paris via satellite.

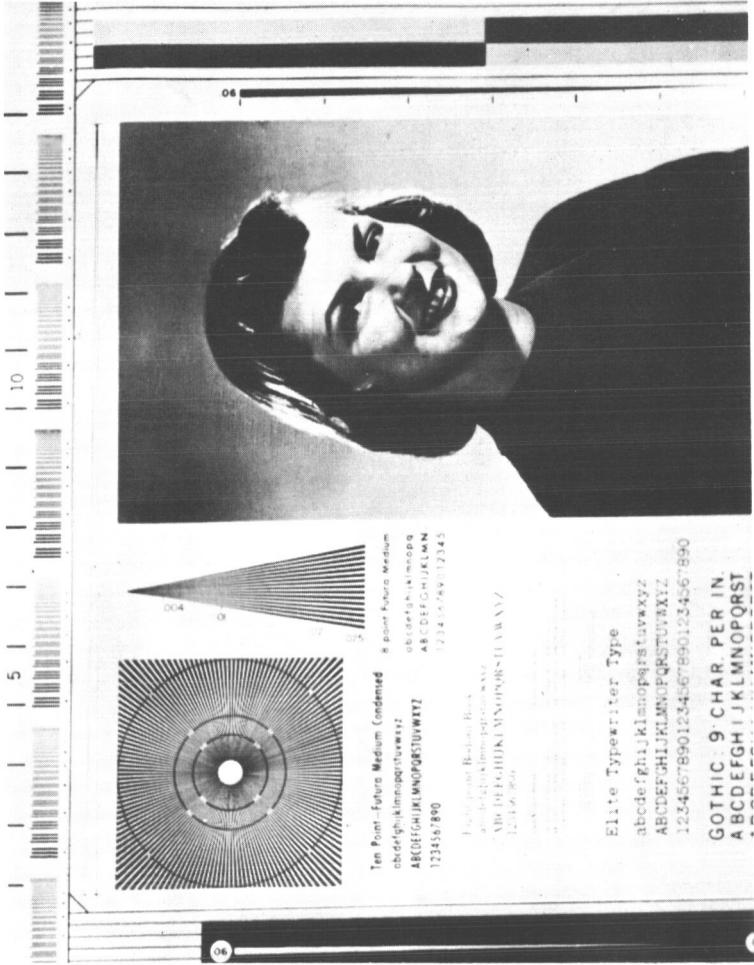


Fig. 29 — Facsimile photograph transmitted and received at Paris after round trip through Telstar I (No correction for Doppler effect).

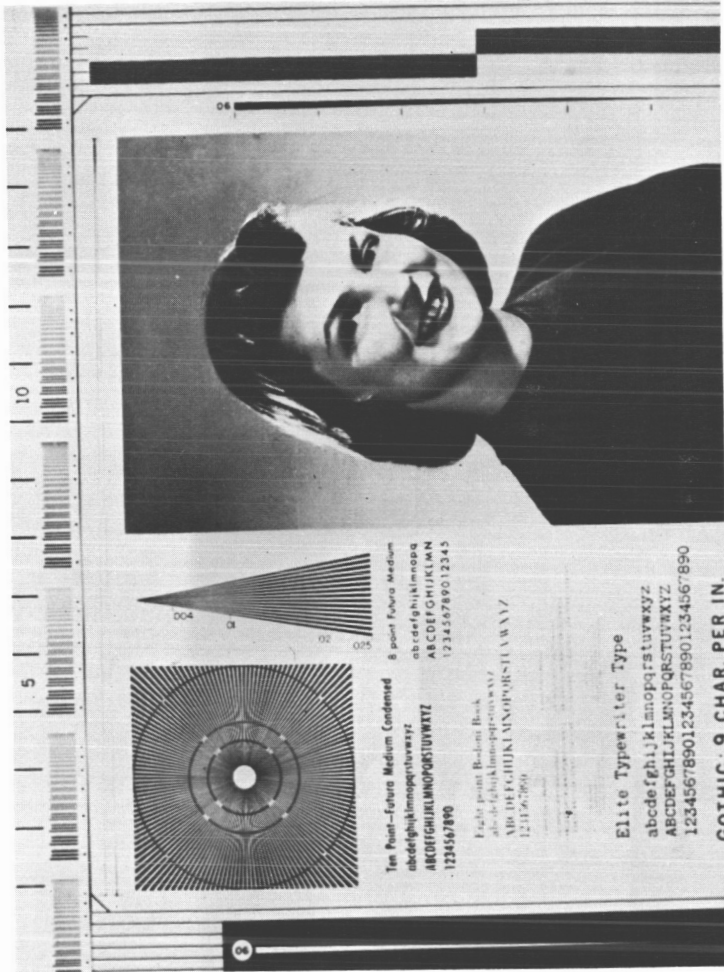


Fig. 30 — Facsimile photograph transmitted and received at Paris after round trip through Telstar I (With Doppler correction).

is transmitted at the highest frequency was used. The deviation, due to Doppler effect, between the frequency transmitted and the frequency received reached a maximum of 28 cps. No error were observed. During a third test, the ratio of signal to white noise at the input of the data transmission receiver was deliberately reduced by 13 db and set at 20 db. The frequency deviation due to Doppler effect was 13 cps maximum and an error rate of 2.5 in  $10^6$  was noted.

These tests show that the quality of the telephone channels for data transmission is excellent. The Doppler effect, which is nevertheless much greater in these tests than in a station-to-station link, is not troublesome in any of the 600 channels transmitted. A very wide margin over the signal-to-noise ratio exists before the error rate becomes significant.

### *System Tests of the Television Link*

Certain passes of the satellite were reserved for the transmission of television pictures on a one-way link between the Andover station, the Goonhilly station, and the Pleumeur-Bodou station.

Especially during passes 6 and 7 (the first two with mutual visibility), pictures transmitted by Andover were received at Pleumeur-Bodou. In Fig. 31 is reproduced the photograph of the first picture received at the beginning of pass 6. During pass 16, the Pleumeur-Bodou station transmitted pictures which were received at Pleumeur-Bodou and Andover.

Later, a large number of passes were reserved for television demonstrations. Passes 123 and 124 in particular were reserved for inaugural demonstrations. Figure 32 is a reproduction of one of the pictures received from the United States at Pleumeur-Bodou on pass 123 and retransmitted directly on the Eurovision network.

All together, the Pleumeur-Bodou station participated in 20 system tests or demonstrations of one-way television in the America-Europe or Europe-America directions, from 10 July to 2 November 1962.

System tests of two-way television between the Andover and Pleumeur-Bodou stations were also performed.

The same norms were adopted as for one-way television, with the exception of the peak-to-peak frequency excursion of the signal, which was reduced by 12 db, or 3.75 Mc. The RF pass band was limited by a pass-band filter of 6 Mc at 3 db.

Figures 33 and 34 are reproductions of a picture received from Andover on one of the transmission channels and of a picture trans-



Fig. 31 — First picture received at Pleumeur-Bodou during Inaugural Program of Mondovision.

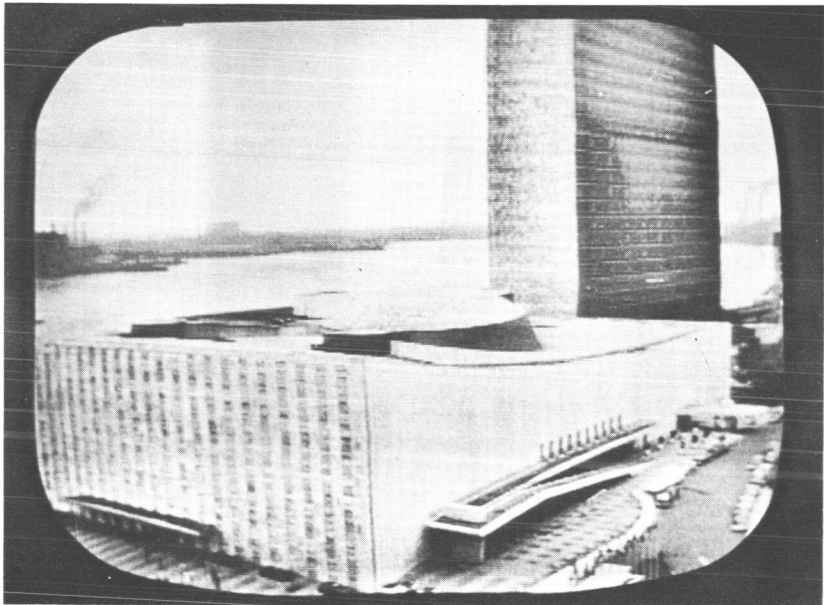


Fig. 32 — Picture received at Pleumeur-Bodou during Inaugural Program of Mondovision.



Fig. 33—Two-way television picture transmitted at Andover and received at Pleumeur-Bodou.

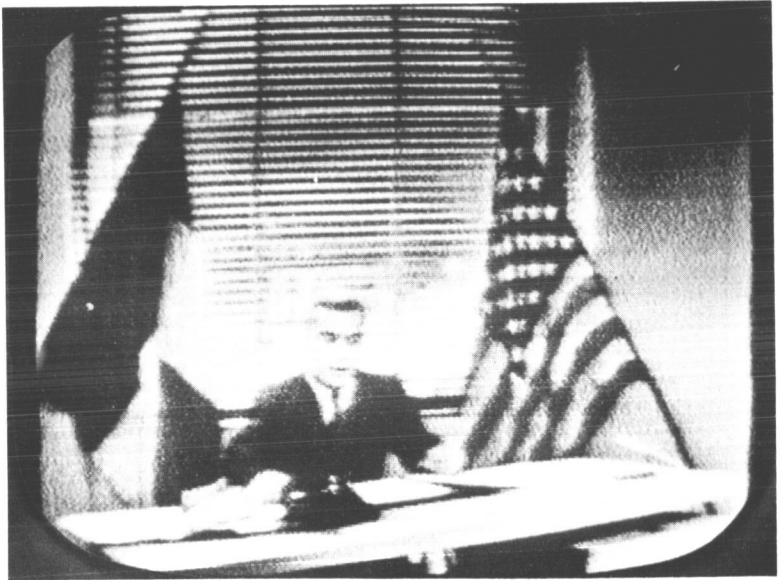


Fig. 34—Two-way television picture transmitted and received at Pleumeur-Bodou after round trip via Andover.

mitted to Andover and retransmitted immediately to Pleumeur-Bodou on the other channel.

The quality of the pictures, although lower than that obtained on one-way television because of the reduced frequency excursion, is nevertheless acceptable.

#### CONCLUSION

The tests which we performed at the Pleumeur-Bodou station with the Telstar I satellite are fully satisfactory. They confirmed our hopes of being able to establish a wideband communications link between continents by the use of a satellite.

We were able to verify that the solutions which had been adopted for the solution of the problems of pointing a highly directive antenna with sufficient accuracy in the direction of a satellite at the moment it appears and then keeping it pointed at the moving satellite, and the problems of transmitting a wideband signal between two widely separated points on the earth without appreciable deterioration were technically valid. We were able to study some of these problems in greater detail and to examine the most adequate solutions for them. Thanks to the experimental facilities we have available, we were able to find the methods which were technically and economically most suitable and which will be usable for the development of a commercially useful system of communications by satellite.

**GOONHILLY DOWNS, ENGLAND**

# The Post Office Satellite Communication System Ground Station at Goonhilly, Cornwall\*

W. J. BRAY and F. J. D. TAYLOR

POST OFFICE ENGINEERING DEPARTMENT

The initial purpose of the Post Office satellite system earth station at Goonhilly Downs, Cornwall, is to obtain information on the performance of experimental communication satellite systems; such information will be of great importance to the designers of systems for commercial operation. To facilitate this dissemination the UK and USA Governments prepared and signed, in February 1961, a Memorandum of Understanding regarding collaboration between the British Post Office and the United States National Aeronautics and Space Administration (NASA) on the testing of experimental communication satellites to be launched by NASA. The first phase of the tests covered Projects Telstar and Relay, both active satellites.

The agreement with the United States covers full interchange of technical information, makes clear that the collaboration is for experimental tests only and is not concerned with commercial exploitation, and does not preclude the use of the Post Office experimental earth station for tests outside the cooperative projects outlined. Similar agreements between the United States and France, Federal Republic of Germany, Italy, and Brazil have since been approved.

The Goonhilly satellite system earth station has been planned and equipped, not only for participation in Projects Telstar and Relay and similar experimental projects, but also with a view to possible operational use at a later date.

The site of the Goonhilly radio station (Fig. 1) has been chosen to be particularly suitable for transatlantic communication in view of its westerly location; also, its southerly latitude is convenient for satellites in equatorial orbits. It is remote from the majority of microwave links in the United Kingdom, so that frequency-sharing with such links is

\* First published in *British Communications and Electronics*, August 1962; reproduced by permission of the Editor.

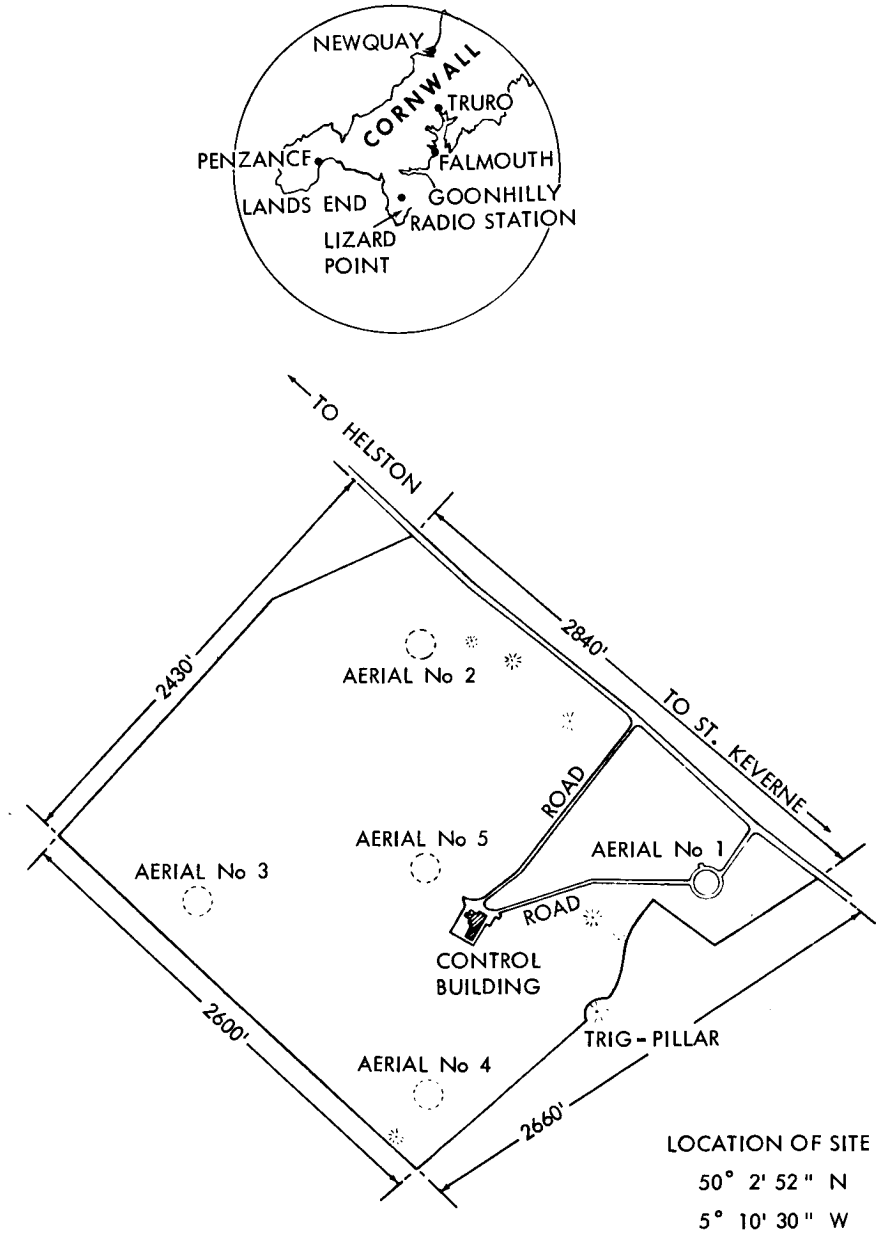


Fig. 1 — Simplified site plan, Goonhilly Radio Station.

facilitated. The horizon angles are predominantly negative with a maximum positive value of about  $0.5^\circ$ , so that satellite orbits involving low angles of elevation can be used. The main station building is located near the centre of the site; the aerial is close to one corner. However, the site is large enough to accommodate additional aerials for experimental purposes or for operational use in the future.

The present equipment for participation in Projects Relay and Telstar includes the following facilities:

- An 85-ft diameter paraboloidal-reflector dish aerial with full steerability over the hemisphere above the horizontal plane;

- Means for steering the aerial automatically from predicted orbital data;

- A 10 kW transmitter operating at 1,725 Mc/s for Project Relay;

- A 5 kW transmitter operating at 6,390 Mc/s for Project Telstar;

- Low-noise receiving equipment for the 4,170 Mc/s communication and 4,080 Mc/s beacon signals transmitted by the Telstar and Relay satellites;

- Terminal equipment for transmission and reception of multi-channel telephone, telegraph and television signals;

- Video and multi-channel telephone and telegraph links to the trunk network; and

- Support communications, including teleprinter and voice circuits to the USA, for the transmission of data and other information concerning the tests.

#### THE STEERABLE AERIAL

The steerable dish aerial (Fig. 2) is designed for operation up to at least 8,000 Mc/s, at which frequency the beamwidth is only about  $0.1^\circ$ . Since the satellites move rapidly across the sky, the aerial is required to track a rapidly moving satellite to within a few minutes of arc. The aerial as a whole rotates on a turntable to provide changes in azimuth, and the dish is rotated about a horizontal axis for elevation changes. In addition, small variations (up to a degree of beam direction) are possible by remotely-controlled movements of the feed at the focus of the dish. The feed for the dish is in the plane of the aperture, an arrangement which, with appropriate feed design, reduces the levels of the minor lobes of the radiation diagram. This is of great importance since, unless the minor lobes are very small, noise can be picked up from the terrain surrounding the aerial which would significantly

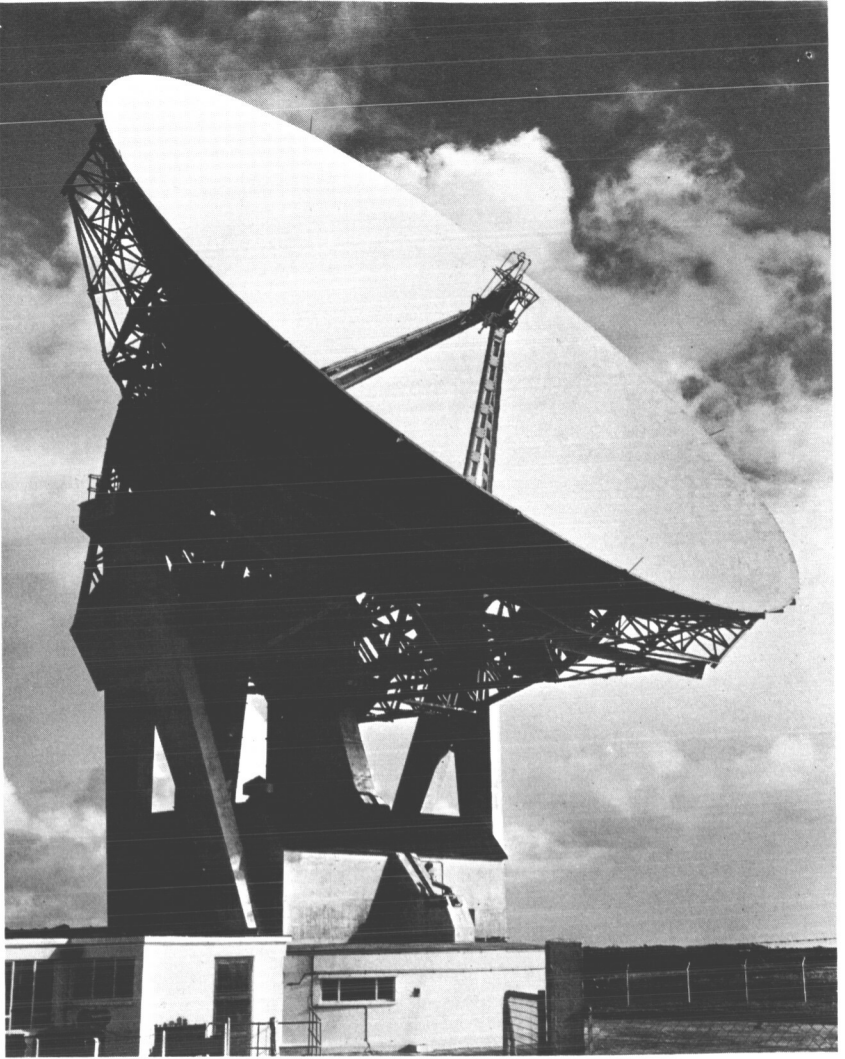


Fig. 2 — The steerable antenna.

degrade the signal-to-noise ratio of the very weak signals received from a satellite.

Since the aerial is not protected by a radome, stability under high wind conditions is achieved by a heavy, sturdy construction using reinforced concrete supporting members, and powerful driving motors. The weight of the movable part of the aerial structure is some 870

tons, and the structure is designed to operate in wind velocities up to 65 mph.

The aerial is automatically steered, using predicted orbital information derived from the NASA worldwide network of Minitrack stations, one of which is operated by the Department of Scientific and Industrial Research at Winkfield, near Slough. This data is received in digital form over a teleprinter circuit from NASA Space Flight Center, USA; it has to be processed in an electronic computer at Goonhilly to give the aerial steering instructions in an appropriate form. To correct for small errors in prediction and errors arising from other causes, the aforementioned manually or automatically controlled aerial beam swinging facility is used. In this operation, the 4,080 Mc/s beacon signal transmitted by the satellite causes the aerial beam to "scan" circularly over a few minutes of arc. Information is thereby derived which enables the appropriate corrections to be applied, initially on a manual basis and later automatically on a "lock-on" basis. A spiral scan of up to  $1^\circ$  is available, if required, to aid in satellite beacon acquisition, but in practice has not been found necessary.

Immediately behind the reflector dish there are two apparatus cabins; one of these accommodates the travelling wave maser amplifier operating at 4,170 Mc/s. The necessary low temperatures for this device are obtained by using liquid helium and liquid nitrogen; evaporated helium is recovered, stored, and compressed by equipment housed in a cabin on the horizontal turntable.

A cabinet behind the reflector also accommodates filters for separating the satellite beacon signal from the satellite communication signal, so that the latter may be amplified separately in the maser. Means for determining the system noise temperature are also provided. Waveguide assemblies with rotary and flexible joints connect the feed at the focus of the reflector with equipment in the cabins at the back of the reflector and on the aerial turntable.

On the horizontal turntable is an apparatus room accommodating the high power stages of the Telstar and Relay transmitters, the low power drive equipment for the transmitters and equipment for translating signals to and from radio frequency and an intermediate frequency of 70 Mc/s.

A cylindrical enclosure in the middle of the apparatus room accommodates the loops of flexible cable used to make connection between the equipment in the moving apparatus room and fixed equipment in the main control building and elsewhere. Rotation of the turntable around the vertical axis is restricted to  $\pm 250^\circ$ , so that cable loops

rather than slip rings can be used. Beneath the horizontal turntable and beyond it there is a chamber and tunnel for the interconnecting cables.

#### MAIN CONTROL BUILDING

In the main buildings (Figs. 3 and 4) from which all experiments are controlled, the principal rooms contain the following:

- Control and experimental apparatus;
- Telegraph equipment;
- Computer and data processing equipment;
- Aerial steering equipment and precise time and frequency standards;
- Aerial steering console; and
- Auxiliary test apparatus, including telecine and television equipment.

#### *Control and Experimental Apparatus Room*

A console is provided for the experiment control (Fig. 5) enabling the availability of the transmitting, receiving, and test equipment and the aerial to be determined at all times, together with voice communication facilities to the operating staff concerned. A similar console is

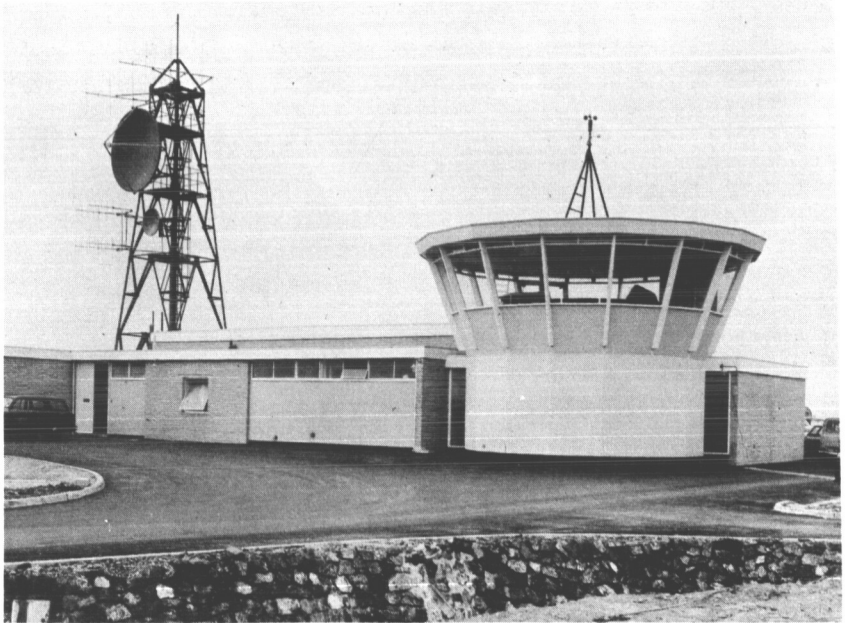
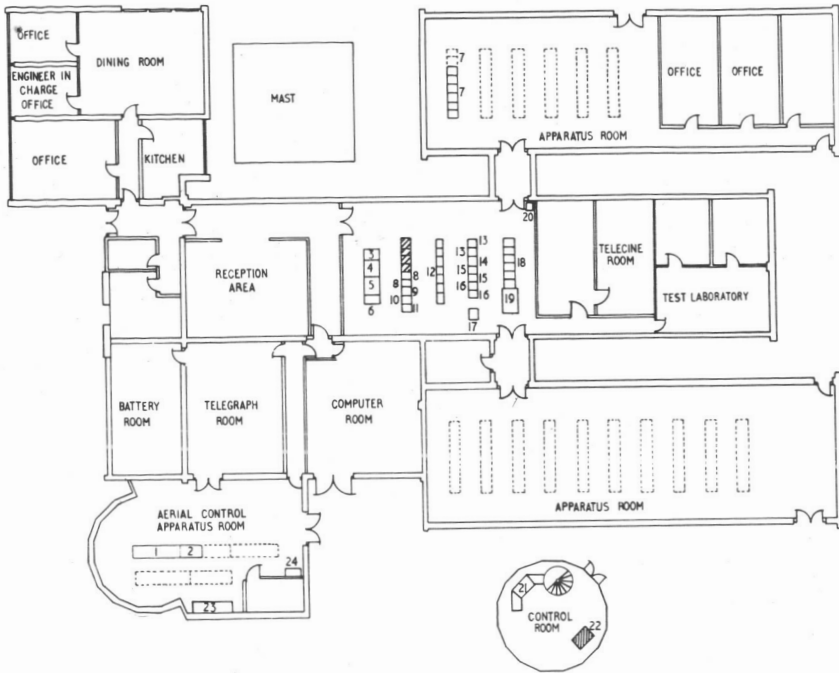


Fig. 3 — External view of the control building.



ITEM	DESCRIPTION
1	AERIAL No.1 CONTROL EQUIPMENT
2	AERIAL No.2 CONTROL EQUIPMENT
3	CONTROLLER'S CONSOLE
4	CIRCUIT SWITCHING CONSOLE
5	BEAM SWINGING EQUIPMENT
6	TX AND RX SUPERVISORY CONSOLE
7	INLAND MICROWAVE LINK EQUIPMENT
8	TINE I. EQUIPMENT
9	EQUIPMENT RACK FOR CIRCUIT SWITCHING CONSOLE
10	MISC APPARATUS RACK
11	D.P.U. RECEIVERS
12	BASEBAND AND IF EQUIPMENT
13	RECORDERS
14	WHITE NOISE TEST EQUIPMENT
15	MISC. TEST EQUIPMENT
16	TV TEST EQUIPMENT
17	CABLE TERMINATING RACK
18	CARRIER AND TRANSMISSION EQUIPMENT
19	DISTRIBUTION FRAME
20	VOLTAGE REGULATOR FOR ITEM 18
21	CONTROL CONSOLE AERIAL No.1
22	CONTROL CONSOLE AERIAL No.2 (PROPOSED)
23	CABLE TERMINATIONS AERIAL No.2
24	MISC APPARATUS RACK

Fig. 4 — Simplified floor plan of the control building.

provided for aerial steering purposes, the latter including visual presentation on cathode ray tubes of the incoming wave direction from the satellite. The equipment in this room includes:

Baseband and intermediate frequency equipment forming part of the transmitting and receiving communication system;

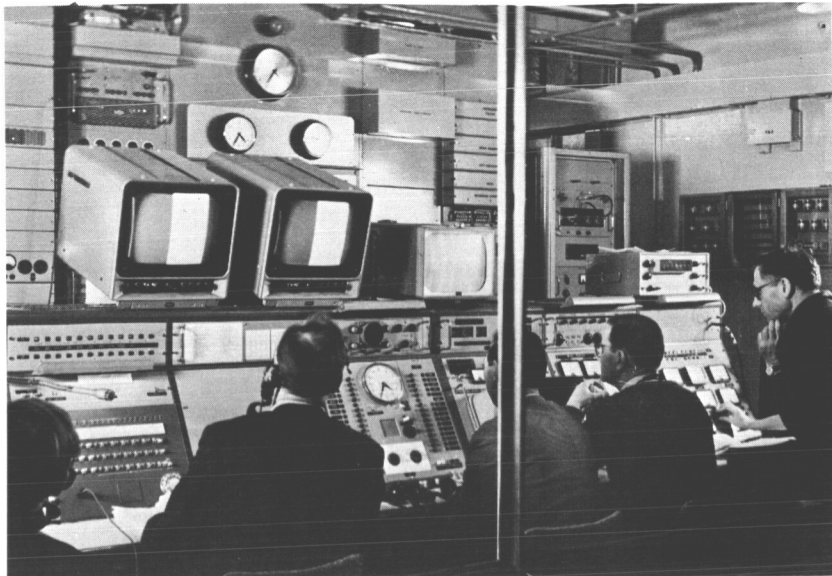


Fig. 5 — The control console suite.

Receivers for the “off-the-air” reception of television broadcast signals;  
 Test equipment;  
 Magnetic tape and other recorders;  
 Satellite beacon signal receivers; and  
 Video and multi-channel telephony terminals.

#### *Telegraph Room*

Separate teletypewriters are provided for:  
 Operational traffic with, and reception of orbital prediction data from, the Goddard Space Flight Center, Greenbelt, Maryland;  
 Communication with the satellite ground station at Andover, Maine, on a private wire basis;  
 Telex facilities;  
 The receipt of local meteorological information (to enable aerial safety precautions to be taken if necessary).

#### *Computer Room*

The principal item in this air conditioned room (Fig. 6) is a National-Elliott Type 803 electronic computer. As noted earlier, orbital data is received in digital form from the USA; this data provides predicted

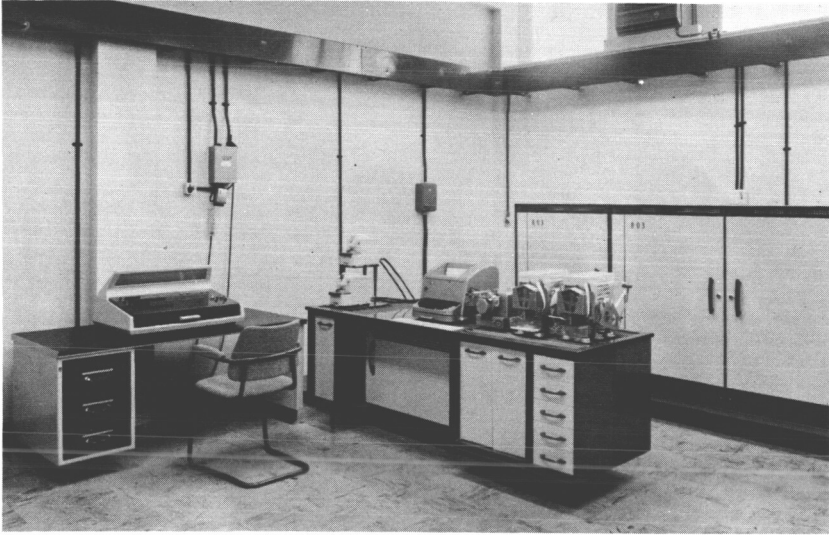


Fig. 6 — The computer room.

X, Y, Z versus time coordinates at one-minute intervals and is recorded on punched tape. The computer processes the data to provide aerial steering instructions also in punched-tape form, the output information for each one-second interval including time, azimuth bearing, rate of change of azimuth, elevation, rate of change of elevation and the slant range to the satellite. The computer programme also makes allowance for changes of apparent satellite bearing due to atmospheric refraction. Telegraph-type tape readers and data recording equipment are provided for processing the received orbital data and for the preparation of the aerial steering tapes.

The manner in which instructions from the computer are passed into the aerial steering equipment is a punched paper tape (Fig. 7). This tape is "read" by the equipment one second in advance, one second at a time, the tape reading equipment positioning the tape for each reading operation from the single "cycle start" hole marking the commencement of each sequence. The time to which the start of each sequence refers is punched into the tape as hours, minutes and seconds in a code which can be read by inspection. This is followed by instructions, in binary code, defining the azimuth and elevation instructions required at that time.

With the exception of a short portion of tape giving a tape identification number, also in a simple code which can be read by inspection,

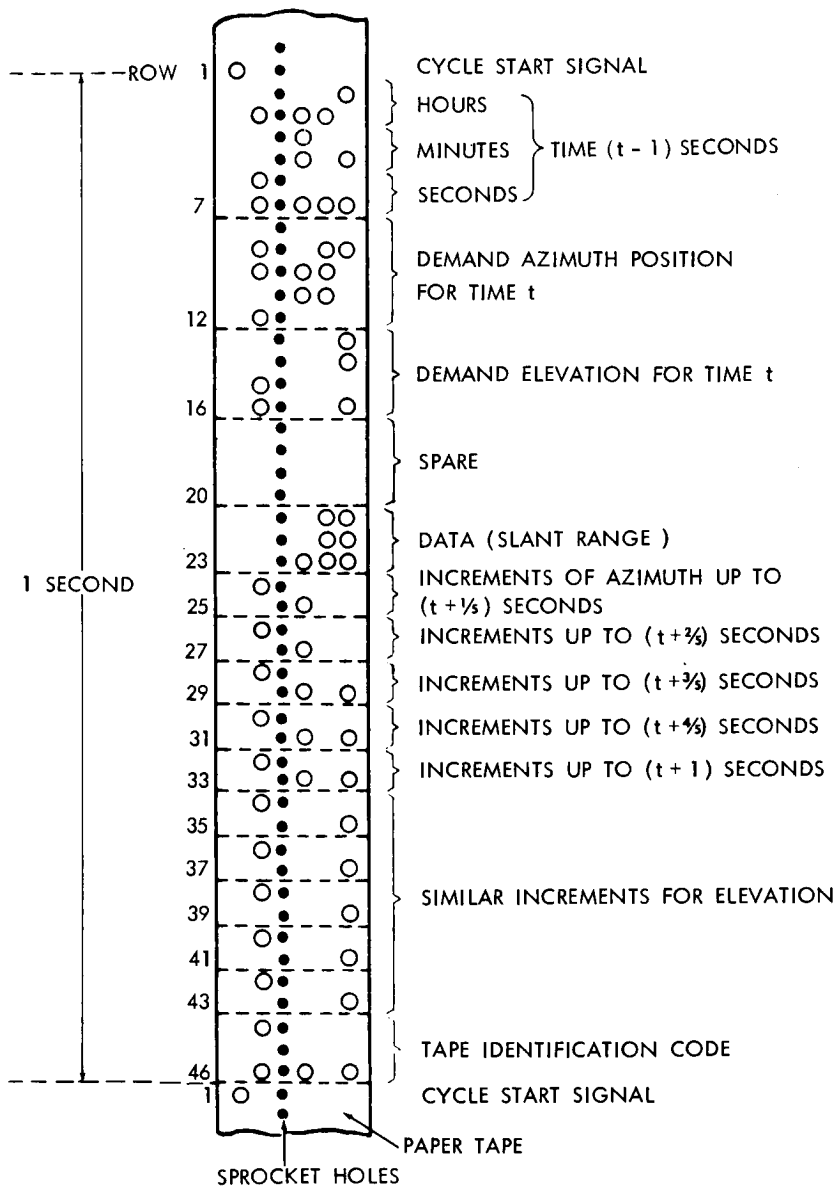


Fig. 7 — A section of control tape.

the remainder of the one second sequence contains a series of increments to the initial demanded aerial directions which enables the equipment to keep the driving motors running at the correct rates for the next demanded position to be reached with minimum error.

#### *Aerial Steering Apparatus Room*

The apparatus in this room enables a comparison to be made between the aerial steering input data in digital form and digital signals derived from read-out units on the aerial azimuth and elevation drives, thus enabling the servo feedback loops to be completed.

A temperature controlled annex to this room accommodates quartz-crystal timing oscillators of high accuracy which, in conjunction with time signal radio-receivers, provide a precise time source adjustable to Universal Time 2.

Steering tapes are received from the computer room for application to the input of the aerial steering apparatus, initiation of aerial movement being dependent upon synchronism between time as recorded on the tape and as generated by the precise time source.

#### *Aerial Steering Console Room (Control Tower)*

The aerial steering console room in the Control Tower (Fig. 8) has been designed and placed to give uninterrupted visibility over the



Fig. 8 — The aerial steering position in the control tower.

whole site. Though every precaution has been taken to ensure safety of personnel, by the provision of mechanical and electrical interlocks, it has been considered desirable that those controlling the movement of the aerial should have full visual surveillance. The aerial is floodlit at night.

Though aerial steering is fully automatic, it has been arranged that the mechanical and electrical conditions of the aerial are displayed to an operator who can observe fault conditions, apply corrections and override the automatic system should any abnormality occur.

#### POWER SUPPLIES

The power supply for Goonhilly radio station is obtained at 11 kV from an electricity substation four miles distant, together with an alternative supply from Helston, eight miles distant. Both supplies are via overhead lines, except for a distance of some 400 yards on site, which is via underground cable. Changeover facilities are provided to enable the second supply to be used in the event of failure of the first. The present supply capacity is 450 kVA; this will ultimately be increased to 800 kVA.

The supply terminates at three transformers. At the aerial site a 250 kVA transformer supplies power for driving motors and a 100 kVA transformer supplies power for electronic equipment, etc. The third transformer, at the control building, is of 100 kVA to provide power for the whole building.

Because of the very small risk of failure of both electricity supplies simultaneously, and because of the large amount of power required, no local standby power is provided except that derived from a 50 V battery to operate emergency lighting, clocks and telephones.

#### SYSTEM CHECKING FACILITIES

It is necessary to be able to check periodically the mechanical alignment of the aerial, the electrical bearing of the aerial beam, and the performance of the transmitting and receiving equipment—independently of a satellite. For these purposes the aerial is fitted with a boresight telescope for ranging on local and distant points of accurately known bearing. In addition, there has been installed at Leswidden, some 21 miles away, apparatus capable of simulating the Telstar and Relay satellites, thus enabling comprehensive overall system tests including tests of the aerial gain and radiation diagram

to be made. Measurements of the aerial tracking characteristics are made using the radio star Cassiopeia A.

#### TRANSMISSION EQUIPMENT

The radio transmission equipment at a satellite system earth station differs markedly from that used in conventional radio-relay systems, for the following reasons:

1. the need for high-power earth station transmitters—with outputs of kilowatts instead of a few watts,
2. the very small signal power, of the order of micro-microwatts, received from satellites, and the resulting low signal-to-noise ratio in the intermediate-frequency passband of the ground station receiver,
3. the use of circularly polarized waves, as compared with linear polarization in most radio-relay systems,
4. the presence of Doppler frequency shifts on the received signals due to the motion of the satellite relative to the earth stations.

The earth station transmission equipment, shown in block schematic form (Fig. 9), enables signals to be transmitted in a 5 Mc/s baseband. Such a baseband could accommodate several hundreds of telephony channels or a television signal of up to 625-line definition or high-speed data transmissions. Multi-channel telegraphy and facsimile signals could alternatively be transmitted in the telephony channels.

The baseband input signals are applied to a 70 Mc/s frequency modulator, the wide-deviation output of which is then passed to up-conversion equipment (for translation to the desired radio frequency), a low-power driver stage and a high-power transmitting amplifier. As the ground-station transmitter frequencies for Telstar and Relay are very different, being 6,390 and 1,725 Mc/s respectively, separate up-conversion, driver and high-power equipment are provided for the two projects. The Telstar high-power transmitter uses a 5 kW travelling-wave tube developed specially by the Services Electronics Research Laboratory, while that for Relay uses an Eimac 10 kW multi-cavity klystron amplifier.

Signals received from a satellite include a c.w. beacon emission on 4,080 Mc/s for tracking purposes, as well as a communications signal on or near 4,170 Mc/s. In view of the limited bandwidth of the maser used as a low-noise first-stage amplifier in the receiver, only the communications signal is amplified in the maser though both signals are amplified in a second-stage comprising a low-noise travelling wave



válve. The beacon signal is selected by a waveguide filter and, after frequency-changing, is applied to a narrow-band beacon receiver.

The communications signal is frequency-changed in a down-converter to an IF of 70 Mc/s and is then applied to one of three FM demodulators. One demodulator is of the conventional limited/discriminator type and is suitable for use only when the received signal-level is relatively high. The second demodulator is of the frequency modulation negative feedback type; it is particularly suitable for multi-channel telephony. The third demodulator comprises a tuned circuit which instantaneously follows the frequency of maximum signal energy, the bandwidth being automatically adjusted according to the received signal level. The second and third demodulators reduce the effective noise bandwidth and thus enable relatively weak signals to be satisfactorily received.

#### TESTS AND TESTING EQUIPMENT

Although objective tests (i.e. measurements of the transmission characteristics between earth station "baseband input" and "baseband output" via the satellite) can provide information on which the suitability of the system for any form of signal transmission can be assessed, it is nevertheless of value also to make subjective assessments. To this end facilities have been provided so that either one-way television pictures or two-way telephony signals can be transmitted for demonstration purposes.

One-way transmission tests via a satellite are carried out either between pairs of similarly equipped earth stations or "in loop". In the latter arrangement, the signals transmitted from a given earth station are received back at the same station.

Under two-way transmission conditions both of a cooperating pair of earth stations energize the same satellite at slightly different frequencies. For two-way telephony transmission the Relay satellite includes two separate receivers operating on slightly different frequencies, but in the Telstar satellite there is only a single wideband receiver. When working on a two-way basis via the Telstar satellite the transmitter powers of the cooperating earth stations must be continuously adjusted so that the signal levels at the distances of the respective earth stations from the satellite.

Many items of test equipment have been provided for the objective tests. These permit the measurement of insertion-gain stability, selective fading, noise levels, television signal transmission characteristics,

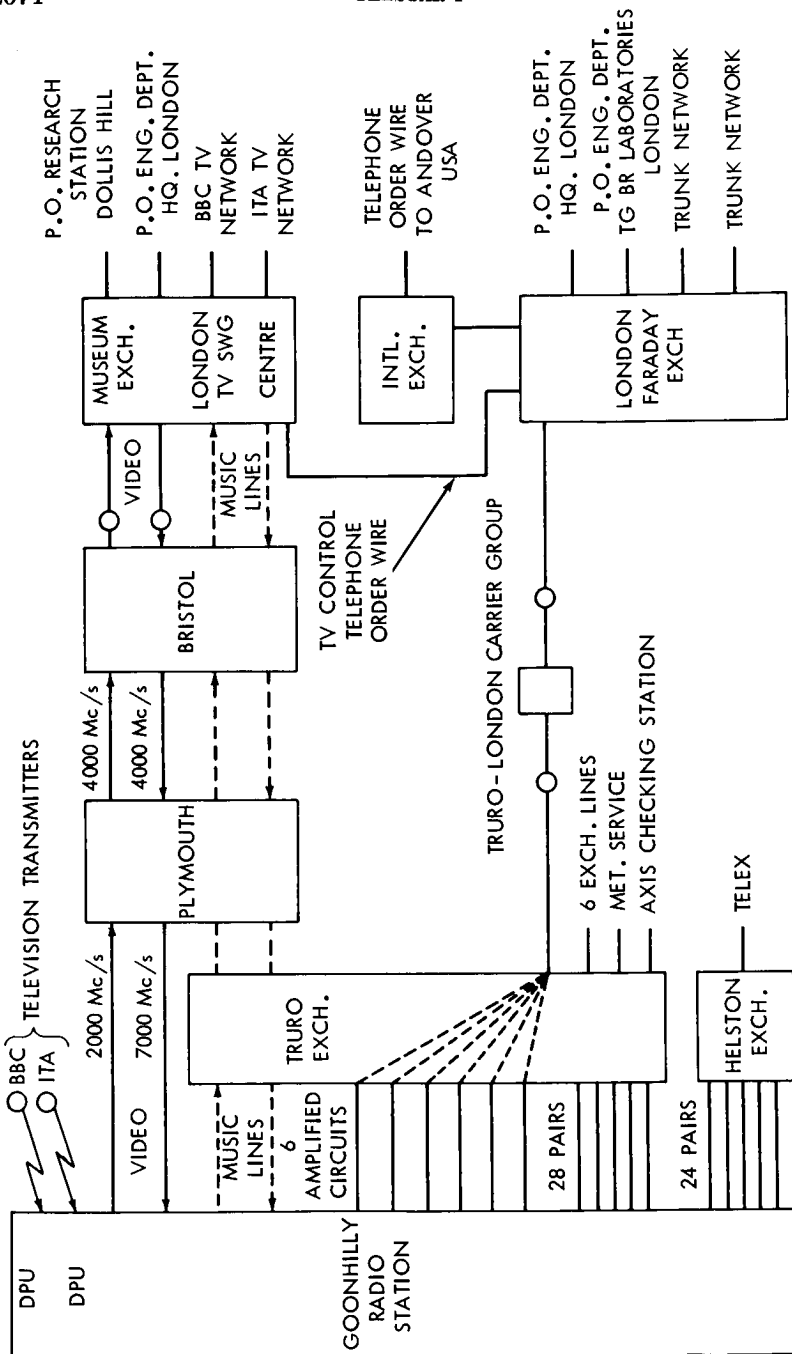


Fig. 10 — Block diagram of the video, telephone (including telephoto) support communications for tests and demonstrations.

telephone and telegraph signal transmission characteristics, received carrier power levels, Doppler frequency shifts and receiving system noise-temperatures, etc. For multi-channel telephony tests, white-noise signals simulating up to 600 telephone channels are available.

In the case of subjective telephony tests baseband equipment has been provided so that twelve two-way circuits assembled in the ranges 12-60 or 60-108 kc/s may be set up. For subjective tests of television transmission, telecine equipment and high-grade picture monitors, suitable for 405, 525, and 625-line standards have been provided.

For telephony demonstrations the audio circuits are connected to the Post Office trunk telephonic network. The audio circuits are also available for carrying out telegraphy, facsimile and data transmission tests via the Post Office Telegraph Branch Laboratories in London. In the case of television demonstrations, the video circuit is connected to the Post Office television distribution network, use being made when necessary of line-standards conversion equipment provided by the broadcasting organizations. The comprehensive network of inland communications is provided for such demonstrations and tests (Fig. 10).

#### CONCLUSION

The station will undoubtedly play a useful part in the acquisition of the information and experience needed for the design and construction of successful operational satellite communication systems. It is of interest to note that the whole of the equipment and facilities provided, including the large steerable aerial, are of British design and manufacture, with the exception of the Eimac klystron used in the Project Relay transmitter.

#### ACKNOWLEDGMENTS

The thanks of the authors are due to their colleagues in the Post Office who contributed to the planning, design, and provision of the Goonhilly satellite communication radio station, and in particular to the staff of the SW Region of the Post Office for their help in the installation phase.

Tribute is also due to the British Telecommunications Industry for its part in providing much of the electronic equipment, to the Services Electronics Research Laboratory for the development of the 5 kW travelling wave tube, and to Husband & Co. and associated contractors for the design and construction of the large steerable aerial. Special

mention should be made of the contractors' staff who worked long hours on the aerial construction, often under extremely adverse weather conditions.

The permission of the Engineer-in-Chief of the Post Office to make use of information contained in this article is gratefully acknowledged.

N67 12306

# The Goonhilly 85-ft Steerable Dish Aerial\*

C. N. KINGTON  
HUSBAND & COMPANY

and

H. E. PEARSON

POST OFFICE ENGINEERING DEPARTMENT

The choice of the basic type of aerial for a satellite communication ground station is of major importance in view of its influence on the overall performance, cost and time to complete the installation. In the case of the Post Office satellite communication earth station at Goonhilly Downs, Cornwall, a decision was made early in 1961 to use an 85-ft diameter steerable paraboloidal dish aerial, without a radome for tests with the Telstar and Relay, and other communication satellites.

Tests with smaller paraboloidal dish aerials with the feed in the aperture plane had shown that a satisfactory electrical performance could be obtained, and experience with the 250-ft diameter radio-telescope at Jodrell Bank had shown that the mechanical problems could be overcome.

An important factor in the present case was the limited time—less than one year—available for the design, manufacture, construction and testing of the aerial.

## DESIGN REQUIREMENTS

To specify for design purposes the requirements for such an aerial it is necessary to know the frequency range and aerial gain required, the feed arrangements and radiation patterns needed, the orbits of the satellites and the proposed method of tracking, the nature of the ground on which the aerial is to be built and the weather under which it must operate.

Radio waves in the spectrum 1000 to 10000 Mc/s are suitable for satellite communication and the Post Office decided for the Goonhilly aerial to limit its interest to the range up to 8000 Mc/s. In the case of

\* First published by the Institute of Electrical Engineers, November 1962.

Projects Telstar and Relay it had been decided that the critical satellite-to-ground link would operate at about 4000 Mc/s, with the ground-to-satellite link operating at about 6000 Mc/s (Telstar) and 1700 Mc/s (Relay). System study showed that an aerial gain of the order of 55 to 60 db was desirable at 4000 Mc/s and an 85-ft diameter 90° dish was chosen, giving a theoretical gain of 58 db.

By careful design of the feed unit mounted at the focus in the plane of the aperture the noise picked up on minor lobes could be minimised. As this would mean some fall-off in illumination toward the edge of the reflector the profile tolerance could be eased in the outer zone. The tolerance  $\pm\lambda/16$ , i.e.  $\pm\frac{3}{16}$  inch in this case, was applied to the central area out to 50-ft diameter, and twice this tolerance between 50-ft and 85-ft diameter. These tolerances were to be maintained under all weather conditions and angles of elevation. Combined feed units for transmitting and receiving were expected to weigh several hundred pounds, and to hold them at the focus quadrupod legs were favoured straddling the centre of the reflector, leaving it free, if desired, for later conversion to Cassegrain feed. Model tests showed that the shadow cast by four legs 90° apart and springing from the bowl on a 35-ft diameter circle would be acceptable. Two of these legs at 90° and 270° could provide direct waveguide access to apparatus cabins at the back of the bowl near its horizontal axis whilst the other two legs at 0° and 180° could carry other services.

To cater for all likely orbits (circular and elliptical) in equatorial, polar or inclined planes and to follow satellites with periods as short as two hours and heights of only a few hundred miles at perigee the aerial must provide hemispherical coverage and be able to move rapidly. For the experimental aerial the velocity and acceleration were limited to 2° per sec and 1.33°/sec<sup>2</sup> respectively, sufficient to track satellites not passing through or near the zenith. The beam-width at 4000 Mc/s, using only 0.2° at the half power points, a tracking accuracy of one-third the beam-width was called for. Steering was required to be from punched tape derived from orbital data transmitted to the Goonhilly Radio Station from the Goddard Space Flight Center. Time information would be provided by a high-precision quartz clock with the facility for checking against radio time signals.

The aerial site on Goonhilly Downs, Cornwall, is on the highest part of the Lizard peninsula with all-round freedom from obstruction above ½° elevation. According to Geological Survey Department records the whole area for at least half a mile beyond the site boundaries rests on solid rock over 1000 ft deep which forms the largest single mass of

Serpentine in Cornwall. The rock is tough, has indistinct cleavage, and is a very suitable base for reinforced concrete foundations on which to mount a precision instrument.

A study of wind records for the Lizard peninsula for the last forty years showed that although high winds peaking up to 90 mph for short periods could be expected almost annually, higher figures were most unlikely, and winds above 100 mph virtually unknown. Using a gust factor of 1.4 appropriate to the terrain it was therefore required that the aerial should have the following properties:

Be fully operational in winds up to  $55 \text{ mph}_{\text{mean}} \times 1.4 = 77 \text{ mph}_{\text{peak}}$ ;

Be structurally and mechanically suitable for working in winds up to  $65 \text{ mph}_{\text{mean}} \times 1.4 = 91 \text{ mph}_{\text{peak}}$ ;

Safely withstand winds up to  $75 \text{ mph}_{\text{mean}} \times 1.4 = 105 \text{ mph}_{\text{peak}}$ .

#### DESIGN CONSIDERATIONS

If a radome is used to protect an aerial from the weather, the aerial itself may be relatively light in construction and the drive/control requirements will be correspondingly less stringent. However, energy losses in receiving through the radome, especially when the latter is wet, may lead to a significant increase of the overall noise temperature of the receiving system. The cost of a light aerial with a radome may also be greater than that of a heavier and more stable unprotected aerial.

The alternative approach, which was adopted for the Goonhilly aerial, is to use a heavy, stiff, and stable supporting structure together with a well balanced, stiff dish to minimise deflections in high winds, driven by motors normally working well below their maximum capacity. The application of these principles has resulted in an aerial of good accuracy and radio efficiency, at relatively low cost.

So far as wind speeds are concerned the first requirement is that the aerial must be designed to survive the maximum winds it can be expected to encounter. Next consideration must be given to the maximum wind speed at which the aerial must remain fully operational, i.e. maintain accuracy of shape when moving at full speed and within the specified following accuracy. The torque required to rotate the aerial in wind is proportional to the square of the wind speed, and the driving horsepower is proportional to the product of torque and angular speed, so that size of the driving motors will increase rapidly as the "full operational speed maximum wind" requirement is raised. It was not considered necessary, at least initially, to provide drives able to con-

tinue rotating the Goonhilly aerial at full speed in winds gusting above 77 mph with the dish at the angles corresponding to maximum wind torque.

The expected satellite orbits were such that operational speeds in excess of  $2^\circ$  per second were unlikely except when a satellite passed over or nearly over the earth station zenith.

The selection of the azimuth speed required careful consideration since this speed, combined with the selected maximum operational wind speed, determines the required horsepower of the azimuth motor. The combined horsepower of the azimuth and elevation drives must also be considered with respect to the total electrical power supply to be provided. For most of the time the aerial was expected to be operating in winds considerably below the maximum and at speeds below its maximum operational speed, i.e. the drive horsepower normally required would be very much below the maximum which may be occasionally required. If the specified maximum azimuth speed or the maximum operational wind speed were higher than was strictly essential, the electrical power requirements and the capacities of the various transformers, switches, etc., would be correspondingly increased.

The azimuth speed was fixed at  $2^\circ$ /sec giving a theoretical maximum drive motor size of 75 hp. The torque/speed calculations for elevation motion, after allowing for unbalanced moving parts, gearbox losses, etc., indicated that a 100 hp drive motor was required. In practice, both elevation and azimuth drives were eventually standardised at 100 hp.

The accuracy with which the aerial can be made to follow a satellite when under automatic control depends on the following factors:

1. The accuracy, rigidity and stability of the structure as a whole and of its major component parts.
2. The accuracy with which the actual angular position in azimuth and elevation can be determined at any time.
3. The reduction to a minimum of any backlash or uncontrolled motion in the drives.
4. The achievement of a stable and accurate but fast-responding servo-control system for the drive motors.
5. The provision of reliable and accurate control signals to control the servo in accordance with the demands of the satellite orbit to be followed.

With regard to these factors, and the fact that orbital information would be available already processed into demanded azimuth and elevation angles at given times, the following basic decisions were made to enable the required following accuracy to be achieved:

The dish supporting structure would be of reinforced concrete, having a relatively high moment of inertia so as to give a steadying effect in gusty winds and high structural stability against deflections from all wind pressures.

Shaft angular position determination would be by use of 16-bit optical shaft encoders, giving a basic resolving power of 1 in 65536 (approx. 20 seconds).

The servo-control system would be of the digital type, receiving incoming demanded angle information on punched tape, comparing the demanded angle for each motion with the actual angle and finally passing an analogue error signal to the servo-system.

The results of the dependent structural, mechanical and electrical decisions emanating from the aforementioned basic decisions are detailed below.

#### GENERAL DESCRIPTION OF THE AERIAL

The general arrangement of the aerial is shown in Figs. 1 and 2, and the components are described below.

##### *The Dish*

Both the structure and the membrane plating of the dish are of steel. The membrane is in 8-gauge Corten sheet, having good corrosion resistant properties, individual plates being screwed to the supporting structure and then continuously welded to give good electrical continuity. Steel was chosen as giving the optimum combination of good strength and rigidity, and relatively low coefficient of expansion with the minimum cost.

The balancing of the dish\* is such that the natural tendency of the dish upper and lower edges to droop downwards as the dish moves from the zenith toward the horizon is automatically opposed by forces in the balance-weight supporting structure. A drainage system is provided for removal of rainwater, and snow may be removed by depressing the dish. The provision of a de-icing system for an installation in South West Cornwall was considered in view of the generally favourable weather conditions.

There are two steel cabins built into the structure behind the dish for housing radio apparatus as near to the focus as possible.

The dish is supported on a prestressed horizontal concrete beam

\* Husband & Co. Provisional Patent No. 12807/61

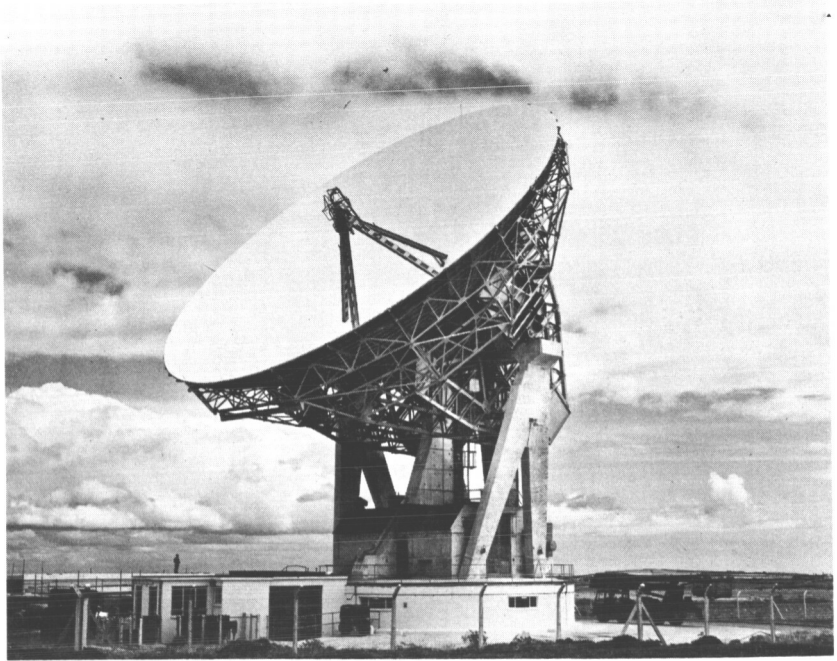


Fig. 1 — The Goonhilly aerial.

via four large split roller bearings of the self-aligning type, one of the centre pair of these being arranged to take axial thrust. The elevation optical shaft angle encoder is driven directly from the thrust bearing by an arm and pin arrangement.

#### *The Dish Supporting Structure*

The dish supporting structure comprises a horizontal concrete beam supported in turn by three reinforced concrete portal frames the outer two of which were precast and lifted into position, and the inner frame cast *in situ*. These portal frames stand on a circular reinforced concrete turntable base, which also carries a large cabin housing radio apparatus and accommodating the main cable-turning device. The latter enables connections to be made between equipment in the moving part of the structure and fixed equipment elsewhere without using slip rings. The concrete cabin is fully screened with continuous copper sheeting.

The lower fixed portion of the mount is also of reinforced concrete, taken down to the rock.

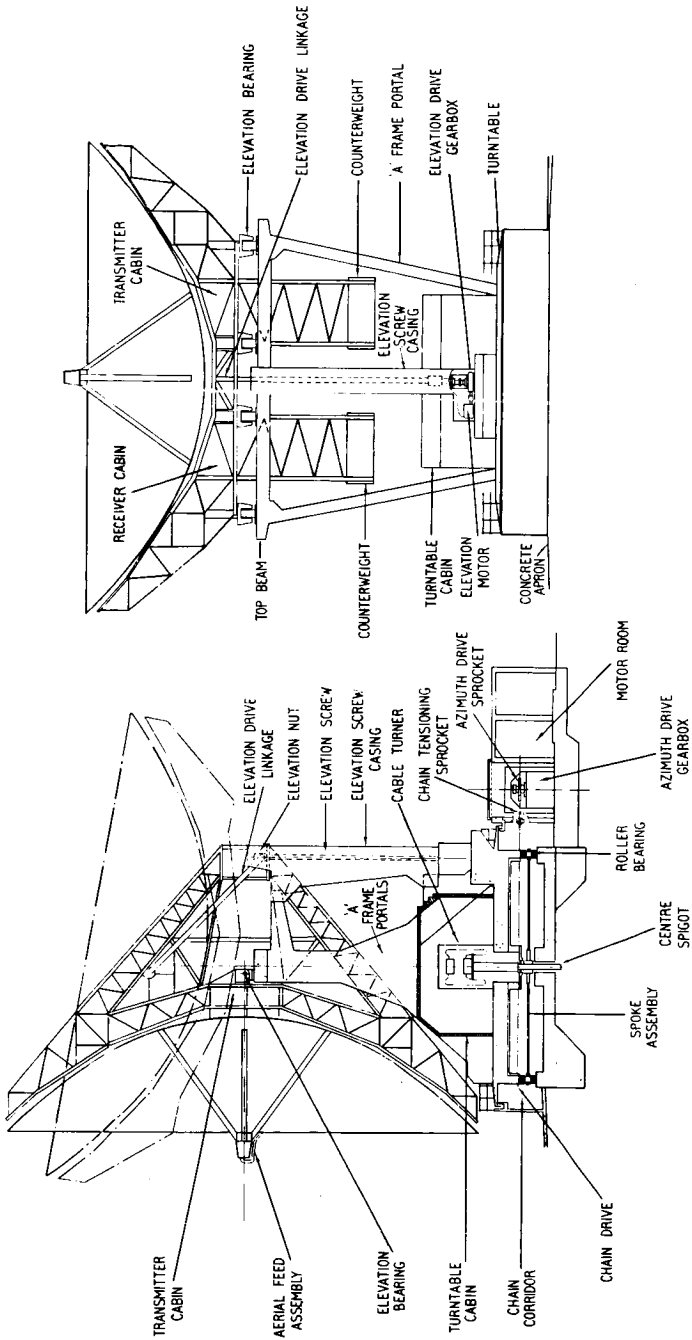


Fig. 2 — Composite sectional view of Goonhilly aerial with the bowl section at zenith.

### *Azimuth Mount*

The moving part of the azimuth mount is carried on 54 tapered rollers, running between an upper and lower track of manganese steel, the tracks being 42 ft 6 in. in diameter, preassembled and accurately machined to the correct conical taper as complete rings. The rollers are carried in a built-up circular frame held in position by 27 tubular spokes with a central hub revolving round a fixed centre pivot. The hub is carried on the centre pivot by a heavy spherical roller bearing and a second similar but larger bearing on the pivot locates the moving part of the mount about the pivot. The arc of travel in azimuth is  $\pm 250^\circ$  from true South providing a  $140^\circ$  overlap on the azimuth circle. Located vertically on the fixed centre pivot post is a rigid tubular tower structure on top of which the body of the azimuth shaft angle encoder is carried. The rotating disc of this encoder is driven from the rigid concrete roof of the turntable cabin previously mentioned. It is thus a feature of the design that both encoders are mounted with their axes on the relevant axis of rotation of the instrument and are driven directly from the axes of rotation.

The rotating part of the azimuth mount is fitted round its periphery with 46 teeth which engage with a 5 in. pitch, cranked-link roller driving chain of accuracy 0.015% on length and 140 tons breaking load. This form of drive was chosen as avoiding the use of large gear wheels or toothed racks whilst providing greater capacity for resisting transient shocks. The chain is provided with tensioning sprockets on both sides of its free length; tension can be adjusted readily by screwing the sprocket mounting blocks in or out in slides. The driving sprocket is mounted on the vertical output shaft of the final bevel gear box; heavy steel frames set in the concrete floor carry an outrigger bearing for the drive sprocket and support the tension sprocket assemblies. The moving part of the aerial, weighing approximately 900 tons, moves silently and smoothly at all speeds, less than 2 hp being required to rotate the aerial at full operational speed in conditions of no wind.

The azimuth final bevel gear box is 8 ft 6 in. high and is preceded by a triple-reduction double-helical unit. The overall reduction ratio from drive motor to aerial is 3000:1 and all couplings are of the oil-filled gear type. The chain has an automatic lubrication system, and phosphor bronze slide supports under the whole of its free length. There is also a combined automatic greasing system for the 108 spherical roller bearings in the taper rollers, the two centre pivot bearings, and for the manganese steel track surfaces.

### *Elevation Mechanical Drive*

The bowl is rocked over its 100° arc in elevation by a steel connecting rod attached to a large nut on a 4-start 10½ in. outside diameter vertical screw, 32 ft long over the screwed portion. The nut is split and has adjustment to enable backlash to be eliminated.

The screw is located inside a fabricated steel box and is carried in bearings at its upper and lower ends. The screw box is attached to the revolving part of the concrete mount and the centre concrete portal frame at its lower end, and its upper end is attached to a concrete cantilever built out at right angles to the horizontal prestressed concrete beam. The screw is driven at its lower end by a single reduction worm box, preceded by a single-reduction double-helical box; the overall reduction between motor and dish being again 3000:1. The reduction ratio of the screw, nut, and connecting rod system itself is 181.5:1. This form of elevation drive avoids the use of large gear wheels or heavy circular racks for the final drive, allows the dish to be supported by a number of bearings along the full length of the supporting structure, eliminates backlash and gives complete rigidity in the highest winds.

### *Azimuth and Elevation Electrical Drives*

The two identical 100 hp dc driving motors for azimuth and elevation are of the traction type with skew slots, fan cooling, and a tachometer generator attached to the non-driving end of the shaft. Each motor has a top speed of 1000 rpm at 480 volts, full load current of 160 amps can be continuously sustained in the stalled condition, and smooth-speed range is 720:1. The couplings between the motors and the first gearboxes also carry brake drums on each of which two solenoid operated brake shoes operate. The azimuth motor shaft is equipped with a manually operated disc brake for parking. Each of the two motors has its own separate Ward Leonard motor-generator set, mounted side by side in a house built at the side of the mount; the same enclosure houses the two azimuth gearboxes and the azimuth drive motor. The Ward Leonard room also contains the ac panel for the two sets and a dc desk for manual control of both aerial motions. One part of the Ward Leonard room has been separated off and houses the helium recovery plant and storage dewars. The room is entirely shielded with copper sheeting to all walls, roof and floor and copper gauze over the windows.

The Ward Leonard system and servo-loop are orthodox but the speed range of 720:1 is considerably greater than that normally used in this

type of plant. The servo-amplifiers and control gear are located in the main control building approximately  $\frac{1}{4}$  mile from the motor-generator sets.

### *Control System*

The digital control system is fully transistorised and there is a separate system for each motion. The aerial can be driven from the control desk either manually or under automatic control from a punched tape (Fig. 3). When under automatic control, motion commences when the tape-start time and actual time coincide. Thereafter demanded angle information read from the tape is stored, passed to an arithmetic unit and then on to the comparator unit, which also receives a statement of the actual angular position from the 16-bit optical shaft angle encoder. The difference between demanded and actual angle is ultimately converted to analogue form and fed into the servo-amplifier equipment which responds accordingly. There is also a facility whereby the differential (rate of change) of error is used to eliminate hunting and overshooting by reducing the rate at which the error is reduced as the value of the error moves towards zero.

The aerial control desk (Fig. 4) carries digital and analogue displays of actual position, a digital display of demanded position, and manual speed controls for both motions, together with drive-motor voltage and current meters. When the aerial is under automatic (tape) control the normal speed controls change their function and can be used to apply a positive or negative correction to the motion so that the actual angular position of the aerial is the selected amount in front of or behind the position demanded by the tape. The desk also carries wind-speed and direction instruments, motor start/stop controls and coloured-lamp signalling systems indicating the state of all safety interlocks of vital parts of the drive equipment. There is also a digital display of control-clock time and another of the time on the tape corresponding to the displayed demanded angles. If synchronism between clock and tape time is lost the aerial stops at the last demanded position. The control desk also carries signal-lamp systems indicating the condition of the drive brakes, drive motor fans and lubrication systems on both motions and also red warning lights indicating that the limit of travel has been reached in either direction on either motion.

In addition to lighting the red signal lamp, operation of a limit switch at the end of the arc of travel also switches off the driving power on that motion and so stops the motion. To restart, a button in a special locked cabinet must be operated, when the aerial will automatically

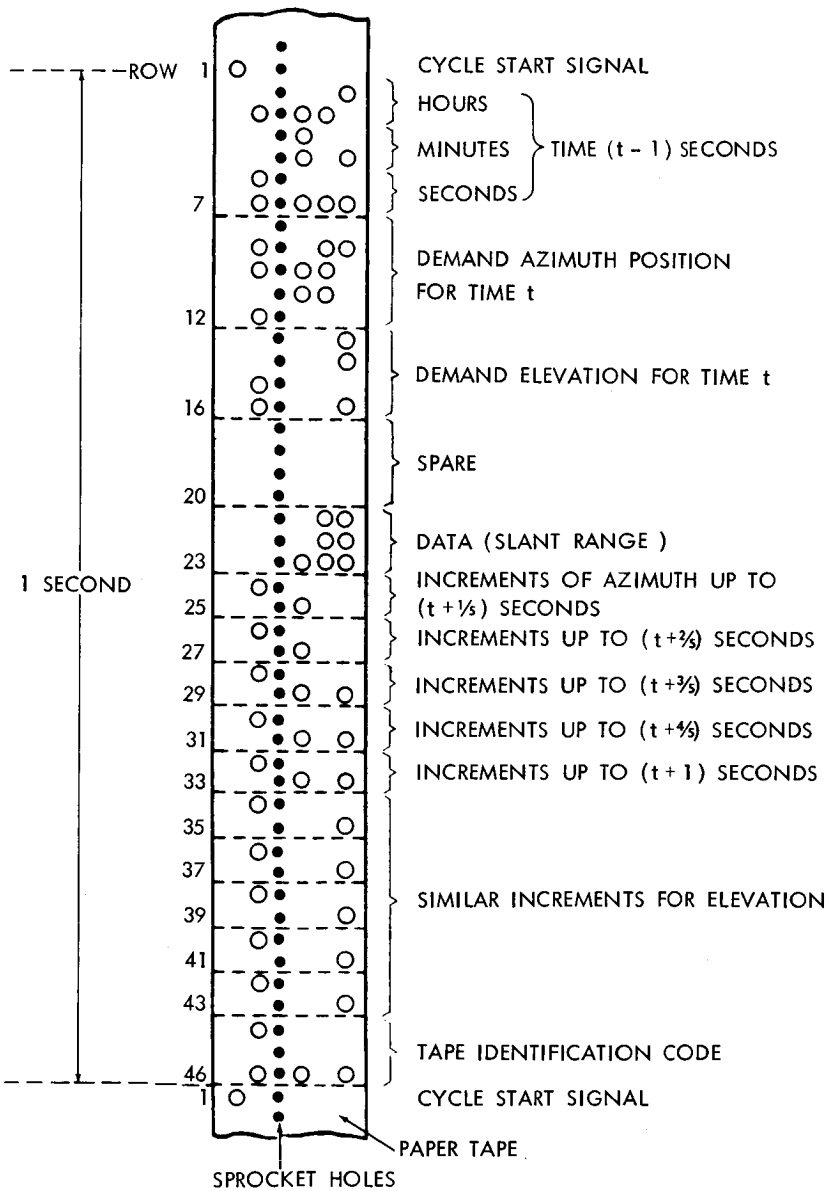


Fig. 3 — A section of control tape.

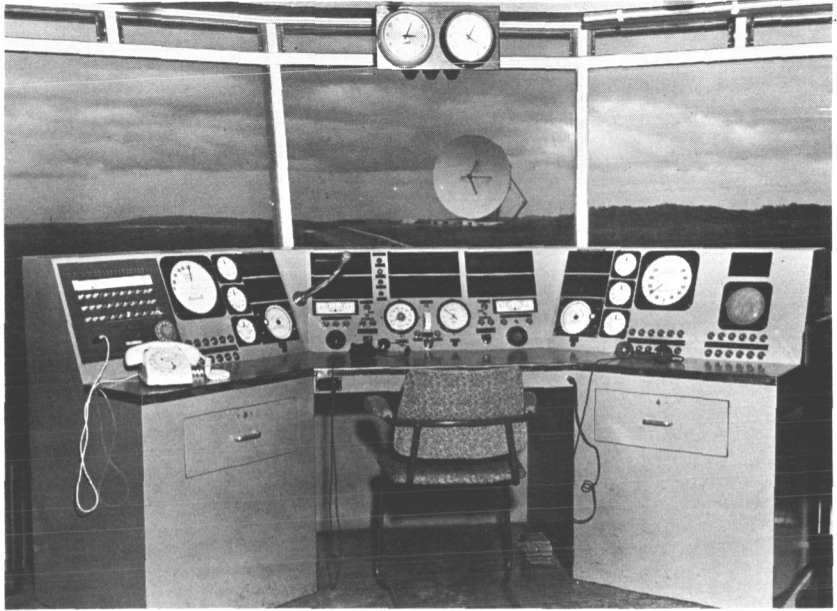


Fig. 4 — The aerial control desk.

move out a certain distance from the limit switch and then stop, after which normal driving procedure may be resumed.

#### CALIBRATION AND TESTING

Profile measurements on the completed dish were made with slip gauges against two accurate templates, one for the inner area and a second for the outer zone. About 1000 measurements were plotted on probability graph paper and showed 99% of the measurements within the tolerances specified with random distribution of error.

Before the dish was moved from its position as built with axis pointing to the zenith, an optical telescope was fitted in one of the cabins behind the dish with its axis truly vertical within 0.2 minutes. This then became the 90° reference condition for the elevation encoder. With the dish set to 60°, 45° and 0° in turn by the encoder, theodolite checks were made of the angle of the peripheral plane, and agreement obtained to  $\pm 15$  seconds.

The azimuth zero on a true South bearing, and checks of the azimuth setting accuracy were obtained by viewing known points at a 5 to 15-mile range through the telescope fitted to the dish. The true bear-

ings of those points were computed by the Ordnance Survey Department to an accuracy of better than one second.

First indications that the finished aerial would point accurately were obtained from successive transit observations through the optical telescope of Alpha Ursa Major. Smooth curves of the azimuth and elevation angles against time as this star moved across the sky showed that under calm conditions a following accuracy of the order of one minute could be expected.

When radio equipment became available for testing the aerial, the horizontal radiation diagram was obtained by measuring the incoming signal strength from a 4000 Mc/s transmission from a test site at Leswidden some 21 miles from Goonhilly. The measured beamwidth was found to be 13 minutes, compared with a theoretical value of 12 minutes, and the first side lobes were correctly spaced on either side of the main beam.

#### CONCLUSIONS

Work on site commenced on 1st June 1961, and the aerial had been tested and provisionally calibrated so that it was in full operation on the 10th July 1962. In the first eighteen months of its working life the aerial has worked satisfactorily with little attention. The British concept of a stiff dish on a sturdy mount without a radome has yielded an aerial of high performance at relatively low cost.

#### ACKNOWLEDGMENTS

Special mention should be made of the excellent cooperation between the main contractors: Messrs. Cleveland Bridge and Engineering Co. Ltd., for foundations and reinforced concrete; Messrs. Markham and Co. Ltd., for turntable and mechanical drives; The Brush Electrical Engineering Co. Ltd., for electric drives and control gear; John Brown Land Boilers Ltd., for the dish structure; and N. G. Bailey and Co. Ltd., for cabling.

The aerial was designed and construction supervised by Husband & Co., Consulting Engineers.

The permission of the Engineer-in-Chief of the Post Office to use information contained in the paper is gratefully acknowledged.

N67 12307

# Computing and Data Transmission for the Prediction Steering of the Goonhilly Satellite-Communication Aerial\*

E. C. SEAMAN and W. E. THOMPSON

POST OFFICE ENGINEERING DEPARTMENT

The Goonhilly satellite-communication aerial uses an 85-ft. diameter paraboloidal reflector with waveguide feed at the focus. The aerial is movable in azimuth and elevation, and is provided with independent feedback control systems for these two motions. During a satellite pass, the aerial must be steered so that its axis points continuously, and with high accuracy, in the direction of the satellite. Of the various possible methods of achieving this result, that based on prediction of satellite position has been adopted for the first transatlantic communication experiments using the Telstar and Relay satellites. The process by which orbital predictions originating in the USA are converted to substantially continuous real-time azimuth and elevation pointing instructions at Goonhilly is described herein.

## PLANNING CONSIDERATIONS

The following considerations influenced the planning of the system. On one hand, data on the observed position of the satellite at known times would be received at the Goddard Space Flight Center, USA from various sources, including the world-wide Minitrack network of tracking stations, and would be processed there to derive the basic parameters of the satellite orbit, from which the future position of the satellite could be predicted. On the other hand, the need at Goonhilly would be to present to the inputs of the azimuth and elevation control systems, 50 times per second throughout a satellite pass, statements of the azimuth and elevation required at each instant (the "demanded" azimuth and elevation) in digital form to the nearest  $2^{-16}$  revolution (0.33 minute of arc).

The passage from orbital elements known in advance at GSFC to angular demands in real time at Goonhilly would involve considerable computation and, at some stage in the process, transmission of data

\* First published by the Institute of Electrical Engineers, November 1962.

across the Atlantic. The computation could be begun in advance at GSFC, continued in advance at Goonhilly, and completed in real time at Goonhilly; the division of the work between these three stages was a matter for practical compromise. Advance computation at GSFC would reduce the computing load at Goonhilly (and at any other stations that might use similar data) but would increase the volume of data to be transmitted. At Goonhilly, the experimental nature of the project would make it appropriate to carry out as much of the remaining computation as possible in advance; for this purpose it would be possible to employ a general purpose computer of well established design, which could also be used part-time for other work such as the analysis of records. The results of the advance computations could be checked before the time of the satellite pass. However, the need for subsequent data storage (e.g. on punched paper tape) would set a limit here, and it would be convenient to leave some simple computing to be carried out in real time by special purpose apparatus in the aerial control equipment.

#### DESCRIPTION OF THE PROCESS

The considerations mentioned above have led to the following arrangements. At GSFC, the satellite position is predicted for intervals of one minute throughout each pass, and is expressed in topocentric Cartesian coordinates, i.e. in a rectangular coordinate system with axes in the direction East, North, and Vertical and origin at the centre of motion of the Goodhilly aerial. Predictions in this form are transmitted to Goonhilly over a transatlantic telegraph circuit, and the receiving teleprinter produces simultaneously a page print and a perforated tape (the "Predictions Tape"). The data for each minute occupy one line of the page print and are accompanied by a "sum of digits" check. The data message includes a statement of the time to which the first prediction for each pass refers, and is sent in a standard format covering not only features visible on the page print but also the incidence of all functional characters (carriage return, shifts etc.) that will be punched on the Predictions Tape. The time taken in transmission is about six seconds for each minute of a satellite pass. When the orbital elements for a particular satellite are well established, predictions can be sent once a week, to cover all the time during the ensuing week that the satellite will be above the Goonhilly horizon.

At Goonhilly, advance computations are carried out by a small general purpose computer. The Predictions Tape is used directly as

data input to the computer, and the first operation is to check the validity of the whole data message (normally covering many passes), applying the sum-of-digits check and examining the tape for errors in format. This operation is quite quick (0.13 second for each minute of pass) and is preferably concurrent with the reception of the data; if an error is detected, all the data for the pass affected are transmitted again.

For those parts of selected passes that are to be used for communication experiments, a further run on the computer, with the Predictions Tape as data input, calculates and prints azimuth, elevation and range for one-minute intervals. This run takes 1.2 seconds of computer time for each minute of pass. The print is useful to show the general nature of each pass. Specifically, it enables the operator to make a decision that is needed because the aerial is not designed to rotate continuously in azimuth, but has a range of movement limited to 500 degrees, so that over a range of 140 degrees any direction has two alternative numerical values; therefore two sets of azimuth values are printed and if one set shows a discontinuity the other must be selected. This decision accompanies the input data to the computer for the next operation.

The next stage represents the main computing operation undertaken at Goonhilly, and comprises the preparation by the computer of a punched paper tape — the "Control Tape" — bearing detailed azimuth and elevation data for the passes of interest. The Predictions Tape again constitutes the data input to the computer. Working in the rectangular coordinate system, fifth-order interpolation is used to derive values for one-second intervals from the one-minute data received from GSFC. Azimuth and elevation are then deduced for the one-second intervals. Finally, second-order interpolation is used to obtain the full details required on the Control Tape, (Appendix 1) and the tape is punched.

The computer programme is so arranged that corrections whose values are predictable can be applied to the calculated quantities in the course of this operation. An obvious need is for a correction in elevation to take account of the effect of atmospheric refraction; this correction is based on prior knowledge and has been included from the outset. If operational experience brings to light any systematic departure of the electrical axis of the aerial from its mechanical axis\* suitable corrections can be added later.

---

\* In this context, the term *mechanical axis* means the direction defined by the readings of the shaft-angle encoders that measure the *actual* position of the aerial.

bits, these sub-routines could be replaced by less precise, and consequently faster, versions.

#### ACKNOWLEDGMENTS

The National Aeronautics and Space Administration evolved the scheme for the telegraphic transmission of data, and have supplied the remarkable accurate predictions on which the steering of the Goonhilly aerial has been based.

## APPENDIX 1

## DETAILS OF CONTROL TAPE

The ultimate requirement is to present to the inputs of the azimuth and elevation control systems of the aerial, in real time 50 times per second, a complete statement of the demanded azimuth and elevation in digital form to the nearest  $2^{-16}$  revolution. This represents 17 bits for azimuth (the range of azimuth motion being 500 degrees = 1.39 revolution) and 15 bits for elevation (100 degrees = 0.28 revolution). It is impracticable to store all these data on punched paper tape, and incremental operation must be adopted.

Suppose that, to describe the demanded azimuth (or elevation), a single incremental value is specified and that this is added to an accumulated number every  $1/50$  second. The result, assuming that the  $1/50$  second discontinuities are smoothed, will be a quantity increasing linearly with time, representing a demand for a constant angular velocity. A real demand, in which the velocity will not in general be constant, can be approximated by changing the value of the increment from time to time; the real curve of angular position as a function of time will then be approximated by a series of chords. The process is analogous to linear interpolation between given values in a mathematical table, and it can be shown that the maximum error that could be incurred (i.e. the maximum possible departure of the chord from the true curve) is given by

$$e = \frac{1}{8} (aT^2),$$

where  $T$  is the time-interval over which a constant increment is added repeatedly,  $a$  the maximum acceleration during this interval, and  $e$  the upper limit to error during this interval.

The solution adopted is to prescribe increments on the tape for intervals of  $1/5$  second, so that any one increment is added 10 times. The formula shows that the error will not exceed 0.4 minute of arc at the maximum acceleration assumed in the structural design of the aerial (1.33 degrees per second per second).

Such increments of azimuth and elevation constitute the main content of the Control Tape. However, a complete specification of demanded azimuth and elevation is essential at the beginning of an automatic run, and is very desirable at intervals afterwards, so that any casual error may not be perpetuated. The complete demanded azimuth and elevation are therefore punched on the tape for intervals of one second. This has the desirable result that the concept of a spe-

cific "starting" condition is avoided; automatic control can begin at any desired time (within about one second) during the period for which a Control Tape has been prepared. The scheme lends itself to a one-second cycle in the punching of the Control Tape and the operation of the digital part of the aerial control equipment.

A 5-track tape is employed; four of the tracks are used for numerical data, the fifth being reserved for a signal indicating the beginning of each one-second cycle. The complete punching scheme for one cycle is shown in Table 1.

TABLE I — PUNCHING OF CONTROL TAPE

Item	Number of rows
Cycle-start signal	1
Time (hr, min, sec)	6
Demanded azimuth	5
Demanded elevation	4
Slant range	3
Five increments of azimuth	10
Five increments of elevation	10
Tape code	3

## APPENDIX 2

## CHECKING OF CONTROL TAPE

The programme which checks a Control Tape determines that:

1. Cycle-start signals appear as prescribed
2. Time, azimuth, elevation, and tape code are within appropriate limits; e.g. the hours in a time must be less than 24, and the minutes and seconds less than 60. For azimuth and elevation this check is applied not only to the completely punched values but also to those that will subsequently be formed in the aerial control system by adding the increments.
3. Time, azimuth, and elevation are continuous: i.e. each time is one second later than the previous time; and each azimuth (or elevation) agrees with that formed by summing the azimuth (or elevation) value and increments of the previous second, due allowance being made for the effects for rounding-off in calculation.

N67 12308

# Digital Techniques Used in the Steering Apparatus of the GPO Steerable Aerial at Goonhilly Downs\*

J. E. MARSHALL, R. J. COULTER, J. K. BINKS,  
K. J. CLARKE, T. STEVENAGE, and G. E. WILLETTS

HAWKER SIDDELEY DYNAMICS LIMITED INDUSTRIAL ELECTRONICS

*A description of the logic design for the digital control equipment is followed by further descriptions of items of particular interest. The means of applying off-sets to the demanded aerial position for overcoming possible inaccuracy of the predicted orbit; and to demand accurately determined velocities manually; means of conversion from pure binary form to provide displays in terms of angles, and the derivation of analogue voltages for the servo-amplifiers are discussed in detail.*

*A critical analysis of the equipment in the light of operational experience concludes the paper.*

AUTHOR

The prime function of the digital control apparatus was to position the steerable aerial in both azimuth and elevation axes in response to information on a punched tape. Due to the need for efficient use of the tape a system of linear interpolation over 200 millisecond intervals was used. The digital equipment performed the interpolation process and calculated the angular position error signal fifty times per second. Actual positions were determined by an optical Gray Code shaft encoder, suitably decoded, and applied to the error arithmetic unit.

Displays were provided showing aerial position, the angle demanded by the tape, control clock time, and the angular corrections which might prove necessary to cancel out inaccuracies of the predicted trajectory. The other requirements of the digital apparatus were to provide accurate velocity signals, set manually, and to produce punched paper tape records of aerial performance. Further signals, concerned

\* First published by the Institute of Electrical Engineers, November 1962.

with the GPO communication equipment, were recorded on the same tape via a digital data logger.

#### SYSTEM DESIGN

##### *Design Parameters*

The following parameters were given:

1. A sample rate of fifty times per second.
2. Accuracy of digital equipment from tape reader to error better than two minutes of arc.
3. A ten volt range in analogue voltages corresponding to  $\pm 42$  minutes of arc error.
4. A standard frequency source of 2 kilocycles per second.
5. Tape information.

Items 1, 2, and 3 were determined by the servo design. Item 4 was a GPO standard. Item 5 will now be discussed in greater detail.

##### *Control Tape Information*

The tape information is given in cycles of a second duration. The demanded azimuth and elevation angles are stated in full form once per second.

Increments to be used for linear interpolation are stated in the following form: each increment corresponds to one tenth of the change in position over 200 milliseconds. There are five such increments for each axis. Each increment is used ten times, making—in all—fifty calculations per second of demanded angle, for each axis.

As the information is renewed once per second any errors occurring in the arithmetic can not endure longer than part of a second. A code identifying the tape is stated once per second. Information corresponding to the aerial gain appropriate to the range of the satellite is given once per second.

Standard resistor-transistor printed circuit logic elements are used throughout. This paper is concerned with the use of logic elements—the electronic design of each element used principles treated in detail in the literature.

##### *Waveform Generation*

It is convenient to use the standard 2 kilocycle signal to define the digit periods directly. The waveforms are derived by division of the 2 waveform, and subsequent groupings using AND gates (Fig. 1).

Each digit period is divided into four non-contiguous phases. The

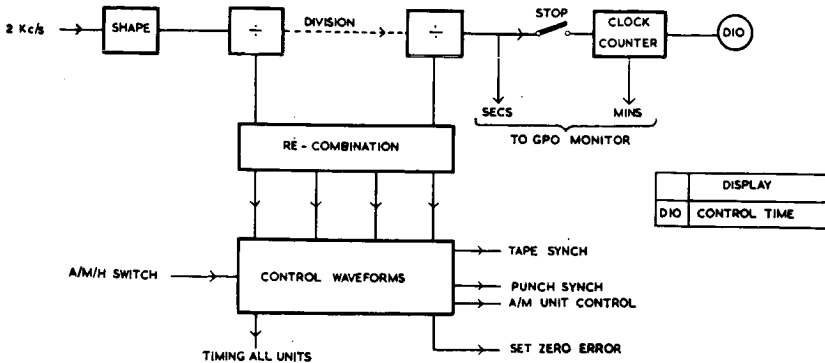


Fig. 1 — Control diagram.

phase waveforms are used as strobes to avoid spurious spikes caused by the AND operation on adjacent edges—this is an established technique.

### Operational Mode

In order to obtain the greatest reliability pure binary serial arithmetic is used for the interpolation and error calculation. The use of serial arithmetic requires serial to parallel conversion for error and tape punching. This is accomplished by the use of shift-registers. The only parallel conversion occurs in the Gray to Binary Conversion of the actual position transducers. Simple serial decoding would result in the most significant digit being produced first in time which is inconvenient for the subsequent arithmetic operations.

### Peripheral Equipment

Logic design for tape reading and tape punching are well established, and will not be treated here in detail. The decoding techniques for the mechanical encoders used for correction and velocity increments is described in detail later.

### Accuracy

The accuracy of two minutes of arc of the digital system is made up of several parts.

1. The accuracy of the shaft encoder.
2. Rounding errors in the arithmetic.
3. Drift in the digital to analogue converter.

The order of 1 and 2 are approximately the quantum step chosen and 3 can be improved by technique. The choice of a 16 bit system; i.e., 216 quanta equivalent to  $360^\circ$  of arc gives a quantum size of 19.77 seconds of arc. This value enables the design figure of 2 minutes to be improved upon under normal circumstances, and leaves error in hand, so to speak, for the rest of the control design.

For accurate interpolation it was necessary to specify the incremental information on the control tape to  $2^{-20} \times 360^\circ$ , the difference in accuracy of the resultant demanded angle and the 16 bit accuracy of actual position is referred to above as rounding error.

#### SYSTEM DIAGRAM

The final realisation of the requirements is shown in Fig. 2. The functions of each black box will be described briefly and the more interesting aspects will be treated in detail.

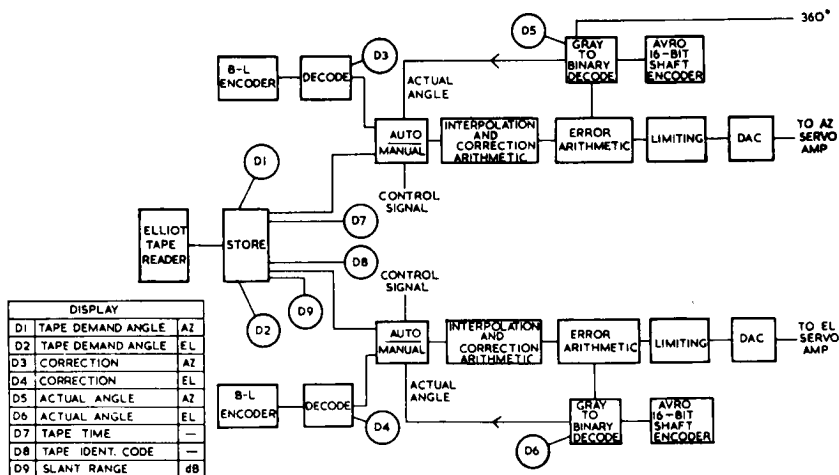


Fig. 2 — System diagram.

#### Tape Reading

The control tape advances one cycle once per second in response to a control signal. This control signal occurs only when the following conditions apply.

When there is coincidence between the control clock and the last time read from the control tape.

When switching from manual to automatic operation so that the store can be "primed" with sensible information.

After the absence of one time coincidence to prevent the reader stopping in the event of a single misread or mispunch. (This is extremely rare of course).

### *Tape Store*

The data from the tape-reader occurs in sets of four parallel digits, the other track of the five track tape being used for synchronisation. Each set of digits is routed, using gating logic derived from counting rows, into an appropriate store.

### *Correction Logic*

A mechanical encoder with a control knob on its input shaft at the control desk is used to derive parallel signals to be used for correction when on AUTOMATIC control. The same parallel signals are used as increments of position for MANUAL control. The mechanical shaft encoder outputs are in coded form to minimise ambiguity of readout. A decode unit converts to parallel signals representing signal and magnitude.

### *Auto/Manual Unit*

The auto/manual unit selects inputs to the arithmetic unit appropriate to the control mode.

On automatic mode the following operations are performed:

From the store are transferred demanded angle at 1 second intervals and increments at appropriate times to the arithmetic units.

From the correction logic the parallel signals are transferred fifty times per second in serial form to the correction arithmetic.

On manual mode the sequence is:

On first switching use actual angle as initial demanded angle.

Use the correction signal as an increment to be added fifty times per second—this will give rise to a uniform velocity; in order to maintain smooth minimum velocity the significance of the parallel digits is reduced by a factor of  $2^{-7}$ .

### *Interpolation and Correction Arithmetic*

The interpolation arithmetic performs the function of adding each tape demanded increment ten times to the accumulated angle. The value of the increment is renewed five times per second. On manual

control the increment remains at a constant value until the encoder shaft at the desk is turned. To avoid ambiguity due to sampling the parallel output while rotating the shaft, a 50 microsecond sampling interval is used.

While the correction signals are used for manual velocity setting their use as corrections as used on "auto" are inhibited.

#### *Error Arithmetic*

The difference between the actual and corrected accumulated angles is calculated in the error arithmetic. Negative errors are prefixed by a bar digit.

#### *Limiting*

As the range of errors is small compared with a full revolution the digital input to the DAC (Digital to Analogue Conversion) is limited. In the event of a large error the appropriate end limit of the DAC is demanded. This enables the DAC to have a sensible dynamic range.

#### *Digital to Analogue Conversion*

The limited parallel digit signal is transferred 50 times per second into the DAC and a signal of  $\pm 5$  volts about a  $+5.0$  volts level is produced. This is appropriate to an error range of  $\pm 42$  minutes or approximately ( $\pm 128$  quanta).

#### *Shaft Encoders*

Avro Sixteen-bit gray-code shaft coders are connected to each axis. These encoders have their own amplifiers which apply signals to the coaxial lines from the aerial site to the steering apparatus room. As the azimuth motion exceeds  $360^\circ$  a signal indicating positive rotation beyond due south is derived from a trip switch. This signal is combined logically with the  $180^\circ$  encoder track signal to produce the digit of significance  $360^\circ \times 2^\circ$  when a full rotation has taken place. This digit is referred to as the 17th bit.

#### *Gray to Binary Decoder*

The gray to binary decoder converts the sixteen parallel digits from the encoder to pure binary form and adds on the 17th bit where appropriate.

On elevation of course the  $180^\circ$  track would not normally be used as the maximum rotation is only  $100^\circ$  of arc, but for reasons of com-

patibility the full information is used. The azimuth and elevation channels are made as identical as possible to make testing and fault finding straight forward.

### *Displays*

The displays shown on the diagram are situated on the control desk with the exception of the slant-range db display which is on the beam swingers console. The derivation of all desk displays is considered in detail later. The slant range display is derived from an accurate dc voltage produced by a digital to analogue converter.

### CONTROL TAPE READING SCHEME

The control techniques for operating the Elliott high speed tape reader have been described elsewhere. A buffer tape reader was used in order to maintain a loop at the input to the high speed reader. This prevents snatching of the tape by the high speed reader which would give rise to reading errors.

### RECORD TAPE PUNCHING

The information to be punched once per second is as follows:

1. Time in hours, minutes, and seconds;
2. Demanded angles at start of second;
3. Error in full form at start of second;
4. Tape identity code;
5. Applied correction; and
6. Data derived from the data logger.

Items 1 and 2 endure for a second and need not be stored again. Items 3, 4 and 5 occur for less than one fiftieth of a second and are stored. The data logger information is held in a store until punching has occurred.

The punch drive scheme was the one recommended by the manufacturer.

The record punch was used on manual operation; also this enabled a check of the equipment to be made conveniently.

### LOGIC TECHNIQUES

Much of the logic design uses well established techniques. While no novelty is claimed for the items which are now described, it was

considered that they are sufficiently interesting to be described in further detail.

### *Design of Interpolation and Error Arithmetic*

With reference to Fig. 3 it will be seen that the demanded angle accumulator is a 24-bit shift register. The most significant digit is the one referred to as the 17th bit, the next 16 in significance are the digits appropriate to the 16 working bits, and the remaining digits are necessary to prevent coarseness of demanded angle after the addition of several increments.

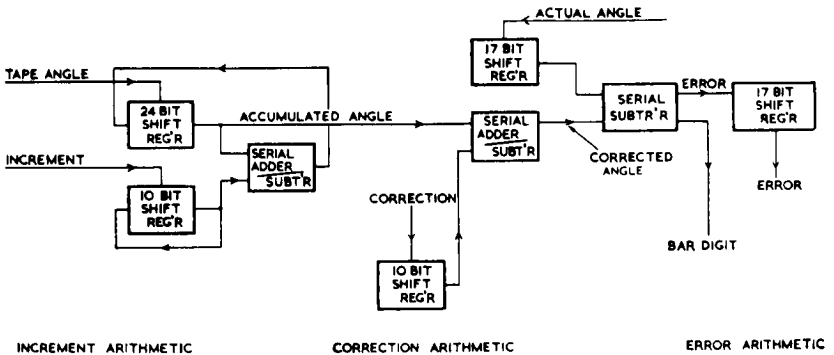


Fig. 3 — Arithmetic scheme.

The 10-bit shift register recirculates to preserve the increment value for succeeding additions. The result of adding or subtracting increments to the demanded angle via the add-subtract unit is recirculated into the 24-bit accumulator. The serial accumulated angle has added to it the correction which has been converted to serial form in the shift register shown. The resultant angle is the complete demanded angle.

The actual angle serialised after the Gray to Binary conversion is subtracted from the demanded angle in a subtractor and the result stored in a 17-bit shift register and used in parallel for the digital to analogue conversion.

Logic (not shown in the diagram) inspects the magnitude of the 17-bit number stored in the shift register. If it is less than  $\pm 128$  quanta digital-to-analogue conversion takes place and produces an error analogue for normal control of the aerial. If the value exceeds  $\pm 128$  quanta but is less than  $\pm 256$  quanta limiting occurs in the

DAC as described above. If the value exceeds  $\pm 256$  quanta protective logic causes the aerial to ignore this gross error condition and to coast for one or two seconds after which emergency stopping action is initiated if the gross error still persists.

*Techniques for Generating a Parallel ten-bit Bi-polar Number*

As it is impossible to predict the trajectory of a satellite, during the initial orbits, to great accuracy it was necessary to enable corrections to be made to the predicted angles on the control tape.

Any errors in the predicted time of arrival can be corrected in advance the actual launch time then being known, by advancing or retarding the control lock by means of switches on the control desk as shown in the control logic diagram Fig. 1.

The correction signal is generated digitally in terms of sign and magnitude for the following reasons: convenience of calculation in the arithmetic, and convenience of display generation.

The two shaft encoders for each motion consisted of an 8 bit gray fine-encoder and a binary encoder which had lagging and leading contacts to overcome ambiguity of read-out due to the gear-box between the encoders. The fine encoders were driven by hand control knobs, one for each motion, on the control desk (Fig. 4).

The encoders were capable of generating a 12-bit parallel number. The 10 least significant tracks were used for the ten digit number and the most significant track for sign. The other track was not used, but was an alternative sign track should it be needed.

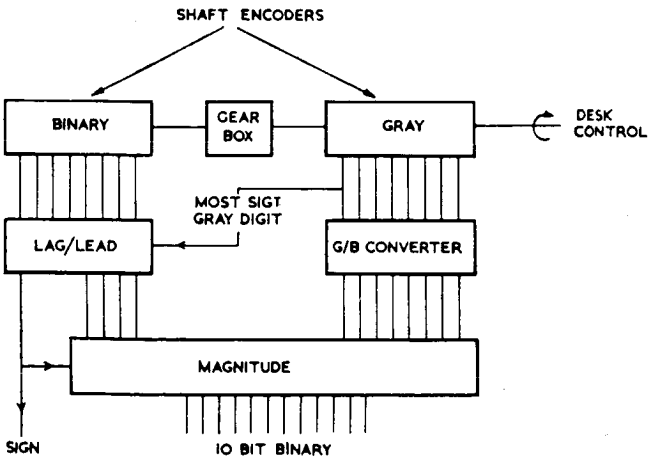


Fig. 4 — Binary code converter.

In this form, of course, negative numbers will not be correctly represented, but by inverting the ten least significant digits when the first track indicates a negative sign (0 for negative, 1 for positive, say) it is possible to approximate to negative numbers, the inaccuracy being one quantum. However, there is an advantage in retaining the accuracy of negative magnitudes in this form as the representation of zero is now two quanta wide. This is convenient as it allows the zero correction to be set more readily. This is also important on manual control where the 10-bit number is used, with the significance of the digits reduced, to produce a velocity signal by accumulation of equal increments. It enables zero velocity to be obtained and held with greater reliability.

As the display of correction was to the nearest minute it was necessary to provide an additional indication of true zero. This was achieved by surrounding the display "zero" with a "green-field".

#### *Means of Obtaining Displays*

##### Elevation and Azimuth Applied Correction Display

The display logic converts two 10-digit binary numbers into degrees and minutes. Angles up to a maximum of 5 degrees are converted and displayed at intervals of 0.5 second. A simplified diagram of the system is shown in Fig. 5.

##### System Outline

A negative pulse sets the binary counter B and the degree and minute counter D to zero and at the same time a positive pulse puts the input binary number into stores S1. A start pulse sets the binary output F to "1" allowing 4 Kc/s pulses to pass through the gate G into the binary counter B and through M into the degree and minute counter D.

When a binary number counted in B and the input binary number stored in S1 are identical, the output from the coincidence logic C becomes "0" resetting the binary output F to "0". This inhibits the input gate G preventing any further count. A positive pulse transfers the completed count in the degree and minute counter D to the stores S2 leaving the system free to make the next conversion. During the next conversion the angle stored in 4, 2, 2, 1 code in S2 is decoded by amplifiers A and displayed as illuminated figures.

The binary to minute conversion is obtained by running counter D slightly less than three times slower than counter B. The minute converter M gives an output minute pulse for every three input pulses except for the 10th minute pulse and every subsequent 29th minute pulse which require four input pulses each.

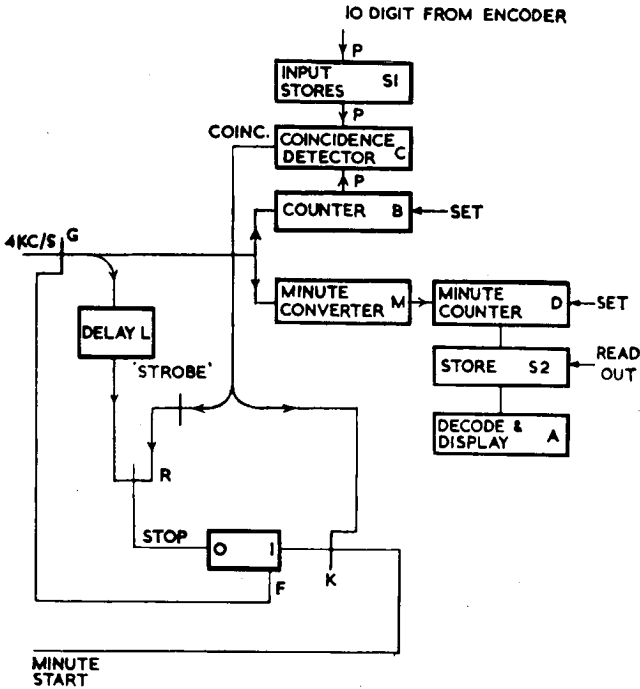


Fig. 5 — Display logic for azimuth and elevation correction.

In the special case of zero binary input the coincidence logic output would be "0" as soon as B had been set to zero. This would not prevent F from going to "12" and a maximum count being obtained. To avoid this the "0" on the coincidence logic is used to prevent the starting pulse from passing through gate K. The edges of the square waves applied to the coincidence logic C from the binary counter B have finite rise and fall times. Because of this there is the possibility that spurious coincidences could occur at the edges of these waveforms. These momentary coincidences would result in negative spikes from the coincidence logic C.

The spikes are prevented from passing through the gate R by strobe pulses which are obtained by delaying the 4 Kc/s pulses at L. The delay time is cut such that strobe pulses are at "0" whenever a spike is present.

When the display reads  $0^{\circ} 0'$  the correction signal may be one or two binary digits causing a slow drift on manual control. The outputs of the three zero amplifiers and the zero outputs of the stores for the

two least significant input digits are connected to a 3 gate. When all the inputs to the gate are 1, the output is a 0; this inhibits the sign amplifiers and gives a 1 on the input to an amplifier whose output is connected to the display. This gives a green field in place of the + or - sign on the display indicating that the manual correction is at true zero.

#### Elevation Readout

The elevation logic converts a 15 digit binary number into degrees and minutes up to a maximum of 100 degrees. The conversion is repeated at one second intervals.

The conversion is done in two stages:

1. The four most significant binary digits are counted; each unit representing an angle of 11 degrees 15 minutes.
2. The remaining 11 binary digits are converted using the method described under Applied Correction Readout. A simplified diagram of the system is shown in Fig. 6.

#### System Outline

A positive pulse puts the binary input number into stores S1, S2 and at the same time a negative pulse sets the counters B1, B2, M and D to zero. A positive pulse starts the degree counter which for each single pulse into B2, counts 11 pulses into D via "or" gate B, and 15 pulses into M via "or" gate A.

When 60 minute pulses have been counted in M the degree pulse carried over to D is delayed at L1 to prevent it reaching the "or" gate B at the same time as one of the degree pulses from the degree counter. When the binary number counted in B2 is identical to the number stored in S2 the output from the coincidence logic C2 becomes a "0" stopping the degree counter.

Sufficient time is allowed for a full count of 15 in B2 if necessary. A negative pulse starts the minute converter which counts out the remaining 11 binary digits. The minute pulses pass the "or" gate A into minute counter M. After sufficient time has been allowed to complete the conversion a positive pulse stores the count in S3 and S4. The angles stored in 4, 2, 2, 1 code in S3 and S4 are decoded by amplifiers A and displayed by digilites.

The degree output from S4 is taken in 4, 2, 2, 1 code to a digital-analogue converter which drives a meter display.

When M is set to zero a delayed pulse is set up in L. This set is prevented from passing into D by inhibiting the gate G with the set pulse. The set pulse is of longer duration than the delayed pulse.

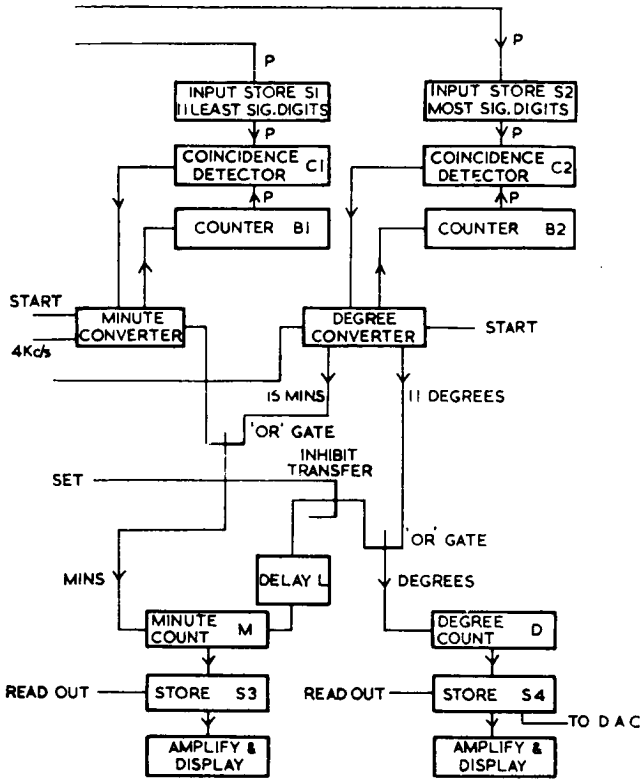


Fig. 6—Display logic for demanded and actual elevation.

When coincidence occurs this prevents any further count. The degree and minute counters  $M$  and  $D$  will then contain a multiple of the angle 11 degrees 15 minutes. The minute converter is described under Applied Correction Readout.

#### Azimuth Readout Tape Demanded and Actual

The azimuth readout converts a 17 digit binary number into degrees and minutes. The angle is displayed in the range  $\pm 250$  degrees at one second intervals.

The conversion is done in three stages:

1. The binary number 01011000111000111 (250 degrees) is subtracted from the input binary number.
2. The first most significant binary digits are counted, each unit representing 11 degrees 15 minutes, as described under Elevation Readout.

3. The remaining 11 binary digits are converted using the method described under applied Correction Readout.

The last two stages in the conversion are identical to the elevation readout except for the added digit, the subtractor unit and the replacement of the input stores by a shift-register. A simplified diagram of the system is shown in Fig. 7.

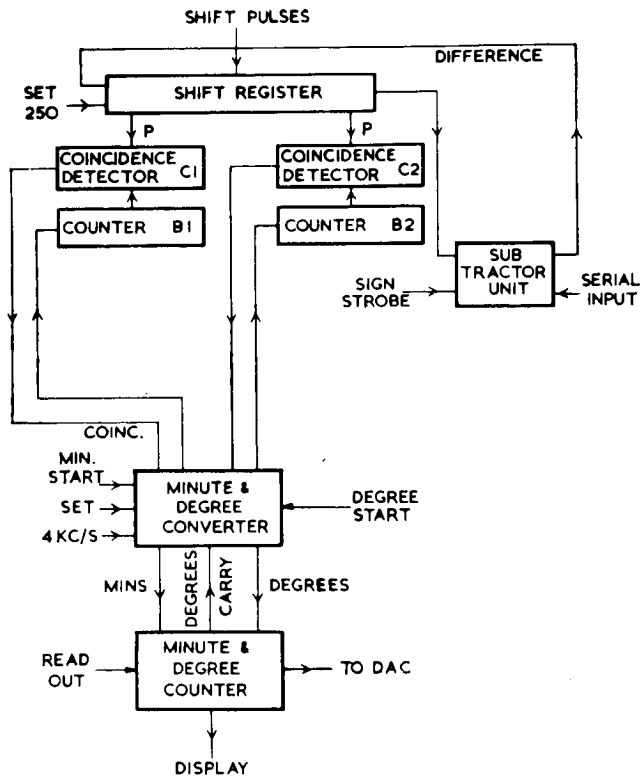


Fig. 7 — Display logic for demanded and actual azimuth.

### System Outline

The binary number to be subtracted (250 degrees) is set in the shift register  $H$ . This number and serial input are then shifted into the subtractor unit, and the differences replaced in  $H$  as it becomes vacated.

When the serial input is greater than 250 the difference (0–250) is positive and is stored in  $H$ . The sign from the subtractor is positive.

When the serial input 0 is less than 250 the difference (0-250) is negative. This is recirculated into the subtractor unit and subtracted from the input which is held at zero. The new difference (250-0) is positive and stored in  $H$  for the rest of the second.

The binary number in  $H$  is converted into degrees and minutes as described under Elevation Readout.

### *Digital to Analogue Conversion Techniques*

The error voltage to be applied to the input of the servoamplifier is in the range 0 to 10 volts, 5 volts representing zero error. This voltage is derived from the output of a summing amplifier of better than 0.1% linearity and drift, which is enclosed in a small constant temperature enclosure—a modular. The input currents to the summing amplifier are derived from a precision voltage source, and precision resistors, also enclosed in the temperature controlled oven. Parallel Transistor switches, with saturated collector-emitter voltages of the digits matches, are driven from stores into which have been transferred the parallel representation of the error. The representation of the error is in bar notation; i.e. the sign digit has significance similar to bar 1, etc. of the familiar logarithm table notation. The error has been generated in this form as it simplifies unipolar switching. In the absence of a bar-digit an input current appropriate to half-scale deflection is applied. In the absence of the least significant digits this is equivalent to zero error.

Full scale positive is produced by energising all switches, full scale negative by all switches being open.

### OPERATIONAL EXPERIENCE

A critical analysis of the design of the digital equipment in the light of operational experience would perhaps best be made by others but the following points are worth making.

Re-organisation of tape-format and the need for linear interpolation over 200 millisecond periods could well be investigated further when a full analysis of all likely orbits is made. This would enable longer periods of tape operation and would reduce storage and simplify the logic.

Control under manual operation could be improved by resetting the demanded accumulator angle to the actual angle once per second. This would prevent an occasional gross error from being perpetuated on manual control.

There is insufficient data yet for prediction of future reliability of the digital equipment but the incidence of reading errors and inaccuracies from other sources is extremely low and augurs well for the future.

It is extremely difficult to design digital compensation networks unless the servo parameters are accurately known. Now that the mechanical parameters are well defined it is thought that digital compensation techniques are worthy of further consideration.

#### CONCLUSIONS

The digital steering apparatus installed at the G.P.O. Radio Station has been described and discussed in detail where it was thought appropriate. This was an example of a digital and analogue servo mechanism of the type where the sample rate was high compared to the bandwidth of the control system. The design of the apparatus was extremely interesting not only for its obvious technical and national interest but for the stimulation it gave to further investigation into the digital control field.

#### ACKNOWLEDGMENTS

The work which this paper described was performed under sub-contract to the Brush Electrical Engineering Co. Ltd.

We acknowledge with gratitude the help of our colleagues at Hawker Siddeley Dynamics, those associated with the project at Brush Electrical Engineering Company, and the GPO W.S. Branch and Goonhilly Site personnel of the GPO and the encouragement of Mr. C. N. Kington of Husband & Company.

# Beam-Swinging Facilities for the Goonhilly Satellite-Communication Aerial\*

C. F. DAVIDSON and W. A. RAWLINSON

POST OFFICE ENGINEERING DEPARTMENT

The mode of satellite tracking adopted at the Goonhilly earth station is to steer the aerial primarily by means of predicted data computed from the satellite orbital parameters and to superimpose, during the passage of the satellite, corrections to remove any prediction errors or aberrations due the transmission path. Predictions have proved to be highly accurate for satellites having a high mass to projected area ratio orbiting at altitudes at which air drag is very small; hence the corrections are small and infrequent.

## SYSTEM DESIGN

Aberrations in the predicted steering data are likely to be greatest during the acquisition phase when the aerial elevation is near zero and when, in consequence, tropospheric ray bending is greatest. It was assessed initially that a beam swing of  $1^\circ$  in all directions from the boresight axis would adequately meet the most extreme condition, i.e. at the time of the earliest satellite passes and prior to refinement of the orbital parameters. Provision was therefore made in the original design for a swing of  $1^\circ$  but experience proved this to be in excess of requirement and it was subsequently reduced to  $\frac{1}{2}^\circ$ . The corresponding shift in the position of the feed unit in the focal plane of an 85-ft focal-plane paraboloid is 3 in.

A beam deviation of  $\frac{1}{2}^\circ$  is equivalent to  $2\frac{1}{2}$  beamwidths (3 db) at the frequency 4080 Mc/s, at which tracking of the Telstar and Relay satellites is performed. At this deviation a degradation in aerial gain of about 2 db is incurred and some beam distortion is present in the form of a coma lobe on the boresight-axis side of the beam. It was envisaged, therefore, that corrections to the predicted steering data

\* First published by the Institute of Electrical Engineers, November 1962.

would be needed, at least in the initial phase of a satellite pass, to ensure that large beam offsets were removed.

The feed-shift mechanism at the aerial focus, by which the beam is offset from the axis, is controlled through a hydroelectric servo system from a console in a control room about  $\frac{1}{4}$  mile from the aerial. This form of control has the advantages, as compared with an all-electric system, of lower weight at the focus, a safer stalling condition, and the removal of most of the moving parts requiring maintenance to positions where they are more easily reached.

After approximate acquisition, the deviations of the satellite from the predicted course are followed by means of a conventional radar mode of tracking. No satisfactory adaptation of the static-split feed (monopulse) system is obvious when diplexed signals with circular polarization are utilized in a focal-plane dish. A conical-scan feed system is therefore used. The requirements, however, are notably different from those common to radar applications in which pulsed signals are generally received from a target whose course is likely to be erratic and evasive. In contrast, the course of a satellite is closely predictable and smooth and the target is a cw beacon on the satellite itself. A slow-speed scan in which the beam rotates about a point 1 db or less from the peak is therefore adequate. A slow speed is essential also to minimize the centrifugal forces encountered in spinning a heavy diplexed feed. The scanning speed is adjustable to avoid synchronism or harmonic relationship with the ripples in the aerial-radiation pattern of a spin-stabilized satellite.

The optimum offset of the rotating beam about the boresight axis depends on the sensitivity of the display equipment and on the allowable loss from the peak gain of the aerial. The latter is of particular importance when, as in Project Telstar, the ground transmit frequency in the diplexed signal is higher than the receive frequency. The trans-

TABLE I — EFFECT OF FEED OFFSET IN AN 85-FT FOCAL-PLANE PARABOLOID

Beam Offset (Degrees)	Feed Offset (in.)	Beacon Signal Loss (db)	Transmit Loss	
			Telstar (db)	Relay (db)
0.061	0.36	1.0	2.5	0.25
0.041	0.24	0.5	1.25	0.12
0.027	0.16	0.25	0.62	0.06

mit beam is then narrower and, for a given offset, introduces a greater loss into the transmit path than in the receive path. For the aperture illumination employed, Table I shows the approximate losses in the transmit and receive paths as the offset is varied. The transmitter frequency for Telstar is nearly 6390 Mc/s and that for Relay 1725 Mc/s. The beacon frequency is the same for both projects: 4080 Mc/s.

The system was provided initially with a conical-scan radius for a 1 db loss in the beacon signal. It was found, however, that the sensitivity of the equipment was sufficient to allow the radius to be reduced to the  $\frac{1}{4}$  db point. The transmit loss and signal modulation at the conical-scan frequency were reduced by this means, especially with respect to the Telstar satellite.

#### DESCRIPTION OF EQUIPMENT

##### *Beam-Swinging Mechanism*

The general arrangement of the beam-swinging mechanism is shown in Fig. 1. The tube marked "Aerial Feed Unit" points towards the apex of the dish and in its central position its aperture is at the focus. The frame, shown as cut away, is mounted on a platform situated about 2-ft outside the focal plane. Two motions of the feed are provided; one is the major beam-swing motion in which the feed aperture can move to any position within a circle originally of 6 in. radius but later limited to 3 in.; the other is the conical-scan motion in which the feed moves circularly with a radius (in the final modification) of 0.16 in. about an axis fixed by the beam-swing motion. The radius of the conical-scan motion is modified simply by changing an eccentric in the motor drive.

The beam-swing motion pivots about gimbals at the rear and is effected by two hydraulic pistons mounted orthogonally in the plane of the main frame. The gimbals have an internal clearance sufficient to allow the waveguide components to be withdrawn through them, without dismantling the main structure. The rear section of the waveguide is flexible to allow movement of the feed relative to the external fixed feeder. The hydraulic pistons are controlled by servo-operated oil valves fed at 800 lb/in.<sup>2</sup> by a pipe line from a hydraulic pump mounted on the roof of the cabin on the azimuth turntable of the aerial.

The gimbals for the conical-scan motion are placed midway on the feed support tube, the far end of which is given a circular motion by a motor mounted outside the beam-swing gimbals. The central dis-

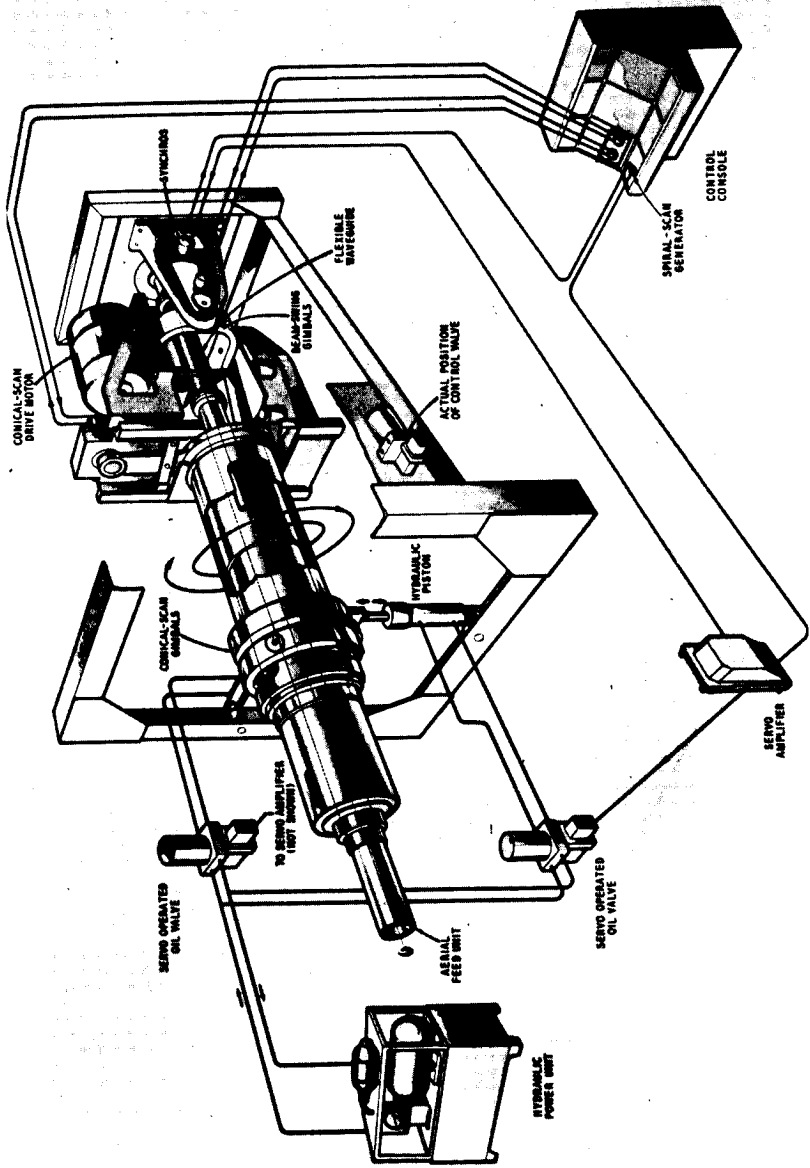


Fig. 1 — Schematic of the waveguide feed system.

position of the conical-scan gimbals results in this part of the mechanism being sensibly in mechanical balance. Counter balance collars are placed on the support tube fore and aft of the gimbals to balance completely particular feed assemblies. The conical-scan drive motor is fed from a small dc control set, originally of the Ward-Leonard type but which is shortly to be changed to the silicon-controlled rectifier type to minimize space, weight and the need of maintenance. The control set is mounted in one of the cabins behind the dish and allows the scanning speed to be regulated between  $\frac{1}{2}$  and 5 cps by remote control.

The whole assembly is designed for minimum maintenance and to withstand the weather conditions encountered on Goonhilly Downs. The weight of the mechanism, exclusive of the external waveguide feeders, is about 900 lb.

#### *Conical-scan Control and Display*

A cathode ray tube display is associated with the conical-scan system to indicate the divergence of the satellite from the scanning axis in direction and angular magnitude up to 8 ft. When the direction of the incoming beacon is off the axis of the conical scan by a small amount the output of the beacon receiver is modulated at the scan frequency. The depth of modulation increases as the deviation off axis increases and determines the length of a radial trace on the cathode ray tube. The direction in which the satellite is off axis determines the phase of the modulation and hence the angular position of the trace. Erroneous indications of direction due to the modulation of the beacon by the satellite spin are readily eliminated by adjusting the conical-scan speed to be non-synchronous with the spin-stabilization speed. A block diagram of the equipment is shown in Fig. 2.

A 50 cps magstrip link relays the rotary motion of the feed to the control console where a resolver is driven to provide the phase reference for the incoming beacon signal. The 2-phase output of the resolver is fed directly to the magnetic deflection coils of the cathode ray tube and the input of the resolver is derived from the beacon signal in the following way. The modulated dc output of the beacon receiver is detected, amplified and fed to a modulator which is so biased that only the positive tips of the input ac wave produce an output. The carrier source to the modulator is a 1.5 kc/s pulse generator in which the pulse width is small. The pulsed output of the modulator is fed to the input of the synchro resolver through a drive amplifier. The necessity for pulsed modulation is twofold; firstly adequate

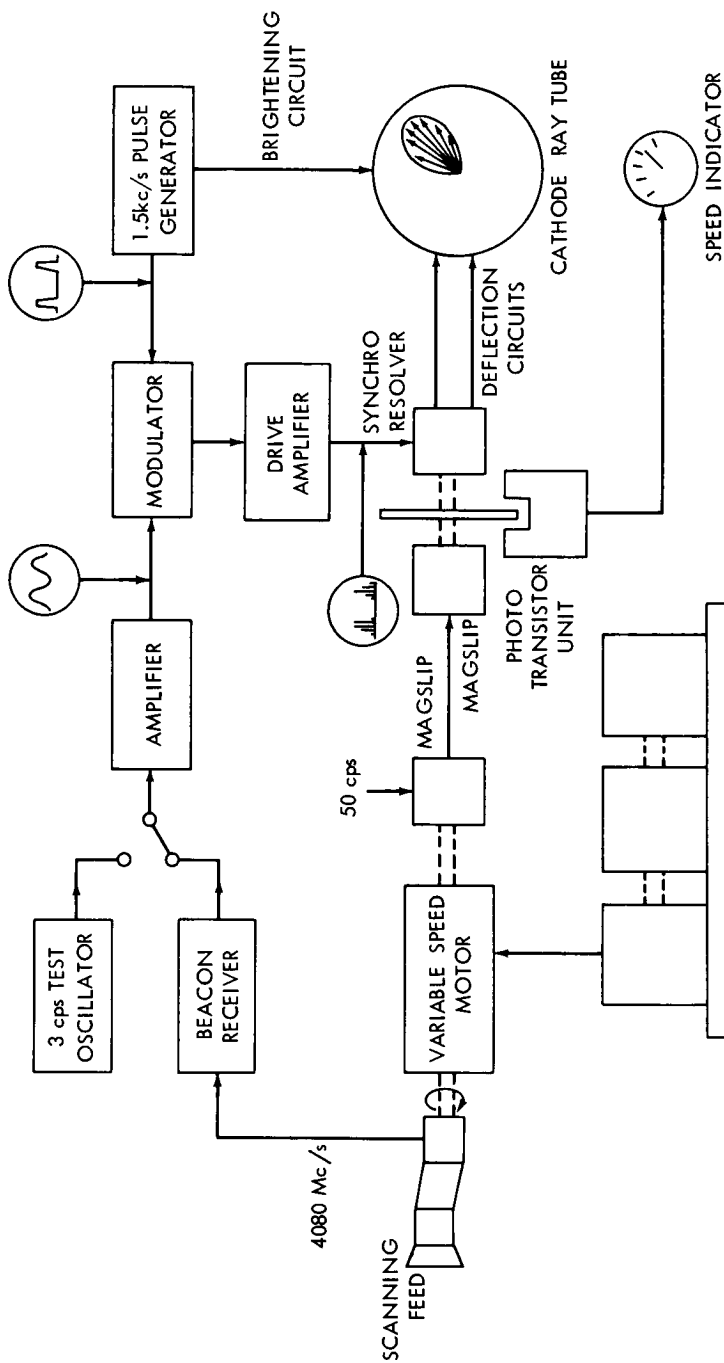


Fig. 2 — The Goonhilly aerial, conical-scan control and display.

transmission through the resolver cannot be obtained at the low conical-scan frequency in use, so translation to a higher frequency is necessary; secondly, it affords a simple means of deriving a radial trace on the cathode ray tube without dc restoration when the input is alternating current. The tips of the forward pulses are brightened to improve the presentation and to blank the small backward pulses. The result is a lobe as shown in the sketch in Fig. 2.

A 3 cps test oscillator is provided in the unit to stimulate the output of the beacon receiver when the equipment is non-operational. The magflip-resolver link is also used to provide an indication of the conical-scan speed. A perforated disc mounted on the coupling between the magflip and the resolver modulates a light beam focussed on a photo-transistor. The output of the transistor is measured on a meter in terms of the conical-scan speed.

#### *Beam-position Control and Display*

The beam-positioning equipment is shown diagrammatically in Fig. 3. The angular offset of the satellite relative to the aerial boresight axis is displayed on two meters calibrated respectively in terms of angular deviation in azimuth and elevation up to 30 ft each side of the central position. The meter display is derived from aerial feed-position indicators (linear transformers) mounted orthogonally on the beam-swing gimbals. The outputs of the transformers are rectified and fed to the relevant centre-zero meter.

Indication that the satellite is acquired is shown on 3 lamps triggered at predetermined stages of acquisition by the depth of modulation imposed on the beacon signal by the conically scanned beam. Indication of complete acquisition is extended to other lamps at points in the earth station where the information is required.

#### *Control Console*

A two-position console, part of a suite of six used for experiment control, houses the conical-scan and beam-position presentation units. A photograph of the two positions is shown in Fig. 4. The conical-scan display cathode ray tube is under the hood on the left hand position. Test facilities for the conical-scan unit, the scan speed indicator and beacon output meter are placed immediately above the hood. The aerial position is displayed digitally on the top panel. The hand control for positioning the aerial beam is on the desk below the cathode ray tube. The original version of this control incorporated a spiral-scan generator for wide-angle search but the high accuracy of the



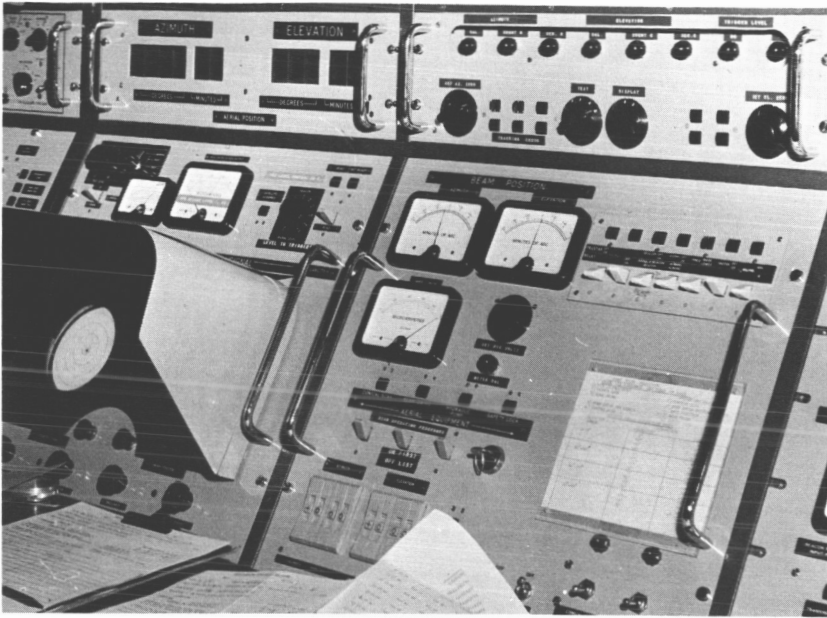


Fig. 4— The beam-swinging console.

predicted data supplied by the GSFC made the provision superfluous and it has been replaced by a "finger-tip" ball-type control.

The right-hand bay of the console houses the beam-position unit and the satellite acquisition circuits. The digital switches, by which the corrections to be applied to the predicted course of the aerial are signalled to the aerial controller, are situated at the bottom left hand corner of the panel.

The operational procedure is:

1. The functioning of the presentation units and the scanning mechanism is checked before each satellite pass in conjunction with the Leswiddden test station about 22 miles away.
2. The conical-scan motion is applied at the commencement of the pass and the radial display reveals any offset of the satellite from the aerial beam.
3. The hand control is used to steer the beam exactly on to the course of the satellite.
4. If the divergence of the beam from the boresight axis of the aerial, as displayed on the beam-position meters, is more than about 4 ft (one-third beamwidth) then azimuth and/or elevation

corrections to the predicted course of the aerial are demanded of the aerial controller to restore the beam to its on-axis position. As the corrections take effect the hand control is adjusted to follow the satellite to its on-axis bearing. This process is repeated as required during the period of the pass.

#### OPERATIONAL EXPERIENCE AND CONCLUSIONS

Experience in Project Telstar showed that the tracking facilities, as originally provided, with an extensive beam-swing capability and automatic spiral-scan facility, were more than adequate. These features have now been modified. It had been expected that acquisition would not be possible until the aerial elevation was about  $5^\circ$  to  $7\frac{1}{2}^\circ$  but, in a very large proportion of the passes the satellite has been sighted while the aerial was waiting at zero elevation, i.e., when the satellite was yet below the horizon. Only very occasionally has acquisition been delayed until the elevation has reached  $2^\circ$ . This fact, and the accuracy of subsequent tracking, reflects very favourably the high accuracy of the predicted data obtained from the Goddard Space Flight Center. After superimposing standard corrections on the predicted steering data to account for tropospheric refraction at low elevations the remaining corrections necessary during the period of a pass have generally totalled no more than 5 ft. Corrections in azimuth have been a little larger, totalling up to 10 ft. Adjustments in tracking by the beam-swing equipment and by overriding the predicted data have, so far, been applied manually. Equipment to track the beam-swinging mechanism automatically has now been developed; further development to provide auto-track facilities for correcting the predicted data from the conical-scan equipment is in hand.

# A 4/6 Gc/s Circularly-Polarized Diplexer for the Goonhilly Satellite-Communication Aerial\*

D. CHAKRABORTY and G. F. D. MILLWARD  
POST OFFICE ENGINEERING DEPARTMENT

The diplexer described transmits some 4 to 5 kilowatts of microwave power and simultaneously receives a signal of the order of a micro-microwatt from a communication satellite, when used in conjunction with the earth-station aerial at Goonhilly.

The earth-station transmitter and received frequencies are 6.39 and 4.17 Gc/s. respectively, the sense of polarization of the transmit signal into the dish aerial being left-handed circularly polarized and that of the received signal from the dish aerial being right-handed. Thus a broadband reciprocal polarizer is required in addition to the diplexer. The details of the diplexer and the broadband polarizer, which constitute one integral unit (Fig. 1) are discussed below.

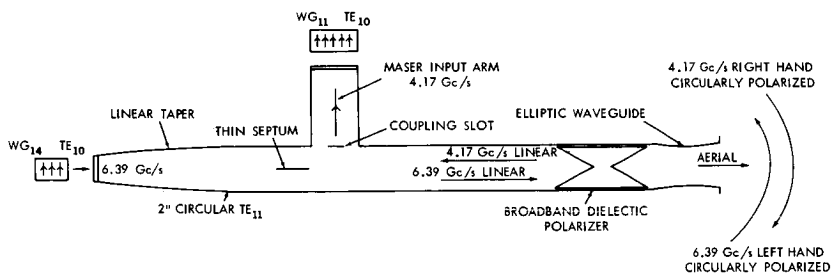


Fig. 1 — A diplexer assembly for circularly polarized waves in the 4 and 6 Gc/s bands.

## THE DIPLEXER

The transmitter power is launched in the  $TE_{11}$  mode in 2-in. circular guide through a linear taper from a rectangular waveguide

\* First published by the Institute of Electrical Engineers, November 1962.

(WG<sub>14</sub>). With the TE<sub>11</sub> mode, separate regions of maximum and minimum power density are produced at 90° intervals around the periphery of the circular guide. If a region of minimum power density due to the transmittal signal is chosen,<sup>1</sup> the received signal may be launched so that its plane of polarization is transverse to that of the transmitted signal in this region. This can be achieved by suitable orientation of the broadband polarizer axis in relation to the axis of the transmit field electric vector. Under these circumstances the minimum coupling region due to transmit field is the maximum coupling region due to received field, and the transmit electric vector is orthogonal to the received field electric vector.

If a narrow slot is cut in this region of the circular guide, it will be non-radiating so far as the transmit field is concerned but will be excited by the received field, since the slot is transverse to the received field electric vector. The coupling slot is common to the round guide and the transverse plane of the rectangular waveguide (WG<sub>11</sub>). The slot will not couple the whole of the received energy to the branched rectangular waveguide, but if a thin polished metallic septum is placed in the circular guide so that the received field electric vector is coplanar with the septum, then the entire received energy will be reflected and coupled to the rectangular waveguide. The field configurations and a cutaway view of the diplexer are shown in Fig. 2.

Considering the diplexer as a third-order waveguide junction (Fig. 2) it is noted that there is a plane of symmetry across the terminals of arm 3. If the septum is placed at appropriate distance from the

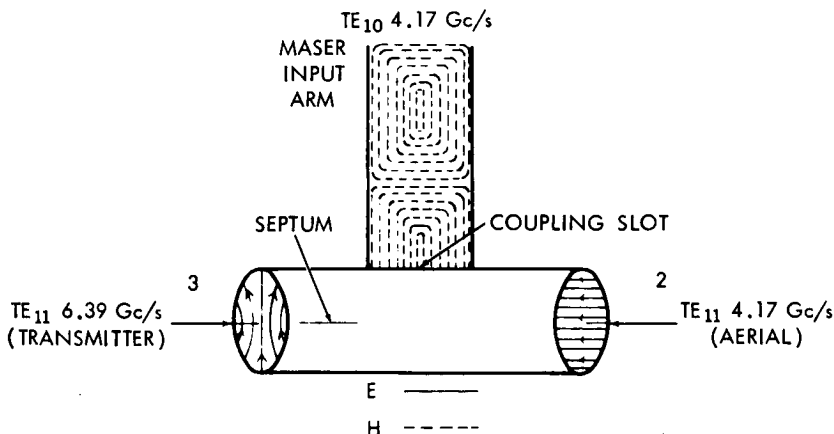


Fig. 2a — Field configuration of the orthogonal TE<sub>11</sub> modes.

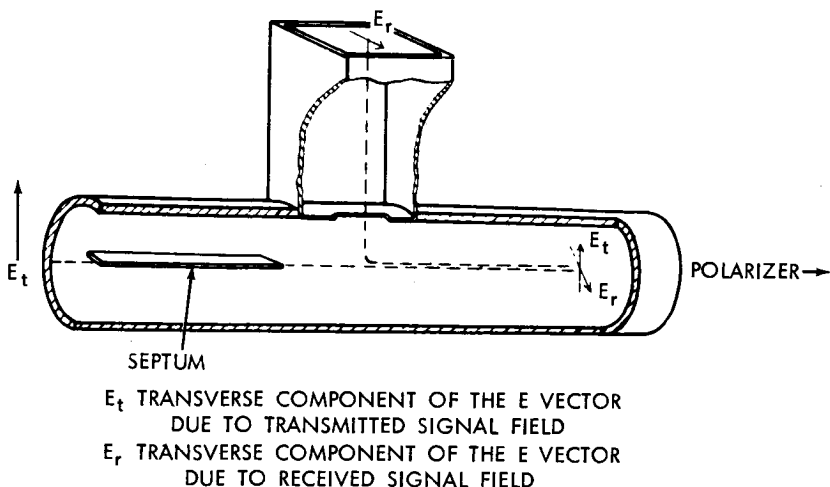


Fig. 2b — The diplexer.

terminal plane of this arm, then the maser input arm (i.e. the waveguide 11 arm) and the aerial arm will behave as a perfect transmission line provided that the impedance in the branched guide is suitably adjusted in relation to the slot impedance  $Z'$ , as shown in the transformer representation of the diplexer (Fig. 3).

The coupling between the aerial arm and maser input arm is achieved through a narrow rounded slot centered in the transverse plane of the rectangular waveguide 11. The interface thickness between the round and the rectangular waveguide is extremely small. The effect of this slot on the fundamental mode of a waveguide may be computed from an equivalent circuit in which the diaphragm is represented by a two terminal impedance shunted across a transmission line which is as-

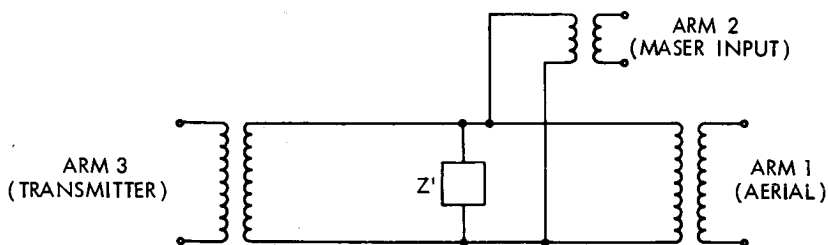


Fig. 3a — Transformer representation of the diplexer.

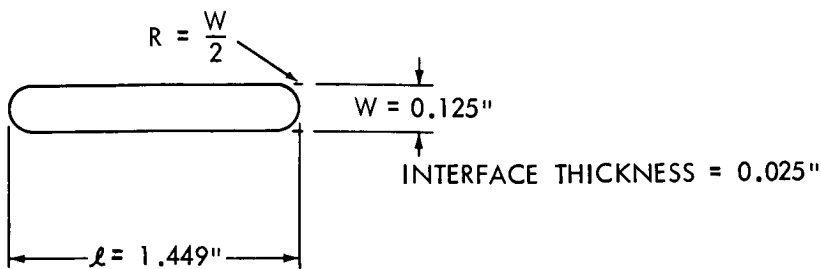


Fig. 3b — Dimensions of the coupling slot.

sumed to carry a fundamental mode of the waveguide. For all practical purposes<sup>2</sup> the reactance function of such a slot is given by the expression:

$$X = \frac{4\pi MZ_0}{ab\lambda_g} \quad (1)$$

where  $M$  is the magnetic polarizability of the slot,  $Z_0$  is the characteristic impedance of the waveguide,  $a$  and  $b$  are the width and the height of the guide,  $\lambda_g$  is guide wavelength.

The approximate value of the magnetic polarizability is

$$M = \frac{\pi}{16} \epsilon w^2, \quad (2)$$

where  $\epsilon$  is the length of the slot and  $w$  is the width of the slot.

According to Slater<sup>3</sup> the approximate resonant length of a thin slot centred on the transverse plane of the rectangular waveguide is given by the expression

$$\epsilon = \frac{\lambda_0}{2} \sqrt{1 + \left(\frac{2aw}{b\lambda_g}\right)^2}, \quad (3)$$

where  $\lambda_0$  is the free space wavelength. For a rounded slot having  $w/l$  less than 0.11, Equation 3 can be further simplified to

$$\epsilon = \frac{\lambda_0}{2} + 0.273w, \quad (4)$$

This empirical relationship agrees well with the experimental measurements and the slot is found to be resonant within the desired frequency range.

## EXPERIMENTAL RESULTS

From Equation 4, the following data are obtained for the slot shown in Fig. 3b.

For a centre-frequency of 4170 Mc/s:

Length of the slot $\ell$	=	1.449 $\pm$ 0.003 in.;
Width of the slot $w$	=	0.125 $\pm$ 0.003 in.;
Wall thickness between the rectangular and round waveguide	=	0.025 $\pm$ 0.001 in.

Fig. 4a shows the insertion loss and the VSWR between the aerial and maser input arm and Fig. 4b shows the discrimination between the transmit and maser input arm. The discrimination achieved over the transmit frequency band exceeds 50 db.

## THE BROADBAND POLARIZER

The principles of the broadband polarizing device may be best understood by considering the characteristics of a circularly polarized

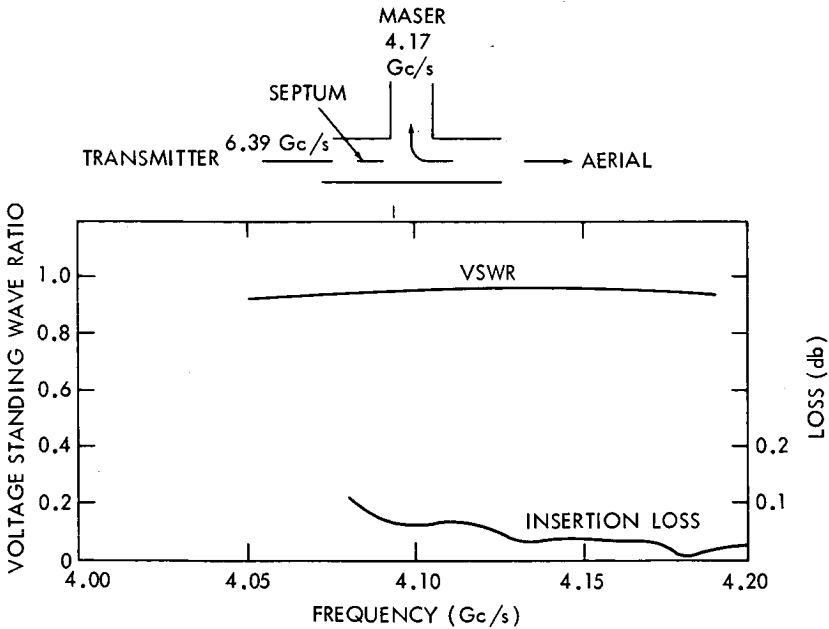


Fig. 4a — Insertion loss between aerial and maser input arm.

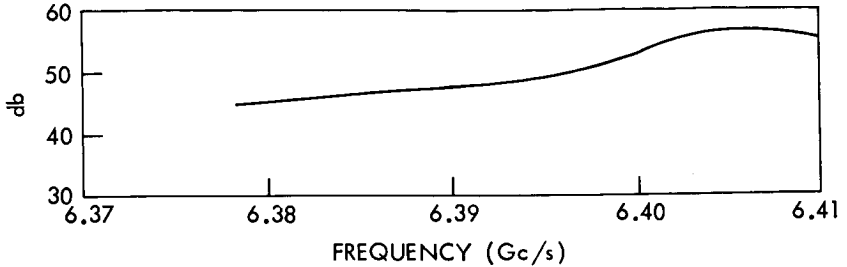


Fig. 4b — Discrimination between transmit and maser input arm.

wave. Consider two linearly polarized waves, propagating in a positive  $Z$  direction in space quadrature as shown in Fig. 5a, and described by

$$E_1 = E_0 \sin(\omega t - \beta Z), \quad E_2 = \gamma E_0 \sin(\omega t - \beta Z + \theta), \quad (4)$$

where  $\gamma$  is constant; and the phase constant,  $\beta = 2\pi/\lambda_0$ .

If we consider  $\theta = \pi/2$  at a plane  $Z = 0$ , then

$$E_1 = E_0 \sin \omega t \quad \text{and} \quad E_2 = \gamma E_0 \cos \omega t; \quad (5)$$

eliminating the time dependence gives the locus of these waves:

$$\frac{E_1^2}{E_0^2} + \frac{E_2^2}{\gamma^2 E_0^2} = 1 \quad (6)$$

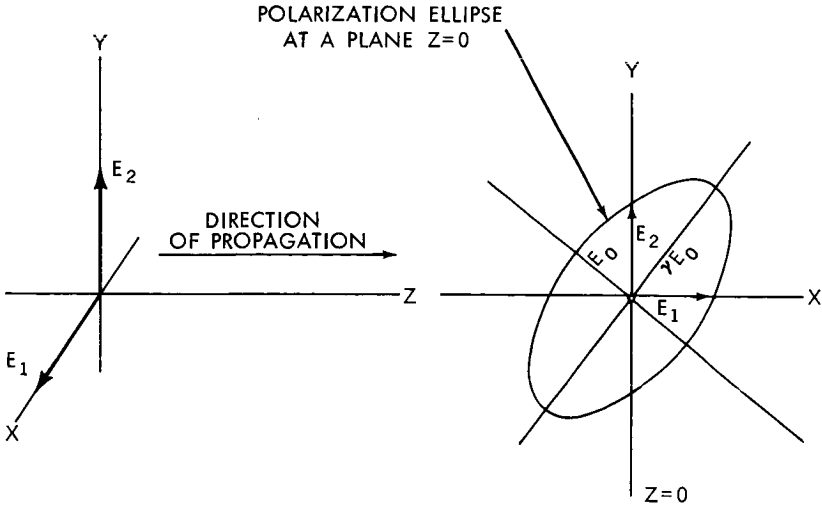
This is the equation of an ellipse with axes  $2 E_0$  and  $2 \gamma E_0$ .

The resultant of these two components traces out this ellipse as it rotates in time. Such a rotating wave is termed an elliptical polarized wave, the polarization ellipse at a plane  $Z = 0$  being shown in Fig 5b. A special case arises if  $\gamma = 1$ , when the locus reverts to a circle giving a circularly polarized (CP) wave. Circular polarization is therefore an ideal case of elliptic polarization, and is generally approximated to in practice by elliptical polarization with an axial ratio approaching unity. Such a wave is also referred to as "Circularly Polarized" without further qualification. The most usual manner of denoting the quality of such a wave is by the following ratio:

$$\frac{\text{Minimum of the transverse component of the electric field}}{\text{Maximum of the transverse component of the electric field}} = \frac{E_0}{\gamma E_0} = \frac{1}{\gamma} \quad (7)$$

#### *Sense of Polarization*

It should be noted that the sense of polarization is ambiguous unless one clearly states the reference plane. The CCIR adopted, at its Xth



(a) Linearly polarized components of an elliptically polarized wave.

(b) Polarization ellipse.

Fig. 5 — Elliptically polarized waves.

Plenary Assembly (Geneva, 1963),<sup>4</sup> a definition according to which a right-handed circularly polarized wave is one in which an observer, looking in the direction of propagation, sees the electric vector rotating clockwise in a fixed reference plane.

### Design of the Dielectric Plate

The two orthogonal components given in Equation 5 may be generated by establishing a linearly polarized wave  $E$  (Fig. 6) at an angle

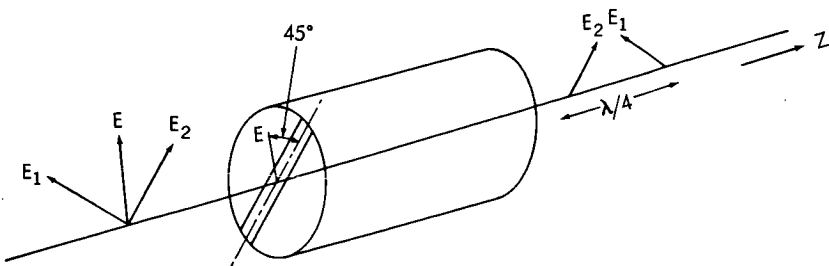


Fig. 6 — Generation of a CP wave.

of  $45^\circ$  to a differential phase shift section, such as a waveguide partially filled with dielectric.

Consider the incident wave  $E$  splitting into two orthogonal components  $E_1$  and  $E_2$ . Assuming the dielectric plate thickness to be considerably smaller than the length of the plate ( $\delta$ ), the wave  $E_2$  in the plane of the plate will be retarded in phase compared to  $E_1$ , and the differential phase shift between  $E_1$  and  $E_2$  will be governed by the following relationship:

$$\phi = 2 \pi \delta \left( \frac{1}{\lambda_{g2}} - \frac{1}{\lambda_{g1}} \right) \quad (8)$$

where  $\lambda_{g1}$  and  $\lambda_{g2}$  are the guide wavelengths for the two orthogonal linearly polarized waves  $E_1$  and  $E_2$ . Clearly the effective dielectric constant  $\epsilon_2$  corresponding to wave  $E_2$  will be greater than the effective dielectric constant  $\epsilon_1$  corresponding to wave  $E_1$  and consequently

$$\phi = 2 \pi \delta \frac{\sqrt{\epsilon_2 - (\lambda_0/\lambda_c)^2} - \sqrt{\epsilon_1 - (\lambda_0/\lambda_c)^2}}{\lambda_0}, \quad (9)$$

where  $\lambda_c$  is the cutoff wavelength of the dominant mode, and  $\lambda_0$  is the free space wavelength.

For broadband operation the differential phase shift  $\phi$  must remain approximately equal to  $90^\circ$  throughout the entire frequency spectrum of interest. The effective dielectric constants  $\epsilon_1$  and  $\epsilon_2$  are not directly computable and hence the length  $\delta$  can only be calculated by finding the propagation constants for the two orthogonal waves  $E_1$  and  $E_2$ . In order to do this one must solve a transverse eigen-value equation for each wave which is due to the boundary conditions at the dielectric-air interfaces. Such a calculation has been made for a polarizer in square guide, and it has been found experimentally that the results hold good in a circular guide having the same cut-off frequency as that of the square guide.

Consider two orthogonal H-waves propagating in the Z direction in a partially dielectric-filled square guide (Fig. 7), E and H being of the form:

$$E = E_0 e^{j(\omega t - \beta z)}, \quad H = H_0 e^{j(\omega t - \beta z)}, \quad \text{and } E_z = 0.$$

$E_y$  is assumed to be continuous over the air-dielectric media I and II and dielectric-air media II and III. The phase shift for the com-



where  $K = \epsilon_1/\epsilon_0$ ; therefore

$$q = s \sqrt{k^2 (K-1) + (\rho/d)^2}. \quad (13)$$

A similar analysis can be made for the perpendicular component but in view of the fact that the thickness of the dielectric wedge is considerably smaller than the length it can be assumed that the phase shift for the perpendicular component is

$$\gamma_1 = \frac{2\pi}{\lambda_g} \text{ per unit length where } \lambda_g \text{ is air-filled guide wavelength.}$$

The following parameters were used for computation of the differential phase shift  $\phi$  (see Equation 8):

$$\begin{aligned} f &= 4170 \text{ Mc/s;} \\ a - b &= 1.75 \text{ in.;} \\ c &= 0.125 \text{ in.;} \\ s &= \frac{C}{2} = 0.0625 \text{ in.;} \\ d &= 0.8125 \text{ in.} \end{aligned}$$

For a dielectric consisting of *PTFE*  $K = 2.01$  and  $k = \frac{2\pi}{\lambda_0} = 0.873$  radian.

Solution of  $\rho$  is obtained from Equations 11 and 13:

$$y = \frac{\tan \rho}{\rho} = \frac{s}{d} \cdot \frac{\cot q}{q};$$

$$\rho = 73.2^\circ = 1.27 \text{ radian.}$$

Therefore

$$\begin{aligned} \gamma_2 &= \sqrt{\left(\frac{2\pi}{\lambda_0}\right)^2 - \left(\frac{\rho}{d}\right)^2} = 0.615 \text{ radian/cm,} \\ \gamma_1 &= \frac{2\pi}{\lambda_g} = \frac{2\pi}{12.2} = 0.515 \text{ radian/cm; and} \\ \phi &= \gamma_2 - \gamma_1 = 0.1 \text{ rad/cm} = 14.6^\circ/\text{inch.} \end{aligned}$$

According to the above calculation the required length of the dielectric wedge is approximately 6.2 in. However, the preceding calculation does not take into account the effect of tapering, and this is difficult to allow for precisely. In order to determine the shape of the wedge (Fig. 8) the following procedure has been adopted.

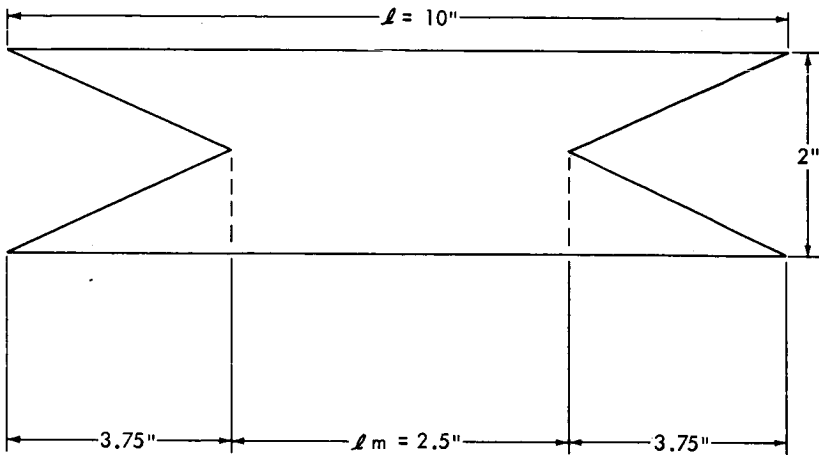


Fig. 8—Dimensions of the polarizer.

Assuming a length of the wedge = 6 in., then the

minimum tapered length  $0.75 \lambda_D$  at 4170 Mc/s = 3.75 in.,

diameter of the circular guide = 2 in.,

mid-section length of the wedge  $\delta_m = (l - 7.5)$  in.

The overall effective area of the wedge is:

$$(6 \times 2) - 7.5 = 12.4$$

$$6 = 9.95 \text{ inches.}$$

Based on the foregoing, a wedge was prepared with an overall length of 10 inches and 3.75 inches tapered length; the measured ellipticities were found to be better than 0.8 over the band 4 to 6.5 Gc/s.

The *PTFE* wedge is held in position inside the 2-in. circular guide by means of eight dielectric pins penetrating slightly into the narrow dimension of the wedge. These dielectric pins are in turn sealed by thin metal sleeves.

#### *Dispersion in Dielectric Plates*

In general the thicker plates have better dispersion characteristics but the discontinuity introduced by a  $\frac{1}{4}$ -in. thick plate is sufficient to cause generations of higher order modes at the transmitting frequency (6.39 Gc/s), and a  $\frac{1}{8}$ -in. thickness has therefore been used. This overcomes the difficulties due to overmoding but increases dis-

persion, the differential phase shift then being no longer constant over the required bandwidth. This has led to the investigation of means for providing compensation for dispersion.

Chu<sup>6</sup> has shown analytically that a slightly distorted circular guide can propagate two distinct transverse electric modes along the two axes of the ellipse. These two modes are usually known as the odd transverse electric ( $OH_1$ ) and the even transverse electric ( $EH_1$ ) waves. If a small section of elliptic guide (slightly distorted circular guide) is used in tandem with the polarizer and by giving proper orientation of the axes of the elliptic guide with reference to the dielectric plate it is possible to give slightly different phase velocities to the two orthogonal components of the circularly polarized wave.

The values of relative phase difference between the even and the odd mode in elliptic guide have been calculated for various values of  $\delta$ . Ellipticities better than 0.9 over the band 4 to 7 Gc/s have been obtained (Fig. 9) using the elliptical guide compensating section in tandem with the dielectric plate polarizer.

The loss of the polarizer comprises two parts, i.e. loss due to dielectric absorption and loss due to imperfect circularity of polarization, the noise temperature due to the polarizer being about  $1.5^\circ\text{K}$ .

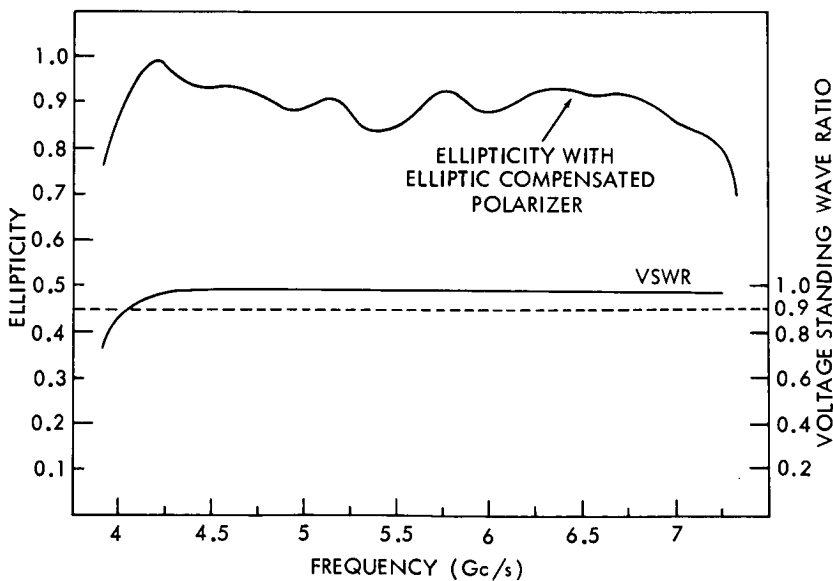


Fig. 9 — Polarizer characteristics.

### Establishment of Field Vectors

Returning to the question of establishing two orthogonal fields for the transmitted and received signal ( $E_t$  and  $E_\gamma$ , Fig. 2b), consider the situation where the received signal from the aerial is to be right-handed circularly polarized and the transmitted signal into the dish aerial is to be left-handed. In both cases the component with suffix 2 (Fig. 10) is phase delayed. The polarizing section must then be oriented with reference to the transmit field electric vector  $E_t$  (Fig. 10a) while the received field electric vector  $E_{\gamma_2}$  (Fig. 10b) is delayed by  $180^\circ$  with respect to  $E_{\gamma_1}$ , the resultant  $E_\gamma$  then being orthogonal to  $E_t$ .

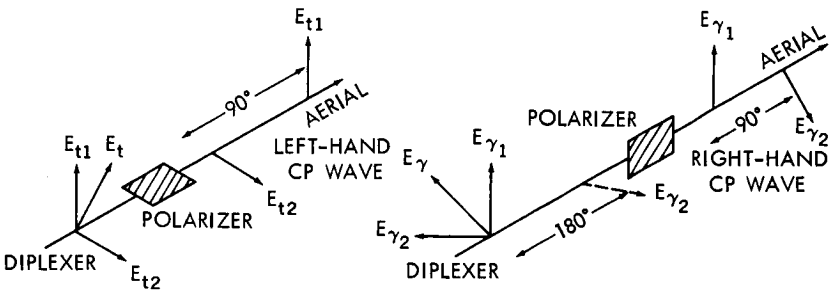


Fig. 10 — Establishment of two orthogonal fields at the diplexer.

### CONCLUSION

The diplexer and the broadband polarizer system described have been successfully used in the Goonhilly Earth Station installation for tests with the Telstar satellite.

A slightly modified version has been used in a combined feed assembly to provide communication via both Telstar and Relay satellites; in this modified version of the diplexer the transmitter power (1.7 Gc/s) for Relay propagates through a 5-inch circular waveguide enclosing the 2-inch waveguide diplexer used for Telstar. This combined feed assembly is described in detail in a companion paper.\*

### REFERENCES

1. Montgomery, C. G., Dieke, R. H., Purcell, E. M., Principles of Microwave Circuits, *M.I.T. Rad. Lab. Series 1943*, New York: McGraw-Hill.
2. Bethe, H. A., Lumped Constants for Small Irises, *M.I.T. Rad. Lab. Report 43-22*, March 24, 1943.

\* See pages 2141-2155.

3. Slater, J. C., *Microwave Transmission*, pp 185-187, New York: McGraw-Hill, 1942.
4. Documents of the Xth Plenary Assembly of the CCIR, Geneva, 1963.
5. Pincherle, L., *Electromagnetic Waves in Metal Tubes Filled Longitudinally with two Dielectrics*, *Phy. Rev.* 66: 118-130, September 1944.
6. Chu, Lan Jen, *Electromagnetic Waves in Elliptic Hollow Pipes of Metal*, *J. Appl. Phys.*, 9, September 1938.

N67 12311

# Primary Feeds for the Goonhilly Satellite-Communication Aerial\*

I. A. RAVENSCROFT

POST OFFICE ENGINEERING DEPARTMENT

The 85-ft. diameter aerial at Goonhilly Downs, Cornwall uses a focal-plane paraboloidal reflector illuminated from a primary feed at the focus. Circularly polarized waves are transmitted and received. For optimum gain and uniformity of the aerial radiation patterns, circular symmetry of the primary feed radiation pattern is desirable. The primary feed has therefore been made circularly symmetric.

The following terms, which are particularly applicable to large-aperture low-noise parabolic-reflector type aerials, are used in the present account of the feed design: *Aerial Gain Factor* (G): the ratio of the actual gain obtained to that of a uniformly illuminated aperture of the same area; *Illumination Efficiency* ( $\epsilon$ ): the ratio of the energy illuminating the reflector to the total energy radiated by the feed; *Radiation Spillover*: the energy radiated by the feed, not illuminating the reflector; *System Figure of Merit*: the ratio of aerial gain to the total receiving system noise-temperature in degrees Kelvin. Other terms and symbols are given in Appendix 1.

Primary feed radiation patterns usually have a field intensity which is maximum in the direction of the vertex and which tapers towards the periphery of the reflector. Spillover is normally permitted to obtain an optimum gain factor. However, for the reception of low-level signals, when the aerial is pointing towards a low-temperature sky, some consideration must be given to spillover which results in the reception of thermal radiation from the earth. The spillover permitted with a receiving aerial may then be less than that with a transmitting aerial for optimum working conditions. The optimum spillover for reception also varies with the aerial elevation, but  $5^\circ$  is an appropriate elevation for consideration since then the sky temperature has the fairly low figure<sup>1</sup> of about  $20^\circ\text{K}$  and the spillover noise temperature is very nearly maximum. At low angles of elevation, approximately one half

\* First published by the Institute of Electrical Engineers, November 1962.

of the spillover energy is at the average sky temperature (assumed to be 6°K) and the other half at the temperature of the earth.

The experiments with the Telstar and Relay satellites require transmitting frequencies at the ground stations of about 6390 and 1725 Mc/s respectively, and a common receive frequency of about 4170 Mc/s. The initial time available for development made it imperative to consider at the outset a separate primary feed design for each experiment. However, a composite feed unit capable of accommodating all three frequencies is now in use.

#### AERIAL GAIN FACTOR AND SYSTEM FIGURE OF MERIT

The gain factor of a parabolic aerial is given by<sup>2</sup>:

$$G = \cot^2 \frac{\psi}{2} \left| \int_0^\psi \left[ G_f(\phi) \right]^{\frac{1}{2}} \tan(\phi/2) d\phi \right|^2 \quad (1)$$

The classes of primary feed patterns considered analytically by Silver<sup>2</sup> are given by:

$$G_f \phi = G_0 \cos^n \phi \quad (2)$$

between the limits  $\phi = +\frac{\pi}{2}$  and  $-\frac{\pi}{2}$ , and where  $n = 2, 4, \dots$  etc.

When  $n = 2$ , the optimum aperture  $\psi$  is about 66° and the gain factor obtained is about 0.83. The primary feed illumination at the reflector periphery is then about -10 db relative to that at the vertex. In the case of the focal plane paraboloidal reflector, the angular aperture,  $\psi$ , is  $\pi/2$  and the gain factor is

$$G_{\pi/2} = \left| \int_0^{\pi/2} \left[ G_f(\phi) \right]^{\frac{1}{2}} \tan(\phi/2) d\phi \right|^2 \quad (3)$$

For the feed pattern given by Equation 2, the gain factor is only 0.57. To obtain a higher value therefore it is necessary to broaden the feed pattern allowing some spillover. This can be considered analytically by assuming a primary feed pattern given by

$$G_f(\phi) = G_0 \cos^n m\phi \quad (4)$$

between the limits  $m\phi = +\pi/2$  and  $-\pi/2$ , and where  $m$  lies between 0.5 and 1.0.

When the gain factor obtained from Equation 3 is plotted against the parameter  $m$ , the curve in Fig. 1 is obtained for  $n = 2$ . This curve

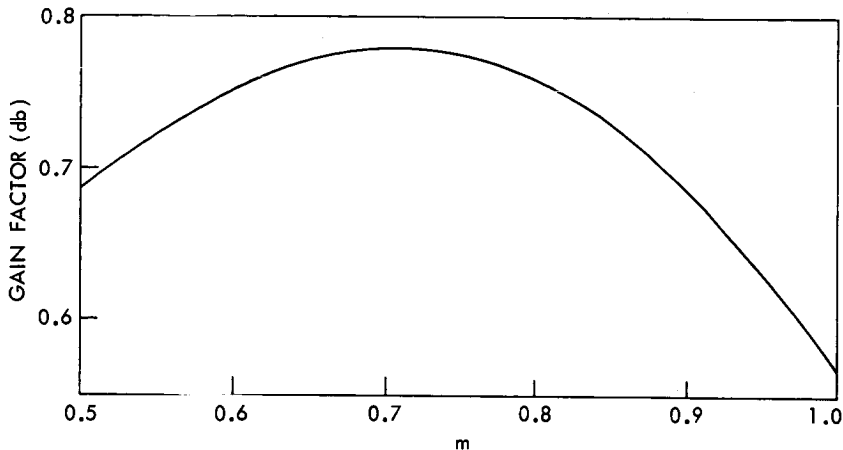


Fig. 1 — Variation of aerial gain factor with  $m$ .

indicates that an optimum gain factor of about 0.78 is obtained with  $m = 0.7$ .

When the effects of radiation-spillover are considered, the following approximate formula for the system noise temperature is obtained:

$$T_s = T_1 + eT_2 + \frac{(1-e)}{2}T_3 + \frac{(1-e)}{2}T_4,$$

where  $T_1$  — noise temperature of the receiving equipment (apart from the aerial)

$T_2$  — sky temperature seen by the aerial main lobe ( $20^\circ\text{K}$  is assumed at  $5^\circ$  elevation)

$T_3$  — average sky temperature, assumed to be  $6^\circ\text{K}$

$T_4$  — effective ground noise-temperature

Curves are plotted in Fig. 2, giving values of figure of merit for an 85-ft. diameter focal-plane aerial with various values of ground noise-temperature and with a receiving apparatus noise-temperature of  $50^\circ\text{K}$ . A ground temperature of  $280^\circ\text{K}$  is the figure assumed where the reflexion coefficient of the earth is zero, i.e. the earth is regarded as a black body radiator. A temperature of  $180^\circ\text{K}$  is where the ground reflexion coefficient is about 0.6, as estimated at Goonhilly Downs, and the case of  $6^\circ\text{K}$  is where the use of an earth-screen is possible, giving an image of the sky in the lower hemisphere of radiation. The latter is an interesting case because the spillover temperature is lower than

that of the main lobe. The condition for maximum figure of merit is then very nearly coincident with the requirements for maximum gain factor, and the effective aerial temperature is less than that of the main lobe. Optimum figures for the three ground temperatures and for apparatus temperatures of 50° and 30°K are summarized in Table 1.

TABLE I — OPTIMUM PERFORMANCE FIGURES OF THE FOCAL-PLANE PARABOLOID FOR VARIOUS GROUND NOISE TEMPERATURES

Ground Temperature (°K)	m	System Figure of Merit (db)	Aerial Gain Factor	System Noise Temp. (°K)
Equipment temperature = 50°K Sky temperature = 20°K				
280	0.8	41.2	0.758	73.1
180	0.77	41.3	0.77	72.8
6	0.69	41.6	0.777	68.6
Equipment temperature = 30°K Sky temperature = 20°K				
280	0.815	42.6	0.75	52.5
180	0.78	42.7	0.765	52.4
6	0.68	43.1	0.777	48.7

Primary feed radiation patterns for m values of 0.8 and 0.69 are shown in Fig. 3.

#### RADIATION FROM A SMALL APERTURE

The radiation patterns of a TE<sub>11</sub> wave from an open-ended circular waveguide have been calculated by Chu<sup>3</sup>, and the normalized patterns are given by:

$$\text{The } E\text{-plane field, } E_{(E\text{-plane})} = \frac{2(1 + \frac{\beta}{k} \cdot \cos \theta) J_1(ka \sin \theta)}{(1 + \frac{\beta}{k}) ka \sin \theta} \quad (5)$$

and the  $H$ -plane field,

$$E_{(H\text{-plane})} = \frac{\left[ \frac{\beta}{k} + \cos \theta \right] \left[ J_0(ka \sin \theta) - J_2(ka \sin \theta) \right]}{\left( 1 + \frac{\beta}{k} \right) \left( 1 - \frac{k^2 \sin^2 \theta}{k_m^2} \right)} \quad (6)$$

At 4170 Mc/s, the  $E$  and  $H$  radiation patterns from a 2 inch circular waveguide (Fig. 4) show that for use as a primary source of a low-temperature aerial the rearward radiation is excessive. It could be reduced by increasing the waveguide aperture, but then the breadth of forward radiation would not be obtained.

A circular flange placed about the waveguide aperture has a marked effect upon both the rearward radiation and the shape of the forward lobe. A feed with a  $3\frac{1}{2}$  inch diameter flange about a 2 inch aperture

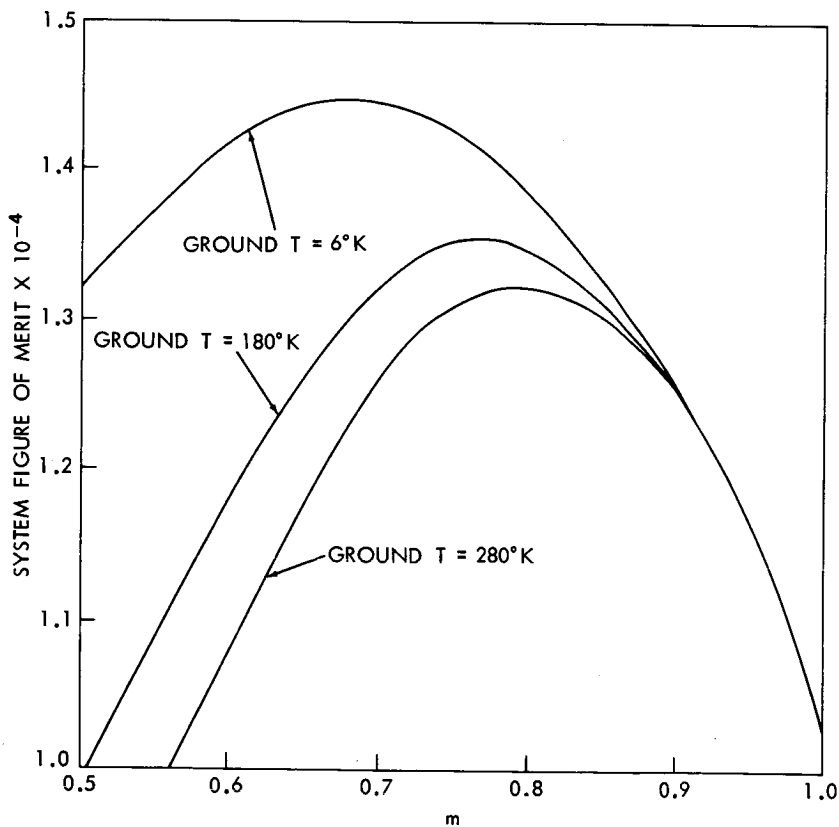


Fig. 2—Dependence of system figure of merit on the radiation pattern of a primary-feed illuminating an 85-ft diameter reflector.

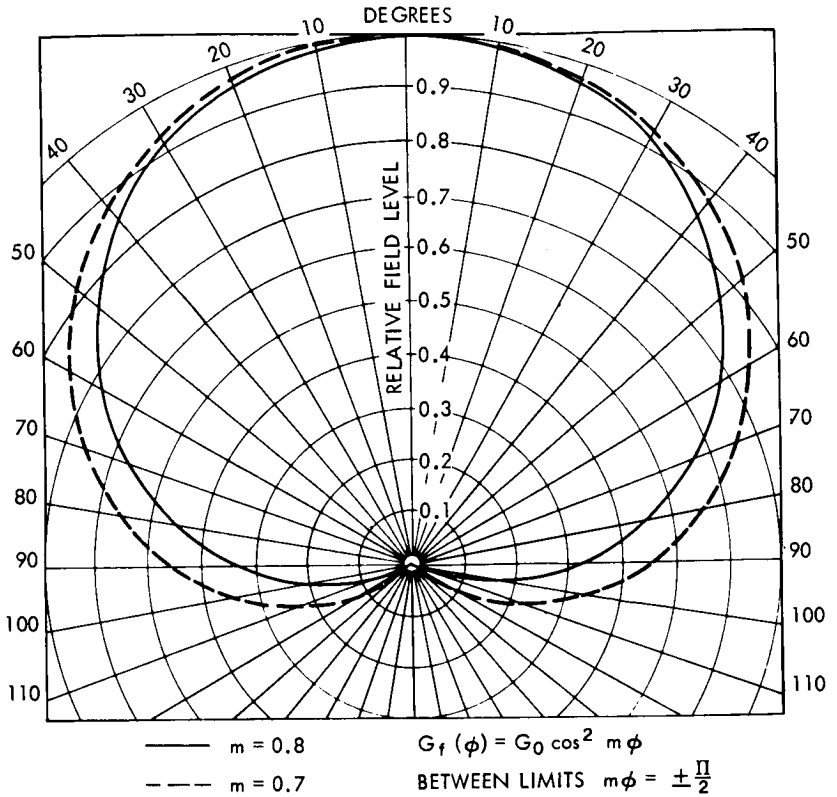


Fig. 3 — Primary feed radiation pattern.

has measured radiation characteristics showing reduced rearward radiation although increased directivity. The aerial gain factor and noise temperature obtained with this feed are estimated to be 0.53 and 5°K respectively. Improved radiation patterns were, however, obtained by placing the flange at critical distances behind the aperture, and further improvements were made by using two or more flanges. Experiments resulting in 3 inch and 4½ inch diameter flanges positioned ¼ and 1½ inches respectively behind the aperture yielded the radiation patterns shown in Fig. 5. Since the waveguide wall adversely affected the pattern, its thickness beyond the 3 inch flange was reduced to a knife-edge. The Telstar feed is based on the above, but the Relay and composite feeds with 5 inch diameter tubes have alternative flange assemblies.

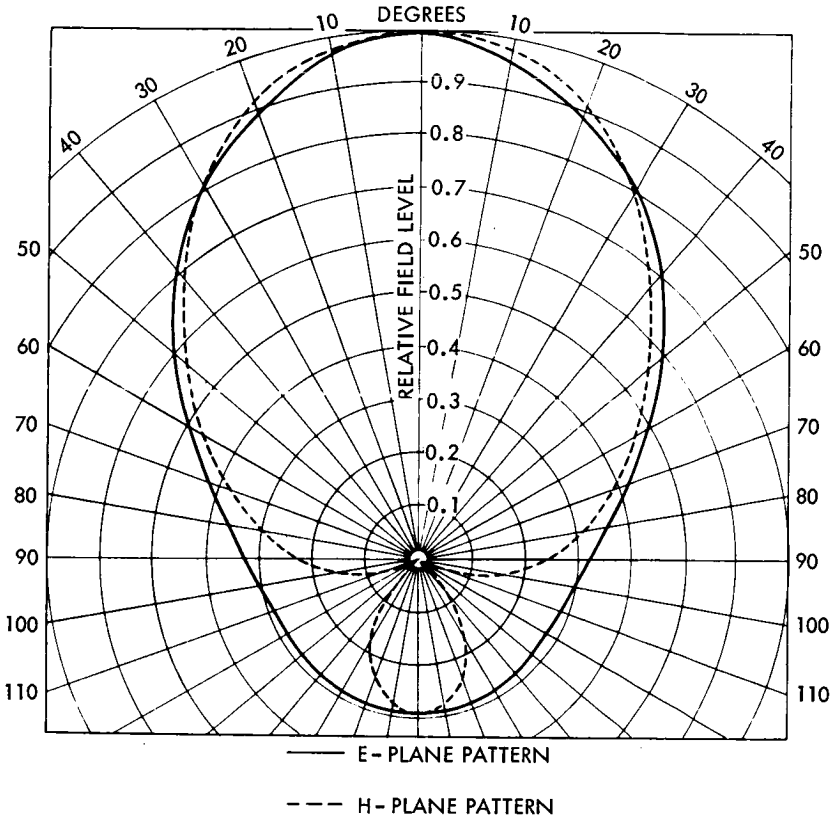


Fig. 4—Radiation pattern (theoretical) of open ended 2" diameter circular waveguide.

#### TELSTAR FEED

##### *General*

The Telstar feed is in the form of a diplexer, the transmit frequency being higher than the receive frequency. Greater emphasis has been given to obtaining optimum operation over the receiving band about 4170 Mc/s. But since the minimum usable aperture at this frequency has a diameter of about 2 inches a more directional feed pattern is obtained at the transmit frequency, resulting in slight aerial beam broadening and reduced gain factor. Since the flanges used for pattern shaping and noise reduction at 4170 Mc/s affect only slightly the 6390

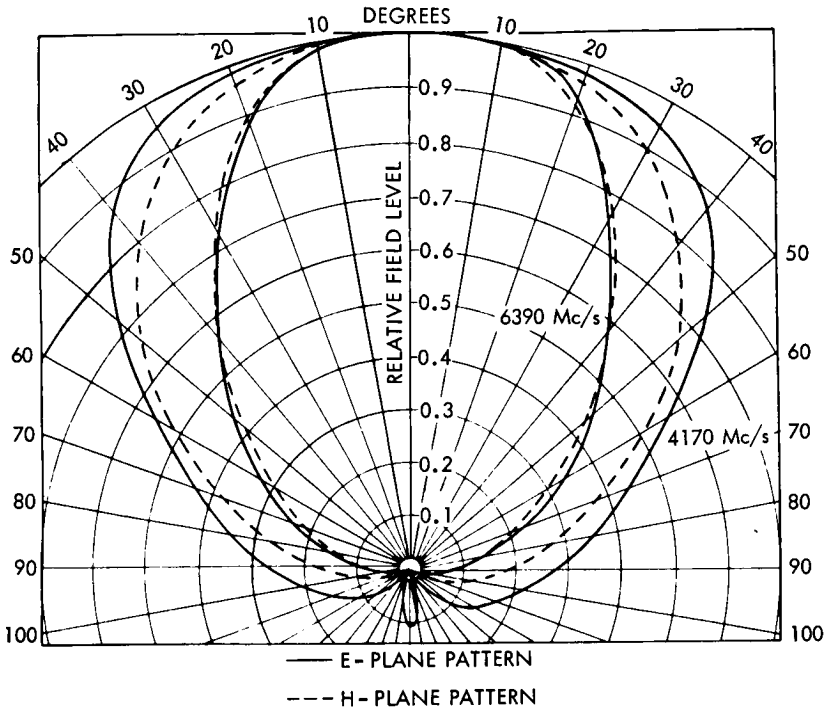


Fig. 5 — Radiation patterns of Telstar feed.

Mc/s pattern, the form of aperture used in the Telstar feed (Fig. 6) is that referred to below.

### Matching

The impedance discontinuity at the feed aperture without compensation is greater at 4170 Mc/s giving a voltage standing wave ratio (VSWR) of about 0.74 compared with 0.96 at 6390 Mc/s. Matching is provided by interposing within the waveguide a section of guide of different impedance. The waveguide section is realized in practice by fitting a dielectric sleeve of the required dimensions within the 2 inch diameter guide. The sleeve has only a small effect on the matching at 6390 Mc/s as the length is about  $0.5\lambda_g$  at this frequency. The position of the sleeve and its thickness are such that improved matching is obtained at 4170 Mc/s.

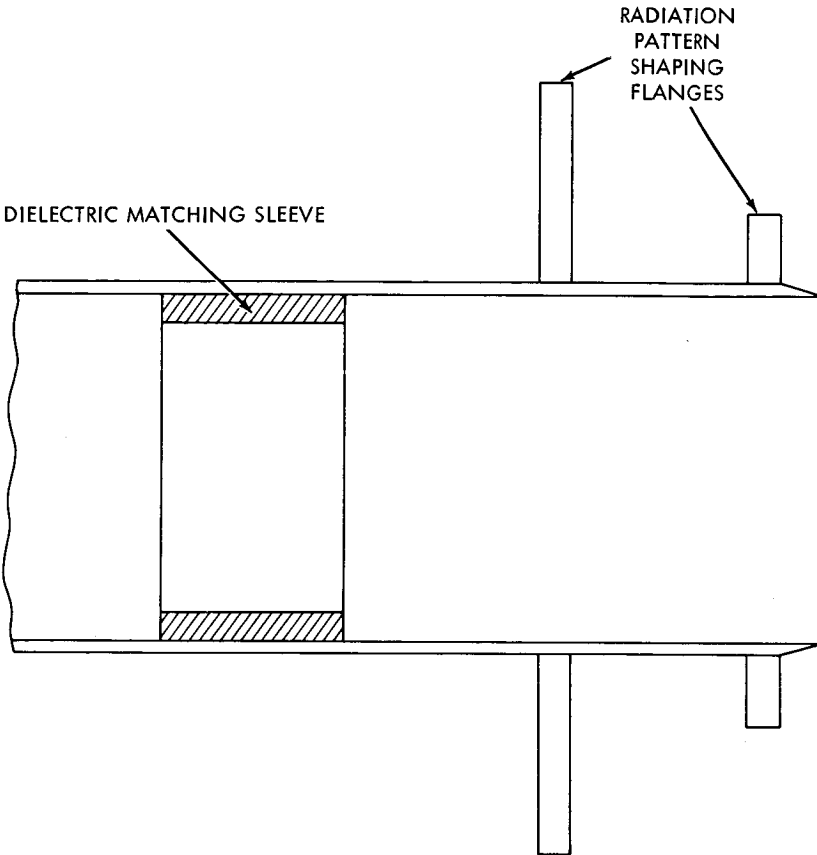


Fig. 6 — Telstar feed.

A VSWR of greater than 0.97 was thus obtained over the transmit and receive frequency bands.

#### *Description*

The Telstar feed (Fig. 6) has the circular brass flanges soldered on the outside of the waveguide, the aperture end of which has been chamfered. The dielectric matching cylinder is of *PTFE* and is set into a slight undercut in the waveguide. Adjustments to the position of the aperture on assembly are made by inserting circular waveguide spacers between the connecting flanges of the primary feed and the waveguide feeder.

### *Feed Performance*

The radiation patterns of the Telstar feed (Fig. 5) show that at the receive frequency the average illumination taper is about  $-13\text{db}$  at  $\pm 90^\circ$ . The aerial gain factor obtained from the feed pattern and the use of equation (3) is estimated to be 0.66. The illumination efficiency is about 0.966 and with a noise-temperature of  $180^\circ\text{K}$  due to the surrounding terrain, the effective increase in system temperature due to spillover is  $2.5^\circ\text{K}$  with the aerial at  $5^\circ$  elevation. The pattern at 6390 Mc/s is considerably more directional and yields a gain factor of 0.51 and an illumination taper of about  $-21\text{db}$  in the focal plane.

Aerial radiation patterns, calculated from the average primary feed patterns, have half-power beamwidths of 12.2 and 8.2 minutes at 4170 and 6390 Mc/s respectively.

### RELAY FEED

#### *General*

In the case of the Relay feed, with the lower transmitting frequency of 1725 Mc/s, compared with the Telstar feed, a larger feed aperture was necessary. Since, however, maximum aerial efficiency and low noise temperature were again required at the receive frequency, it was imperative to consider the design of individual primary sources for transmission and reception. Of the types of feed investigated, a coaxial aperture was considered effective, the 1725 Mc/s signal being transmitted through a coaxial waveguide in the  $\text{TE}_{11}$  coaxial mode, and the 4170 Mc/s signal being received in the associated hollow inner conductor and supported in the  $\text{TE}_{11}$  circular-waveguide mode. Since the cut-off wavelength of the inner guide is less than the transmit wavelength, the highpower signal is rapidly attenuated along the receiving guide.

#### *Description*

The feed assembly (Fig. 7) has waveguide size  $\text{WG}_8$  coupled to a power divider which divides the waveguide into two half-section guides. These diverge to allow the inclusion of a  $\text{WG}_{11}$  binomially-stepped corner in a waveguide combining section. The transducer following transforms the  $\text{WG}_{11}$  waveguide to 2 inch circular guide and the two half-section  $\text{WG}_8$  waveguides to septate 5 in. diameter coaxial guide. The wedges through the transition provide mechanical rigidity as well as continuity of mode transformation. The septate coaxial guide is coupled to a coaxial section in which the transmitted signal

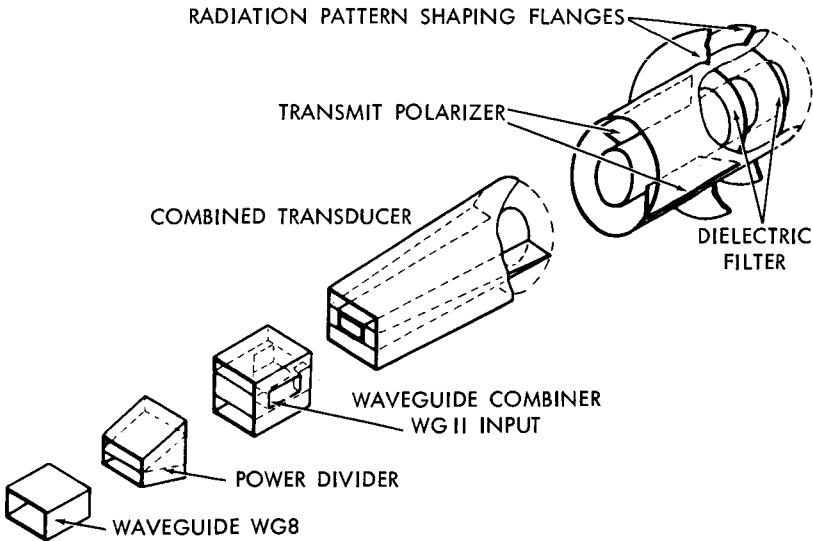


Fig. 7 — Relay feed.

is converted from linear to circular polarization through a matched pair of dielectric quarter-wave plates, of PTFE, having low-loss and a high melting point. The principle of operation of this polarizer, although in coaxial guide, is similar to that used in the Telstar feed, which has been described in a companion paper\*. A dielectric filter near the coaxial aperture, whilst permitting low-loss transmission at 1725 Mc/s, provides substantial reflection at the receive frequency thus reducing radiation of noise from the "high-temperature" transmit aperture. The filter is positioned relative to the aperture to obtain a broad radiation pattern at the receive frequency consistent with low-level spillover. Circular flanges about the outer conductor provide pattern shaping at the transmit as well as the receive frequency.

The dielectric polarizer<sup>4</sup> and the matching in the inner waveguide are similar to those in the Telstar feed.

#### COMPOSITE FEED

##### *Description*

The composite feed (Figs. 8 and 9) comprises the component parts of the Relay and Telstar feeds. The Relay transducer is however sep-

\* See pages 2127-2140.

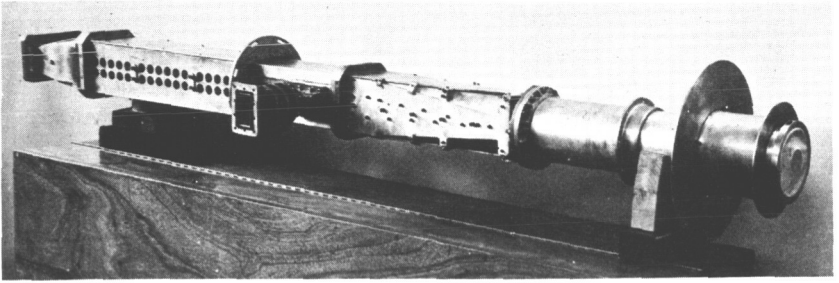


Fig. 8 — Telstar/Relay composite feed unit.

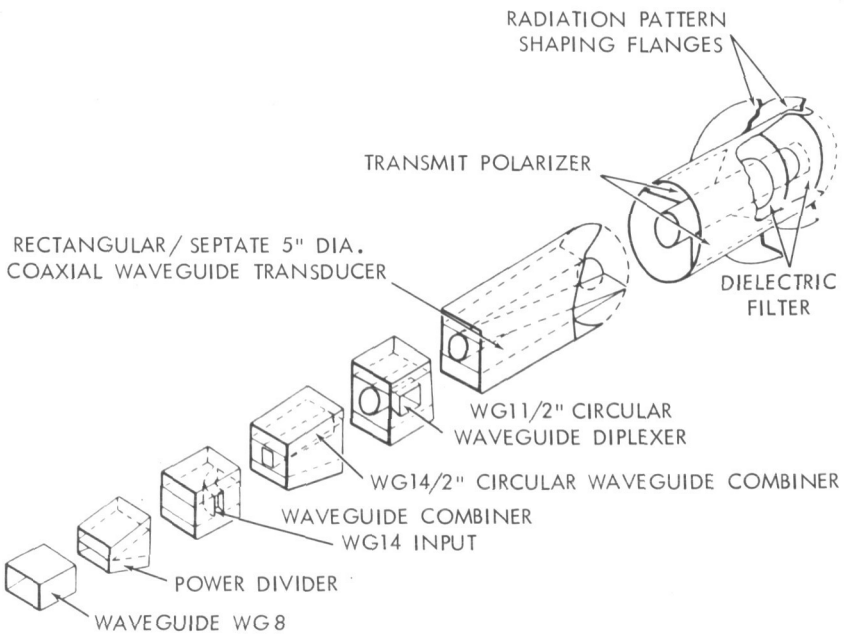


Fig. 9 — Composite Feed

arated to perform the waveguide transformations at different parts of the assembly.

The waveguide from the Relay transmitter is again coupled to a power divider to provide the two half-section guides allowing the inclusion of a  $WG_{14}$  bend. The components in the centre guide are then in the same sequence as in the Telstar feed and comprise a  $WG_{14}$  2 inch circular waveguide transducer,  $WG_{11}$  2 inch circular waveguide

diplexer<sup>4</sup>, dielectric polarizer<sup>4</sup> and the aperture matching section. In the transmitting outer guide the two half sections of WG<sub>8</sub> sandwich the inner guide as far as the second transducer, where the rectangular guides are transformed to septate coaxial guide. The coaxial section is then similar to that in the Relay feed.

In the Telstar experiments, the inner guide and its components are used, the 5 inch diameter aperture and flanges functioning only to shape the radiation pattern. In the Relay experiments, the WG<sub>8</sub> 5 inch diameter coaxial guide carries the transmitting signal, and the internal circular guide receives the satellite signal, the diplexer transferring it to the main receive waveguide feeder.

### *Performance*

The impedance matching into the composite feed gives a voltage standing wave ratio (VSWR) of 0.97 at 1725 Mc/s. The matching characteristic measured over a frequency range is that shown in Fig. 10.

The ellipticity ratio of the circularly polarized fields within the coaxial waveguide is about 0.98. The radiation pattern at the transmit frequency has a field intensity taper of  $-10\text{db}$  in the focal plane, and gives an aerial gain factor of about 0.67. The receive pattern is very similar to that of the Telstar feed and gives a gain factor of 0.66 and an illumination efficiency of 0.967.

### MODEL AERIAL TESTS

During the period of feed development, some considerable experience was obtained with a 10 ft. diameter focal-plane reflector modelled on the Goonhilly aerial. The model primary feeds were sealed to operate

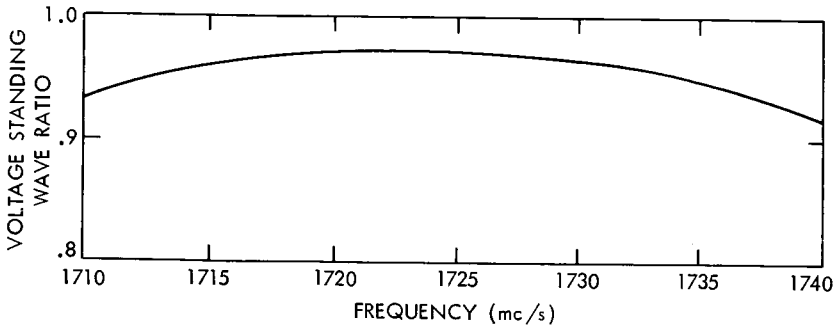


Fig. 10 — Composite feed, overall matching characteristic.

at about 11 Gc/s. A typical radiation pattern obtained with a model Telstar feed, vertically polarized (Fig. 11) shows that apart from the main lobe and immediate side lobes;

1. At bearings up to  $\pm 20^\circ$  relative to the electrical axis, the radiation is largely due to scatter from the tetrapod structure. This was shown by measurements with the tetrapod removed and the feed supported by thin nylon cords.
2. At bearings between  $\pm 20^\circ$  to  $\pm 90^\circ$  the radiation is predominately primary feed spillover.

The pattern with horizontal polarization showed a greater level of primary feed spillover consistent with the larger level measured in this plane in the primary feed radiation pattern (Fig. 6).

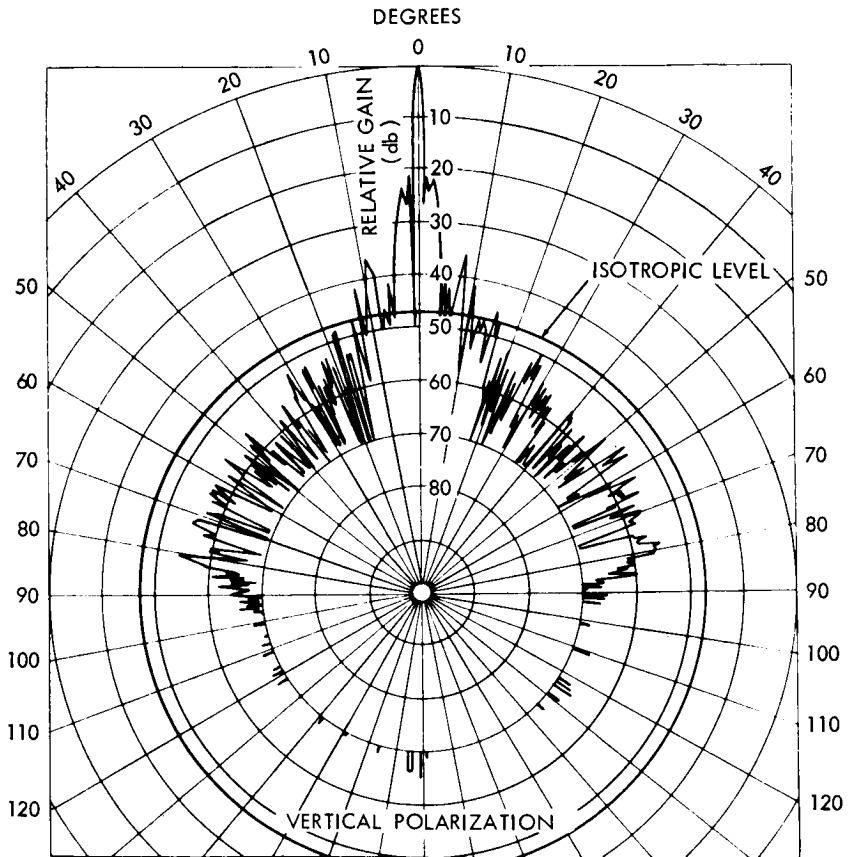


Fig. 11 — H-plane radiation pattern of model aerial with Telstar feed scaled to operate at 11.1 Gc/s.

## CONCLUSIONS

Using idealized primary feed radiation patterns for guidance, it is evident that the permissible spillover is dependent upon the effective noise-temperature of the surrounding terrain, and to a lesser extent on the noise-temperature of the system receiving equipment. Where the equipment and ground temperatures are about 50 and 180°K respectively, a primary feed illumination taper of about -15db is required for an optimum figure of merit at low angles of aerial elevation. The effect of spillover is then to increase the system noise temperature by about 2.8 degrees, the gain factor being 0.77. However, if it were possible to reduce the effective ground temperature further, then the spillover could be increased to provide a greater aerial gain factor.

Experiments with circular flanges about a circular-waveguide aperture have resulted in primary feed patterns giving gain factors of about 0.65 and an effective noise temperature increase of about 2.5°K due to spillover (ground temperature = 180°K). The illumination taper at the reflector periphery is about 19db. If it were possible to broaden the feed pattern further to increase the gain factor, a closer approach to the ideal could be obtained.

## REFERENCES

1. Hogg, D. C., Problems in Low Noise Reception of Microwaves, *I.R.E. Trans., Nat. Symp. on Space Electronics and Telemetry*, 1960, p8-2.
2. Silver, S., Microwave Antenna Theory and Design, *M.I.T. Radiation Laboratory Series No. 12*.
3. Chu, L. J., Calculation of the Radiation Properties of Hollow Pipes and Horns, *J. Appl. Phys.*, 11: 603-610, September 1940.

## APPENDIX I

*List of Symbols*

- $G$  = Aerial gain factor  
 $e$  = Illumination efficiency  
 $\psi$  = Angular half-aperture of aerial, i.e. angle subtended by reflector periphery to the focus  
 $\phi$  = Angle subtended to focus  
 $G_f(\phi)$  = Gain function of primary feed radiation pattern  
 $G_0$  = Primary feed gain when  $\phi = 0$   
 $G_{\pi/2}$  = Aerial gain factor when  $\psi = \pi/2$   
 $\beta$  = phase constant =  $\frac{2\pi}{\lambda} \sqrt{1 - \frac{\lambda^2}{\lambda_c^2}}$   
 $k$  =  $w (\mu\epsilon)^{\frac{1}{2}}$   
 $k_m$  =  $\sqrt{k^2 - \beta^2}$   
 $\mu$  = permeability of medium (henrys)  
 $\epsilon$  = dielectric constant of medium (farads)  
 $\lambda$  = free space wavelength  
 $\lambda_c$  = waveguide cut-off wavelength  
 $\lambda_g$  = guide wavelength  
 $w$  =  $2\pi \times$  frequency  
 $a$  = radius of waveguide  
 $\theta$  = angle subtended to centre of waveguide aperture  
 $J_n(\chi)$  = Bessel's function of  $n$ th order

# Waveguide Feeder System for the Goonhilly Satellite-Communication Earth Station\*

I. F. MACDIARMID and S.C. GORDON

POST OFFICE ENGINEERING DEPARTMENT

There are two features which distinguish the feeder arrangements at a satellite earth station from those used in conventional microwave line-of-sight links. The first is the importance of low loss in all waveguides and components and the second is the need for rotating joints. Losses are important in the receive direction because they contribute significantly to the overall system noise temperature while, in the transmit direction, not only do they waste expensive transmitter power but localized points of high loss can give rise to the formation of arcs when the power is applied. Rotating joints are required on the elevation axis of the aerial to permit waveguide connection between apparatus in the turntable cabin and on the dish.

In the installation at Goonhilly, three separate waveguide connections are required between the turntable cabin and the focus platform; one each for the Telstar and Relay transmitters operating at 6390 and 1725 Mc/s respectively, and one for the receiver feed, routed via the maser cabin on the back of the dish and operating at 4170 and 4080 Mc/s. Dominant-mode rectangular waveguide is used for these runs, and the components and installation practices used follow normal practice as far as possible.

## MAIN WAVEGUIDE RUNS

Fig. 1 shows the layout of the main waveguide runs. Rectangular waveguide is used in sizes WG 8, 11 and 14 for the 1725, 4170 and 6390 Mc/s runs, respectively. Copper waveguide, using electrolytic copper, is employed to minimize the losses.

It can be seen from the sketch that a relatively large number of bends or corners are required on each waveguide run, including some

\* First published by the Institute of Electrical Engineers, November 1962.

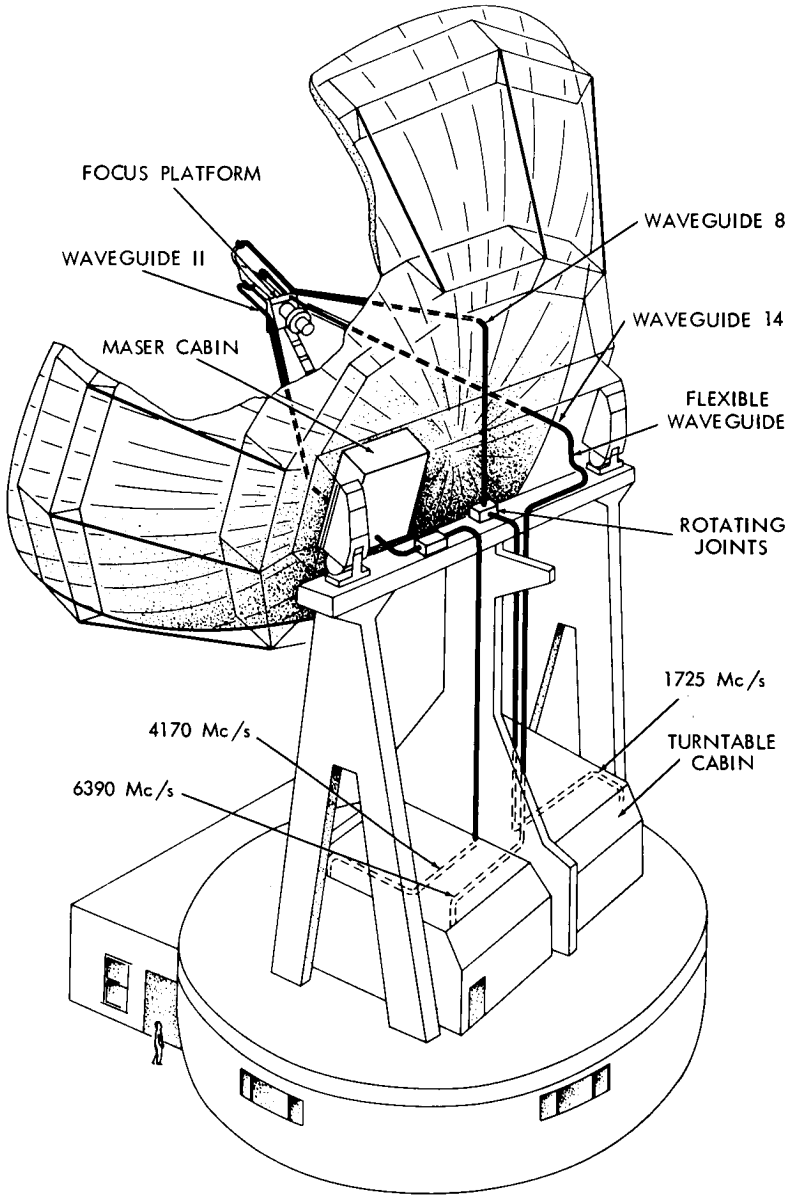


Fig. 1 — Main waveguide runs.

at special angles as at each end of the tetrapod legs. Fabricated corners of the simple mitred type are used in the  $WG_8$  run. Typically, these give a measured VSWR of 0.995 at band centre (1725 Mc/s), the VSWR remaining greater than 0.99 over a bandwidth of  $\pm 20$  Mc/s. In the  $WG_{11}$  run, binomially-matched fabricated corners are used because the required bandwidth is greater—the beacon signal at 4080 Mc/s must be accommodated in addition to the communication signal at 4170 Mc/s. The VSWR of these corners is typically 0.995 at 4170 Mc/s and greater than 0.99 at 4080 Mc/s. In the  $WG_{14}$  run the compactness of the fabricated corner is of less importance than in the larger sizes and also the high power-density of the transmitted signal makes the use of fabricated corners inadvisable. Bends which are made by bending copper waveguide on a suitable mandrel are therefore used. The VSWR of such bends is typically 0.985 at 6390 Mc/s.

The use of large mean powers in waveguide systems is less common than the use of large peak powers. However, experience has shown that waveguide systems carrying large mean powers are subject to the formation of arcs at power levels of more than an order of magnitude below those which might be expected to give trouble from voltage breakdown. No adequate theory exists for this type of breakdown but it is known that one cause is localized over heating of lossy particles such as dust, swarf or shreds from rubber sealing rings. A consequence of the lack of an adequate theory of c.w. breakdown is that it is not possible to design a component with any assurance that it will not breakdown in service unless it has been tested at full power. Special precautions were taken during the installation of the waveguide runs to ensure that the interior surfaces of all waveguide and all components were kept scrupulously clean, particularly in the case of the  $WG_{14}$  installation where the power density is very high. The flange joints on the  $WG_8$  runs were improved by using metallic gaskets.

The performance of the  $WG_{11}$  and  $WG_{14}$  runs were measured after installation with the following results. The  $WG_{11}$  between the maser cabin and the focus platform gave a VSWR of between 0.91 and 0.96 in the frequency range 4070–4185 Mc/s. The attenuation, calculated from VSWR measurements with a short-circuiting plate over the guide, was 0.262 db compared with the theoretical figure of 0.188 db for plain copper guide of the same length. The  $WG_{11}$  run between the turntable cabin and the rotating joint on the elevation axis gave a VSWR of between 0.89 and 0.98 over the frequency range 4060–4175 Mc/s and the attenuation was 0.67 db compared with a theoretical figure of 0.52 db. The  $WG_{14}$  run between the turntable cabin and the

focus platform gave a VSWR of between 0.82 and 0.97 over the frequency range 6350–6430 Mc/s and the attenuation was 1.94 db as compared with a theoretical figure of 1.76 db.

#### ROTATING JOINTS

Rotating joints are required at the elevation axis of the aerial to permit the waveguide connections from the dish to be extended down to the joint, another polarizer and stepped transition convert the circularly polarized wave back to the normal  $TE_{01}$  wave in rectangular guide. The insertion loss of the complete rotating joint is 0.035 db at 4170 Mc/s and the VSWR is nearly constant at 0.95 over the range of angles of rotation which are used and over the frequency range 4080–4183 Mc/s. The rotating joint for the 1725 Mc/s waveguide run is similar in principle to that just described but uses waveguide turnstiles to convert from rectangular guide to circularly polarized waves in circular guide. This arrangement leads to a shorter axial length. Initially, some doubts were experienced about the bandwidth of this type of joint but the performance has proved to be adequate. At mid-band frequency, 1725 Mc/s, the VSWR is about 0.99 irrespective of angle of rotation while at  $\pm 20$  Mc/s the VSWR varies between 0.95 and 0.99 with angle of rotation.

#### WAVEGUIDE FOR RECEIVER INPUT

The losses which occur between the primary feed at the focus of the dish and the input port of the maser are of particular importance because they contribute significantly to the overall system noise temperature. Unfortunately, a large number of waveguide components is required in this part of the system in addition to the plain waveguide, and this increases the difficulty in making the total loss small. The path between the primary feed and the maser includes the broad-band polarizer and diplexer (described elsewhere), flexible waveguide to permit the feed to be moved, some 31 ft of waveguide between the diplexer and the maser cabin, and the rather complex assembly of components within the maser cabin which is illustrated in Fig. 2. The assembly in the maser cabin is required to provide the desired test facilities and to provide an alternate path for the beacon signal which lies outside the pass band of the maser.

Of the components in the maser cabin, the filter which separates the beacon signal from the communication signal could have the greatest potential for introducing loss in the communication channel. However

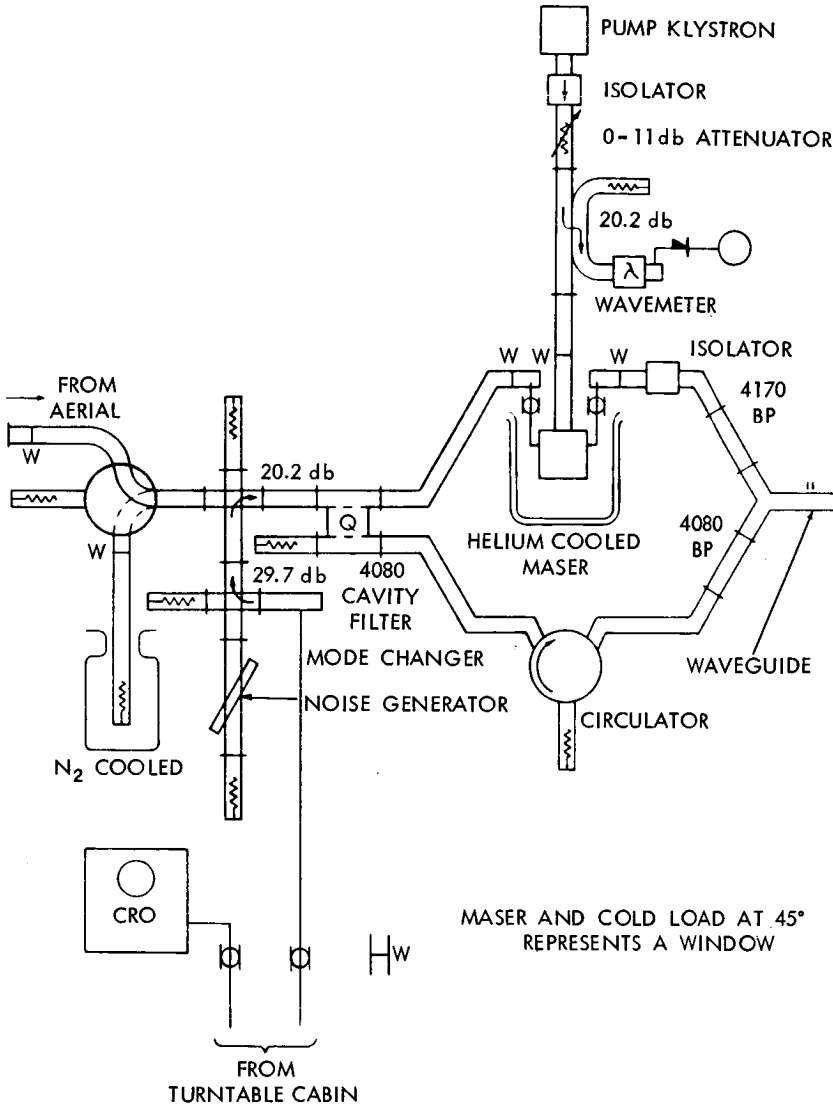


Fig. 2 — Schematic of equipment in aerial cabin.

by employing a resonant cavity coupler for the beacon channel this loss is only 0.033 db at 4170 Mc/s, and the loss in the beacon path is 1.3 db at 4080 Mc/s. The coupling loss between the beacon guide and communication channel output is 33 db so the extra contribution to system noise is negligible.

The filter pair which combines the communication and beacon signals at the output of the maser and a similar pair which is fitted in the turntable cabin and feeds the two receivers, are of straightforward design and use apparatus in the turntable cabin. A separate joint is required for each frequency band but the basic principle of them all is the same. This is that the  $TE_{01}$ -mode wave in rectangular guide is converted to a circularly polarized (or rotating)  $TE_{11}$ -mode wave in circular guide. The joint itself is in the circular guide and uses a simple choked flange, the rubbing contact occurring at the high-impedance junction between the two quarter-wave sections of the choke. After the joint, the wave is converted back again to the dominant mode in rectangular guide. This class of rotating joint was chosen for economy in design effort as some of the components used in it are also required for other purposes.

The 6390 Mc/s version of the rotating joint was not completed in time for the initial installation at Goonhilly and a length of flexible (twistable) rectangular waveguide was installed instead. This was arranged so that it is straight when the aerial elevation is  $45^\circ$ , the maximum bending thus being  $\pm 45^\circ$ . This arrangement has proved so successful that it is doubtful whether it is worthwhile replacing it with the more complex rotating joint.

Fig. 3 shows a sketch of the 4170 Mc/s rotating joint. To minimize the axial length of the unit, a binomially corrected stepped transition is used to convert the  $TE_{01}$  wave in rectangular guide to a  $TE_{11}$  wave in circular guide. A constant guide-width is maintained throughout the intermediate rectangular steps of the transition to simplify the problem of obtaining a theoretical starting point for the design. The final dimensions are, however, obtained by experimental modifications of the initial design. In its final form the transition has a VSWR in excess of 0.98 from 4070 Mc/s to greater than 4300 Mc/s, the figure for 4170 Mc/s being about 0.99. The  $TE_{11}$  wave in the circular guide is converted to a circularly polarized wave by the finline polarizer. This contains a copper fin inserted into circular guide at an angle of  $45^\circ$  to the plane of polarization of the linearly polarized incident  $TE_{11}$  wave, and retards the phase of the resolved component of the incident wave which is parallel to the fin by  $90^\circ$  with respect to the component which is at right angles to the fin. The circularly polarized wave which emerges has the necessary circular symmetry to permit the joint to be rotated without introducing variations in its transmission properties. The joint itself is of the simple choke-flange type with a rubbing contact at the current null in the choke. Time did not permit the

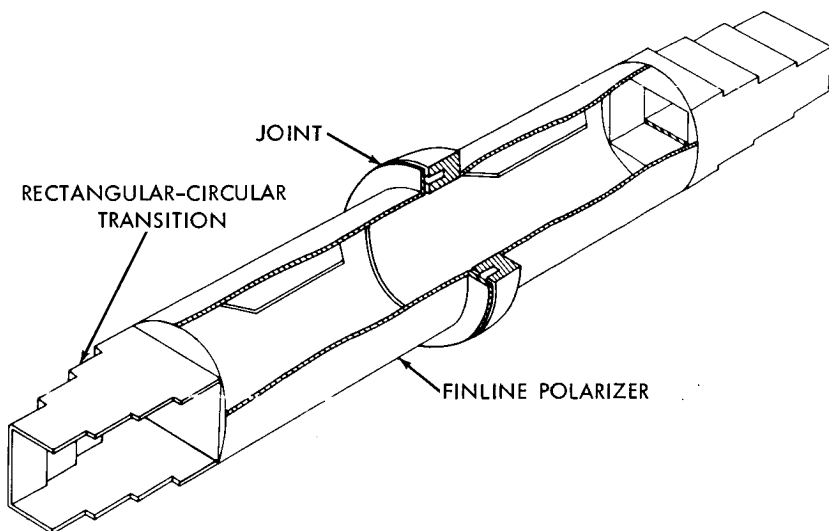


Fig. 3 — Rotating joint.

investigation of more sophisticated joints but present indications are that the simple type is quite adequate. Following the joint, another polarizer and stepped transition convert the circularly polarized wave back to the normal  $TE_{01}$  wave in rectangular guide. The insertion loss of the complete rotating joint is 0.035 db at 4170 Mc/s and the VSWR is nearly constant at 0.95 over the range of angles of rotation which are used and over the frequency range 4080–4183 Mc/s. The rotating joint for the 1725 Mc/s waveguide run is similar in principle to that just described but uses waveguide turnstiles to convert from rectangular guide to circularly polarized waves in circular guide. This arrangement leads to a shorter axial length. Initially, some doubts were experienced about the bandwidth of this type of joint but the performance has proved to be adequate. At mid-band frequency, 1725 Mc/s, the VSWR is about 0.99 irrespective of angle of rotation while at  $\pm 20$  Mc/s the VSWR varies between 0.95 and 0.99 with angle of rotation.

#### WAVEGUIDE FOR RECEIVER INPUT

The losses which occur between the primary feed at the focus of the dish and the input port of the maser are of particular importance because they contribute significantly to the overall system noise tem-

perature. Unfortunately, a large number of waveguide components is required in this part of the system in addition to the plain waveguide, and this increases the difficulty in making the total loss small. The path between the primary feed and the maser includes the broad-band polarizer and diplexer (described elsewhere), flexible waveguide to permit the feed to be moved, some 31 ft of waveguide between the diplexer and the maser cabin and the rather complex assembly of components within the maser cabin which is illustrated in Fig. 2. The assembly in the maser cabin is required to provide the desired test facilities and to provide an alternate path for the beacon signal which lies outside the pass band of the maser.

Of the components in the maser cabin, the filter which separates the beacon signal from the communication signal could have the greatest potential for introducing loss in the communication channel. However by employing a resonant cavity coupler for the beacon channel this loss is only 0.033 db at 4170 Mc/s, and the loss in the beacon path is 1.3 db at 4080 Mc/s. The coupling loss between the beacon guide load and communication channel output is 33 db so the extra contribution to system noise is negligible.

The filter pair which combines the communication and beacon signals at the output of the maser and a similar pair which is fitted in the turntable cabin and feeds the two receivers, are of straightforward design and use three quarter-wave-coupled triple-post cavities. The isolator which follows the maser and the circulator in the maser by-pass are provided to ensure that the filters, which are designed on an insertion loss basis, are correctly terminated and so give their design performance.

In view of the importance of knowing the very small losses introduced by individual components an experimental equipment for measuring very small losses has been developed. An analysis of the loss figures for the pre-maser waveguide components is given in Table 1.

It can readily be shown that a matched network of loss  $L$  (input/output power ratio) at a temperature  $T_0$ , inserted between an aerial of noise temperature  $T_a$  and a low-noise receiver (e.g. a maser) at a temperature  $T_r$ , increases the effective aerial temperature by  $T_0(L - 1)$ . Thus the total effective noise temperature of the system referred to the aerial is

$$T_a + T_0(L - 1) + LT_r.$$

By inserting the figures of Table I this becomes

$$(T_a + 42 + 1.14 T_r)^\circ\text{K},$$

or referred to the maser input,

$$(0.87 T_a + 37 + T_r)^\circ\text{K}.$$

As the system noise temperature measured at the maser input, with the aerial pointing at zenith, is  $56^\circ\text{K}$  and the effective maser noise temperature is of the order of  $13^\circ\text{K}$ , the component of the noise temperature due to the waveguide losses cannot differ very much from the estimated figure of  $37^\circ\text{K}$ . While this figure is large, it can be seen from the Table that there is not much scope for a substantial reduction unless the first-stage amplifier can be placed nearer the feed. The largest single component is the waveguide run between the diplexer and the maser cabin. Consideration is being given to using oversized rectangular and even circular guide, for the straight portion of the run down the tetrapod leg, but the maximum saving would only be some  $7^\circ\text{K}$ . Cooling of the waveguide run has been investigated, but it is not considered worth-while.

TABLE 1 — ANALYSIS OF LOSSES IN PRE-MASER WAVEGUIDE COMPONENTS

Component	Loss (db)
Diplexer (incl. polarizer)	0.100
Connecting section (incl twist and 1 corner)	0.074
External WG <sub>11</sub> (incl. flexible section and 2 corners)	0.232
Internal WG <sub>11</sub> (incl. 1 window and 2 corners)	0.021
Waveguide switch	0.028
Directional coupler	0.048
Internal WG <sub>11</sub> (incl. 5 corners)	0.047
Beacon separation filter	0.033
Total	0.583

## CONCLUSIONS

The special features of the waveguide installation on the aerial at Goonhilly have been outlined and performance data have been given. The installation and all its components have functioned successfully in the manner expected. The most significant feature is the relatively large contribution which the waveguide installation between the pri-

mary feed and the maser makes to the system noise temperature. This is not due to any one cause but arises partly from the distance involved and partly from the necessary complexity of the arrangements. While it can be expected that further work will lead to a reduction in the losses in this part of the system, it seems unlikely that any very large reduction will prove possible unless the first-stage amplifier can be placed nearer the feed.

N67 12313

# The Travelling Wave Maser Amplifier in the Goonhilly Radio Station\*

J. C. WALLING and F. W. SMITH

MULLARD RESEARCH LABORATORIES

*The design and performance of the 4170 Mc/s travelling wave maser at present installed at the GPO Radio Station, Goonhilly Downs, is described. Means of increasing the bandwidth of the device are discussed.*

AUTHOR

## SYSTEM REQUIREMENTS AND MASER SPECIFICATION

The signal entering the first stage of the Goonhilly receiver is very small, about  $10^{-12}$  watts, and the bandwidth of the system is some tens of megacycles. If the received signal is to be amplified and detected with an acceptable signal to noise ratio then it is essential that the noise contribution made by the first stage amplifier should be as small as possible. It was therefore decided that the first stage amplifier should be a solid state travelling wave maser (TWM) having sufficient net gain to make the noise contribution of the second stage amplifier insignificant. The specification for this TWM is as follows:

Signal Frequency	4170 Mc/s
Gain (minimum)	20 db
Bandwidth to 3 db points	25 Mc/s
Noise temperature	15°K
Input VSWR	0.666 over the operating band
Operating life per filling of liquid helium	8 hrs.

## DESIGN OF THE MASER

The overriding consideration in the design of this maser was the need to produce an engineered and operating device within some six or seven months of the initiation of the project. Sophistication in the

\* First published by the Institute of Electrical Engineers, November 1962.

design therefore was subordinate to expediency and as far as possible use was made of immediately available materials and techniques.

### *Active Materials*

Because of its ready availability in large single crystals and also because of its proven characteristics synthetic ruby was selected as the active material. Previous experience indicated that the best orientation for maser operation at frequencies below 7 kMc/s is that in which the applied magnetic field is at right angles to the c-axis of the ruby. In this orientation the ground state of the  $\text{Cr}^{3+}$  ion is split by the combined action of the crystal fields and the applied magnetic field according to the energy level diagram of Fig. 1.

It has been found experimentally that when the separation of levels 1 and 2 corresponds to a frequency of 4170 Mc/s the greatest inversion of the populations of these levels can be obtained if the pump is applied between levels 1 and 4, i.e., at a frequency of 30,150 Mc/s. In ruby having a Cr to Al ratio of 0.05 atoms per cent we find that 1-4 pumping produces an inversion ration of 2.7 at 1.4°K.

Operation at 1.4°K involves reduction of the liquid helium bath pressure to about 2.5 mm Hg. In practice this is accomplished within less than half an hour of filling and in an experimental system such as this where operation over more than three successive satellite passes is rarely required this is no disadvantage.

Assuming that the excitation at the signal frequency is by an RF magnetic field circularly polarised in the plane perpendicular to the applied field (a condition which is closely approximated in practice) and using the table of transition probabilities prepared by Chang and Siegman<sup>3</sup> we calculated by the method outlined<sup>2</sup> that 1-4 pumping in 0.05% ruby at 1.4°K will produce a value of  $Q_m$  of  $-15/\eta$ .  $Q_m$  is the magnetic quality factor of the structure and is essentially a measure of the ratio of the energy stored in the structure to the power absorbed by the maser material,  $\eta$  is the filling factor of the maser and is the ratio of the mean square RF magnetic field over the volume of the maser crystal to that over the volume of the propagating structure. Although filling factors up to 0.5 are theoretically possible in a TWM experience suggests that 0.2 is a practical figure. Taking  $\eta = 0.2$  we have  $Q_m = -75$  as a basis for design.

### *Non-Reciprocity*

A travelling wave maser exhibits some non-reciprocity by virtue of the fact that circularly polarised field of opposite sense interact to

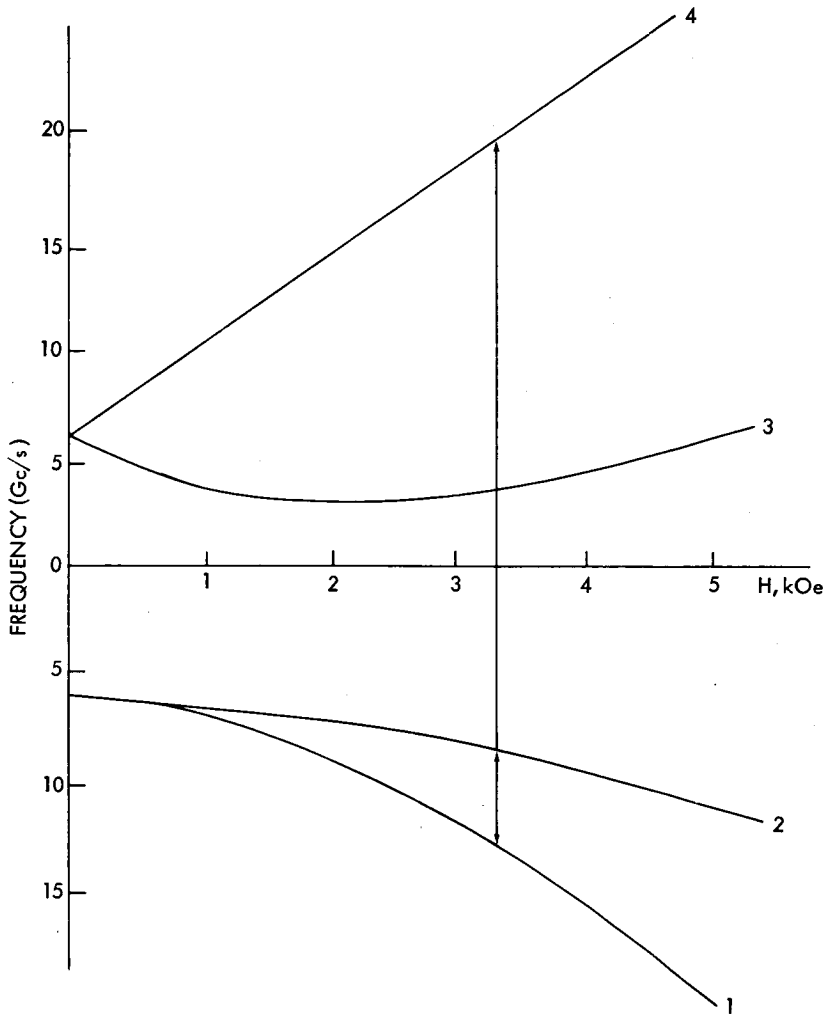


Fig. 1 — Energy level diagram (Ruby,  $\theta = 90^\circ$ ).

different extents with the active ions<sup>4</sup>. However, additional non-reciprocal backward loss must be provided if a completely stable device is to be obtained. Polycrystalline yttrium iron garnet is a suitable material for this purpose as its absorption line width is reasonably narrow (about 150 oersteds) even at liquid helium temperature. Because of its high susceptibility only a small volume of this material needs

to be incorporated in the maser. The dimensions of the yttrium iron garnet (YIG) are adjusted in order that resonant interaction at the signal frequency can be obtained with the same applied field as is required to give the correct ruby energy level splitting. In the present case the field is 3,280 oersteds and an appropriate shape for the YIG is a flat disc of aspect ratio 0.1 with the plane of the disc perpendicular to the applied field.

Obviously it is necessary that the YIG discs should be incorporated in the TWM in such a way that they are acted upon by a substantially circularly polarised RF field of opposite sense to that acting upon the ruby. This is accomplished by making use of a comb slow wave structure as described in the following section.

### *Slow Wave Structure*

The small signal gain of a TWM can readily be expressed in terms of two quality factors,  $Q_m$  the magnetic  $Q$  discussed above and  $Q_0$  the intrinsic  $Q$  of the propagating structure determined by ohmic and dielectric losses and also the forward loss of the YIG. If  $r$  is the slowing factor (the ratio of the group velocity in the propagating structure at the signal frequency to the free space velocity of light) and  $N$  is the number of free space wavelengths in the structure the net gain of the device, expressed in db is

$$G = 27.3 rN \left( \frac{1}{Q_m} - \frac{1}{Q_0} \right).$$

A structure having a slowing factor of 100 and an active length of 1.6 free space wavelengths (which is a convenient figure at a frequency of 4170 Mc/s) will therefore give an electronic gain of 58 db if  $Q_m = -75$ .

A suitable slow wave structure for the TWM is then one having this slowing factor and containing regions in which the RF magnetic field is circularly polarised, the structure must also be such as to allow propagation of the pump frequency, not necessarily in a slow mode.

All these requirements can be met by structures consisting essentially of an array of parallel conductors in which the RF magnetic field is substantially circularly polarised, the senses of polarisation on the two sides of the array being opposite.

A comb structure<sup>1, 5</sup> is used in the present maser and has dimensions as indicated in Fig. 2, the positioning of the ruby, dielectric and YIG discs in the structure is apparent from this figure.

The dispersion characteristic for this structure when containing liquid helium is similar to that shown in Fig. 3, and the slowing factor

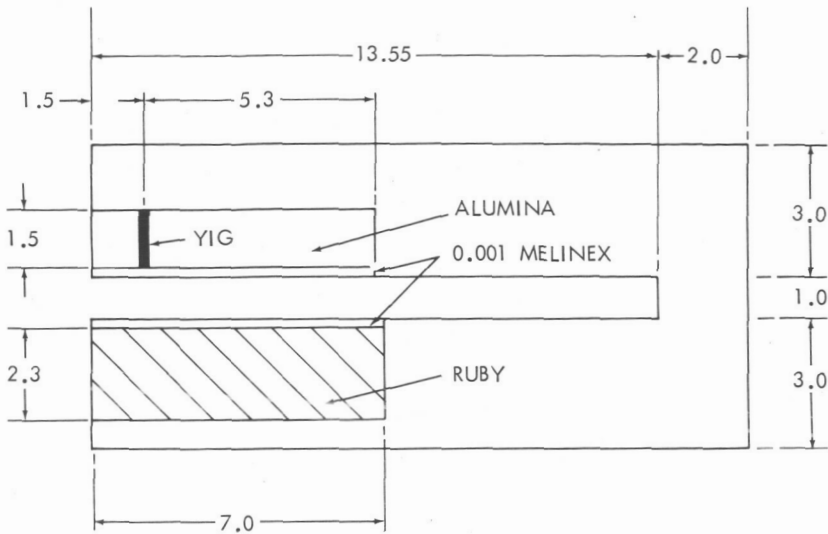


Fig. 2a — Cross-section of the 4170 Mc/s comb structure.

at the signal frequency is 110. The comb is milled from a block of high conductivity copper, this form of construction tending to minimize conductor losses. (The slowing factor of 110 quoted above was inferred from the observed pass band of the structure, subsequent measurements of the  $\omega\beta$  characteristic of a similar comb suggest that this is over-estimated by about 10%.)

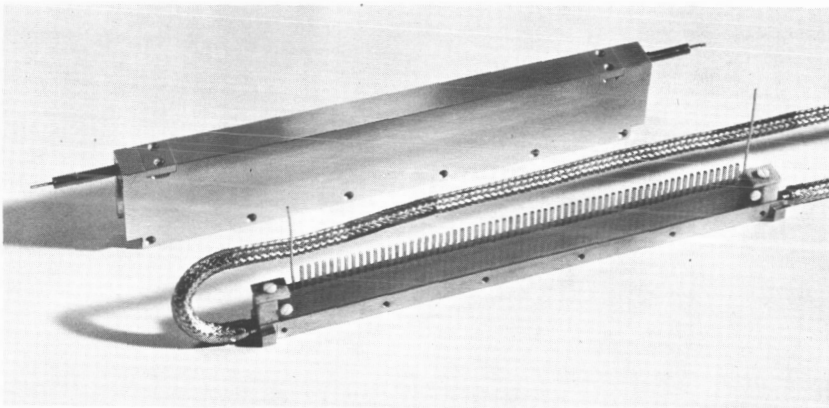


Fig. 2b — The comb structure.

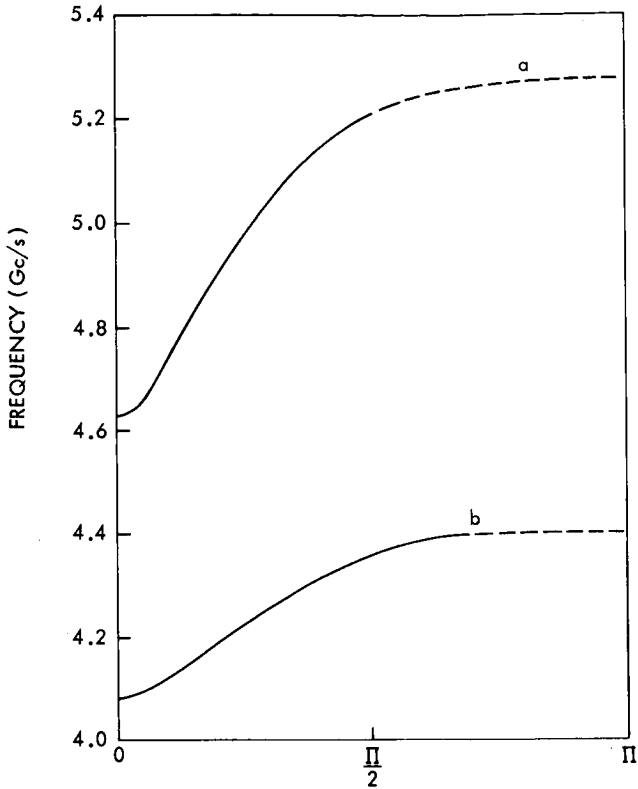


Fig. 3 — Phase change per conductor.

### *Input Leads*

The input and output leads to the maser are air dielectric coaxials of low thermal conductivity (silver plated copper nickel). The leads have an outside diameter (od) of 15 mm and a characteristic impedance of 72 ohms. It is important that these leads have a low electrical loss as they make the main contribution to the maser noise temperature. At the cryostat head these leads terminate in vacuum sealed wave guide to coaxial transitions. At their lower end the leads have tapered transitions to 5 mm od coaxials having *P.T.F.E.* dielectric. These latter coaxials are matched to the comb by means of the arrangement shown in Fig. 4. Some adjustment of the separation between the matching conductor and the first finger of the comb is

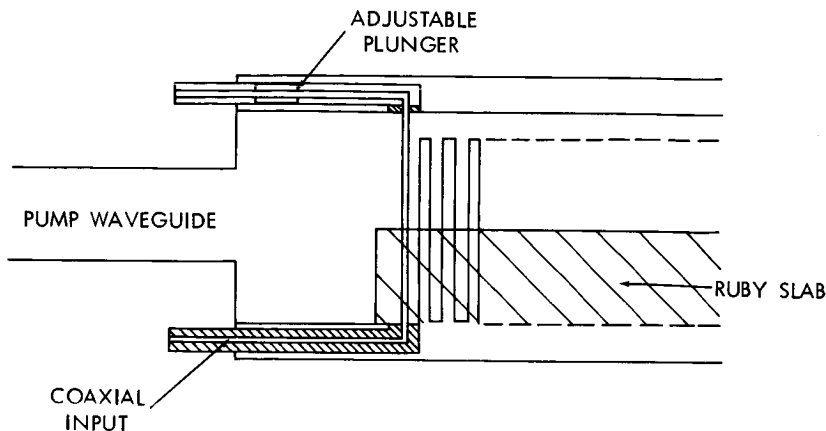


Fig. 4 — Schematic of matching unit.

necessary if the optimum match is to be secured over the pass band of the structure.

The pump power at 30,150 Mc/s is supplied by way of thin walled (0.2 mm) copper nickel waveguide with the internal dimensions of WG<sub>22</sub>. Approximately 40 mW is required to saturate the pump transition, this output power is obtained from selected R9518 klystrons.

In this connection we may note that operation at 1.4°K calls for substantially less pump power than does operation 4.2°K and thus although, with a given pump source, pump frequency stabilization may be necessary for 4.2°K operation it is not necessary for 1.4°K operation. No pump frequency stabilization is provided in the present maser.

### *Maser Packaging*

The final form of the maser package depends on the form of magnet used. Superconducting magnets by virtue of their light weight and very high stability are attractive for use with masers operating at liquid helium temperatures and at the outset of the development of the Goonhilly maser it was hoped to make use of superconducting magnets. It soon became apparent, however, that the construction of a superconducting magnet giving the requisite field homogeneity was a matter of some difficulty and in view of the short time available for development a permanent magnet version of the maser package was constructed as a parallel development. The permanent magnet version of the maser is illustrated in Fig. 5 in which the trimming coils used to adjust the field of the permanent magnet are clearly visible.

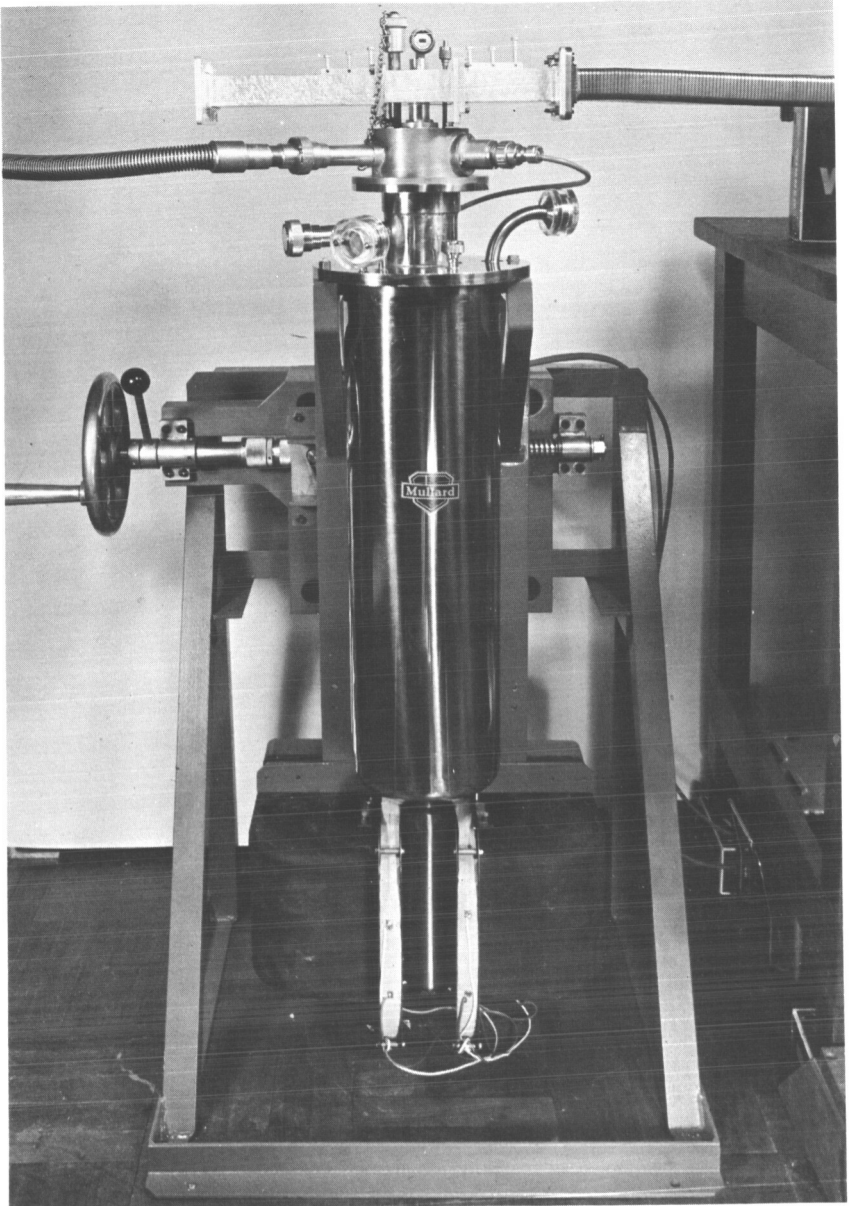


Fig. 5 — Maser package with permanent magnet.

Following the work of Cioffi<sup>6</sup> on the use of superconducting screens in magnetic circuits a superconducting magnet has been developed in which satisfactory operation of this maser in the laboratory has been obtained. Superconducting magnet masers have however not been employed in the Goonhilly system.

#### MASER PERFORMANCE

##### *Laboratory Operation*

In the permanent magnet shimmed to provide a field of 3280 oersted uniform to better than 0.1% over the volume of the ruby the maser gives in the laboratory the performance summarized as follows:

Operating temperature	1.4 °K
Electronic gain	50 db
Bandwidth to 3 db points	16 Mc/s
Field	3280 oersteds
Pump frequency	30, 150 Mc/s
Noise temperature	15 ± 4 °K
Isolator backward loss	60 db
Isolator forward loss	3 db
Structure loss	8 db
Net forward gain	39 db
Input VSWR	1.4
Operating life/filling of He	8 hrs.

Saturation effects become apparent at an input power of -65 dbm. The effect of possible breakthrough from the Goonhilly 6390 Mc/s transmitter on the maser performance was investigated in the laboratory and with the maximum power available (100mW) at this frequency incident on the maser the performance at 4170 Mc/s was unaffected, and subsequent site experience confirmed this.

The recovery time of the maser after saturation at 4170 Mc/s is 150 milliseconds.

##### *Bandwidth*

The specification bandwidth of 25 Mc/s is slightly greater than can be achieved in a TWM in a uniform magnetic field and giving a net gain in excess of 20 db (Fig. 6). This was realized at the outset of the project and the maser was therefore designed to give a higher gain

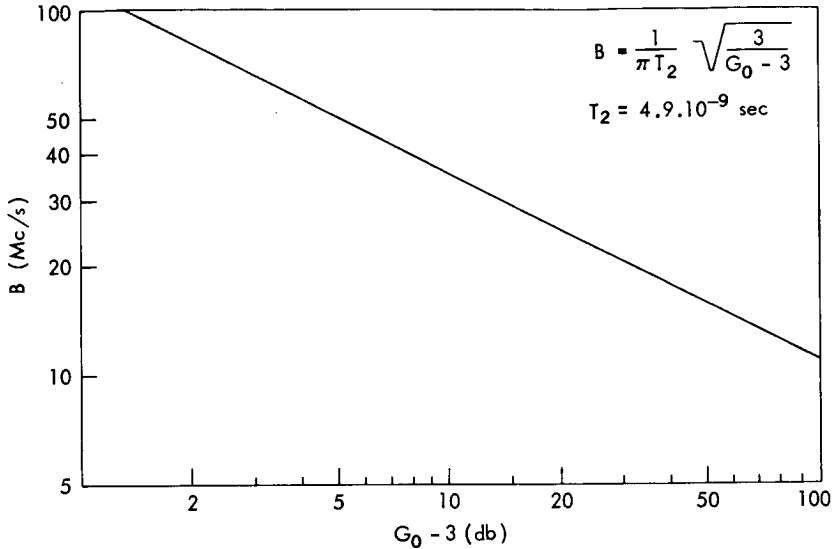


Fig. 6 — Bandwidth versus electronic gain ( $G_0$ ) for TWAM in a uniform field.

than the specified 20 db in a uniform field in order that ultimately the bandwidth could be increased for instance by field staggering. (Another reason why the maser was designed for high gain was that the operating temperatures which would be obtained at Goonhilly were uncertain in view of the considerable length of pipe between the maser and the helium pump—in the event  $1.4^\circ\text{K}$  was readily achieved.)

The bandwidth of a TWAM can be increased in practice by staggering either the crystal orientation or the magnetic field along the length of the maser. Orientation staggering is however undesirable as it results in an unfavorable exchange of gain for bandwidth.

The bandwidth resulting from various forms of field staggering has been calculated on the assumption of a Lorentzian line shape and is plotted against peak electronic gain in Fig. 7. Clearly a substantial increase in bandwidth can be obtained by the simple expedient of introducing a step in the magnetic field by suitably shimming the magnet.

In Fig. 9 the observed gain of the maser is plotted against frequency for the case in which a step is introduced in the magnetic field by means of 0.006" steel shims on the magnetic pole faces (magnet pole gap = 2.25").

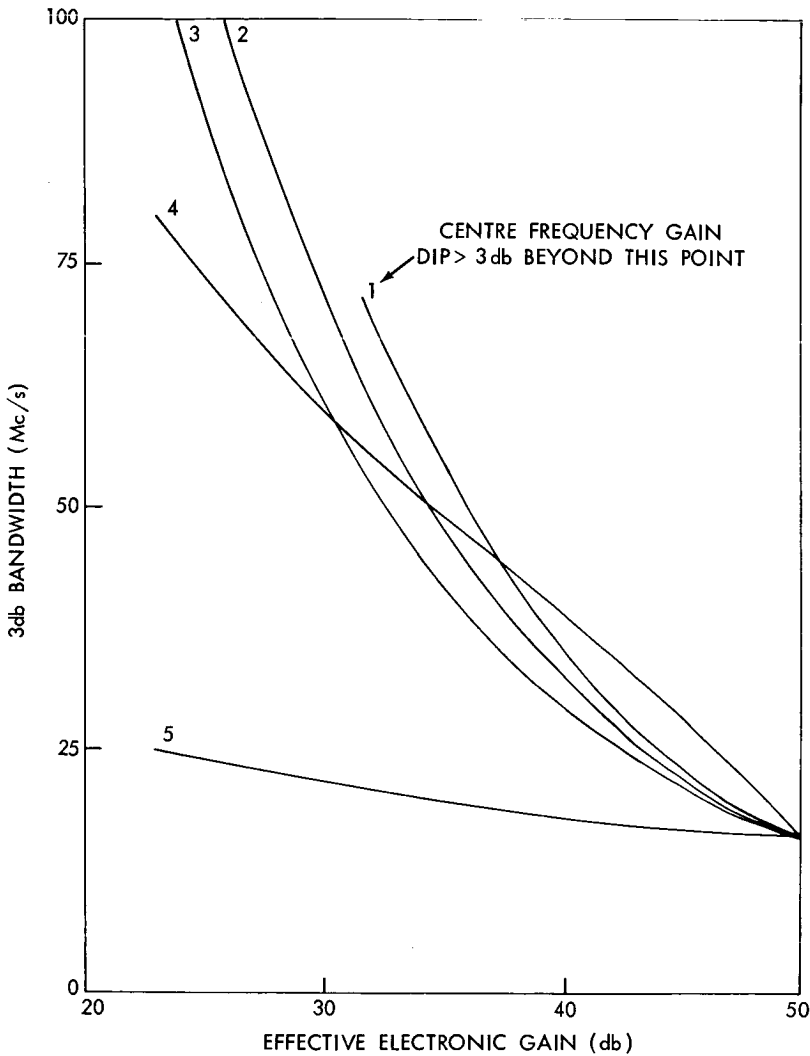


Fig. 7—Bandwidth curves for maser with electronic gain of 50 db in uniform magnetic field with operating temperature  $1.4^{\circ}\text{K}$  and  $T_2 = 5.10^{-9}$  sec: (1) Magnetic field variation—single step; (2) Magnetic field variation—sinusoidal; (3) Magnetic field variation—linear; (4) Gain equalisation; and (5) Operating temperature variation.

*Site Operation*

The uniform field permanent magnet version of the maser was installed in the Goonhilly aerial in June, 1962 (Fig. 9) in a cabin at the back of the dish and gave a similar performance to that measured in the laboratory. It was, however, not possible to obtain consistently an operating life of eight hours per filling of liquid helium when operating at  $1.4^{\circ}\text{K}$ , this being presumably due in part at least to the continuous movement of the aerial during satellite tracking. Changes in elevation of up to  $100^{\circ}$  are possible and for this reason the maser is mounted at  $45^{\circ}$  to the vertical when the dish is pointing to the horizon (Fig. 6).

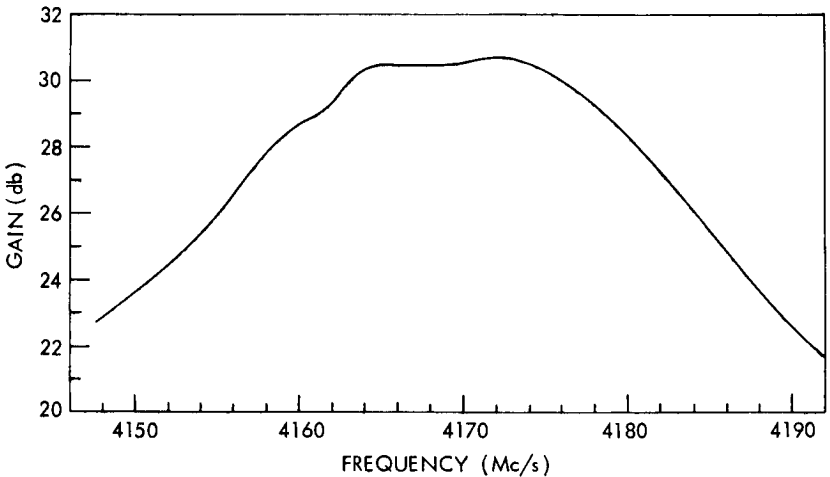


Fig 8 — Net gain-frequency characteristic of broad-band maser.

Following the initial Telstar experiments which were carried out using the maser in a uniform magnetic field the bandwidth of the device was increased by shimming the magnet as described above. A further improvement made has been the replacement of the small helium dewar vessels illustrated in Fig. 5 by substantially larger vessels as shown in Fig. 10. The use of the larger vessel has increased the continuous operating time per filling of liquid helium from less than eight hours to about 2 days.

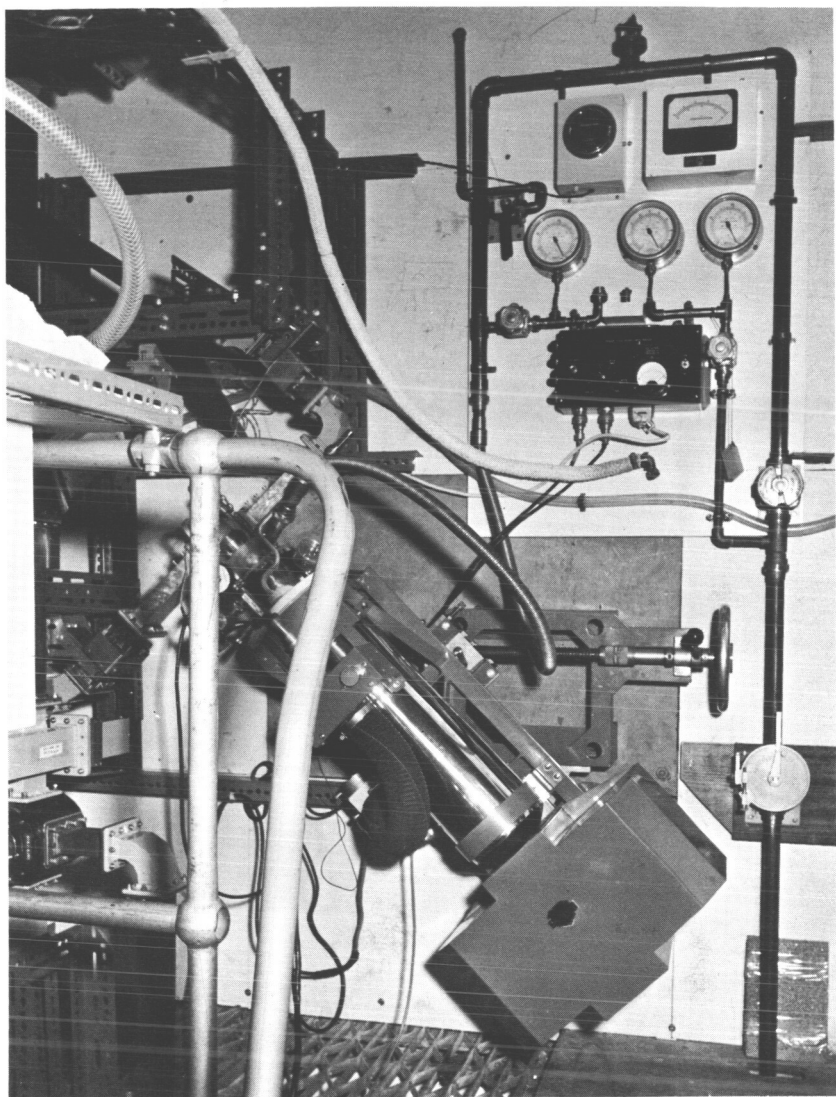


Fig. 9 — Maser installed at Goonhilly.



Fig. 10 — Maser with large dewar at Goonhilly.

## ACKNOWLEDGMENT

The design, construction, and testing of this maser was completed in six months. This rapid development would not have been possible without the enthusiastic and able cooperation of Messrs. J. M. W. Cook, J. D. A. Day, E. L. Hentley, D. G. Stevenson, M. C. Kite and other of the authors' colleagues at Mullard Research Laboratories which they gratefully acknowledge. The authors would also like to acknowledge the generous assistance in respect of equipment and installation given by Dr. H. N. Daghish and Mr. M. R. Child of the GPO Research Establishment, Dollis Hill.

## REFERENCES

1. DeGrasse, R. W., Schulz-DuBois, E. D., and Scovil, H. E. D., The Three-Level Solid State Traveling-Wave Maser, *Bell Syst. Tech. J.* 38(2): 305-334, March 1959.
2. Walling, J. C., Travelling-Wave Maser, *Low Noise Electronics*, (K. Endresen, ed.): 225-234, Oxford. New York: Pergamon Press; Published for and on behalf of Advisory Group for Aeronautical Research and Development, NATO, 1962.
3. Chang, W. S., and Siegman, A. E., Characteristics of Ruby for Maser Applications, *Electronics Laboratories*, Stanford, TR 156-2 (PB 136586), September 30, 1958.
4. Osborn, J. A., Demagnetizing Factors of the General Ellipsoid, *Phys. Rev.* 67: 351-357, June 1945.
5. Butcher, P. N., An Introduction to the Theory of Solid-State Masers with Particular Attention to Traveling-Wave Maser, *IEE Proc.* 107B(34): 341-351, 352-353, July 1960.
6. Cioffi, P. P., Approach to the Ideal Magnetic Circuit Concept through Superconductivity, *J. Appl. Phys.* 33(3): 875-879, March 1962.

# The Helium System of the Maser Installation at the Goonhilly Satellite-Communication Earth Station\*

H. N. DAGLISH and M. R. CHILD

POST OFFICE ENGINEERING DEPARTMENT

A travelling-wave solid-state maser amplifier is used to provide the first stage of amplification in the receiving system at the communication-satellite earth-station at Goonhilly Downs. While the maser itself was built by an industrial research laboratory, the auxiliary supplies and equipment essential for the operation of the maser were designed and built by staff of the Post Office Research Station. A major part of this auxiliary equipment consists of apparatus for handling the helium refrigerant.

## GENERAL DESCRIPTION

The maser is a microwave amplifier in which the amplification takes place in a single crystal of "pink" ruby-crystalline alumina containing a small percentage of chromium. Microwave power, at a frequency of about 30 Gc/s, is injected into the crystal and temporarily disturbs the thermal equilibrium of outer electrons in the chromium ions in the crystal. Some of the energy stored in this way is available to amplify a low-level signal at a frequency of 4.17 Gc/s. The particular frequencies involved are determined by an applied steady magnetic field. The particular property of the amplifier which makes it so important for use in satellite communication is its ability to amplify extremely weak radio signals whilst introducing a negligible amount of additional background noise. A disadvantage is that it will only operate at very low temperatures. The present equipment requires a temperature lower than 2°K (i.e. -271°C) and the only possible method of obtaining such a low temperature is to immerse the amplifier in liquid helium. This normally boils at 4.2°K, but the lower temperature required for the maser can be produced by causing the

\* First published by the Institute of Electrical Engineers, November 1962.

helium to boil at a reduced pressure. A large vacuum pump must therefore be incorporated into the apparatus.

If the maser and all the associated equipment could have been mounted in close proximity, the installation would have been relatively straightforward. However, to make use of the unique low-noise properties of the maser, it was essential that it should be mounted as near as possible to the focus of the 85-ft. parabolic reflector, whilst the remainder of the equipment had to be mounted in the rotating cabin or at ground level.

It was not practicable to mount the maser actually at the focus because of its weight and because there was already a considerable amount of aerial-feed equipment at the focus. The maser was therefore

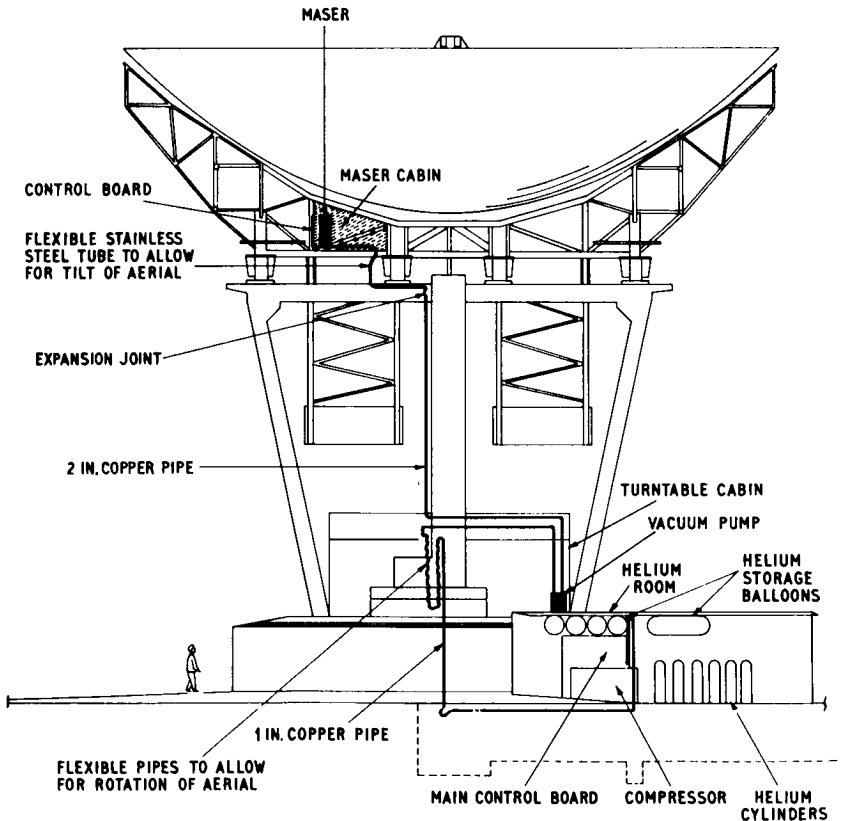


Fig. 1 — Position of the maser and helium equipment on the Goonhilly aerial.

housed in a cabin constructed on the back of the parabolic reflector, and connected by waveguide to the feed equipment at the focus.

Thus the complete installation consists of the helium control equipment associated with the maser, a vacuum line along and down the aerial structure to the vacuum pump, together with the equipment for controlling the flow of helium gas from the vacuum pump and storing this helium for return to the liquefaction plant. The location of the various items is indicated diagrammatically in Fig. 1.

During operation, the axis of the aerial may be tilted between horizontal and  $10^\circ$  beyond vertical, and consequently all the equipment in the maser cabin, including the klystron and magnet power supplies, a small oscilloscope, a nitrogen-cooled reference load and the maser itself, must operate satisfactorily when tilted by  $100^\circ$ . To prevent refrigerant from spilling from the maser as the aerial tilts, it was mounted at an angle of  $45^\circ$  to the axis of the aerial, so that the maser axis is never more than  $55^\circ$  from vertical. However, access to the aerial cabin to fill the maser with refrigerant is only possible when the aerial axis is horizontal, so that the maser must be capable of being tilted in its cradle from the normal operating position through  $45^\circ$  to the vertical position for filling. The helium-gas handling system must also provide for the maser to be tilted inside the cabin, and, when the aerial is in use, for the cabin to tilt with respect to the ground without restricting the flow of helium gas. Sections of corrugated stainless-steel tube are used to provide this flexibility.

Special quick-release waveguide flanges were designed to permit the maser to be tilted through  $45^\circ$  into the filling position, as shown in Fig. 2.

#### LIQUID HELIUM AND LIQUID NITROGEN

Liquefied gases are usually contained in metal "dewar" vessels, which are spherical flasks with a double wall, the space between the walls being evacuated to provide thermal insulation. The latent heat of helium is so low that this form of thermal insulation is inadequate. The maser is therefore mounted inside a double vacuum-insulated dewar, with the outer vessel containing liquid nitrogen. Equipment was provided for re-evacuating the insulating spaces in the maser dewar when necessary.

Double dewars must also be used for transporting and storing liquid helium. All supplies of liquid nitrogen and liquid helium are despatched by rail from a liquefaction plant in London to Cornwall two or three times a week.

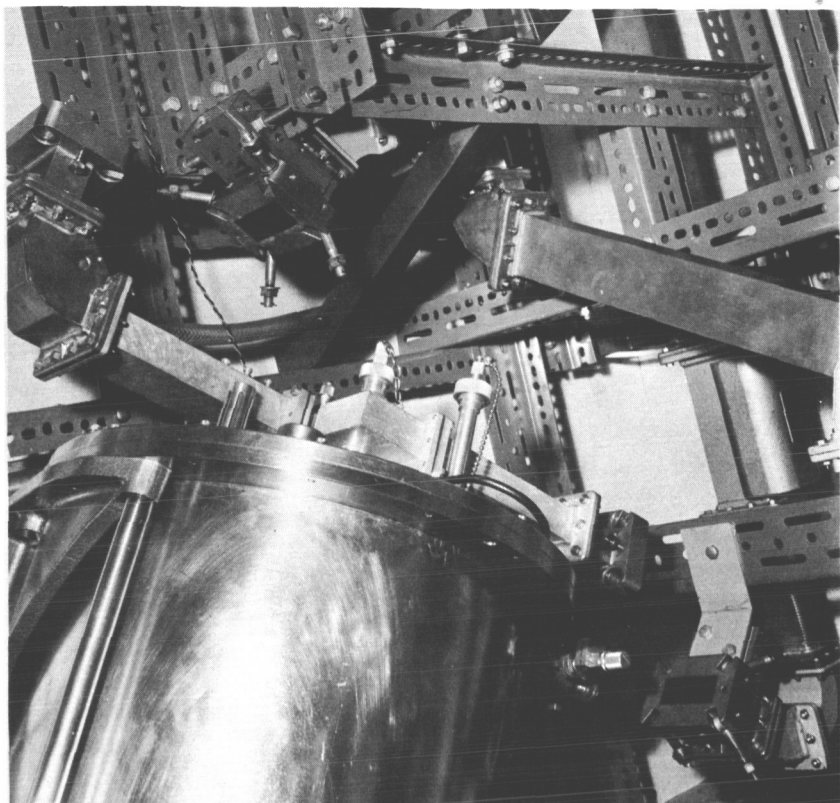


Fig. 2 — The top of the maser tilted to show the quick release flanges.

The temperature of liquid helium is lower than the freezing point of both oxygen and nitrogen, and it is necessary to take precautions to prevent air from freezing inside the neck of the dewar vessels. A non-return valve must therefore be fitted to the dewars, allowing helium gas to boil away from the liquid, but preventing air from entering.

#### COOLING THE MASER

The maser is mounted in its tipping cradle on one wall of the maser cabin, as shown in Fig. 3. Above it on the wall is a control panel that enables the flow of helium gas to be regulated, and the pressure in the maser to be measured. A flexible stainless-steel tube connects the maser to the control panel. Electrical monitoring equipment is also

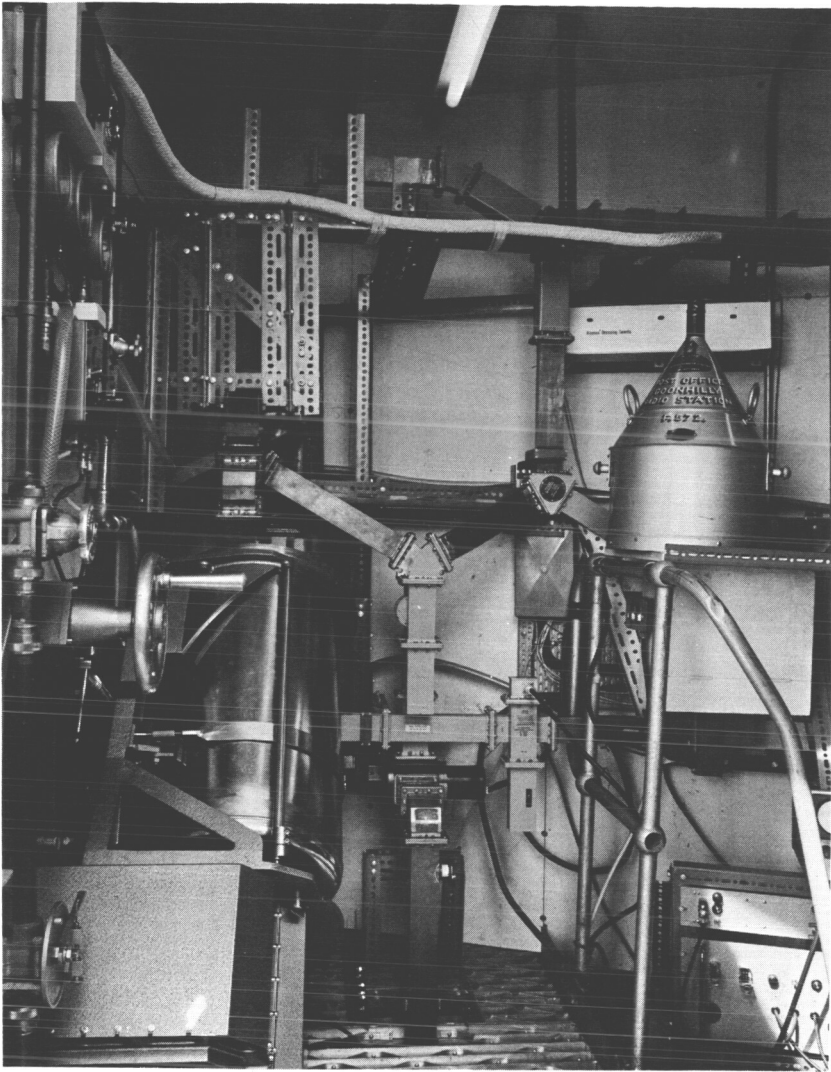


Fig. 3—The maser in the operating position showing the 12 litre dewar.

mounted on this panel, indicating the output of the klystron oscillator and the level of helium in the maser.

Figure 4 shows dewars of liquid helium and liquid nitrogen being lifted by a hydraulically-operated platform to the portal beam of the aerial, from which they can be carried to the maser cabin. Here, the liquid-nitrogen dewar is connected to an insulated transfer tube



Fig. 4—Dewars of liquid helium and liquid nitrogen being lifted to the maser cabin.

permanently installed in the cabin. Compressed nitrogen from a cylinder is used to force the liquid nitrogen along the thermally-insulated tube into the outer part of the maser dewar.

When the outer vessel of the maser dewar is full of liquid nitrogen, the inner vessel is filled with liquid helium. The helium-storage dewar is placed on a hydraulically-operated lift-platform beside the maser dewar, and a transfer tube is inserted into the two dewars. This transfer tube, which can be seen in Fig. 5, has a vacuum-insulated double wall, to prevent the boiling of helium inside the transfer tube due to heat entering through the walls. A bladder attached to the helium-storage dewar is used to start the helium transfer. A gentle squeezing action agitates the liquid in this dewar, causing increased evaporation. The gas pressure so produced forces the liquid helium through the transfer tube. As the level of the helium rises in the maser dewar, the storage dewar and transfer tube are raised to keep the outlet of the transfer tube above the liquid surface in the maser dewar.



Fig. 5 — Helium transfer into the maser.

Great care must be exercised during the transfer to prevent air or water entering the dewars. When the dewar containing the maser is full, the transfer tube is rapidly removed and the entry port sealed. During the helium transfer, a considerable amount of liquid is evaporated in cooling the structure to  $4.2^{\circ}\text{K}$ . The helium gas so evolved

passes along the flexible tube to the control panel, and thence into the helium collection system.

Immediately the maser dewar has been filled and the filling port sealed, the pressure must be reduced to a few torr (mm Hg) in order to lower the helium temperature from  $4.2^{\circ}\text{K}$ . The rate of change in the pressure must be controlled carefully in order to prevent the risk of damage to the maser. A special adjustable throttle valve was designed to control the rate of change of pressure during the initial stage of pump-down.

The version of the maser installed initially was built into a relatively small commercial helium dewar. More recently, a new dewar has been installed to give an extended maser operating life. This dewar (Fig. 3) holds approximately 12 litres of liquid helium.

The operating procedures devised for the small dewar have proved quite adequate for the new installation. The principal change has been an increase in the time needed to fill the dewar because of the greater volume of liquid, and the increased mass of metal to be cooled. Operationally the increased helium capacity has enabled several successive TELSTAR and RELAY passes to be used without refilling the maser. It has also been possible to carry out the maser filling some hours in advance of a satellite experiment, when this has been desirable.

#### THE MAIN VACUUM LINE

As already mentioned, the nearest position to the maser which could be used for the vacuum pump was in the turntable cabin. The main vacuum line between the maser cabin and the pump therefore had to be about 80 ft. in length. Two-inch diameter copper pipe was used, with joints and bends assembled from commercial fittings, silver soldered into position. The pipeline was constructed in sections on the ground and these sections were joined by vacuum flanges sealed with rubber rings and bolted together by stainless-steel bolts.

A great deal of care was taken in assembling the system, to eliminate possible sources of contamination or leakage. Apart from directly reducing the purity of the recovered helium, any volatile contamination in the pipeline would increase the background pressure in the system, making subsequent detection of possible leaks much more difficult. The success of the whole installation depends upon the quality of the silver-soldered joints and upon the cleanliness of the system, and elaborate cleaning and leak testing procedures were devised and followed during the installation.

The 2-in. pipe is supported by a series of brackets fixed to the wave-guide ladder which runs alongside the vertical centre member of the concrete aerial structure. The weight of the pipe is taken on a special flange located near the base of the ladder and a flexible stainless-steel section near the top permits small residual movements.

#### THE VACUUM PUMP

In order to handle large quantities of helium, a vacuum pump of large capacity is needed. The rate at which helium gas would be evolved could not be known in advance, as it depends upon the constructional details of the maser structure. A large margin of safety was therefore desirable when specifying the required pump performance. A pump with a capacity of 36 cubic ft/min. was fitted; this was the largest available air-cooled vacuum pump, air cooling being very desirable to avoid the necessity for an additional water-circulation system on the aerial.

A remotely controlled valve is used to provide a low impedance path round the pump while the maser is being filled.

#### THE HELIUM RECOVERY APPARATUS

The output from the vacuum pump cannot be exhausted to the atmosphere in the usual way, but must be piped away for recovery. Accordingly, a 1 in. diameter copper pipe is connected to the output of the pump to carry the helium over the transmitting equipment to the rotating joint at the centre of the turntable cabin. To carry the helium through this rotating joint four 17 ft. lengths of nylon-reinforced PVC tube are used, hanging as U-loops, connected in parallel. As the aerial rotates, the loops wind round a central pylon, permitting a movement of  $\pm 250^\circ$  from the central position. From the bottom of the central pylon the copper pipe goes through underground ducts to the helium room, which is part of the building housing the aerial control gear.

The total length of the 1 in. pipe is about 120 ft. and the same care over cleanliness was observed in its fabrication as for the 2 in. vacuum section.

The helium room (Fig. 6) contains a large control panel to handle the helium gas which is now at atmospheric pressure. This panel is fitted with over 20 vacuum-type valves to interconnect the pipe which brings the helium gas from the vacuum pump, the temporary gas store, and the compressor. A flowmeter is included, to monitor the rate of evolution of helium gas from the maser.

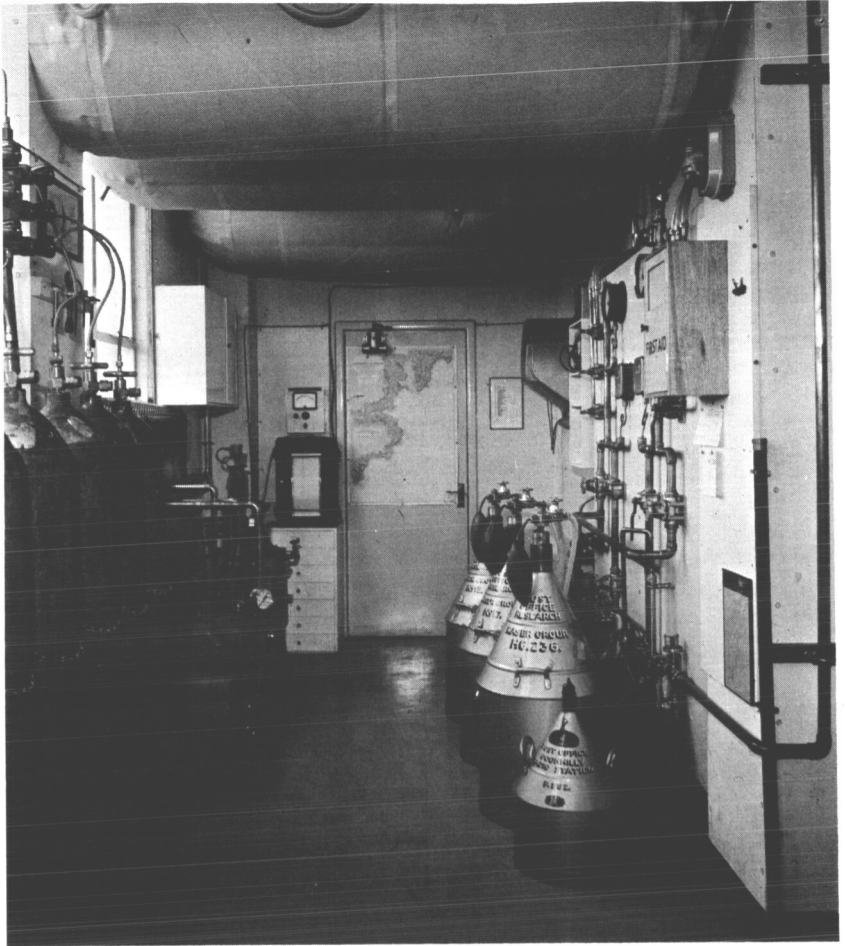


Fig. 6 — The helium collection room.

The helium store consists of rubberized-canvas balloons suspended beneath the ceiling, each balloon holding up to 17 ft of helium. The initial installation of six balloons has been increased to 16, to give adequate storage for extended periods of maser operation.

For return to the liquefaction plant, the contents of the balloons must be compressed into steel cylinders. A modified commercial air compressor is used to compress the helium to 1,000 lb/in.<sup>2</sup> Additional facilities are required to collect gas released from the sump and the starting bypass valve, which are normally open to the atmosphere in

an ordinary air compressor. Helium, which is a monatomic gas, becomes hotter than diatomic oxygen or nitrogen during compression. To avoid damaging the compressor by over-heating, it must not be used for more than 10-15 minutes at any one time when compressing helium. The full cylinders are returned by rail to the liquefaction plant in London, for the cycle to begin again.

Also visible in Fig. 6 is the continuous chart recorder, connected to the resistance thermometers in the maser dewar. A continuous indication of helium level is thus always available.

#### CONCLUSION

The helium system at Goonhilly was commissioned on 25th June, 1962, having been completely designed and constructed in four months. The general features of the system have proved satisfactory in operation, requiring little modification to the original conception, although a number of changes have been introduced to simplify the filling of the maser with liquid helium.

The great care taken in construction and operation of the helium system has been justified by the high level of purity attained for the returned gas.

N67 12315

# A Low-Temperature Thermal Noise Source for Use at the Goonhilly Satellite-Communication Earth Station\*

H. N. DAGLISH

POST OFFICE ENGINEERING DEPARTMENT

A matched waveguide termination was required as part of the noise temperature calibration facility in the receiving system at the Goonhilly earth-station. For routine measurement of overall system noise temperature, this termination is at ambient temperature. For other noise measurements, and in particular for the measurement of the effective input noise temperature of the maser, the waveguide termination is cooled to 77°K by immersion in liquid nitrogen.

## DESIGN OF THE TERMINATION

AUTHOR

The termination consists of an absorptive pyramidal load mounted inside a length of thick-walled copper waveguide, which provides an approximation to a constant temperature enclosure, even when only partially immersed in refrigerant. The adjacent section of waveguide has thin walls, made of an alloy of low thermal conductivity, in order to reduce the rate at which heat leaks into the refrigerant. A thin internal layer of silver ensures adequate electrical conductivity. The internal dimensions of the waveguide are those of RCSC WG<sub>11</sub>, (i.e. 2.372" by 1.122"). Fig. 1 shows two slightly different mechanical constructions of the waveguide structure.

Before deciding on the type of absorptive material to be used, samples of various materials were tested by repeated cycles of immersion in liquid air. Of the two materials which were found suitable, one was a suspension of iron powder in a synthetic resin ("poly-iron"), cast in the laboratory, in a suitable mould, and the other was a commercial material, machined into the appropriate shape.

The samples were alternately cooled and warmed for several days, until it was established that when the temperature changes were not

\* First published by the Institute of Electrical Engineers, November 1962.

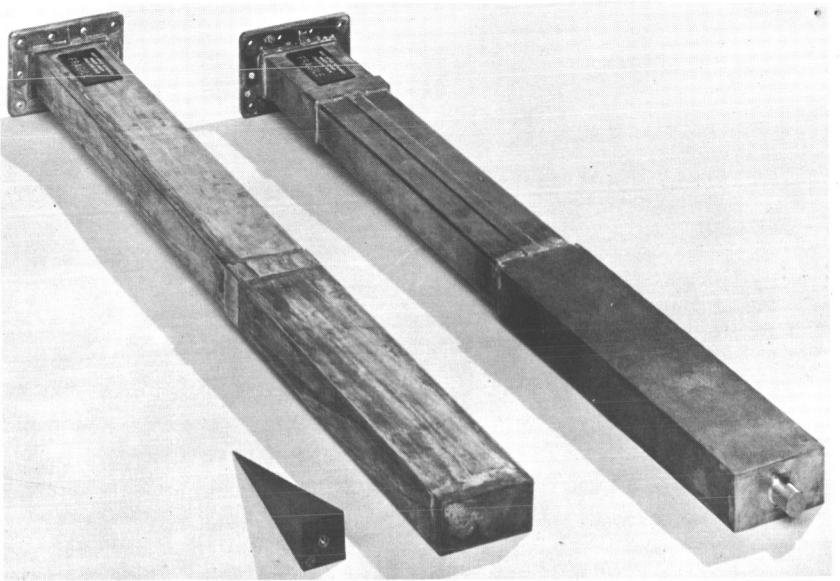


Fig. 1 — Alternative types of cold termination and a poly-iron pyramid load.

too sudden, serious cracking was unlikely, provided that water was excluded. However, if the samples were wet, the surface of the material became crazed and eventually broke up. It was therefore necessary to take suitable precautions to exclude condensed water vapour from the completed termination.

The shape chosen for the polyiron load is shown in Fig. 2. A symmetrical pyramidal shaped load, mounted centrally in the waveguide was found to be preferable to an assymetric, wedge-shaped load attached to the side of the guide. The pyramidal load appears to be less likely to introduce small changes in impedance due to the absorptive material twisting or warping when cooled. The mounting screw is sealed with solder to prevent refrigerant leaking into the waveguide.

The residual VSWR of a termination using this type of load is, in general, better than 0.99 across the 3.8-4.3 Gc/s band.

#### INSTALLATION AT GOONHILLY

The general arrangement of the installation at Goonhilly Radio Station is shown in Fig. 3. The equipment is located in the receiver cabin on the back of the parabolic reflector. The termination is mounted

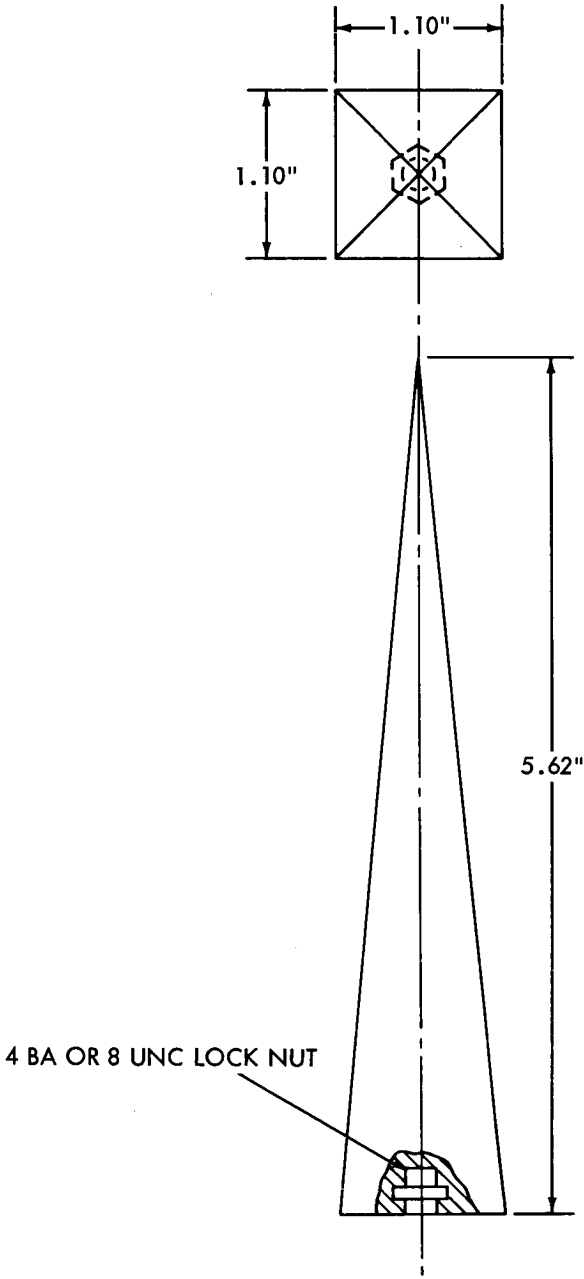


Fig. 2 — Poly-iron pyramid load.

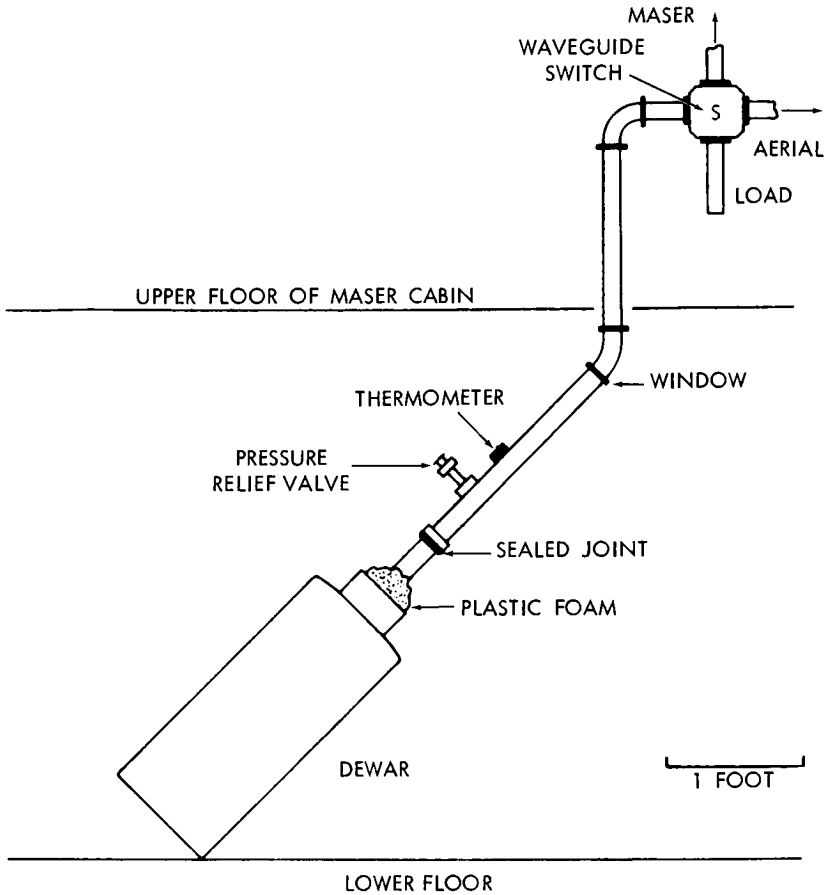


Fig. 3—Layout of cold load at Goonhilly.

beneath the upper floor which is used for maser operation. To prevent loss of liquid nitrogen when the aerial is moved in elevation, the termination and the metal dewar vessel surrounding it are mounted at  $45^\circ$  to the axis of the aerial. A binomially-corrected  $45^\circ$  waveguide corner was designed (with optimum performance at the receiver centre frequency of 4.17 Gc/s.) to connect the termination to the remainder of the waveguide.

To prevent the continuous entry of water vapour and oxygen which would condense in the cooled section of waveguide, a window is required. A simple uncorrected window of "Melinex" (ICI trademark

for polyethylene terephthalate film) was found suitable. A thickness of 0.004" introduced less than 0.005 db of attenuation, and no measurable change in the VSWR of the termination. The flanged joints between the window and the load were sealed with neoprene gaskets. A spring-loaded relief valve was provided to prevent an excess pressure accidentally arising inside the waveguide and possibly rupturing the window and damaging the maser.

The VSWR of the termination was measured at the waveguide switch, at a frequency of 4.17 Gc/s. The value, 0.970, remained constant when the termination was cooled from 290°K to 77°K.

When the termination is used for the two-temperature method of measuring the maser noise temperature, it is necessary to correct for the additional thermal noise generated in the uncooled waveguide between the load and the maser. This amounts to 10°K.

The second termination for the two-temperature measurements is provided by a second pyramidal load at ambient temperature. This can be temporarily installed in the main waveguide in place of the usual flexible connexion to the aerial feed. The thermal noise from the two loads can thus be compared by rotating the waveguide switch.

#### CONCLUSION

A waveguide-mounted thermal noise source for operation either at 77°K or at ambient temperature has been devised and installed as part of the receiver equipment at Goonhilly earth station, and used for noise temperature calibration throughout the experiments with the Telstar and Relay satellites.

N67 12316

# Demodulation Techniques for Use at Goonhilly Satellite-Communication Earth Station\*

R. W. WHITE and R. J. WESTCOTT

POST OFFICE ENGINEERING DEPARTMENT

As part of the programme of experimental and development work to determine the optimum demodulating techniques for communication satellite systems, three types of demodulators have been investigated at the Goonhilly earth station:

1. A conventional demodulator of the type used in 960-channel telephony or television microwave radio-relay links;
2. A frequency modulation feed-back demodulator in which the deviation of the signal is reduced before it reaches the final discriminator; and
3. A variable-bandwidth 'dynamic-tracking' demodulator in which the resonant frequency of a narrow bandwidth tuned circuit is moved rapidly to follow the nominal instantaneous frequency of the incoming signal.

The conventional demodulator will not be discussed in detail here; however, information is given on two specialised demodulators.

Up to a point, the baseband signal-to-noise ratio at the output of a broadband frequency-modulated microwave system can be improved by increasing the deviation. To accommodate the wider deviation signal, increased receiver bandwidth is required. If the noise temperature and gain of the receiver remain constant, the increased bandwidth will result in more noise reaching the limiter stage which precedes the discriminator. Thus, for the same received signal level the IF signal-to-noise ratio will be decreased.

So long as the instantaneous peaks of noise at the limiter input always remain a decibel or two below the carrier level, normal operation of the demodulator is maintained, i.e. changes of  $x$  db up or down in the carrier level will result in corresponding changes of ap-

\* First published by the Institute of Electrical Engineers, November 1962.

proximately  $x$  db in the ratio of signal-to-basic noise measured at the baseband output. But when the peaks of noise are approximately equal to the carrier, a "threshold" condition is reached where any further decrease in carrier-to-noise ratio results in a much more than directly corresponding decrease in baseband signal-to-noise ratio.

For signals above the threshold level, good conventional demodulators of the types used in line-of-sight microwave links perform quite satisfactorily and nothing is to be gained by using more complex demodulating equipment. This will probably be the state of affairs under normal conditions in operational satellite systems. But when abnormally low-level signals have to be received, or when the noise level is unusually high (e.g. due to heavy rainfall) it is highly desirable that the demodulator should have the lowest possible threshold level. That is to say the demodulator should continue to operate down to the lowest practicable signal level before the output signal-to-noise ratio crashes catastrophically; under these conditions very complex demodulating equipment is justified, even if it lowers the operational threshold by only a few decibels.

A number of techniques are known or have been proposed for obtaining a lower threshold, but the basic principle of all involve either enhancement of the carrier or restriction of the effective bandwidth before demodulation. Baseband signal processing after demodulation (e.g. low-pass filtering) can affect the overall signal-to-noise ratio obtainable with any form of demodulator, but will normally have only a second-order effect on relative performance of various demodulators and a virtually negligible effect on attainable threshold levels.

#### FREQUENCY MODULATION FEED-BACK DEMODULATOR

##### *Design Features*

The frequency modulation feed-back demodulator<sup>1,2</sup> follows the general principles laid down by Enloe<sup>3</sup>, and is shown in block schematic form in Fig. 1. It accepts an input signal at a mean frequency of 70 Mc/s, up-converts to a mean frequency of 3590 Mc/s and then down-converts again to 75 Mc/s. The local oscillator for up-conversion is crystal controlled; but the oscillator used for down-conversion is a klystron which is frequency modulated in such a manner that the deviation of the final IF signal is reduced. The modulating signal for this klystron is obtained from the output of the final 75 Mc/s demodulator.

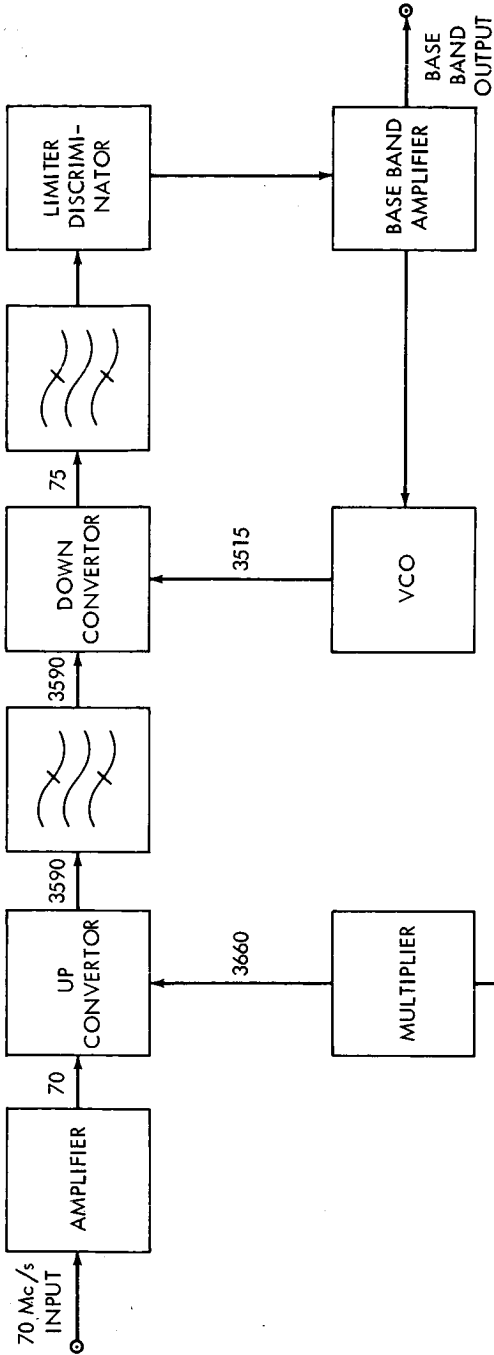


Fig. 1 — FM-FB Demodulator: Simplified Block Diagram.

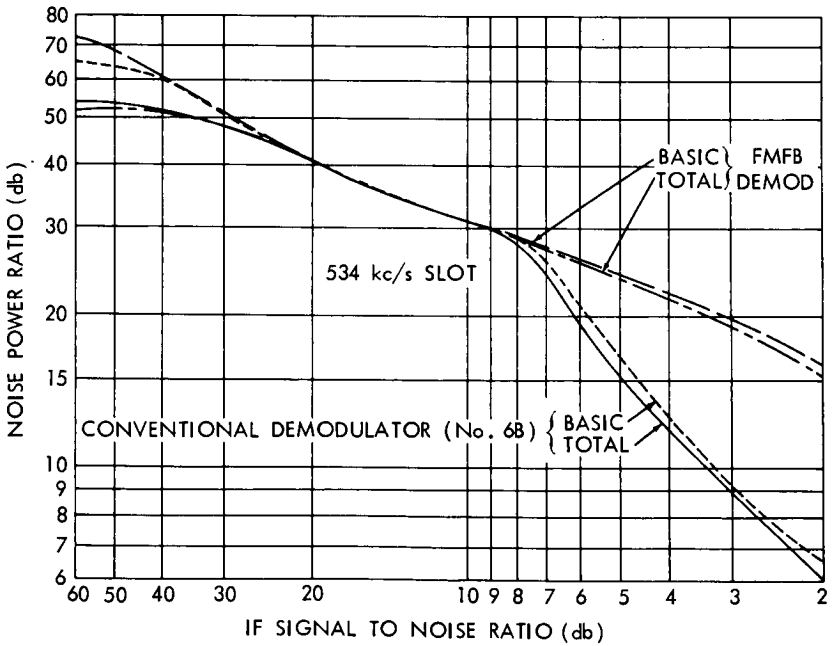
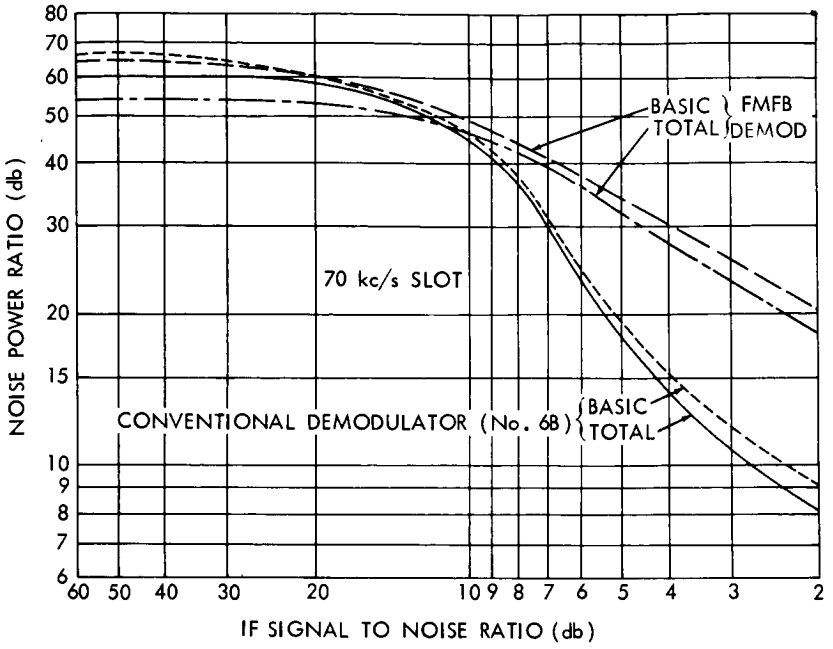


Fig. 2 — FMFB Demodulator: Comparison with Conventional Demodulator (No. 6B) with 240-channel Noise Loading.

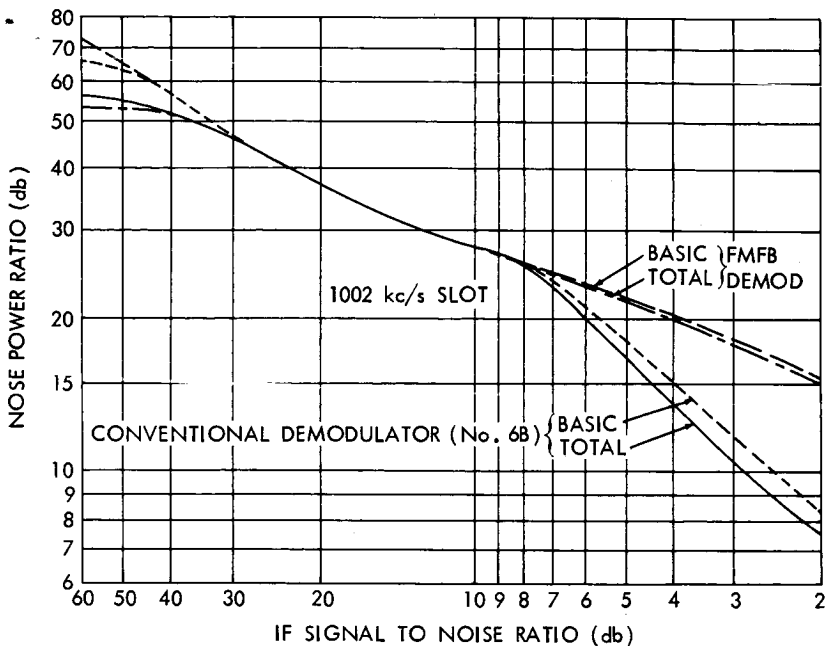


Fig. 2 (continued)

The version of this demodulator which is installed at Goonhilly normally operates at one or the other of two fixed bandwidths; however, experiments have been carried out using continuously variable bandwidth facilities, so that the operating conditions can be more accurately adjusted to optimum for the signal level or modulation being received.

*Performance*

For television signals the threshold of the FM feed-back demodulator is some 4 to 5 db below that for a conventional demodulator when operated at adequate bandwidth to allow satisfactory reception of both the video signal and the sound sub-carrier.

The performance for 240-channel telephony signals is indicated by the curves in Fig. 2. It will be noticed that the FM feedback demodulator provides appreciable improvement over a conventional demodulator (No. 6B) at values of IF signal-to-noise ratio below 10 db; however, a further improvement in this region would be required to meet accepted international standards of performance.

Fig. 3 shows the baseband frequency response under open and closed-loop conditions.

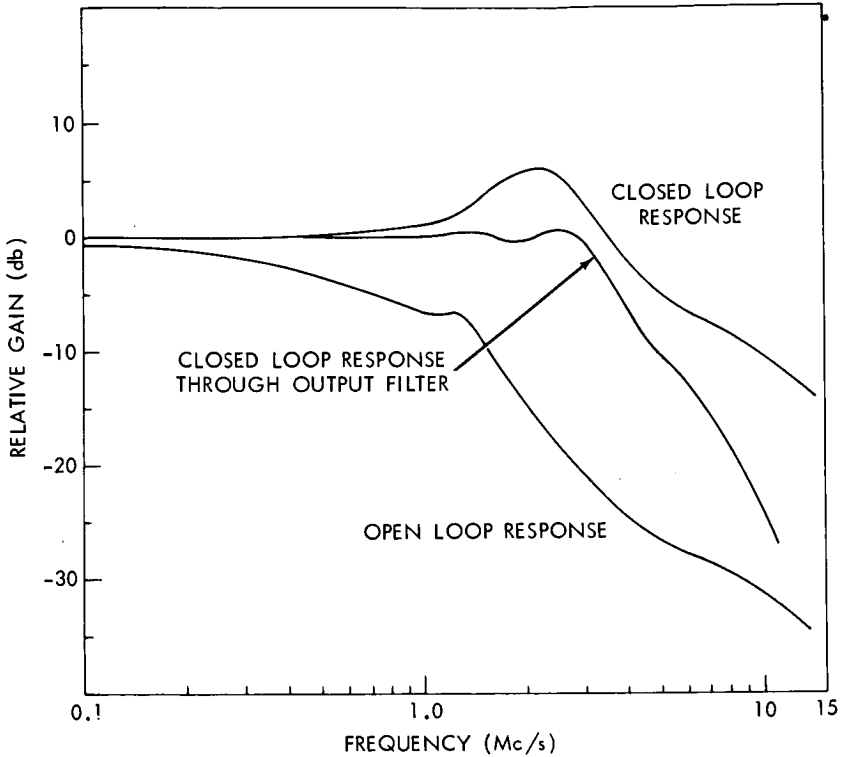


Fig. 3 — FMFB Demodulator; Baseband Frequency Response.

#### DYNAMIC-TRACKING VARIABLE-BANDWIDTH DEMODULATOR

##### *Principles Involved*

Automatic control of the IF bandwidth prior to limiting is already quite well known as a method of improving threshold performance of a receiver demodulator in fairly low deviation FM systems. In essence such an arrangement maintains normal receiver bandwidth until the input signal drops to a level close to threshold, but for still lower levels of signal the effective bandwidth of the receiver is progressively reduced. This reduced bandwidth lowers the total noise and hence the threshold, at the cost of rapidly rising distortion. The occasional rises in inter-modulation noise which result from restricted bandwidth are generally to be preferred to the relatively severe bursts of noise

which occur when a fading signal drops below threshold—especially in lightly-loaded telephony systems.

An automatic bandwidth control arrangement of this type is particularly useful for rapidly fading signals and was used very successfully in Post Office tests on a tropospheric—scatter link during 1959-60; but it is not suitable for use in wide-deviation television systems.

It has been pointed out by Baghdady<sup>4</sup>, that in many wide-deviation FM systems only limited parts of the total signal bandwidth are carrying essential information at any specific moment, and that it should be possible to improve the threshold by a narrow-band IF filter—provided that the filter could be tuned rapidly enough to follow the changing location of the main energy in the signal spectrum. Baghdady describes such a system in outline and calls the device a “dynamic selector”.

*Design Features*

A simplified block diagram of the demodulator is shown in Fig. 4. A single tuned circuit is used as the variable filter, and a varactor

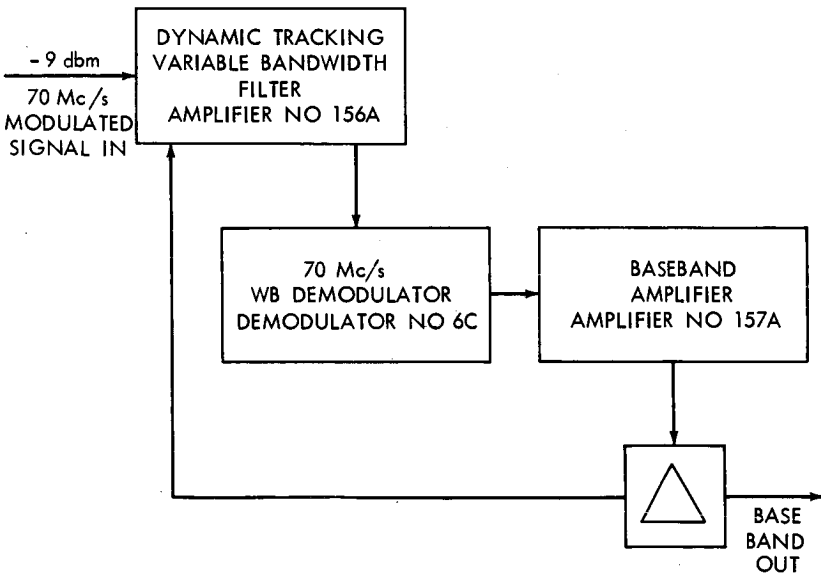


Fig. 4—Goonhilly Radio Station; Dynamic Tracking Demodulator.

diode forms the tuning element. Variation of the bandwidth is accomplished by altering dc current through a thermistor bead.

The relationship between frequency and voltage which the varactor diode provides is distinctly non-linear, but this is compensated by shaping networks in the video amplifier.

A number of different ways of varying bandwidth were tried; but the majority of these resulted in tuning changes, and a thermistor was found to be the most satisfactory device.

The 3 db bandwidth of the tuned circuit is adjustable from about 2 to 20 Mc/s, but the narrowest bandwidth is rarely useable in practice. A useful feature of the arrangement is that, under wide-band (i.e. high signal level) conditions, the overall performance becomes virtually that of the associated high-grade conventional demodulator. The automatic bandwidth control is adjusted to maintain full bandwidth until the signal falls to within a decibel or two of threshold, and then decreases bandwidth at a rate of approximately 2 to 1 for a 3 db drop in signal.

### *Performance*

For television reception under the usual conditions used for tests on Telstar and Relay, this modulator gives an average threshold improvement of about 4 or 5 db. The improvement is greatest on fairly uniform areas of grey, or on areas of slowly changing brightness; but is limited by noise in regions where there is a sudden change in brightness, due to inability of the narrow-band circuit to follow fast enough. This feature can result in some roughness of vertical edges under conditions of very low signal-to-noise ratio, which can be considerably reduced by fly-wheel synchronization, or synchronizing-pulse restoration.

The dynamic-tracking demodulator gives optimum results only if the incoming television signal includes a dc component, i.e. when specific frequencies correspond to the synchronizing pulse, black and white levels in the video waveform. It is less effective if the earth-station transmitter originating the signals uses no pre-emphasis and mean-frequency automatic frequency control. Furthermore, if the bandwidth restriction is excessive, cross modulation from the video channel into the sound-sub-carrier channel may occur.

The variable-bandwidth dynamic tracking demodulator is considered unsuitable for multi-channel telephony, and it is probable that a simple variable-bandwidth system (i.e. without the tracking feature) may be preferred.

## POSSIBILITIES FOR FURTHER IMPROVEMENT OF DEMODULATOR PERFORMANCE

*Noise Limiting Techniques*

At the output of a wide-band demodulator operating at or just below threshold, the noise peaks are very narrow. It is suggested that a peak-clipping device might be used at that point to restrict the video signal to limits appropriate to the white and synchronising pulse levels, and if the bandwidth is subsequently restricted, (e.g. to 3 Mc/s) the amplitude of the noise peaks will be still further reduced. The clipping must take place before the video bandwidth is restricted.

It is possible that still further suppression of these short duration noise peaks could be obtained by arranging for automatic variation of the clipping levels, especially if the main signal can be very slightly delayed and advance information on its levels obtained from an earlier part of the circuit.

*Alternative Sound Channel Arrangement*

The use of a sound sub-carrier at 4.5 Mc/s necessitates, for television a minimum IF bandwidth of slightly over 9 Mc/s. If this sub-carrier is eliminated an IF bandwidth of just over 6 Mc/s would give a full-bandwidth video response. In difficult reception conditions some restriction of video bandwidth is permissible and the effective IF bandwidth could then be further reduced. For example, a 2.5 Mc/s IF bandwidth would represent an improvement of about 10 db in threshold relative to a conventional demodulator of 25 Mc/s bandwidth.

## CONCLUSIONS

When the carrier/noise ratio is appreciably greater than that corresponding to threshold conditions, a conventional demodulator is to be preferred. At carrier/noise ratios (measured in 25 Mc/s bandwidth) less than 10 db there is some benefit from the specialised demodulators, and at carrier/noise ratios less than 6 db there is a marked benefit.

It is possible that further development work on noise limiting techniques in demodulators might result in yet better performance, and there is no doubt that elimination of the sound sub-carrier, e.g. by transmission of the sound on pulses within the synchronizing interval of the television signal, would greatly increase the threshold margin for television under difficult conditions.

## REFERENCES

1. Chafee, J. G., The Application of Negative Feedback to Frequency Modulation, *Bell Sys. Tech. J.*, 18, July 1939.
2. Ruthroff, C. L., Project *ECHO*: F.M. Demodulators with Negative Feedback, *Bell Sys. Tech. J.*, 40, July 1961.
3. Enloe, L. H., Decreasing the Threshold in F.M. by Frequency Feedback, *Proc. I.R.E.*, January 1962.
4. Baghdady, E. J., Analog Modulation Systems, *Lectures on Communication Theory*, pp. 439-555, New York: McGraw-Hill, 1961.

# A High Power Travelling Wave tube for Satellite Communications\*

N67 12317

M. O. BRYANT, A. THOMAS, and P. W. WELLS

SERVICES ELECTRONICS RESEARCH LABORATORY

*This paper describes the CW travelling wave tube used by the General Post Office in their ground transmitter for Project Telstar. It operates in the 6000 Mc/s band with a maximum power output of about 5 kw and a bandwidth of great than 100 Mc/s. The factors influencing the design of the valve and its performance are discussed in some detail.*

## AUTHOR

The experimental communication satellite Telstar requires a ground transmitter at 6390 Mc/s giving a power of more than 2 kW with a bandwidth of about 50 Mc/s. The valve used by the General Post Office to produce this power in their station at Goonhilly Downs is a travelling-wave amplifier using a 'clover leaf' slow-wave structure<sup>1</sup> to interact with the electron beam. Amplifiers of this type have been the subject of much research in recent years<sup>2, 3, 4, 5, 6</sup> which showed that the requirements for Telstar could probably be best satisfied by a similar device. This valve has already been briefly described in the Press<sup>7</sup>. In the present paper the most important factors influencing the design and performance are described in more detail and the potential capability of clover leaf travelling wave amplifiers for CW operation is discussed. Fig. 1 shows the main features of the valve which will be described in the following paragraphs.

### REASONS FOR CHOOSING A CLOVER LEAF TRAVELLING WAVE TUBE

For a CW output power of several kilowatts at centimetre wavelengths travelling wave tubes with the familiar helical wire circuit are impracticable at present because their thermal dissipation is too low. If a travelling wave tube is to be used it must have a more massive circuit, such as a periodically-loaded waveguide. Stagger-tuned

\* First published by the Institute of Electrical Engineers, November 1962.

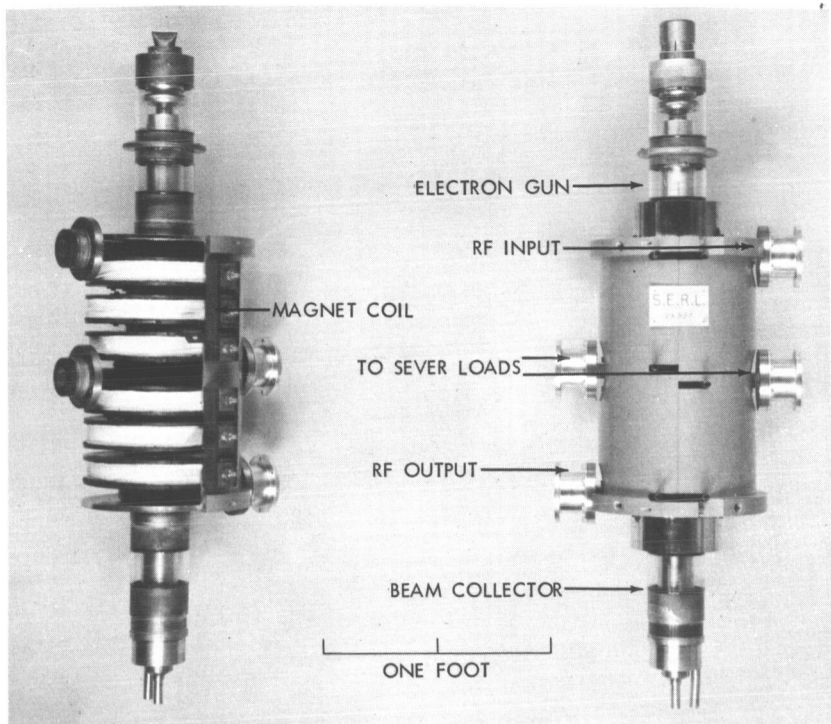


Fig. 1—The C-band travelling wave tube. The valve on the left has the protection covers removed to show more detail.

multicavity klystron amplifiers might also be considered. These are capable of very high CW output powers,<sup>8</sup> but the bandwidth obtainable at kilowatt power levels is barely 1%<sup>9</sup>—and that only at relatively poor efficiency. Furthermore, in any communication system it is desirable that the transmitter be tunable over a large fraction of the allocated frequency range in order to avoid a multiplicity of frequency variants. Although klystrons can be mechanically tuned by a few percent it is very difficult to maintain the stagger-tuning of the cavities required for maximum bandwidth.

Travelling wave tubes with periodically-loaded wave guide circuits have greater bandwidth and in our experience are much easier and more reliable to make. There are several types of circuit which might be considered. The choice between them is a rather complicated one and has been elaborated elsewhere<sup>2, 3</sup>. The clover leaf structure is considered to be the best available at present because of its very high power

handling capacity, relative freedom from instabilities and high gain per unit length. At kilowatt powers its bandwidth is rather limited, but more than adequate for the amount of traffic likely to be handled by one transmitter, and it can be voltage-tuned over a frequency range of about 5%.

A diagram of the clover leaf structure is shown in Fig. 2. It consists essentially of a circular waveguide, operating in the  $TM_{01}$  mode, which is periodically loaded by thin irises. Alternatively it may be regarded as a series of coupled cavities forming a band pass filter. The cavities are inductively coupled by radial slots and there is also a small amount of capacitive coupling through the beam hole. The structure is very simply made from two varieties of copper stampings which are stacked and brazed together inside a copper shell forming the vacuum envelope.

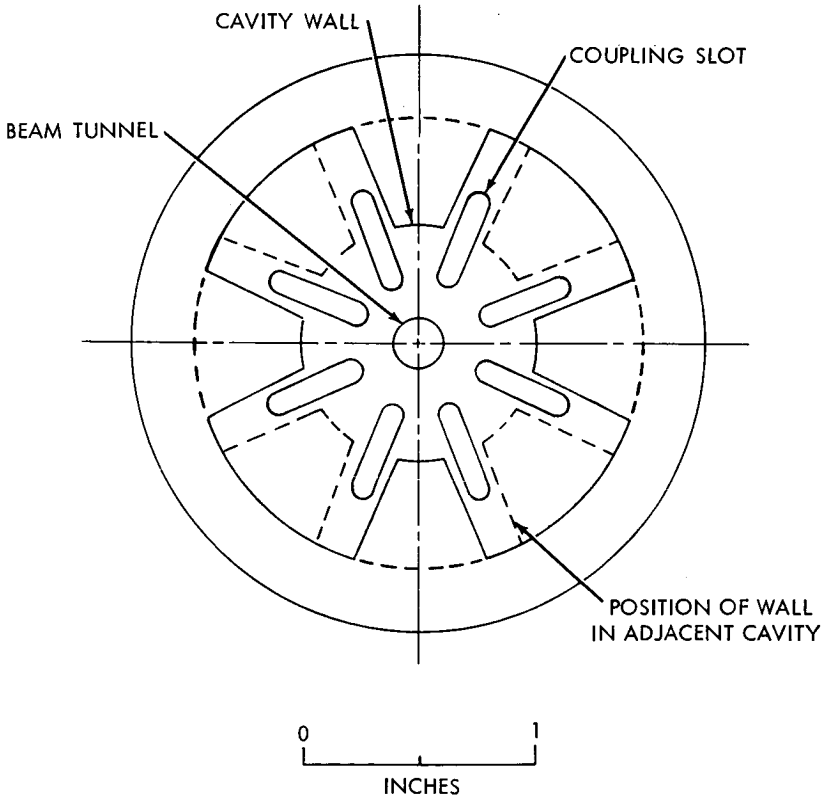


Fig. 2 — The clover leaf structure.

## OPERATING PARAMETERS AND PERFORMANCE

At output powers of a few kilowatts the clover leaf structure offers a bandwidth at fixed beam voltage of 1-2%, with a tuning range of about 5% for a beam voltage variation of less than 2:1. The best choice of voltage and current for a particular valve is governed by a number of factors. One of the most important of these is that the maximum space charge density in the beam shall not be too high. Excessive space charge prevents the formation and maintenance of the very sharp electron bunches necessary for high gain and efficiency. In the present case the choice was dictated by the performance of an existing electron gun which had been developed for another valve but was used in order to carry out this development in the very short time available.

This gun gives a constant dc beam power of about 28 kW over a voltage range of 20-32 kV, the beam current being controlled independently by a separate electrode. At the high voltage end of this range a much higher beam power can be reached, the maximum of 32 kV being about 46 kW. Fig. 3 shows the output power of the valve for four beam voltages at a constant beam power of 28 kW. At each beam voltage the R.F. drive power is kept constant at the value giving maximum bandwidth. An output of greater than 3 kW is obtained from 6290 Mc/s to 6660 Mc/s, a range slightly greater than 5%. The gain and efficiency are reduced at the high frequency end of the tuning range, largely as a result of the high space charge density in the beam at low voltages. A rather small variation of gain and power output with voltage would be obtained if the operating range were somewhat higher, say 25 kV-40 kV.

The power handling capacity of the clover leaf structure is very much greater than can be achieved with the present gun. Using a beam power of 46 kW at the high voltage end of the tuning range a CW output of 10 kW has been obtained without difficulty with a gain of 30 db. With a new electron gun operating at higher voltage the dc power input to the tube could be even further increased, with a corresponding increase in power output.

## THE ELECTRON BEAM

The diameter of the electron beam is about 3 mm. and the maximum current 1.4 amp, corresponding to a current density of 20 amp/cm<sup>2</sup>. This is well beyond the capability of existing cathodes and the beam is therefore formed from a cathode with about ten times the beam area. The beam is converged electrostatically and then introduced into

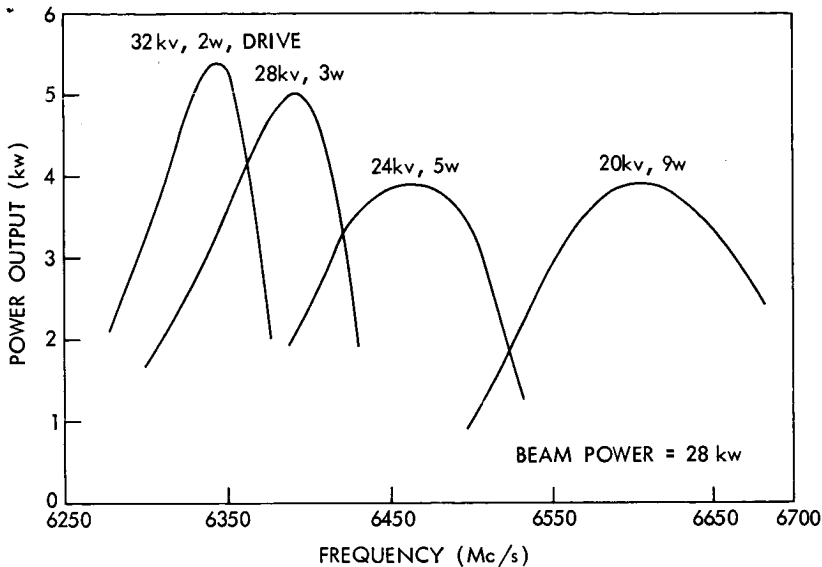


Fig. 3 — Output power of the valve.

an axial magnetic field of 1100 gauss which prevents it from spreading until it has travelled through the R.F. circuit. In a valve of this power it is essential to minimize heat input to the circuit from electron bombardment and the design of the focusing system requires great care. In the present case less than 1% of the dc beam current is intercepted on the slow-wave structure at maximum RF output. Considerable assistance in reaching this low figure is obtained by using an electromagnet whose coils are wound directly on the body of the valve thus ensuring very good alignment of the magnetic field with the beam. The virtue of this type of magnet has been demonstrated with previous valves,<sup>4</sup> but a new technique for making the coils has now been adopted.<sup>10</sup> They are wound from 1 in.  $\times$  0.01 in. O.F.H.C. copper tape, interleaved with 0.003 in. glass fibre tape and impregnated with a self-setting porcelain cement. This method of construction gives very good heat dissipation and also allows the coils to be baked on the tube at up to 450°C. during outgassing on the pumps. Thus the magnet is available for focusing the electron beam while the valve is on the pump, which is a great advantage. It also permits valves to be rebuilt and processed, thereby effecting worthwhile economies. For a field of 1100 gauss the coils require a current of 40 amp and consume a power of 1600 W.

## STABILITY

In order to avoid excessive feedback in high gain travelling wave tubes, caused by internal reflections, some form of isolation in the slow-wave structure is needed. In high power tubes such isolation is provided by introducing one or more breaks, or severers, in the structure. At these severers any power on the circuit is dissipated in resistive loads and the RF signal is propagated solely as current and velocity modulations on the electron beam, which act in the forward direction only. In this tube the gain is such that only one sever is necessary. Because the mean power is so high the sever terminations are not placed inside the valve, but the structure is matched through waveguide transitions into loads outside the vacuum envelope. These loads are required to dissipate up to 200 watts, depending on the power output and the proportion reflected.

## COLLECTOR DEPRESSION

In a travelling wave tube only a small proportion of the dc beam energy can be converted into RF and the remainder is wasted in heating the collector cooling water. This situation can be improved by holding the collector at a negative potential with respect to the RF circuit. By this means electrons are slowed down before hitting the collector and hence the power wasted and the amount of cooling water needed are reduced. In practice, the extent to which the collector potential can be depressed is limited by the number of electrons accelerated back into the slow-wave structure by the biasing field. This problem becomes more acute the higher the mean power in the electron beam but even if only a modest amount of collector depression can be used it may effect an economy in dc power of many kilowatts. With the present design<sup>5</sup> the maximum depression that can be used is about 40% of the cathode potential. At a beam power of 28 kW this depression reduces the collector power by about 12kW giving a maximum efficiency of dc to RF conversion of 34%.

## ACKNOWLEDGMENTS

The authors would like to express their thanks to the many people at SERL who have contributed to this development. The paper is published by permission of the Admiralty.

*References*

1. Chodorow, M., and Craig, R. A., Some New Circuits for High Power Travelling Wave Tubes, *Proc. I.R.E.* 45(8), August 1957.
2. Gittins, J. F., Rock, N. H., and Sullivan, A. B. J., An Experimental High Power Pulsed Travelling Wave Tube, *J. Electronics and Control* 3(3), September 1957.
3. Bryant, M. O., Gittins, J. F., and Wray, F., An Experimental CW Power Travelling Wave Tube, *J. Electronics and Control* 6(2), February 1959.
4. Bryant, M. O., Gittins, J. F., and Wray, F., Improvements in a CW Power Travelling Wave Tube, *J. Electronics and Control* 7(6), December 1959.
5. Bryant, M. O., Thomas A., and Wells, P. W., A High Power CW Travelling Wave Tube, *J. Electronics and Control* 12(1), January 1962.
6. Ruetz, J. A., and Yocom, W. H., High Power Travelling Wave Tubes for Radar Systems, *I.R.E. Trans. Military Electronics, MIL-5*, 2, April 1961.
7. Bryant, M. O., The Five-Kilowatt Travelling Wave Tube, *Brit. Comm. and Electronics* 9(8), August 1962.
8. McCune, E., Maltzer, I., and Zitelli, L. T., A 20 kW CW X-band Klystron Amplifier, *Microwave J.* 4(8), August 1961.
9. Bryant, M. O., and Lea-Wilson, C. P., Some Experiments on Broad-band CW Power Klystrons at X-band, *J. Electronics and Control* 6(6), June 1959.
10. Thomas A., A bakeable magnet for high power travelling wave tubes, *J. Sci. Instr.* 40(131), March 1963.

# The Output Stage for the Ground Transmitter at Goonhilly\*

N67 12318

A. R. PETHERHAM

ASSOCIATED ELECTRICAL INDUSTRIES LIMITED

The power output amplifier of the transmitter for the Goonhilly project uses a travelling tube, type VX527 delivering 4 kW at 6,390 Mc/s, with a bandwidth of about 100 Mc/s. This amplifier, together with its power supplies and driver stage is located in a cabin, situated on the turntable underneath the aerial. Input signals for the transmitter are received in the cabin from the main control room at a frequency of 70 Mc/s; they are converted to the nominal 6,390 Mc/s before being amplified to about 3 watts by the driver TWT and fed via a waveguide link to the output stage.

The output stage, described below, was designed and manufactured by A.E.I. Electronic Apparatus Division, Leicester, England, during the first half of 1962.

## THE TRAVELLING WAVE AMPLIFIER

The travelling wave tube, which was designed and built for the Goonhilly Station by the Services Electronics Research Laboratory, at Harlow, England is illustrated in Fig. 1. Fig. 2 is a schematic diagram of its power supply, based on SERL recommendations, and Fig. 3, the associated RF circuitry.

The tube is of the type in which an electron beam passes firstly through a hole in the anode and then through the centre of a clover-leaf slow wave structure before striking the collector. Amplification takes place due to the interaction between the beam and the fields associated with the structure, which has input and output waveguide windows at its ends and is at earth potential. The dc power supplies are therefore required for three electrodes and for the focusing magnet, while water and air are required for cooling.

Table I lists the characteristics of the tube at different frequencies and, as may be seen from Fig. 2, voltages are available from the power

\* First published in *British Communications and Electronics*, August 1962.

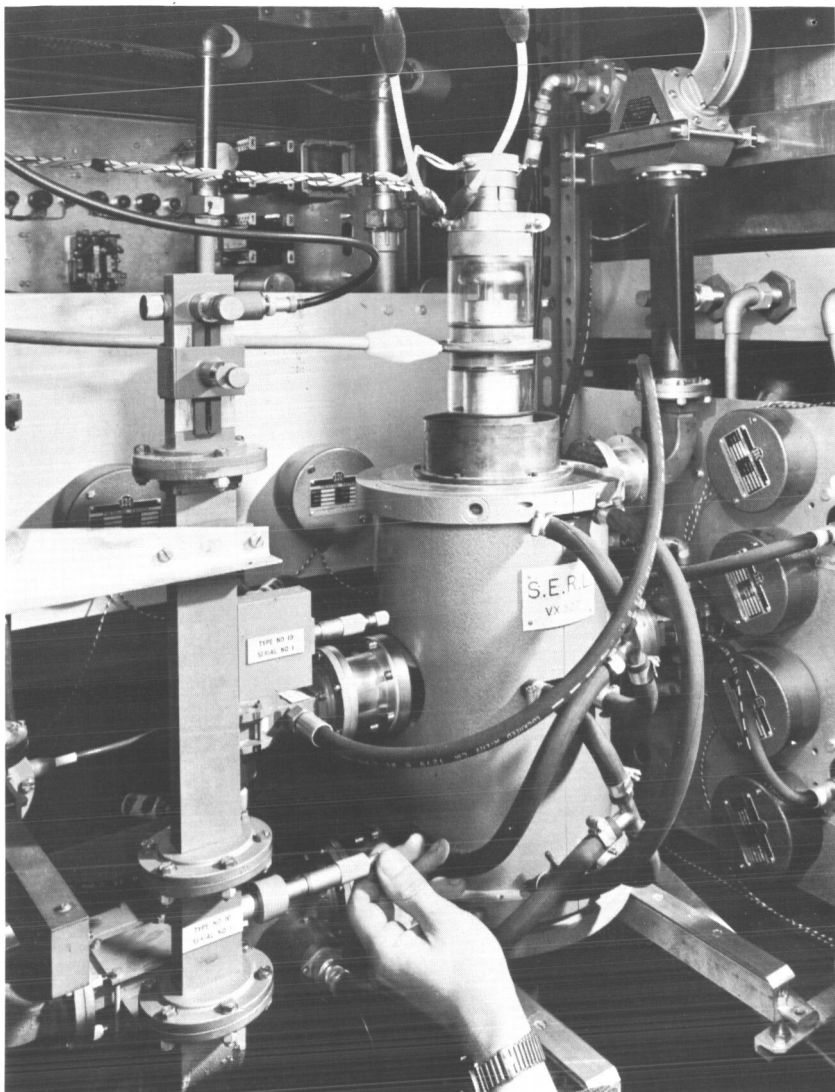


Fig. 1 — The SERI travelling wave amplifier.

supplies to tune the tube for maximum power over the full range of 6,275 Mc/s to 6,550 Mc/s.

It will also be seen from Fig. 2 that the collector is not connected to the slow wave structure at earth potential, but is held negative by the collector bias supply.

• TABLE I — CHARACTERISTICS OF TRAVELLING WAVE TUBE VX527

Frequency	Minimum 6,275 Mc/s	TELSTAR 6,390 Mc/s	Maximum 6,550 Mc/s
Beam Voltage (Cathode to Slow-Wave Structure)	32kv	25kv	20kv
Beam Current	0.8 amps	1.1 amps	1.4 amps
Collector Voltage	21.5kV	17kV	13.5kV
Collector Bias Voltage	10.5kV	8kV	6.5kV
Anode Current	< 1mA	< 1mA	< 1mA
Magnet (Hot)	Voltage 40V Current 40A		
Heater	Voltage 6.5V ac Current 8.5A		

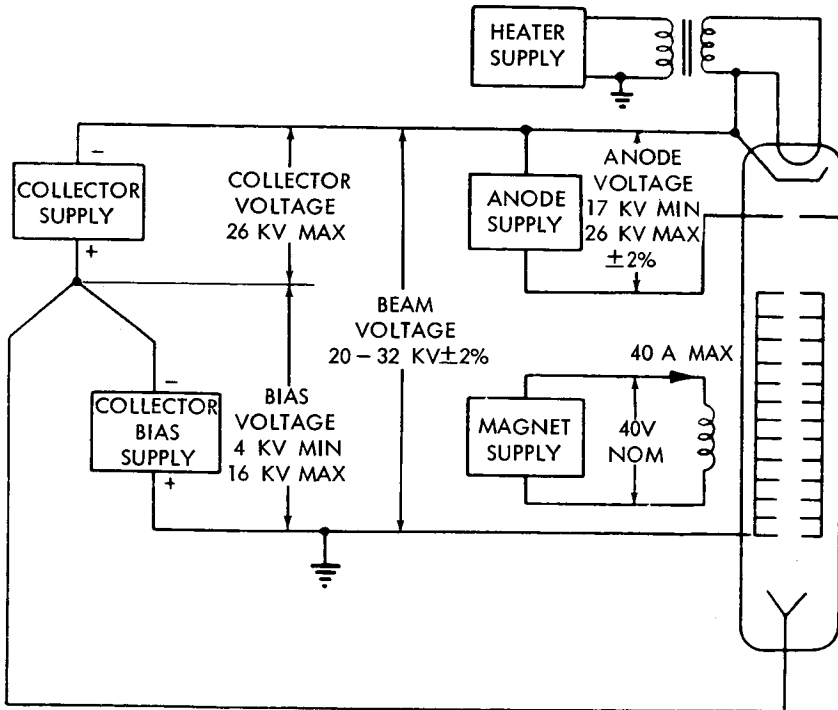


Fig. 2 — Schematic diagram of Telstar output stage power supply.

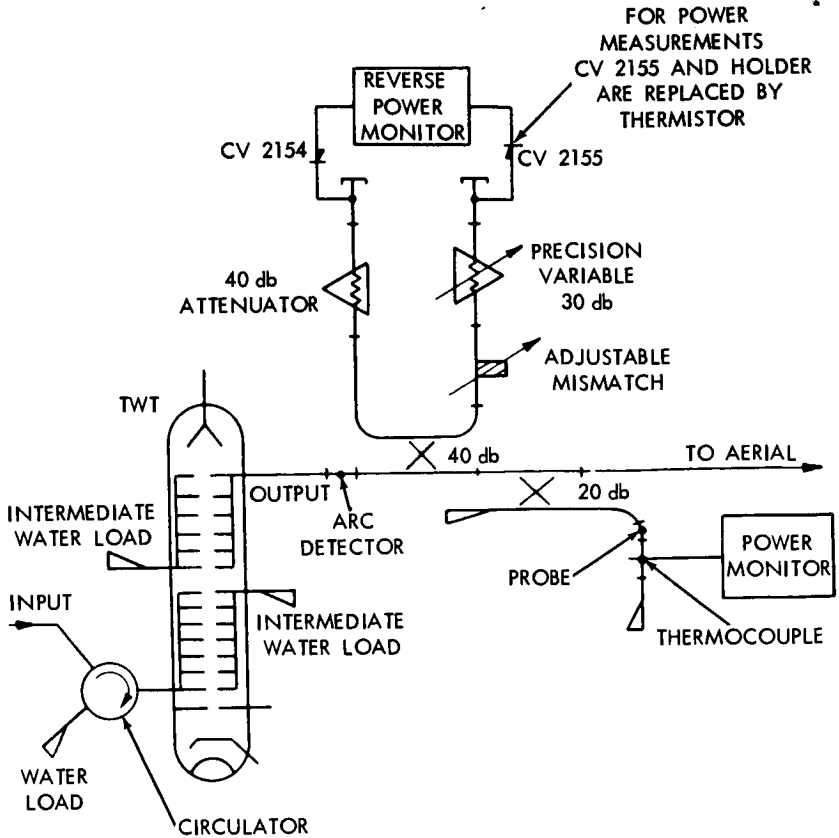


Fig. 3 — Telstar output stage waveguide system.

Operation of the tube is controlled by the cathode-slow wave structure voltage, called the beam voltage, and if the collector bias supply is omitted, the beam current must be supplied at this voltage. This is not necessary however, since the electrons may be allowed to slow down by the action of the collector bias before striking the collector. It will be seen that at the Telstar frequency, a collector voltage of only 17 kV is required compared with a beam voltage of 25 kV, giving a saving of over 8 kW, since the bias power is small in comparison.

This form of bias is also known as collector depression and when used gives a tube efficiency of 22% with a collector input of 18 kW

Part of the electron beam is, however, intercepted by the slow wave structure due to imperfect focusing and other causes and this forms a

load on the collector bias supply, which increases with drive power and may reach 15mA. The leakage current flowing from earth to collector in the cooling water must also come from the collector bias supply and it is in the order of 20 mA when distilled water is used.

Interception of the electron beam also occurs at the anode to some extent but the current is usually less than 1ma.

The electron beam is focused by an electromagnet wound with aluminum strip directly on to the outside of the slow wave structure.

#### STABILIZATION OF ELECTRICAL SUPPLIES

To keep the travelling wave tube operating correctly, the beam and anode voltages must be stabilized against variations of the mains supply and against voltage drift due to component warm-up. Failure to do this results in loss of gain and therefore of power output, but also causes the gain to depend on frequency, resulting in distortion of the transmitted signals. Similarly ripple voltages must be limited to .25% peak in order to keep phase modulation of the output at an acceptable level in the transmission of, for example, colour television.

Since neither side of the collector supply is at earth potential when depression is used and since the bias current is less than 5% of the collector current, it is convenient to stabilize the beam voltage by controlling only the bias voltage. Stabilization against slow changes is carried out by varying the ac input voltage to the bias supply using a motor driven variable ratio transformer, while faster transients and ripple are reduced by means of a dc coupled series valve and LC filters. A conventional system is used in which a small fraction of the beam voltage is compared with a neon reference and the difference amplified to supply the grid of the series valve. If low frequency drifts make the operating point of the series valve wander too far from the optimum, a voltage discriminator across the valve causes the variable transformer to re-adjust the input voltage.

The anode voltage is stabilized in a similar manner, although neither side of the anode supply is at earth potential. Since the supply is fed from the mains some method of transferring power and monitoring and protection signals between earth and anode circuit potential is required. The solution chosen involves having the variable ratio transformer and its motor control circuits at earth potential and all the other stabilizer components including the rectifiers and smoothing at anode potential. Connection between the two is by means of transformers insulated for the high voltage, and the control circuits as well

as the power circuit use mains frequency. This system requires only a small number of components and has been proved to be reliable.

During the turning on procedure, bias, collector and anode supplies are controlled without stabilization by raise and lower switches working in the motor drive circuits, and at the correct working point, indicated by a lamp, the operator switches the stabilizer into circuit.

The magnet supply is stabilized to prevent the current from falling during the initial warming-up period, and to hold it to within  $\pm 1$  amp of the nominal 40 amps. However, it has been shown that the VX527 is very tolerant to changes of magnet current and will work satisfactorily over a range of more than 10 amps.

The TWT cathode heater is energized from a constant voltage transformer. The heater is run up to full power over a period of 5 minutes and then allowed to settle for a further 5 minutes before the electrode voltages are applied. A protection circuit prevents application of the e.h.t. to the tube before the correct operating voltage is reached.

#### COOLING OF THE TRAVELLING WAVE TUBE

In addition to the input and output waveguide windows, the TWT has two intermediate windows fitted with water cooled loads to absorb reverse power. The output window is supplied with 2 ft<sup>2</sup>/min. of free air to cool it while the other three windows are connected in a series air circuit and supplied with 1 ft<sup>2</sup>/min. This air is obtained from a single cylinder compressor providing oil free air at 100 psi. In order to dry the air, it is cooled so that the excess water condenses and can be removed. The pressure is then reduced to 10 psi at which point the relative humidity has been reduced to less than 35%. Carbon piston rings with a life of over 5000 hours are fitted in the compressor to remove the need for lubrication of the bore.

The TWT also requires liquid cooling, both for the collector and for the slow wave structure/magnet assembly. Distilled water is used in a closed cycle system lessen corrosion and to reduce the leakage current flowing from earth to the collector and it is pumped at 120 psi with a flow of 14 gallons per minute through the TWT cooling system to a forced-air-cooled heat exchanger mounted on the cabin roof. Separate pressure switches and flow meters are fitted in four parallel flow paths supplying the collector, the structure, the intermediate window loads and an RF dummy load which can be connected to the output window.

To prevent the water from freezing in the heat exchanger in cold weather, it is continually circulated via a 6 kW immersion heater when the transmitter is off.

#### RF POWER MEASUREMENT

For single way working between two ground stations via Telstar it is normal practice to run the transmitter at its full power. However when two way working experiments are in progress, using two closely spaced frequencies in the satellite pass band, it is necessary to ensure that the single strength at the satellite is approximately the same for both signals. This means that the transmitted power must be continuously reduced during passes in which the satellite approaches the transmitter and to cope with these requirements, two methods of power measurement are provided. As may be seen in Fig. 3, one method uses a 20 db coupler feeding a thermocouple, the output of which is amplified by a magnetic amplifier to drive a meter with a scale linear from 1 to 5 kW. This is satisfactory for general use, but below 500 watts it is not accurate enough for two way working.

A second method of measuring power is to meter the crystal current in the forward arm of the reverse power monitor. The crystal current is calibrated against the thermocouple at full power and a decibel scale may then be considered linear to at least 15 db below 4 kW with an accuracy of better than 1 db. The basic calibration for both systems is obtained from a thermistor bridge.

#### FAULT PROTECTION

The TWT is expensive and care must be taken to prevent damage caused by any faults occurring in the system. Failure of the water and air cooling is detected by pressure and flow switches, and failure of the magnet or heater excitation by no-volt relays, while overload relays detect excessive electrode currents. All these trips bring out the contactor supplying the electrode voltages as well as the contactor supplying the circuit causing the trip. However, this system is not necessarily adequate when the fault results in excessive interception of the beam current by the anode or slow wave structure since there may be sufficient energy stored in the components of the smoothing circuits to damage these electrodes even if the main supply could be removed instantaneously. This condition is dealt with in a few microseconds by a pulse circuit operated from the rapid increase in electrode current which causes the e.h.t. supplies to be short-circuited

through ignitron and thyatron crowbars. In each case the stored energy is diverted into resistors which dissipate it until the normal overload relays open the contactor to clear the fault currents produced.

If arcing should occur in the output waveguide, it will either start at, or run towards the output window where an arc detector is fitted. This is a photoelectric relay whose photocell looks into the waveguide through a slot so that an arc passing the slot causes the relay to operate and fire the crowbars.



Fig. 4 — A general view of the Telstar ground transmitter at Goonhilly.

Protection against mismatches in the output guide is given by a reverse power monitor. Forward power is measured by a crystal fed through a variable attenuator and a variable mismatch used for setting the sensitivity, and reverse power is measured by a crystal fed through a fixed attenuator. The ratio of the RF fields feeding the two crystals is proportional to the reflection coefficient in the main waveguide and the crystals are connected in a circuit driving a dc amplifier which operates a relay to switch off the drive to the TWT. The use of two crystals in this way reduces the effect of transmitter power variations on the tripping point.

### MECHANICAL ARRANGEMENT

The equipment is fitted into six cubicles, three of which are on a common baseplate for convenience of interconnection (Fig. 4). All cubicles are 7 ft. 6 in. high but are of varying plan dimensions to fit the available space in the transmitter cabin.

Components at a high potential to earth are mounted in boxes made from proprietary extruded aluminium sections, which is a convenient way of ensuring well-rounded corners to prevent corona. Other electronic components are mounted on swing frames inside the cubicles, which have doors front and back, and trays fitted on these frames may be repaired in situ or removed for servicing, although for safety of personnel it is not possible to close the main supply isolator when any of the cubicle doors are open. Fault location is simplified by a comprehensive system of lamps which indicate the part of the circuit that has initiated a shut down.

The cubicles are cooled by extractor fans mounted near the roof feeding an external common duct which is led outside the cabin through a diverter which permits the hot air to be fed into the cabin to economize on heating in cold weather. The larger transformers are filled with non-inflammable oil and are sealed and fitted with bursting diaphragms which have separate vents leading directly to the outside of the cabin. The cabin is air conditioned to avoid difficulties due to condensation on high voltage insulators.

### REFERENCE

1. Bryant, M. O., Thomas, A., and Wells, P. W., A High Power CW Travelling Wave Tube, *J. Electronics and Control* 12(1), January 1962.

N67 12319

# Results of Tests at Goonhilly Using the Experimental Communication Satellites Telstar I and Telstar II\*

W. J. BRAY, F. J. D. TAYLOR, and R. W. WHITE

POST OFFICE ENGINEERING DEPARTMENT

The first active communication satellite—Telstar I—was launched from Cape Canaveral by the National Aeronautics and Space Administration (NASA) on 10th July, 1962, and was later followed by Relay and Telstar II. Since the 10th July, 1962, many tests and demonstrations of television, multi-channel telephony and telegraphy, facsimile and data transmission have been made via these experimental satellites. In addition, much data has been accumulated on microwave propagation, earth-station receiving system noise temperatures and satellite tracking accuracy. Such tests and data will be of considerable value for the planning and design of future operational communication-satellite systems.

The aim of this lecture is to review the results obtained from the tests with the Telstar Satellites and to draw some broad conclusions as to their implications. Since it will not be possible to present all the data, a representative selection has been made.

Several communication-satellite earth stations, including those at Andover, Maine, and Pleumeur-Bodou, France, took part in the tests. The results presented, however, are mainly those obtained from measurements made at the British Post Office earth-station at Goonhilly, Cornwall. It is to be noted that much additional data on the performance of the communication satellites themselves, and on the intensities of radiation in space and its effect on the lives of solar cells and other components in satellites, has been obtained by the Bell Telephone Laboratories and NASA via telemetry transmissions from the satellites.

The cooperative programme of tests between the various earth stations has been coordinated by a *Ground Station Committee*. This Committee, which is chaired by NASA, includes representatives of NASA,

---

\* Read before the Institute of Electrical Engineers, November 1962.

and the administrations concerned with operation of the stations and the satellite designers.

Before discussing the tests it will perhaps be of value to outline briefly the characteristics of the Telstar satellites and their orbits, and the characteristics of the Goonhilly earth-station.

#### THE TELSTAR AND RELAY SATELLITES AND THEIR ORBITS

The main characteristics of the Telstar and Relay satellites are shown in Table I.

TABLE I — CHARACTERISTICS OF THE TELSTAR SATELLITES

SATELLITE	TELSTAR I	TELSTAR II
DATE OF LAUNCH	10th JULY, 1962	7th MAY, 1963
PRESENT STATUS (NOVEMBER 1963)	FAILED 21st FEBRUARY, 1963	OPERATIONAL
TRANSMISSION CHARACTERISTICS		
Transmit Frequency (Mc/s)	4170	4170
Beacon Frequency (Mc/s)	4080	4080
Receive Frequency (Mc/s)	6390	6390
Radiated Power (Watts)	2	2
Transponder Bandwidth (Mc/s)	50	50
ORBIT		
Perigee (Statute Miles)	590	600
Apogee (Statute Miles)	3500	6700
Inclination (Degrees Relative to Equator)	45	43
Period (Minutes)	158	225

It will be seen that, although Telstar I failed, it is believed finally, on 21st February, 1963, Telstar II is operating effectively at the present time.

Both satellites transmit on the same frequencies in the 4000 Mc/s band with radiated power about two watts; the receive frequencies, i.e. the frequencies of the earth-station transmitters, are in the 6000 Mc/s band.

Both satellites are in highly elliptical orbits with different maximum (apogee) heights, but have approximately the same inclinations of the orbital planes relative to the Equator.

The increased height of the Telstar II orbit compared with the

Telstar I results in slant ranges up to 10,000 miles or more. The longer range without increased transmitted power result in significantly lower received signal levels at the earth stations, and place stringent requirements on the earth-station receiving system in respect of aerial gain and overall noise temperature. However, the greater height also results in a longer orbital period and the mutual visibility between Andover and Goonhilly may extend up to an hour or more on certain passes.

#### CHARACTERISTICS OF THE GOONHILLY EARTH-STATION

In its present form the Goonhilly earth station has been designed and built primarily to enable tests with experimental communication satellites to be made, but also to be capable of development into an operational station at a later stage if required. For this reason it incorporates extensive testing equipment and other facilities that would not necessarily be part of an operational station.

#### *Steerable Aerial*

The steerable aerial at Goonhilly employs an 85-ft. diameter parabolic reflector with a feed in the aperture plane, Fig. 1. Unlike the aerials at Andover and Pleumeur-Bodou, the Goonhilly aerial is designed to operate without a radome. The dish can be rotated in azimuth through  $\pm 250$  degrees, and in elevation from 0 to 100 degrees, by servo-controlled motor drives. The aerial is steered on the basis of predicted orbital data, with either manual or automatic fine correction of any residual errors in the data. The predicted data, which corresponds to the X, Y, Z co-ordinates of the satellite position at 1-minute intervals of time, is supplied over a teleprinter link from the Goddard Space Flight Centre, up to a week or so in advance of each satellite pass. From it is derived, via a computer at Goonhilly, azimuth and elevation angle pointing data at 1-second intervals of time. The latter data is recorded on punched tape and used to control the aerial steering system.

Any errors in aerial pointing are determined by causing the aerial beam to scan conically over a very small angle, e.g. 0.03 degree. The resulting amplitude modulation of the microwave beacon signal received from the satellite is detected and used to correct the aerial pointing, by either manual or automatic remote-control of the position of the feed at the focus.

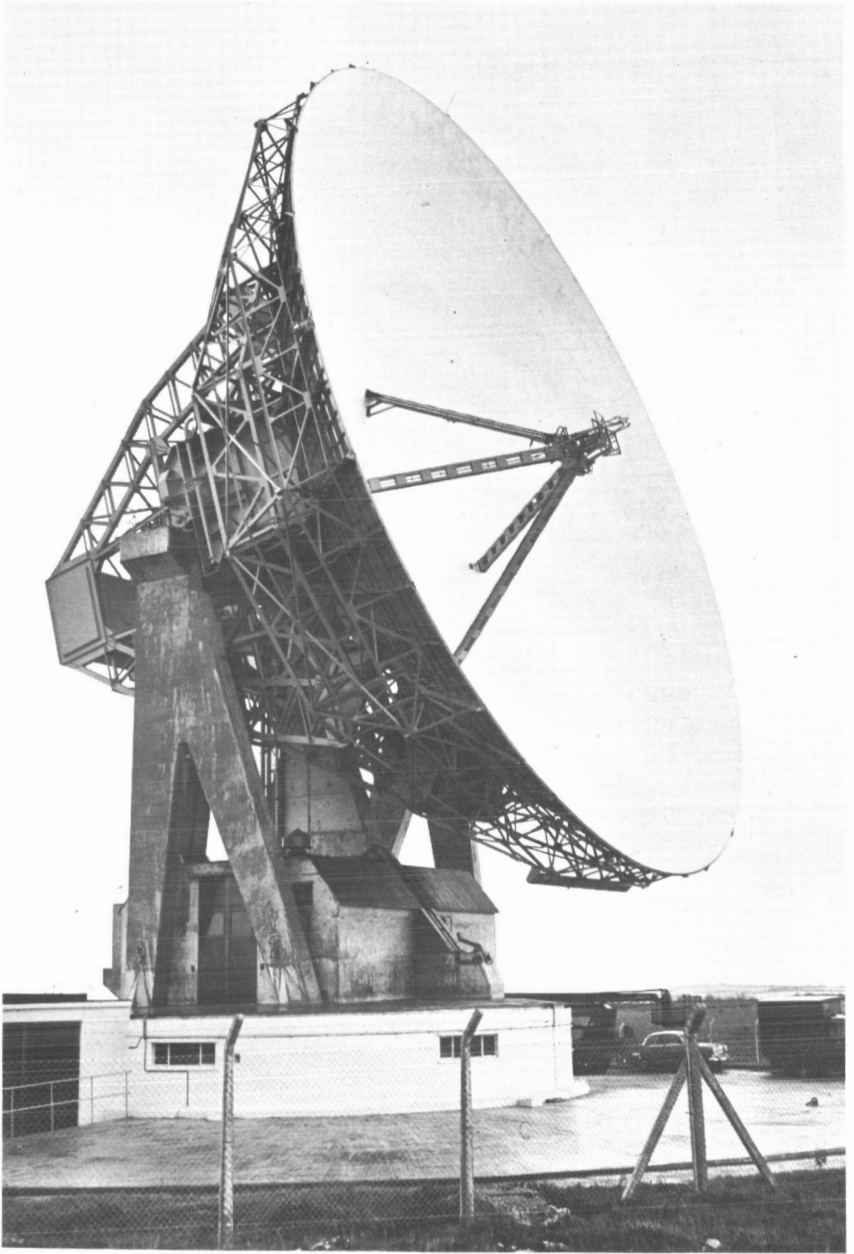


Fig. 1 — General view of Goonhilly aerial.

*Aerial Gain and Radiation Diagram*

The accurate measurement of the gain of large-aperture microwave aerials is a matter of some difficulty, since the test transmitter or receiver must be located at least several miles away if a sufficiently plane wave is to be achieved. If tower-mounted test aerials are used, undesirable ground reflections are liable to arise thus causing errors. However, the radio star Cassiopeia A provides a source of known and stable amplitude free from such limitations. Measurements of the gain of the Goonhilly aerial at 4170 Mc/s using Cassiopeia A indicate a gain of 55.6 db (excluding waveguide losses) relative to an isotropic aerial, as shown in Table II.

TABLE II — CHARACTERISTICS OF GOONHILLY AERIAL

CHARACTERISTIC	GAIN OR LOSS (db)		
	FREQUENCY Mc/s)	1725	4170
<b>GAIN OF IDEAL AERIAL</b>			
Gain with uniform illumination	53.4	61.1	64.8
Loss due to tapering	1.8	2.0	3.0
Gain with tapered illumination	51.6	59.1	61.8
<b>ADDITIONAL LOSSES DUE TO</b>			
Feed support shadowing	1.5	1.5	1.5
Reflector profile inaccuracies	0.4	2.0	4.8
Total	1.9	3.5	6.3
<b>GAIN OF ACTUAL AERIAL</b>	<b>49.7</b>	<b>55.6</b>	<b>55.5</b>

The gain at 4170 Mc/s is some 3.5 db less than that of an ideal aerial with the same feed radiation pattern, the loss being mainly due to dish profile inaccuracies (these being less than 3/16 inch or  $\lambda/16$  at 4170 Mc/s over the area of the dish within the 45-ft. diameter); the remaining losses are due to scattering from, and aperture blocking by, the feed supporting structure. It is to be noted that the feed pattern is heavily tapered, the radiation intensity at the rim of the dish being some 18 db below that at the centre, in order to reduce noise pick-up from the ground. The aerial gains at 1725 and 6390 Mc/s are 49.8 and 55.5 db, the losses being 1.8 and 6 db respectively, relative to an ideal aerial. The larger losses at 6390 Mc/s are due to the greater effect of profile inaccuracies as the frequency is increased.

The aerial radiation diagram at 4170 Mc/s, for angles up to  $\pm 6^\circ$  from the main lobe, is shown in Fig. 2. For angles between  $\pm 10^\circ$  and  $\pm 90^\circ$  the minor lobes are at least 50 db below the main lobe, and beyond  $\pm 90^\circ$  they are at least 70 db below. The high discrimination provided by such aerials is, of course, a major factor in avoiding interference to and from terrestrial radio-relay systems, and other satellites, using the same frequency bands.

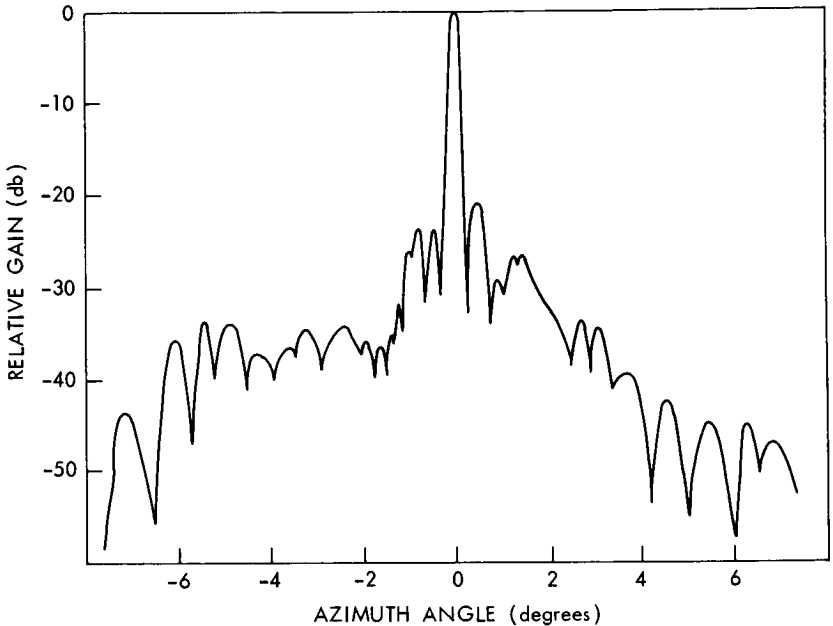


Fig. 2 — Goonhilly aerial horizontal radiation diagram.

The main lobe of the radiation diagram at 4170 Mc/s is shown in greater detail in Fig. 3, which gives a comparison between the measured and computed values. The amplitudes of the first pair of minor lobes are somewhat larger than the computed values, due to scattering from the feed supporting structure. The width of the main lobe at 4170 Mc/s is about 12 minutes of arc at 3 db below the maximum amplitude, and only nine minutes at 6390 Mc/s; thus pointing accuracies of less than a few minutes of arc are essential if significant losses of received signal strength at earth station and satellite are to be avoided.

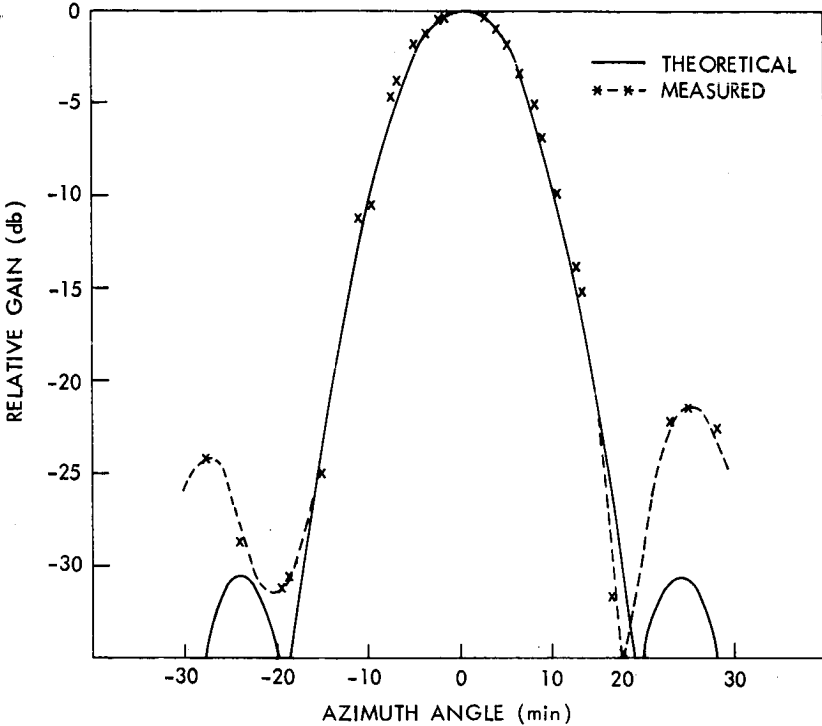


Fig. 3 — Goonhilly aerial main lobe radiation diagram.

#### *Receiving System Overall Noise Temperature*

The signals received from Telstar—even allowing for the gain of the 85-ft. aperture aerial—may be only of the order of a micro-microwatt, and a low-noise receiving system is therefore essential. The Goonhilly receiver incorporates a liquid-helium cooled maser operating at about  $2^{\circ}\text{K}$ , the equivalent noise temperature at the maser input being about  $12^{\circ}\text{K}$ . However, the losses in the waveguide feeders, filters and other components between the maser and the aerial feed increase the overall receiving system noise temperature to about  $55^{\circ}\text{K}$  when the aerial is pointing at the zenith, as shown in Fig. 4. As the aerial moves from the zenith towards the horizon, additional noise is picked up from the atmosphere and, for angles of elevation below a few degrees, from the ground via the minor lobes of the radiation diagram. Fig. 4, shows curve (c), the calculated noise contribution from a “standard” atmosphere. The difference between the measured overall noise temperatures shown in curves (a) and (b) represents an improvement of some  $15^{\circ}\text{K}$

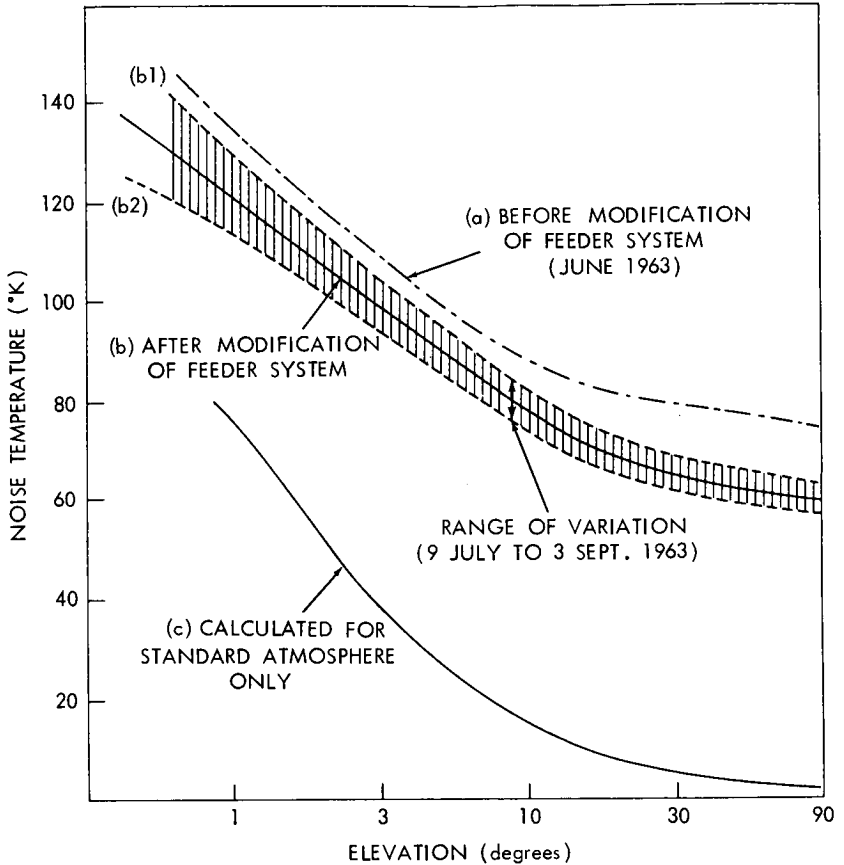


Fig. 4 — Overall noise temperature variation with elevation angle.

due to a reduction of the feeder system losses by 0.2 db. Of particular interest is the limited range of variation of the noise temperature at given angles of elevation over a period of some two months with changing atmospheric conditions, i.e. clear skies interspersed with rain, cloud and occasional ground mist. It is believed that this small range of variation is in part due to the absence of a radome, which when wet could contribute significantly to the overall noise temperature.

#### *Transmitters*

The transmitter used at Goonhilly for tests with Telstar produces an output of up to 5 kW at 6390 Mc/s; the maximum effective radi-

ated power, allowing for the aerial gain and the feeder losses, is some 5000 megawatts.

#### RESULTS OF TESTS AND DEMONSTRATIONS

##### *Characteristics of Received Carrier*

The characteristics of the received carrier of primary interest are: the variation of level during a satellite pass, especially at low angles of elevation; and the Doppler frequency shift due to the motion of the satellite relative to the earth stations.

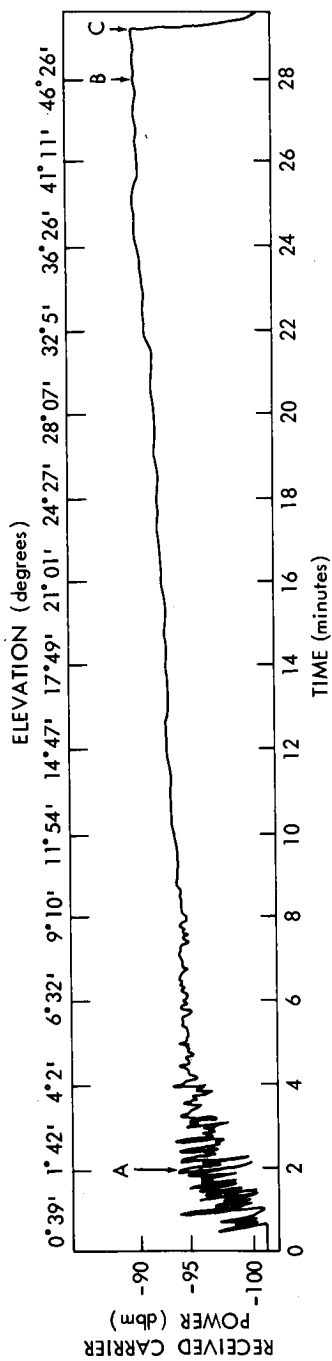
The variation of received carrier level during a typical pass of Telstar I is shown in Fig. 5. It indicates:

1. acquisition of the satellite with the aerial beam only 0.5 degree above the horizontal;
2. fluctuations of level of a few decibels for angles of elevation up to about three degrees, due to the tropospheric layers and irregularities; and
3. a steadily increasing level from about three degrees elevation, to the end of the pass.

Study of the variations of received carrier level for low angles of elevation is of considerable importance for the design of operational communication satellite systems, since the coverage obtainable and therefore the number of satellites required depends on the minimum angle of elevation at which signals can be consistently received. The fact that the horizon at Goonhilly is not more than 0.5 degree above the horizontal has facilitated such studies. Statistical data of the variation of received carrier level at low angles of elevation, obtained during a number of satellite passes, is shown in Fig. 6. It is considered that reliable operation can be achieved for angles of elevation down to about three degrees; however, more data are needed to confirm this provisional result.

For angles of elevation above about three degrees, the received carrier level can be calculated with good accuracy from the free-space transmission equation, allowance being made for the satellite "look angle", i.e., the angle which determines the effective gain (or loss) of the satellite aerial along the direction between the satellite and the earth station.

Fig. 7 shows a comparison between the measured and calculated received carrier powers for a typical pass. It also shows the Doppler frequency shift of the carrier during the pass, due to the rate of change



AT A THE SATELLITE WAS 7000 MILES FROM GOONHILLY  
 AT B THE SATELLITE WAS 3000 MILES FROM GOONHILLY  
 AT C THE SATELLITE TRANSMITTER WAS SWITCHED OFF

Fig. 5 — Variation of received carrier power with elevation angle and time during a typical pass.

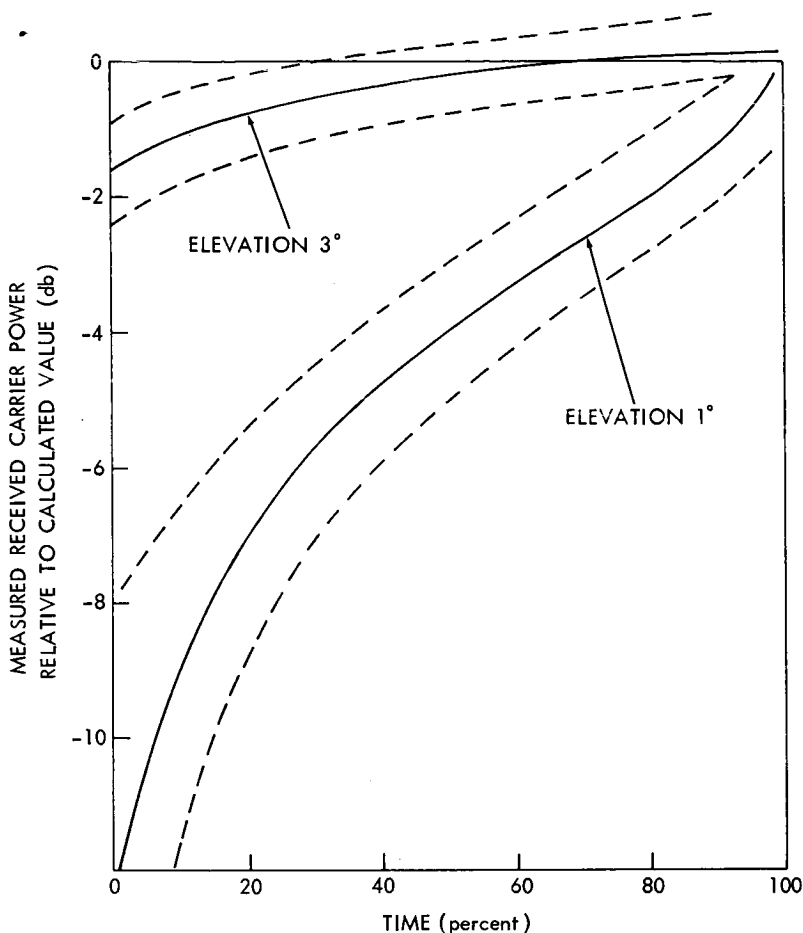


Fig. 6—Variation of received carrier level at low angle of elevation.

of path length between the earth stations via the satellite. The varying small difference between the measured and calculated values is due to frequency drift of the oscillators in the satellite and earth stations.

The Doppler frequency shift may be up to some 80 kc/s on the 4170 Mc/s received carrier (i.e. up to 2 parts in  $10^5$ ) in the case of the Telstar satellites, for a loop connection via the satellites (i.e. from one earth station to the satellite and back to the same earth station). For earth stations on opposite sides of the Atlantic the Doppler shift rarely exceeds 1 part in  $10^5$ , and is generally appreciably less. Such shifts of the carrier frequency are not significant in the wide-band

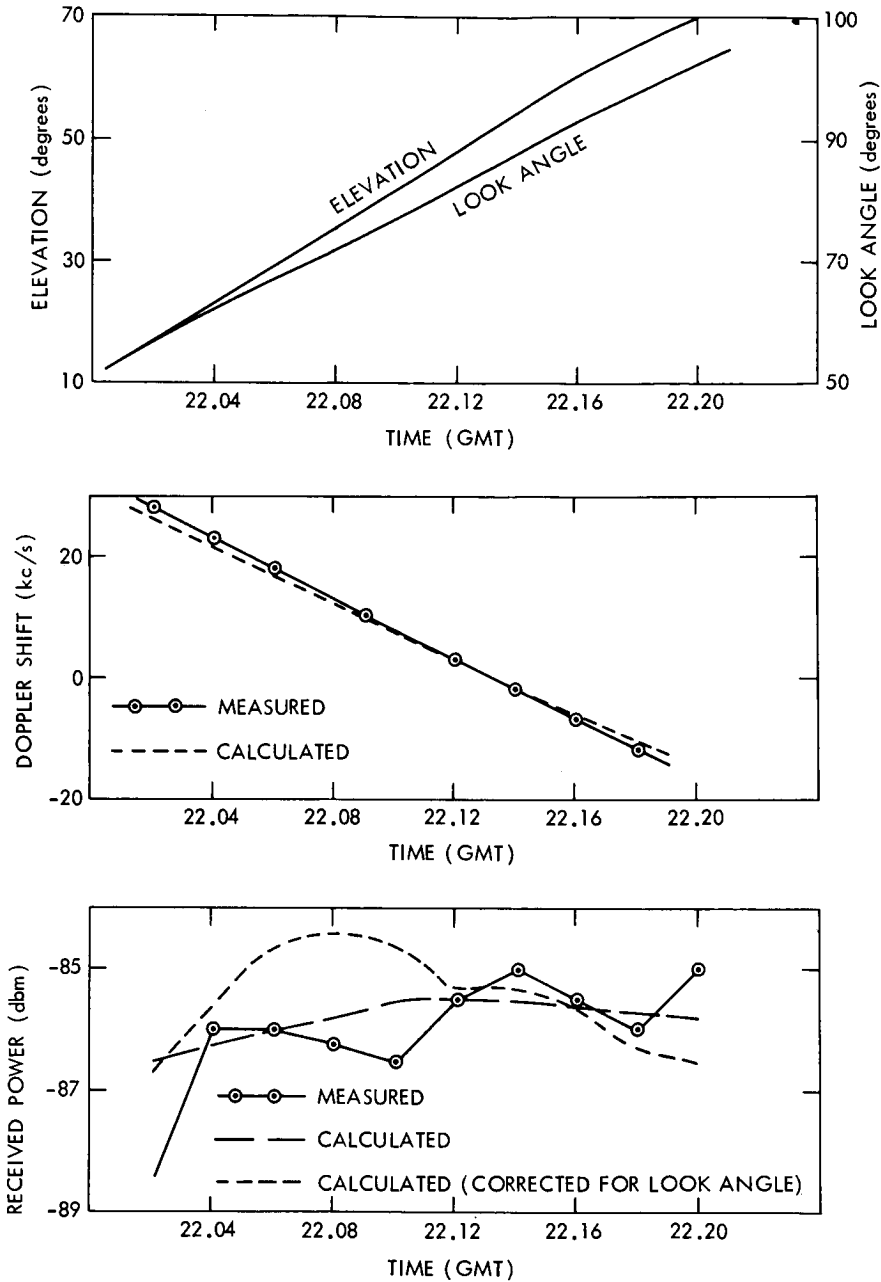


Fig. 7 — Comparison of measured and calculated received carrier power and doppler shift.

RF or IF channels of the FM communication systems; they are important, however, in the narrow-band beacon channel which has to be tuned to allow for the shift. Doppler frequency shifts of up to 1 or 2 parts in  $10^5$  also occur in the baseband signals; the effects for various types of baseband signal will be discussed later.

### *Selective Fading and Multi-path Effects*

Observations have been made on many occasions to determine whether frequency selective fading or multi-path effects, e.g., due to partial reflections from tropospheric layers, are present. Such effects might be expected to occur, for example, at low angles of elevation with glancing incidence on the tropospheric layers.

Frequency selective fading can be investigated by transmitting a frequency-modulated carrier with a deviation of several megacycles per second and observing the received signal on an IF spectrum analyser; multi-path echo signals can be investigated by transmitting a narrow pulse (e.g., 0.2 microsecond pulse-width) and observing the received baseband signal.

Although many observations have been made, no evidence of selective fading or multi-path effects within the limits of resolution of the equipment have been detected for angles of elevation above about three degrees. This favourable result is attributable in part to the very high directivity of the earth-station aerial, which discriminates markedly against any tropospheric reflections more than a fifth of a degree off-beam, and partly to the smaller reflection coefficients for angles of incidence of greater than a few degrees relative to the mainly horizontal layers.

Below about three degrees elevation of the earth-station aerial beam, the received carrier level fluctuations indicate reflections from tropospheric discontinuities. However, even in this region, the relative delays of such signals are so small that they do not give rise to significant selective fading or echo effects.

The foregoing observations are confirmed by the excellent transmission quality of the satellite link for television and multi-channel telephony signals, referred to later.

### *Satellite Tracking Accuracy*

For angles of elevation above about three degrees, errors in uncorrected aerial pointing relative to the wave arrival direction rarely exceed 10 minutes of arc, and are generally less than 5 minutes of arc.

for satellite orbits predicted up to two weeks in advance. The manual or auto-track fine correction systems enable even these small errors to be reduced to one or two minutes of arc.

These results indicate the practicability in operational systems of using aerials with beamwidths of only 10 minutes of arc, i.e. with gains of up to about 60 db, provided that such regular operation does not extend below about three degrees elevation relative to the horizon. Below about three degrees elevation, ray bending due to atmospheric refraction plays an increasingly important role; in the case of a satellite the true direction of which is horizontal, the aerial must be pointed about 0.6 degree above the horizontal, for a "standard" atmosphere. In practice the amount of refraction varies somewhat about the "standard" value and small fluctuations of wave arrival direction occur at low angles of elevation.

#### *Television Transmission*

It is to be noted that a sound channel is normally provided with

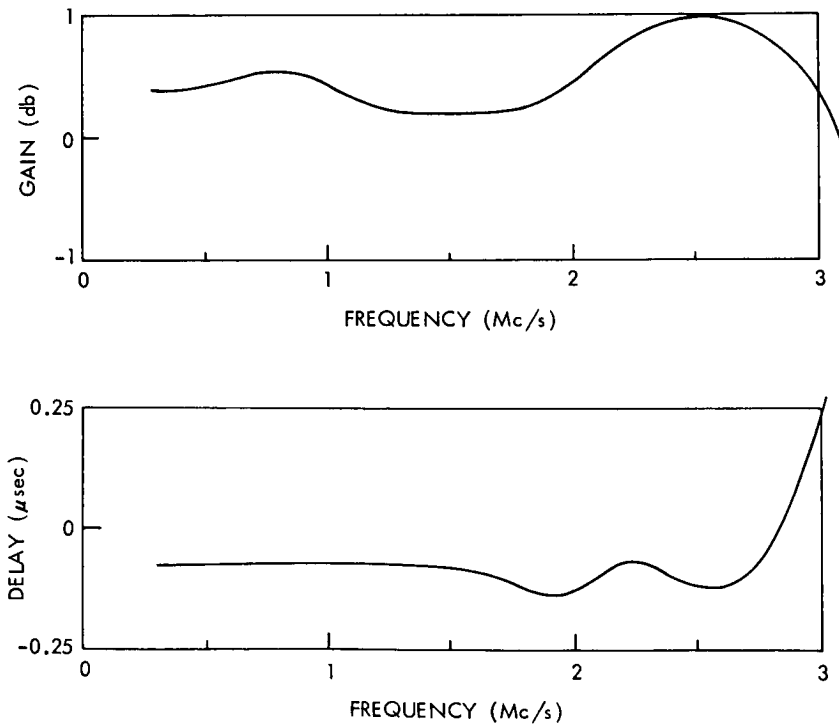


Fig. 8—Insertion-gain and group-delay frequency characteristics of video channel.

the television channel, using a 4.5 Mc/s frequency-modulated sub-carrier in the baseband. This requires that a 3 Mc/s low-pass filter be inserted in the television channel; the results reported are with such a filter in use, except where indicated otherwise.

#### VIDEO CHANNEL TRANSMISSION CHARACTERISTICS

Typical video channel gain and delay/frequency responses, measured at Goonhilly via the Telstar satellites in loop, are shown in Fig. 8. As would be expected in a frequency-modulation system, the loop-gain stability is good, the variation being generally less than  $\pm 0.2$  db.

The video waveform response, measured with a sine-squared pulse ( $2T = 0.3 \mu\text{sec}$ ) and bar signal with the satellite in loop is shown in Fig. 9. The corresponding K-rating factor, which defines the waveform distortion, is less than 2%.

The good quality of the satellite video channel is shown by Fig. 10, a typical test card on the US 525-line television standard transmitted from Andover, Maine, to Goonhilly. Multi-path and echo signals are imperceptible; such imperfections as are apparent on close examination of the received test card are due to the bandwidth restriction imposed by the 3 Mc/s low-pass filter on the nominal 4.5 Mc/s bandwidth video signal.

Doppler frequency shifts have no effect on the quality of the received monochrome video signals, since they correspond to a slow variation of transmission time of a few tens of milliseconds during each pass and this is imperceptible to viewers.

#### COLOUR TELEVISION TRANSMISSION

During the 60th and 61st passes of Telstar I, on 16th/17th July, 1962, the first transmissions of colour television signals were made from Goonhilly, with the co-operation of the Research and Designs Departments of the BBC who provided a colour-slide scanner and picture-monitor equipment. The signals, which were on 525-line, 60 frames/second National Television System Committee (NTSC) standards, comprised captions, test cards and still pictures used to assess colour quality. The transmissions were made initially from Goonhilly to the Telstar I satellite and back to Goonhilly, and were also monitored by Andover. Fig. 11 shows typical colour test cards before and after transmission.

Similar colour television transmission tests were also carried out on the 88th pass on the night of 19th-20th July, 1962; these included transmissions from Andover to Goonhilly. The success of these tests

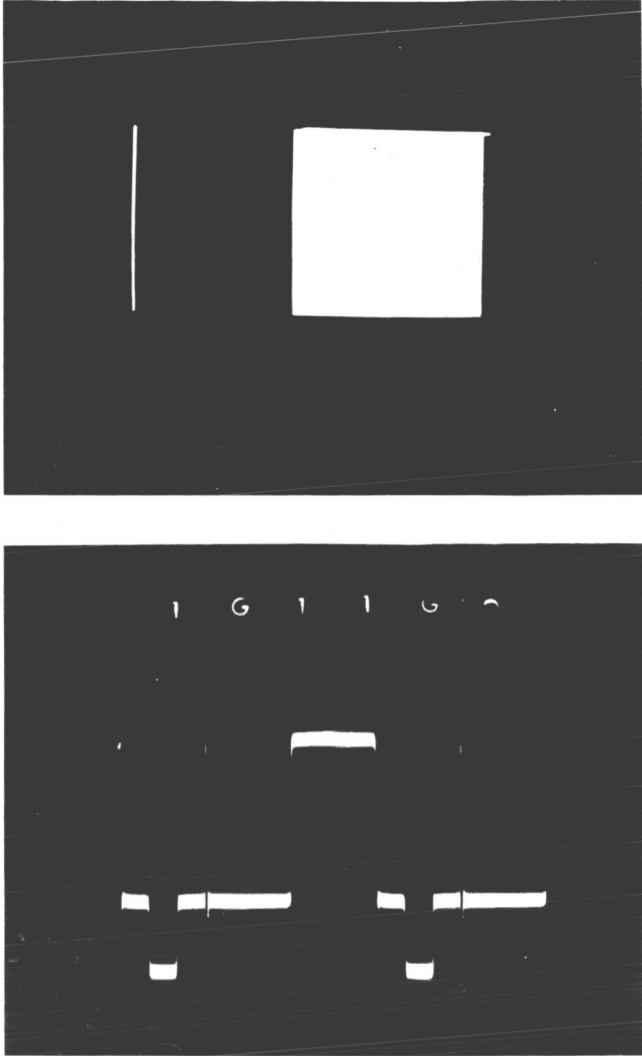


Fig. 9— Video waveform (sine-squared  $2T$  pulse and bar) response.

is a striking demonstration of the excellent transmission quality of the satellite link; in particular it was observed that there was no perceptible deterioration of colour quality due to Doppler frequency shifts. It also appeared that the Doppler frequency shift of up to some 40 c/s of the 3.58 Mc/s chrominance sub-carrier was within the lock-in range of typical colour receivers.

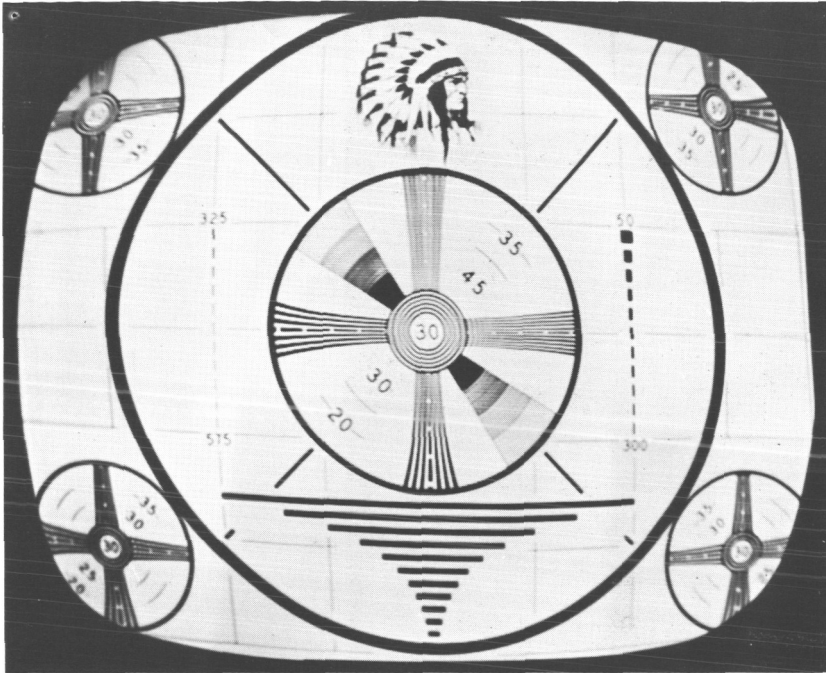
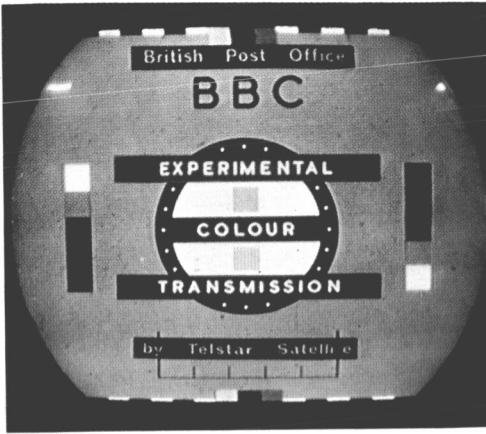


Fig. 10 — Typical test card (US 525-Line) received at Goonhilly.

#### VIDEO SIGNAL-TO-NOISE RATIO

For most passes of the Telstar satellites, and for angles of elevation above a few degrees, the measured overall weighted video signal (peak-to-peak, black-to-white) to RMS noise ratio has been in the range from about 40 to 50 db, corresponding received carrier-to-noise ratios in a 25 Mc/s IF band exceeding some 10 db. The measured values have agreed, within one or two decibels, with the calculated values allowing for satellite range and look angle, the receiving system noise temperature and other characteristics.

Under the above conditions it is possible to use a normal frequency modulation demodulator to recover the video modulation from the carrier. However, conditions arise occasionally when, due to abnormally long distance of the satellite, unfavourable satellite look angles or low angles of elevation at the earth station, the received carrier-to-noise ratio has been less than 10 db. For example, such conditions have arisen at times with Telstar II, due to the greater apogee height and longer ranges compared with Telstar I. Under these conditions a fre-



Picture as transmitted to  
Telstar from Goonhilly Downs



Picture returned to Goonhilly  
Downs by Telstar



Picture transmitted from US  
to Goonhilly Downs via Telstar

Fig. 11 — Colour television transmission via Telstar.

quency-following negative-feedback (FMFB) demodulator, or variable-bandwidth dynamic-tracking demodulator (DTVb) can be used and have been shown to give satisfactory results for carrier-to-noise ratios, measured in a 25 Mc/s band, of only 6 db and usable results at even smaller ratios. The DTVb demodulator uses a narrowband filter, the centre-frequency of which follows the instantaneous frequency of the FM carrier, the filter bandwidth being adjustable to suit the prevailing noise conditions. Fig 12 shows a comparison of the performance of the FMFB and DTVb demodulators with a normal FM demodulator under conditions of low carrier-to-noise ratio.

#### USE OF VIDEO PRE-EMPHASIS AND DE-EMPHASIS

It has generally been preferred at Goonhilly to use video pre-emphasis and de-emphasis, since this reduces the mean deviation of the frequency modulated carrier without reducing the overall signal-to-noise ratio. The smaller mean deviation has two advantages:

1. It reduces crosstalk from the video channel into the sub-carrier audio channel due to residual non-linearity of the FM system;
2. It improves the overall performance of the video channel under low carrier-to-noise ratio conditions by minimising effects due to maser bandwidth limitations.

#### VIDEO-TO-AUDIO CROSSTALK

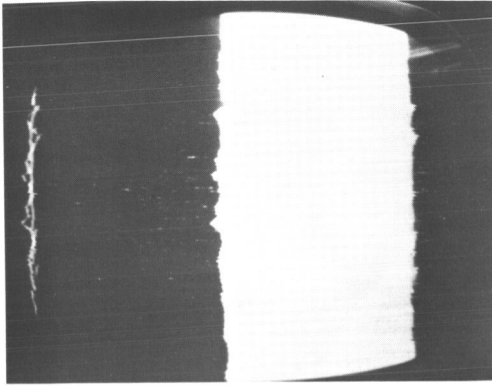
Without video pre-emphasis the audio noise due to crosstalk from the video channel has varied from about -30 to -40 dbm (weighted), depending on picture content; with video pre-emphasis, values ranging from -44 to -48 dbm have been obtained.

#### *Multi-Channel Telephony Transmission*

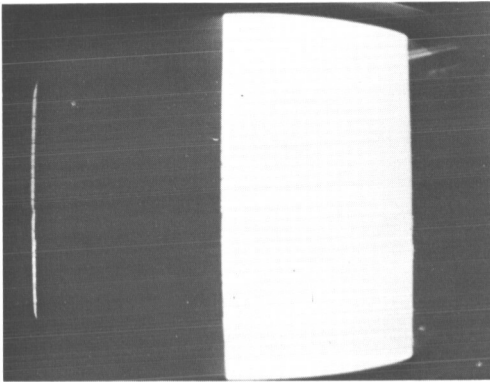
Multi-channel telephony tests are especially important since the economic viability of communication satellite systems will depend to a considerable degree on their ability to accommodate large numbers of telephone channels, subdivided into both small and large blocks of channels.

The multi-channel telephony tests carried out with the Telstar satellites have been of two types:

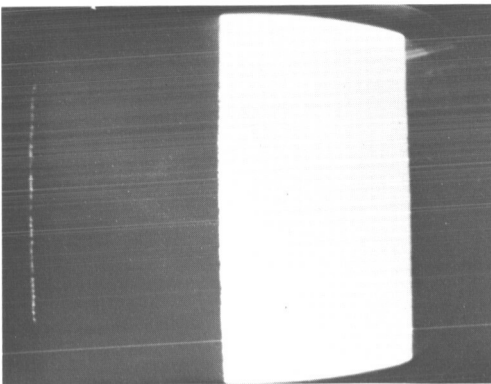
1. Two-way tests (e.g. demonstrations between telephone subscribers) using blocks of 12 or 24 channels in the baseband from 12 to 108 kc/s;
2. One-way tests of 300 or 600 simulated telephone channels, using white noise in the baseband from 60 to 2540 kc/s.



Standard Demodulation  
C/N  $6.7 \pm 0.5$  db



DTV B Demodulation  
C/N  $6.7 \pm 0.5$  db



FMFB Demodulation  
C/N  $6.7 \pm 0.5$  db

Fig. 12 — Comparison of FMFB, DTVB and normal demodulator.

### 12/24 CHANNEL TWO-WAY TELEPHONY TESTS

For two-way transmission of 12 or 24 telephone channels the broadband transponder in the Telstar I or II satellite is energised simultaneously by two earth stations, their transmissions being spaced by 10 Mc/s. This represents a somewhat inefficient use of bandwidth, but the arrangement is convenient for experimental purposes in that only one transponder is needed in the satellite for two-way tests.

The weighted noise in the 3.1 kc/s-wide telephony channels, measured at a point of zero relative level, ranges in general from about  $-55$  dbm to  $-65$  dbm, when working with the larger earth stations.

The two-way telephone channels have been used for many subjective tests and demonstrations between telephone subscribers and the results have been fully comparable with other high-quality long-distance transmission systems.

### ONE-WAY TESTS WITH 300/600 SIMULATED TELEPHONE CHANNELS

As mentioned earlier, large numbers of telephone channels carrying speech and other signals may be conveniently simulated by white noise with a uniform spectrum occupying the same frequency range as the telephone channels, e.g. 60 to 1300 kc/s for 300 channels and 60 to 2540 kc/s for 600 channels.

In order to determine the performance of a transmission system, narrow slots are inserted in the spectrum of the white-noise test signal, the slots being centred on 70, 534, 1248 and 2438 kc/s. The slots enable any noise, whether basic, i.e. of thermal origin, or due to intermodulation between the signals in the telephone channels, to be measured at the output of the transmission system under test. The loading of the transmission system, i.e. the RMS frequency deviation produced in a frequency-modulation system, by the multi-channel signal, can be varied by adjusting the level of the white-noise test signal at the input of the system. As the loading is increased the level, at the output of the system, of basic noise in the slot channels decreases and the intermodulation noise increases. Thus, an optimum loading condition giving the best overall signal-to-noise ratio can be determined.

Furthermore, the effect of pre-emphasis of the multi-channel signal before transmission can be readily assessed by means of a white-noise test signal. Pre-emphasis is useful in frequency modulation systems for multi-channel telephony, since in the absence of pre-emphasis the basic noise spectrum tends to be "triangular", the signal-to-basic noise ratio in the high-frequency baseband channels being worse than in the low-frequency channels; with pre-emphasis a more uniform

distribution of signal-to-noise ratio in the baseband can be obtained. However, in choosing the amount and shape of the pre-emphasis characteristic a compromise is necessary, since too much pre-emphasis introduces excessive intermodulation noise in low-frequency telephone channels.

White-noise test signals are also useful for comparing the multi-channel telephone performance of FMFB and standard demodulators under conditions of low received carrier-to-noise ratio.

The application of these principles to simulated multi-channel telephony tests using the Telstar satellites will now be discussed. Figs. 13 and 14 respectively shows the results of 300 and 600 channel white-noise loading tests with Telstar, the loading being varied about a "normal" value for the simulated multi-channel signal, the deviation produced by a test-tone of 1 mW at zero level point in a telephone channel then being 400 kc/s r.m.s. The results indicate that an optimum deviation is some 5 db higher than the nominal value. However, with a somewhat higher carrier-to-noise ratio, the optimum deviation would tend to move downwards.

The tests have also shown that with a standard FM demodulator system threshold occurs for a carrier-to-noise ratio, in a 25 Mc/s band, of about 10.5 db; with the FMFB demodulator the corresponding ratio is about 6.5 db, an improvement of 4 db.

In an operational system meeting international circuit standards, the test tone-to-weighted noise ratio would be expected to exceed 50 db, compared with the values of 46 to 56 db shown in the 300-channel tests and 37 to 45 db in the 600-channel tests. However, it should be borne in mind that the experimental Telstar satellites do not employ significant aerial gain at the satellites; in an operational system using attitude-stabilized satellites aerial gains of up to 15 db would be possible and would yield a corresponding improvement in signal-to-noise ratio. Furthermore, the linearity of the experimental system is by no means optimum; improved RF/IF delay equalization and more linear modulators and demodulators should be possible with further development. Given such improvements it is expected that at least 1000 telephone channels to international circuit standards should be achievable on each radio carrier, using satellite transmitter powers of no more than a few watts. With large blocks of telephone channels correction of Doppler frequency shifts would be necessary, as discussed later.

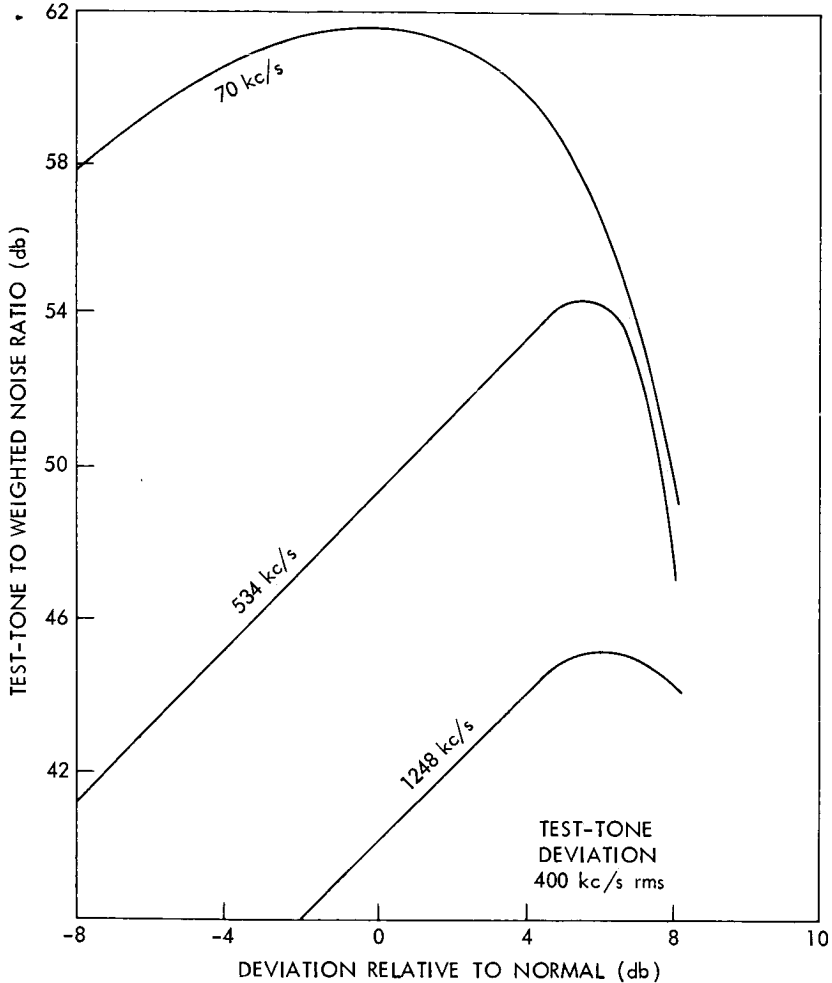


Fig. 13 — 300-Channel white-noise loading test.

#### FACSIMILE TRANSMISSION

A number of tests of facsimile transmission have been made via the Telstar satellites, using individual audio channels in the 12/24 channel groups and standard facsimile transmitters and receivers.

The facsimile transmissions were of two types: a double-sideband amplitude modulated audio tone, e.g. 1300 cps; and a frequency-modulated audio tone, e.g. with 1500 cps for white and 2300 cps for black.

In general, the amplitude-modulated transmissions are more sus-

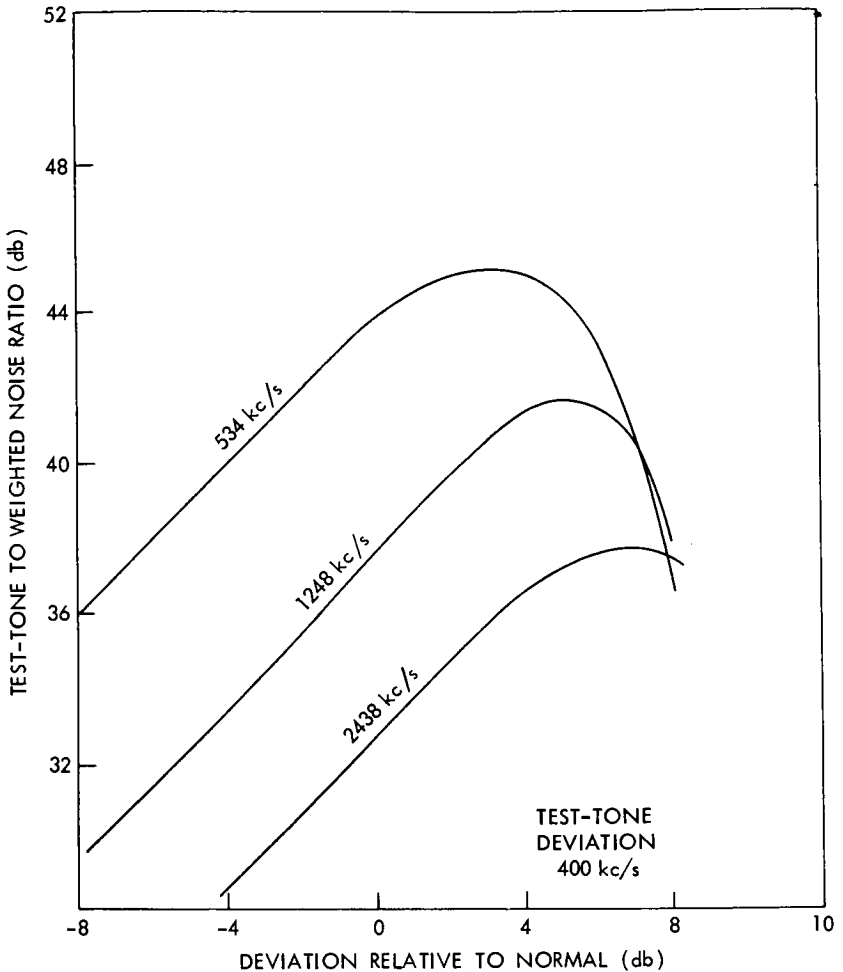


Fig. 14 — 600-Channel white-noise loading test.

ceptible to impairment due to noise or variations of loss in the transmission path, than are the frequency-modulated transmissions, and are thus a more searching form of test.

Fig. 15 shows the CCITT test charts transmitted via Satellite—the upper chart with frequency modulation and the lower chart with amplitude modulation.

The principal defect likely to occur in facsimile transmission via a satellite link, unless special means are taken to prevent it, is 'skew' of the received picture due to the gradually changing transmission

delay as the path length via the satellite changes. For typical Telstar orbits, which are highly elliptical, this might be up to 10 milliseconds in a picture transmission time of 7.5 minutes, i.e. up to 2 parts in  $10^5$  compared with the CCITT recommended limit for skew of 1 part in  $10^5$ .

In an operational satellite system using a medium-altitude circular equatorial orbit the rate of change of transmission delay would be less than for the Telstar orbits, and would be within the CCITT limit for skew.

#### VF TELEGRAPHY AND DATA TRANSMISSION

Many tests of V.F. telegraphy transmission have been made via the Telstar satellites, using individual audio channels in the 12/24 channel groups. Standard frequency-modulation VF telegraph terminal equipments were used with the following characteristics:

120 cps channel spacing and a frequency deviation of  $\pm 30$  cps (CCITT standard); and

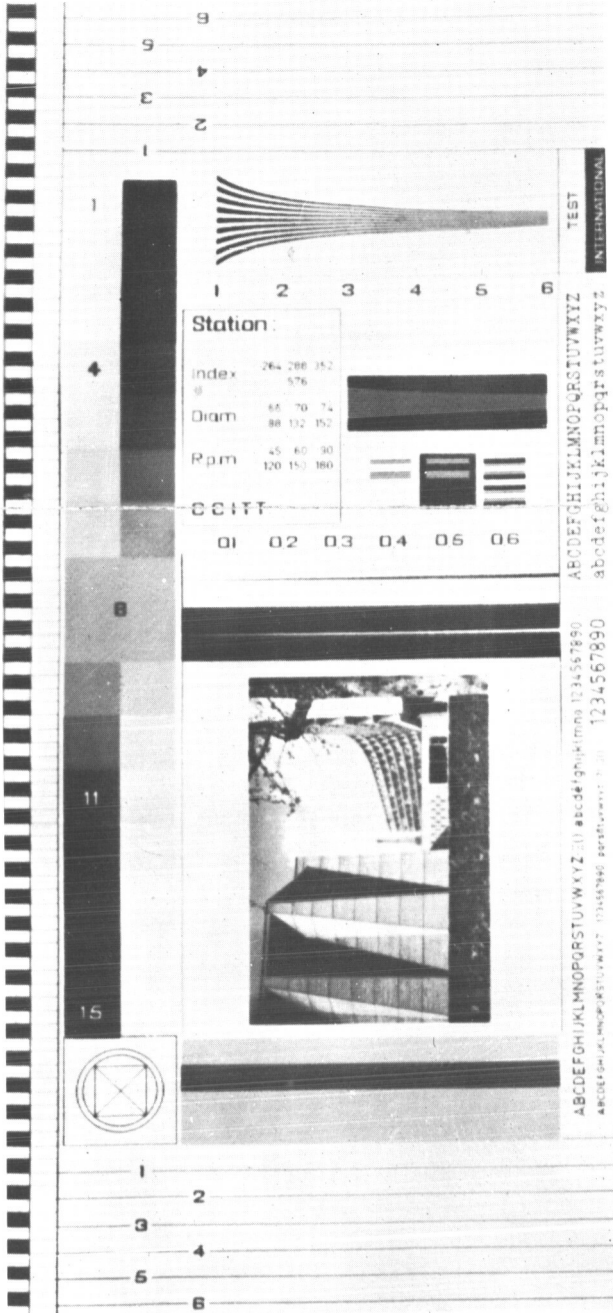
170 cps channel spacing and a frequency deviation of  $\pm 35$  cps (US standard).

The tests were in three main classes:

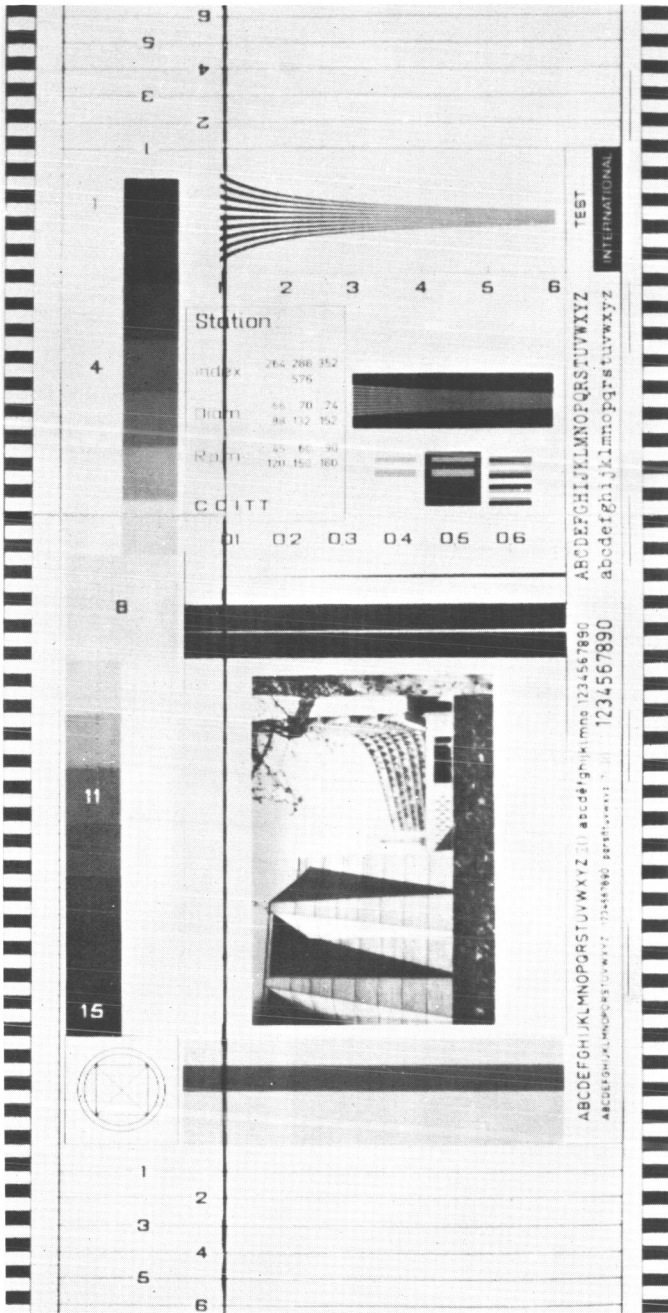
1. *Demonstrations, in co-operation with American telegraph common carriers, between Telex subscribers in London and New York.* Although some difficulties were encountered initially, apparently due to differences between British and American VF telegraph equipments, most of the demonstrations were successful and it was concluded that the satellite link did not contribute any significant adverse factor.

2. *Tests over the loop London-Andover-London, using 50-baud signals and CCITT standard terminal equipment.* The start-stop distortion round the loop was not higher than 16% for a normal pass, and even when the signal-to-noise ratio was lower than would normally be expected, the distortion did not exceed 25%. On a number of passes a synchronous telegraph test set was used to determine the error rate. In a total of 150,000 signal elements transmitted, only one error was counted. A detailed analysis of the distortion during a representative pass (Telstar I Pass No. 787, 4th October, 1962) indicated a mean value varying during the pass from 2.5 to 4%, with a standard deviation of from 3 to 3.7%, as shown in Fig. 16.

The gradual increase in the mean value of the distortion is attributed



(upper chart)



(lower chart)

Fig. 15 — Facsimile transmission.

to a Doppler shift in the order of 1 cps in the mean carrier frequency of the telegraph channel.

It was concluded that the basic error-rate of the satellite link was about the same as that of a long-distance circuit provided by conventional means.

3. *One-way tests between New York and London using US standard terminal equipment.* Up to 18,000 characters (126,000 signal elements) were transmitted without error on typical passes.

For the channels in the 12/24 channel groups used for the various telegraph tests, Doppler frequency shifts were less than 1 or 2 cps, and thus did not present a major source of distortion. However, it was noted, that while the gradually changing transmission time caused no difficulty for start-stop teleprinter systems, an adequate range of automatic speed correction is necessary for isochronous systems. In future operational satellite communication systems using larger blocks of channels with higher baseband frequencies than the 12/24 channel groups used in the tests it will be necessary to correct for Doppler frequency shifts, e.g., by the use of pilot reference frequency carriers, path-delay correction or by other means. Consideration will also need to be given to compensation for the change of transmission delay in switching from satellite-to-satellite, which may be up to 10 or 20 milliseconds, equivalent to one element of a 50-baud teleprinter signal, in some types of satellite system.

In addition to the VF telegraphy tests, a number of low, medium and high-speed data transmission tests have been made via the Telstar satellites by the American Telephone and Telegraph Co. with, it is understood, satisfactory results. Some of the high-speed data transmissions were made from Goonhilly at 875 kilobauds, using quadruple-phase modulation of a 2.6 Mc/s carrier in the baseband of the satellite link. The ability of the link satisfactorily to transmit such high-speed data is due in large measure to the absence of multi-path and echo effects.

During medium-speed data transmissions (1200 bauds), made from London over an audio channel looped at Andover, a total of two million signal elements were transmitted during two Telstar passes with only one error.

#### STANDARD CLOCK COMPARISON

About six weeks after launch, Telstar I was used to compare the precision clocks at Goonhilly and Andover, and since these could be checked against their respective national standards it was possible to

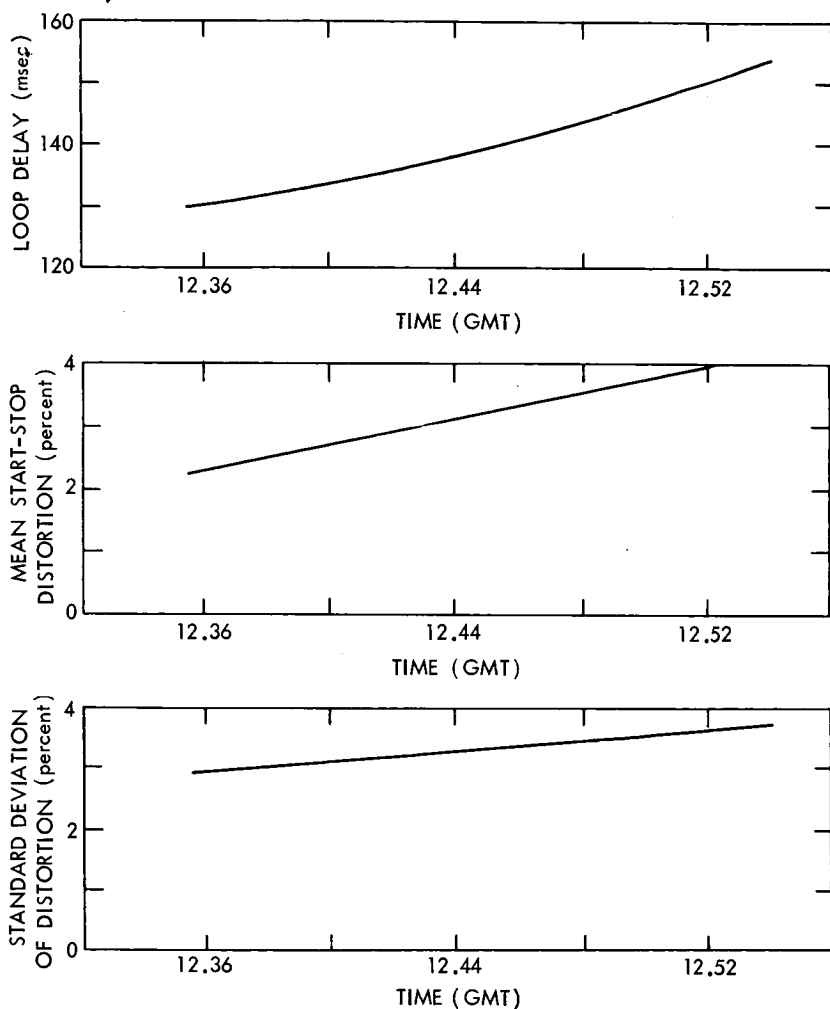


Fig. 16—VF telegraphy test variation of loop delay and distortion during pass. assess the difference between UK and USA standards of time. The Royal Observatory and US Naval Observatory collaborated in these tests, in which the national standards were compared with an accuracy some two orders better than had been achieved by any other means.

A simple diagram of the arrangement is shown in the upper part of Fig. 17, while the lower part indicates the basic principle involved.

The earth station transmitter frequencies were spaced approximately 10 Mc/s, as for a two-way telephony test, and IF bandwidths of about 5 Mc/s were used in the receivers. Each earth-station transmitted

timing signals from its own clock as short pulses producing a carrier deviation of some 2 Mc/s, each station also retransmitted incoming pulses from the other station. The retransmitted pulses were attenuated by 6 db, i.e. were transmitted with a deviation of 1 Mc/s, to enable transmitted and re-transmitted pulses to be identified.

If the clocks are in synchronism, the local pulses are applied simultaneously at Stations A and B. After a short interval of time 't', of the order of 40 milliseconds, each pulse arrives at the other station, and after an almost identical interval each pulse arrives, but with half amplitude, back at the originating station. Apart from very small corrections which may have to be applied for differences in transmission time through equipment, cables, etc. in the two directions, each station should then receive the other's pulses precisely midway between its own sent and looped-back pulses. If, however, the clock at B is ahead of that at A by an amount  $\Delta t$ , then A will receive B's pulses  $\Delta t$  before the mid-position.

During these tests the Controller of Experiments at Goonhilly devised a very simple but effective display and measuring arrangement using a television monitor. By synchronising the line and frame time bases to 10 kc/s and 50 cps local clock pulses, the raster was converted into an open and accurate time scale, the transmitted and received pulses being applied as brightness modulation. This display allowed the difference between the clocks to be read readily and directly from a scale calibrated in microseconds. By using photographic recording of the raster display, an overall accuracy of about a microsecond is achievable in clock comparisons via satellites.

#### CONCLUSIONS

In this broad survey it has only been possible to present representative results from the considerable volume of experimental data that has been accumulated since the launch of Telstar I.

Nevertheless, the results obtained from the tests and demonstrations to date have confirmed the expectation that active communication satellites could provide high-quality stable circuits for television, multi-channel telephony, VF telegraphy, facsimile and data transmission. The very good results obtained with colour television signals a stringent test of any transmission system—and in the tests with 600 simulated telephone channels, are particularly note-worthy. With further development it is considered that it will be possible to transmit at least a thousand telephone channels, of international circuit perform-

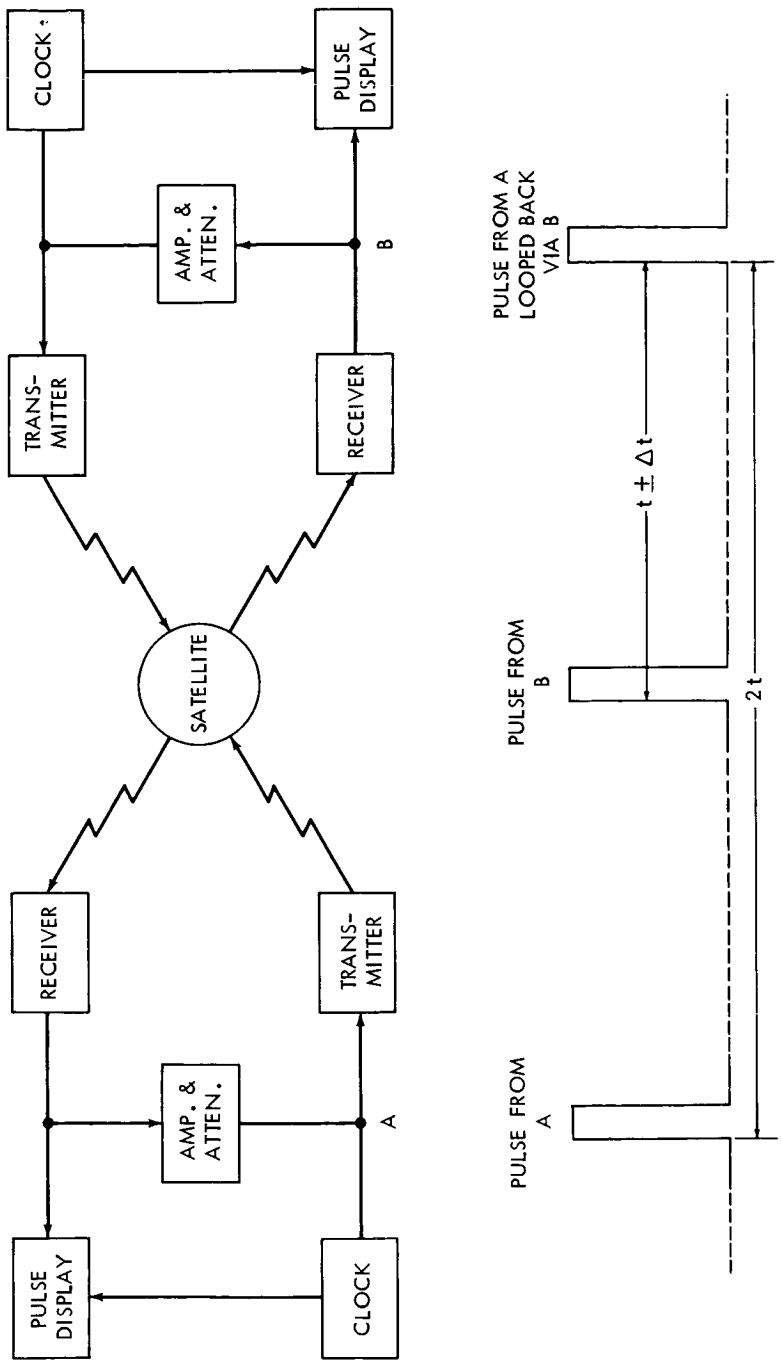


Fig. 17 — Precision clock comparison.

ance standards, on each radio carrier; communication satellites with twice or three times this capacity can be envisaged.

The propagation results obtained at Goonhilly have been particularly interesting since they have revealed the possibility of reliable operation down to elevation angles of only a few degrees. This conclusion has a marked bearing on the coverage provided by a communication satellite and the numbers of satellites required to provide world-wide coverage. It is also of interest that at no time has interference (e.g. from radio-relay systems sharing the same frequency band or from other man-made sources) been detected on the satellite link.

The practicability of tracking satellites, to within some ten minutes of arc, from orbital data predicted up to a fortnight in advance, with automatic fine correction to within a minute or two of arc, has been established.

Standard clock comparisons across the Atlantic have been made with an accuracy of about a microsecond, some two orders better than with other means of comparison.

Finally, it is believed that the results obtained at Goonhilly and the other earth stations participating in the NASA co-operative programme of communication satellite tests will be of considerable value for the design of future operational systems.

#### ACKNOWLEDGMENTS

The authors would like to thank their colleagues in the Post Office Engineering Department who contributed to the tests and demonstrations described in this lecture, and in particular the staff of the Telegraph Branch who provided information on the VF telegraphy and facsimile tests. Their thanks are due to the BBC and ITA for their help in the television demonstrations, the staff of the cooperating earth stations at Andover and Nutley, and to NASA and members of the Ground Station Committee for their help in planning many of the tests. They also wish to acknowledge the co-operation of the Royal Observatory and the US Naval Observatory in the clock comparison tests, and that of the American Telephone & Telegraph Co. and other US common-carriers in telephony, VF telegraphy and television transmission tests.

The permission of the Engineer-in-Chief, General Post Office, to make use of information contained in the lecture and the permission of the Institute of Electrical Engineers to reproduce it is gratefully acknowledged.

**TELSTAR II**

N67 12320

# Communications and Radiation Experiments with Telstar II

BELL TELEPHONE LABORATORIES

## INTRODUCTION

Telstar II has been used for numerous tests and demonstrations since it was launched on May 7, 1963. A monthly tabulation of the passes worked for either technical tests or demonstrations is presented in Table I. Many stations have participated with Andover in the tests and demonstrations worked. These stations are listed below:

COMHIL	Goonhilly Downs, England
COMBOD	Pleumeur-Bodou, France
COMTEL	Fucino, Italy
COMITT	Nutley, New Jersey
COMCAN	Cape Kennedy, Florida
COMDEL	Holmdel, New Jersey
COMDOD	Camp Roberts, Salinas
COMDOD	Fort Dix, New Jersey
COMIBA	Tokyo, Japan

This report presents the results of tests made on Telstar II shortly after launch in May 1963, the results of similar tests made during March and April 1964 and a comparison of the results of the two groups of tests. Evaluations of the results presented indicate no significant unpredicted change in the performance of Telstar II during the eleven months covered by this report. Although no data on Telstar I is included in this publication, comparison of the data obtained on Telstar II with previously published data on Telstar I indicate no discernible difference.

A preliminary report on the radiation experiment for which Telstar II is equipped is also included. The data reported in this area generally agrees with theoretical expectations quite closely.

The final section of this report outlines the differences in implementation between Telstar I and Telstar II. This includes differences in electronics as well as orbit. The differences in electronics are minor and are associated with the 4080 Mc telemetry transmission capability of Telstar II. The orbits are appreciably different, with Telstar II's orbit being much more elliptic.

TABLE I — TABULATION OF TELSTAR II PASSES WORKED

Month		Technical Tests	Demonstrations
May	1963	25	6
June	1963	20	22
July	1963	18	8
August	1963	33	6
September	1963	24	8
October	1963	11	13
November	1963	9	1
December	1963	7	0
January	1964	17	1
February	1964	40	0
March	1964	39	3
April	1964	25	1

This report is divided into five additional sections as indicated below:

Results of tests performed on Telstar II shortly after launch.

Results of recent tests on Telstar II.

Comparison of results reported in the aforementioned sections.

Preliminary results of Telstar II radiation experiment.

Differences in instrumentation of Telstar I and Telstar II.

Detailed descriptions of Telstar, the Andover, Maine ground station and all subsystems of each have been published in previous reports and will not be included as part of this report. A bibliography of these reports is given below.

*Preliminary Report Telstar I — July-September 1962*

This document was prepared by Bell Telephone Laboratories, Incorporated on behalf of American Telephone and Telegraph Company

and transmitted to NASA under cover of a letter from Mr. E. F. O'Neill of the Laboratories to Mr. C. P. Smith of NASA.

*Bell Laboratories Record — April 1963*

This issue of the Record was devoted entirely to the Telstar Project.

*The Bell System Technical Journal — July 1963*

This was a three volume issue, the contents of which were submitted to NASA as a final report on Telstar I.

TELSTAR II — TEST RESULTS OBTAINED SHORTLY AFTER LAUNCH

*Introduction*

This section presents the results of the initial series of communications tests conducted shortly after the launch of the Telstar II satellite on May 7, 1963 (11:54.73 UT). All of the tests were made on an Andover loop, i.e., transmission from Andover to the satellite and back to Andover. A detailed description of the test procedure is given in the Project Telstar Experiment Plan.

The following tests conducted are described below: carrier power, baseband transmission, noise, nonlinearity, and video tests.

*Carrier Power*

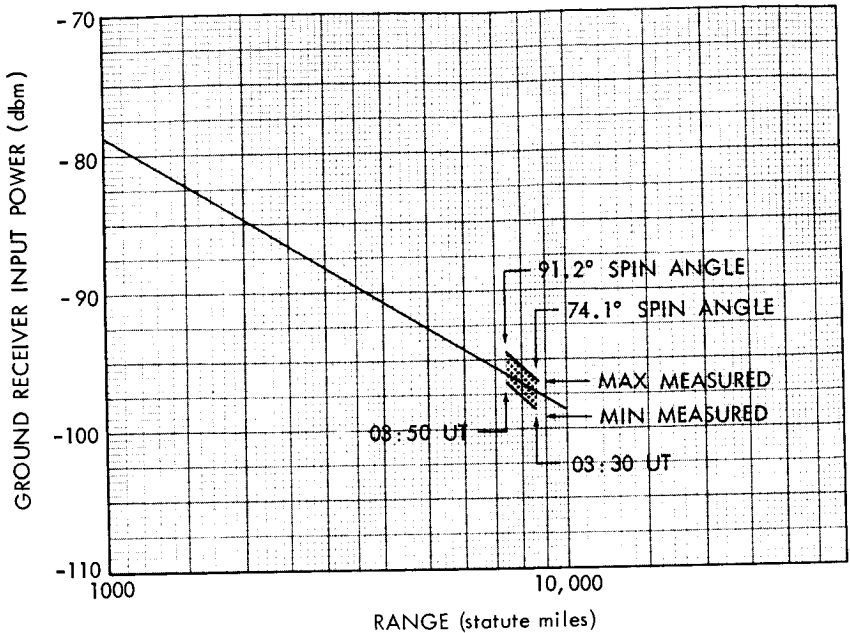
Received Carrier Power

The 4.17 Gc carrier transmitted by the satellite is measured by monitoring the ground radio receiver's AGC voltage. Variations of this voltage are recorded on paper tape during each operating pass. The calibration is referenced to the maser input.

The signal transmitted to the satellite is at 6.39 Gc. The satellite monitors the received carrier power in a manner analogous to that used at the ground receiver, i.e., by monitoring the AGC control voltage of the satellite's IF amplifier. In this case, however, instead of a continuous recording, the information is sampled and returned to earth once per minute via the telemetry system.

Received Carrier Power vs. Range

The 4.17 Gc received carrier power was measured at Andover during pass 11 on May 9, 1963 from 03:30 to 03:50 UT. The measured values are plotted in Figure 1 with spin angle as a parameter. The expected value of the received carrier power for a 90° spin angle is plotted as



RADIATED POWER	+33.0 dbm
SATELLITE ANTENNA GAIN AT 90° SPIN ANGLE	0 db
EARTH STATION ANTENNA GAIN	+57.8 db
MISC GRD STATION LOSSES	0.4 db

Fig. 1 — Ground receiver input power, 4170 Mc — Telstar II, pass 11.

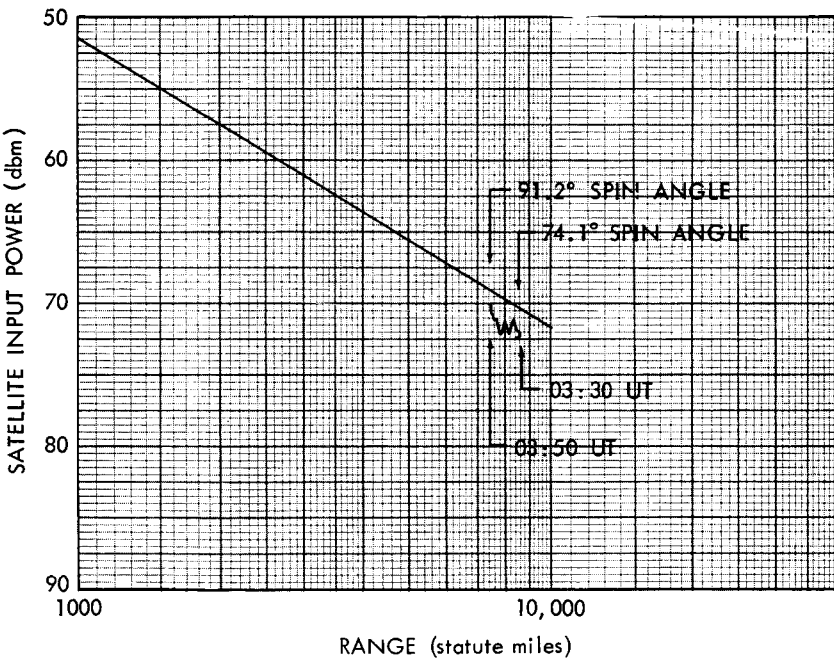
a straight line. The constants used in the calculations are given in the figure. The figure shows the spin modulation of the carrier, caused by ripples in the antenna pattern at constant latitude, is in the order of  $\pm 1.0$  db. The difference between the measured and calculated values can be accounted for by the variation in the spin angle loss to within an average of 0.7 db during the pass.

The 6.39 Gc received carrier power at the satellite was also measured during pass 11 on May 9, 1963 from 03:30 to 03:50 UT. The measured values are plotted in Figure 2 with spin angle as a parameter. Included in Figure 2 is a plot of received carrier power for a 90° spin angle and

the constants used in the calculations. Fluctuations about the average of  $\pm 1$  db were measured. This is to be expected since the values were measured once per minute and the peak-to-peak ripples in the antenna patterns at constant latitude are on the order of 2.5 db. When spin angle variations are considered, the difference between the measured and calculated values averaged about 1 db during the pass.

*Baseband Transmission*

Baseband transmission characteristics were measured on the base-



TRANSMITTER POWER	63.0 dbm
EARTH STATION ANTENNA GAIN	61.5 db
MISC GRD STATION LOSSES	1.4 db
SATELLITE CABLE LOSS	2.0 db
SATELLITE ANTENNA GAIN	0 db

Fig. 2 — Satellite input power, 6390 Mc — Telstar II, pass 11.

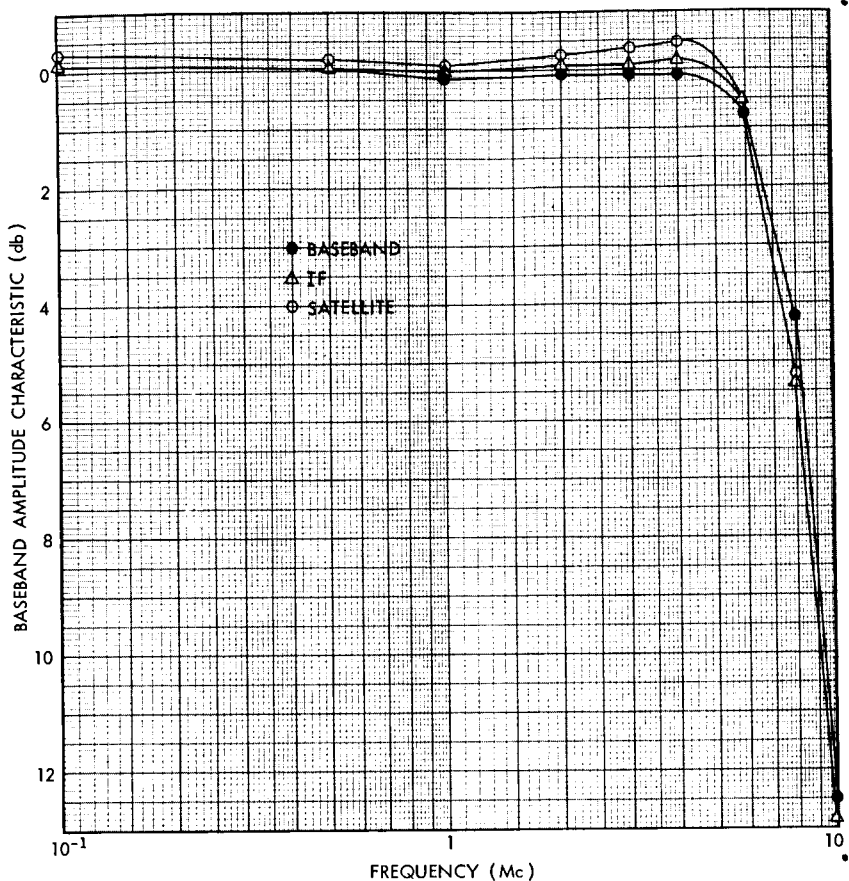


Fig. 3—Baseband amplitude characteristics, standard FM receiver—Telstar II, pass 11.

band, IF and satellite loops when using the standard FM receiver and its associated circuitry without clampers, diplexers or band limiting filters. Measurements made on pass 11 directly after launch on May 9, 1963 are plotted in Figure 3. The FM deviator-Standard Receiver combination have a negligible effect on the transmission shape, which is set by the video circuits of the baseband loop. The difference between the transmission shapes measured on the IF and satellite loops is shown in Figure 3 and represents the combined effect of the RF and satellite equipment. No significant change in shape from the IF to the satellite loops is indicated.

## \*Noise

## Baseband Noise Spectrum

Measurements of baseband noise were made on the down path video circuits and the satellite system using the standard FM receiver in the circuit without clampers, diplexers or band limiting filters. Measurements made from the test area on pass 11 directly after launch on May 9, 1963 are plotted in Figure 4. Curve 2 represents the noise measured on the down path video circuits. Curve 1 represents the noise measured on the satellite at 03:46 UT on May 9, 1963 during pass 11. Curve 1 is representative of the noise spectrum measured at 1 minute intervals during the pass (a total of 17 separate measurements of the baseband noise spectrum were made in the time available). At the time of measurement the received carrier powers were  $-71.0$  and  $-96.0 \pm 1$  dbm at the satellite and ground receiver, re-

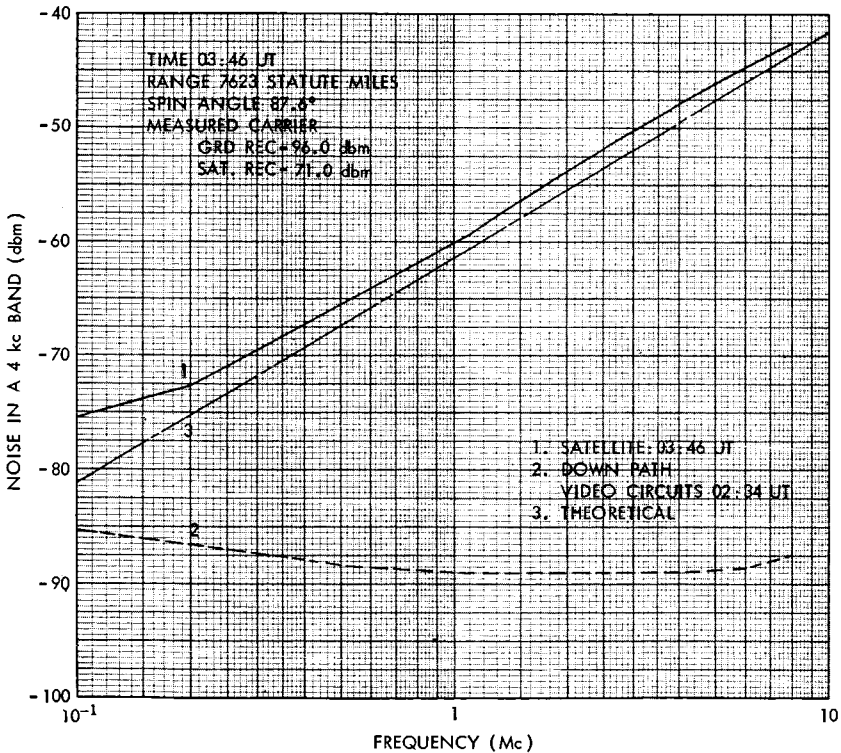


Fig. 4 — Baseband noise spectrum, standard FM receiver — Telstar II, pass 11.

spectively. The corresponding calculated values based on the constants\* of the system given in Figures 1 and 2 and including a correction to account for the  $87.6^\circ$  spin angle loss were  $-69.6$  and  $-95.7 \pm 1$  dbm, respectively. Using the calculated values of received carrier powers, a ground receiver noise temperature of  $39^\circ$  Kelvin and assuming a 13 db satellite noise figure, the computed value of the noise in a 4 kc band centered at 1 Mc was  $-61.4$  dbm at the test area. The measured value of the noise was  $-60.1$  dbm at the test point. From FM theory the noise should increase at 20 db/decade. Curve 3 in Figure 4 (the center line) represents the expected value of the noise as a function of frequency. The difference between Curves 1 and 3 can be accounted for by measurement error. The spectrum is essentially triangular down to about 500 kc where the baseband video circuits and low frequency fill begin to be noticeable.

#### Telephone Noise

The thermal noise in any channel of a 600 channel telephone system can be determined from the baseband noise spectrum. In the calculations made, the constants in Table II were assumed.

TABLE II — TELEPHONE NOISE MEASUREMENT CONSTANTS

Average Talker Power at 0 TL	-11 dbm
Activity Factor for Multichannel Telephony	0.25
Average Power in a 600 Channel Load at 0 TL	+10.8 dbm
Peak Factor for a 600 Channel Load	12.0 db
Full Load Test Tone at 0 TL	+22.8 dbm
Full Load Test Tone at Test Area	+5.2 dbm
Transmission Level in Test Area	-17.6 db TL
0 dbm of White Noise in a 3 kc Band	88 dbrn C'

The noise measured at the area is 17.6 db lower than would be measured at a 0 TL point. Further, since the baseband noise is measured in a 4 kc band, it must be reduced by 1.2 db to get the equivalent noise in a 3 kc telephone channel. Making the above corrections and converting from dbm to dbrn "C" message weighted, the noise expected in any channel may be determined from the baseband noise spectrum. This was done for nine different channels using the CCITT frequency allocation for a 600 channel system and for the conditions that prevailed during Telstar II, pass 11 shown by Curve 1 in Figure 4. The results are given in Table III.

TABLE III — TELEPHONE NOISE MEASUREMENT RESULTS

Channel Number	Group Number	Super Group Number	Frequency (kc)	Noise (dbm "C" Message Weight)
12	5	2	548-552	39.1
1	1	3	800-804	42.3
1	1	4	1048-1052	44.6
1	1	5	1296-1300	46.6
1	1	6	1544-1548	48.1
1	1	7	1792-1796	49.5
1	1	8	2040-2044	50.7
1	1	9	2288-2292	51.7
1	1	10	2536-2540	52.7

Television Noise

The weighted peak-to-peak signal to rms noise was measured on Telstar II, pass 11 directly after launch on May 9, 1963 from 03:39:40 UT to 03:56:00 UT. The results of the measurements are plotted in Figure 5. At that time the ground receiver and satellite input powers were recorded and are shown in Figures 1 and 2 respectively; the ground receiver noise temperature measured was 39° Kelvin. The calculated values of received carrier powers are given in Figure 70

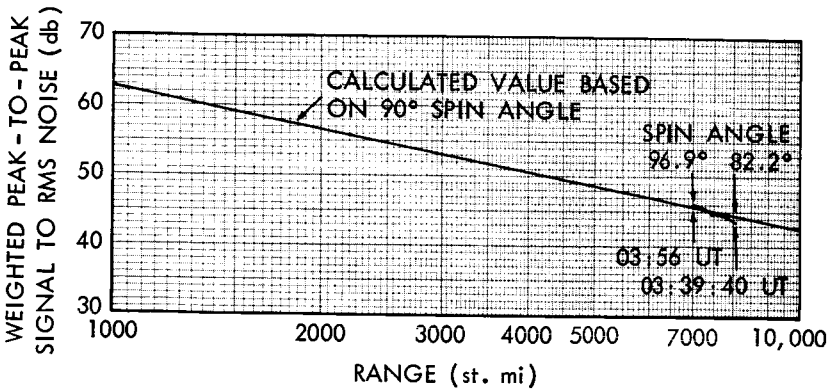


Fig. 5 — Weighted television signal-to-noise ratio — Telstar II, pass 11.

(page 2318). Using the calculated values of received carrier powers, the applicable measured receiver noise temperature of 39° Kelvin and assuming a satellite noise figure of 13 db the unweighted peak-to-peak signal to rms noise can be calculated from the following expression:

$$\frac{S_{p-p}}{N_{\text{rms}}} = \frac{3f_{p-p}^2}{\left(\frac{\phi_V}{S_V} + \frac{\phi_G}{S_G}\right) f_m^3},$$

where

- $f_{p-p}$  = peak-to-peak frequency deviation, cps,
- $\phi_V$  = satellite receiver noise density, watts/cps,
- $\phi_G$  = ground receiver noise density, watts/cps,
- $S_V$  = satellite receiver power in watts,
- $S_G$  = ground received power in watts,
- $f_m$  = top baseband frequency, cps.

Under a 10.6 db weighting factor, the weighted peak-to-peak signal to rms noise was determined and is compared to the measured values in Table IV. As can be seen from the table, the measured and calculated values are in good agreement when spin angle losses are included.

TABLE IV — WEIGHTED PEAK-TO-PEAK SIGNAL TO RMS NOISE

Time	Measured Value	Calculated
03:39:00	43.9	44.2
03:46:00	45.0	44.9
03:49:00	45.2	45.2
03:53:00	46.0	45.6
03:56:00	46.3	45.8

### Nonlinearity

#### Envelope Delay Distortion

The envelope delay distortion discussed in this section is generated in the IF and RF circuitry of the system causing cross modulation in FM systems. Envelope delay distortion was measured by the two frequency sweep method described in detail on page 2288.

Each of the RF and IF portions of the system contributes to the

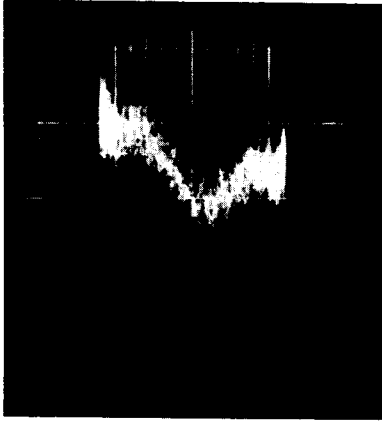


Fig. 6—Envelope delay distortion, satellite loop, FMFB receiver—Telstar II, pass 5, May 8, 1963. Vertical sensitivity =  $5.0 \eta$  sec/small div; horizontal sensitivity = 2.0 Mc/small div.

over-all envelope delay distortion. Delay equalizers with the inverse characteristic of the IF envelope delay distortion have been provided for the IF loop. Envelope delay distortion tests have been made indicating a negligible contribution for this portion of the system.

Figure 6 shows the envelope delay distortion measured on a satellite loop during pass 5 directly after launch on May 8, 1963 at 05:42 UT. The EDD measured can easily be equalized (see page 2287).

#### Differential Phase and Gain

Differential phase and gain measurements were made on Telstar II, pass 17 shortly after launch at 02:15 and 02:18 UT on May 10, 1964. Video duplexers, clammers and bandlimiting filters were not included in the circuit. The standard FM receiver was used. The 3:58 Mc signal was set at 14 db below the low frequency 15.75 kc signal which was adjusted to a 1 volt peak-to-peak amplitude at the test area corresponding to a 14 Mc peak-to-peak frequency deviation.

Figures 7 and 8 show the differential phase and gain measured on the baseband loop. Figures 9 and 10 show the differential phase and gain measured on the satellite loop. It should be noted that the system was not delay equalized at the time of measurement. Delay equalization would improve the differential phase shown in Figure 9.

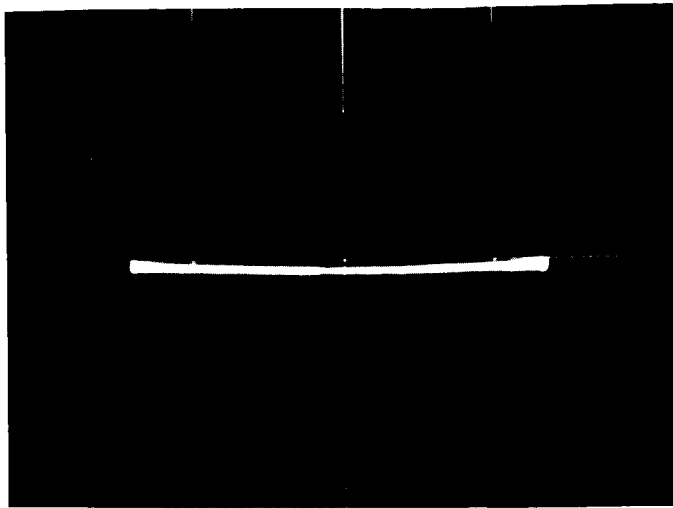


Fig. 7—Differential phase, baseband loop, standard FM receiver, Telstar II. Horizontal sweep: 1 div = 1 Mc; vertical sweep: 1 div = 1°.

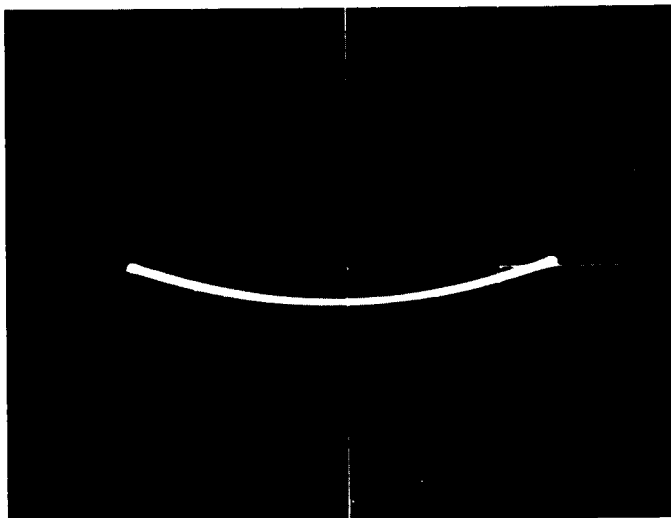


Fig. 8—Differential gain, baseband loop, standard FM receiver—Telstar II, Horizontal sweep: 1 div = 1 Mc; vertical sweep: 0.2 db.

### *Video Tests*

The first video transmissions over Telstar II are shown in Figures 11, 12, and 13. Figure 11, a monoscope test pattern, is the first signal

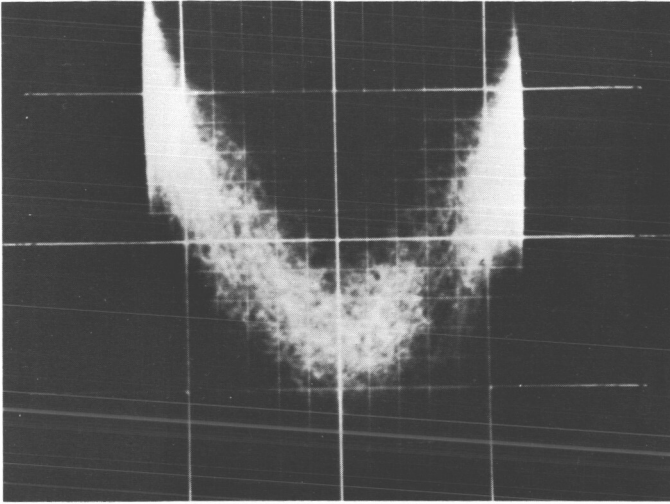


Fig. 9—Differential phase, satellite loop, standard FM receiver—Telstar II, pass 17, May 10, 1963. Horizontal sweep: 1 div = 1 Mc; vertical sweep: 1 div =  $2^\circ$ .

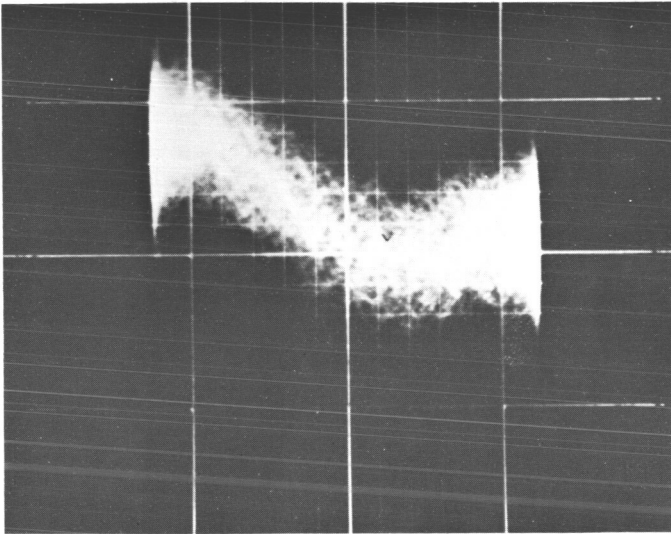


Fig. 10—Differential gain, satellite loop, standard FM receiver—Telstar II, pass 17, May 10, 1963. Horizontal sweep: 1 div = 1 Mc; vertical sweep: 1 div = 0.4 db.

received from the satellite on pass 4, May 7, 1963. Figures 12 and 13 are subsequent video tape transmissions on passes 4 and 5, respectively.

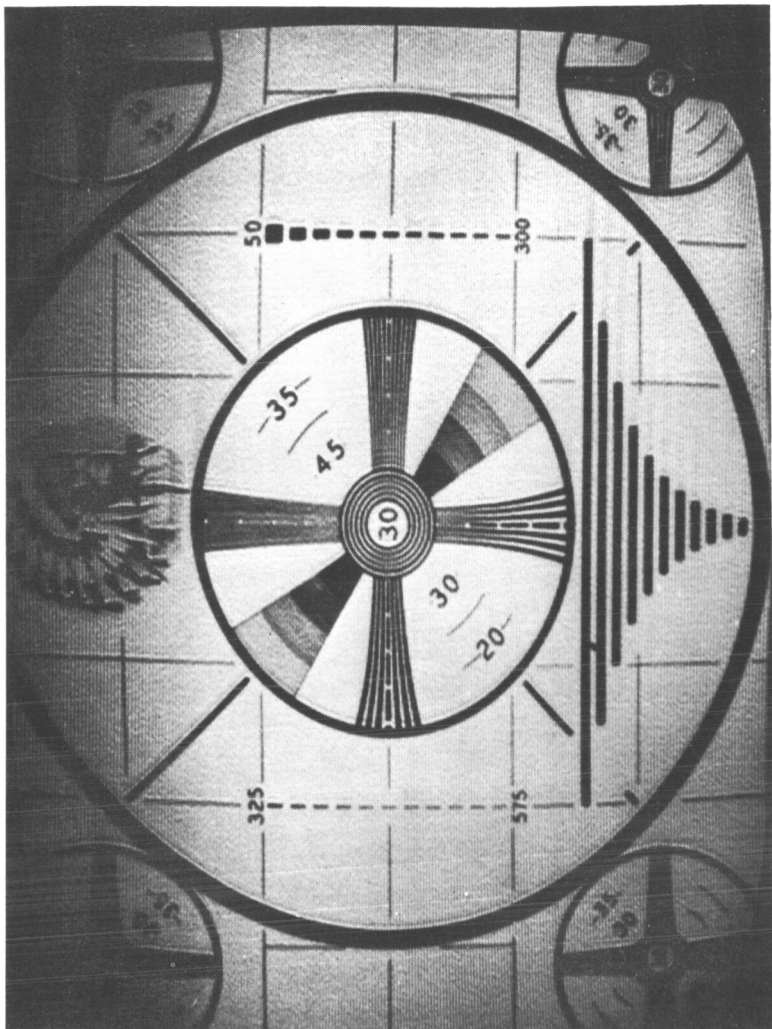


Fig. 11 — Monoscope video transmission — Andover to Telstar II to Andover — Telstar II, pass 4, May 7, 1963.

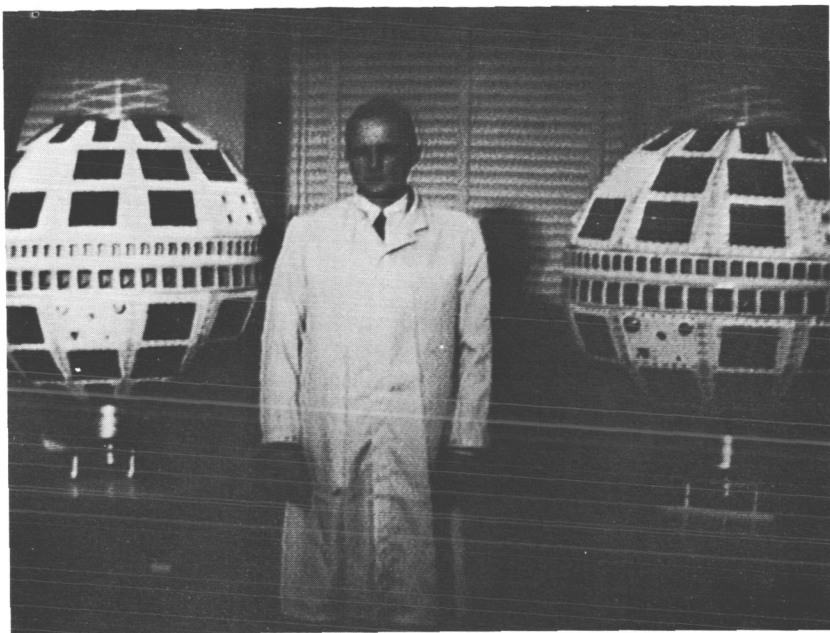


Fig. 12 — Video transmission, tape — Andover to Telstar II to Andover — Telstar II, pass 4, May 7, 1963.

The circuit used for these two passes included video-audio duplexers, 3.5 Mc linear phase filters and the FM feedback receiver.

A direct evaluation of the systems performance can be made by comparing Figure 14 with 11. Figure 14 is the signal as produced by the monoscope generator. Figure 11 is the same signal received a few minutes later from the satellite on pass 4. Both the effects of noise and band limitation are evident and this was to be expected in view of the range and bandlimiting effect of the video-audio diplexer and 3.5 Mc linear phase filter.

#### TELSTAR II—TEST RESULTS PERFORMED RECENTLY

##### *Introduction*

This section presents the results of the recent series of communications tests conducted with the Telstar II satellite. All the tests were made on an Andover loop, i.e., transmission from Andover to the satellite and back to Andover. The data presented in this section is in good agreement with values obtained experimentally.

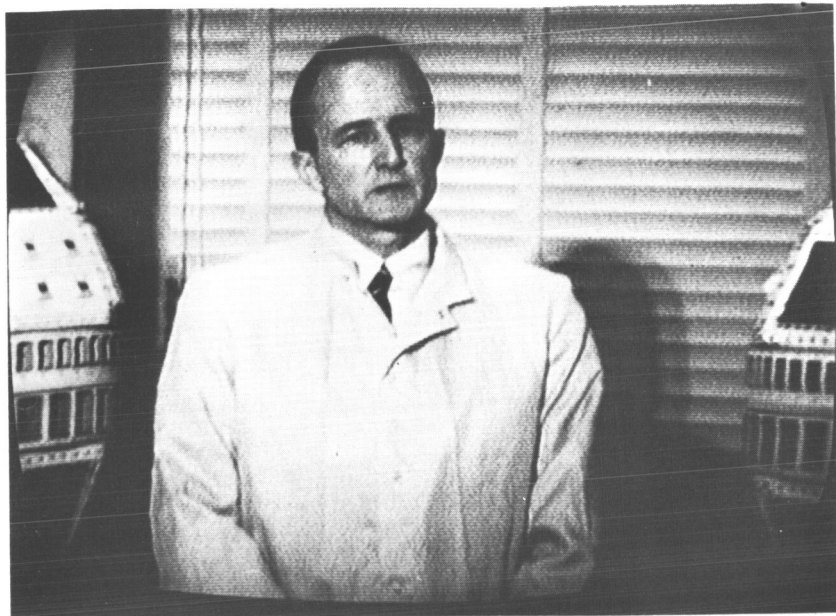


Fig. 13— Video transmission, tape— Andover to Telstar II to Andover— Telstar II, pass 5, May 7, 1963.

### *Carrier Power*

#### Received Carrier Power

In view of the importance of received carrier power measurements in the analysis of satellite performance and because of the many variables involved, many measurements were made during the testing period.

The received carrier power in the communications channel was measured continuously during all tests and demonstrations by monitoring the voltage of the AGC circuit of the ground receiver. The received carrier power at the satellite was measured at 1 minute intervals and relayed to the ground via the telemetry system.

Measurements of the ground received carrier power are accurate to within  $\pm 1.0$  db. Measurements of the satellite input power are accurate to within  $\pm 1.5$  db. When range, spin angle and measurement inaccuracies are considered, the measured values agree with the predicted values.

#### Received Carrier Power vs. Range

A plot of the 4.17 Gc received carrier power versus range measured

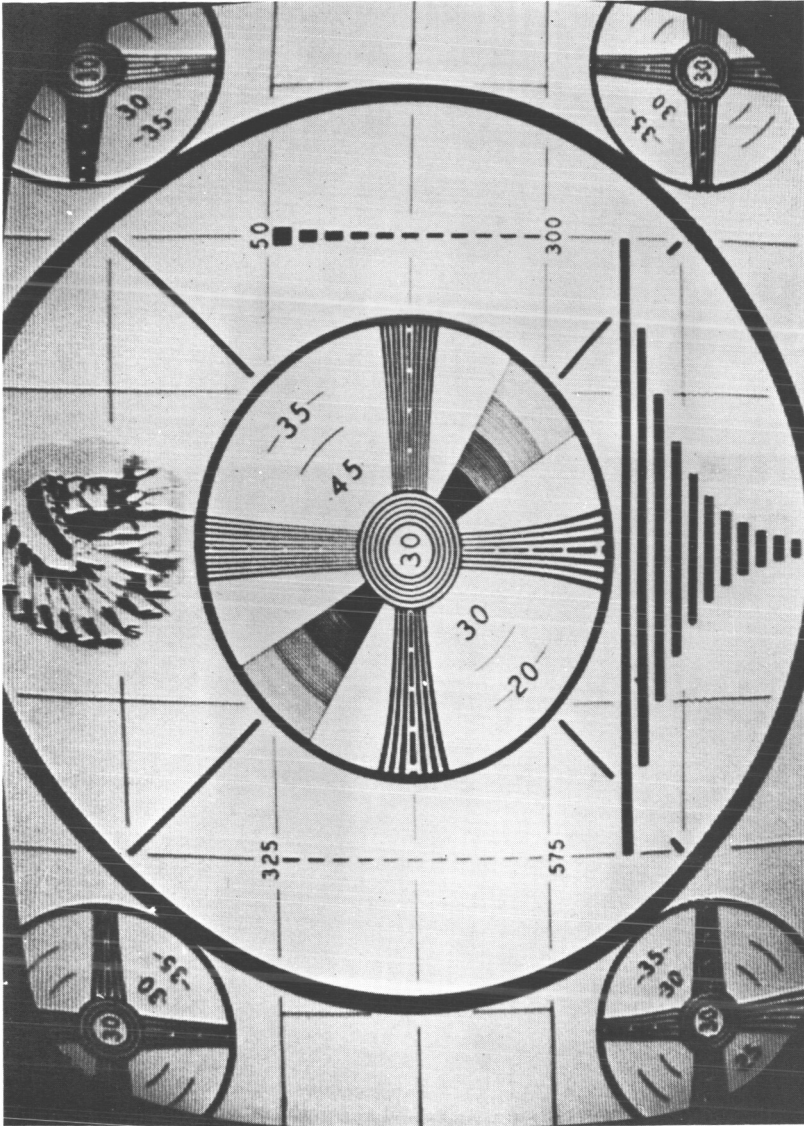
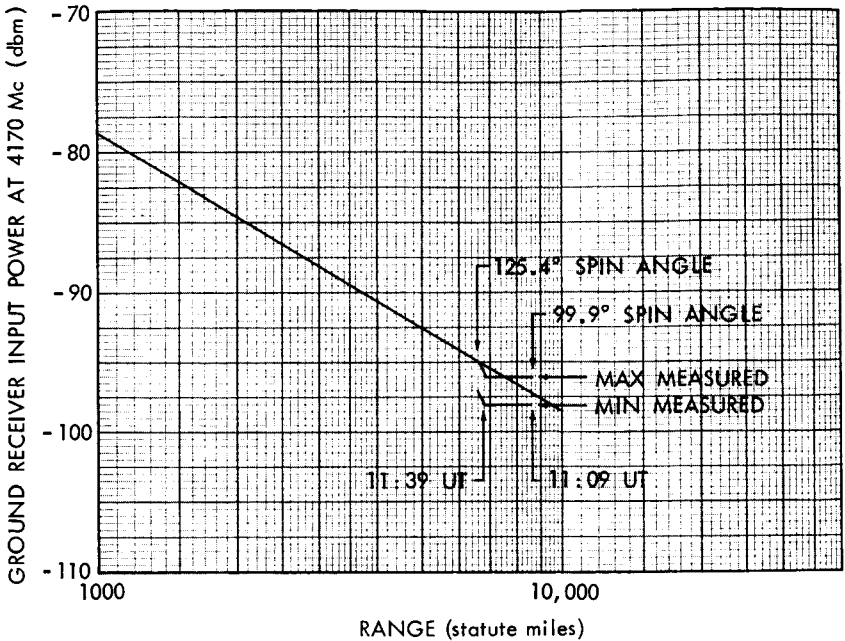


Fig. 14 — Monoscope video transmission — Andover to Telstar II to Andover — Telstar II, pass 5, May 7, 1963.



RADIATED POWER	+ 33 dbm
SATELLITE ANTENNA GAIN AT 90° SPIN ANGLE	0 db
EARTH STATION ANTENNA GAIN	57.8 db
MISC GRD STATION LOSSES	0.4 db

Fig. 15 — Ground receiver input power, 4170 Mc — Telstar II, pass 1989.

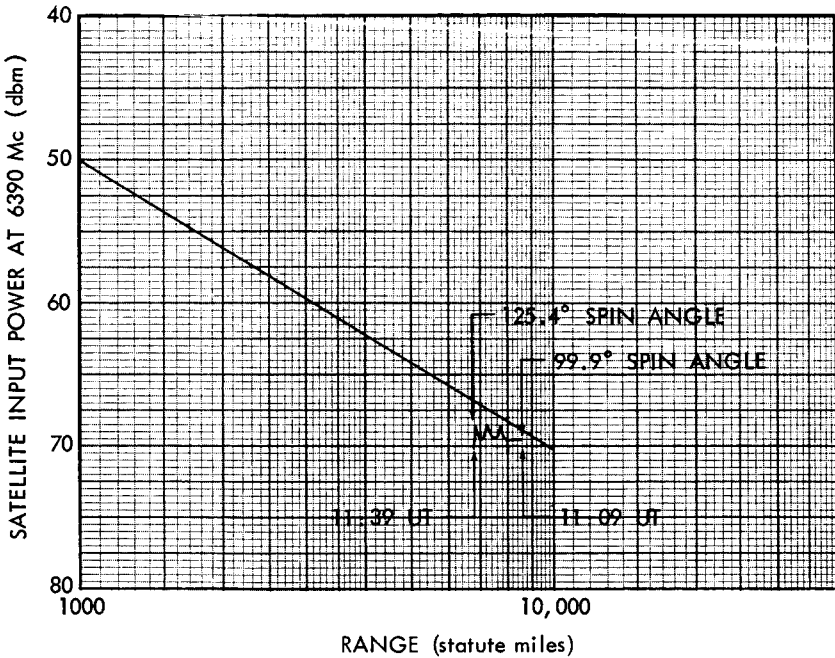
at Andover during pass 1989 is given in Figure 15. The expected value of received carrier power at a 90° spin angle is plotted in the figure as a straight line. The system constants used in the calculations are given in Table V.

As illustrated in Figure 15 the spin modulation of the carrier is in the order of  $\pm 1.0$  db. The difference between the measured and calculated values can be accounted for by the variation of the spin angle to within an average of 0.5 db during the pass.

Figure 16 is a plot of the satellite received carrier power versus range for pass 1989. The expected value of the 6.39 Gc received carrier power at the satellite, based on the assumptions given in Table 5, is

TABLE V — SYSTEM CONSTANTS

System Constants	Frequency (Mc)	
	6390	4170
Transmitter Power	64.3 dbm	34.7 dbm
Earth Station Antenna Gain	61.5 dbm	57.8 db
Misc. Ground Station Losses	1.4 db	0.4 db
Satellite Antenna Gain at 90° Spin Angle	0.0 db	0.0 db
Satellite Cable Loss	2.0 db	1.7 db



TRANSMITTER POWER	+64.3 dbm
EARTH STATION ANTENNA GAIN	61.5 db
MISC GRD STATION LOSSES	1.4 db
SATELLITE CABLE LOSS	2.0 db
SATELLITE ANTENNA GAIN AT 90° SPIN ANGLE	0 db

Fig. 16 — Satellite input power, 6390 Mc — Telstar II, pass 1989.

shown as a straight line for a spin angle of  $90^\circ$ . Fluctuations of about the average of  $\pm 1.0$  db were measured. When spin angle variations are considered, the difference between the measured and calculated values averaged about 0.5 db during the pass.

### Baseband Transmission

Baseband transmission characteristics were measured on the baseband, IF and satellite loops when using the standard FM receiver and its associated circuitry without clampers, diplexers, or band limiting filters. Typical of measurements made recently were those made on Telstar II, Pass 2249 on April 23, 1964 (Figure 17). No significant

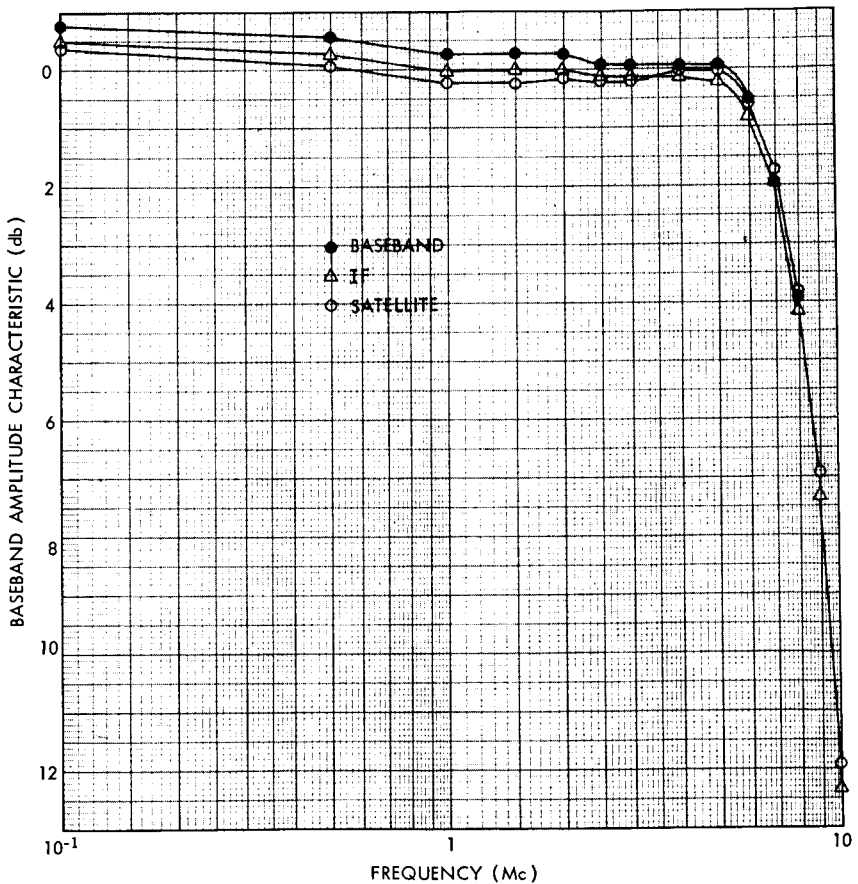


Fig. 17 — Baseband amplitude characteristic, standard FM receiver — Telstar II, pass 2249.

change in shape was measured when the FM deviator-Standard receiver was added to the baseband loop. Figure 17 also shows that a comparison of the IF and satellite loops show no significant change was measured when the RF and satellite equipment was added to the loop. In all cases the loops are essentially flat out to 6 Mc to within 1 db.

Since the IF characteristic of the FM feedback receiver is controlling when it is used with the satellite loop and since this information has been reported previously in the Bell System Technical Journal this information will not be presented.

## Noise

### Baseband Noise Spectrum

In view of the many parameters affecting the systems baseband noise spectrum (e.g., satellite slant range, spin angle, satellite input power, ground receiver input power, noise temperature) repeated measurements were made to insure valid data. Typical measurements made from the test area are shown in Figure 18. The measurements were made using the standard FM receiver in the circuit without clampers, diplexers or bandlimiting filters. Curve 1 represents the noise measured on the satellite loop. Curves 2 and 3 represent the noise measured on the IF and baseband loops, respectively. All curves have been corrected for the transmission characteristics measured. Curves 2 and 3 indicate a negligible noise contribution to the satellite loop.

Curve 1 is a plot of the noise measured on Pass 1989 at 11:31:00 UT on March 13, 1964. It is representative of the noise spectrum measured at 1 minute intervals during the pass. (A total of 24 separate measurements of the baseband spectrum were made in the time available.) At that time the ground receiver and satellite input powers measured  $-97 \pm 1$  and  $-69.5$  dbm, respectively. The corresponding calculated values based on the constants of the system noted previously in Table 5 and including a correction to account for the loss due to a spin angle of  $118^\circ$  were  $-97.6 \pm 1$  and  $-69.3$  dbm, respectively. Using the calculated values of receiver carrier powers, a ground receiver noise temperature of  $37^\circ$  Kelvin and assuming a 13 db satellite noise figure, the computed value of the noise in a 4 kc band centered at 1 Mc was  $-60.2$  dbm at the test area. The measured value of the noise was  $-59.9$  dbm at the test point. From FM theory the noise should increase at 20 db/decade. Curve 4 in Figure 18 (the dashed line) represents the

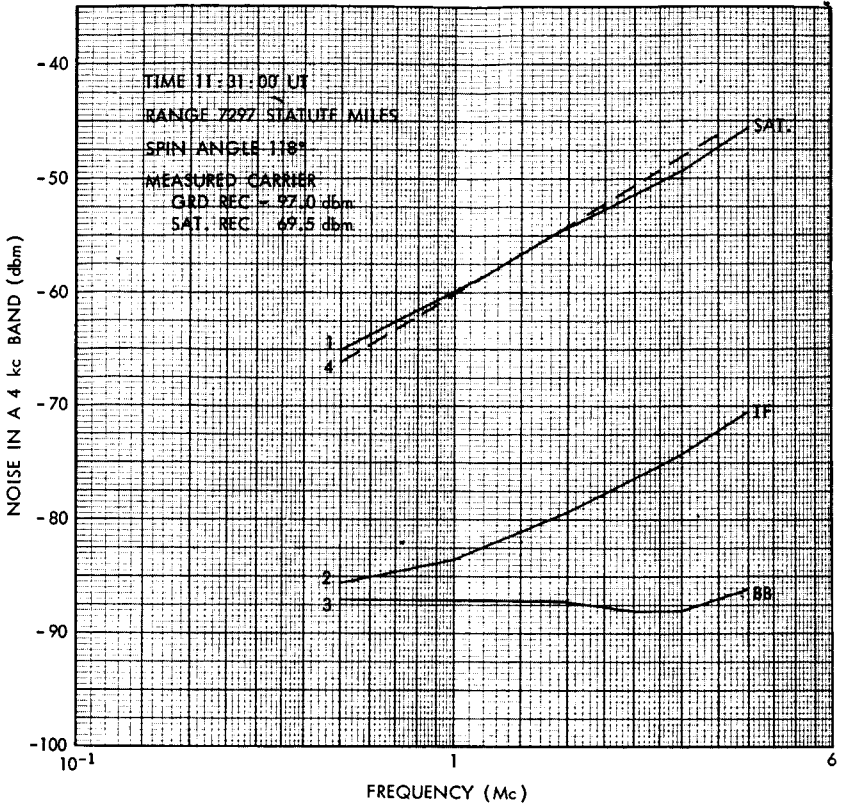


Fig. 18 — Baseband noise spectrum, standard FM receiver — Telstar II, pass 1989.

expected value of the noise as a function of frequency. The difference between the curves 1 and 4 can be accounted for by measurement error. The spectrum over the frequencies measured is essentially triangular.

#### Telephone Noise

The thermal noise in any channel of a 600 channel telephone system can be determined from the baseband noise spectrum. In the calculations made, the constants in Table VI were assumed.

Since the noise was measured with the 37B Transmission Measuring Set having a 4 kc bandwidth, the level must be reduced by 1.2 db to obtain the equivalent noise in a 3 kc band (the assumed bandwidth of an actual telephone channel). Further, since the noise is measured

TABLE VI — TELEPHONE NOISE MEASUREMENT CONSTANTS

Average Talker Power at 0 TL	-11 dbm
Activity Factor for Multichannel Telephony	0.25
Average Power in a 600 Channel Load at 0 TL	+10.8 dbm
Peak Factor for a 600 Channel Load	12.0 db
Full Load Test Tone at 0 TL	+22.8 dbm
Full Load Test Tone at Test Area	+5.2 dbm
Transmission Level in Test Area	-17.6 db TL
0 dbm of White Noise in a 3 kc Band	88 dbrn C

at the test area, a -17.6 TL point, the noise must be increased by 17.6 db to obtain the noise that would have been measured at 0 TL. Making the above corrections and converting from dbm to dbrn "C" message weighted, the thermal noise expected in any channel may be determined from the baseband noise spectrum. This was done for nine different channels using the CCITT frequency allocation for a 600 channel system and for the conditions that prevailed during Telstar II Pass 1989 as noted above and shown by Curve 1. The results are given in Table VII.

TABLE VII — TELEPHONE NOISE MEASUREMENT RESULTS

Channel Number	Group Number	Super Group Number	Frequency (kc)	Noise (dbrn "C" Message Weight)
12	5	2	548-552	40
1	1	3	800-804	42.8
1	1	4	1048-1052	44.8
1	1	5	1296-1300	46.5
1	1	6	1544-1548	47.9
1	1	7	1792-1796	49.2
1	1	8	2040-2044	50.1
1	1	9	2288-2292	51.2
1	1	10	2536-2540	51.8

### Television Noise

The noise in the video channel was determined from the baseband noise spectrum by integrating the spectrum plotted as Curve 1 of Figure 18. The unweighted peak-to-peak to rms noise calculated was 34.3 db. The applicable curve of the latest Bell System weighting network was used to modify the spectrum of Curve 1 and the weighted

peak-to-peak to rms noise was calculated to be 44.9 db. The data for the baseband noise spectrum was taken on Pass 1989 at 11:31 UT on March 13, 1964. At that time the ground receiver and satellite input powers calculated were  $-97.6 \pm 1$  and  $-69.3$  dbm, respectively; the ground receiver noise temperature was  $37^\circ$  Kelvin. Using these values and assuming a satellite noise figure of 13 db, the unweighted peak-to-peak signal to rms noise can be calculated from the following expression:

$$\frac{S_{p-p}}{N_{\text{rms}}} = \frac{3f_{p-p}^2}{\left(\frac{\phi_r}{S_r} + \frac{\phi_g}{S_g}\right) f_m^3}$$

where

- $f_{p-p}$  = peak-to-peak frequency deviation (cps),
- $\phi_r$  = satellite receiver noise density (watts/cps),
- $\phi_g$  = ground receiver noise density (watts/cps),
- $S_r$  = satellite received power (watts),
- $S_g$  = ground received power (watts),
- $f_m$  = top baseband frequency (cps).

The unweighted peak-to-peak signal to noise calculated was 33.4 db and the corresponding weighted peak-to-peak signal to noise calculated was 44.0 db. These compare favorably with the measured values of 34.3 and 44.9 db, respectively.

The weighted peak-to-peak signal to rms noise was measured directly on many passes since the launch of Telstar II. Typical measurements are given in Table VIII below:

TABLE VIII — TELEVISION NOISE-WEIGHTED PEAK-TO-PEAK SIGNAL TO RMS NOISE

Pass	Receiver	Time (UT)	Range (SM)	Spin Angle (Degrees)	Weighted Peak-to-Peak Signal RMS Noise (db)
1811	Standard	15:40-16:03	6109-2731	123.4 149.3	46.1-50.3
1989	Standard	11:09-11:39	8522-6721	99.0 126.0	46.1-45.0

The measurements taken are also plotted as a function of range and spin angle in Figure 19 along with the expected peak-to-peak signal to rms noise for a  $90^\circ$  spin angle. Calculations indicate the

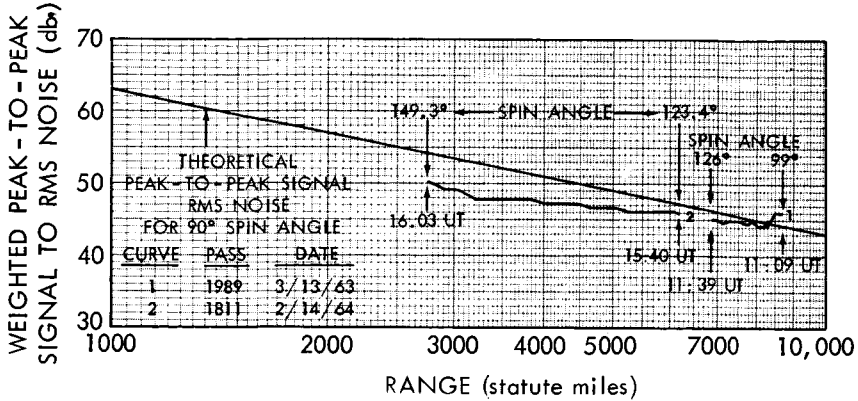


Fig. 19 — Weighted television signal-to-noise ratio — Telstar II, passes 1989 and 1811.

measured values agree with those calculated within 1.5 db when spin angle losses are considered.

*Nonlinearity*

Envelope Delay Distortion

The envelope delay distortion discussed in this section is generated in the IF and RF circuitry of the system causing cross modulation in FM systems. The envelope delay distortion was measured by the two-frequency sweep method, using the standard test set used on the TD2 and TH radio systems. In this method the carrier is swept approximately  $\pm 12$  Mc with a 100 cycle sine wave applied to the B0 klystron of the FM deviator so that the output at IF is swept from 62 to 86 Mc. Simultaneously a 278 kc sine wave is applied at the video input to the FM deviator to provide a peak deviation of about 200 kc. The 100 cycle and 278 kc signals are recovered and separated at the FM receiver video output. The 100 cycle sine wave is used for horizontal scope deflection. The 278 kc tone which has been phase modulated by the transmission delay distortion of the system is compared in phase with a 278 kc crystal controlled oscillator located in the delay set receiver. The crystal controlled oscillator is phase locked to the long-term average phase of the received 278 kc tone. The phase variations are used for vertical scope deflection with a sensitivity of 5 nanoseconds per small division.

Each of the RF and IF portions of the system contributes to the

over-all envelope delay distortion. Delay equalizers\* with the inverse characteristic of the IF envelope delay distortion have been provided for the IF loop. (The IF loop includes the FM deviator, FM receivers and ground receiver IF amplifier combination.) Envelope delay distortion tests have been made indicating a negligible contribution for this portion of the system.

Figure 20 shows the envelope delay distortion measured on a satellite loop during pass 2255 at 01:24 UT on April 24, 1964. This is typical of many measurements made since the launch of Telstar II. Delay

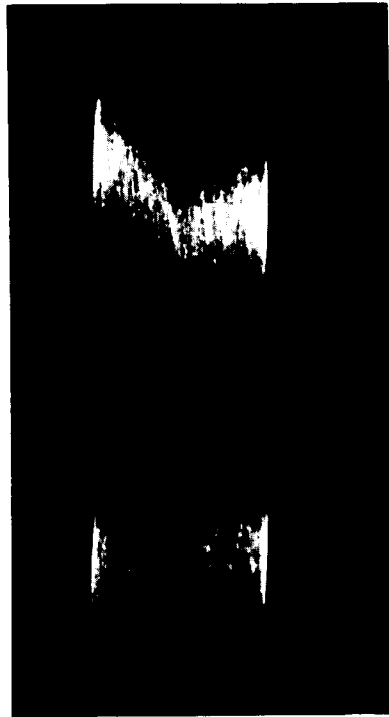


Fig. 20—Envelope delay distortion, satellite loop, FMFB receiver. Telstar II, pass 2255, April 24, 1964. Top: Time 01:24 UT—No RF Equalization. Bottom: Time 01:28 UT—RF Equalized. Sensitivities: Vertical = 5.0  $\eta$  sec/small div. Horizontal = 2.0 mc/small div.

\* The delay equalization provided for Telstar II is identical to that provided for Telstar I reported in Vol. 2, p. 1598.

equalization has been provided for the RF portion of the system which includes the ground transmitter, the satellite and the RF portion of the ground receiver. Figure 20 also shows the equalized envelope delay distortion measured on a satellite loop during pass 2255 at 01:28 UT on April 24, 1964.

#### Differential Phase and Gain

Differential phase is a measure of the phase nonlinearity of a system over the RF bandwidth corresponding to the frequency deviation of the picture portion of the video signal. Differential gain is a measure of the amplitude nonlinearity of the system.

The measurements were made by transmitting two test signals, one at a low frequency (15.75 kc) adjusted to sweep  $\pm 7$  Mc at 74 Mc; the other, a fixed frequency at 3.58 Mc applied at a power level 14 db below that of the low frequency signal. The test signals are applied to the video lines in the test area. At the receiving end of the system, the 15.75 kc tone drives the horizontal sweep and either the gain or phase variations of the 3.58 Mc tone may be selected to drive the vertical sweep.

Figures 21 and 22 show the differential phase and gain measured on the baseband loop. Figures 23 and 24 show the differential phase

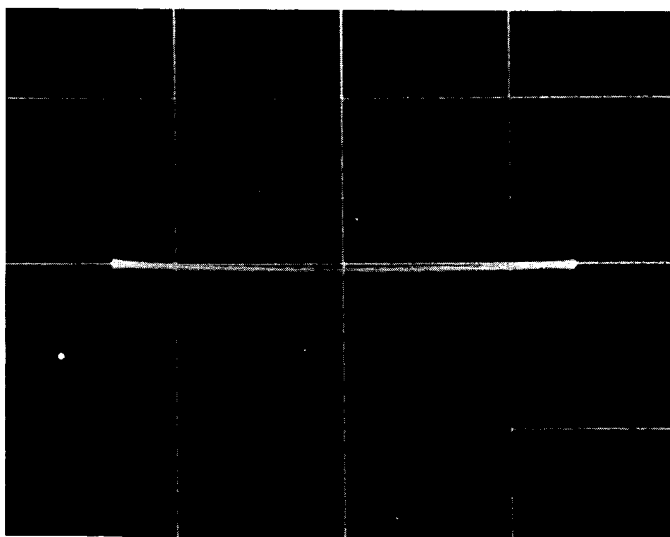


Fig. 21—Differential phase, baseband loop, standard FM receiver — Telstar II. Horizontal Sweep: 1 div = 1 Mc. Vertical Sweep: 1 div =  $1^\circ$ .

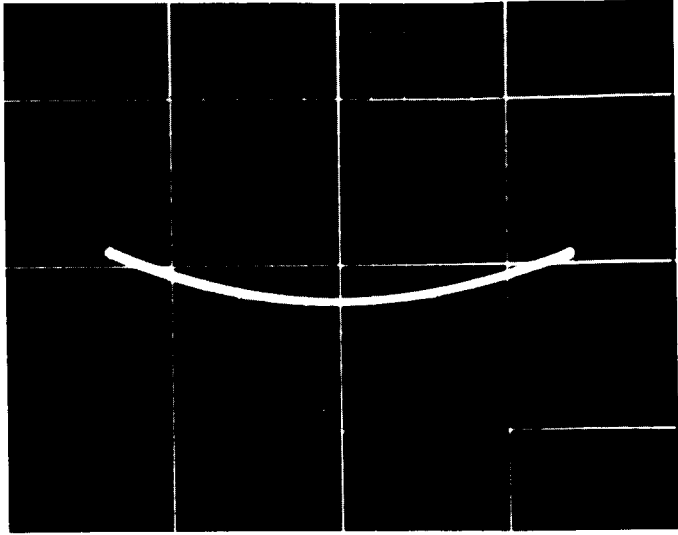


Fig. 22 — Differential gain, baseband loop, standard FM receiver — Telstar II. Horizontal Sweep: 1 div = 1 Mc. Vertical Sweep: 1 div = 0.2 db.

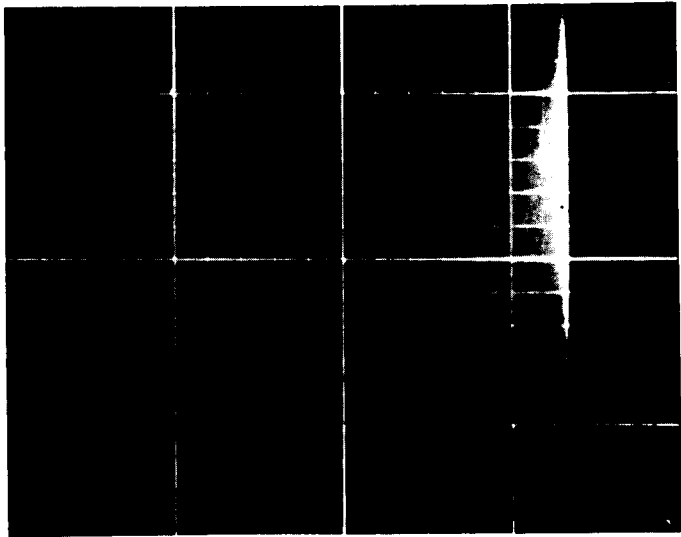


Fig. 23 — Differential phase, satellite loop, standard FM receiver — Telstar II, pass 1804, February 13, 1964. Horizontal Sweep: 1 div = 1 Mc. Vertical Sweep: 1 div = 1°.

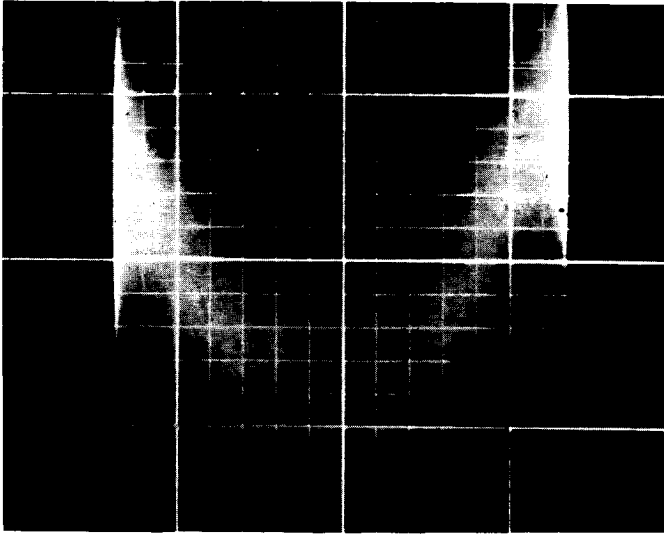


Fig. 24 — Differential gain, satellite loop, standard FM receiver—Telstar II, pass 1804, February 13, 1964. Horizontal Sweep: 1 div = 1 Mc. Vertical Sweep: 1 div = 0.2 db.

and gain measured with the satellite loop on pass 1804 on February 13, 1964. These are typical of many measurements made since the launch of Telstar II. It should be recalled that the system was not delay equalized at the time of the measurement, and since the differential phase is related to envelope delay distortion the differential phase recorded here would be reduced by delay equalization.

### *Video Tests*

Typical photographs of test patterns taken recently through Telstar II are presented in this section. Such photographs afford a means of rapidly evaluating a satellite performance. Telstar II, pass 2282 on April 28, 1964 was used to photograph the monoscope, multiburst, sine-squared window, and stairstep test patterns on the test trunk, baseband, IF and satellite loops. The standard receiver and its associated circuitry was used without pre-emphasis. Other conditions pertaining to each photograph are given in Table IX, an index of the photographs taken. This table lists for each photograph the type of signal, the loop used, the receiver or receiver line used, the type of presentation and sweep rate as well as whether or not audio diplexers are included in the circuit. Figures 25 through 33 were taken on a

TABLE IX — TELSTAR II, PASS 2282, PHOTOGRAPHIC INDEX, APRIL 28, 1964

Figure	Type of Signal	Circuit	Audio Duplexers	Receiver	Monitor	Oscilloscope	Oscilloscope Sweep
25	Monoscope	Test Trunk Loop	Out	—		✓	Line
26	Monoscope	Test Trunk Loop	Out	—	✓		Line
27	Multiburst	Test Trunk Loop	Out	—	✓		Line
28	Multiburst	Test Trunk Loop	Out	—	✓		Line
29	Sin <sup>2</sup> Window	Test Trunk Loop	Out	—	✓		Field Line
30	Sin <sup>2</sup> Window	Test Trunk Loop	Out	—	✓		Field Line
31	Sin <sup>2</sup> Window	Test Trunk Loop	Out	—	✓		Line
32	Stairstep	Test Trunk Loop	Out	—	✓		Line
33	Stairstep	Test Trunk Loop	Out	—	✓		Line
34	Monoscope	Baseband Loop	Out	Std Rec. Line	✓		Line
35	Monoscope	Baseband Loop	Out	Std Rec. Line	✓		Line
36	Multiburst	Baseband Loop	Out	Std Rec. Line	✓		Line
37	Multiburst	Baseband Loop	Out	Std Rec. Line	✓		Line
38	Multiburst	Baseband Loop	Out	Std Rec. Line	✓		Line
39	Sin <sup>2</sup> Window	Baseband Loop	Out	Std Rec. Line	✓		Field Line
40	Sin <sup>2</sup> Window	Baseband Loop	Out	Std Rec. Line	✓		Field Line
41	Stairstep	Baseband Loop	Out	Std Rec. Line	✓		Line
42	Stairstep	Baseband Loop	Out	Std Rec. Line	✓		Line
43	Monoscope	IF Loop	Out	Std FM Rec.	✓		Line
44	Monoscope	IF Loop	Out	Std FM Rec.	✓		Line
45	Multiburst	IF Loop	Out	Std FM Rec.	✓		Line
46	Multiburst	IF Loop	Out	Std FM Rec.	✓		Line
47	Sin <sup>2</sup> Window	IF Loop	Out	Std FM Rec.	✓		Field Line
48	Sin <sup>2</sup> Window	IF Loop	Out	Std FM Rec.	✓		Field Line
49	Sin <sup>2</sup> Window	IF Loop	Out	Std FM Rec.	✓		Field Line
50	Stairstep	IF Loop	Out	Std FM Rec.	✓		Field Line

51	Stairstep	IF Loop	Out	Std FM Rec.	✓	Line
52	Monoscope	IF Loop	In	Std FM Rec.	✓	Line
53	Monoscope	IF Loop	In	Std FM Rec.	✓	Line
54	Multiburst	IF Loop	In	Std FM Rec.	✓	Line
55	Multiburst	IF Loop	In	Std FM Rec.	✓	Line
56	Sin <sup>2</sup> Window	IF Loop	In	Std FM Rec.	✓	Field
57	Sin <sup>2</sup> Window	IF Loop	In	Std FM Rec.	✓	Line
58	Sin <sup>2</sup> Window	IF Loop	In	Std FM Rec.	✓	Line
59	Stairstep	IF Loop	In	Std FM Rec.	✓	Line
60	Stairstep	IF Loop	In	Std FM Rec.	✓	Line
61	Monoscope	Satellite Loop	In	Std FM Rec.	✓	Line
62	Monoscope	Satellite Loop	In	Std FM Rec.	✓	Line
63	Multiburst	Satellite Loop	In	Std FM Rec.	✓	Line
64	Multiburst	Satellite Loop	In	Std FM Rec.	✓	Line
65	Sin <sup>2</sup> Window	Satellite Loop	In	Std FM Rec.	✓	Line
66	Sin <sup>2</sup> Window	Satellite Loop	In	Std FM Rec.	✓	Field
67	Sin <sup>2</sup> Window	Satellite Loop	In	Std FM Rec.	✓	Line
68	Stairstep	Satellite Loop	In	Std FM Rec.	✓	Field
69	Stairstep	Satellite Loop	In	Std FM Rec.	✓	Line

test trunk loop and represent the purest form of the signal with the least equipment external to the source. Figures 34 through 42 were taken on a baseband loop representing a condition which includes all video circuitry to and from the radome FM deviator and FM receiver. No appreciable degradation of the signals can be noticed. Figures 43 through 51 were taken on an IF loop with the standard FM receiver without audio diplexers. Again no visible degradation of the test signal is noticeable. Figures 52 through 60 were taken on the same IF loop with the standard FM receiver but this time with audio diplexers included in the circuit. The only noticeable effect of adding the diplexer is that of bandlimiting by the 3.5 Mc linear phase filter shown by Figures 54 and 55. Finally, Figures 61 through 69 were taken on the satellite loop with the standard FM receiver and audio diplexing equipment included in the circuit. This represents the normal operating condition and as can be seen from the photographs no appreciable degradation can be attributed to the satellite except for the expected increase in noise.

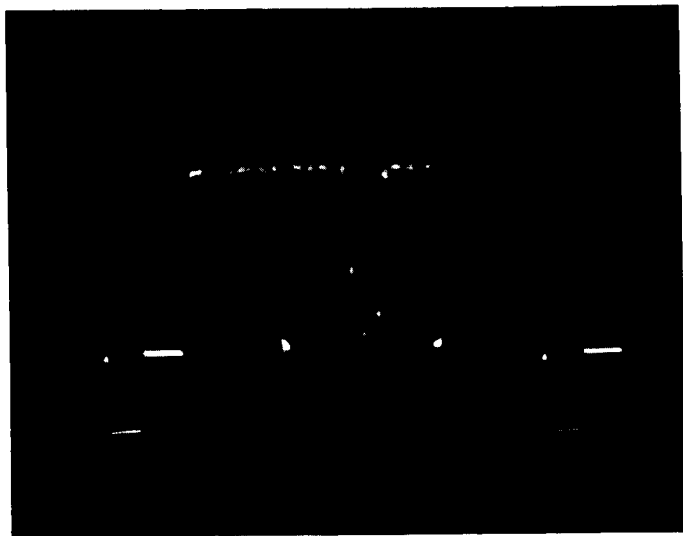


Fig. 25—Monoscope test pattern, test trunk loop, no diplexers; vertical calibration: 4 div = 1 volt. Telstar II, pass 2282, April 28, 1964.

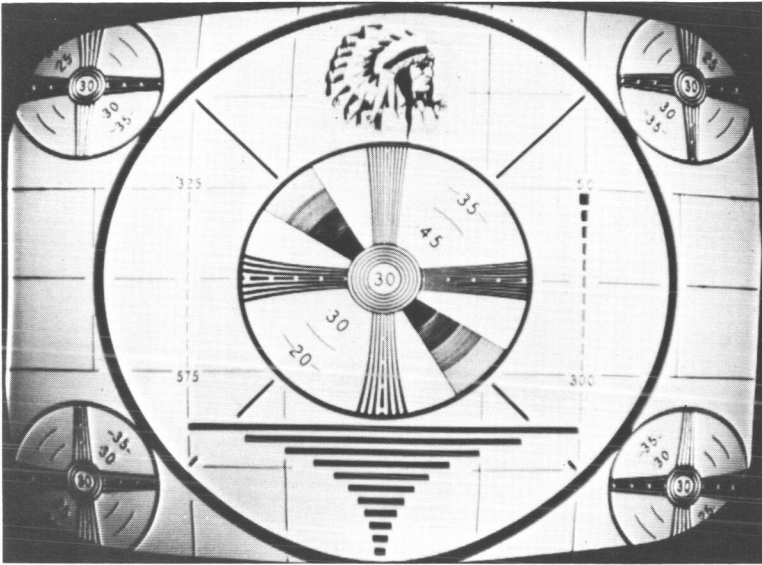


Fig. 26 — Monoscope test pattern, test trunk loop, no diplexers. Telstar II, pass 2282, April 28, 1964.

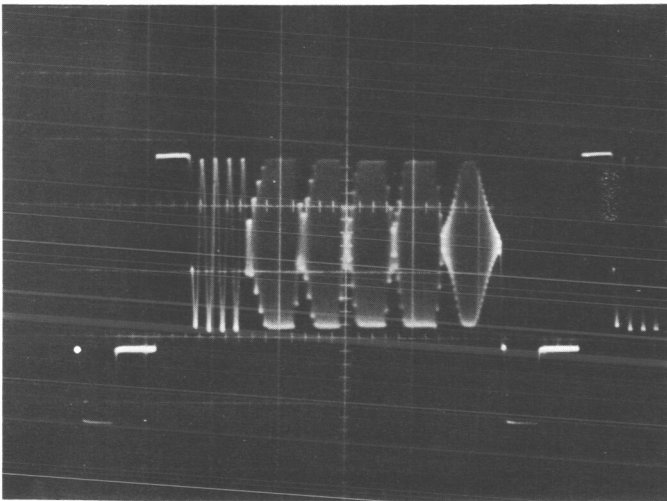


Fig. 27 — Multiburst test pattern, test trunk loop, no diplexers: vertical calibration: 4 div = 1 volt. Telstar II, pass 2282, April 28, 1964.

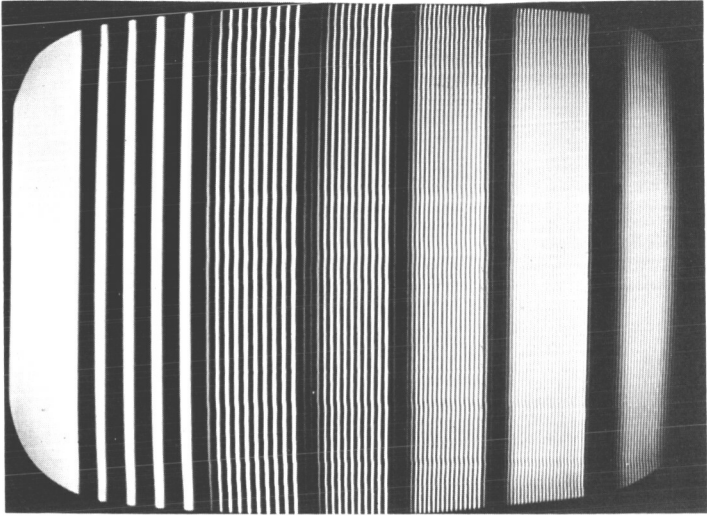


Fig. 28 — Multiburst test pattern, test trunk loop, no diplexers. Telstar II, pass 2282, April 28, 1964.

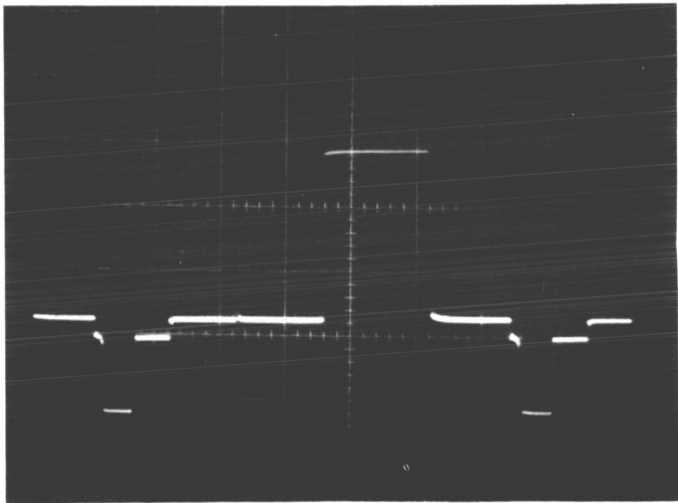


Fig. 29 — Sin<sup>2</sup> window test pattern, test trunk loop, no diplexers; vertical calibration: 4 div = 1 volt. Telstar II, pass 2282, April 28, 1964.

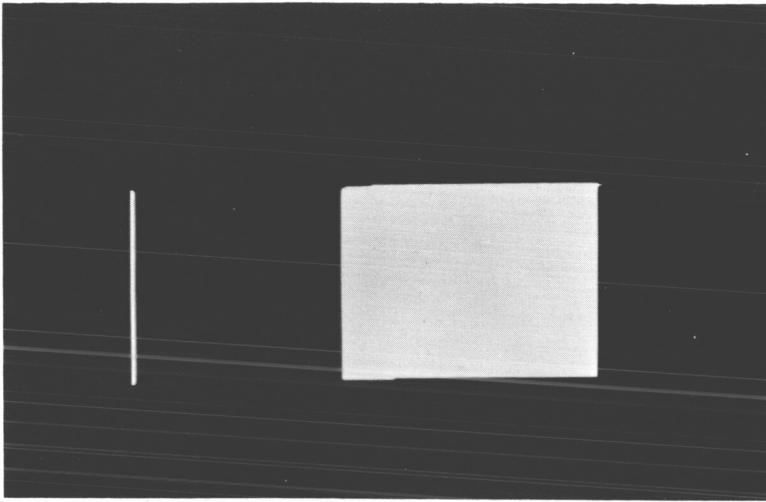


Fig. 30 —  $\text{Sin}^2$  window test pattern, test trunk loop, no diplexers. Telstar II, pass 2282, April 28, 1964.

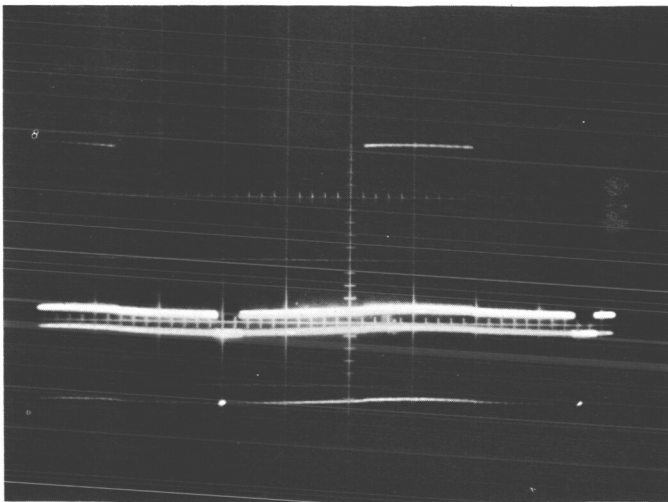


Fig. 31 —  $\text{Sin}^2$  window test pattern, test trunk loop, no diplexers; vertical calibration: 4 div = 1 volt. Telstar II, pass 2282, April 28, 1964.

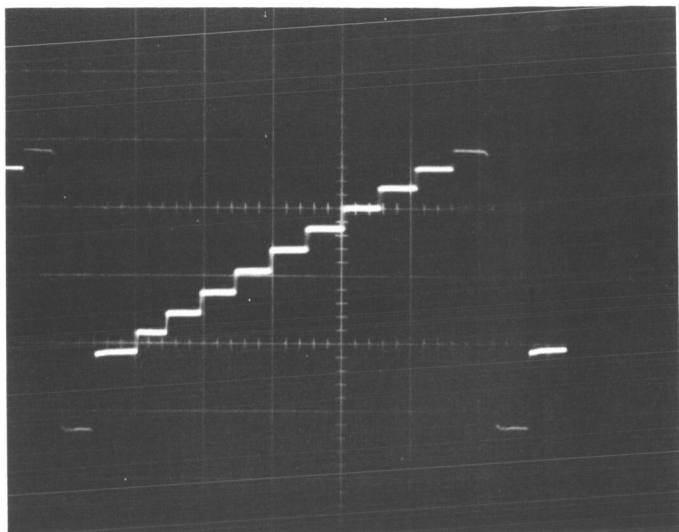


Fig. 32 — Stairstep test pattern, test trunk loop, no diplexers; vertical calibration: 4 div = 1 volt. Telstar II, pass 2282, April 28, 1964.

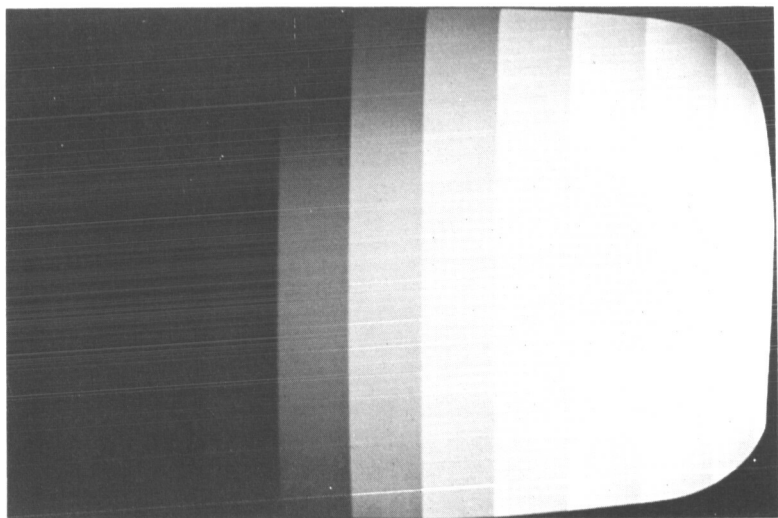


Fig. 33 — Stairstep test pattern, test trunk loop, no diplexers. Telstar II, pass 2282, April 28, 1964.

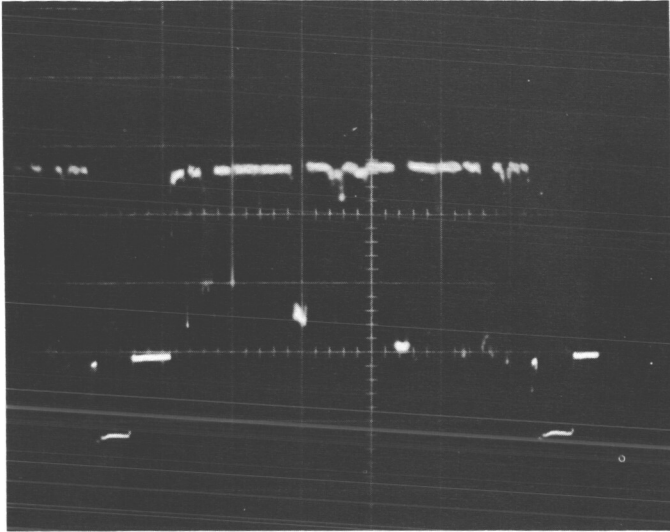


Fig. 34—Monoscope test pattern, baseband loop, no diplexers, standard receiver line; Vertical Calibration: 4 div = 1 volt. Telstar II, pass 2282, April 28, 1964.

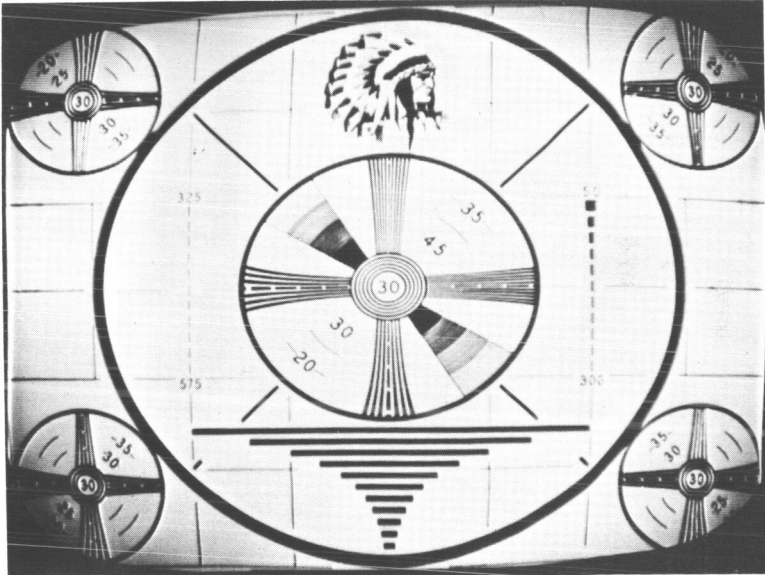


Fig. 35—Monoscope test pattern, baseband loop, no diplexers, standard receiver line. Telstar II, pass 2282, April 28, 1964.

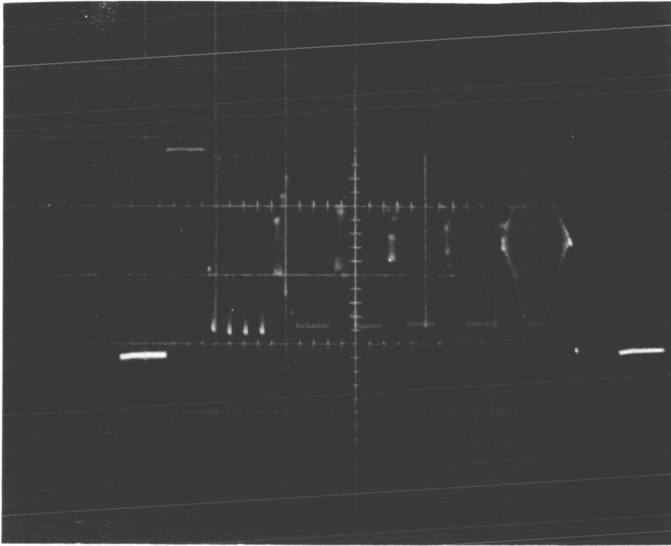


Fig. 36 — Multiburst test pattern, baseband loop, no diplexers, standard receiver line; Vertical Calibration: 4 div = 1 volt. Telstar II, pass 2282, April 28, 1964.

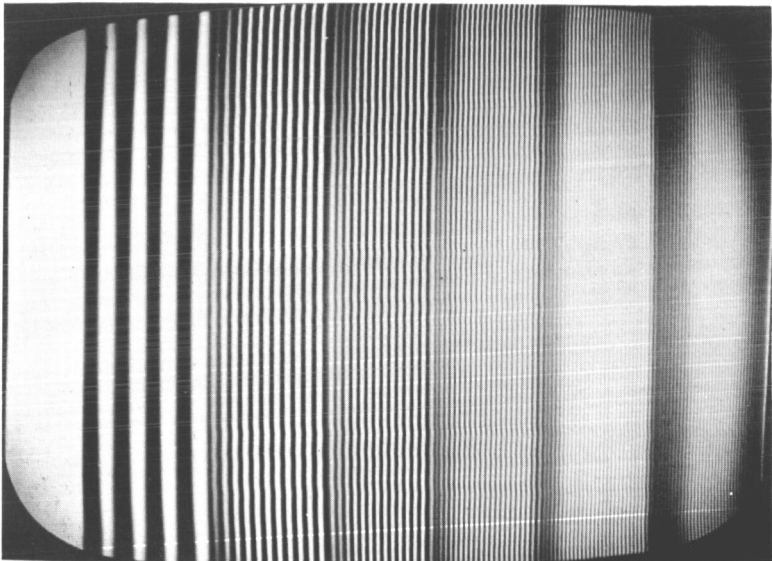


Fig. 37 — Multiburst test pattern, baseband loop, no diplexers, standard receiver line. Telstar II, pass 2282, April 28, 1964.

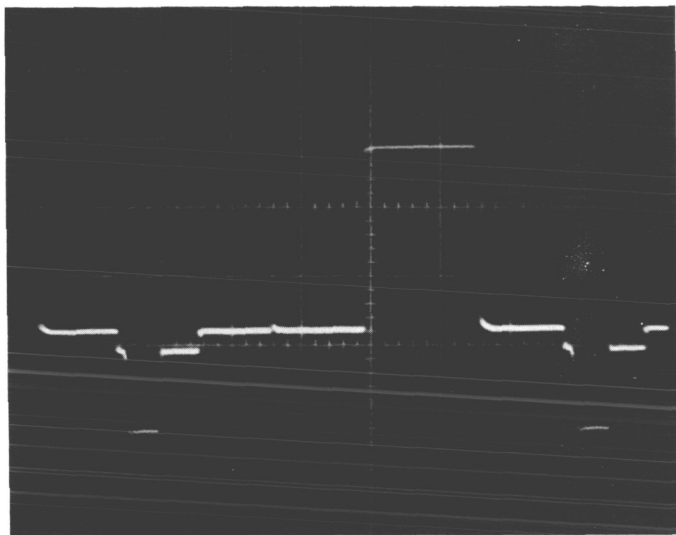


Fig. 38— $\text{Sin}^2$  window test pattern, baseband loop, no diplexers, standard receiver line; vertical calibration: 4 div = 1 volt. Telstar II, pass 2282, April 28, 1964.

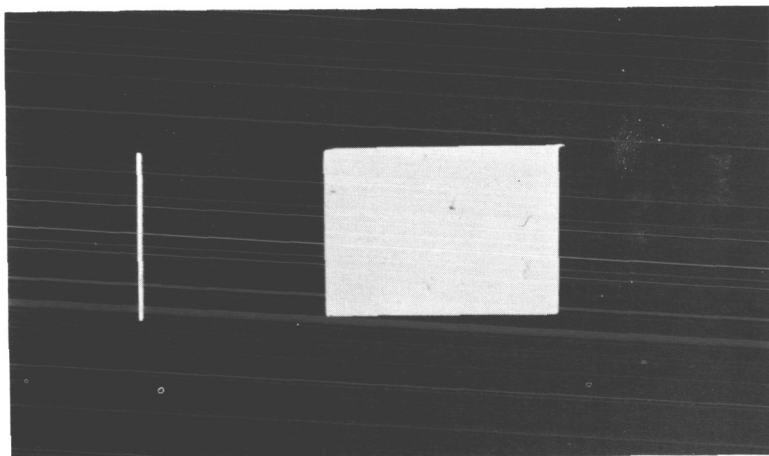


Fig. 39— $\text{Sin}^2$  window test pattern, baseband loop, no diplexers, standard receiver line. Telstar II, pass 2282, April 28, 1964.

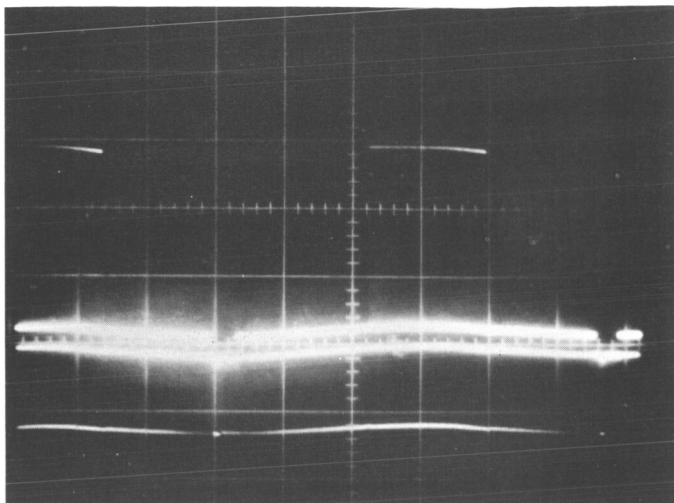


Fig. 40 —  $\text{Sin}^2$  window test pattern, baseband loop, no duplexers, standard receiver line; vertical calibration: 4 div = 1 volt, Telstar II, pass 2282, April 28, 1964.

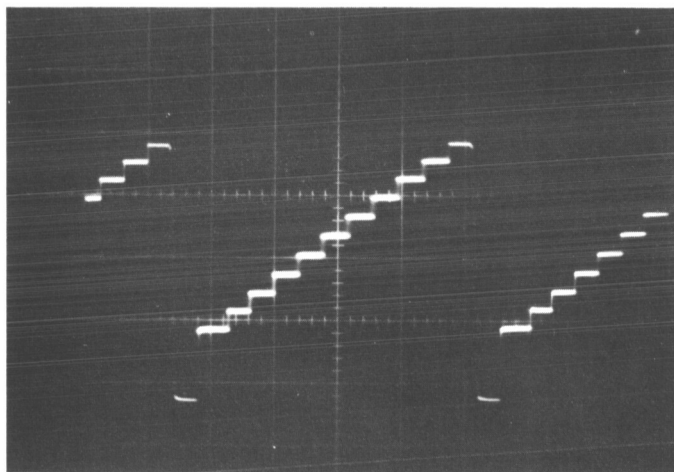


Fig. 41 — Stairstep test pattern, baseband loop, no duplexers, standard receiver line; Vertical Calibration: 4 div = 1 volt, Telstar II, pass 2282, April 28, 1964.

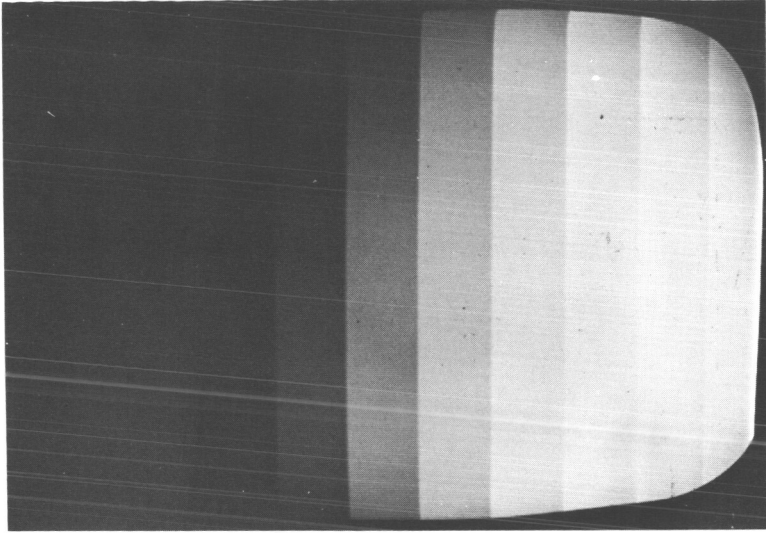


Fig. 42 — Stairstep test pattern, baseband loop, no duplexers, standard receiver line. Telstar II, pass 2282, April 28, 1964.

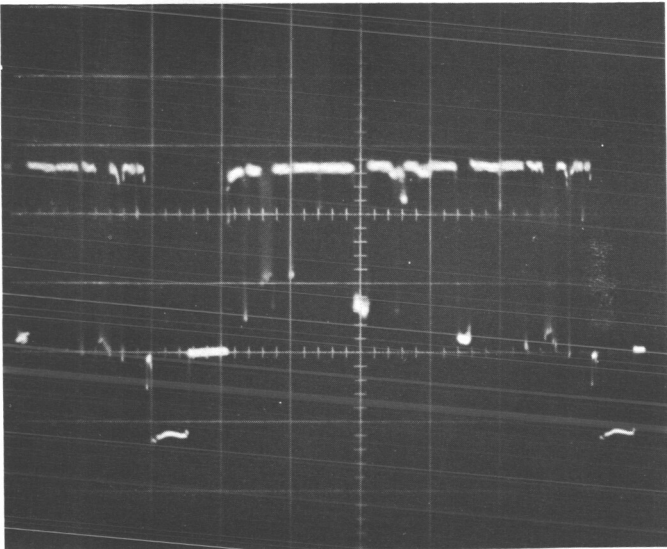


Fig. 43 — Monoscope test pattern, IF loop, no duplexers; standard FM receiver, vertical calibration: 4 div = 1 volt. Telstar II, pass 2282, April 28, 1964.



Fig. 44 — Monoscope test pattern, IF loop, no diplexers, standard FM receiver. Telstar II, pass 2282, April 28, 1964.

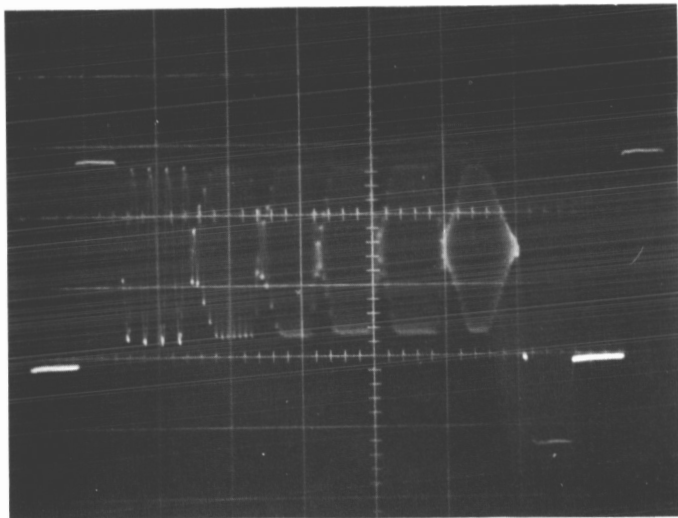


Fig. 45 — Multiburst test pattern, IF loop, no diplexers, standard FM receiver; vertical calibration: 4 div = 1 volt. Telstar II, pass 2282, April 28, 1964.

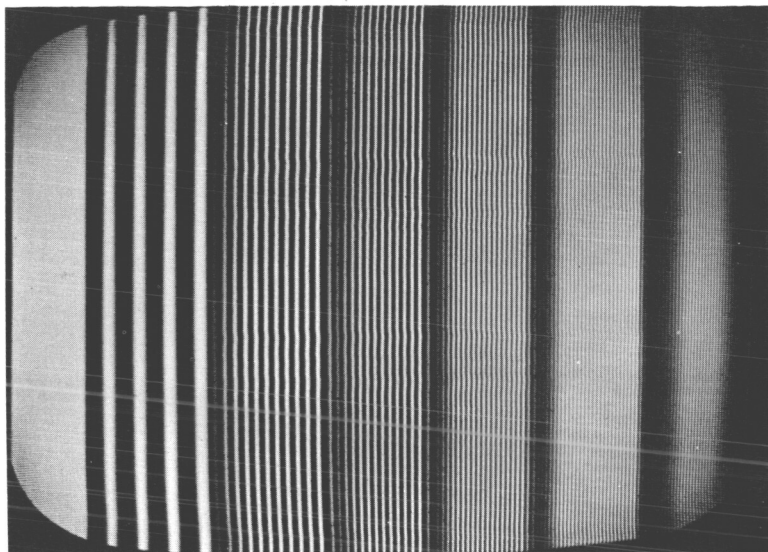


Fig. 46 — Multiburst test pattern, IF loop, no duplexers, standard FM receiver. Telstar II, pass 2282, April 28, 1964.

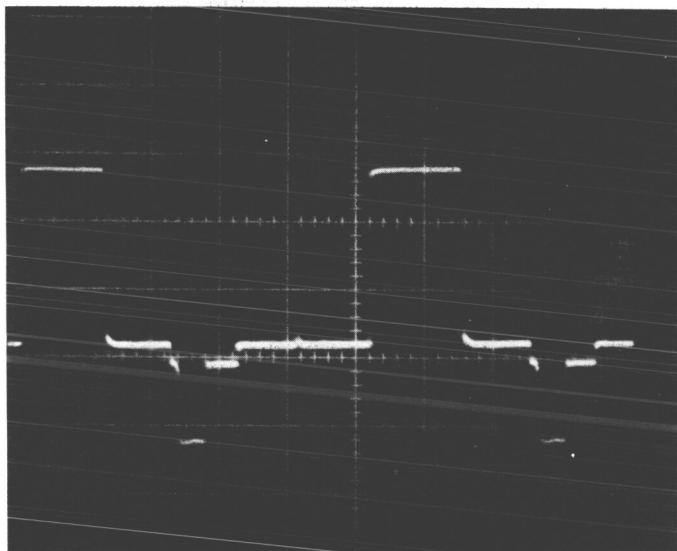


Fig. 47 —  $\text{Sin}^2$  window test pattern, IF loop, no duplexers, standard FM receiver; vertical calibration: 4 div = 1 volt. Telstar II, pass 2282, April 28, 1964.

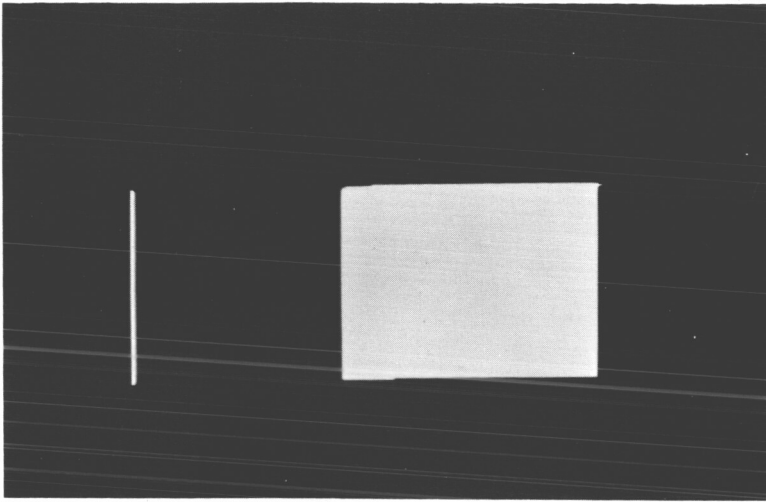


Fig. 30 —  $\text{Sin}^2$  window test pattern, test trunk loop, no diplexers. Telstar II, pass 2282, April 28, 1964.

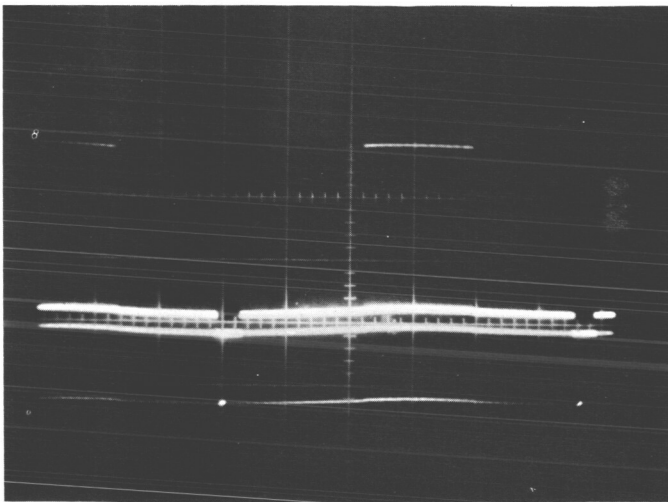


Fig. 31 —  $\text{Sin}^2$  window test pattern, test trunk loop, no diplexers; vertical calibration: 4 div = 1 volt. Telstar II, pass 2282, April 28, 1964.

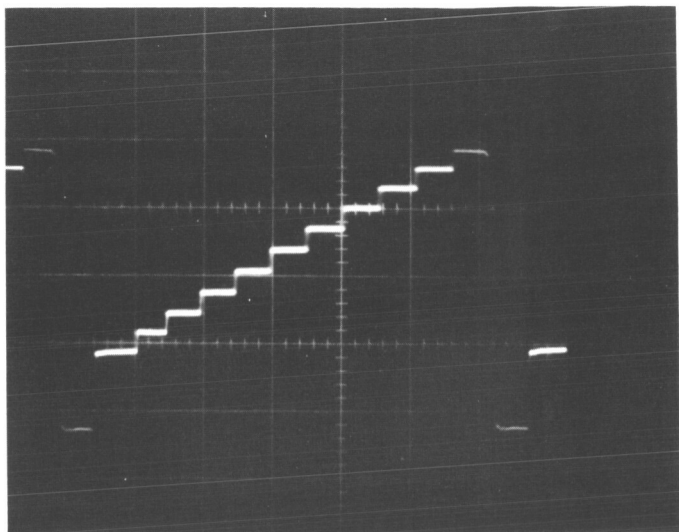


Fig. 32 — Stairstep test pattern, test trunk loop, no diplexers; vertical calibration: 4 div = 1 volt. Telstar II, pass 2282, April 28, 1964.

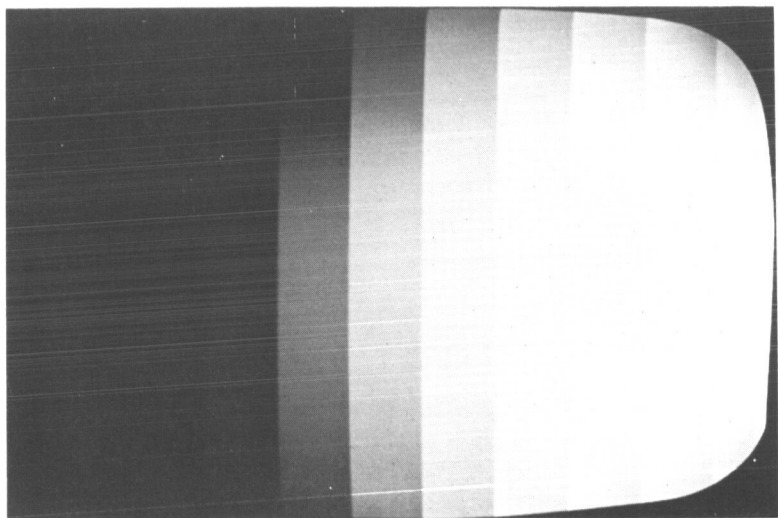


Fig. 33 — Stairstep test pattern, test trunk loop, no diplexers. Telstar II, pass 2282, April 28, 1964.

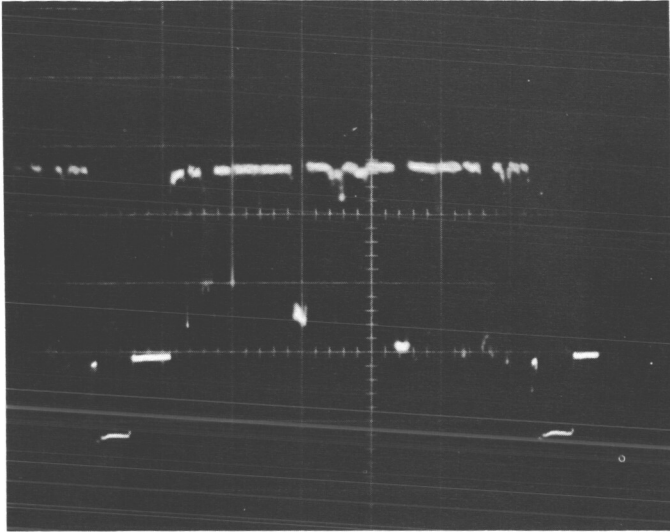


Fig. 34—Monoscope test pattern, baseband loop, no diplexers, standard receiver line; Vertical Calibration: 4 div = 1 volt. Telstar II, pass 2282, April 28, 1964.

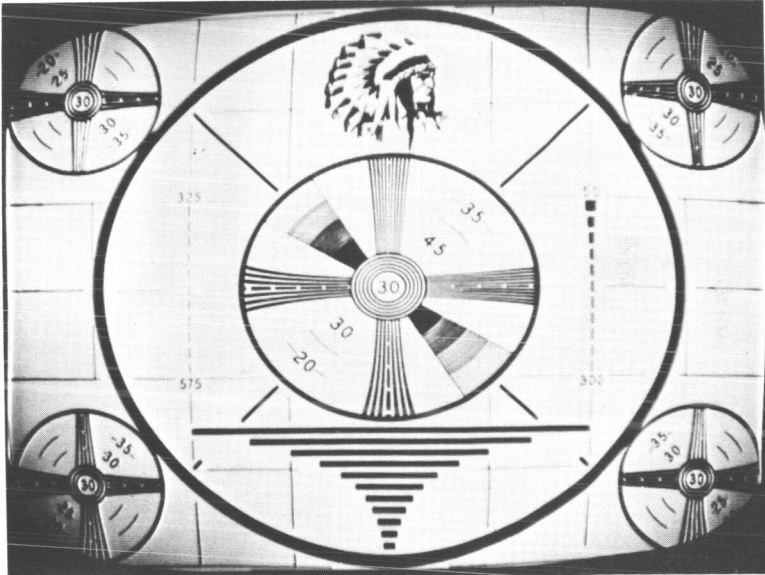


Fig. 35—Monoscope test pattern, baseband loop, no diplexers, standard receiver line. Telstar II, pass 2282, April 28, 1964.

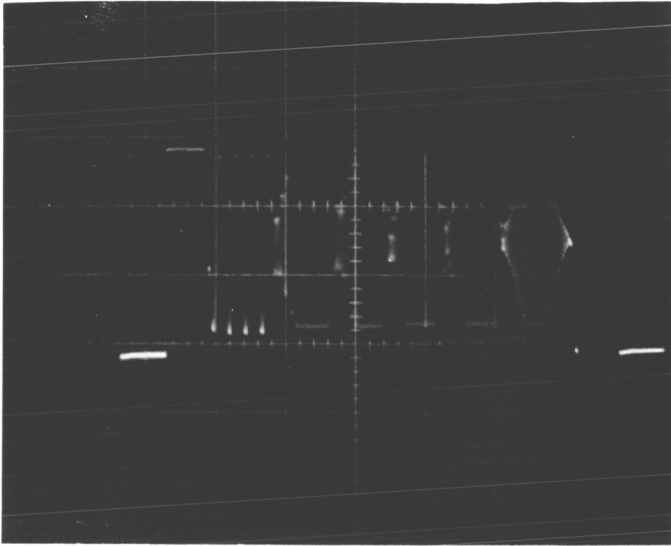


Fig. 36 — Multiburst test pattern, baseband loop, no diplexers, standard receiver line; Vertical Calibration: 4 div = 1 volt. Telstar II, pass 2282, April 28, 1964.



Fig. 37 — Multiburst test pattern, baseband loop, no diplexers, standard receiver line. Telstar II, pass 2282, April 28, 1964.

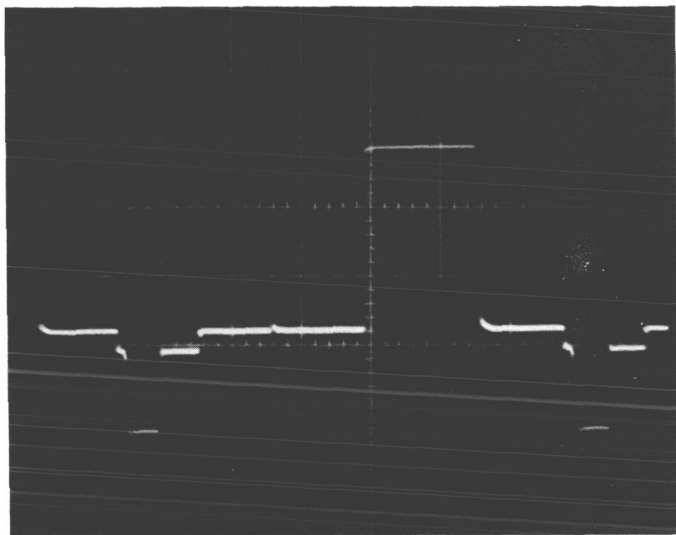


Fig. 38 —  $\text{Sin}^2$  window test pattern, baseband loop, no diplexers, standard receiver line; vertical calibration: 4 div = 1 volt. Telstar II, pass 2282, April 28, 1964.

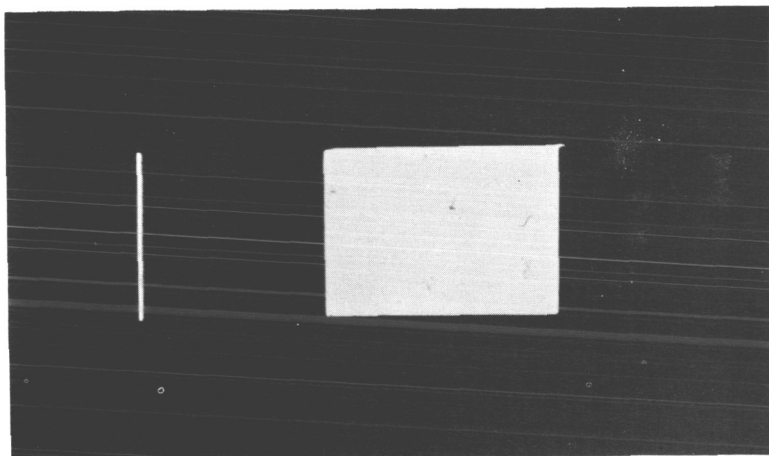


Fig. 39 —  $\text{Sin}^2$  window test pattern, baseband loop, no diplexers, standard receiver line. Telstar II, pass 2282, April 28, 1964.

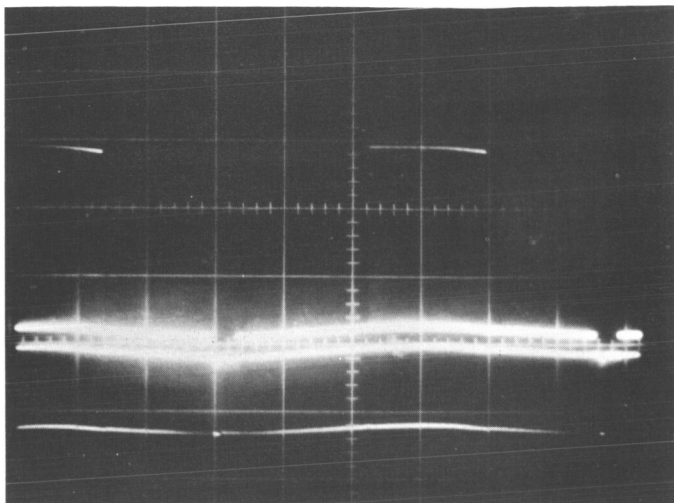


Fig. 40 —  $\text{Sin}^2$  window test pattern, baseband loop, no duplexers, standard receiver line; vertical calibration: 4 div = 1 volt, Telstar II, pass 2282, April 28, 1964.

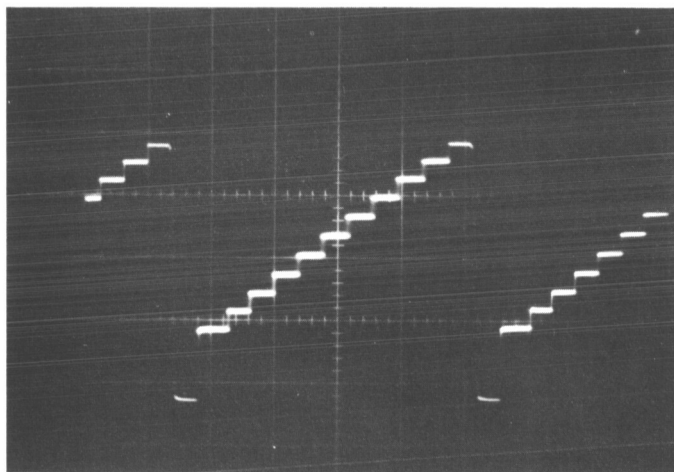


Fig. 41 — Stairstep test pattern, baseband loop, no duplexers, standard receiver line; Vertical Calibration: 4 div = 1 volt, Telstar II, pass 2282, April 28, 1964.

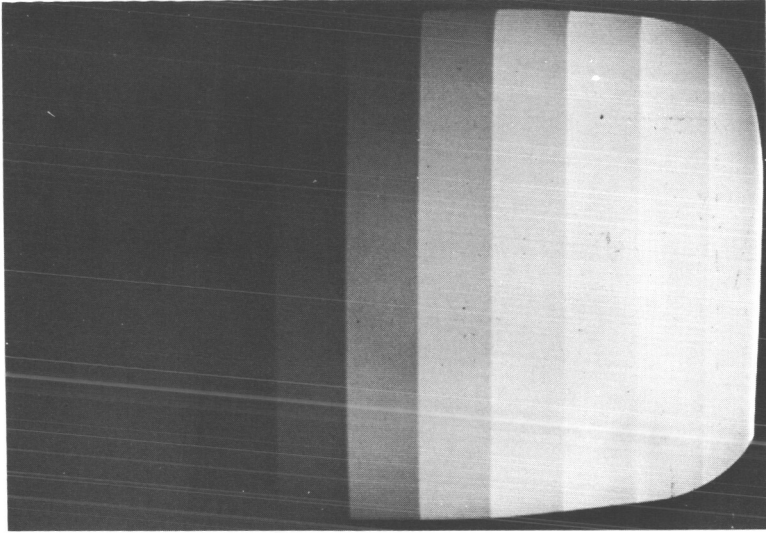


Fig. 42 — Stairstep test pattern, baseband loop, no diplexers, standard receiver line. Telstar II, pass 2282, April 28, 1964.

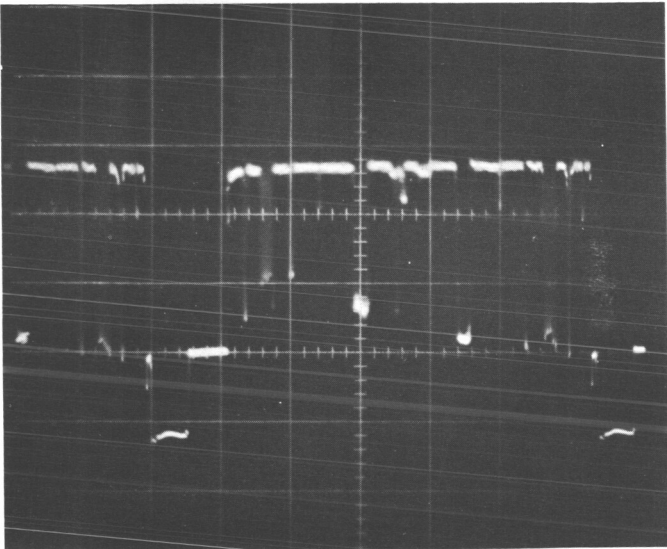


Fig. 43 — Monoscope test pattern, IF loop, no diplexers; standard FM receiver, vertical calibration: 4 div = 1 volt. Telstar II, pass 2282, April 28, 1964.

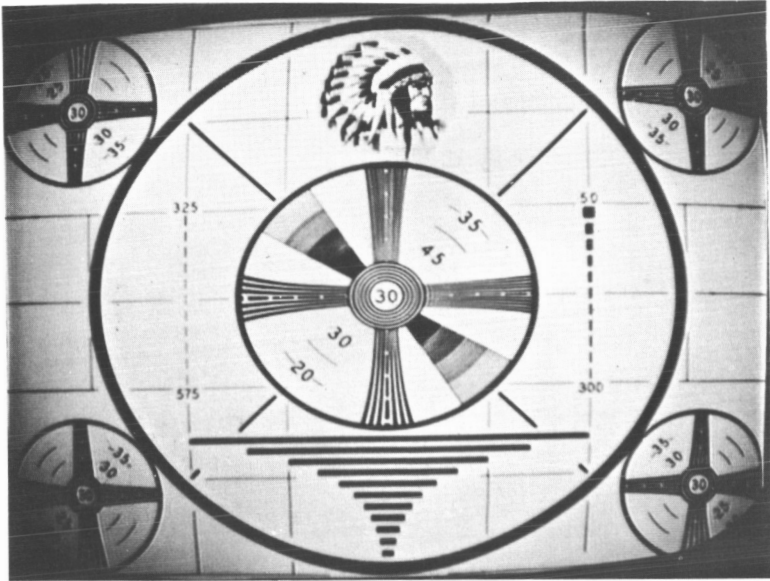


Fig. 44 — Monoscope test pattern, IF loop, no diplexers, standard FM receiver. Telstar II, pass 2282, April 28, 1964.

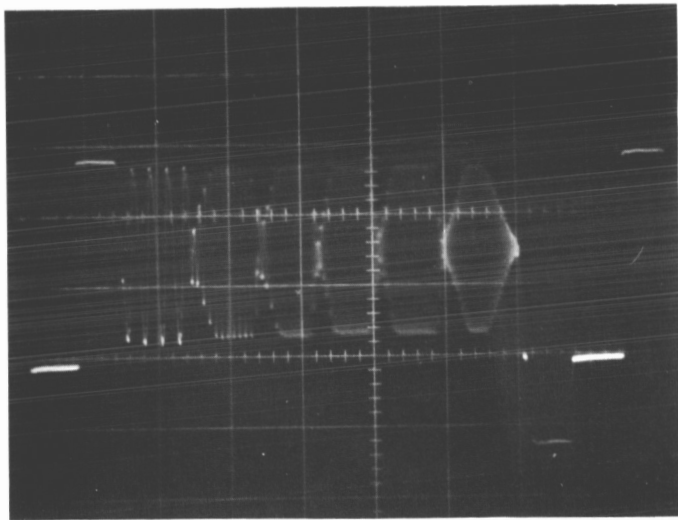


Fig. 45 — Multiburst test pattern, IF loop, no diplexers, standard FM receiver; vertical calibration: 4 div = 1 volt. Telstar II, pass 2282, April 28, 1964.

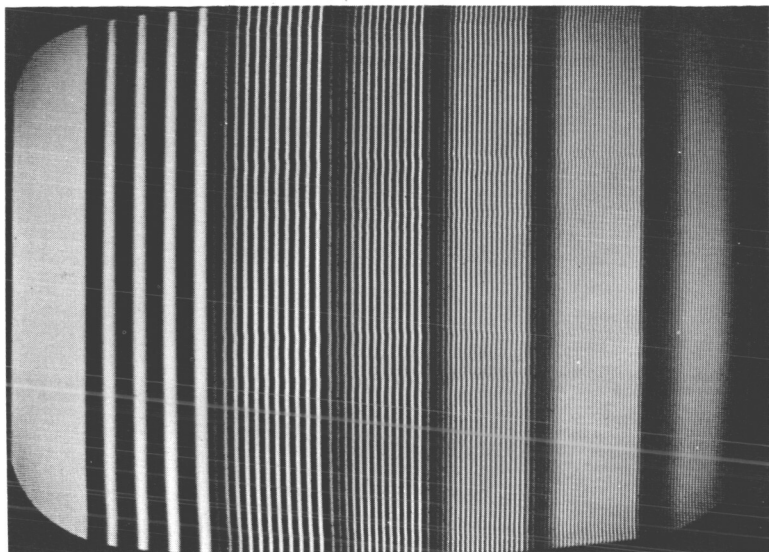


Fig. 46 — Multiburst test pattern, IF loop, no duplexers, standard FM receiver. Telstar II, pass 2282, April 28, 1964.

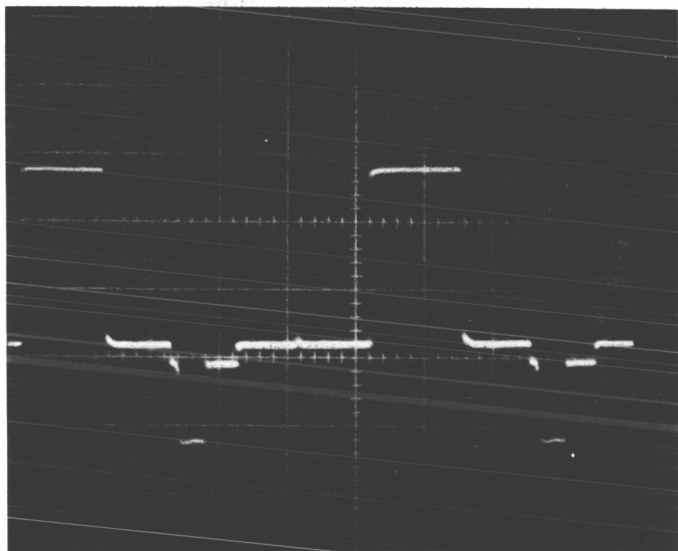


Fig. 47 —  $\text{Sin}^2$  window test pattern, IF loop, no duplexers, standard FM receiver; vertical calibration: 4 div = 1 volt. Telstar II, pass 2282, April 28, 1964.

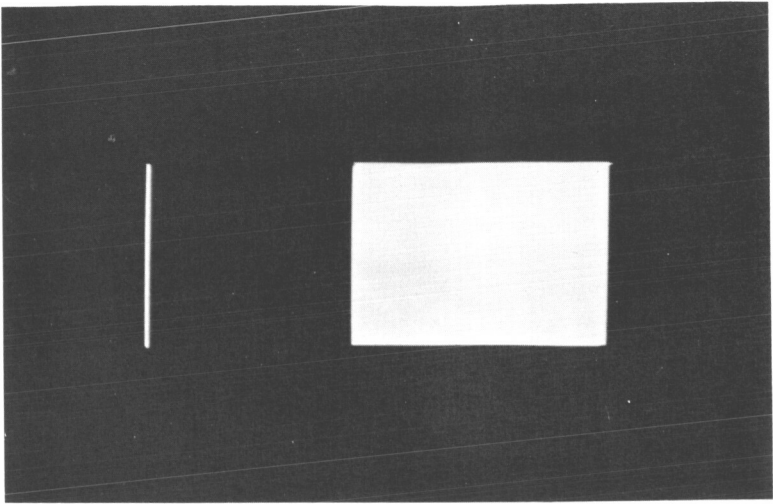


Fig. 48— $\text{Sin}^2$  window test pattern, IF loop, no diplexers, standard FM receiver. Telstar II, pass 2282, April 28, 1964.

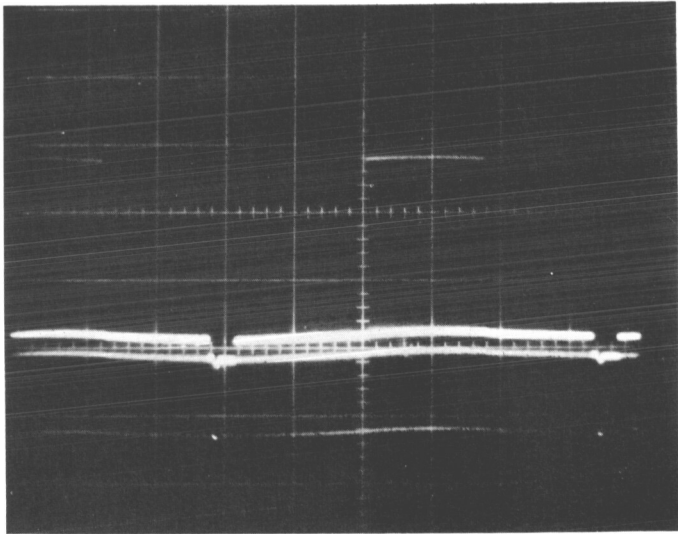


Fig. 49— $\text{Sin}^2$  window test pattern, IF loop, no diplexers, standard FM receiver; vertical calibration: 4 div = 1 volt. Telstar II, pass 2282, April 28, 1964.

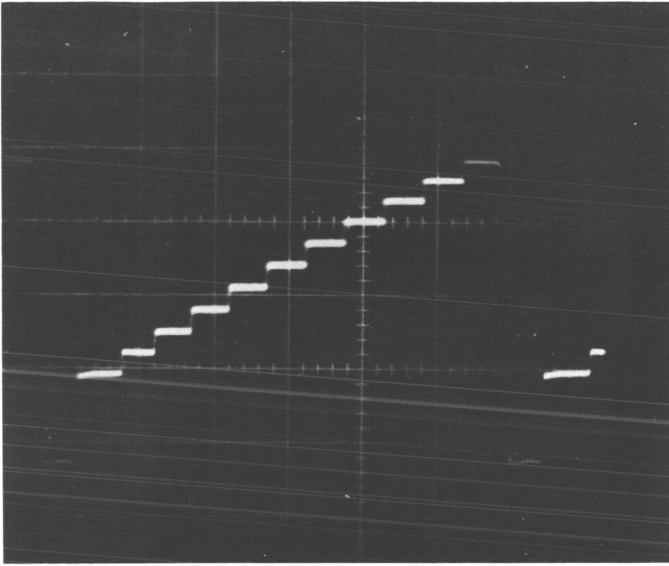


Fig. 50—Stairstep test pattern, IF loop, no diplexers, standard FM receiver; vertical calibration: 4 div = 1 volt. Telstar II, pass 2282, April 28, 1964.

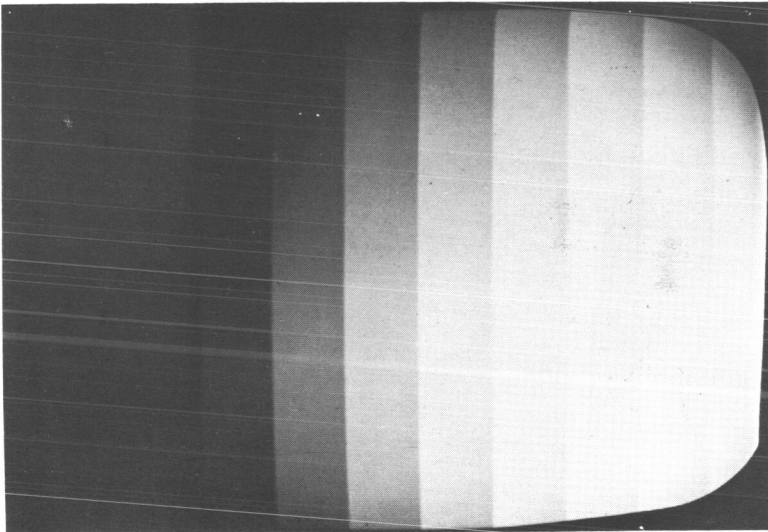


Fig. 51—Stairstep test pattern, IF loop, no diplexers, standard FM receiver. Telstar II, pass 2282, April 28, 1964.

## TEST RESULT COMPARISON

*Introduction*

Earlier sections of this report presented the results of initial communication tests conducted on Telstar II shortly after launch in May of 1963 and the results of communications tests conducted recently in April 1964. This section presents a comparison of the data analyzed in the two previous sections. As detailed in the following sections no noticeable degradation of the satellite has taken place and its performance now is the same as it was shortly after launch.

*Carrier Power*

## Received Carrier Power

The results have been discussed of received carrier power tests conducted on Telstar II directly after launch on pass 11 (May 9, 1963) and those conducted recently on pass 1989 (March 31, 1964), respectively. This section compares the results of the two passes to determine if there has been any change in satellite performance during this period. No significant changes were noted as discussed below.

## Received Carrier Power versus Time

The 4.17 Gc received carrier power measured on pass 11 on May 9, 1963 from 03:30 to 03:50 UT is plotted in Figure 70 as a function of time with the range and spin angle parameters shown. The average expected value is also plotted based on the constants given in Figure 1. (Spin angle losses have been included in these computations.) Comparison of the two indicates good agreement. Similar measurements made on pass 1989 on March 13, 1964 are plotted in the lower half of Figure 70 along with the expected calculated value based on the same constants as given in Figure 15. Comparison of the expected and measured values again indicate good agreement. Since both passes show good agreement with the expected theoretical value, it can be concluded that the satellite performance has not changed in this respect and that the 4.17 Gc transmitted power has not changed.

The 6.39 Gc received carrier power at the satellite measured on passes 11 and 1989 are plotted in the top and bottom, respectively, of Figure 71. The expected value of the received carrier power is also plotted in the figure for each pass as a function of time. Spin angle and range are also given as parameters. The values of the constants used for the computations are given in Figures 2 and 16 for passes 11

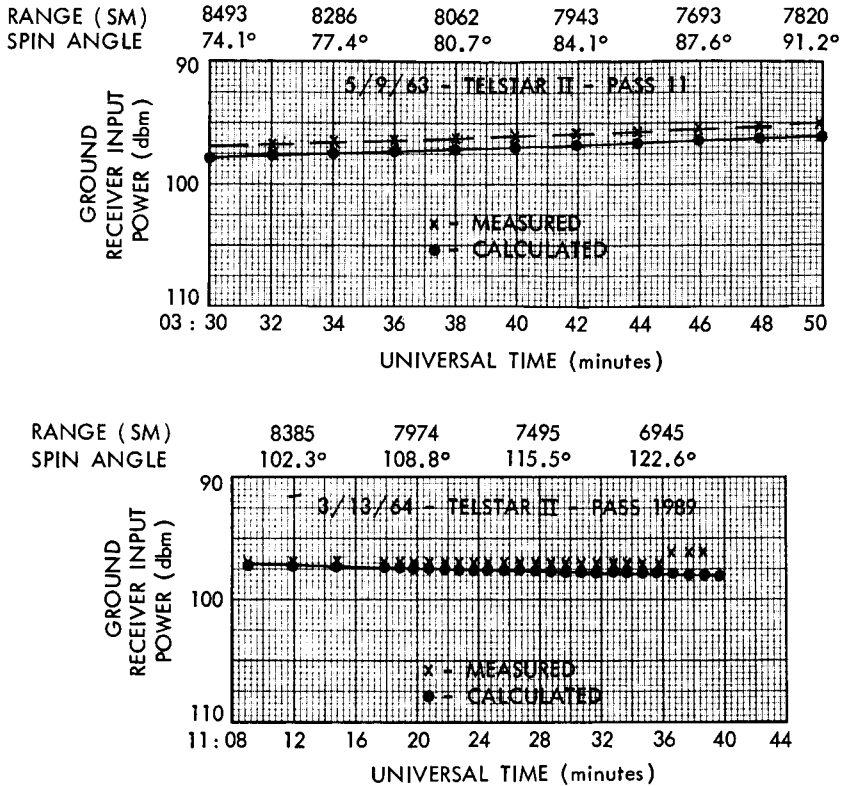


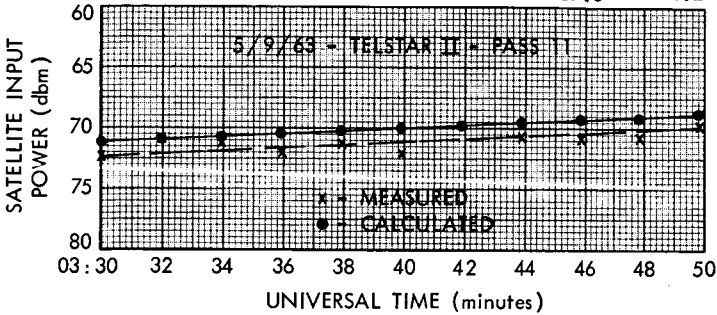
Fig. 70 — Ground receiver input power, 4170 Mc — Telstar II, passes 11 and 1989.

and 1989, respectively. A comparison of the measured and calculated values show good agreement for each pass again indicating no change in the satellite during this period.

#### Baseband Transmission

Baseband transmission characteristics were measured on the baseband, IF and satellite loops when using the standard FM receiver and its associated circuitry without clampers, duplexers, or band limiting filters. Measurements made on pass 11 directly after launch on May 9,

RANGE (SM)	8493	8286	8062	7943	7693	7820
SPIN ANGLE	74.1°	77.4°	80.7°	84.1°	87.6°	91.2°



RANGE (SM)	8385	7974	7495	6945
SPIN ANGLE	102.3°	108.8°	115.5°	122.6°

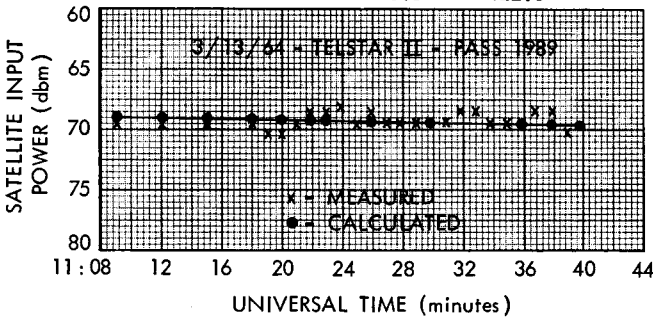


Fig. 71 — Satellite input power, 6390 Mc — Telstar II, passes 11 and 1989.

1963 were discussed on page 2265 and those made recently on pass 2249 (April 24, 1964) were discussed on page 2267. A comparison of the data plotted in Figures 3 and 17 show the baseband and IF loops have not changed significantly in that period. The transmission characteristics of the satellite loop as measured on pass 11 and pass 2249 has been replotted in Figure 72 for convenience. The slight difference in shape of the two transmission characteristics can be attributed to a change in the RF equipment used and to measurement error. It can be concluded that no significant change in the transmission characteristic due to the satellite was measured.

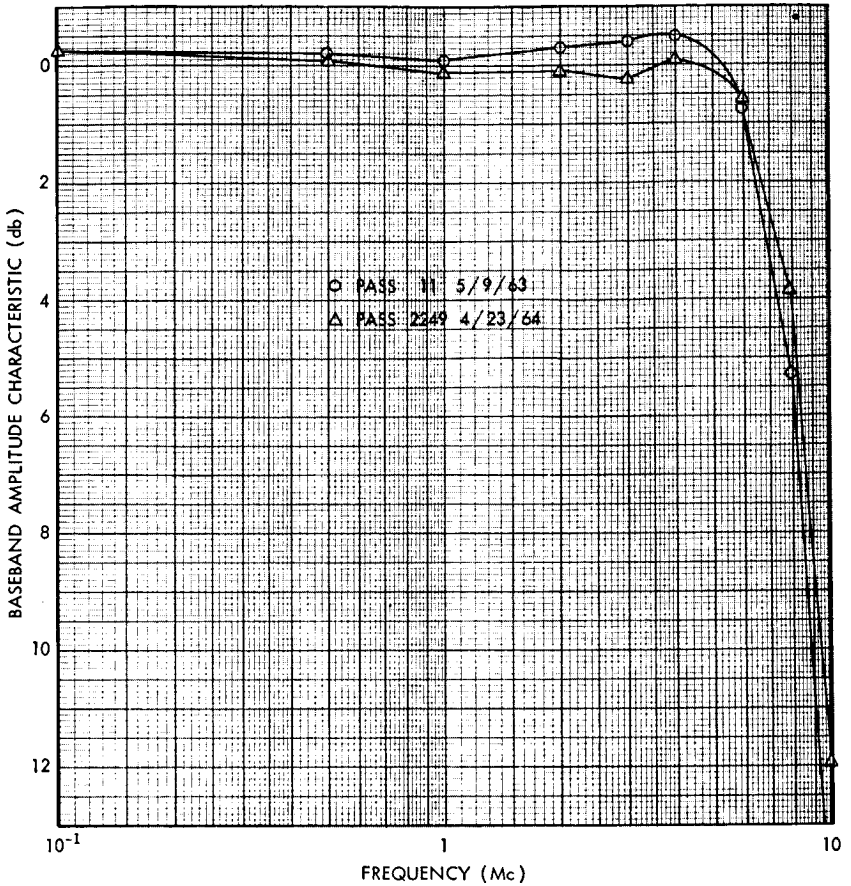


Fig. 72 — Baseband amplitude characteristic, standard FM receiver — Telstar II, passes 11 and 2249

### Noise

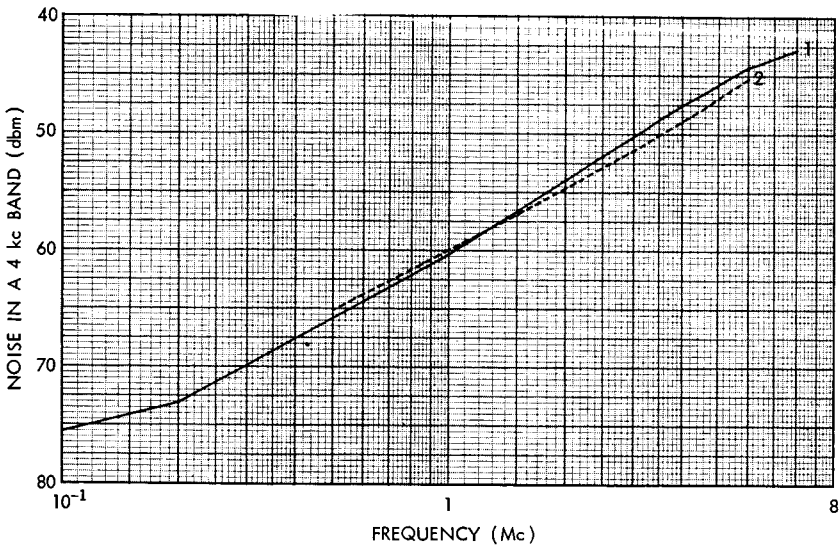
#### Baseband Noise Spectrum

Measurements of the baseband noise spectrum made on pass 11 directly after launch on May 9, 1963 and those made recently on pass 1989 (March 13, 1964) have been discussed. A comparison of the data obtained on both passes indicates good agreement. For convenience the data obtained on the satellite during passes 11 and 1989 has been replotted in Figure 73 as Curves 1 and 2, respectively. Associated information such as range, spin angle, received carrier powers and

noise temperature and the calculated value of the noise at the test area is also given in the Figure 73. The slight difference between the two spectra can be attributed to the slightly different transmission characteristics, the difference in range and spin angle and to measurement error. It can be concluded that no significant change in the baseband noise characteristic due to the satellite was measured.

Telephone Noise

The thermal noise in nine channels of a 600 channel telephone system were calculated from the baseband noise spectrum measured



	<u>1</u>	<u>2</u>
PASS	11	1989
DATE	5/9/63	3/13/64
TIME - UT	03:46	11:31
RANGE - SM	7623	7297
SPIN ANGLE	87.6°	118°
MEASURED CARRIER		
GRD REC	-96.0 dbm	-97.0
SAT. REC	-71.0 dbm	-69.5
NOISE TEMPERATURE	39°K	37°K
CALC. NOISE AT 1 Mc	-61.4 dbm	-60.2

Fig. 73— Baseband noise spectrum standard FM receiver— Telstar II, passes 11 and 1989.

during pass 11 directly after launch on May 9, 1963 (see page 2271). Similar calculations were made from measurements taken recently on pass 1989 (March 13, 1964). The results were discussed on page 2284. The results of both measurements are repeated below in Table X. Associated information such as range, spin angle, received carrier powers, and the noise temperature prevailing during the passes at the time of measurement are given in Figure 73.

TABLE X — TELEPHONE NOISE MEASUREMENT RESULTS

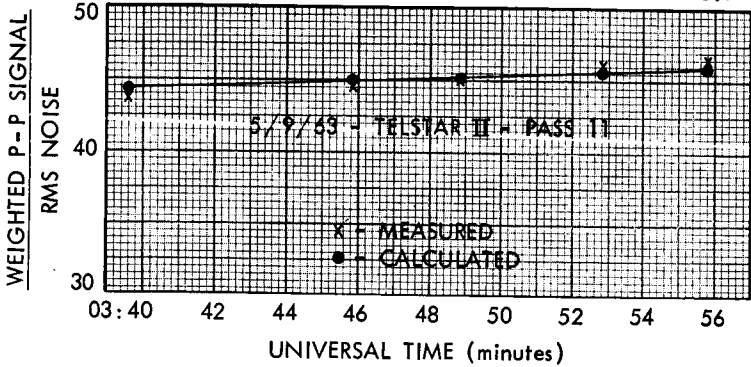
Channel Number	Group Number	Super Group Number	Frequency (kc)	Noise dbrn "C" Message Wt.	
				Pass 11	Pass 1989
12	5	2	548-552	39.1	40.0
1	1	3	800-804	42.3	42.8
1	1	4	1048-1052	44.6	44.8
1	1	5	1296-1300	46.6	46.5
1	1	6	1544-1548	48.1	47.9
1	1	7	1792-1796	49.5	49.2
1	1	8	2040-2044	50.7	50.1
1	1	9	2288-2292	51.7	51.2
1	1	10	2536-2540	52.7	51.8

The slight differences ( $\pm 0.9$  db) between the noise measured in each pass can be accounted for by the slightly different transmission characteristic, the differences in range and spin angle, and to measurement error. It can be included that no significant change in channel noise can be attributed to a change in satellite performance.

#### Television Noise

The results of weighted peak-to-peak signal to rms noise measurements made on Telstar II directly after launch on pass 11 (May 9, 1963) and those made recently on pass 1989 (March 31, 1964) have been discussed previously. For convenience, the data obtained on passes 11 and 1989 have been replotted as a function of time with range and spin angle data as parameters in Figure 74. The upper part of the figure shows the data taken on pass 11 and the lower part of the figure shows the data taken on pass 1989. In each case, the expected value of the peak-to-peak signal-to-rms noise has been calculated based on the average values of received carrier powers determined from the range and spin angle data shown in the figure, the noise temperature

RANGE (SM)	7962	7561	7354	7130	6903
SPIN ANGLE	82.2°	87.6°	91.2°	94.0°	96.9°



RANGE (SM)	8385	7974	7495	6945
SPIN ANGLE	102.3°	108.8°	115.5°	122.6°

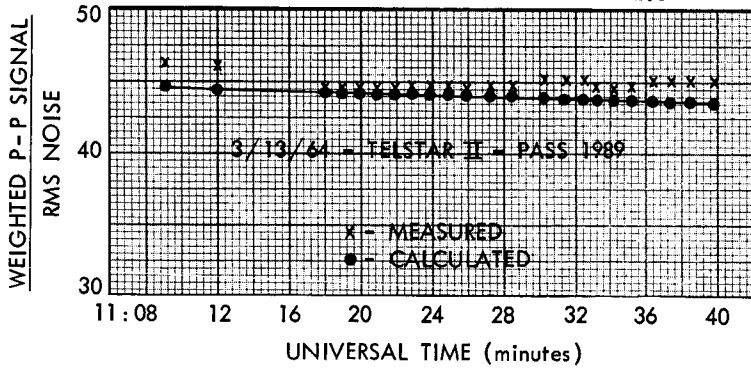


Fig. 74 — Weighted television signal-to-noise ratio — Telstar II, passes 11 and 1989.

measured during the pass and an assumed satellite noise figure of 13 db. Comparison of the expected and measured values shows good agreement in each case. Since both passes show good agreement with the expected theoretical values, it can be concluded that the satellite performance has not changed in this respect since launch.

## *Nonlinearity*

### Envelope Delay Distortion

The results of envelope delay distortion measurements made on Telstar II directly after launch on pass 5 (May 8, 1963) and those made recently on pass 2255 (April 24, 1964) have been discussed on pages 2272 and 2287. A comparison of the unequalized envelope delay distortion measured on each pass can be made by comparing Figure 6 with the top portion of Figure 20. As can be seen from the figures no change in the unequalized envelope delay distortion characteristics has taken place since the launch of Telstar II. It can therefore be concluded that the satellite contributions to the over-all envelope delay distortion of the system have not changed during the interval between tests.

### Differential Phase and Gain.

Measurements of differential phase and gain made on pass 17 shortly after launch at 02:15 and 02:18 UT on May 10, 1964 and the measurements made recently on pass 1804 on February 13, 1964 have been discussed. A comparison of the differential phase and gain measured on the satellite loop on pass 17 (Figures 9 and 10) with the differential phase and gain measured on the satellite loop on pass 1804 (Figures 23 and 24) indicates good agreement between the measurements. It can therefore be concluded that no change in the satellite contribution to the differential phase and gain has been measured since launch.

### *Video Tests*

Video transmissions over Telstar II photographed directly after launch on passes 4 and 5 (May 7, 1963) and test patterns photographed recently on pass 2282 (April 28, 1964) have been discussed on page 2291. A comparison of the results indicates no change in the satellite has taken place in the interval between tests. Figure 75 shows the monoscope test pattern received from the satellite on pass 4, May 7, 1963. Figures 76 and 77 show the same monoscope test pattern received on pass 2282, April 28, 1964. The circuits used when each photograph was taken were identical. The circuit was in each case a satellite loop which included the FM feedback receiver with video-audio diplexers and 3.5 Mc linear phase filters. Figure 76 is an oscilloscope presentation while 77 is a monitor presentation of the same

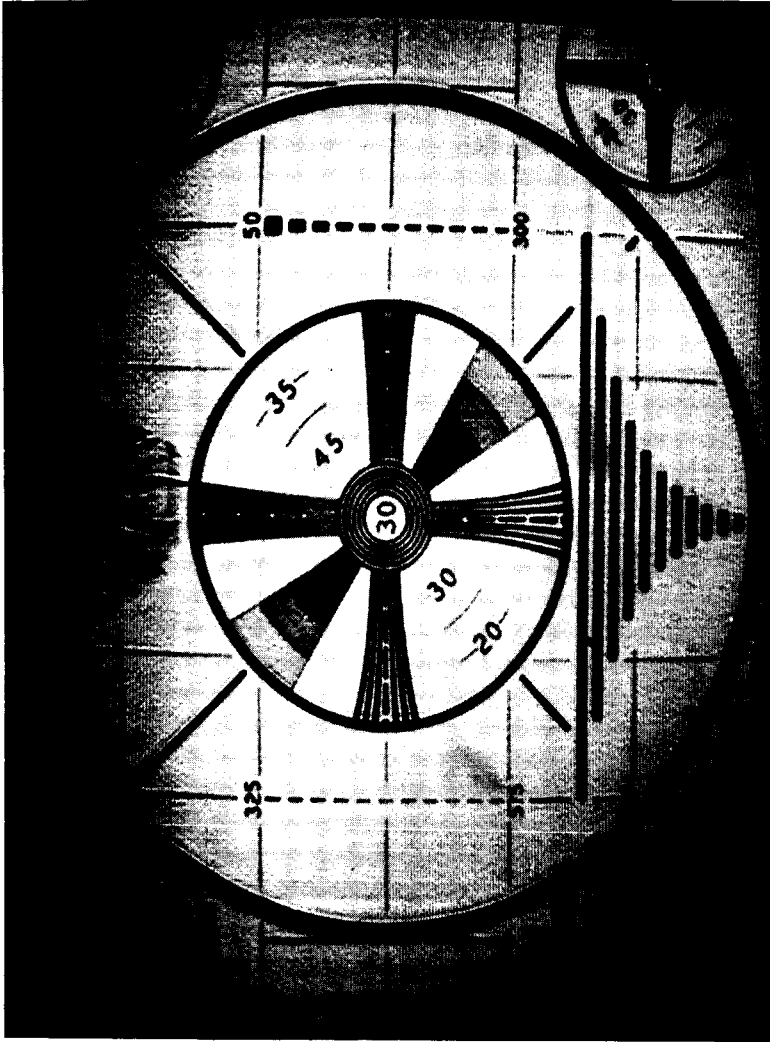


Fig. 75 — Monoscope video transmission — Andover to Telstar II to Andover — Telstar II, pass 4, May 7, 1963.

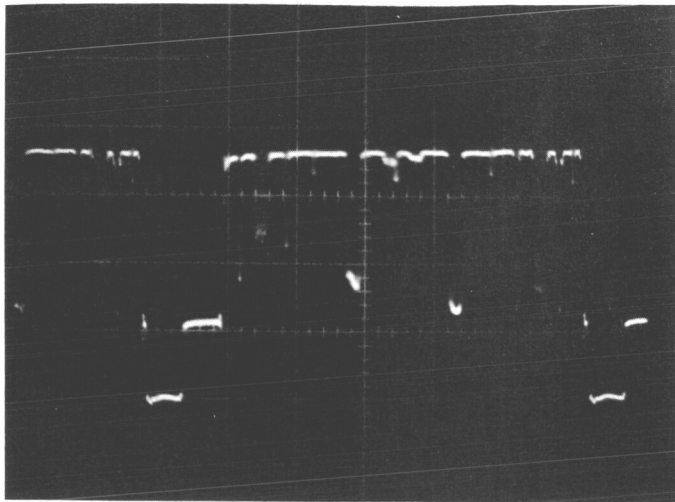


Fig. 52—Monoscope test pattern, IF loop, with diplexers, standard FM receiver; vertical calibration: 4 div = 1 volt. Telstar II, pass 2282, April 28, 1964.

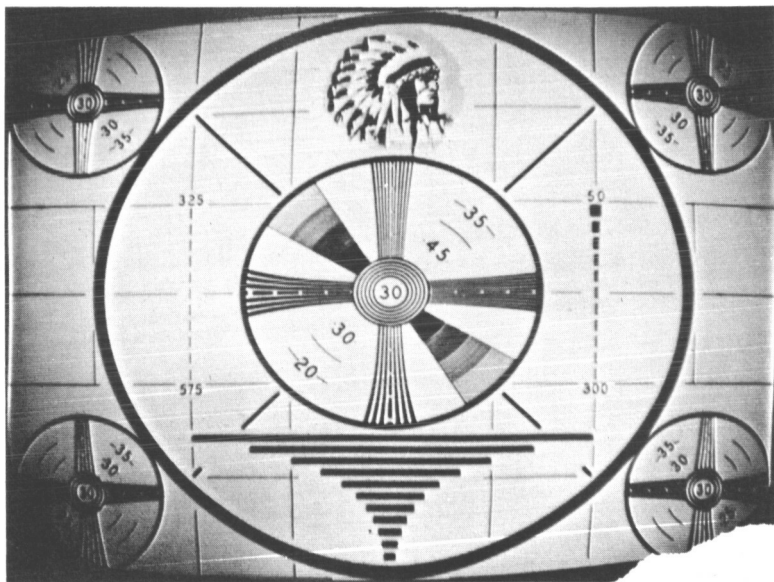


Fig. 53—Monoscope test pattern, IF loop, with diplexers, standard FM receiver. Telstar II, pass 2282, April 28, 1964.

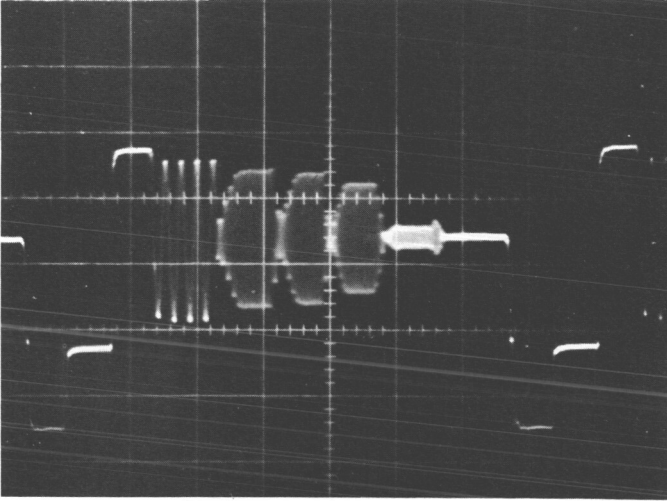


Fig. 54—Multiburst test pattern, IF loop, with diplexers, standard FM receiver; vertical calibration: 4 div = 1 volt. Telstar II, pass 2282, April 28, 1964.

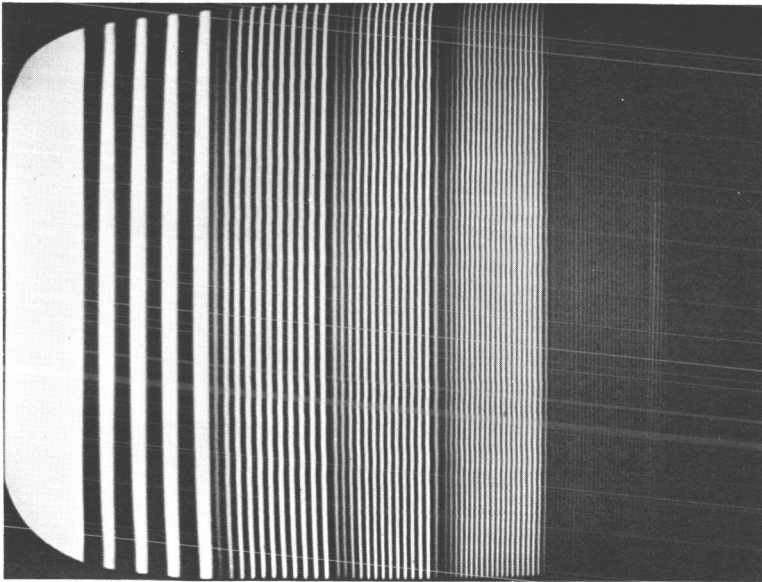


Fig. 55—Multiburst test pattern, IF loop, with diplexers, standard FM receiver. Telstar II, pass 2282, April 28, 1964.

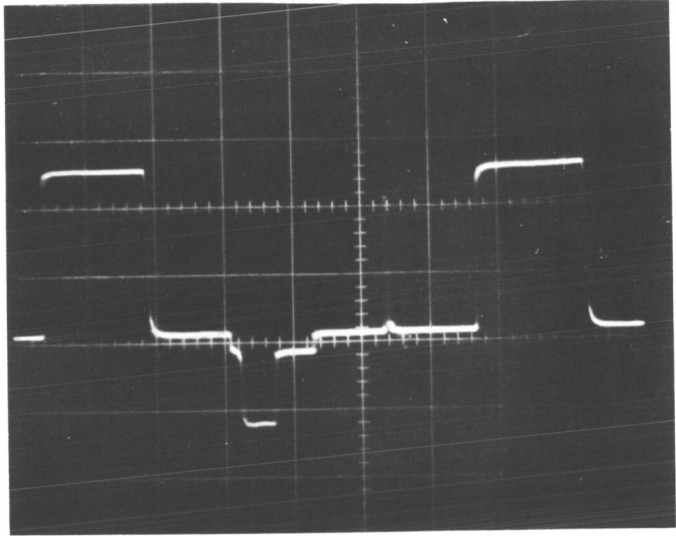


Fig. 56— $\text{Sin}^2$  window test pattern, IF loop, with duplexers, standard FM receiver; vertical calibration: 4 div = 1 volt. Telstar II, pass 2282, April 28, 1964.

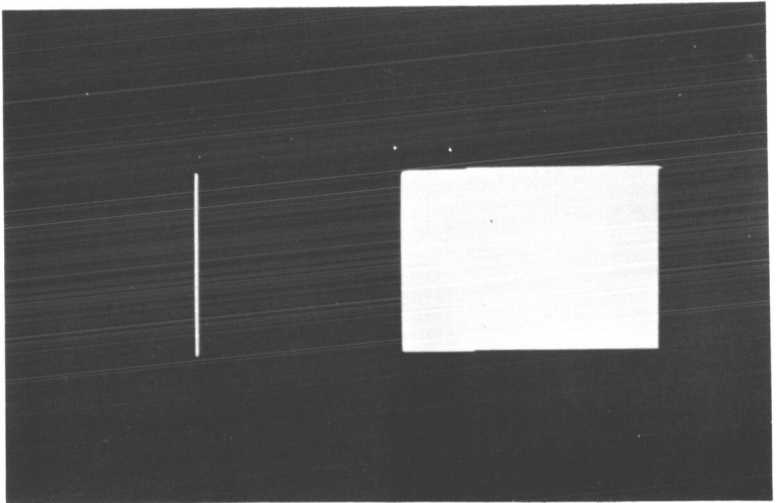


Fig. 57— $\text{Sin}^2$  window test pattern, IF loop, with duplexers, standard FM receiver. Telstar II, pass 2282, April 28, 1964.

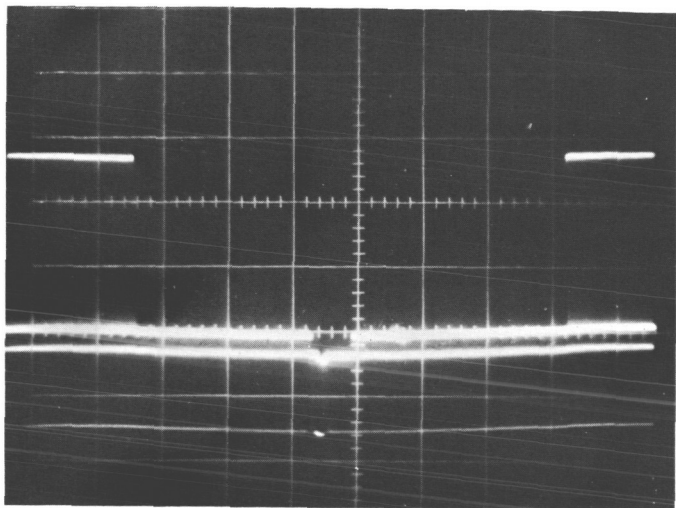


Fig. 58— $\text{Sin}^2$  window test pattern, IF loop, with diplexers, standard FM receiver; vertical calibration: 4 div = 1 volt. Telstar II, pass 2282, April 28, 1964.

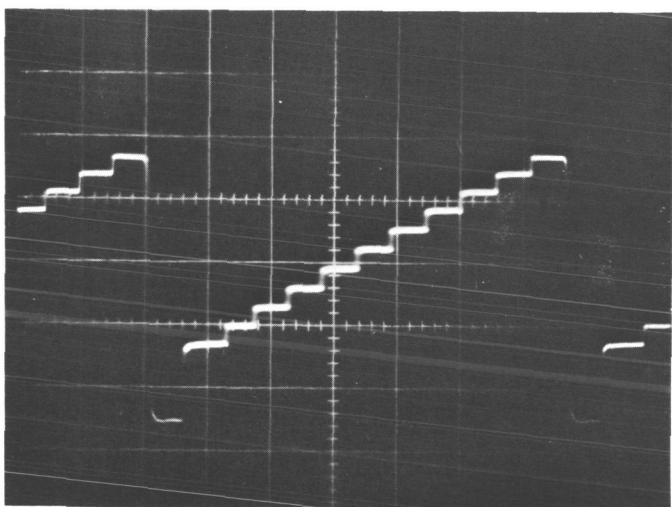


Fig. 59—Stairstep test pattern, IF loop, with diplexers, standard FM receiver; vertical calibration: 4 div = 1 volt. Telstar II, pass 2282, April 28, 1964.

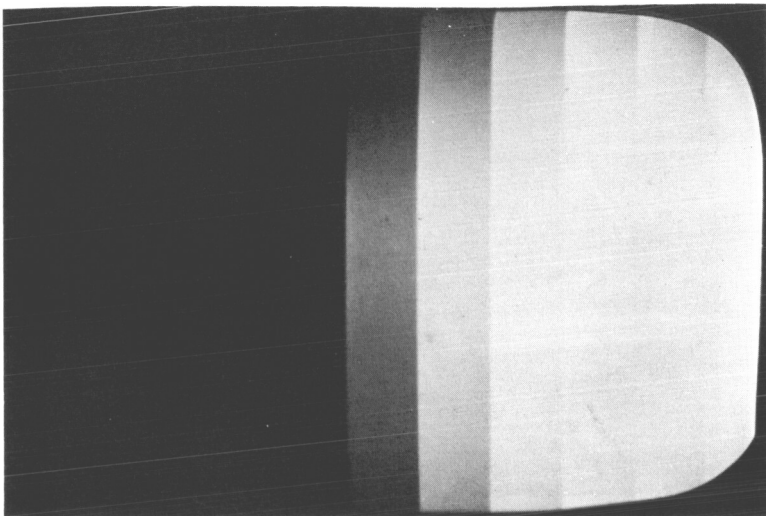


Fig. 60 — Stairstep test pattern, IF loop, with diplexers, standard FM receiver. Telstar II, pass 2282, April 28, 1964.

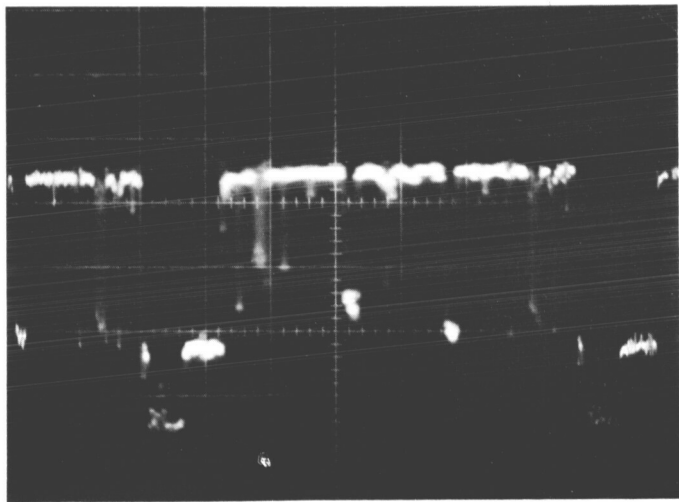


Fig. 61 — Monoscope test pattern, satellite loop, with diplexers, standard FM receiver; Vertical Calibration: 4 div = 1 volt, 06:46:45 UT, 7466 SM. Telstar II, pass 2282, April 28, 1964.

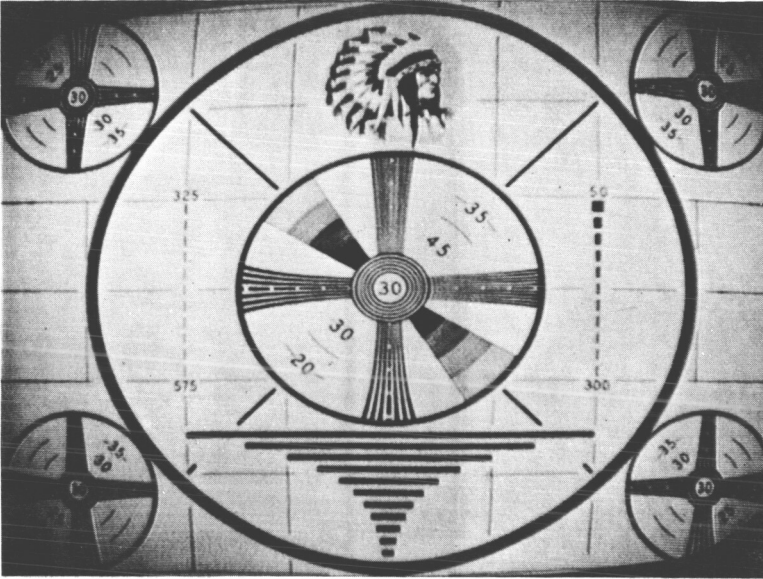


Fig. 62 — Monoscope test pattern, satellite loop, with diplexers, standard FM receiver. 06:46:45 UT, 7466 SM. Telstar II, pass 2282, April 28, 1964.

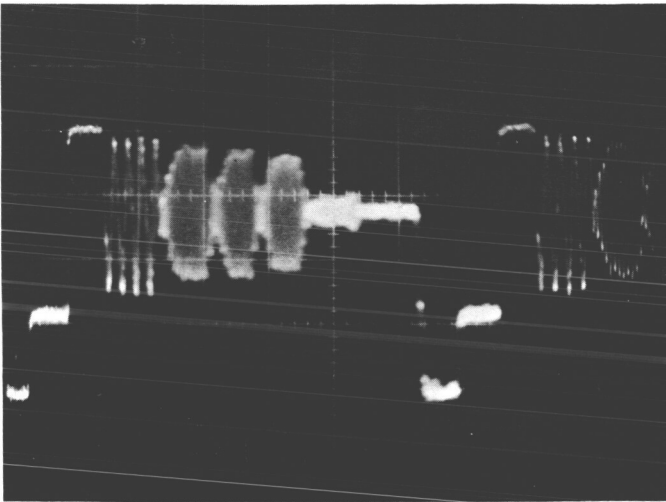


Fig. 63 — Multiburst test pattern, satellite loop, with diplexers, standard FM receiver; vertical calibration: 4 div = 1 volt, 06:48:40 UT, 7456 SM. Telstar II, pass 2282, April 28, 1964.

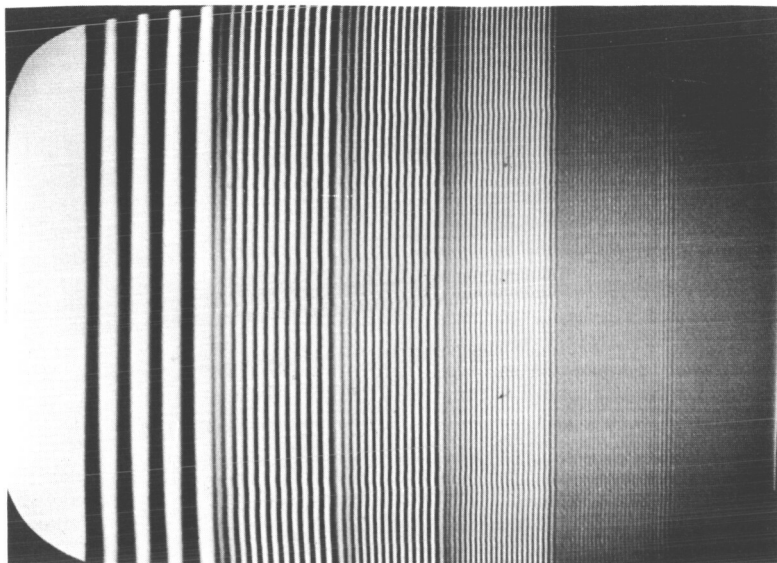


Fig. 64 — Multiburst test pattern, satellite loop, with diplexers, standard FM receiver. 06:48:50 UT, 7456 SM. Telstar II, pass 2282, April 28, 1964.

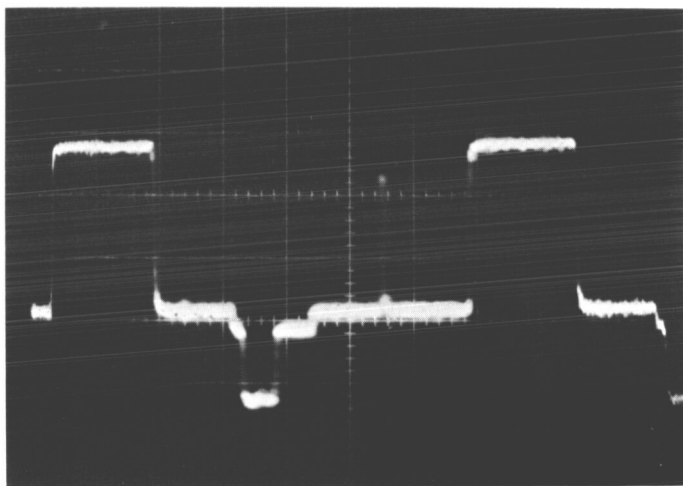


Fig. 65 —  $\text{Sin}^2$  window test pattern, satellite loop, with diplexers, standard FM receiver; vertical calibration: 4 div = 1 volt. 06:50:10 UT, 7452 SM. Telstar II, pass 2282, April 28, 1964.

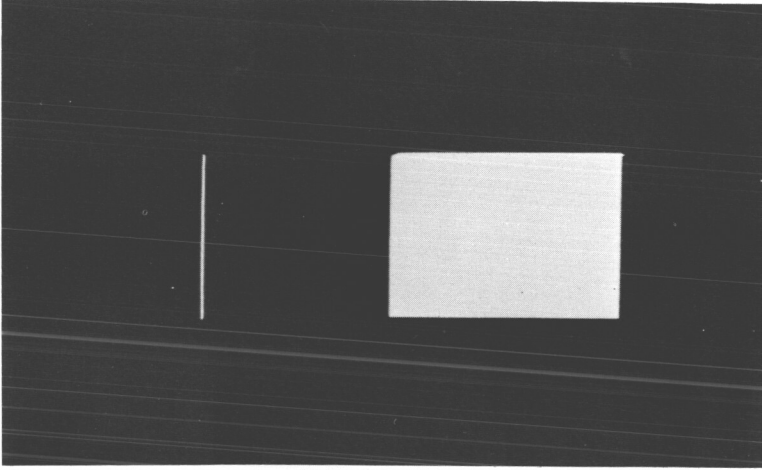


Fig. 66 —  $\text{Sin}^2$  window test pattern, satellite loop, with diplexers, standard FM receiver. 06:50:10 UT, 7452 SM. Telstar II, pass 2282, April 28, 1964.

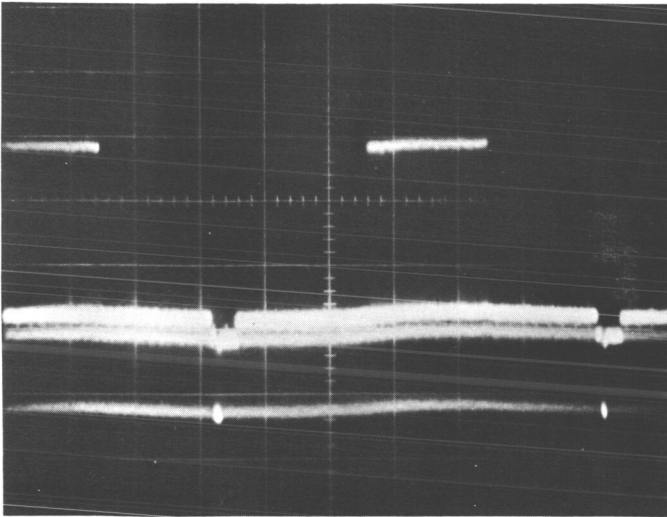


Fig. 67 —  $\text{Sin}^2$  window test pattern, satellite loop, with diplexers, standard FM receiver; vertical calibration: 4 div = 1 volt. 06:50:00 UT, 7452 SM. Telstar II, pass 2282, April 28, 1964.

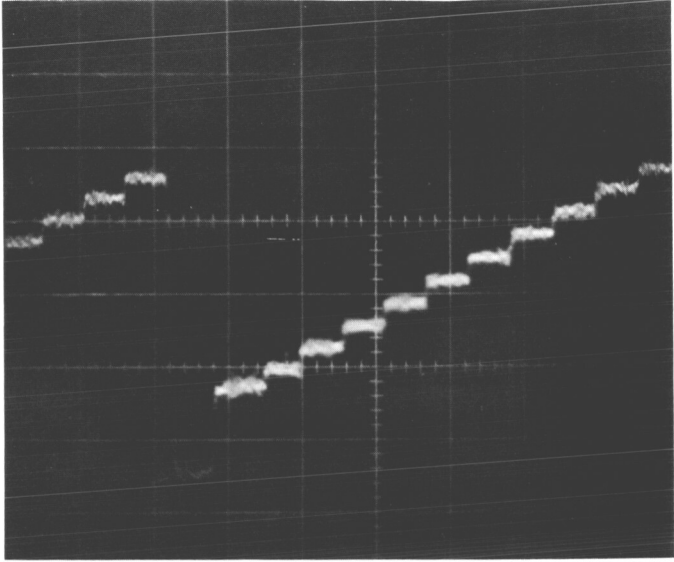


Fig. 68—Stairstep test pattern, satellite loop, with diplexers, standard FM receiver; vertical calibration: 4 div = 1 volt. 06:52:30 UT, 7436 SM. Telstar II, pass 2282, April 28, 1964.

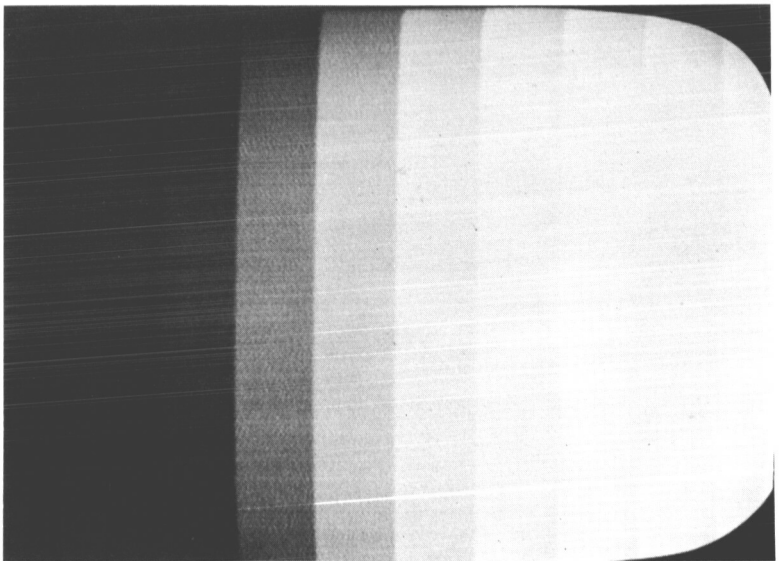


Fig. 69—Stairstep test pattern, satellite loop, with diplexers, standard FM receiver. 06:52:30 UT, 7436 SM. Telstar II, pass 2282, April 28, 1964.

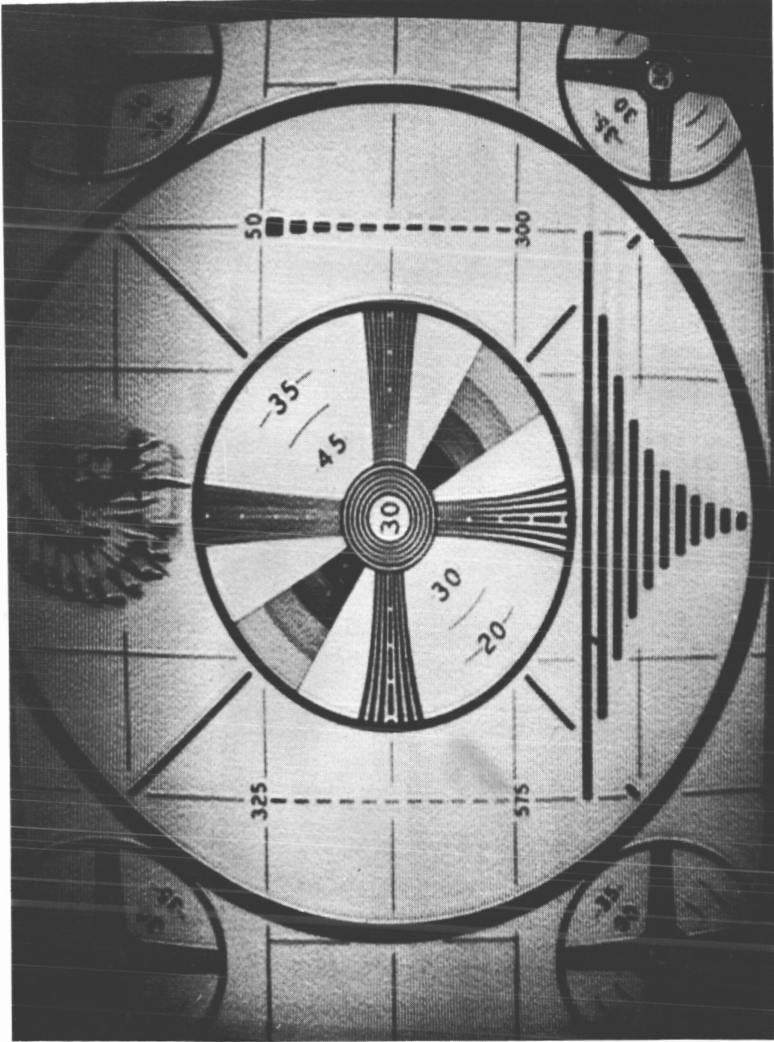


Fig. 75 — Monoscope video transmission — Andover to Telstar II to Andover — Telstar II, pass 4, May 7, 1963.

pattern. Comparing Figures 77 and 75 resulted in the conclusion that the satellite performance at present is the same as it was directly after launch.

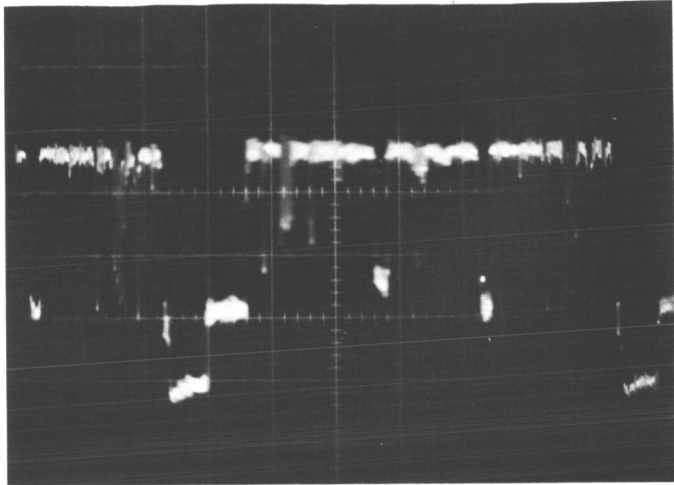


Fig. 76— Monoscope test pattern, satellite loop, with diplexers, FMFB receiver; calibration: 4 div = 1 volt. 07:06:00 UT, 7300 SM. Telstar II, pass 2282, April 28, 1964.

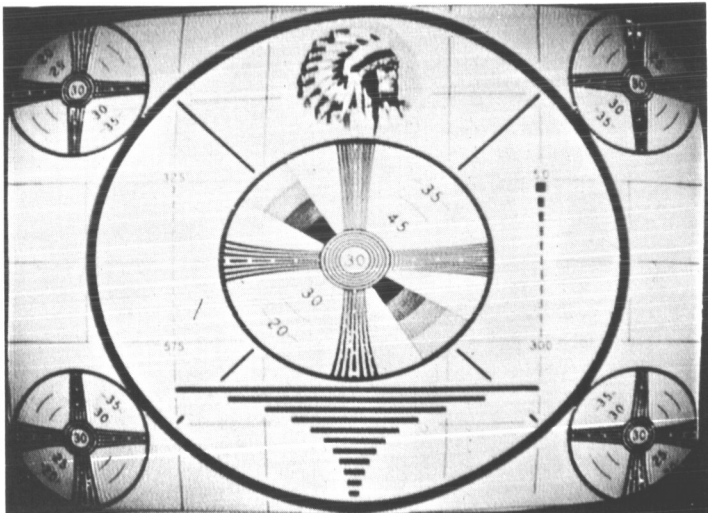


Fig. 77— Monoscope test pattern, satellite loop, with diplexers, FMFB receiver. 07:06:00 UT, 7300 SM. Telstar II, pass 2282, April 28, 1964.

## TELSTAR II RADIATION EXPERIMENTS — PRELIMINARY RESULTS

*Introduction*

## General

This section gives a preliminary description of the distribution of several classes of energetic particles mapped out by the particle-radiation experiments on Telstar II, and compares the distributions with those obtained from Telstar I. The integral radiation exposure of Telstar II is also calculated and compared with that of Telstar I. The radiation damage effects, which were observed directly in the solar power plant and in the radiation damage experiments are presented and compared with the damage to be expected on the basis of the orbital integrals.

## Charged Particle Experiments

The charged particle experiments on Telstar II (Table XI) are basically the same as those on Telstar I (Reference 1). The lower energy threshold of the electron detector on Telstar II was moved up so that it would measure directly the intensity of electrons capable of damaging the solar cells or penetrating the canister, and the detector was made omnidirectional. The energy range over which the intermediate energy proton detector is effective was moved from the 26-34 Mev range covered in Telstar I to 18-28 Mev in order to get additional spectral information. The low and high energy proton experiments were not changed although the corresponding detectors differed somewhat in calibration. In addition some minor improvements were made in the circuits and telemetry.

The Telstar II particle radiation results presented here were reduced from the 370 hours of telemetry acquired between days 127 and 197, 1963 (May 7 and July 16, 1963).

## Radiation Damage Experiments

The radiation damage experiments were the same on Telstar II as on Telstar I. Results are presented from approximately 300 days in orbit.

*Particle Experiments*

## General

*Coordinates.* The relevant coordinates for a given datum point are: the kind of particle; the particle energy  $E$ ; the flux  $F$ ; the time  $t$  at which the measurement was made; and the position,  $B-L$  or  $R-\lambda$ , in magnetic coordinates.

TABLE XI — ORBITAL PARAMETERS AND THE PARTICLE RADIATION EXPERIMENTS FOR TELSTARS I AND II

	<u>TELSTAR I</u>	<u>TELSTAR II</u>
Launched	JULY 10, 1962 (DAY 191)	MAY 7, 1963 (DAY 127)
Apogee (NM)	3043	5830
Perigee (NM)	512	530
Inclination	44.8°	42.8°
Particle Energies from Various Particle Experiments		
Electrons	SEMIDIRECTIONAL >215 kev >315 >420 >660	OMNIDIRECTIONAL > 750 kev > 900 >1200 >1400
Protons, omnidirectional	26 - 34 Mev > 50	18 - 28 Mev > 50
Protons, semidirectional	2.5 - 25 Mev IN 9 RANGES	2 - 30 Mev IN 9 RANGES

The location of a flux measurement is given in magnetic coordinates because the flux is governed by the magnetically determined charged particle orbits. The best magnetic coordinates in current use are the  $B$ - $L$  and  $R$ - $\lambda$  sets proposed by McIlwain (Reference 2). Values of  $B$  and  $L$ , and  $R$  and  $\lambda$  are arrived at as follows. The actual magnetic field of the earth is mapped onto a dipole field using the adiabatic invariants of the particle motion. Because the dipole field has axial symmetry, and symmetry about the equatorial plane, a quarter of a meridian plane gives a complete representation. Position in this quarter plane may be specified using either the magnetic dipole coordinates  $R$  and  $\lambda$  or the magnetic shell coordinates  $B$  and  $L$ . In the  $R$ - $\lambda$  set,  $R$  is the distance from the center of the dipole and is measured in earth radii,  $R_e$ , and  $\lambda$  is the latitude angle in degrees (Figure 78). In the  $B$ - $L$  set,  $L$  is the magnetic shell parameter, which is the distance, in earth radii, of a magnetic line of force from the dipole in the dipole equatorial plane; and  $B$  is the magnetic induction (field strength) in gauss. The  $R$ - $\lambda$  coordinates resemble geographic coordinates and will

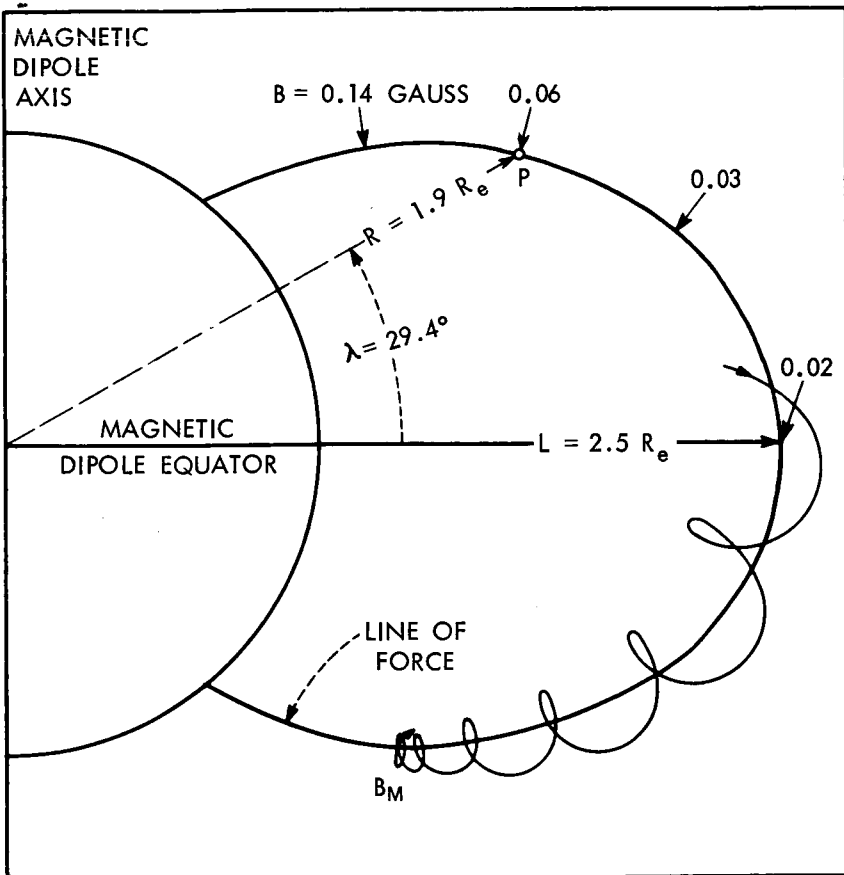


Fig. 78 — The motion of a charged particle trapped in a dipole magnetic field. The particle is confined near the magnetic shell  $L = 2.5 R_e$  and is mirroring at field strength  $B_m$ . The  $B$ - $L$  coordinates of the point  $P$  are  $B = 0.06$  gauss and  $L = 2.5 R_e$ . The  $R$ - $\lambda$  coordinates of the point  $P$  are  $R = 1.9 R_e$  and  $\lambda = 29.4^\circ$ .

be preferred in the following discussion because their meaning is intuitively more obvious.

*Treatment of the Data.* The data reduction procedure for Telstar II as indicated in Figure 79 is completely analogous to that for Telstar I (Reference 3). An omnidirectional counting rate (OCR) is calculated for the high and intermediate energy proton channels, and each of the nine low-energy proton channels, and four electron channels. From a knowledge of the satellite ephemeris, spin axis orientation, counter calibration, and the time, the various other coordinates are

associated with the OCR. The OCR is proportional to the flux. The constant of proportionality is the detector efficiency, which depends on the energy spectrum of the particles. Because the energy spectrum of the protons and electrons being measured varies with both time and position in the radiation belts, the detector efficiency also varies. For this reason some of the results will be presented in terms of the OCR, which represents the data directly, and will be converted to flux where necessary at a later stage in the analysis. The experimental uncertainties of the detector calibrations leave an uncertainty in the derived flux which may be as large as a factor of 1.5.

*Presentation of the Reduced Data.* The procedure described in the above paragraph leads to a description of the radiation belts in terms of the coordinates enumerated above. As a simple analytical expression for the belts is not presently known, the description is presented graphically. There are, however, more coordinates than can be plotted simultaneous. Therefore a variety of graphs have been made, plotting against two of the coordinates, using one or more as parameters in the plot, and fixing the values of the remainder in the way that seems most reasonable. The various plots are described in detail in Reference 3.

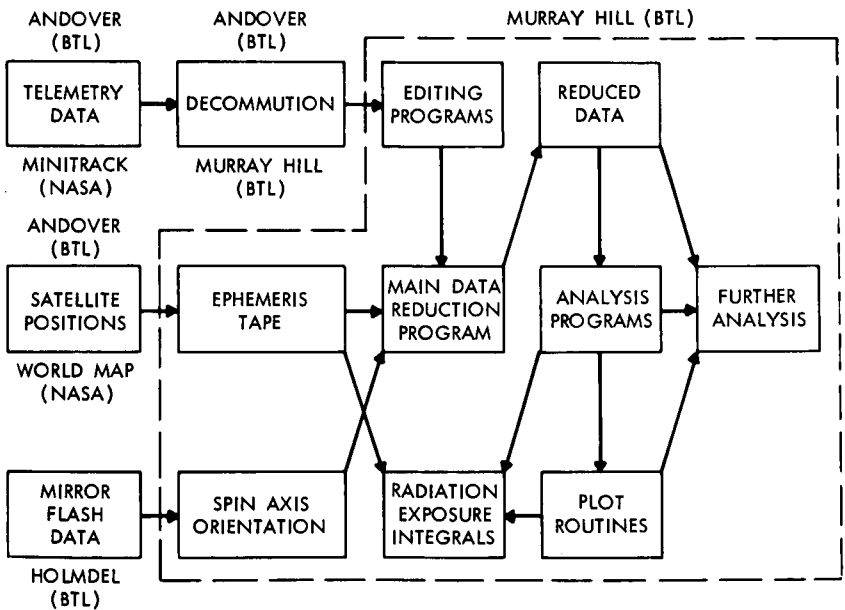


Fig. 79 — The reduction procedure for the particle radiation data.

## Results of the Electron Experiments

The results of the electron experiments on Telstar I (Reference 3) were referred to electron channel 3, which was most sensitive to electrons with energies between 420 and 640 kev but retained significant sensitivity to electrons with energies between 640 kev and 1000 kev and above. For simplicity these electrons shall be referred to as those above 0.5 Mev. The results of the electron experiments on Telstar II will likewise be referred to channel 3, but on Telstar II channel 3 is primarily sensitive to electrons with energies greater than 1.2 Mev. The results from the two satellites cannot be compared without taking the energy spectrum of the electrons into account. This spectrum varies dramatically with space and time as was shown by measurements on Telstar I (Reference 3), Explorer XV (References 4 and 5), and other satellites. However, the differential spectrum.

$$N(E) = N_0 \exp -(E/E_0), \quad (1)$$

where

$N(E)$  = the number of electrons with energies  
between  $E$  and  $E + dE$  Mev,

$E_0$  = 1.2 Mev,

and

$N_0$  = constant

gives a good fit to measurements in the center of the inner belt and a reasonable fit in the center of the outer belt (Reference 6). This spectrum is used to correlate the Telstar I and II results even though it is only approximately correct and is clearly much too hard a spectrum to apply to the region of the slot between the inner and outer belts on most occasions.

*Temporal Variations.* A record of the spacial distribution of electrons above 0.5 Mev between July 10, 1962 and February 21, 1963 was obtained from Telstar I. After about 200 days in orbit this detector began to show signs of radiation damage, and results obtained after the early part of December, 1962 have not been presented. Telstar II took up the record on May 7, 1963, measuring electrons above 1.2 Mev and is still returning data. Figure 80 is a plot of the omnidirectional flux of electrons with energies greater than 0 Mev (the spectrum of Equation 1 is assumed) against time for three small regions of space. The record is not complete because the orbits of the satellites take

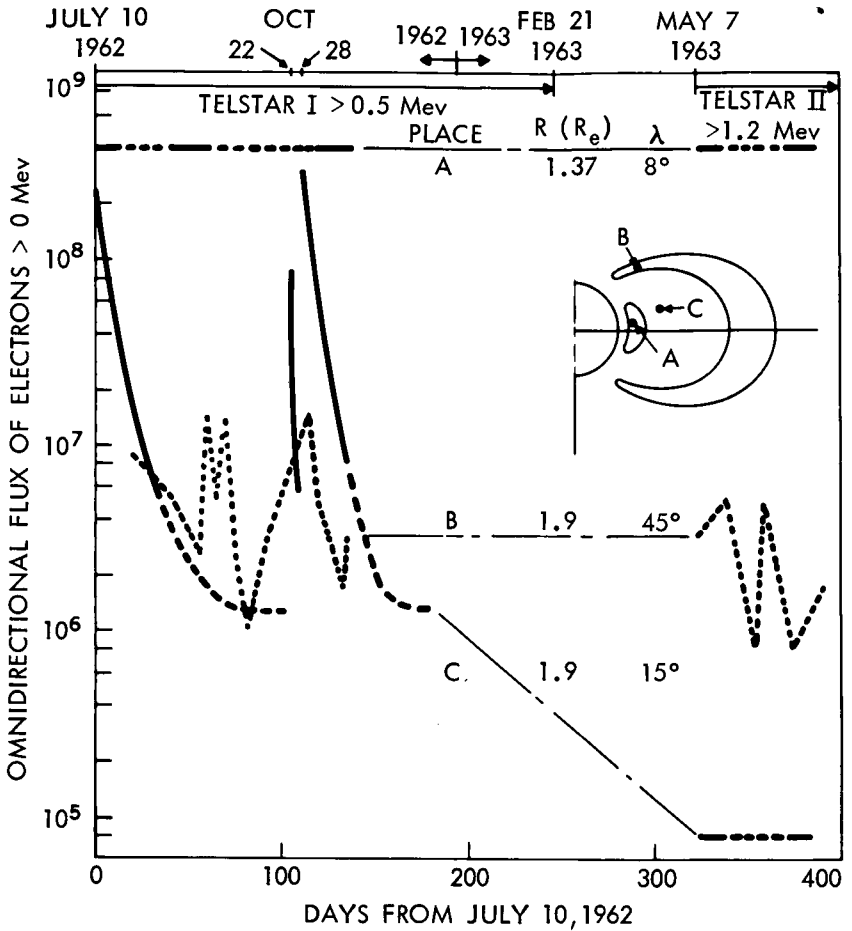


Fig. 80—The electron flux versus time for three positions in space (see inset). The flux has been normalized to flux above 0 Mev using the spectrum  $N(E) = N_0 \exp(-E/1.2 \text{ Mev})$ .

them through the three specified regions only during certain intervals of time. This point is discussed in more detail on page 3348. Point A, Figure 80 (inset), with coordinates  $R = 1.37 R_e$  and  $\lambda = 8^\circ$  is near the center of the inner belt. Here, within the accuracy of the measurements, detector calibrations, and the spectral correction no change in intensity over a period of a year has been observed (Reference 7). These electrons are believed to be the residue of the Starfish nuclear test of July 9, 1962. In contrast, the flux at point B ( $R =$

$1.9 R_e$ ,  $\lambda = 45^\circ$ ) near the tip of the horn of the outer belt has fluctuated by more than an order of magnitude. The changes in slope of curve *B* represent points at which occasional samples of the intensity in this region were obtained and the curve is not to be taken as a continuous record. There is undoubtedly some correlation between the fluctuations in this region and solar and magnetic disturbances, but the mechanism is not yet understood. The most violent fluctuations in intensity have been observed to occur in the slot between the inner and outer belts. Point *C*, at  $R = 1.9 R_e$  and  $\lambda = 15^\circ$  is typical of this region. When Telstar I was launched the slot was full of electrons, presumably from the Starfish test of the previous day (Reference 8). These electrons decayed rapidly and after about 90 days the intensity at point *C* seemed to have reached equilibrium two orders of magnitude below its initial value. The Russian nuclear tests of October 22, and 28, 1962 increased the intensity again and on October 28 it was two and a half orders of magnitude higher than the previous week. The electrons injected by the Russian tests decayed faster than the electrons observed immediately after July 10, and equilibrium appeared to have been reached by early December. Up to July 21, 1963 Telstar II had observed no activity near point *C*. As noted earlier, the spectral correction assumes an energy spectrum which is too hard for the slot. This results in an underestimate of the number of lower energy electrons between the inner and outer belts when Telstar II data are used, and is at least partially responsible for the fact that the intensity at point *C* as calculated from Telstar II data is a factor of 20 smaller than the "equilibrium" estimate arrived at using the data from Telstar I.

*Flux Map.* The Telstar II data for electrons with energies above 1.2 Mev have been used to create a map of the electron belts, Figure 81. The plotting coordinates are  $R$  and  $\lambda$ , and intensity appears as a parameter in the plot. In the data for the first 70 days in orbit the inner belt was quite stable and the outer belt shows normal short-term fluctuations. Figure 82 is representative of the flux distribution over this period. The Telstar I data (heavy lettered contours) as taken from Figure 9 of Reference 3 are shown for comparison. They are representative of the quasi equilibrium period immediately preceding the Russian high altitude nuclear test on October 22, 1962. Equation 1 is used again in comparing the Telstar II results to those of Telstar I.

The center of the inner belt (contour 1), during May, June, and July of 1963 was located at an  $R$  of about  $1.32 R_e$  and had an omnidirectional intensity of about  $7 \times 10^8$  electrons/cm<sup>2</sup>-sec above 0 Mev.

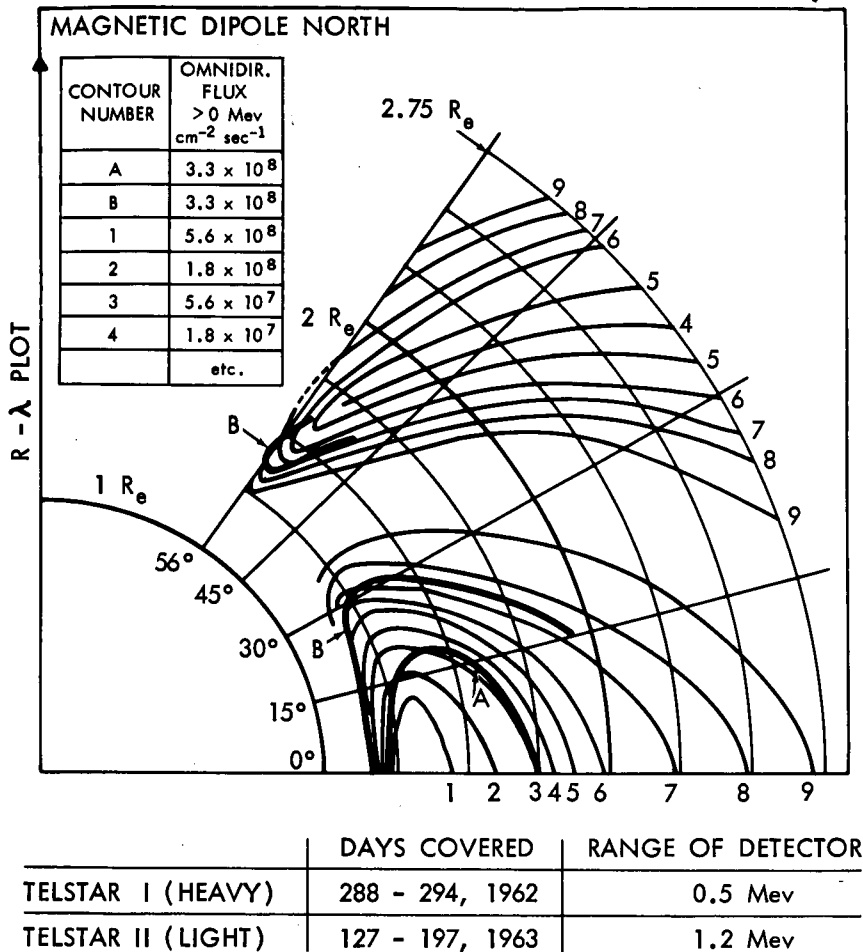


Fig. 81 — Isointensity contours for electrons from Telstar I and II data. The flux has been normalized to flux above 0 Mev using the spectrum  $N(E) = N_0 \exp(-E/1.2 \text{ Mev})$ .

In mid-October of 1962 the center of the inner belt was at  $R$  of about  $1.45 R_e$  and the intensity was about  $8 \times 10^8$  electrons/cm<sup>2</sup>-sec above 0 Mev. The difference in intensity is not significant as it is well within the uncertainties of the measurements. Lower energy electrons have their flux maxima at higher altitudes than higher energy electrons, presumably because the higher energy electrons are less easily scattered by the residual atmosphere at low altitudes. This fact must be par-

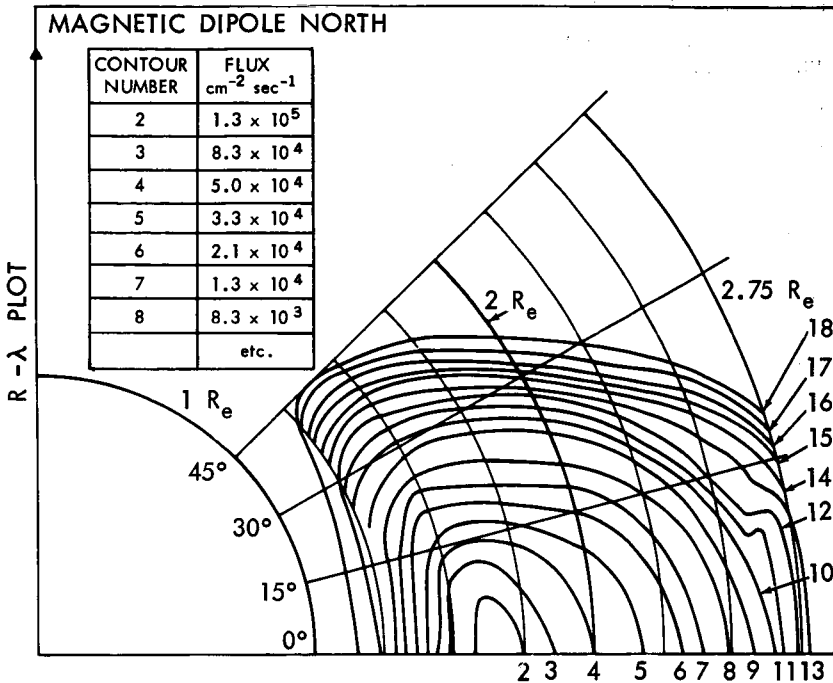


Fig. 82 — Isointensity contours for protons with energies greater than 50 Mev. Data are from Telstar I and II.

tially responsible for the difference in the locations of the Telstar I and II electron maxima. However, the outer slope of the inner belt was still contracting in October of 1962, and a continued contraction would contribute to a decrease in the altitude of the maximum flux. Figure 5-4 also shows that the outer slope of the inner belt flux mountain is much steeper during the early summer of 1963 than during the early fall of 1962. Part of this greater steepness must be assigned to a softening of the energy spectrum with increasing  $R$  coupled with the different effective energy sensitivities of the detectors as noted in the discussion of curve C of Figure 80. However, a continued contraction of the inner belt would also steepen the outer slope and this is undoubtedly contributing to the observed difference in the falling off of the flux as one proceeds towards the center of the slot.

On Day 264, 1963 (September 21) a magnetic storm increased the

electron intensity by a factor of about 10 in the near equatorial region ( $B < .05$  gauss) between  $L = 2.6$  and  $3.4 R_e$ . The orbital configuration was that of Figure 90 at this time. Therefore, no observations from the equatorial regions between  $L = 1.5$  and  $2.6 R_e$  are available. The electron intensity between  $L = 2.6$  and  $3.4 R_e$  returns to its earlier value over a period of about six weeks.

### Results of the Proton Experiment

*General.* The proton measurements from the Telstar satellites have two features in common:

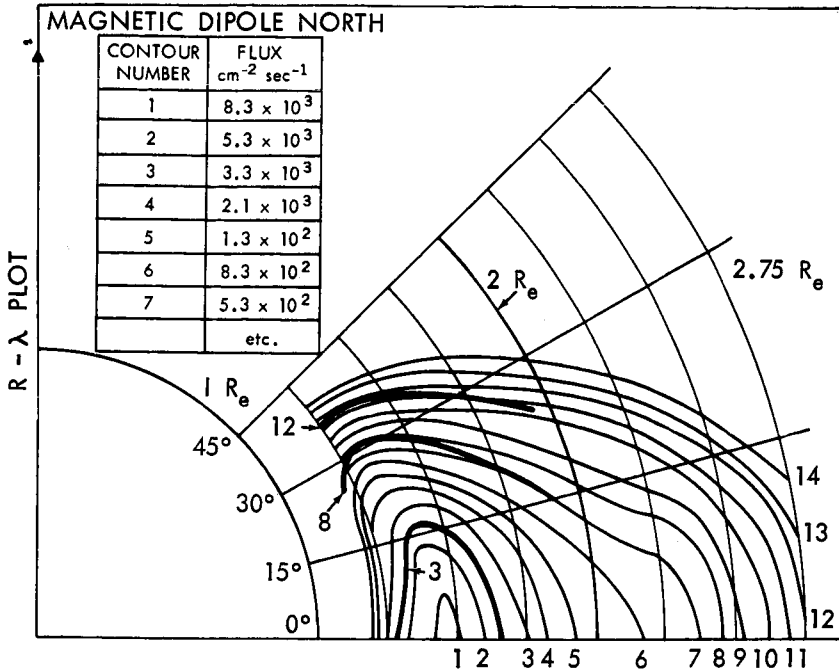
They show no gross temporal variations.

With the exception of the low energy proton detector whose behavior will be discussed separately on page 2344 below, the detectors showed no effects of exposure to the space environment during either the seven months that Telstar I returned data or the three months of Telstar II data discussed here.

These two features allowed the elimination of time as a variable. The reduction of the coordinate space by one dimension provides a major simplification in the results. It also permits the construction of more accurate contour maps as there is no need to keep separate data taken at times far apart, an important consideration in regions where data are sparse.

*Flux Map for Protons with Energies Above 50 Mev.* The data from the high energy proton detector on Telstar II are presented in Figure 82. The three heavy contours are Telstar I data taken from Figure 18 of Reference 3. Successive contours are only a factor of 1.6 apart in flux, a fifth of a decade on a logarithmic scale. The agreement between the two detectors is very good, and the differences are within the uncertainties of the instruments. An interesting feature is the stretching of the isointensity contours in the equatorial region toward higher altitudes for geocentric distances beyond  $2 R_e$ . This feature had previously been observed by Explorer XV (Reference 5) and could not have been predicted from the Telstar I data.

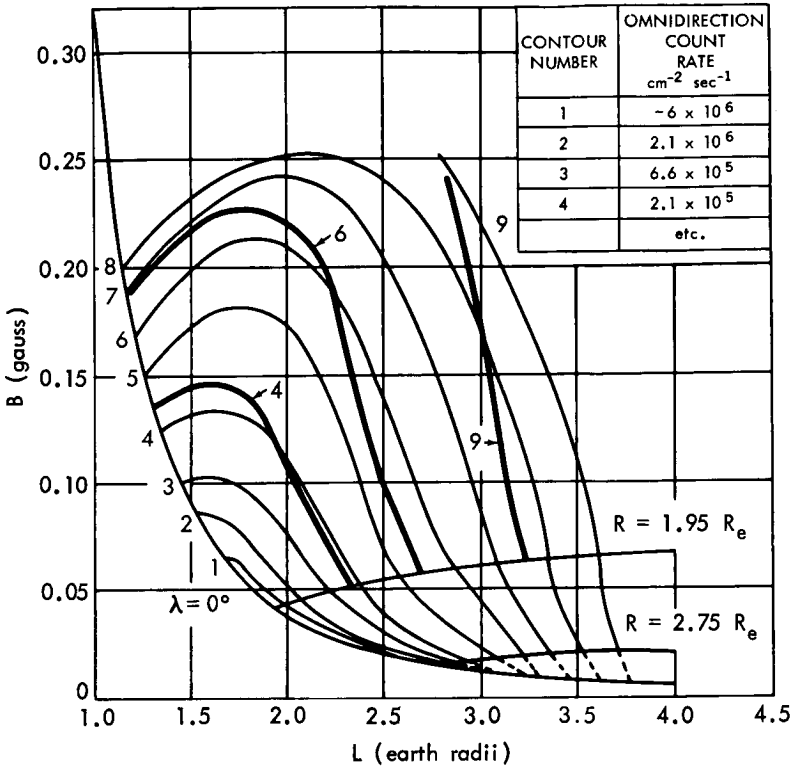
*Flux Map for Protons with Energies Between 18 and 28 Mev.* Figure 83 is a flux map made from the intermediate energy proton data received from Telstar II. As in Figure 82 the contours are separated in intensity by  $1/5$  of a decade on a logarithmic scale. The intensity falls off quite slowly with increasing altitude near the magnetic equator until a geocentric distance of about  $2.7 R_e$  is reached. Then the flux appears to begin a rapid decline with increasing altitude, but the data does not extend to high enough altitudes to say whether or not



TELSTAR I (HEAVY)	DAYS 191, 1962 - 52, 1963
TELSTAR II (LIGHT)	DAYS 127, 1963 - 197, 1963

Fig. 83— Isointensity contours for protons with energies between 18 and 28 Mev. Data are from Telstar II and were acquired between day 127 and 197, 1963. this sharp decline continues. The kinks in contours 11, 12, and 13 near  $R = 2.7 R_e$  and  $\lambda = 10^\circ$  are not well enough resolved in the data to allow any further discussion. The corresponding detector on Telstar I measured protons in the energy range from 26-34 Mev and so the contours for Telstars I and II cannot be compared directly.

*A Map of the OCR from the 4-13 Mev Channel of the Low Energy Proton Detector.* The 4-13 Mev channel (channel 9) has been selected from the nine channels of the low energy proton detector because this channel is stable over the periods of time considered, and is comparable in energy range to a low energy proton detector on Explorer XV (Reference 4). Contours of constant omnidirectional counting rate in  $B-L$  space have been plotted in Figure 84. The data are bounded by the line  $\lambda = 0^\circ$ , the projection of the magnetic equatorial plane in  $B-L$  coordinates, and the high altitude limits of Telstars I and II, which are geocentric distances of  $R = 1.95$  and  $R = 2.75 R_e$ , respectively. The contours are separated by a factor of  $\sqrt{10}$  in intensity, that is,



	TIME PERIOD (DAYS)	ENERGY (APPROX)
TELSTAR I (HEAVY)	206 - 220, 1962	4.2 - 12 Mev
TELSTAR II (LIGHT)	127 - 197, 1963	4.0 - 13 Mev

Fig. 84—Isointensity contours for protons with energies between 4 and 13 Mev. Data are from Telstar I and II.

half a decade on a logarithmic scale. The nominal energy ranges of the Telstar I and II detectors are somewhat different, and the agreement between the first 70 days of Telstar II data and the data (heavy lines of Figure 84) from the third and fourth week that Telstar I was in orbit is quite satisfactory in the region of space which is common to the orbits. The differences in OCR cannot be interpreted as signifying a secular change. The highest intensity contour from Telstar II clings to the equator as a long tongue reaching out to a geocentric distance of nearly  $2.6 R_e$ . Naive extrapolation of the Telstar I data would have predicted counting rates nearly two orders of magnitude

lower near the equator at  $R = 2.5 R_e$ , and the higher intensity indicated by Telstar II was not expected. Explorer XV (Reference 4), which monitored the radiation between  $R = 1.1$  and  $4.7R_e$  for  $\lambda \leq \pm 30^\circ$  in November and December of 1962, and January of 1963 with a detector sensitive to protons between 4 and 12 Mev, did not show this tongue of protons along the equator. The discrepancy may be caused by differences in the responses of the detectors or changes in the belts between the dates of the two measurements. An hypothesis that convincingly explains these diverse results has not yet been found.

*The Proton Energy Spectrum.* The proton energy spectrum in the radiation belts is a strong function of position at low altitudes, and is complex even at higher altitudes. To reduce the scope of the discussion only the energy spectrum in the plane of the magnetic equator is considered. Figure 85 is a plot of the proton fluxes in the equatorial plane as a function of geocentric distance. All the curves rise steeply at low altitudes as the atmospheric density decreases. The peak intensity occurs at lower altitude for the higher energy protons as predicted by theory (Reference 9) and confirmed by many measurements.

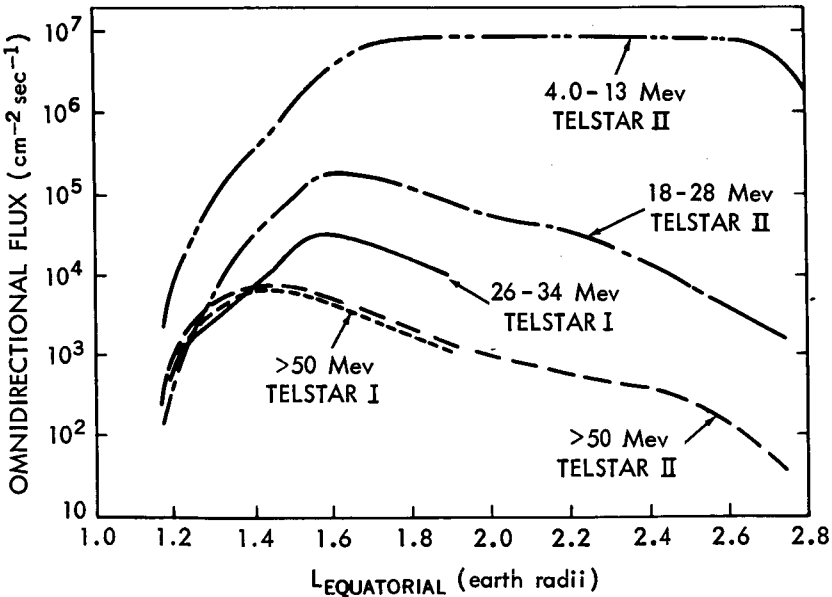


Fig. 85 — Proton fluxes in the plane of the magnetic equator as measured by Telstar I and II. (The efficiency of the 4.0-13 Mev detector is arbitrarily set equal to unity.)

With the exception of the 4 to 13 Mev protons, which have an anomalously flat peak, the intensities fall with a further increase in altitude at rates which are about equal on the average (though not in detail). The Telstar I and II data for protons above 50 Mev show very good agreement.

It is clear from Figure 85 that the differential energy spectrum falls rapidly with increasing energy at all but the lowest altitudes. A differential spectrum of the form

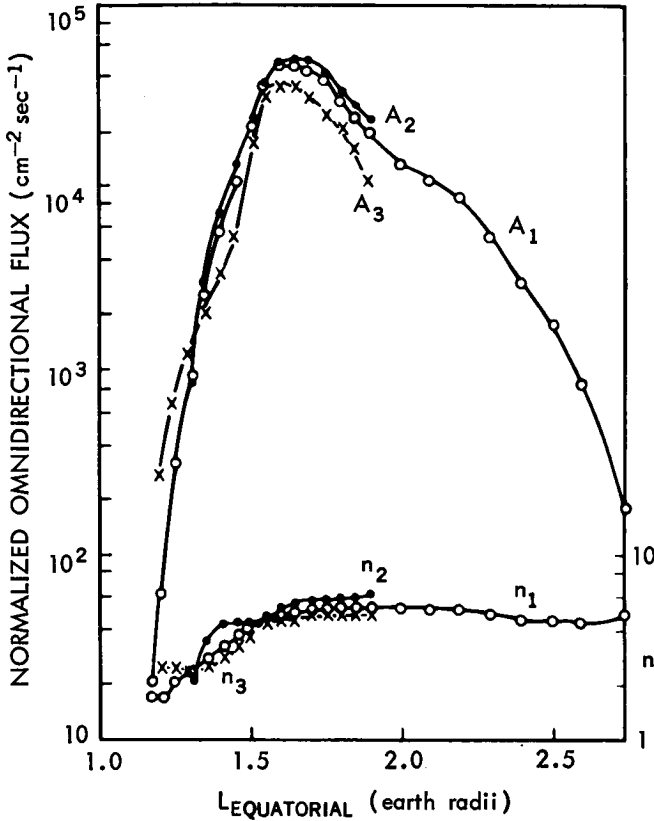
$$N(E) = A_i (E/E_0)^{-n_i} \quad (2)$$

has been fitted to the higher energy data of Figure 85. In this expression  $N(E)$  is the number of protons with energies between  $E$  and  $E + dE$ , and  $E_0$  is 18 Mev. The subscript  $i$  indicates which pair of the three higher energy channels is used to determine the constants  $A$  and  $n$ . Figure 86 is a graph of the parameters thus determined. Above a geocentric distance of about  $1.4 R_e$  the model fits the data quite well, and between about  $1.6$  and  $2.7 R_e$ ,  $n$  is nearly constant and approximately equal to 5. The values of  $A_1$ ,  $A_2$  and  $A_3$  (corresponding to the pairs indicated in the legend of Figure 86) are also in good agreement. These results indicate that a power law spectrum is a reasonable approximation to equatorial protons in this energy range between  $R \approx 1.4$  and  $2.7 R_e$ , and that  $n \approx 5$  for  $2.7 R_e > R > 1.6 R_e$ . Below  $R \approx 1.4 R_e$  the power law spectrum is not a good fit as may be concluded from the inconsistency among the values of  $n_i$  in this region.

The nominal energy ranges of the 9 low energy proton channels are listed in Table XXII. Figure 87 is a plot of 77 minutes of telemetry from this detector. The telemetry was taken by the Minitrack station at Johannesburg starting at 16:57 UT on day 127, 1963, 5 hours after Telstar II was injected into orbit. The  $\log_{10}$  (OCR) of the nine channels is plotted against time in minutes from the beginning of the pass. Note that on a log scale a difference of one division corresponds to a factor of 10 between counting rates. Each of the nine channels is read out once every three minutes, and is represented on the plot by its channel number. The solid line is the value (not the log) of the magnetic shell parameter  $L$  which may be read off the scale directly in  $R_e$ . The value of the magnetic induction  $B$  may be derived from the dotted curve by applying the scaling factor.

$$B = (\text{Ordinate} - 1)/10 \text{ gauss.} \quad (3)$$

The configuration of the channels in order of decreasing counting rate, with 7, 4, and 1 on top followed by a gap and then the remaining



i	SOURCE
1	18 - 28 Mev and 50 Mev, TELSTAR II
2	18 - 28 Mev, TELSTAR II; and 26 - 34 Mev, TELSTAR I
3	26 - 34 Mev and 50 Mev, TELSTAR I

Fig. 86—Differential energy spectra for protons in the magnetic equatorial place fitted to  $N(E) = A_1 (E/18 \text{ Mev})^{-n_1}$ .

channels except for 3, which appears below the others, is typical of a spectrum that decreases rapidly with increasing energy. Either a power law spectrum,

$$N(E) = AE^{-n},$$

or an exponential spectrum

$$N(E) = K \exp(-E/E_c),$$

TABLE XXII — NOMINAL ENERGY RANGES FOR THE 9 CHANNELS OF THE LOW ENERGY PROTON DETECTOR ON TELSTAR II

Channel	Bias	Discriminator	Nominal Energy Range (Mev)
1	Low	Low	2.8-3.2 and 4.9-7.0
2	Low	Intermediate	3.3-4.6
3	Low	High	4.0-4.1
4	Intermediate	Low	2.2-3.1 and 8.2-14
5	Intermediate	Intermediate	3.2-3.8 and 6.8-80
6	Intermediate	High	4.0-6.6
7	High	Low	2.0-3.0 and 17-30
8	High	Intermediate	3.2-3.8 and 13-16
9	High	High	4.0-13

where  $K$ ,  $A$ ,  $n$ , and  $E_c$  are constants will give rise to the observed 7, 4, 1 configuration. For an exponential spectrum the value of  $E_c$  required to fit the data in channels 1, 4, and 7 is between 0.5 and 1 Mev. With these values of  $E_c$  the exponential spectrum extrapolates in a very unreasonable way to 18 Mev, giving fluxes which are orders of magnitude too low. Extrapolating the power law spectrum to 18 Mev gives the right order of magnitude for the flux, and the discussion will be confined to this spectral form. Exponents of the power law spectra that fit the data from channels 7, 4, and 1 at a few points have been derived, Table XXIII.

The value of  $n = 3.3$  at  $L = 2.6 R_c$  from Table XXIII is derived from data close enough to the equator ( $B \approx B_0$ ) to be compared to

TABLE XXIII — EXPONENTS FOR THE POWER LAW DIFFERENTIAL ENERGY SPECTRUM (EQUATION 2) FROM THE LOW ENERGY PROTON DETECTOR

Orbit Number	Day 1963	Time (UT)	$B$ (gauss)	$L$ ( $R_e$ )	$BO^*$ (gauss)	$n$
1	127	17:56	.018	2.6	.0177	3.3
1	127	17:17	.018	3.0	.0115	4.4
1	127	17:01	.022	3.2	.0095	4.5

\*  $B_0$  is the equatorial value of  $B$  for the  $L$  in the previous column. The fluxes in Figure 85 and results in Figure 86 are for  $B = B_0$ .

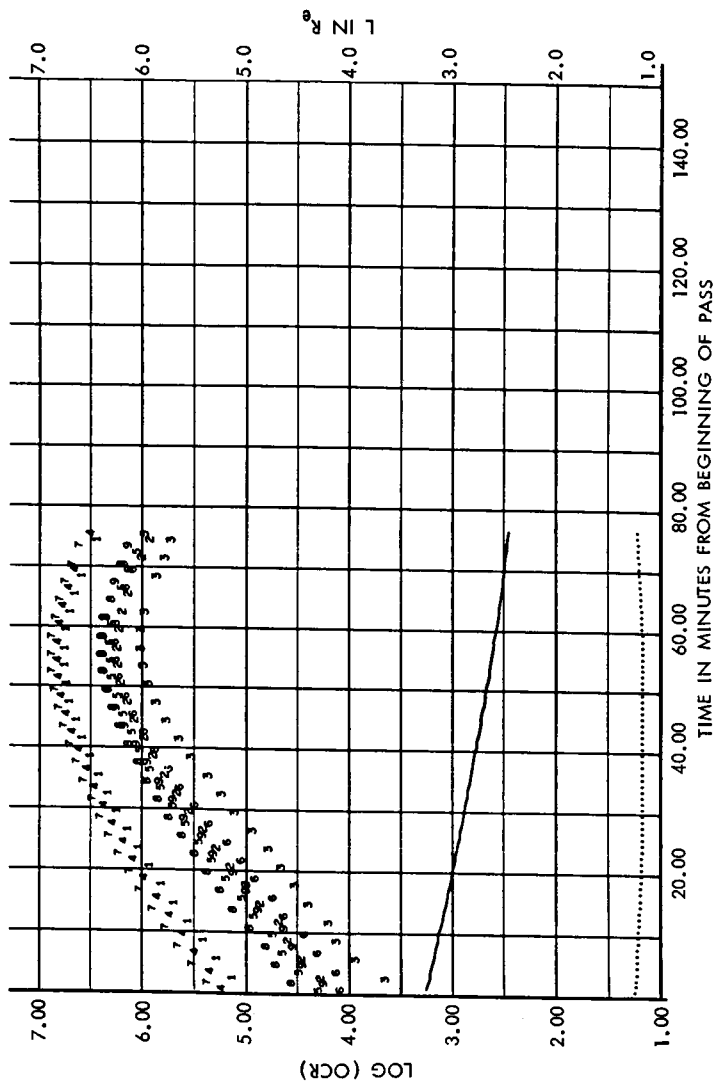


Fig. 87 — Data from the nine proton channels in the energy range 2-30 Mev on Telstar II. The channels are described in Table 5-2. The scale on the ordinate is  $\log_{10}$  (OCR) for the nine channels, and  $L$  is in earth radii for the solid line.  $B$  may be derived from the dotted curve by applying the scaling factor  $B = (\text{Ordinate} - 1)/10$  gauss. The data commence at 16:57 on day 127, 1963, and were acquired by the Minitrack station at Johannesburg on orbit 1.

the value of  $n = 4.4$  at  $L = 2.6 R_e$  in Figure 86. The difference between the two values indicates that the energy spectrum of the protons in the 2-3 Mev range is harder than in the 18-50 Mev range. A single value for the exponent in the power law spectrum will not fit the data from 2-50 Mev. In a steep power law spectrum channels 7, 4, and 1 are completely dominated by the lowest energy protons that they measure. This makes the results quite sensitive to the values chosen for the bottom of the energy range. The power law spectrum, while giving the correct general configuration, does not order all the remaining channels correctly. This may indicate that a simple power law spectrum does not describe the details of the proton energy distribution even in this restricted energy range and region of space, or that the energy edges of the various channels are not precisely enough known to allow the exponent to be accurately determined.

The data in Figure 88 were recorded by the Minitrack station at Santiago de Chile on orbit 2, about three hours after the data of Figure 87. At the beginning of the pass the satellite was at an altitude of 1200 nautical miles, at  $L = 1.6 R_e$  and  $B = .152$  gauss (far from the  $B_0 = .076$  gauss of the magnetic equator). In this part of space the energy spectrum is quite flat, and channel nine with its wide energy range in the lower half of the 2-25 Mev band predominates. As the satellite moves to higher  $L$  values and lower  $B$  values (toward the center of the radiation belt), the energy spectrum changes. A cross-over occurs at  $L = 2.3$  and  $B = .07$ , where the spectrum has become steep enough so that the lowest energy channels have the highest counting rates as in Figure 87. The relative positions of the channels on the plots give the energy spectrum. The intensity, which shows a steady increase in some channels (e.g. 7) and a local minimum in others (e.g. 9), is given by the absolute positions of the plotted points. About forty minutes before the end of the pass the satellite reaches an  $L$  value of  $2.8 R_e$  and travels along this magnetic shell ( $\pm 0.25 R_e$ ) from  $B = .030$  gauss to  $B = .015$  gauss, which is close to the equatorial value of  $B_0 = .0142$  gauss. During this 40 minutes the satellite moves from a dipole magnetic latitude of  $25^\circ$  to one of about  $7^\circ$ , and as may be seen from the pattern of Figure 88, the energy spectrum remains almost unchanged while the intensity increased by a factor of 8.

*Radiation Damage to the Low-Energy Proton Detector.* The data acquired by the Johannesburg Minitrack station on orbit 8, are displayed in Figure 89. These data, which were recorded 23 hours after the data in Figure 87, come from the same region of the radiation belts. In particular at 17:37 UT on day 127, Telstar II was at position

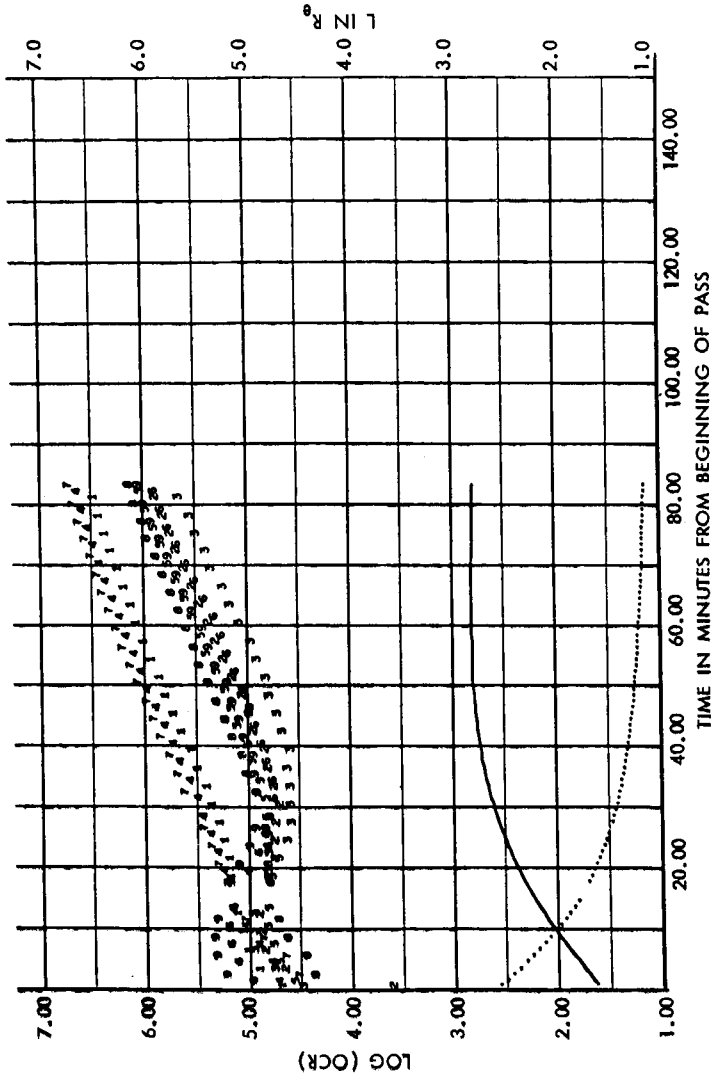


Fig. 88 — Data from the nine proton channels in the energy range 2-30 Mev on Telstar II. The channels are described in Table 5-2. The scale on the ordinate is  $\log_{10}$  (OCR) for the nine channels, and  $L$  is in earth radii for the solid line.  $B$  may be derived from the dotted curve by applying the scaling factor  $B = \text{Ordinate} - 1/10$  gauss. The data commence at 19:40 UT on day 127, 1963, and were acquired by the Minitract station at Santiago de Chile on orbit 2.

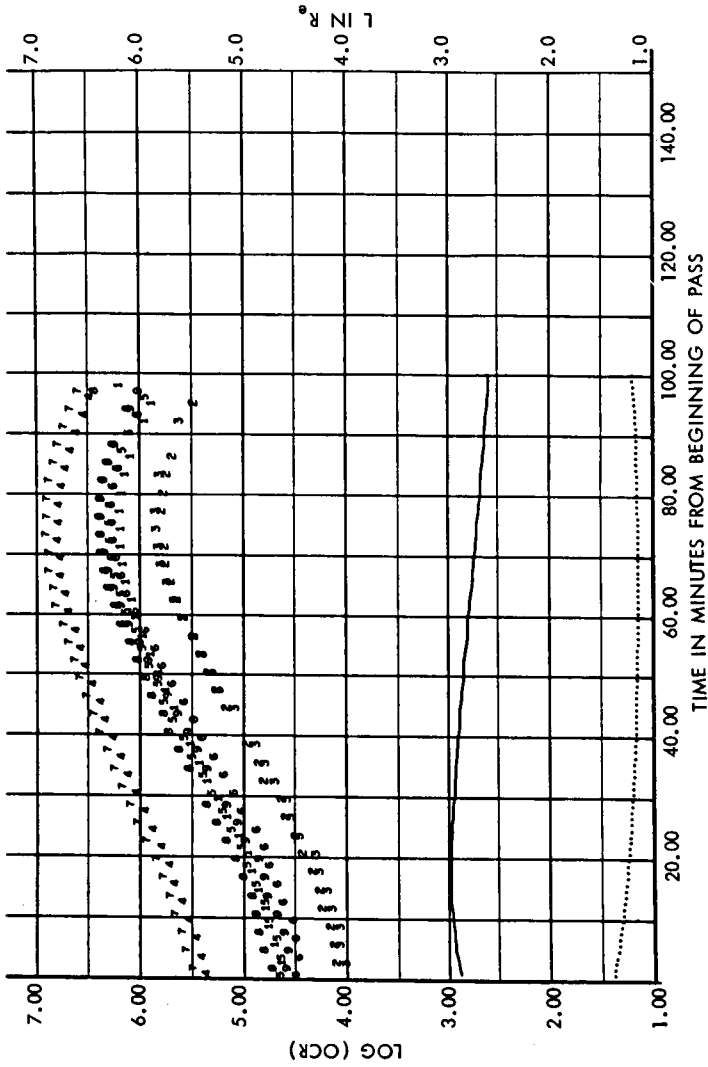


Fig. 89 — Data from the nine proton channels in the energy range 2-30 Mev on Telstar II. The channels are described in Table 5-2. The scale on the ordinate is  $\log_{10}$  (OCR), for the nine channels, and  $L$  is in earth radii for the solid line.  $B$  may be derived from the dotted curve by applying the scaling factor  $B = (\text{Ordinate} - 1)/10$  gauss. The data commence at 18:45 UT on day 128, 1963 and were acquired by the Minitrack station at Johannesburg on orbit 8.

$L = 2.775 R_e$ ,  $B = .0165$  gauss, and at 19:50 UT on day 128, Telstar II was at position  $L = 2.775 R_e$ ,  $B = .0152$  gauss. As seen in Figure 88, a difference of .0013 gauss is completely insignificant insofar as the energy spectrum of these low-energy protons in this region of space is concerned. The configuration in Figure 89, however, is quite different from the configuration of Figure 87. Channel 1 has dropped into the center of the second group of channels, and channel 2 has dropped down and joined channel 3. This is part of a pattern of changes in the low energy proton detector which becomes discernible by orbit 3, 12 hours after the satellite was launched. These changes are attributed to radiation damage to the bulk of the detector. The radiation defects created in the silicon of the detector interfere with the collection of holes and electrons by the electric field in the detector and decrease its efficiency. The damage is most important at low bias (channels 1, 2, 3) because of the small electric field in the detector. It is most important for the lowest discrimination level in this bias range (channel 1) because the damage is most severe in the region penetrated by the lowest energy particles. In contrast to the effects in channels 1, 2 and 3, the measurements from channels 7, 8, and 9 relatively unaffected by the damage. Similar observations were made on detectors flown on Telstar I and Relay I (Reference 10). There are differences in the low energy proton exposure of these satellites, but the large damage differences observed seem to indicate a difference in sensitivity of the devices to low energy proton damage, a feature which requires further investigation.

#### The Radiation Exposure of the Satellite

*General.* The radiation exposure of the satellite is given by the expression:

$$S = \int_{T_i}^{T_f} F(t) dt, \quad (5)$$

where  $S$  is the radiation exposure in particles per  $\text{cm}^2$ ,  $F(t)$  is the omnidirectional flux of the particles in question at the satellite,  $t$  is time, and  $T_i$  and  $T_f$  are the times which define the beginning and end of the period for which the exposure is calculated. The flux is a function of time because the position of the satellite changes with time, and also, in the case of electrons, because the flux itself may change with time. When  $T_i$  and  $T_f$  are midnights of succeeding days,

$$F = S/(T_f - T_i) \quad (6)$$

is called the daily average omnidirectional flux. When  $T_i$  is the time of launch and  $T_f$  some later time,  $S$  is called the cumulative exposure to time  $T_f$ . The cumulative exposure will be treated in conjunction with the radiation damage in a later section.

In practice the integral of Equation 5 has been approximated by a sum. This is done, as described in Reference 3, by dividing  $B$ - $L$  space into boxes by a grid assigning a value to the flux in each box, adding up the time spent in each box, and taking the sum of the flux-time products. For the calculations presented here, a grid which divided  $B$ - $L$  space into 2501 boxes was used. The grid size is varied so that the boxes are small in the important regions of space. This approximate method introduces an error of less than 5% in the exposure for the orbits considered here.

*Orbits.* The radiation exposure depends on how much time the satellite spends in the more intense regions of the radiation belts. This, in turn, depends on the orbital configuration. The orbital ellipse of Telstar II is quite eccentric, apogee is at about  $2.75 R_c$  and perigee at about  $1.1 R_c$ , and the line of apsides precesses  $360^\circ$  in about 300 days. Figures 90, 91 and 92 are plots of the Telstar II orbit in  $R$ - $\lambda$  space for various positions of the line of apsides. Figure 90 shows the orbital configuration on day 134, when apogee and perigee are both over the equator (the line of apsides is in the geographic equatorial plane of the earth). The lines  $A$  and  $B$  represent the envelope of all orbits on that day, and Telstar II is confined to the region of the radiation belts between  $A$  and  $B$ . This region does not contain high fluxes of 18-28 Mev protons as may be seen by comparing Figure 90 to Figure 83. Orbits 1 and 3 for day 134, 1963 are plotted in detail and marked at 10 minute intervals.

Between days 134 and 208 apogee moves northward. By day 171 the envelope of the orbits has shifted to the configuration shown in Figure 91. Orbits 2 and 6 are plotted, and the satellite is seen to spend more time in regions in which the 18-28 Mev proton intensity is appreciable. On day 208, 1963 apogee is full north (Figure 92) and the orbits are passing through the maximum of the 18-28 Mev proton intensity at  $R = 1.65 R_c$ ,  $\lambda = 0^\circ$ . The line is once more the envelope of all the orbits on this day. Note how much more time the satellite spends at apogee than at perigee. These three orbital configurations may also be examined in conjunction with Figure 79 to get some insight into the variations in the radiation exposure to electrons.

The orbit of Telstar I had approximately the same perigee and inclination as that of Telstar II, however the apogee of Telstar I was only

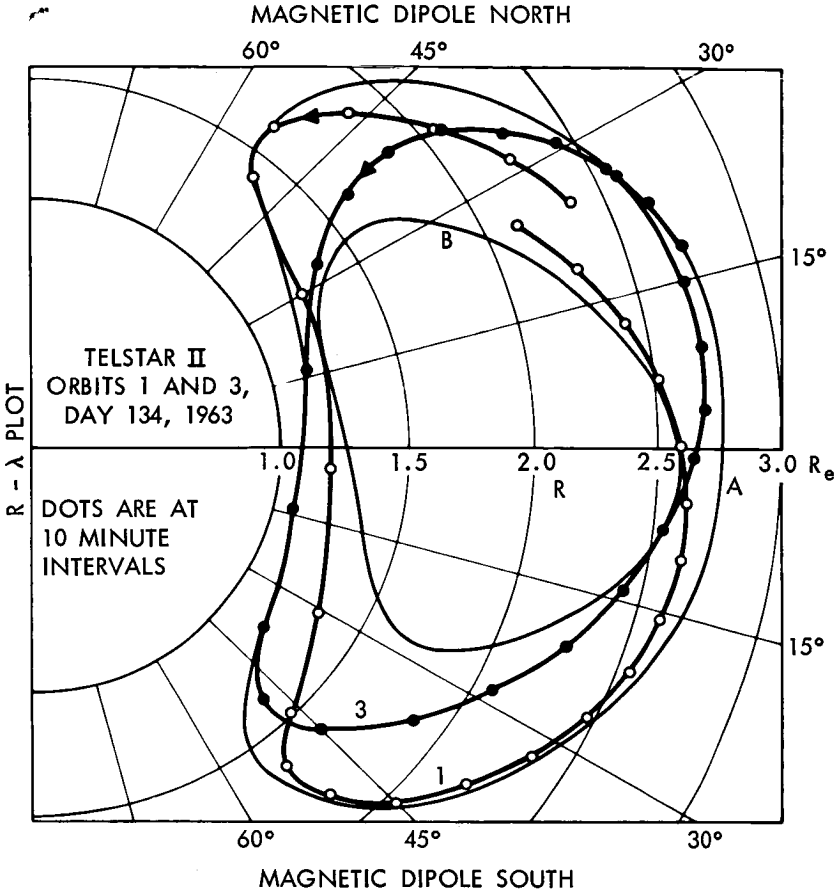


Fig. 90 — Telstar II: Orbits 1 and 3 on May 12, 1963 plotted in  $R-\lambda$  coordinates. Apogee and perigee are both over the geographic equator. The dots represent 10 minute intervals along the orbits. The lines A and B are the external and internal envelopes of the six orbits for this day.

$1.95 R_e$ . The resultant orbital configurations in  $R-\lambda$  space for Telstar I are similar to those of Telstar II, but are radially compressed (Reference 3) by being confined below  $R = 1.95 R_e$ . This confinement forces Telstar I to cross the equator much closer to the maximum of the 18-28 Mev proton belt for all orbital orientations. The difference in the behavior of the radiation exposure of the two satellites is also substantial for electrons and for protons of other energy ranges.

*Radiation Exposure to 18-28 Mev Protons.* Protons with energies above 15 Mev can penetrate the shields on the solar cells in the main

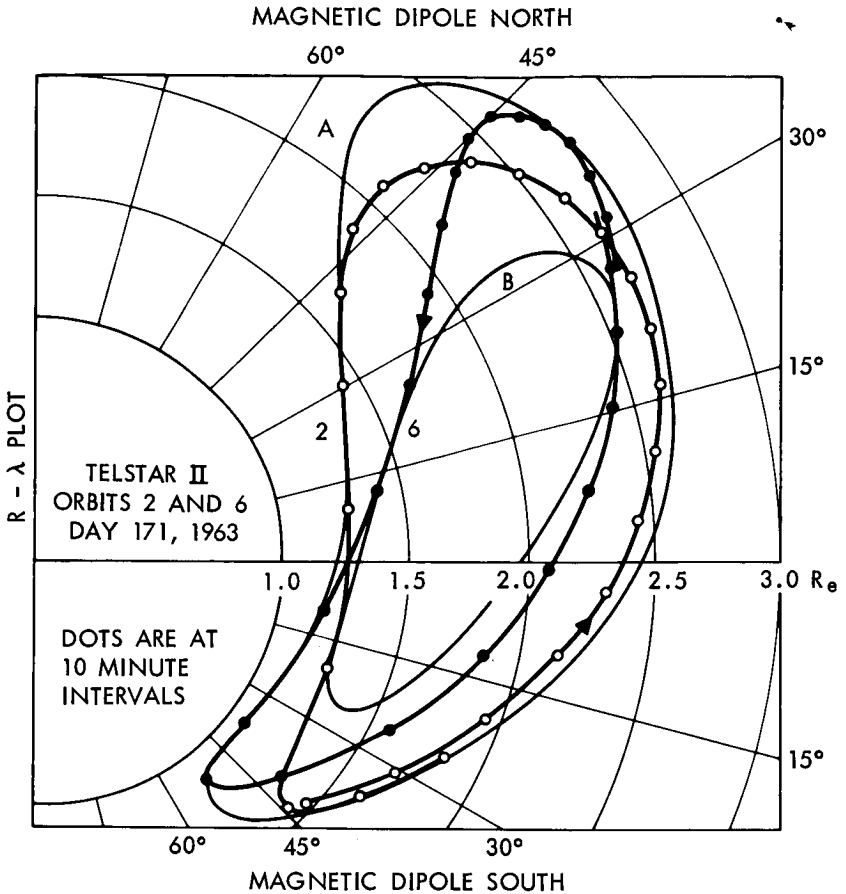


Fig. 91 — Telstar II: Orbits 2 and 6 on June 18, 1963 plotted in R- $\lambda$  coordinates. The latitude of apogee is 28°N. The dots represent 10 minute intervals along the orbits. The lines A and B are the external and internal envelopes of the six orbits for this day.

power plants of the Telstar satellites. The protons with energies just above 15 Mev are the most damaging and also, because the energy spectrum rises steeply at lower energies, the most numerous. These protons were calculated to have caused about half of the damage to the power plant on Telstar I (Reference 3). They are the major cause of solar cell degradation on Telstar II. Because the protons in the radiation belts have shown no gross temporal variation in this energy range, Telstar I was presumably exposed to the same distribution of 18-28 Mev protons as Telstar II (only Telstar II made measurements

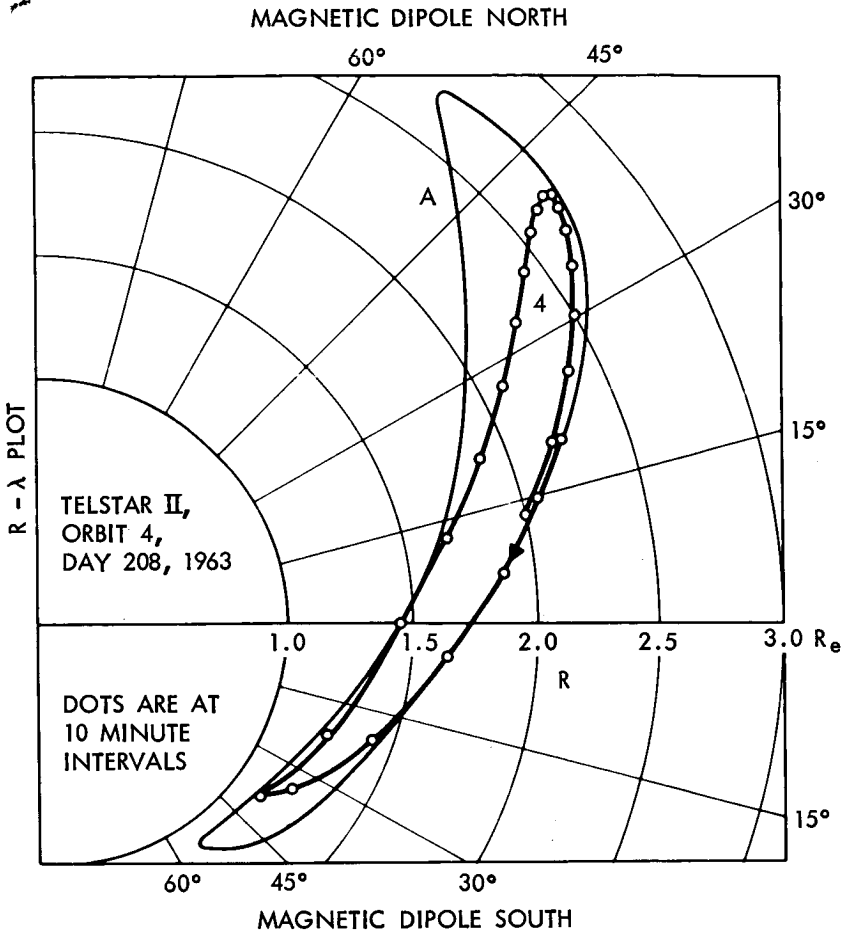
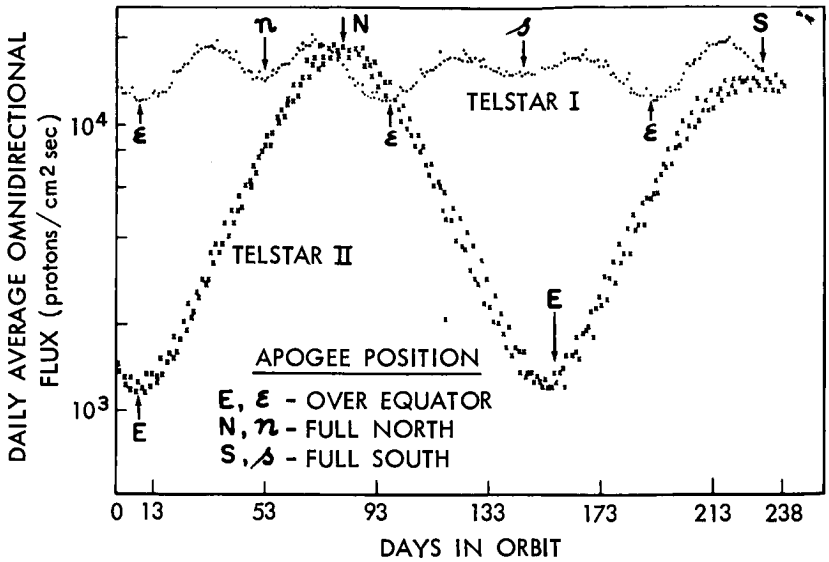


Fig. 92 — Telstar II: Orbit 4 on July 25, 1963 plotted in R-λ coordinates. The latitude of apogee in 43°N. The dots represent 10 minute intervals along the orbit. The line A is the external envelope of the six orbits for this day.

of the 18-28 Mev range). The daily average omnidirectional flux of protons between 18 and 28 Mev is plotted against days in orbit for both Telstars in Figure 93. The points are integrations over the actual orbits. The letter *E* points to the time when the orbital configuration of Telstar II corresponds to that of Figure 90, at N the orbital configuration is that of Figure 92. The ratio of the daily average exposure on day 208, 1963 (the 81st day in orbit) to that on day 134, 1963 (the 7th day in orbit) is 15. The effects of the variations in the exposure

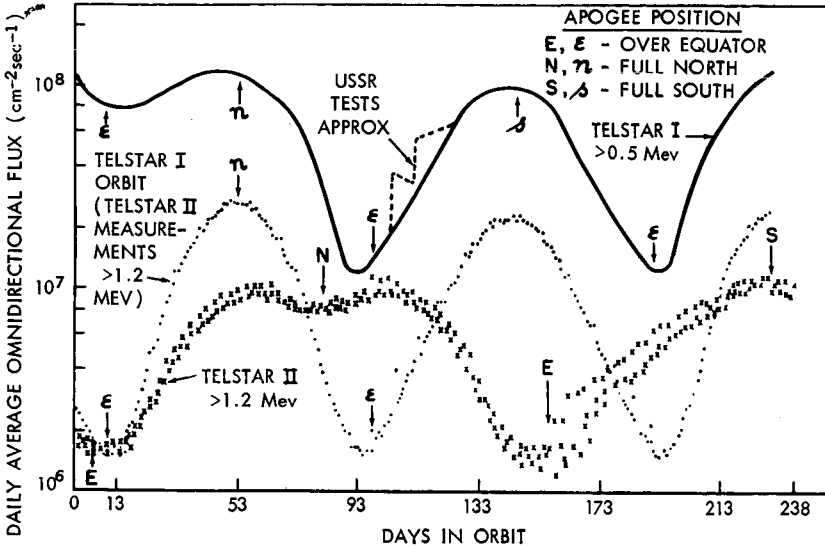


TELSTAR	AVERAGE OMNIDIRECTIONAL FLUX cm <sup>-2</sup> sec <sup>-1</sup>
I	$1.5 \times 10^4$
II	$7.3 \times 10^3$

Fig. 93 — The radiation exposure of the Telstar satellites to protons with energies between 18 and 28 Mev.

on the rate at which the solar power plant degrades is discussed on pages 2354-2361. The lower apogee of Telstar I keeps it much closer to the maximum of the proton distribution, so that the daily average exposure of Telstar I to these protons varies by a factor of only 1.5. As a result the long term average exposure of Telstar II to protons with energies between 18 and 28 Mev, which is  $7.3 \times 10^3/\text{cm}^2\text{-sec}$ , is half the long term exposure of Telstar I to the same particles, which is calculated to have been  $1.5 \times 10^4/\text{cm}^2\text{-sec}$ .

*Radiation Exposure to Electrons.* The radiation exposure of Telstar II to electrons capable of damaging the solar cells ( $E > 1.2$  Mev) can be calculated straightforwardly. However, the comparison with Telstar I is complicated by the time dependence of the flux and the differences in the energy ranges of the measurements. The top curve in Figure 94 is reproduced from Reference 3 (with a change in scale) and represents the daily average exposure of Telstar I to electrons with



TELSTAR	AVERAGE OMNIDIRECTIONAL FLUX $\text{cm}^{-2} \text{sec}^{-1}$	ELECTRON ENERGY	DATE OF FLUX MAPS
I	$6.5 \times 10^7$	$>0.5 \text{ Mev}$	JULY - OCT 1962
I	$3.6 \times 10^7$	$>1.2 \text{ Mev}$	JULY - OCT 1962
I	$1.0 \times 10^7$	$>1.2 \text{ Mev}$	MAY - JULY 1963
II	$0.6 \times 10^7$	$>1.2 \text{ Mev}$	MAY - JULY 1963

Fig. 94—The radiation exposure of the Telstar satellites to high energy electrons.

energies above 0.5 Mev. The fluxes were anomalously high, particularly when Telstar I was launched. The long term exposure of Telstar I to electrons above 0.5 Mev was  $6.5 \times 10^7/\text{cm}^2\text{-sec}$ , and, assuming the energy spectrum of Equation 1, the exposure to electrons with energies above 1.2 Mev was  $3.6 \times 10^7/\text{cm}^2\text{-sec}$ . The x's in Figure 94 give the daily average exposure of Telstar II to electrons with energies above 1.2 Mev. The long term average for Telstar II is  $0.6 \times 10^7$  electrons/ $\text{cm}^2\text{-sec}$  with energies above 1.2 Mev, or about 1/6 the value for Telstar I. However, note from the dotted curve in Figure 94, that if Telstar I had been launched in May of 1963 it would have been exposed to an average of only  $1.0 \times 10^7$  electrons/ $\text{cm}^2\text{-sec}$  with energies above 1.2 Mev.

*Radiation Exposure to Low-Energy Protons.* The energy spectrum of protons in the 4-13 Mev range rises steeply toward lower energies

as described on page 2339. This means that the flux map, Figure 84, of protons measured by channel 9 is more representative of the distribution of 4-5 Mev protons than those in the upper part of the energy band of the channel. These protons lie closer to the equator and also extend to higher altitudes than the higher-energy protons previously discussed. The orbital integrals gave an average daily exposure to the low-energy protons that is a factor of 1.6 higher when both apogee and perigee lie over the equator (Figure 90), than when apogee is far north (Figure 92). This variation is  $180^\circ$  out of phase with the variation of the 18-28 Mev protons, and the implications are considered in connection with the lightly shielded radiation damage transistors discussed below.

### *Radiation Damage*

#### General

The radiation damage in Telstar II is substantially different both in magnitude and in time variation from that observed in Telstar I. The effects in the main solar cell power plant and in the radiation damage transistor experiment illustrate these differences clearly. They will be considered in the paragraphs to follow, and interpreted in connection with the particle exposure of the satellite and the laboratory determined damage effectiveness of electrons and protons with energies such as are found in space.

#### Solar Power Plant

*General.* Figure 95 shows the comparison between the average output current of the solar power plants of Telstars I and II. The values are obtained by averaging a sequence of telemetry readings each of which represents the instantaneous value of the current at a particular phase in the orientation of the satellite with respect to the sun as the satellite rotates on its spin axis. The orientation is determined from the solar aspect experiment as discussed in connection with Telstar I (Reference 3). As the satellite spin rate gradually decreases there are passes in which the telemetry frame time and the satellite spin rate are nearly commensurate and a sequence of measurements from the telemetry does not permit an adequate average to be taken. Data from such passes have not been used. The average current has been corrected to the mean solar distance.

The curve drawn through the Telstar I data has the shape to be expected from laboratory experiments assuming the damaging particle flux is constant in time. The curve has been adjusted by sliding it

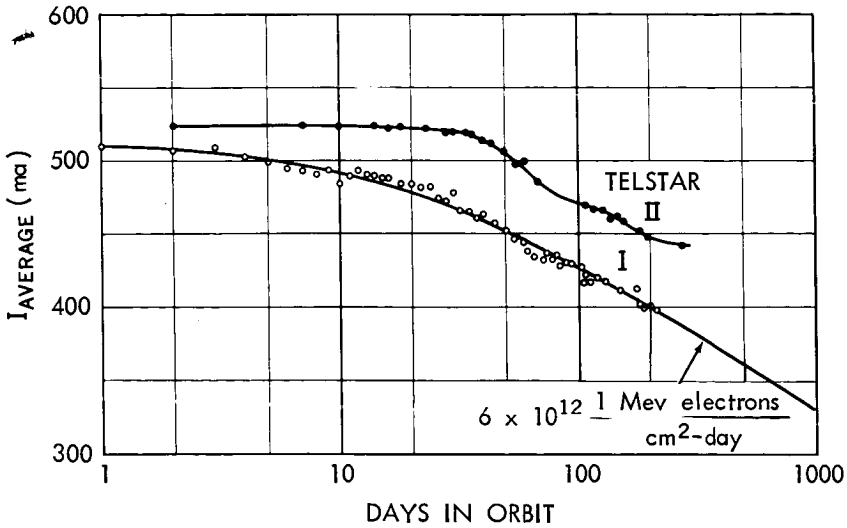


Fig. 95—The average solar power plant currents for Telstar I and II as they decrease with time in orbit.

along the horizontal axis in this semilogarithmic plot to give the best visual fit to the data. Numerically this point corresponds to the damage that would have been sustained by the Telstar I solar cells if they had been exposed to a flux of  $6 \times 10^{12}$  1-Mev electrons/cm<sup>2</sup>-day at normal incidence and without solar cell shielding. This damage equivalence is discussed more fully below. The Telstar II data in Figure 95 have quite a different shape from those of Telstar I, indicating that the damaging flux in this case is not constant in time. The curve is simply drawn through the measured points. The shape is considered again below but it is clear from the trend of the curve that the magnitude of the average damaging flux is less in Telstar II's orbit by a factor of between two and four.

*Integral Particle Exposure.* The orbital differences between the two satellites have been discussed above together with the time varying particle exposure of the satellite computed from the measured particle fluxes. The cumulative exposures to 18–28 Mev protons and to electrons are plotted in Figures 96 and 97. Since a solar cell degrades approximately the logarithm of the number of particles to which it has been exposed (Reference 1), log-log plots of this type illustrate the approximate sensitivity of the cells to damage. The dashed lines of Figure 96 for 18–28 Mev protons, are the long term average exposure, taken over at least half a period of precession of the line of apsides of the

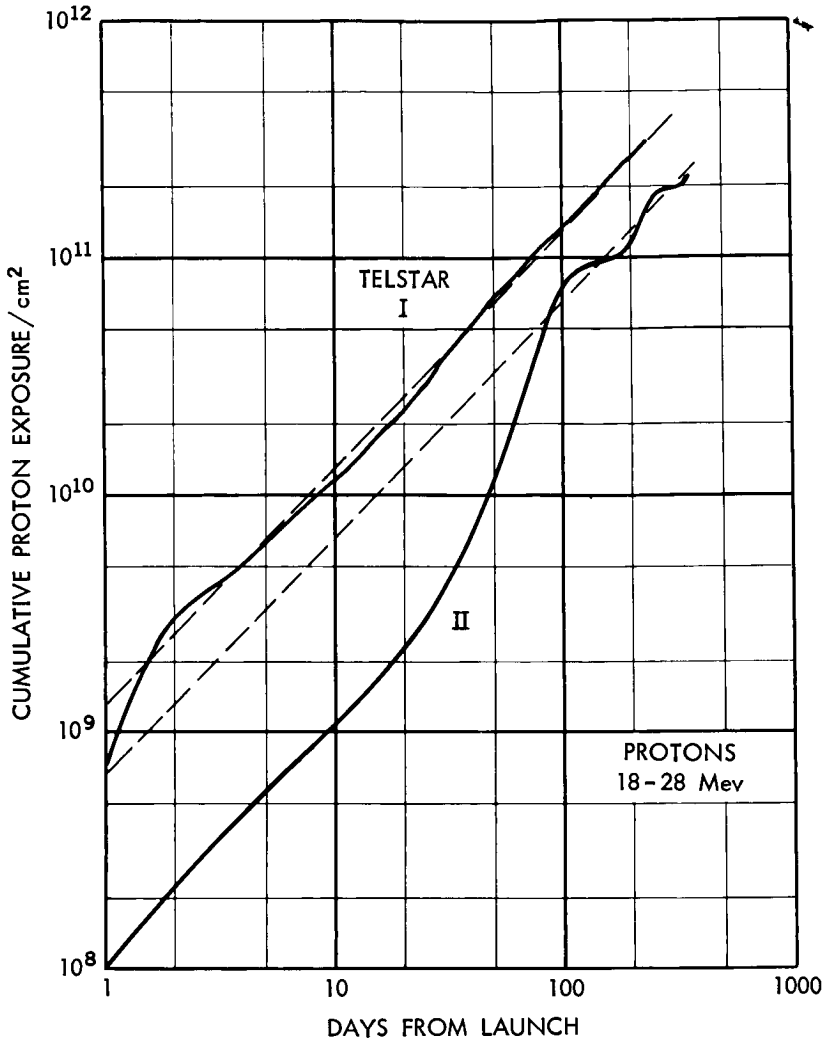


Fig. 96—The cumulative exposure of Telstar I and II to 18-28 Mev protons. The dashed line represents exposure at the long time average rate.

orbits. The departures of the solid curves from the dashed lines arise from the orbital variation. In Telstar I the differences are quite small, but in Telstar II the cumulative flux is below the average by a large amount for about the first 50 days in orbit. This effect is consistent with the long period in Figure 95 during which the power plant shows very small changes. Because of the nature of the logarithm of a cumu-

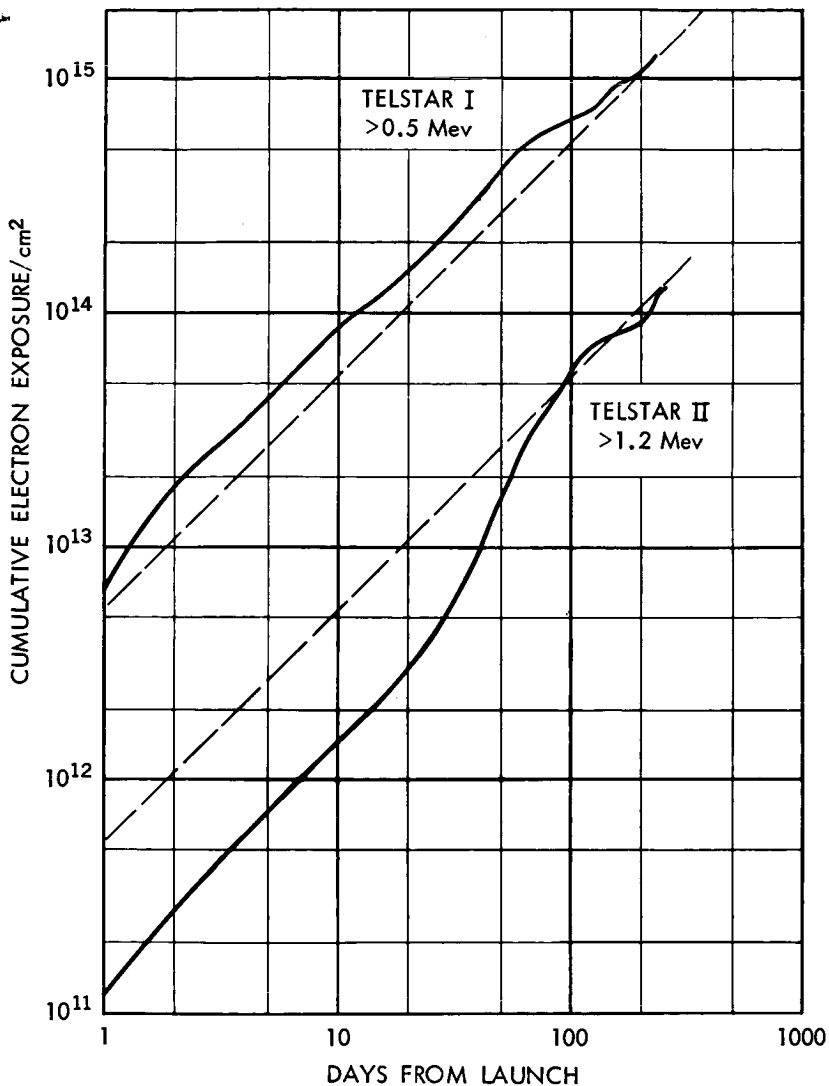


Fig. 97 — The cumulative exposure of Telstar I and II to electrons. The dashed line represents exposure at the long time average rate.

lative flux the fractional difference of the cumulative from the average becomes quite small after a single cycle of maximum and minimum exposure, which is half of the apsidal period of the satellite (about 150 days for Telstar II). These same trends are also evident in the electron exposure of Telstar II in Figure 97. The cumulative flux for

Telstar I is above the extrapolated long term average because the decay of anomalously high electron fluxes found following Telstar I's launch lowers the long term average.

*Effective Time in Orbit.* The solar cell power plant current can be examined in the light of the nonuniform time history of the particle exposure by plotting the observed current against an effective rather than a real time in orbit. The effective time is the time it would take to achieve the cumulative exposure at the average rate. Thus for Telstar II in Figure 96 the proton flux accumulated in 10 days is equivalent to that which would have been accumulated in 1.6 days at the average rate. The effective time in orbit is dependent on the exposure of the satellite to electrons and protons of various energies taking into account their relative damaging effectiveness. However, the most important contributor to the damage that the particle experiments of Telstar II measure directly is the 18–28 Mev proton group, and this single group has been used to determine the effective time in orbit. The results for the solar power plant are shown in Figure 98. The points are now well represented by a curve corresponding to damage under a uniform flux (such as the curve of Telstar I in Figure 95). The magnitude of the equivalent flux is approximately  $2.3 \times 10^{12}$  1-Mev electrons/cm<sup>2</sup>-day, about 2.6 times less than in Telstar I. The

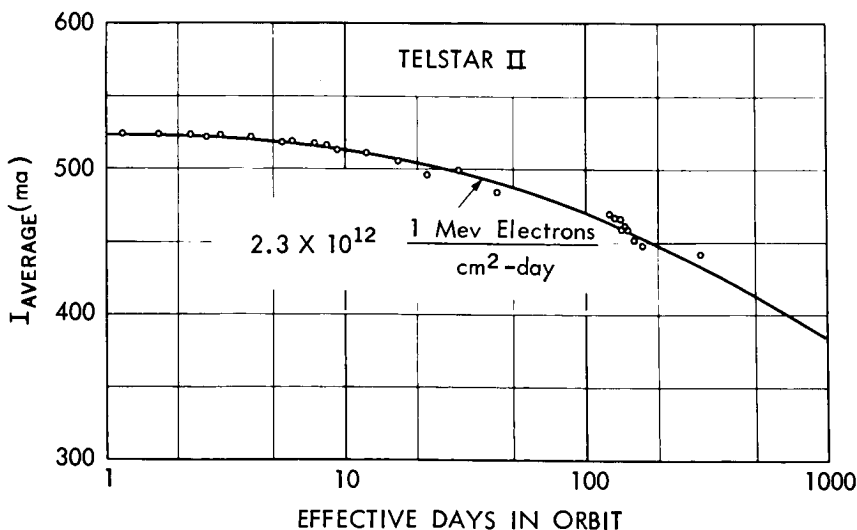


Fig. 98—The average solar power plant current from Telstar II as a function of the effective time in orbit as deduced from exposure to 18–28 Mev protons.

group of points at about 150 days seem to show a systematic deviation from the curve. This is not yet quantitatively understood but is believed to occur because only one group of particles has been used in establishing the effective time scale.

The magnitude of the damage observed can now be compared with that computed using the particle fluxes discussed on pages 2354-2355 and the damage equivalence of these particles. It has been convenient to refer all damage to the 1-Mev electron equivalence as shown for protons in Figure 99 (Reference 11). The particles incident on the solar cells in space arrive approximately uniformly from all directions. The figure gives the damage produced by one omnidirectional proton incident on a cell shielded with a thickness  $w$ , in terms of the number of 1-Mev electrons which at normal incidence on a bare cell would

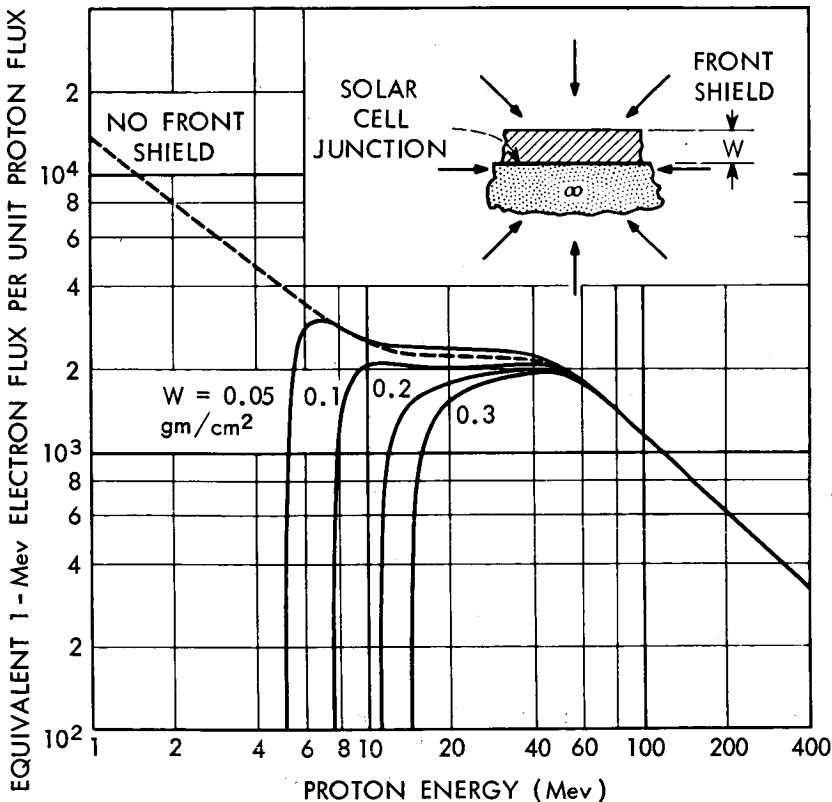


Fig. 99—The damage-equivalent 1-Mev electron flux as a function of the energy of a monoenergetic isotropic flux of protons incident on n-on-p solar cells with various front shielding. The back shield is assumed to be infinitely thick.

produce the same resultant loss of current. For the Telstar II solar cells  $w$  equals  $0.3 \text{ g/cm}^2$  (the same as Telstar I) so that only protons with energies greater than 15 Mev can contribute to damage. For any given proton spectrum an equivalent flux can be determined as the properly weighted average of the equivalent flux for monoenergetic protons of different energies, as given in the figure.

The parameters of the power law differential energy spectrum were deduced from measurements of the 18–28 and  $> 50$  Mev detectors on Telstar II (see pages 2337–2339). It was found that an energy dependence of approximately  $E^{-5}$  satisfied the equatorial proton distribution between  $R \sim 1.4$  and  $2.7 R_e$ . The same technique may be used to derive the average spectrum of the proton exposure of the satellite. The particle exposure to the 18–28 and  $> 50$  Mev protons have similar, but not identical, variations with the Telstar II orbital precession, so that the effective spectrum changes with time. Over a long term, the average differential proton spectrum is found to vary as  $E^{-4.1}$ . In such a spectrum the equivalent 1-Mev electron flux is computed to be  $3.8 \times 10^8$  per particle in the 18–28 Mev range. With an average exposure of 18–28 Mev protons of  $6.3 \times 10^8/\text{cm}^2\text{-day}$  from Section 5–3.2, the 1-Mev equivalence is found to be  $2.4 \times 10^{12}/\text{cm}^2 \text{ day}$ .

The case for electrons can be handled in the same way. Figure 100 gives the damage equivalence for monoenergetic electrons of different energies in an omnidirectional flux at different thicknesses of shielding. At  $0.3 \text{ gm/cm}^2$  only electrons of more than 1.2 Mev are important and it is these that have been measured in the Telstar II experiment. The electrons at still higher energies have been determined in other satellites and it is found that the spectrum is very hard in the region at which the major contribution to the Telstar II exposure is produced, namely in the inner and outer belt maxima. A representative spectrum is exponential with an e-folding energy of about 1.2 Mev. Electrons in such a spectrum have a damage equivalence at  $0.3 \text{ gm/cm}^2$  of 0.92 1-Mev electrons for each measured electron above 1.2 Mev. With an average daily flux of  $5.2 \times 10^{11}/\text{cm}^2\text{-day}$  above 1.2 Mev the equivalent damage of the electrons is approximately  $5 \times 10^{11}/\text{cm}^2 \text{ day}$ , about 20% of the damage equivalence of the protons. The total damage equivalence is then  $2.9 \times 10^{12}/\text{cm}^2 \text{ day}$ . This value is to be compared with  $2.3 \times 10^{12}/\text{cm}^2 \text{ day}$  which was found to represent a best fit to the data in Figure 98. The 25% discrepancy between the observed and computed values is not unreasonable in view of the approximations that have been made in obtaining this comparison and the experimental uncertainties of the particle fluxes and of the

damage equivalence of these particles, particularly the protons (Reference 12).

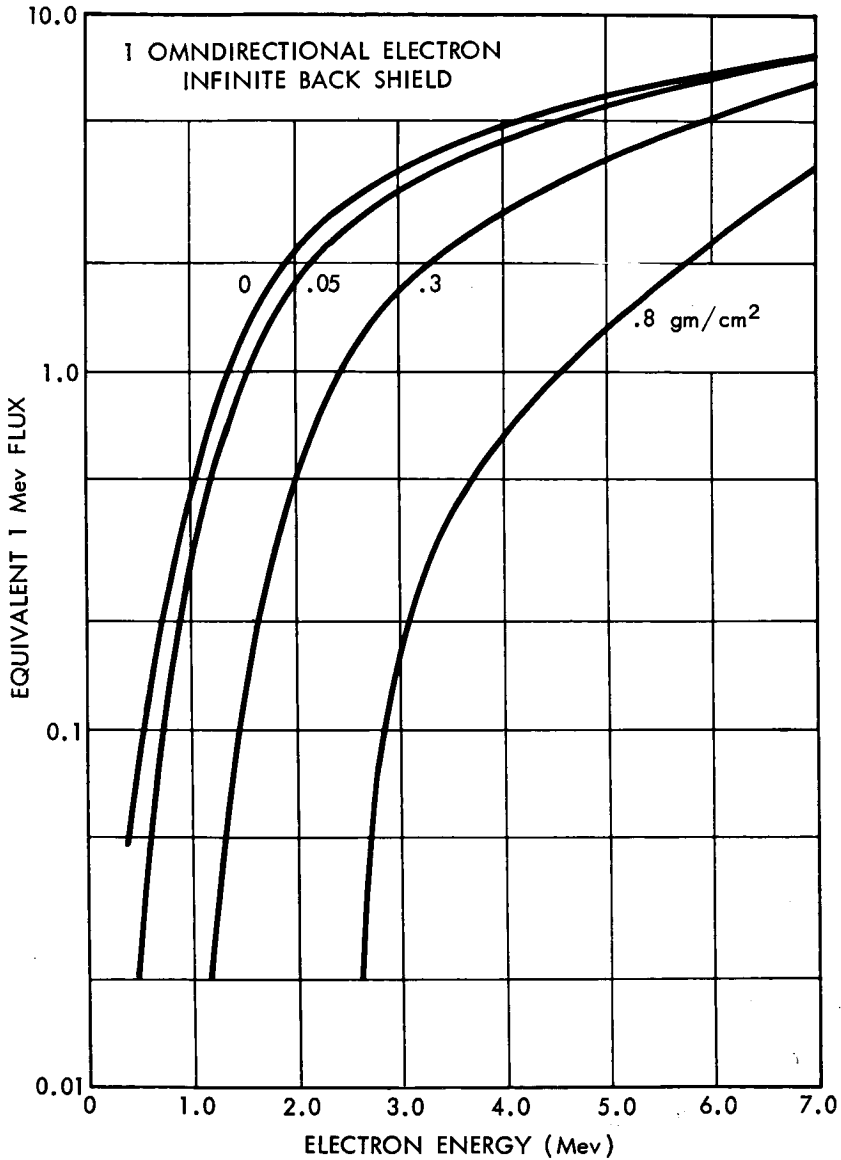


Fig. 100—The damage-equivalent 1-Mev electron flux as a function of the energy of a monoenergetic isotropic flux of electrons incident on n-on-p solar cells with various front shielding. The back shield is assumed to be infinitely thick.

### Damage-Measuring Transistors

The changes in the gain of the radiation damage measuring transistors on Telstar II are shown in Figure 101. The devices are the same as those carried on Telstar I, broad base n-p-n silicon transistors with a high damage sensitivity in their common base current gain (Reference 1). Pairs of these devices at each of three shielding thicknesses are included in the experiment. Figure 102 is, for comparison, the set of results obtained on Telstar I. As in the solar cell case discussed above, the magnitude and time variation of the damage in Telstar II are quite different from those of Telstar I. The curves for different shielding thicknesses do not all have the same shape in Figure 101. They would have if the flux were uniform in size, more nearly the case in Figure 102 for Telstar I. The very pronounced flatness of the 285 mg/cm<sup>2</sup> curves of Figure 101 in the region of day 150 is a direct reflection of the flatness of the accumulated proton exposure in Figure 96. The individual devices in each pair at a given shielding thickness (Figure 101) have very similar shapes in time. There are, however, differences in the extent of the gain change between members of the same pair arising from differences in the sensitivity of the devices which are not adequately accounted for by computing the relative gain.

Determination of the variation of damage rate with shielding thick-

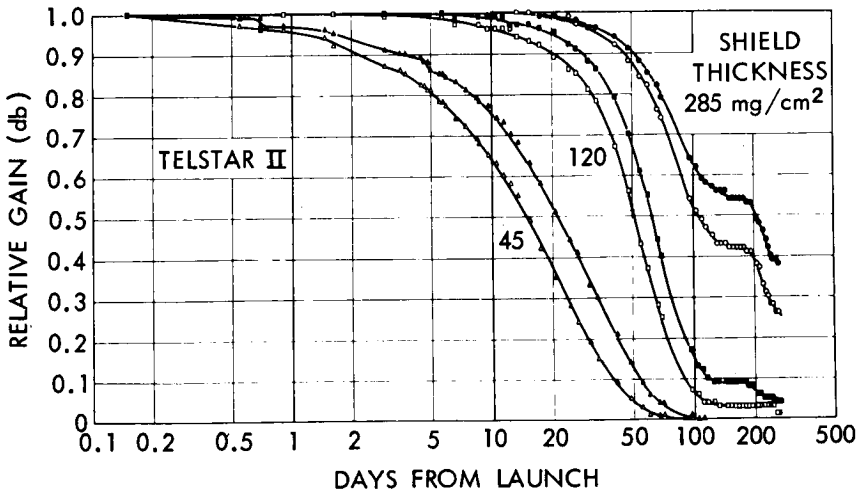


Fig. 101 — The relative gains of the radiation damage transistors on Telstar II as a function of time in orbit.

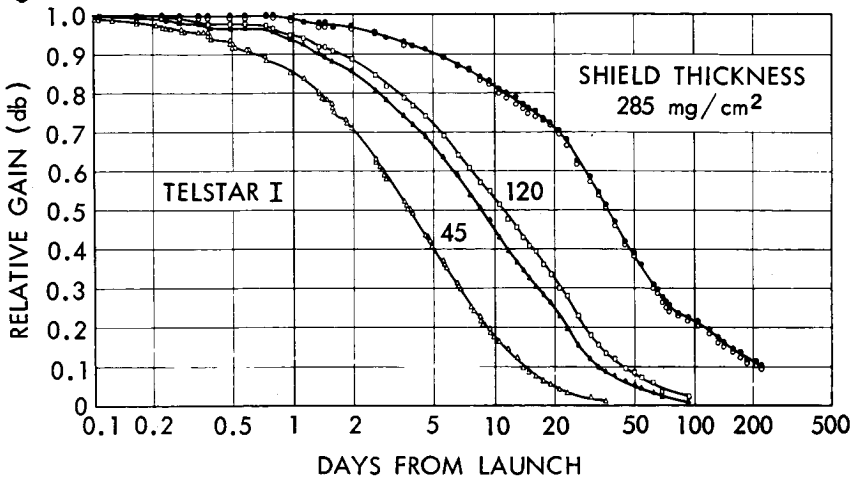


Fig. 102—The relative gains of the radiation damage transistors on Telstar I as a function of time in orbit.

ness cannot be made as directly in Telstar II as in Telstar I because of the time variation of the damaging flux exposure. Since damage to the 45, 120 and 285 mg/cm<sup>2</sup> shielded transistors depends critically on protons above 5, 8 and 15 Mev, respectively, it is insufficient to use 18–28 Mev protons to infer the effective time scale for all. The devices shielded with 45 mg/cm<sup>2</sup> suffer a major part of their damage in the first month in space (Figure 101). During this time apogee of the satellite orbit moves from slightly south of the equator at launch to about 15°N of the equator so the variation in exposure is small. Using the measured distribution of 4–13 Mev protons from Telstar II as representative of the particles primarily affecting the lightly shielded devices, the maximum exposure of the satellite is found to occur when apogee is near the equator, in contrast to the situation for both the high energy protons and the electrons. The maximum exposure to these particles exceeds the average exposure by a factor of about 1.4. Comparing the two devices at 45 mg/cm<sup>2</sup> with the two at 285 mg/cm<sup>2</sup> at a relative gain of 0.4 in Figure 101, the more lightly shielded devices have been damaged approximately 10 times more rapidly. This ratio must be increased by a factor of approximately 1.5 to adjust for the difference in the effective solid angle through which particles can reach the transistors under the two shielding conditions. The edges of the entrance hole (see Figure 9 in Reference 1) provide a sharp cutoff at approximately  $\pi$  steradians for the 5 Mev protons. The 15 Mev protons, however, have an effective solid angle of approximately  $1.5 \pi$  steradians.

At about 200 days in orbit the cumulative exposure and the cumulative exposure at the average rate are essentially equal for 18–28 Mev protons. Thus the results for the most heavily shielded devices correspond approximately to the average exposure to the higher energy protons while the results for the least heavily shielded devices correspond to the maximum exposure to low energy protons. The results assert that the damage effectiveness of the latter is approximately 15 times the former. Comparing the two cases at an average exposure for each energy group the factor is only  $15/1.4 = 11$ . Such a factor between the damage rate for thinly and thickly shielded devices is inconsistent with the differential proton spectrum of  $E^{-4.1}$ , which predicts a ratio of approximately 100. Electrons are providing only a small fraction of the damage and hence do not serve to reduce significantly the damage variation of the shielding thickness as they would tend to do. The failure of the damage rate to rise as rapidly with a reduction in shielding thickness as anticipated was also observed in connection with Telstar I (Reference 3). The explanation for these results may depend on the details of the energy spectrum of the proton exposure between 5 and 18 Mev although the number of protons in the 4–13 Mev range measured by Telstar II does not disagree with the extrapolation of the spectrum from higher energies by anything like a factor of 10. The discrepancy may alternatively indicate a lower sensitivity of the radiation damage transistors to low energy protons than anticipated from a knowledge of their structure and the relative damage measured with monoenergetic protons on solar cells (Reference 12). It is interesting to note that although the absolute rate of damage for Telstar I and Telstar II differs by more than a factor of 2, the comparison between thinly and thickly shielded devices is almost identical.

### *Summary*

This preliminary study of the results of the radiation experiments on Telstar II confirms and extends many of the results from Telstar I (Reference 3). The proton distribution in space in the energy range from 18 Mev to more than 50 Mev agrees very well with that from Telstar I in the parts of the radiation belts traversed by both satellites. The proton spectrum near the magnetic equator and at radial distances greater than that of the maximum of the highest energy proton group is found to be satisfactorily represented by an inverse power law. Very large fluxes of low energy protons, dominantly at the bottom of the 2–13 Mev energy range, are found to be present and

highly damaging to the semiconductor particle detector measuring them. Electron measurements were made in a higher energy range on Telstar II than on Telstar I. They show the characteristic inner and outer Van Allen belt structure, the former being quite stable with time, the latter showing many small variations and one major perturbation in September 1963. The absolute electron fluxes agree quite well with those observed by Telstar I in early October 1962, except in the region of the slot between the inner and outer belt where the spectrum assumed in making the comparison is apparently inapplicable.

The radiation damage in the main solar power plant of the satellite is well accounted for by the particles to which the satellite was exposed. A large variation in the rate of damage is also found to correspond very well to the time variation of the calculated exposure of the satellite with the precession of the satellite's orbit. The radiation damage measuring transistors show this same time variation in their rates of degradation with time in orbit. The dependence of the damage rate on shielding thickness in these devices is very much the same as in Telstar I. In both cases, however, the increase of the rate of damage with decreasing shielding thickness is smaller than anticipated.

#### TELSTAR I AND TELSTAR II — DIFFERENCES

##### *Introduction*

Physically the differences in Telstar I and II are as follows:

- a. Telstar II has provisions for microwave telemetry so that telemetry can be obtained after the two-year timer turns off the VHF beacon.
- b. Telstar II has radiation detectors capable of detecting particles of higher energy levels than Telstar I.
- c. Telstar II has vacuum encapsulated transistors in one of the command decoders. These transistors should not be subject to surface ionization and therefore will be affected by radiation only through bulk damage. Data indicates that significant bulk damage will not occur before an exposure of  $10^8$  rads. Telstar II will have received this level of radiation at the end of about 90 years in space.
- d. Telstar II measures canister pressure by using a 1-lb/in<sup>2</sup> pressure switch and a continuous-reading pressure gauge (max. indication 12.7 lb/in<sup>2</sup>) whereas Telstar I has a 1-lb/in<sup>2</sup> and 5-lb/in<sup>2</sup> pressure switches.
- e. Telstar II has telemetry channels to check the output of each

S relay driver.

- f. Telstar II has a  $1\frac{1}{4}$  db pad between the VHF antenna and antenna diplexer. This improves the margin against parasitic oscillations in the VHF beacon circuit.
- g. The orbits of the two satellites are different:

	<i>Telstar I</i>	<i>Telstar II</i>
Apogee	3507 st. miles	6713 st. miles
Perigee	592 st. miles	604 st. miles
Orbital Inclination	44.9°	42.8°
Orbital Period	158 minutes	225 minutes

### The Communications Repeater

The communications repeater for Telstar II as shown in Figure 103 is the same as the one in Telstar I except for the microwave telemetry. When the proper commands are sent to the satellite, the telemetry signal is used to phase modulate a transistor frequency multiplier in the circuits which generate the microwave beacon signal. The modulation index, caused by telemetry is so small that the modulated micro-

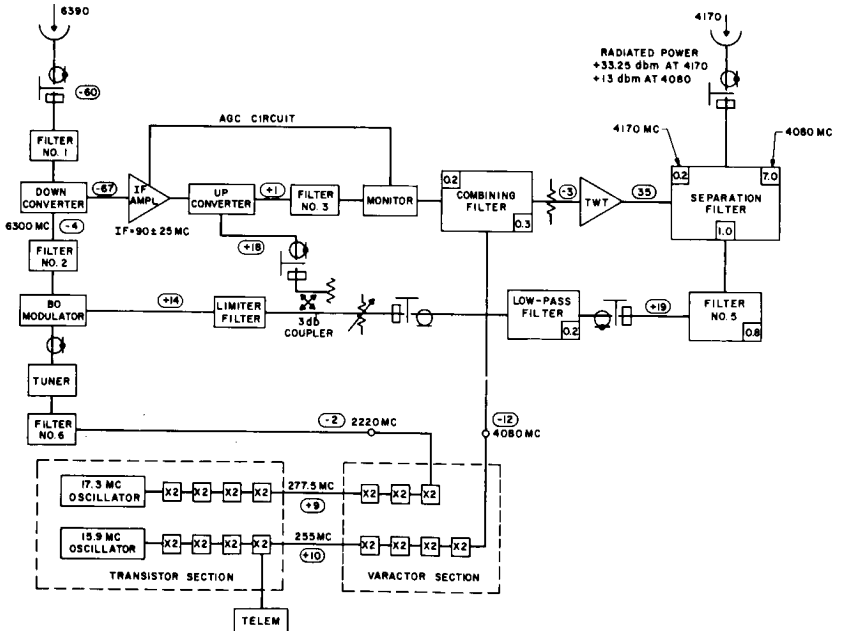


Fig. 103 — Telstar II communications repeater.

wave beacon carrier drops only a fraction of a db below its unmodulated value.

Telemetry channels are provided to show the proper levels of the signals at the varactor frequency multipliers, the local oscillator signals for the up and down converters, and the received signal at 6390 Mc. There are also telemetry data to show TWT currents and temperatures at several points. Except for temperature changes which were expected, the telemetry data show no degradation of the communications circuit since it was first assembled.

The antenna patterns for the two models are the same except for small variations in the ripples in the pattern.

*Satellite Command and Telemetry*

The block diagram of the satellite command and telemetry circuits are shown in Figure 104. This diagram applies to both Telstar I and Telstar II. The command system for Telstar II has not had any of the radiation problems associated with Telstar I. There still remains the

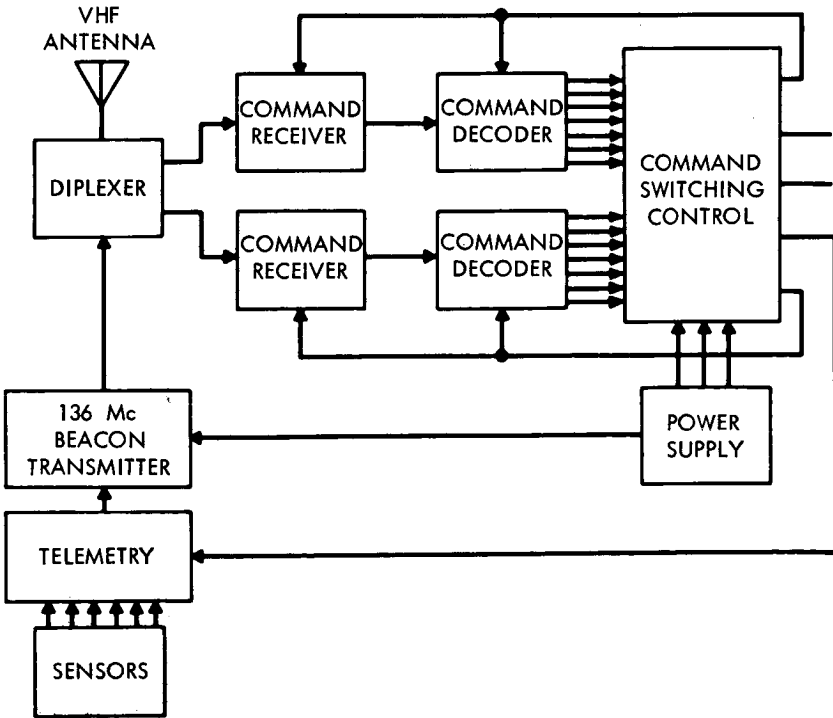


Fig. 104 — Telstar II satellite command and telemetry circuit.

unexplained problem, not restricted to the Telstar satellites, of false commands. There have been since launch, an average of about two commands per month which have been executed by the satellite which are unexplained. An extensive program has been carried out to explain these false commands but no concrete explanation accounts for all these commands.

### Canister Temperature

There are several thermistors located near the skin of the canister and all show essentially the same temperature. The upper dome temperatures for Telstar I and II are both shown in Figure 105. The thermal shutters which were provided to change the emissivity of the canister, partially compensate the canister temperature for changes of

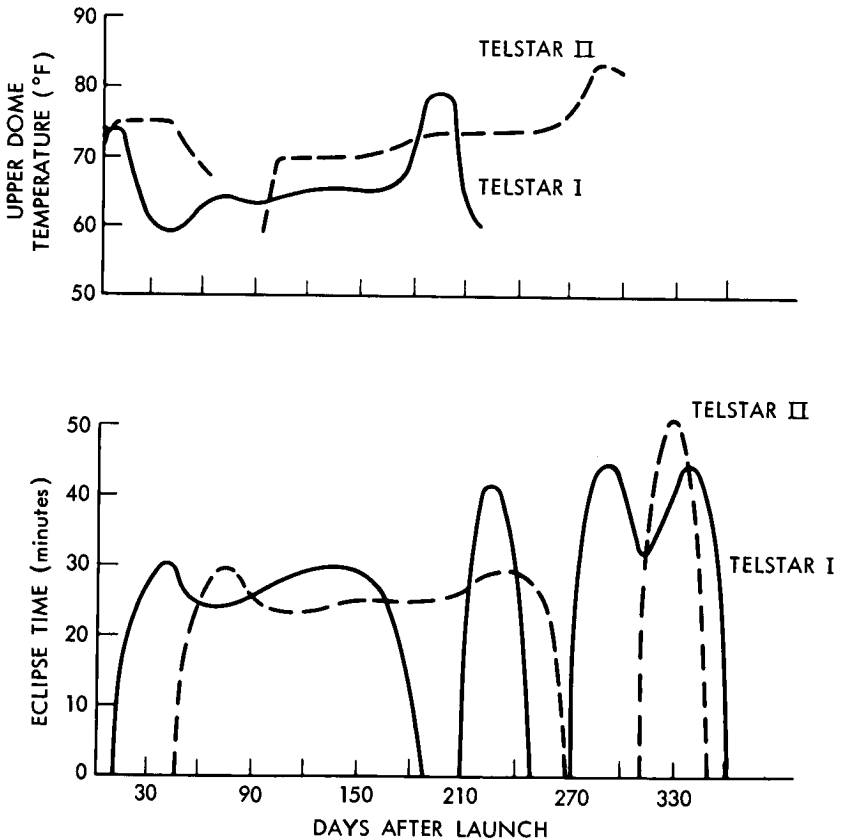


Fig. 105 — Telstar I and Telstar II upper dome temperatures and eclipse times.

the skin temperature. Both satellites show the dependence of temperature on eclipse time. Also, both satellites show that after the satellite comes out of eclipse, some 180 to 270 days after launch that the canister temperature is greater than the initial value in a full sunlit orbit. This increase in canister temperature, even though the solar current decreases with time, is attributed to a slight increase in the absorptivity-to-emissivity ratio ( $\alpha/\epsilon$ ) of the satellite skin. Ultraviolet radiation is known to increase the solar absorptivity of the exterior white surface of the satellite. Also, thermal cycling as the satellite goes through eclipses may cause the white aluminum oxide to flake off the surface.

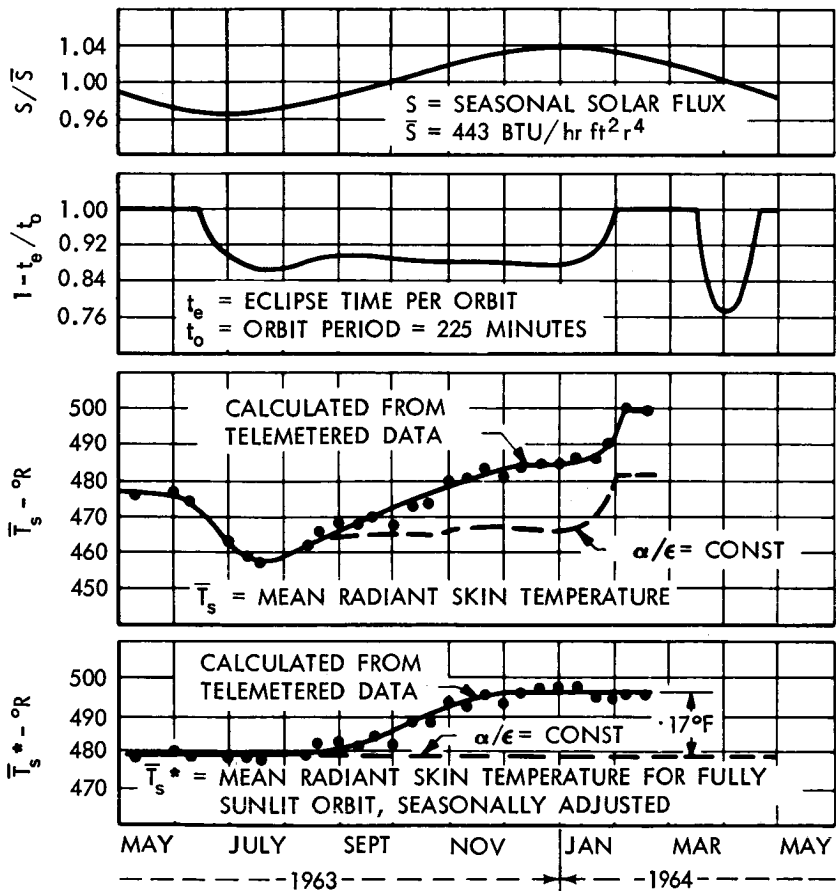


Fig. 106 — Telstar II eclipse and skin temperature data.

Figure 106 shows data to substantiate the change in  $\alpha/\epsilon$ . If the data in the top two curves are used, the calculated mean radiant temperature would be as shown in the dotted curve in the graph second from the bottom. The solid curve calculated from telemetry data shows that the mean radiant skin temperature has increased. The mean radiant skin temperature for a fully sunlit orbit and adjusted for the seasonal variation of solar flux would be constant if the  $\alpha/\epsilon$  of the satellite had not changed. The bottom graph in Figure 106 shows the  $\alpha/\epsilon$  has changed since launch.

#### *Canister Pressure*

The canister pressure is plotted as a function of time in Figure 107. The pressure within the electronics package has gradually increased from 9.5 psia at the time the canister was sealed to beyond 12.7 psia. The latter figure corresponds to the upper bit level limit of the particular telemetry channel used to measure pressure. The pressure rise is due to continuing effusion of  $\text{CO}_2$  from the polyurethane foam used in the canister. The pressure has a strong temperature dependence which has been duplicated in the laboratory. During the eclipse period in March 1964 (see Figure 105) the pressure will be below the 12.7 psia value. The pressure is not expected to ever exceed atmospheric pressure.

#### *Spin Rate and Solar Aspect*

The top graph in Figure 108 shows how rapidly the spin rates of

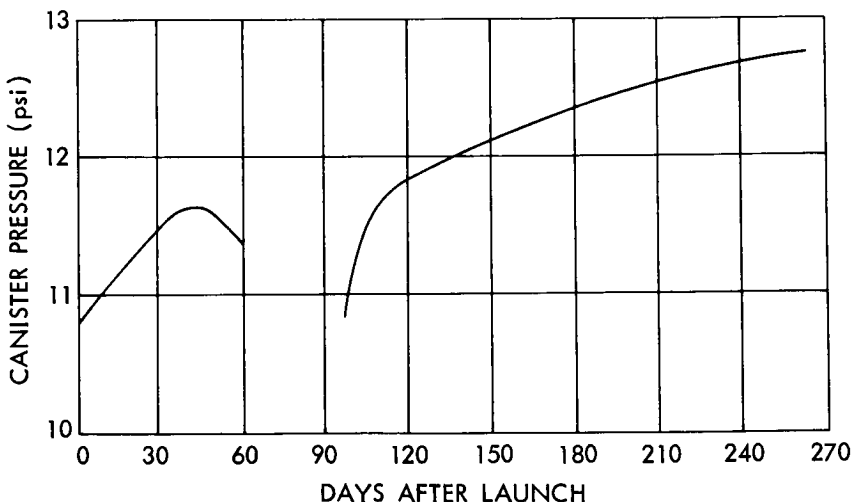


Fig. 107 — Telstar II canister pressure versus time.

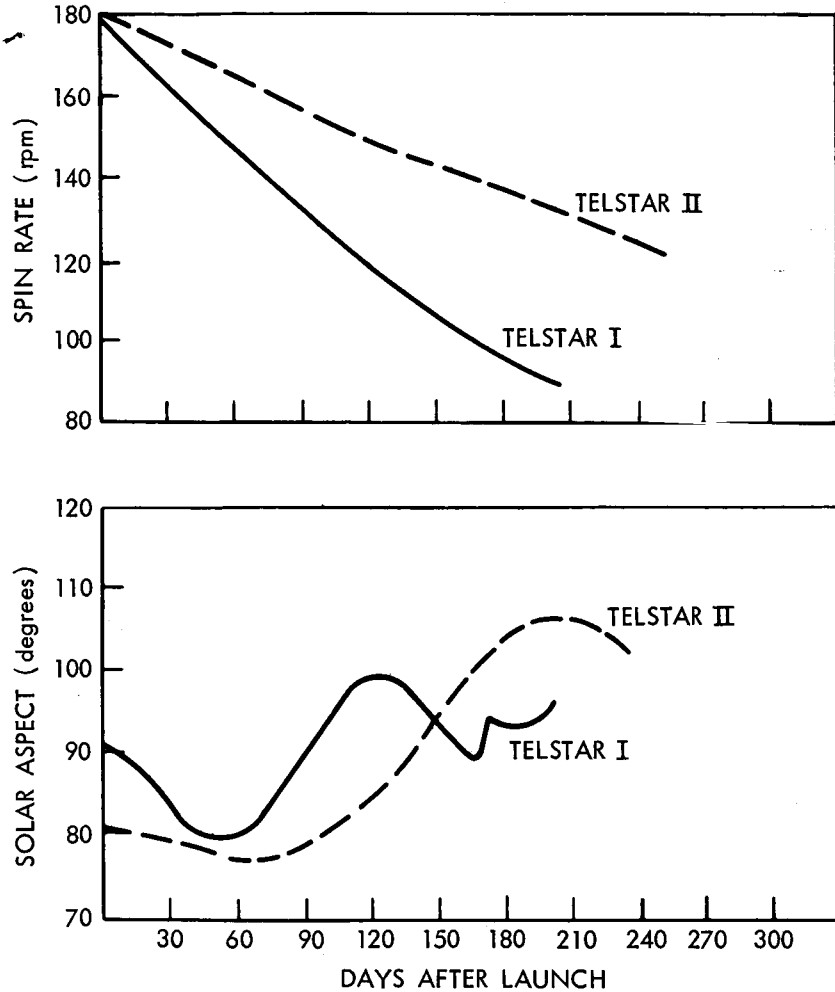


Fig. 108—Telstar II spin rates and solar aspect.

Telstar I and II have changed since launch. The Telstar II spin rate decay is less than that of Telstar I because of the difference in orbit; the higher apogee of Telstar II means it experiences a weaker geomagnetic field and thus the induced eddy currents are less.

Both Telstar I and II are spin oriented and were launched so that the sun's rays would be approximately perpendicular to the spin axis; solar aspect angle is approximately 90°. The lower graph in Figure 108 shows how the solar aspect angles for the two satellites have changed since launch. The abrupt change in the angle for Telstar I resulted

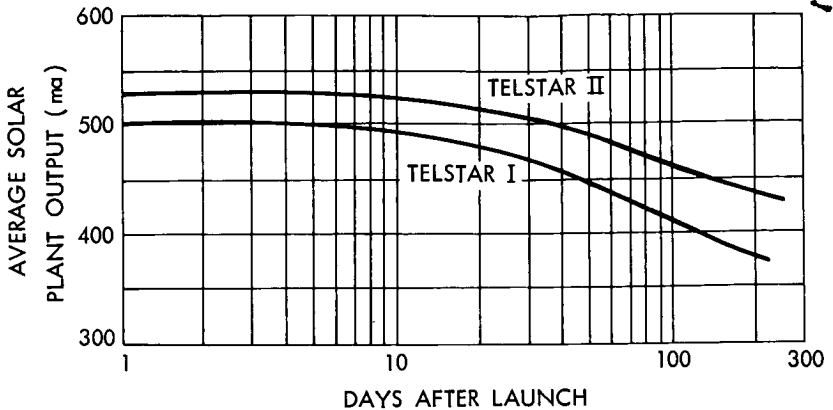


Fig. 109 — Telstar solar currents.

from planned correction of the angle by use of the torquing coil in the satellite. The torquing coil in Telstar II was used in May 1964.

#### *Solar Current*

The solar currents for Telstar I and II shown in Figure 109 are corrected for mean solar distance and are averaged over one revolution of the satellite. The initial current for Telstar I is less than that for Telstar II because there were two faulty solar cell groups of 12 cells each shorted out in the former prior to launch. The slower degradation in the solar plant in Telstar II reflects the lower total radiation dose experienced because of the higher apogee for this satellite.

#### *Conclusions*

The Telstar II satellite has performed in a proper and predictable manner. The telemetry data from the satellite and data taken on the ground show no measurable change in the satellite except for predictable things such as temperatures and solar plant degradation. There is no reason to believe that the life expectancy will be less than prelaunch predictions.

#### REFERENCES

1. Brown, W. L., et al. "The Spacecraft Radiation Experiments," *Bell Syst. Tech. J.* 42(4-1): 899-942, July 1963.
2. McIlwain, C. E., "Coordinates for Mapping the Distribution of Magnetically Trapped Particles," *J. Geophys. Res.* 66(11): 3681-3691, November 1961.
3. Brown, W. L., Gabbe, J. D., and Rosenzweig, W., "Results of the Telstar Radiation Experiments," *Bell System Tech. J.* 42(4-3): 1505-1560, July 1963.

4. Brown, W. L., "Trapped Particle Population from Telstar and Explorer 15 Observations," *Am. Geophys. Union Trans.* 44(1): 76, March 1963 (Title only).
5. McIlwain, C. E., "The Radiation Belts, Natural and Artificial," *Science*, 142(3590): 355-360, October 18, 1963.
6. Carter, R. E., Reines, F., Wagner, J. J., and Wyman, M. E., "Free Antineutrino Absorption Cross Section. II. Expected Cross Section from Measurement of Fission Fragment Electron Spectrum," *Phys. Rev.* 113(1): 280-286, January 1, 1959.
7. Van Allen, J. A., and Lin, W. C., "Fifteen-Month History of the Artificial Radiation Belt Due to the Starfish Nuclear Burst," *Am. Geophys. Union Trans.* 45(1): 84-85, March 1964 (Abstract).
8. Hess, W. N., ed., "Collector Papers on the Artificial Radiation Belt from the July 9, 1962, Nuclear Detonation," *J. Geophys. Res.* 68(3): 605-758, February 1, 1963.
9. Lenchek, A. M., and Singer, S. F., "Geomagnetically Trapped Protons from Cosmic-Ray Albedo Neutrons," *J. Geophys. Res.* 67(4): 1263-1287, April 1962.
10. Brown, W. L., Davidson, L. W., and Medford, L. V., "Relay I Technical Report," January 1964.
11. Smith, K. D., et al, "The Solar Cells and Their Mounting," *Bell Syst. Tech. J.* 42(4-3): 1765-1816, July 1963.